Università degli Studi di Urbino Carlo Bo

Dipartimento di Scienze Pure e Applicate (DiSPeA)

Ph.D. in Scienze di Base e Applicazioni
Curriculum Scienze della Terra
XXXIII cycle

Textural and petrologic study of the subvolcanic mafic and ultramafic ejecta of Piton de la Fournaise as a key to unravel the shallow magmatic crystallization processes at La Réunion Island (Indian Ocean)

ACADEMIC DISCIPLINE:

GEO/07 (Petrologia e Petrografia)
GEO/08 (Geochimica e Vulcanologia)

Coordinator: Prof. Alessandro Bogliolo

Supervisor: Prof. Alberto Renzulli

Co-Supervisors: Prof. Andrea Di Muro

Dott. Andrea Luca Rizzo

Ph.D. student: Gaia Brugnoni

ACADEMIC YEAR
2019-2020

"Se le cose le vuoi veramente

accadono".

A Mirco

Index

I. Abstract

The Réunion Island consists of two juxtaposed volcanic massifs, the oldest Piton des Neiges (in the north-west) and the youngest, presently active Piton de la Fournaise (in the south-east). A third, poorly known buried volcano, named Les Alizés was mainly defined through exploratory drilling and constitutes the basement of Piton de la Fournaise (Lénat et al., 2012). The construction of Piton de la Fournaise *sensu stricto* started at about 400-450 ka. Its lavas are mainly transitional basalts defining a differentiation trend towards mugearites, intermediate in character between the alkaline and tholeiitic series, both aphyric ("cotectic basalts") and olivine-rich ("oceanites"). They slightly differ from Les Alizés aphyric basalts ("abnormal group") that belong to the more alkalic (K_2O-rich) series, with higher MgO and lower CaO and SiO_2 contents. The moderate chemical heterogeneity has been since long attributed to a combination of slight mantle source heterogeneity and influence of clinopyroxene fractionation at mantle/underplating depth. Magmas stored at crustal depths and erupted at the summit area are quite homogeneous and result from the hybridization process of "tholeiitic" and "alkaline" end members (Di Muro et al., 2014; Boudoire et al., 2018; Vlastelic et al., 2018).
The present Ph.D. work deals with a petrological study of mafic and ultramafic ejecta of the "Bellecombe Ash Member" (BAM, ≈ 5.5-3.0 ka), in order to unravel the pre-eruptive conditions of basalt crystallization and possibly matching the various recognized petrographic groups of the subvolcanic igneous rocks with the whole extrusives (Piton de la Fournaise, Piton des Neiges, Les Alizés) combining mineralogy, petrographic texture and geochemistry. Large caldera forming events such as that of the Bellecombe Ash Member, the largest explosive activity produced by Piton de la Fournaise involve, as ejecta, a large fraction of the crustal magmatic plumbing system and allowed to i) access to a rare snapshot of the magmatic processes (cumulate vs. liquid composition; volatile exsolution and percolation; melt and rock assimilation) occurring below one of the most active basaltic volcanoes of the world, and ii) study the magmas driving these rare but very hazardous geological events. The petrological study of more than one hundred samples, representative of the ejecta within the Bellecombe Ash Member, emphasizes the presence of many subvolcanic mafic and ultramafic igneous rocks: dunites, wherlites, ophitic gabbros, sub-ophitic gabbros, poikilitic gabbros, doleritic gabbros, micro-monzogabbros and porphyrogabbros. Cumulate cognates *sensu stricto* are present, often with quenched basaltic glass entrapped interstitially and in minerals (melt inclusions), with no disequilibrium textures recognized in the subvolcanic crystal frameworks. Other subvolcanic clasts (e.g. doleritic gabbros) may simply represent slowly-cooled equivalents (with no crystal-liquid fractionation) of the erupted cotectic basalts. Chemistry of both minerals (olivine, clinopyroxene, feldspar, oxides and phlogopite) and interstitial glass from the subvolcanic ejecta has been performed by EMPA. It is worth to note

that porphyrogabbros emphasize a wide range of feldspars, as interstitial crystals between the large olivine phenocrysts, represented by plagioclase, anorthoclase and sanidine, defining a complete miscibility feldspar curve. Olivines of each mafic and ultramafic lithotype ejecta show different forsterite contents and the whole compositional range is from Fo_{69} (sub-ophitic gabbros) to Fo_{90} (dunite), with an overall range in CaO contents from 0.05 to 0.4 wt.%. A fluid inclusion chemical and thermobarometric study (CO_2, H_2O and noble gases) was made on selected olivine, clinopyroxene, and feldspar crystals. Noble gases and CO_2 content in fluid inclusions of the studied ejecta reveal variable concentrations and elemental ratios (e.g. He/Ar*), indicating, for the whole mafic and ultramafic suite of the Piton de la Fournaise magmatic plumbing system a wide range of depths, from the underplating zone to the submarine base of the edifice and various extent of magmatic degassing. The above barometric data have been also confirmed by fluid inclusion study by Raman spectroscopy analyses. A comprehensive geochemical comparison among the analysed mafic and ultramafic ejecta (major and trace elements by ICP-OES-MS) and the whole compositional spectrum of the Piton de la Fournaise and Les Alizés volcanic rocks available from literature was also carried out. Major and trace elements geochemistry allowed to confirm the three fractional crystallization trends already defined by the literature, namely gabbro- wherlite- and dunite-fractionations which well agree with the erupted basalts in the Réunion Island in the last 500 ka. A wide range of textures in these ejecta results from variable P-T gradients in the subvolcanic environment of crystallization. In particular the CO_2-H_2O fluid inclusion and thermobarometric studies carried out by Raman spectroscopy on selected single crystals (olivine and clinopyroxene) permitted to better understand the depths of crystallization of the samples. The study of the mafic and ultramafic subvolcanic igneous rocks of Piton de la Fournaise entrapped in the BAM eruption allow to target the transcrustal plumbing system still active during large caldera forming events. Compositions of the interstitial glass and minerals in some subvolcanic ejecta has been also compared with small volumes of evolved liquids (trachytes) detected as pumiceous components in the products of the Bellecombe Ash Member caldera-forming eruption and the old Piton des Neiges volcano. In general, the textural and petrologic study of the subvolcanic ejecta of Piton de la Fournaise provides new insights on the magmatic plumbing system and the subvolcanic crystallization processes at La Réunion Island. Some peculiarities on the processes of crystallization in the magmatic plumbing system were pointed out, with respect previous knowledges. Some ejecta defined as porphyrogabbros could represent oceanite magmas stored at crustal levels where, the interstitial basaltic melts supporting the abundant olivine crystals gave rise to a sanidine- and phlogopite-bearing micro-cryptocrystalline groundmass. This micro-cryptocrystalline groundmass could be really considered cogenetic with trachytic liquid, which may be erupted as

glassy pumice if the undercooling would be high enough to preclude groundmass crystallization. The overall textural and geochemical data of the investigated mafic-ultramafic ejecta, do not only reflect different mode of subvolcanic crystallization (cumulate *sensu stricto* vs. slowly-cooled equivalents of the steady state basalts which are represented by the doleritic gabbro and some of the subophitic gabbro ejecta) but also (i) the interaction between basaltic liquids and cumulates already formed at crustal level of the Piton de la Fournaise plumbing system and (ii) the possibility that small pockets of liquids may also evolve to trachytic compositions. The compositional range from basalt to basaltic trachyandesite of the interstitial glass found in the intrusive clasts, indicate that the melt was entrapped within the crystal frameworks and quenched during the eruption. This likely suggests the clast were disrupted from the wall rocks and transported very fast to the surface, mostly as cognates. If not entrapped interstitially during *in situ* crystallization, silicate liquid could be also expelled from the crystal frameworks, forming separated melt pockets or larger body, e.g. slightly differentiated sills.

Fluid inclusion barometry (Raman analyses) and noble gases and CO_2 from fluid inclusion crushing extraction and mass spectrometer analyses indicate the dunites are the intrusive ejecta from the deepest levels, approximately at the underplating levels of formation (~13 km b.s.l.). Wherlites should have crystallized close to the submarine base of the edifice (~6 km b.s.l.), whereas the mafic subvolcanic samples are even shallower. Nevertheless, a large composite intrusive ejecta (B108) emphasizes the coexistence of mesoscale ultramafic-mafic patchy microdomains (wherlite to plagioclase-wherlite to troctolite to gabbro) at intermediate crustal level of crystallization, below 0.3 GPa according to the liquidus curves of the La Reunion magmas (Fisk et al., 1988). Textures in this composite ejecta can be the result of basaltic melts interacting with wherlitic cumulates at relatively low pressure, leading to the instability of clinopyroxene and high dissolution of olivines (now highly rounded), with a high loss of temperature of the system. In this way at the same pressure, but lower temperature, plagioclase is the *liquidus phase* and therefore wherlitic cumulates interacting with basaltic melts at relatively low pressure can produce plagioclase-wherlite and troctolite patchy microdomains at the mesoscale. Similar interactions between batches of basaltic magmas and cumulates already present in the magmatic plumbing system are also highlighted by other wherlites (i.e. B28 sample) coupled with olivine dissolution/reaction leading also to clinopyroxene.

Finally, the presence of loose quartz xenocrysts in products at the Langevin Caldera, possibly with aqueous inclusions with low-salinity and low CO_2 content and an enrichment of some trace elements (e.g. Li, Al, Sr) at their rims could suggest the involvement of the hydrothermal system of Piton del la Fournaise during explosive eruptions of the volcano.

1 Introduction

Réunion Island is a large and dominantly effusive basaltic volcanic oceanic system in the southernmost part of the Mascarene Basin (Indian Ocean), 800 km east of Madagascar, located at the youngest end of the hot spot track, which produced the Deccan Trapps. The island consists of two juxtaposed volcanic massifs, the oldest Piton des Neiges (in the north-west) and the youngest, presently active Piton de la Fournaise (in the south-east). A third, poorly known buried volcano, named Les Alizés was mainly defined through exploratory drilling and constitutes the basement of Piton de la Fournaise. The construction of Piton de la Fournaise *sensu stricto* started at about 400-450 ka. Piton de la Fournaise is one of the most active intra-plate volcanoes of the world. The main eruptive centre corresponds to the poly lobate U-shaped Enclos Fouqué caldera. The horseshoe-shaped geometry was interpreted as the result of a huge flank landslide, occurring with the emplacement of the Bellecombe Ash Member. Bellecombe Ash Member is the main tephra identified all around the Enclos Fouqué caldera, corresponding to a sequence of ash, crystal and lithic-rich deposits, (Bachèlery, 1981; Mohamed-Abchir, 1996; Ort et al., 2014), erupted between 4880 ± 35 yr BP and 2340 ± 30 yr BP (Morandi et al., 2016; Bachèlery et al., 2015). This deposit is thought to be emplaced during violent phreatic/phreatomagmatic events related to the flashing of an extensive hydrothermal system during the collapse of the Enclos Fouqué caldera (Bachèlery, 1981; Fontaine et al., 2002; Upton et al., 2000).
The possibility of studying deposits of the Bellecombe Ash Member allow to access to a rare snapshot of the magmatic processes (cumulate vs. liquid composition; volatile exsolution and percolation; melt and rock assimilation) occurring below one of the most active basaltic volcanoes of the world. As the large explosive event of the Bellecombe Ash Member could have disrupted the subvolcanic plumbing system of both Piton de la Fournaise and Les Alizés, the whole crystallization/fractionation trends of the studied mafic and ultramafic ejecta will be compared with those of the main extrusive products of the La Réunion Island oceanic system inferred by the literature.

2 Geological and volcanological setting

The Indian Ocean started to open around 175 Ma (Schettino and Scotese, 2005). The early stages of Gondwanan break-up separated Africa from a block composed of Madagascar, India, Australia and Antartica (Coffin and Rabinowitz, 1987; Smith and Sandwell, 1997). Around 83 Ma the Mascarene Basin opened, marking the separation of Madagascar and India (Bernard and Munschy, 2000; Dyment, 1991a). The Mascarene basin rift became extinct at ≈61 Ma, when the spreading jumped to a new location, between the Seychelles and India, to become the Central Indian Ridge. The Seychelles and Madagascar are micro-continents isolated by episodes of sea floor spreading. The other

plateaus, Laccadives, Maldive, Chagos, Mascarene, Mauritius and La Réunion islands are widely regarded as volcanic constructions of the La Réunion hotspot can be traced back to the emission of the Deccan Trapps at the K-T boundary in the late Cretaceous era (Duncan, 1990; Duncan et al., 1989; Georgen et al., 2001; Storey, 1995; Berthod et al., 2020; Fig. 2.1). When the hotspot was near the mid-ocean spreading ridge, it produced complex structural and geochemical interactions (Ito et al., 2003; Morgan, 1978; Sleep, 2002). Mascarene Basin has been the subject of numerous studies because it is a key area to understand the geodynamics of the early stages of the Indian Ocean. Based on radiometric dating of subaerial rocks, current effusive rate and volumetric estimates of the island, La Réunion is thought to be active since at least 5 Ma (Gillot et al., 1994; Lénat et al., 2001; Berthod et al., 2020) with the edification of two successive shield volcanoes.

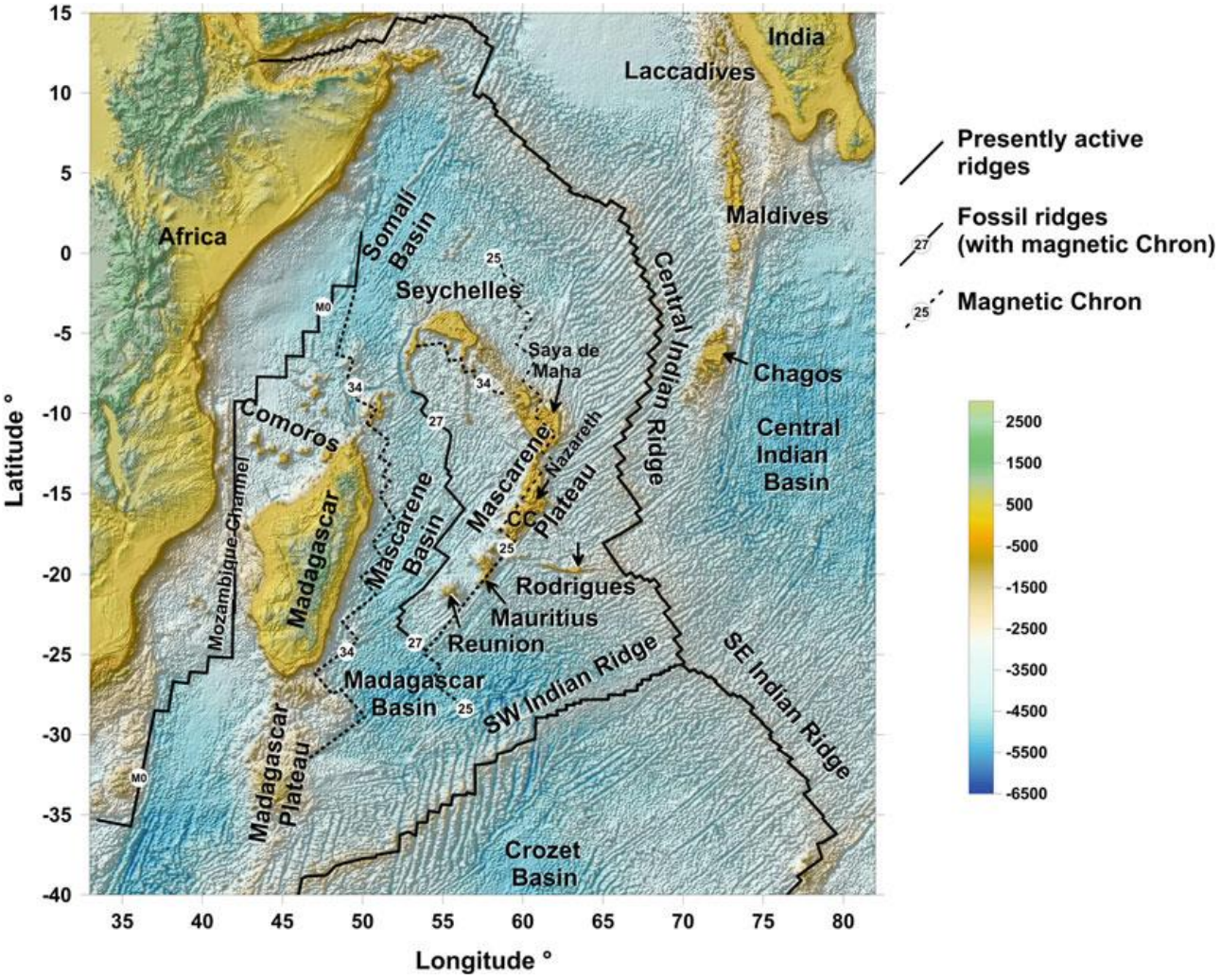

Fig. 2.1 - Geodynamic setting of La Réunion. The magnetic chronos are taken from Müller et al. (1997).

2.1 La Réunion

La Réunion (21.0°S; 55.5°E) lies in the middle of an approximately 350 km-wide zone bounded by the Mauritius transform fault to the SE and by the Mahanoro-Wilshaw transform fault to the NW. Another structural boundary, to the SW, is a trough identified as an extinct spreading centre. La Réunion is a huge volcanic oceanic system in the southernmost part of the Mascarene Basin, in the Indian Ocean (Fig. 2.1.1). The island is a large cone of about 51500 km^3, is elliptical in shape (50x70 km) with a NW-SE orientation, and rises on the ocean floor (about 4200 m below sea level) to 3070 m above sea level and its base diameter is of about 210 km.

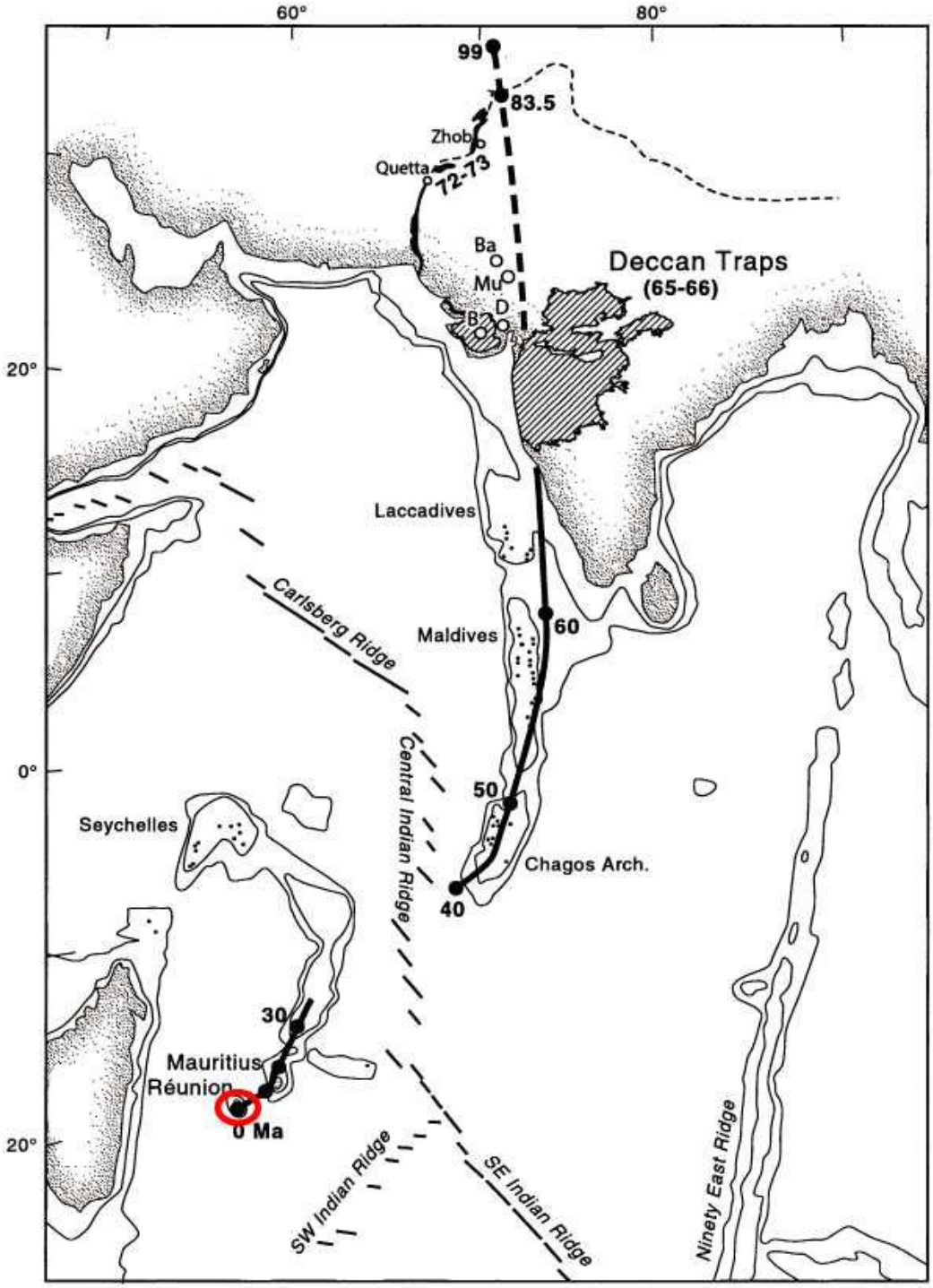

Fig.2.1.1 - The heavy line in the map indicates the model 0-99 Ma track of the Réunion hotspot, assuming a stationary hotspot and that plate reconstructions are accurate. The age is in Ma. The Réunion Island is indicated in the map with a red circle (Kent et al., 2002; Duncan, 1990).

The island of Réunion is situated 700 km east of Madagascar and is composed of two juxtaposed volcanic massifs, the oldest Piton des Neiges (in the north-west) and the youngest, presently active Piton de la Fournaise (Piton de la Fournaise, in the south-east; Fig. 2.1.2), respectively 3070 and 2600 m above sea-level. A third, poorly known buried volcano, named Les Alizés, has been recognized below

Piton de la Fournaise on the eastern submarine flank and was mainly defined through exploratory drilling. It constitutes the basement of Piton de la Fournaise (Gailler and Lénat, 2010; Lénat et al., 2001a; Malengreauet al., 1999; Smietana, 2011; Smietana et al., 2010; Fig. 2.1.3).

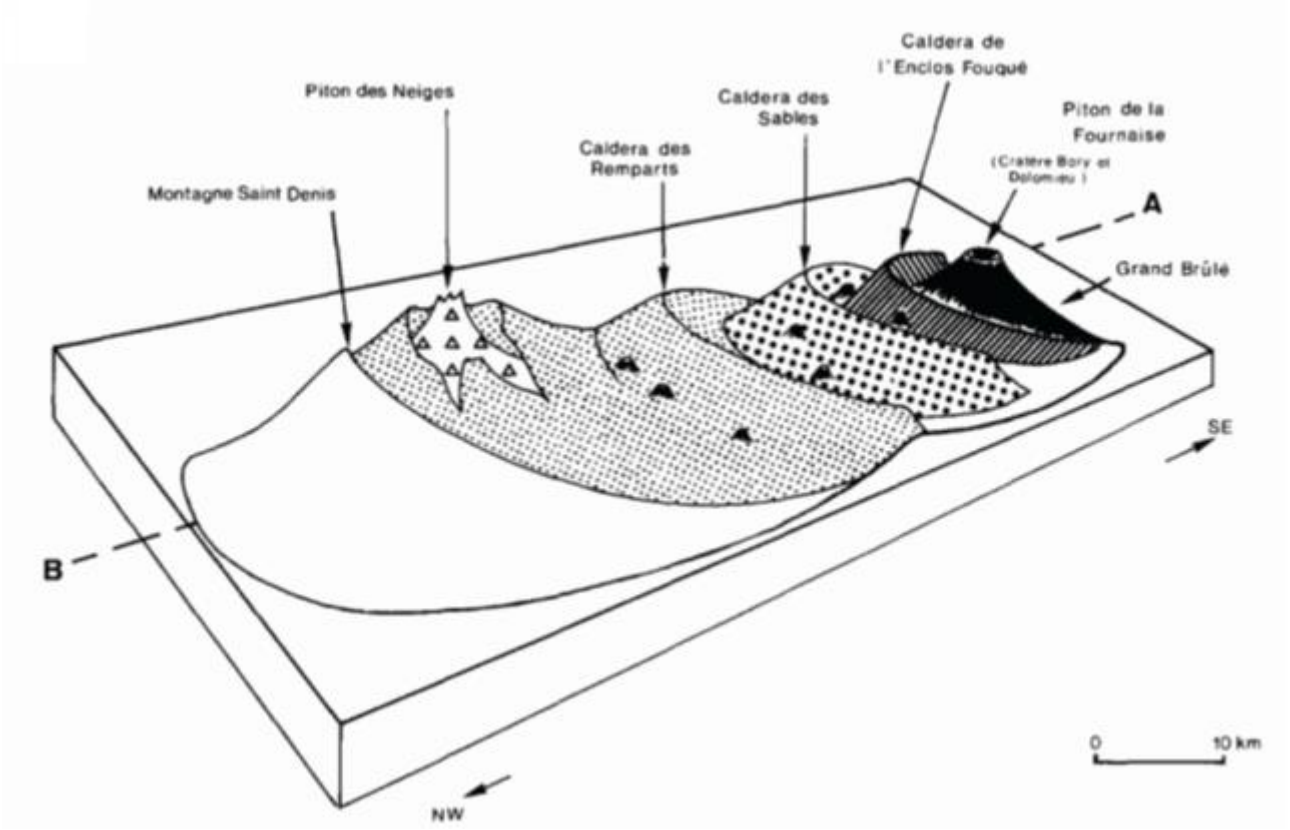

Fig. 2.1.2 - Evolutionary diagram of construction of La Réunion Island with the succession of nested collapses (from NW to SE) over time (Gillot et al., 1994; Smietana, 2011).

The whole edifice appears as a flattened cone, 220-240 km in diameter and 7 km in height, with a very large submarine base, about 210 km in diameter (Saint-Ange et al., 2011, 2013; Le Friant et al., 2011; Sisavath et al., 2011, 2012; Babonneau et al., 2013; Michon et al., 2016). Its contact with the quasi-flat sediments of the ocean bottom is clear, at depths of around -4000 m. In the transition zone between the lower flanks of the edifice and the abyssal plain, there are almost continuous sediment waves, concentric to the edifice, except where major canyons reach the abyssal plain (Le Friant et al., 2011; Oehler et al., 2008). These concentric features are classically attributed to turbidity currents (Le Friant et al., 2011; Wynn et al., 2000), but they could correspond to the folding of ductile pelagic sediments in response to compressive strain created at the front of advancing debris avalanches (Oehler et al., 2008). The volcanic edifice does not correspond to a perfectly shaped cone, although the base of the whole island is almost circular (Le Friant et al., 2011). The submarine cone is composed of four main fan-shaped bulges which are separated by major canyon systems (Labazuy,

1996; Oehler et al., 2008). In La Réunion, products of flank destabilization and erosion are widely distributed on the submarine slopes (Gailler and Lénat, 2010; Saint-Ange et al., 2013). These deposits are related to spreading, which implies slow deformation, and rapid mass movement, like debris avalanches or sediment transfer by shallow landsliding and turbidity currents (Oehler et al., 2008; Le Friant et al., 2011). A widespread extension of volcaniclastic products emphasize the importance of remobilization process on La Réunion Island. The part of the submarine flanks of Piton de la Fournaise that are directly built by lava-flows are only few portions. Among volcaniclastic deposits, large volume of debris avalanche deposits has been identified on the submarine flanks of Piton de la Fournaise (Oehler et al., 2004; Lénat et al., 2009; Le Friant et al., 2011; Saint-Ange et al., 2013). These deposits reveal the occurrence of old large flank collapse affecting Piton de la Fournaise.

The geological maps of La Réunion island (Oehler et al., 2008; Lebas, 2012) show surface rocks resulting from both constructional and destruction processes. On the submarine surface, few constructional features (cones, eroded piles of lava flows) have been recognized. Most of these features are located close to the coast in continuation of the on land southwest and northeast rift zones of Piton de la Fournaise. Pristine, small monogenic cones and flat-topped cones on the north and northeast flanks indicate small eruptions outside of the main volcano centres during the construction of La Réunion (Gailler and Lénat, 2010; Oehler et al., 2008). Debris avalanche deposits are the most extensive and voluminous formations in the submarine domain (Oehler et al., 2008). They have built four huge submarine bulges to the south, west, north and east of the island, forming fans 20-30 km wide at the coastline and 100-150 km wide at their ends, 70-80 km offshore. Submarine flanks have relatively gentle slopes ranging between 2° and 5° on average (Saint-Ange et al., 2011; Michon et al., 2016). In La Réunion, products of flank destabilization and erosion are widely distributed on the submarine slopes; this is the reason why the flanks of La Réunion are less steep than other volcanic islands, like Hawaii (10° to 15°; Michon et al., 2016). These deposits are related to slow deformation (spreading) and rapid mass movements, like debris avalanches or sediment transfer by shallow landslides and turbidity current (Oehler et al., 2008; Le Friant et al., 2011; Michon et al., 2016). The importance of remobilization processes on La Reunion Island results in a widespread extension of volcanoclastic products and a very wide submarine base of the volcanic edifice compared to the size of the island itself (Babonneau et al., 2016). The portion of the submarine flanks built by lava flows accumulations are rare. They essentially correspond to the submarine extensions of the subaerial NE and SE rift zones. The smooth surface that characterizes the shallowest part (from sea level to 1800 m deep) of the NE rift zone submarine extension is in a good morphologic continuity with the subaerial slopes. However, the incision of deepest relief

together obtained on pillow lavas dredged 1400 and 2100 m depth on this area (Smietana, 2011) clearly indicate that the NE rift zone is built on an older edifice, probably Les Alizés volcano (Lénat et al., 2001a).

La Rèunion is built on Upper Cretaceous to Paleocene oceanic crust. Although the onset of La Réunion volcanism is unknown; it is probably younger than 10 Ma and therefore a thick sequence of oceanic sediments should already have blanketed the basaltic crust when the hotspot volcanism started. Seamounts were built up after formation of the oceanic crust and some are probably buried beneath La Réunion (Lénat, 2016).

Seismic studies show that there is virtually no or very weak lithospheric flexure beneath La Réunion, whereas a large body of underplating material has been demonstrated beneath the southwest part of the island (Charvis et al., 1999; Voogd et al., 1999; Gallart et al., 1999). This absence of flexure is supported by the gravity data (Lénat, 2016). The absence of a large flexure contrasts with most similar oceanic volcanoes and suggests a dynamic equilibrium where positive buoyancy of the plume would contribute to the dynamic support of the load of La Réunion. The scale models suggest that the most important factor controlling the buoyant flow of the plume material is the presence of mechanical discontinuities at the lithospheric scale. On the base of this geometry of the ocean floor, it has been estimated that the subaerial part of the edifice of La Réunion represents only 4% of the total volume of the whole volcanic system (Michon et al., 2016).

With different geophysical approach, the interior of the submarine flanks of La Réunion have been studied, showing negative Bouguer anomalies, which more or less mimics the four bathymetric bulges described above (Oehler et al., 2008).

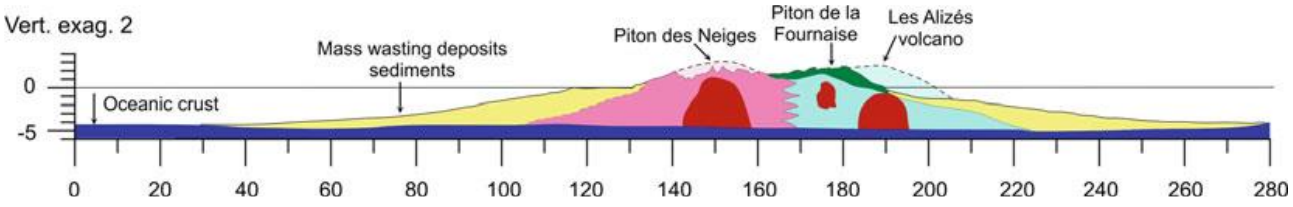

Fig. 2.1.3 - A summary view of the internal structure of La Réunion (Bachelery et al., 2015).

2.2 Piton des Neiges

Piton des Neiges, whose oldest recognized outcropping lava flows are 2.2 Ma old basalts (McDougall, 1971; Quidelleur et al., 2010), is located in the north-west of the island and is the largest of the three volcanoes. It has been dormant for less than 30 ka (Deniel et al., 1992; Gillot and Nativel, 1982; McDougall, 1971; Salvany et al., 2012). After a period of apparent quiescence, Piton des Neiges then erupted differentiated alkaline lavas between 350 and 29 ka.

The evolution of Piton des Neiges volcano over more than 2 Ma, involving volcanic and volcano-tectonic activity and high erosion rates, has resulted in a complex geology exposed in deep valleys. The internal structure of Piton des Neiges volcano has been studied with several approaches. The main feature of the interior of the volcano is the presence of a huge intrusive complex which creates a large positive gravity anomaly. This complex emerges at various places at the bottom of the Salazie and Cilaos Cirques as gabbro outcrops; some syenites and micro-syenites are also observed (Berthod et al., 2020). Various models (Gailler and Lénat, 2012) suggest that the volcanic-subvolcanic complex may extend down to the base of the edifice and it is overlaid by lava flows, pyroclastics, landslide deposits and sills and dykes in the central part (Chevallier and Vatin-Pérignon, 1982; Maillot, 1999; Rançon, 1982).

2.3 Les Alizés

Les Alizés, in the south-west of the island, is poorly known, as it constitutes the basement of the youngest Piton de la Fournaise volcano. The discovery of a large positive gravity anomaly near the eastern coast of Piton de la Fournaise (Gérard et al., 1980; Rousset et al., 1989), in the area called Grand Brûlé, produced a debate in the scientific community (Lebas, 2012; Salvany et al., 2012). A drill hole provided the proof that the structure responsible for the gravity anomaly was a hypovolcanic intrusive complex, mostly composed of gabbros and other cumulates (Rançon et al., 1989), encountered between about 1000 and 3000 m b.s.l. (bottom of the drill hole). The geothermal gradient and the relatively low temperature at the bottom of the drill hole (≈140° C) indicated that the complex was old and inactive (Rançon et al., 1989). The 5-8 km wide complex is elongated in a north-south direction in plan view (15-18 km). Subsequent gravity measurements and modelling showed that the dense structure was independent from the structures of Piton de la Fournaise volcano (Gailler et al., 2009). Les Alizés volcano could have emerged at about the same period as Piton des Neiges (around 2 Ma), considering the age of about 3.5 Ma for pillows lava near 2000 m b.s.l. (Bachelery et al., 2015). Large flanks landslides probably were responsible for the massive destruction of Les Alizés volcano (Merle et al., 2010; Oehler et al., 2008; Fig. 2.3.1). The reconstruction of the history of building and erosion/burial of Les Alizés volcano is one of the main issues in the understanding of the evolution of La Réunion, but large uncertainties remain.

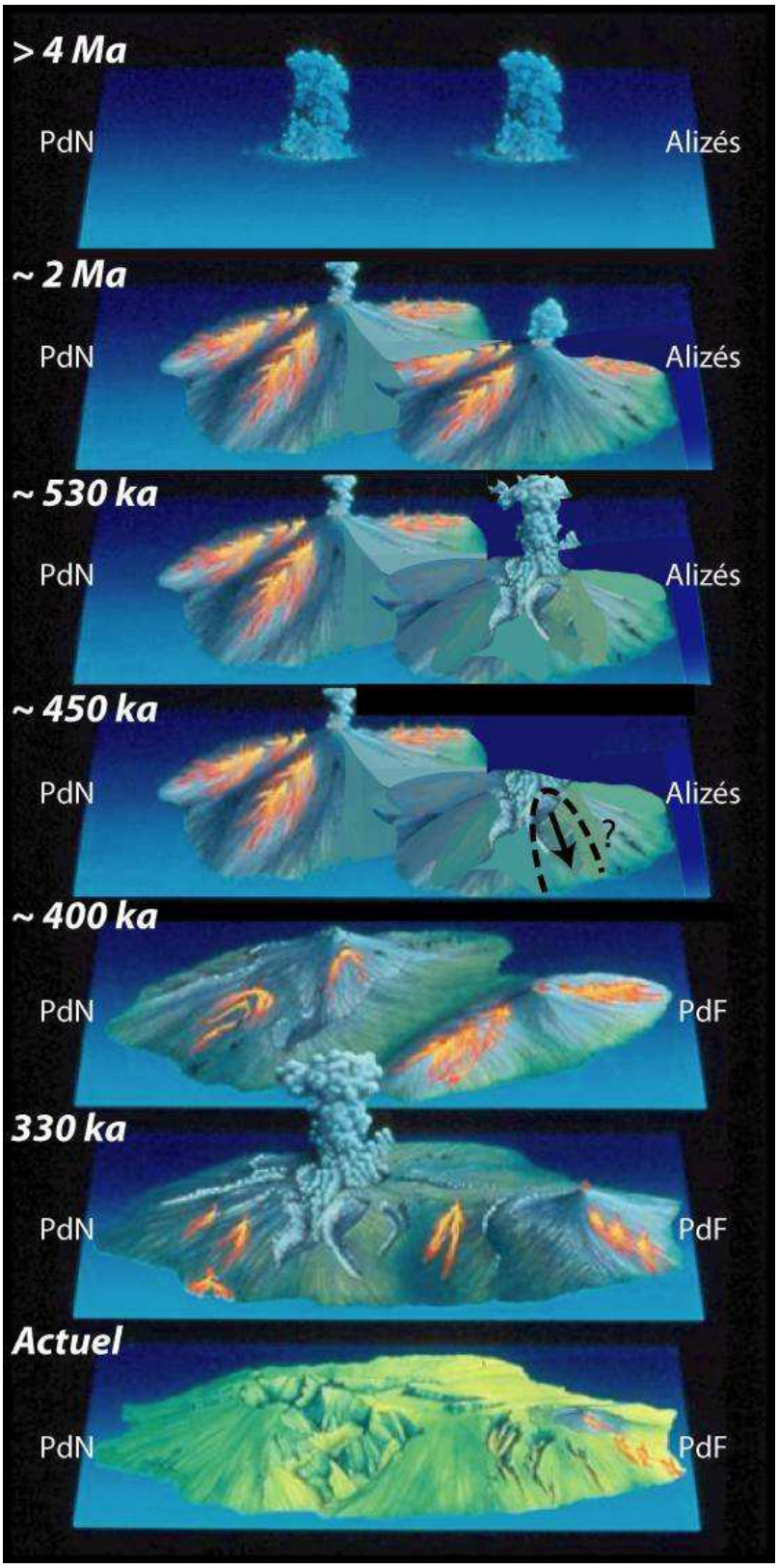

Fig. 2.3.1 – Iconography representing the different stages of construction of La Réunion island (Bachelery and Mairine, 1991; Smietana, 2011).

2.4 Piton de la Fournaise

Piton de la Fournaise occupies the south-eastern part of the island, and is a highly active basaltic shield volcano, with most of its activity restricted to effusions from its Central Cone and along rift zone (Michon et al., 2016). Deep valleys have been incised into the areas not covered by young volcanic deposits, providing exposures that enable the reconstruction of certain parts of the volcano's evolution. Piton de la Fournaise has been extensively studied using geological, petrological, geochemical and geophysical monitoring approaches (Fig. 2.4.1). Les Alizés volcano may have produced a large explosive activity occurred around 450 ka, causing a period of quiescence of Piton des Neiges and the birth of Piton de la Fournaise (Smietana, 2011).

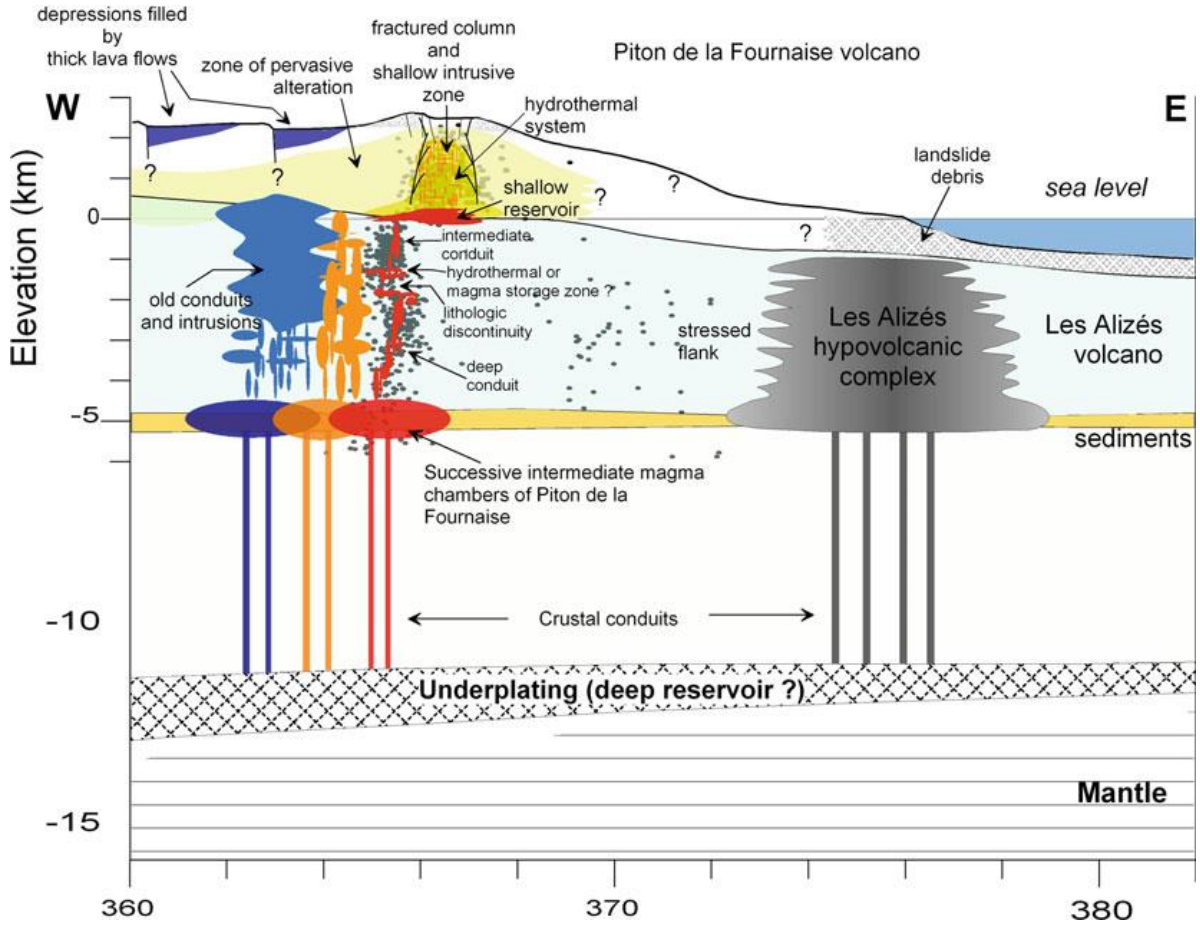

Fig. 2.4.1 - Interpreted W-E geological section of Piton de la Fournaise (Lénat et al., 2012). Horizontal coordinates: UTM km WGS84.

The oldest dated rocks of the Piton de la Fournaise volcano (up to 535 ka; Gillot and Nativel, 1989; Kluska, 1997) are found at the bottom of deep valleys (Rivière des Remparts, Rivière Langevin, Rivière de L'Est) and in La Plaine des Palmistes. Up to 400-450 ka the lavas are plagioclase-rich basalts (locally called "Roches Pintades Series"; Albarède et al., 1997), and they are significantly different from the subsequently emitted basaltic lavas of Piton de la Fournaise. Similar plagioclase-rich basalts are found in Piton

des Neiges, but they are about 200 ka younger than the Piton de la Fournaise ones (Bachelery et al., 2015 and reference therein).

The oldest on-land outcrops are dated at about 530 ka (Gillot and Nativel, 1989) and have been grouped into a single Pintades lava unit (Bachèlery, 1981; Bachèlery and Mairine, 1990; Mairine and Bachèlery, 1997; Merle et al., 2010), observed at the base of all lava sequences in the deep valleys incising Piton de la Fournaise (Rivière de Remparts, Rivière de l'Est and Rivière Langevin). The pintades lava unit, consisting of feldspar-rich basalt to mugearite, does not belong to the Piton de la Fournaise series *stricto sensu* since it includes differentiated rocks, richer in alkali in bulk composition than typical Piton de la Fournaise lavas (Albarède et al., 1997; Luais, 2004; Smietana, 2011). It can represent the upper part of its basement, possibly related to the old Les Alizés volcano (Merle et al., 2010).

Chevallier and Bachèlery (1981) proposed two coeval volcanic centres for this old phase of Piton de la Fournaise, one located north of the Plaine des Sables and the other one close to the current location of the summit of Piton de la Fournaise. The Ancient Piton de la Fournaise then experienced alternating episodes of volcanic destruction and reconstruction, destructive episodes of the edifice being characterized by giant landslides and summit caldera collapses (Merle et al., 2010). The oldest recognized landslide occurred at about 290 ka.

2.5 The Enclos Fouqué caldera and Bellecombe Ash Member

The main eruptive centre was located at the same place of the today's Central Cone, but some researchers suggests the possibility of the occurrence of an intermediate location before activity attained the present one (Letourneur et al., 2008). The age of the eastward migration of the eruptive centre remains controversial (Merle et al., 2010). The eastward migration could have taken place at about 150 ka, concurrently with the formation of the Morne Langevin caldera (Bachèlery and Mairnìine, 1990). Several collapse-related structures can be identified in the morphology of Piton de la Fournaise and have been interpreted as the scars of huge landslides or the scarps of collapse calderas. The youngest one corresponds to the polylobate U-shaped Enclos Fouqué caldera (which is opened in the east and connected to the Grand Brûlé depression). The horseshoe-shaped geometry was interpreted as the result of a huge flank landslide (Fig.2.5.1a; Bachèlery, 1981; Chevallier and Bachèlery, 1981; Duffield et al., 1982; Lénat et al., 1989; Labazuy, 1996; Merle and Lénat, 2003; Oehler et al., 2004, 2008; Michon and Saint-Ange, 2008). Another interpretation was that the Enclos Fouqué caldera results from coalescent caldera collapses and the Grandes Pentes correspond to the head of an eastwards directed flank landslide (Fig.2.5.1b; Bachélery, 1981). Two additional interpretations interpreted the Enclos Fouqué caldera as an hydrothermal collapse caldera triggered

by the lateral deformation of the hydrothermal system caused by a landslide (Fig.2.5.1c; Merle and Lénat, 2003) or a vertical collapse of the Grand Brûlé (Fig.2.5.1d; Michon and Saint-Ange, 2008). A second possibility is that it occurred after the Plaine des Sables caldera formed at about 65 and/or 40 ka (Bachèlery and Mairine, 1990; Gillot and Nativel, 1989; Merle et al., 2010; Staudacher and Allègre, 1993). A new edifice built east of the ancient volcanic centre after the collapse of the Plaine des Sables. The formation of the most recent 8 km-wide caldera, termed Enclos Fouqué caldera, stopped its activity. This event marked the most recent major volcano-tectonic event in the history of Piton de la Fournaise whose timing and dynamics remains unclear. Caldera formation has been initially associated with the emplacement of the Bellecombe Ash Member, a sequence of ash deposits cropping along the western area of the Enclos Fouqué caldera (Bachèlery, 1981; Mohamed-Abchir, 1996; Ort et al., 2014). An age of 4745 ± 130 yr BP is usually assumed as an older limit for this caldera collapse event and the beginning of the Bellecombe paroxysmal explosive events (Mohamed-Abchir, 1996; Staudacher and Allègre, 1993). This age corresponds to a radiocarbon dating of the uppermost lava flows of the Bellecombe scarp (Bachèlery, 1981). The recent rappraisal of the existing radiocarbon data, enriched by new dating, suggests that Bellecombe ashes groups several explosive events, whose age ranges between 4880 ± 35 yr BP and 2340 ± 30 yr BP (Morandi et al., 2016; Bachèlery et al., 2015). Seismological data indicate that above 7.5 km below sea level, the plumbing system is almost exclusively restricted to the Enclos Fouqué caldera (Nercessian et al., 1996; Aki and Ferrazzini, 2000; Battaglia et al., 2005; Prôno et al., 2009). The magmatic activity related to this part of the volcanic system progressively led to the building, on the floor of the Enclos Fouqué caldera, of the 400-m-high steep Central Cone capped by the Bory crater and the Dolomieu caldera. This cone and to a lesser extent the Enclos Fouqué caldera are cut by hundreds of eruptive fissures that formed during the recent history of Piton de la Fournaise.

A recent reappraisal of historical reports combined with new geological observations suggests that the historical activity of the Central Cone was characterized by a lava lake activity centred on the current inactive Bory crater (Michon et al., 2013). This lava lake fed the largest recent pahoehoe lava field, the Enclos Fouqué lava field (Lénat et al., 2001), between 1733 and 1750 CE.

The main tephra identified all around the Enclos Fouqué is the “Bellecombe Ash unit”. It corresponds to a complex sequence of ash, crystal and lithic-rich deposits (Bachèlery, 1981; Mohamed-Abchir, 1996). This deposit is thought to be emplaced during violent phreatic/phreatomagmatic events related to the flashing of an extensive hydrothermal system during the collapse of the Enclos Fouqué caldera (Bachèlery, 1981; Fontaine et al., 2002; Upton et al., 2000). The ages of the caldera formation and related Bellecombe Ash unit are poorly constrained and are likely comprised in a time

span ranging between the emplacement of the lavas forming the uppermost part of the Enclos Fouqué walls that underlay Bellecombe and Partage ashes (4745 ± 130 BP, 3340 ± 1012) and that of the crystal and lithic-rich Bellecombe and Partage ashes themselves (several ages between 4175 ± 145 and 2320 ± 90 BP). That ashes with age of 2140 ± 80 BP drape the lower and inner wall of Bellecombe cliff (Vergniolle and Bachèlery, 1982). This possibly represents the upper age for a series of caldera-forming events. Most of the eruptive products, lavas and tephras, cropping out inside the Enclos Fouqué caldera are much younger than 2320 BP, actually younger than 1750 CE, final age of the widespread pahoehoe lava field named “champ de lave de l’Enclose Fouqué” (CLEF) by Lénat et al. (2001).

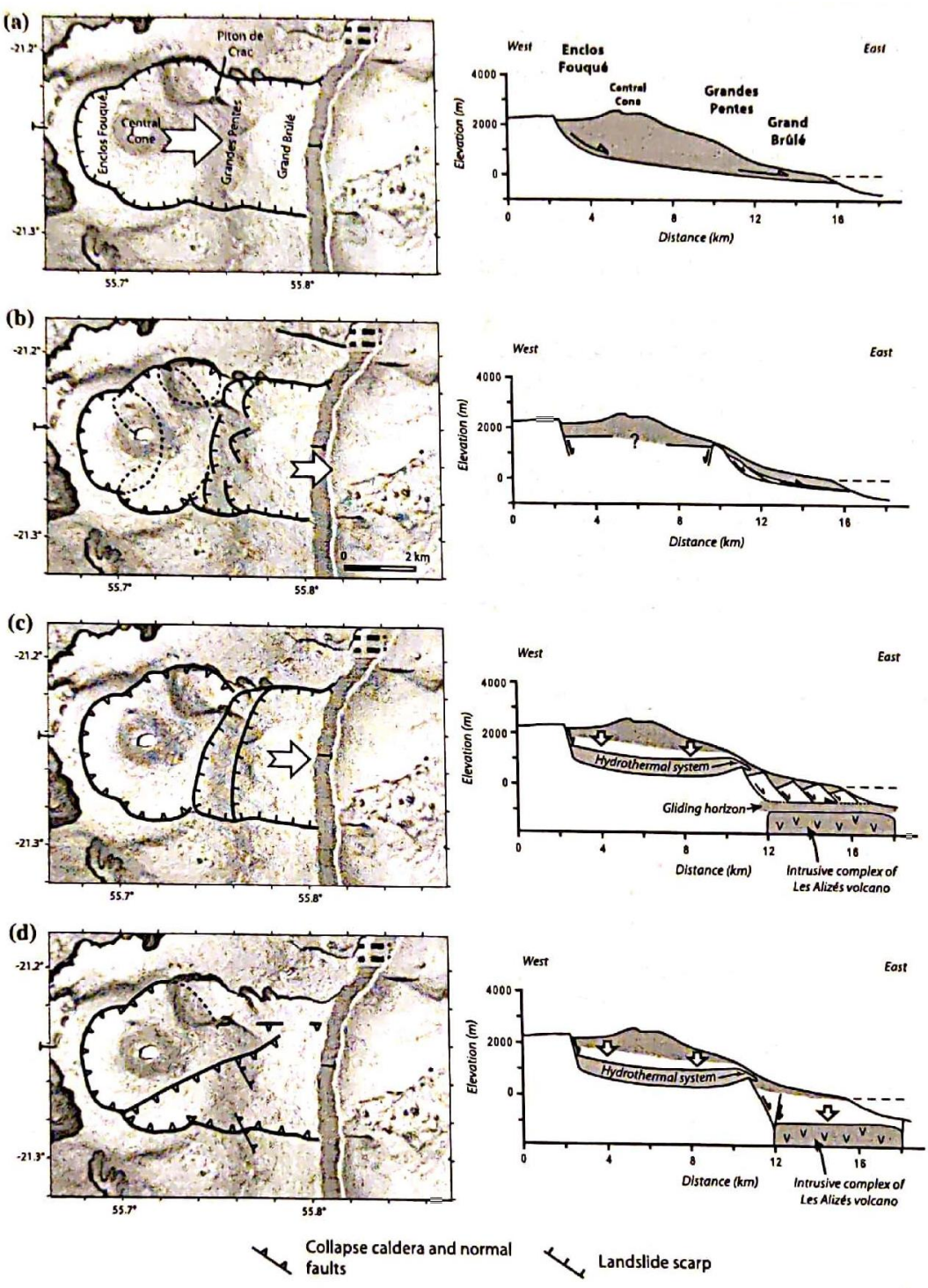

Fig. 2.5.1 - Interpretations of the horseshoe-shaped structure composed of the Enclos Fouqué, the Grand Brûlé and the Grandes Pentes areas (Michon et al., 2016). a) The U-shaped structure as the result of a huge flank landslide; b) The Enclos Fouqué caldera results from coalescent caldera collapses and the Grandes Pentes correspond to the head of an eastwards directed flank landslide; the Enclos Fouqué caldera as an hydrothermal collapse caldera triggered by the lateral deformation of the hydrothermal system caused by c) a landslide or d) a vertical collapse of the Grand Brûlé.

The Plaine des Sables is another larger structure well developed west of the Enclos Fouqué, limited by a north-south trending scarp.

This structure would result from a vertical collapse of the edifice (Bachélery, 1981), a large flank landslide toward the east (Duffield et al., 1982; Gillot et al., 1994; Oehler et al., 2004, 2008), or the deformation of the hydrothermal system in a way similar to the one proposed for the Enclos Fouqué (Merle and Lénat, 2003).

Geological data suggest the occurrence of older collapse structures related to the Ancient Piton de la Fournaise (older than 60 ka) Evidenced, also, a twofold construction of Piton de la Fournaise. Between 530 and 60 kyrs, the volcanic centre located in the current Plaine des Sables led to the building of the western part of the massif. The volcanic centre migrated eastwards to its current location, possibly at 60-40 kyrs (Bachélery and Mairine, 1990; Gillot and Nativel, 1989; Merle et al., 2010; Staudacher and Allègre, 1993). Then Piton de la Fournaise experienced caldera collapses and recurrent phreatomagmatic eruptions especially between 4880 and 2340 yr BP as evidence by the Bellecombe ash deposits (Michon et al., 2016). Most of the recent volcanic activity is now currently focused restricted inside the Enclos Fouqué caldera where lava flow accumulation and rare explosive events built the 400-m-high Central Cone.

3 The erupted magmas of Piton de la Fournaise

3.1 Magmas series and magma types

The presence of a geothermal well in the eastern flank of the Piton de la Fournaise in the Grand Brulé area (x = 187.823, y = 38.646, z = 172 m) located on an oceanite flow erupted in 1961 allowed the study of Piton de la Fournaise products for the first ~ 4 km. The exploration geothermal well was drilled in 1985 by the French Company for Geothermal and Renewable Energy Development (CFG) on the eastern flank of the Piton de la Fournaise volcano. The study of the section represent the sequence of rocks intersected through the entire depth of the borehole, from ground level (0 m, 172 m a.s.l.), to the bottom (3003.5 m). Twelve principal units have been distinguished representing the essential lithofacies of the succession (Rancon et al., 1985):

- 0-108 m: subaerial lava flows, massive to scoriaceous olivine basalt and oceanite. The vesicles in some flows are occupied by zeolites and calcite.
- 108-390 m: subaerial lava flows cut by intrusions. Olivine basalt and rare oceanite cut by dykes and/or sill of the same composition.
- 390-440 m: subaerial flows, represented by scoriaceous to massive olivine basalt and aphyric basalt, little altered except for the presence of quartz, calcite and zeolites in the vacuoles.

- 440-556 m: subaerial-submarine transition zone. Subaerial flows of olivine basalt and aphyric basalt and submarine flows of vitric olivine basalt.
- 556-616 m: submarine basalt flows. Olivine basalt and aphyric basalt with thick argillaceous intervals and fragments of vitric basalt most probably representing altered hyaloclastic breccia.
- 616-890 m: subaerial flows, comprising various scoriaceous olivine basalt and aphyric basalt.
- 890-1010 m: submarine flows, predominantly microlitic and vitric rocks.
- 1010-1129 m: lavas intruded by gabbro. Sheets of leucogabbro and biotite melagabbro have been injected into aphyric, locally vitric, basalt.
- 1129-1920 m: layered gabbro: alternations several meters thick of melagabbro and microleucogabbro.
- 1920-2468 m: submarine lavas with basic to ultrabasic intrusions, essentially sheets of melagabbro and microgabbro injected into vitric basalt and hyaloclastite, with intervals several meters thick of peridotite (Ol+Cpx+Fe-Ti and Cr oxides).
- 2468-2820 m: wherlite and dunite. A massive intrusive ultramafic sequence with sparse intervals of several decimetres thick of altered microgabbro.
- 2820-3003.5 m: massive dunite with layers of unaltered, relatively plagioclase-rich gabbro. The fractures in the gabbros are filled with calcite-zeolite-quartz-chlorite assemblages and veinlets of serpentine.

Lavas of Piton de la Fournaise are subdivided into four different compositional groups, which correspond to the activity inside and outside the Enclos Fouqué caldera:

The Steady State Basalt (SSB) is the most abundant group in the recent activity of the volcano. These lavas are transitional basalts with a narrow range of compositions, of MgO = 5-8 wt% and CaO/Al_2O_3 = 0.75-0.85 (Albarede et al., 1997; Famin et al., 2009; Villemant et al., 2009; Salaun et al., 2010; Fig. 3.1.1). SSB lavas host olivine, clinopyroxene, plagioclase and spinel in variable but generally low proportions (the latter mainly as inclusions in olivine; Pichavant et al., 2016).

Picritic lavas, also termed oceanites (Lacroix, 1936), are characteristic of the volcanic activity of la Réunion Island, being found at Piton de la Fournaise but also at Piton des Neiges. The composition of these lavas range from MgO = 8-28 wt% and CaO/Al_2O_3 = 0.75-0.85. They contain millimetric to centimetric crystals of olivine embedded in a cryptocrystalline to glassy groundmass. Oceanites of La Réunion Island are much studied but their significance is still not completely clear. Oceanite whole rock

compositions clearly plot on olivine control lines (Salaun et al., 2010) suggesting that their chemistry reflects the proportion of olivine crystals present in the rock. An important observation is that the composition of matrix glasses in oceanites is nearly constant and similar to SSB bulk rocks (Welsch et al., 2009). Most workers consider oceanites result from a general mechanism of shallow incorporation of olivine crystals into a basaltic parental magma. Di Muro et al. (2014) shows the heterogeneous composition and origin of recycled olivines and constrain the olivine accumulation at shallow depth (>1 kbar).

The Differentiated Lavas group has been defined mainly from differentiated lavas erupted near the end of activity of Piton des Neiges (Upton and Wadsworth, 1966). These lavas are characterized by a strongly decreasing CaO and increasing Al_2O_3 at decreasing MgO (MgO = 2-6 wt%, CaO/Al_2O_3 = 0.2-0.8; Fig.3.1.1). Differentiated alkaline lavas are found during the early stages of activity of the Piton de la Fournaise (Albarede et al., 1997) but are uncommon among recent products. This group includes chemically evolved terms such as hawaiites, mugeraites and benmoreites and, in the recent activity, rare trachytic pumices (Vlastelic et al., 2011; Vlastelic et al., 2021). Recent study (Smietana, 2011) has suggested that the early-differentiated alkaline lavas (the Pintade unit) do not belong to the Piton de la Fournaise series but rather should be associated with the activity of the older Les Alizés volcano.

The Abnormal Group (AbG) is compositionally different from the three others. It comprises lavas with MgO = 8-11 wt% and CaO/Al_2O_3 = 0.60-0.80, and shows enrichments in Fe, Mg, Ti, Na, K and depletion in Ca relative to SSB basalts. AbG-type compositions are rarely observed inside the Enclos Fouqué caldera, being mostly found at eccentric vents or at recent vents west to the central cone (Lénat et al., 2012). This group of lavas has got mixed geochemical features, some suggesting primitive character (e.g. high MgO) and others indicating a differentiated evolution similar to that shown by the Differentiated lavas group (e.g. low CaO/Al_2O_3 and high K_2O). It seems clear, however, that the Abnormal Group lavas does not evolve directly from Steady State Basalts-like parental liquids (Bachelery et al., 2015 and reference therein).

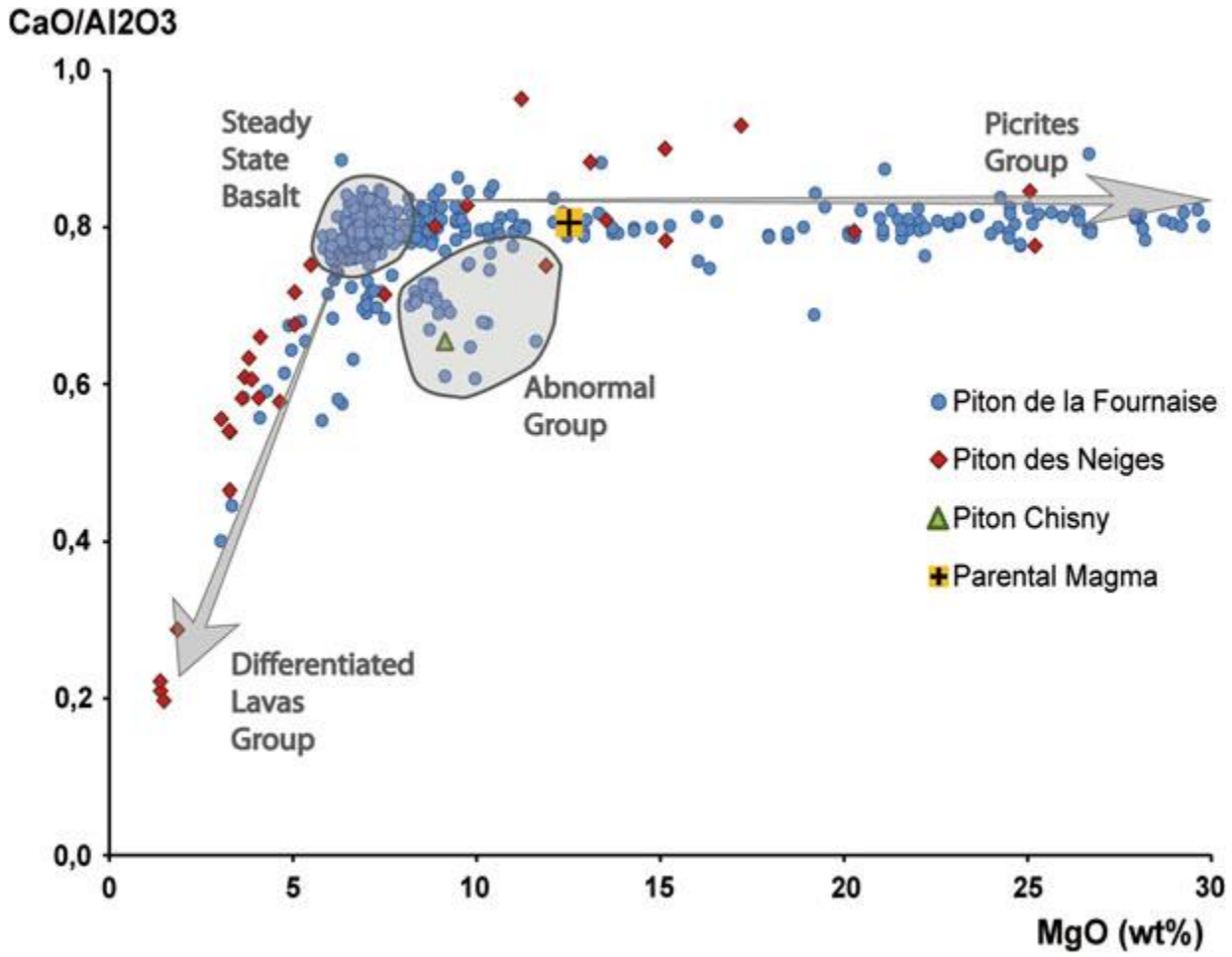

Fig. 3.1.1 – CaO/Al_2O_3 vs. MgO plot for Piton de la Fournaise and Piton des Neiges magmas. The four different magma groups and one representative sample of parental magma are shown (Bachelery et al., 2015 and reference therein).

Piton de la Fournaise basalts range from tholeiitic to alkaline series. He, Nd and Sr isotopic homogeneity of La Réunion lavas has been emphasized (Fisk et al., 1988; Graham et al., 1990). Some geochemical variabilities has been interpreted to reflect melting of different source components intrinsic to La Réunion mantle plume, and superimposed crustal processes including magma contamination and fractionation. Clinopyroxene and olivine fractionation ("wherlitic trend") has been proposed to generate Abnormal Group compositions (Kornprobst et al., 1979, 1984) and to drive tholeiitic basalts in the field of alkaline basalts (Albarède et al., 1997).

4 Phase relationships

Olivine, clinopyroxene, plagioclase and Cr-spinel are found systematically in Piton de la Fournaise products. Ti-rich magnetite is also present, together with sulphides. Ilmenite and amphibole are rare (Albarede et al., 1997). The four main crystalline phases are found in a variety of textural types, occurring as phenocrysts, microphenocrysts and microlites (Salaun et al., 2010; Welsch et al.,

2009, 2013). However, the characteristics of the mineral phase assemblage are specific of the distinct lava groups.

SSB lavas host olivine, clinopyroxene, plagioclase and spinel in variable but generally low proportions. Textural evidence suggests that, in SSB, clinopyroxene and plagioclase crystallize together with olivine, this lava group being often designated as "cotectic". The olivine + plagioclase + clinopyroxene + spinel four phase assemblage is also typical of the AbG Group. Early AbG lavas from Piton Chisny are crystal-poor (< 2 vol%) and have only phenocrysts of olivine and Cr-spinel.

Oceanite lavas of the Picrite group contain macrocrysts of olivine, mesocrysts of either olivine or an assemblage of clinopyroxene and plagioclase, and microcrysts of olivine + clinopyroxene + plagioclase + spinel ± Ti-magnetite (Welsch et al., 2009).

Piton de la Fournaise basalts generally contain small amounts of plagioclase. However, plagioclase is the dominant phase in the Differentiated Lava group from Piton des Neiges and early Piton de la Fournaise (Upton and Wadsworth, 1966; Albarede et al., 1997). Olivine compositions at Piton de la Fournaise are rarely highly forsteritic. Histograms of Fo contents yield frequency maxima at 86 (early activity; Albarede et al., 1997), 81 and 84 (1977-1998 activity; Boivin and Bachèlery, 2009; Villemant et al., 2009), 85-86 (Chisny lavas; Brugier, 2012) and 83 and 88 for both the Chisny ultramafic cumulate nodules (Brugier, 2012) and the dunite nodules (Sobolev and Nikogosian, 1994).

Texturally, the occurrence of deformed olivines has led to the inference that many crystals at Piton de la Fournaise are xenocrysts of earlier cumulates (Albarède et al., 1997). Clinopyroxene compositions are mostly augite, some extending into the fields of diopside and salite (Boivin and Bachèlery, 2009; Welsch et al., 2009). Boivin and Bachèlery (2009) distinguished two pyroxene compositional groups, one with an average composition $En_{49}Fs_{9}Wo_{42}$ (Mg-augite) and the other $En_{48}Fs_{12}Wo_{40}$ (augite). They suggested that the former group, with higher Al/Ti ratios, crystallized at higher pressures than latter. Plagioclase in recent (1977-1998) Piton de la Fournaise products ranges from An_{45} to An_{80} (Boivin and Bachelery, 2009). Spinels (both inclusions in olivine and isolated crystals dispersed in the matrix) are mostly chromites with Cr/(Cr + Al) around 70 and Mg/(Mg + Fe_t) between 50 and 65. They have TiO_2 contents between 2 and 3 wt%, increasing with decrasing Mg/(Mg + Fe_t), and Fe^{3+}/(Fe^{3+} + Al + Cr) of 10-15 % (Brugier, 2012). Spinel compositions at Piton de la Fournaise do not show systematic variations with magma types (Sobolev and Nikogosian, 1994; Albarède et al., 1997; Welsch et al., 2009; Brugier, 2012).

Data on matrix glass concerns the SSB and Picrite groups and, to a lesser extent, the AbG group. The composition of the matrix glass in most Piton de la Fournaise products is similar to SSB bulk rocks (MgO = 5.5-6 wt%, CaO/Al_2O_3 = 0.79-0.82); it is in equilibrium with

olivines in the range Fo_{75-80} (Welsch et al., 2009). Matrix glasses with MgO contents as high as 8-9 wt% have been analysed in 2007 products (Villemant et al., 2009; Di Muro et al., 2016). The 1998-2007 matrix glasses define a unique evolution trend starting from these high-MgO glasses and ending at ~5.5 wt% MgO (Villemant et al., 2009; Salaun et al., 2010).

Melt inclusions are common in olivine crystals from Piton de la Fournaise. Primary inclusions are either glassy or recrystallized. Secondary inclusions are mainly fluid inclusions. These occur along healed fractures in olivine and are associated with glass and crystals in variable proportions (Sobolev and Nikogosian, 1994; Bureau et al., 1998a; Famin et al., 2009). Compositions of primary glassy inclusions (recalculated for post-entrapment crystallization in olivine) range from 8 to 10 wt% MgO (Bureau et al., 1998a), 8-11.5 wt% MgO (Famin et al., 2009) to up to ~14 wt% MgO (Sobolev and Nikogosian, 1994; Di Muro et al., 2016).

H_2O and CO_2 concentrations in glass inclusions are generally < 1 wt% and < 500 ppm (Bureau et al., 1998b; Famin et al., 2009). However, certain samples have H_2O and CO_2 concentrations largely exceeding these values, with H_2O up to ~ 1.6 wt% and CO_2 up to ~ 2800 ppm (Bureau et al., 1998b; 1999). The secondary fluid inclusions contain essentially pure CO_2 with a large range of densities, from 0 to 0.8 g/cm^3 (Bureau et al., 1998; Famin et al., 2009; Di Muro et al., 2016).

5 Thermobarometric constraints and oxygen fugacity

Information on temperature of Piton de la Fournaise magmas comes from different methods. First, optical pyrometry and thermocouple measurements in the field provide direct data on lava temperatures, from 872°C and up to 1170°C with a frequency maximum between 1100 and 1150°C. Second, magma temperatures have been computed from olivine-liquid equilibrium. When applied to olivine phenocryst cores and their host bulk lava, grouped values are obtained, close to 1200°C for the 1977-1998 products (Boivin and Bachèlery, 2009). As a variant of this method, the MgO content of the melt (from the analysis of glass inclusions) at equilibrium with olivine yields temperature (e.g. Helz and Thornber, 1987) between 1170 and 1215°C (Bureau et al., 1998a, b) and between 1192 and 1236°C (Famin et al., 2009; Di Muro et al., 2016). It should be noted however that results with methods based on glass inclusion compositions depend on procedures adopted to correct for post-entrapment olivine crystallization. Third, thermometric measurements on melt inclusions have yielded homogeneization temperatures from 1170 to about 1215°C (Bureau et al., 1998).

Oxygen fugacities between NNO+0.7 to NNO-1.8 have been computed from the olivine-liquid equilibrium (Boivin and Bachèlery, 2009). Most values are however <NNO, and so Piton de la Fournaise magmas evolve under moderately reducing conditions (Bachelery et al., 2015 and

reference therein). Pichavant et al. (2016) reported a fO_2 value of the Piton de la Fournaise magmas which is reasonably well defined, around NNO-0.5. This makes the average Fe_2O_3/FeO of basaltic liquids at Piton de la Fournaise slightly higher than commonly assumed (the proportion of Fe_2O_3 is 18% and not 15%; e.g. Fisk et al., 1988). Experiments by Fisk et al. (1988) have provided a framework for interpreting the genesis and evolution of Piton de la Fournaise magmas. The Fisk et al. (1988) data imply minimum pressures of 250-500 MPa for clinopyroxene to crystallize before plagioclase. Fractionation of olivine together with clinopyroxene would also require a minimum of 250-500 MPa from their data. Still higher crystallization pressures (a minimum of 800-1000 MPa for compositions < 11 wt% MgO) would be necessary for fractionation of clinopyroxene alone. Assuming that all Piton de la Fournaise primitive magmas crystallize in the sequence olivine-clinopyroxene-plagioclase (Albarede et al., 1997; Welsch et al., 2009), then the Fisk et al. (1988) experimental results would lead to the conclusion that magma fractionation takes place for the most part at the base of the crust or in the mantle. The crust-mantle boundary beneath La Réunion is located at 12-15 km depths (Gallart et al., 1999; Lénat et al., 2012) or 320-400 MPa. Hence, the 250-500 MPa minimum pressure required by the Fisk et al. (1988) data makes it possible that crystallization of either olivine + clinopyroxene or olivine + clinopyroxene + plagioclase takes place at the base of the crust. It is worth noting that both melt and fluid inclusions are consistent with fluid-melt saturation and fluid entrapment at crustal pressures, and that petrological evidence for crystallization pressures above 400-500 MPa (Bureau et al., 1998, 1999; Di Muro et al., 2016) is presently lacking.

These difficulties lead to an alternative interpretation of the Fisk et al. (1988) data, reminding that their experiments were performed under volatile-free conditions. Numerical runs using the MELTS software have been performed for a parental Piton de la Fournaise magma composition (Famin et al., 2009; Welsch et al., 2009), in presence of 1 wt% H_2O and 0.1 wt% CO_2 and for fO_2 set at the FMQ buffer (about 0.7 log unit below NNO). They show that clinopyroxene crystallizes second after olivine at 100 MPa (Welsch et al., 2009), at pressures much lower than the 250-500 MPa minimum pressure range found by Fisk et al. (1988). Nevertheless, recent study (Boudoire et al., 2019) individuate in clinopyroxene phenocrysts from "clinopyroxene-bearing" lavas from peripheral eruptions a minimum average pressure of 3.1±0.6 kbar. The highest pressures are recorded in clinopyroxene from dunite-wherlite enclaves erupted as lithics from the polygenetic Chisny cone, with an average of 5.6±0.8 kbar.

6 Methods

In this chapter, all the methods used to investigate the mafic and ultramafic ejecta of the Bellecombe Ash Member as well as some quartz xenocrysts were described.

6.1 Inductively Coupled Plasma Optical Emission Spectroscopy and Inductively Coupled Plasma Mass Spectroscopy (ICP-OES and ICP-MS)

Samples were crushed and finely powdered in agate mortar. Major and trace element analysis of bulk-rocks were carried out at the Centre de Recherches Pétrographiques et Géochimiques (CNRS-SARM) in Nancy (France) by Inductively Coupled Plasma - Optical Emission Spectrometry (ICP-OES) and Inductively Coupled Plasma - Mass Spectrometry (ICP-MS; see Carignan *et al.* (2001) for a review of the protocols and of reference materials).

Relative errors for major elements are < 1 % (SiO_2 and Al_2O_3), < 2 % (MgO, FeO and CaO), < 5 % (Na_2O, K_2O and TiO_2). Relative trace element errors are < 5 % with exception for Sc (< 15%) and Th, Cr (< 10%). The analytical results were reported in the appendix (see chapter 17).

6.2 Electron Micro Probe Analyses (EMPA)

An electron probe micro-analyser is a microbeam instrument used primarily for the *in situ* non-destructive chemical analysis of minute solid samples. EMPA is also informally called an electron microprobe, or just probe. Electron micro-probe analyser is an analytical instrument largely diffused to determine the quantitative chemical composition of small volume (few μ^3) of sample in non-destructive form, primarily by wavelength-dispersive spectroscopy. Analyses of single phase minerals (olivine, clinopyroxene, feldspars, oxides, biotite and interstitial or glass inclusion) were performed with a Cameca SX100 microprobe at University of Hannover, operated at accelerating voltage of 15 kV and 15 ηA beam current. The beam was focused to 1μ. Na and K were analysed first with counting times of 8 s to minimize alkali volatilization. Counting time for other elements was 10 s. Standards used for calibrations were natural mineral standards. During each microprobe session, analytical precision and accuracy was verified by measuring the mineral standards. The analytical results were reported in the appendix (see chapter 17).

6.3 Isotopic and elemental composition of light noble gases and CO_2 analysis

The isotopic and elemental composition of light noble gases (He, Ne, and Ar) and CO_2 was determined in fluid inclusions (FI) hosted in crystals of olivine, clinopyroxene and feldspars at Istituto Nazionale di Geofisica e Vulcanologia, Sezione di Palermo (INGV - Palermo). These crystals were separated by handpicking under a binocular microscope from the 1-0.5 mm-sieved fraction of the mafic and ultramafic subvolcanic ejecta of the Bellecombe Ash Member (Piton de la Fournaise). The crystals were carefully separated (0.4 - 1.9 g), cleaned in an ultrasonic bath following internal protocol (Rizzo et al., 2018). These crystals were split into two aliquots: the first

was loaded into a stainless-steel crusher capable of holding up to six samples simultaneously for noble-gas analysis, and the second was used for determining the concentration and isotope ratio of CO_2. Noble gases trapped inside primary (when present) and secondary fluid inclusions were released by in-vacuo single-step crushing at about 200 bar. This procedure is the most conservative in order to minimize the contribution of cosmogenic ^{3}He and radiogenic ^{4}He possibly grown/trapped in the crystal lattice (Kurz, 1986; Hilton et al., 1993, 2002; Rizzo et al., 2018). The CO_2 measurement was performed during noble-gas extraction at the time of crushing by quantifying the total gas pressure (CO_2 + N_2 + O_2 + noble gases) and subtracting the residual pressure of N_2 + O_2 + noble gases after removing CO_2 using a "cold finger" immersed in liquid N_2 at −196°C. Gases were then cleaned in an ultra-high vacuum (10^{-9} - 10^{-10} mbar) purification line, and all the species of the gas mixture except noble gases were removed. Helium (^{3}He and ^{4}He) and neon (^{20}Ne, ^{21}Ne and ^{22}Ne) isotopes were measured separately by two different split-flight-tube mass spectrometers (Helix SFT-Thermo). The values of the $^{3}He/^{4}He$ ratio are expressed as R/Ra (where Ra is the $^{3}He/^{4}He$ ratio of air, which is equal to $1.39*10^{-6}$). The analytical uncertainty of the He isotopic ratio is generally < 1.2%. The R/Ra values were corrected for atmospheric contamination based on the $^{4}He/^{20}Ne$ ratio (Sano and Wakita, 1985) and are expressed hereafter as Rc/Ra values. Argon isotopes (^{36}Ar, ^{38}Ar and ^{40}Ar) were analyzed by a multicollector mass spectrometer (GVI Argus), with an analytical uncertainty generally < 1.1%. The uncertainty in the determinations of the elemental He, Ne, and Ar contents was < 5% after considering natural variability and the assumption of residual (not crushed) crystals for weight normalization of the number of moles of gas. Typical blanks for He, Ne and Ar were < 10^{-15}, < 10^{-16} and < 10^{-15} mol, respectively. ^{40}Ar values were corrected for atmospheric contamination ($^{40}Ar^{*}$) according with the following formula: $^{40}Ar^{*} = {}^{40}Ar_{m} - (({}^{40}Ar/{}^{36}Ar)_{air} \times {}^{36}Ar_{m})$, where $^{40}Ar^{*}$ represents the corrected ^{40}Ar, and the "m" subscript indicates "measured".
Quantities of noble gases are reported either in moles of gas or as cm^3 STP (Standard Temperature and Pressure); it should be noted that although STP is usually defined as 273.15 K and 101.325 kPa (= 1 bar), some definitions use 100.000 kPa (McNaught and Wilkinson, 1997). As a consequence, noble gas concentrations are usually expressed as moles (or cm^3 STP) per gram of rock or fluid. Sometimes these are converted to percent or ppm of the noble gas by weight, as is common for other elements in many branches of geochemistry (Burnard et al., 2013).

6.4 Scanning Electron Microscopy Backscattered Electron Energy Dispersive Spectroscopy (SEM-BSD-EDS)

The Scanning Electron Microscopy Backscattered system equipped at the Department of "Scienze della Terra e dell'Ambiente" of University of Pavia was only used on wherlitic sample B28 and on layered

ultramafic to mafic sample B108a, for the investigation of the different textures and compositions. Polished thin section B28 and B108a were analysed by a Scanning Electron Microscopy Tescan series 3xMU operating in backscattered Electron imaging mode equipped with EDAX Energy Dispersive Spectrometer (Fe-SEM-EDS) for major elements analyses, using a 20 keV accelerating voltage. Beam current and spot size were 0.4 nA and 3µm respectively. The counting times on peak and background were 100 s. Maps of samples were surveyed using 20 keV, a working distance of 15.8 mm, 32 frame, resolution of 1024x800 and max counts per channel of 256. The analytical results both for samples B108a and B28 were reported in the appendix (see chapter 17).

6.5 Laser Ablation Inductively Coupled Plasma Mass Spectroscopy (LA-ICP-MS)

The Laser Ablation-Inductively Coupled Plasma-Mass Spectrometer (LA-ICP-MS) system equipped at the Department of "Fisica e Geologia" of University of Perugia was only used for the investigation of the quartz xenocrysts. The instrument is composed by a commercial New Wave UP213 (New Wave, UK) LA system coupled with a Thermo Electron X7 (Thermo Electron Corporation, Waltham, USA) ICP-MS. The laser ablation system is a frequency quintupled Nd:YAG laser, whose fundamental wavelength of 1064 nm is converted into 213 nm by means of three harmonic generators. The commercial ablation cell (NewWave, UK), capable to support both thin sections and cylindrical resin chips, has been modified in order to mount together both reference materials and unknown samples. In addition, special adjustments have been developed on the ablation cell for the lodging of 'large' samples (up to c.a. 5 cm). Helium is preferred over argon as a carrier gas to enhance the transport efficiency of ablated aerosol (Eggins et al., 1998). The helium carrier gas exiting the ablation cell is mixed with argon make-up gas before entering the ICP torch; this configuration permits the maintenance of stable and optimum excitation condition. LA-ICP-MS measurements are carried out using time resolved analysis operating in a peak jumping mode. The laser repetition rate and the laser energy density are fixed to 10 Hz and ~10 J/cm^2, respectively. The LA-ICP-MS system is optimized for dry plasma conditions prior to each analytical session on a continuous linear ablation of NIST SRM 612 glass standard by maximizing the signals for selected masses (La^+ and Th^+) and reducing oxide formation by minimizing the ThO^+/Th^+ ratio. For the operating conditions outlined above, background intensities are typically 20-200 cps for Sc, V, Cr and Ga, 10-20 cps for Rb, Sr and Pb and < 10 cps for all other elements. Analyte sensitivities vary as a function of the amount of material reaching the torch, the ionization efficiency, isotope abundance, and mass. For the operating conditions outlined above and for a laser beam of 40 µm sensitivities range between 690 and 6230 $cps/\mu g*g^{-1}$.

6.6 Raman spectroscopy analyses

This is a versatile non-destructive technique for fluid inclusion analysis. For barometric studies on representative phases of mafic and ultramafic samples, Raman spectra were acquired on polished crystals at the Ludwig Maximilian University of Munich (LMU Lab. of crystallography; Resp. of the Raman lab: Dr. M. Kaliwoda) using an XPlora One spectrometer (Jobin Yvon) equipped with an Olympus microscope at 100x magnification. Analytical conditions were: excitation wavelength: 532 nm, filter: 50%, hole 100, slit 50, gratings 1800, acquisition time: 150s x 2.

Raman spectroscopy was tentatively used on the quartz xenocrysts. It has a wide field of application ranging from qualitative detection of solid, liquid and gaseous components to identification of polyatomic ions in solution. Raman technique is commonly used to calculate the density of CO_2 fluids, the chemistry of aqueous fluids, and the molar proportions of gaseous mixtures present as inclusions. The main advantages of this technique are the minimal sample preparation and the high versatility. The analyzed samples of quartz xenocrysts are both doubled-polished thin sections (Q1, Q13, Q16 and Q19) and crystals *tal quale* (Q14, Q15, Q17 and Q18).

The analyses were performed by the confocal integrated micro/macro-Raman spectrometer "Labram HR800" (HORIBA JOBIN YVON) of the "Centro interdipartimentale G.Scansetti" (Department of "Scienze della Terra", University of Torino). Excitation line at 532 nm (solidstate Nd laser and 180 mW of emission power) was used, with a grating of 600 grooves/mm and a slit ranging from 100 to 300 µm; the corresponding spectral resolution was 2-4 cm^{-1}. Each spectrum was collected in confocal setting with a hole of 200 µm. The laser was focussed on the sample using an Olympus BX41 microscope. An objective 100× (spot size resolution of ca. 1 × 1 × 3 µm) was used on thin sections, whereas an objective 20x (spot size resolution of ca. 5 × 5 × 15 µm) was used on sample *tal quale*. Each spectrum was collected by 2-5 accumulations of 20-120 s. The calibration of the instrument has been checked daily using the 521 cm^{-1} silicon peak and the 1332 cm−1 diamond peak (precision ≤ 1 cm-1). Spectra were acquired using Labspec5 software in the 100- 1800 and 3100-4200cm^{-1} domains.

6.7 X-ray powder diffraction analyses

X-ray powder diffraction is a very versatile technique. In qualitative and quantitative analyses of unknown materials, the analyst must reduce preferred orientation so that the diffraction pattern can be reduced and matched to standards for identification. Materials with equal crystal shapes and no cleavages that produce flat samples usually yield random samples using any specimen preparation method. If the particles have any crystallographically related shape, the shape will make achieving randomness difficult. As the difference between the maximum and minimum dimensions of the particle increases, it becomes more difficult to make random samples.

The easiest way to reduce particle size effects is to grind the sample in a mortar and pestle and obtain sample powdering. After that, the powder of sample were put into a sample holder, commonly made of aluminium, with a depression or cavity in which to mount the sample. In a diffractometer, the X-rays are generally diffracted from the top of the sample. The cavities are usually designed so the surface of the sample is on the diffractometer axis. It is the half-depth of the penetration of the X-ray beam in the sample that determines the effective diffracting surface and hence the specimen displacement error that shifts the resultant peak position. The X-ray penetration into a specimen will depend on incident angle, absorption, and elemental composition of the sample. Very low average atomic number compounds allow considerable penetration of the X-ray beam, resulting in peak displacement and broadening.

The oscillating electric field of a light wave will interact with the electrons in matter to cause coherent scattering. Each scattering point maybe treated as a new source of spherical waves. Thus, waves scattering from two objects will expand in space round the objects until they interfere with each other. Their interaction will produce constructive interference at certain angles of view and destructive interference at other angles depending on the distance between the scatterers and the wavelengths of the radiation. When a periodic array of objects each scatter radiation coherently, the concerted constructive interference at specific angles is called diffraction (Jenkins and Snider, 1996).

X-ray diffraction analyses were performed at the X-ray laboratory of University of Urbino “Carlo Bo” on some xenocrysts supposed to be quartz. For the X-ray diffraction analyses was used the side-loading technique. The type of holder employed has a rectangular hole punched through it. The first step is to attach a microscope slide to the top surface using scotch tape or clamps. The holder is then turned over and the powder carefully loaded into the cavity. The cavity is filled by applying gentle pressure to the powder as the cavity is filled up. A cover is then placed over the holder again so that the microscope slide is uppermost. When the specimen is to be exposed, the top microscope slide is carefully removed.

7 The subvolcanic ejecta of the Bellecombe Ash Member and comparisons with literature

7.1 Petrography

The petrographic study of more than one hundred samples (109), representative of the mafic and ultramafic subvolcanic ejecta of the Piton de la Fournaise emphasizes the presence of several lithotypes (see Table 7.1.1; all tables with the analytical results were reported in the appendix on chapter 17). Cumulate cognates *stricto sensu* are present, often characterized by abundant quenched glass entrapped interstitially and in minerals (melt inclusions), with no disequilibrium textures induced into the subvolcanic crystal frameworks. Wager et al. (1960) recognized that such a mechanism of enlargement of cumulus crystals at constant temperature could only take place at or near the top of any pile of crystals. They called this style of growth adcumulus growth. The adcumulus process gradually reduced the volume of intercumulus liquid by mechanically pushing it out of the pile and could result in vanishingly small quantities being preserved. Any intercumulus liquid remaining as the result of continued accumulation of crystals was termed trapped liquid which crystallized to the pore material. This liquid, and the subsequently crystallized pore material, necessarily had the composition of the contemporary magma. By contrast, orthocumulates are characterized by zoned cumulus minerals and a variety of postcumulus material, representing crystallization during cooling from original intercumulus liquid trapped interstitial pore spaces.

A wide range of textures in these ejecta results from crystal-liquid fractionation, variable P-T gradients in the subvolcanic environment of crystallization and/or reactions (peritectic?) between continuously rising basaltic magmas and the intrusive piles of products.

These clasts also allow to compare the compositions of the interstitial glass in the subvolcanic ejecta with small volumes of evolved liquids, which are trachytes from petrographic observation, detected as pumiceous components in the products of Bellecombe Ash Member, Langevin caldera and Piton des Neiges.

Other subvolcanic clasts (e.g. doleritic gabbros) may simply represent slowly-cooled equivalents of basalts, rather than cumulates, with no crystal-liquid fractionation.

Brugier (thesis, 2016) investigated some different lithotypes of mafic and ultramafic ejecta at La Réunion Island (Fig. 7.1.1): ol-rich cumulates, Cpx-rich veins in banded wherlite, massive gabbros with phlogopite-bearing veins from Piton des Neiges, gabbroic xenoliths from Piton Chisny.

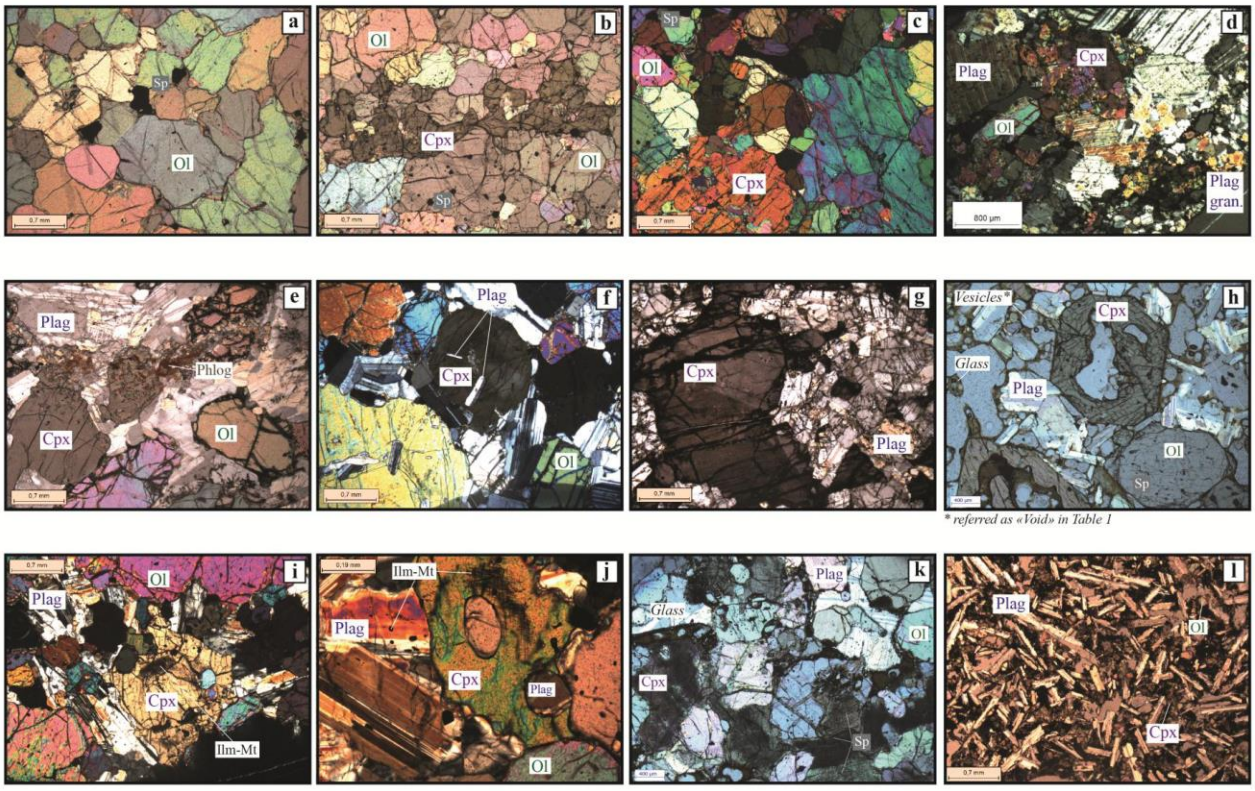

Fig. 7.1.1 - Photomicrographs of representative thin sections of the different rock types; from Brugier et al. (2016). (a) Cumulative texture of rounded olivine in dunite xenolith. Note the interstitial Cr-spinels (from Plaines des Sables). (b) Clinopyroxene-rich vein in banded wherlite (from Plaines des Sables). (c) Large (cm size) Cpx in wherlite (from Plaines des Sables). (d) Gabbroic xenolith from Piton Chisny. (e) Phlogopite-bearing vein in the Piton des Neiges massive gabbro. (f) Massive gabbro showing zoned Cpx with Plg inclusions (from Salazie Cirque). (g) Gabbroic inclusion from a Piton des Neiges ignimbrite. (h) Gabbroic xenolith from the Bellecombe Tephra. (i) Gabbroic xenolith from Piton Haüy. (j) Plg inclusions in Cpx and the crystallographically-oriented ilmenite exsolutions (from Plaines des Sables). (k) Cpx phenocrysts strongly darkened by Cr-spinel exsolutions in gabbroic xenolith (from Plaines des Sables). (l) Dolerite sample (from Plaines des Sables).

In Piton des Neiges samples from cirque of Salazie eroded intrusive complex (Berthod et al., 2020) were recognized several lithotypes (Figg. 7.1.2 and 7.1.3), both ultramafic (Site 1 and Site 2: dunite, wherlite, plg-wherlite) and mafic (Site 3 and Site 4: olivine gabbros, gabbros, ferrogabbros).

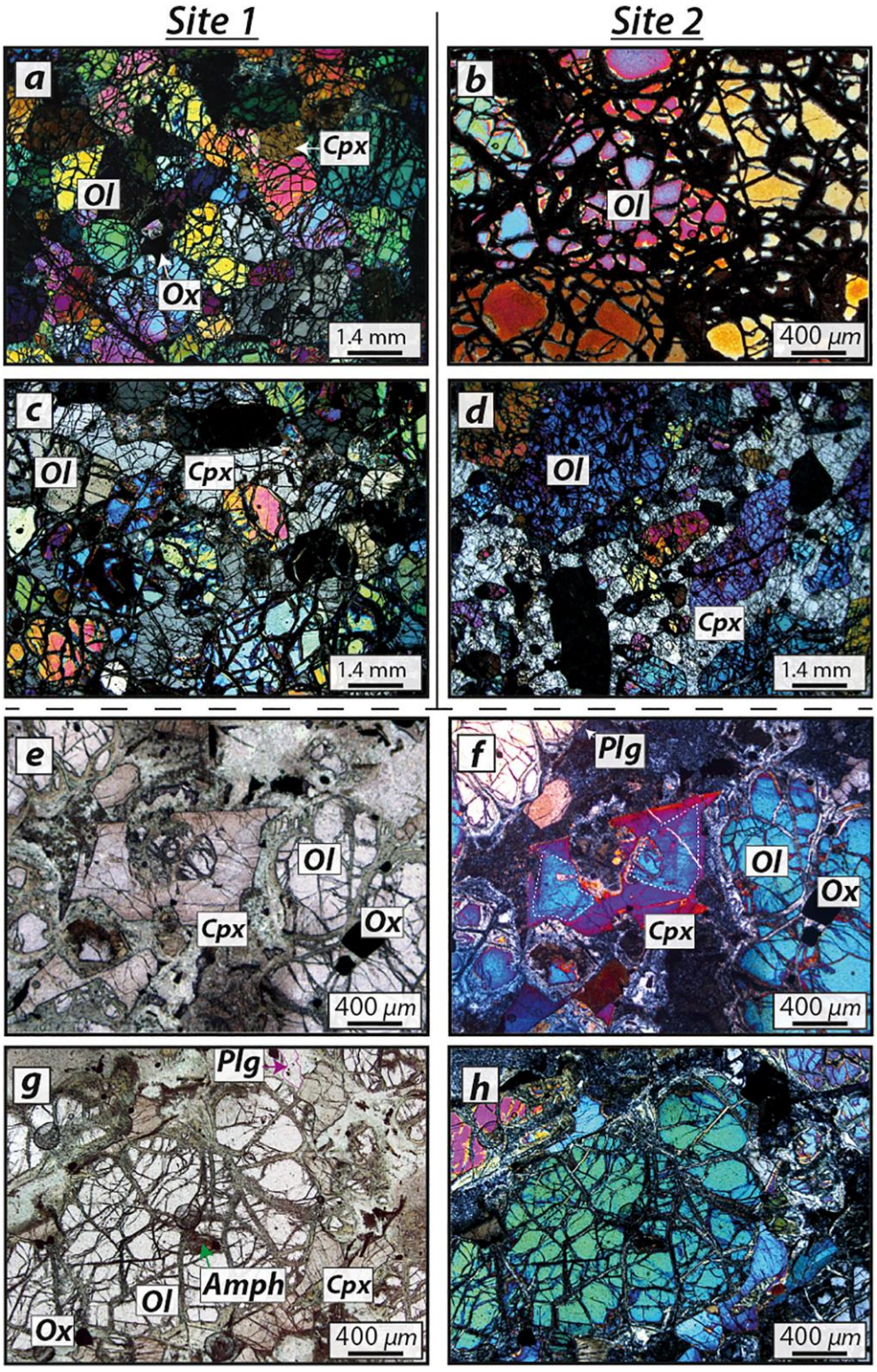

Fig. 7.1.2 - Representative parageneses and textures of samples collected at Cirque of Salazie eroded intrusive complex; from Berthod et al. (2020). Sites 1 and 2. a) Dunite from Site 1 made of anhedral grains of olivine in cumulus position, and anhedral crystals of clinopyroxene and oxides in interstitial position. b) Dunite from Site 2 with only olivine crystals. c) and d) Wherlite samples from Sites 1 and 2, respectively, in which the olivine is euhedral and in cumulus position, and clinopyroxene is poikilitic. e) and f) Wherlite from Site 2 made of rounded grains of olivine and euhedral, sector-zoned crystals of clinopyroxene in cumulus position, and plagioclase in interstitial position. g)

and h) Plagioclase-wherlites from Site 2 displaying a mesocumulate texture with euhedral olivine in cumulus position, and clinopyroxene and plagioclase in interstitial position.

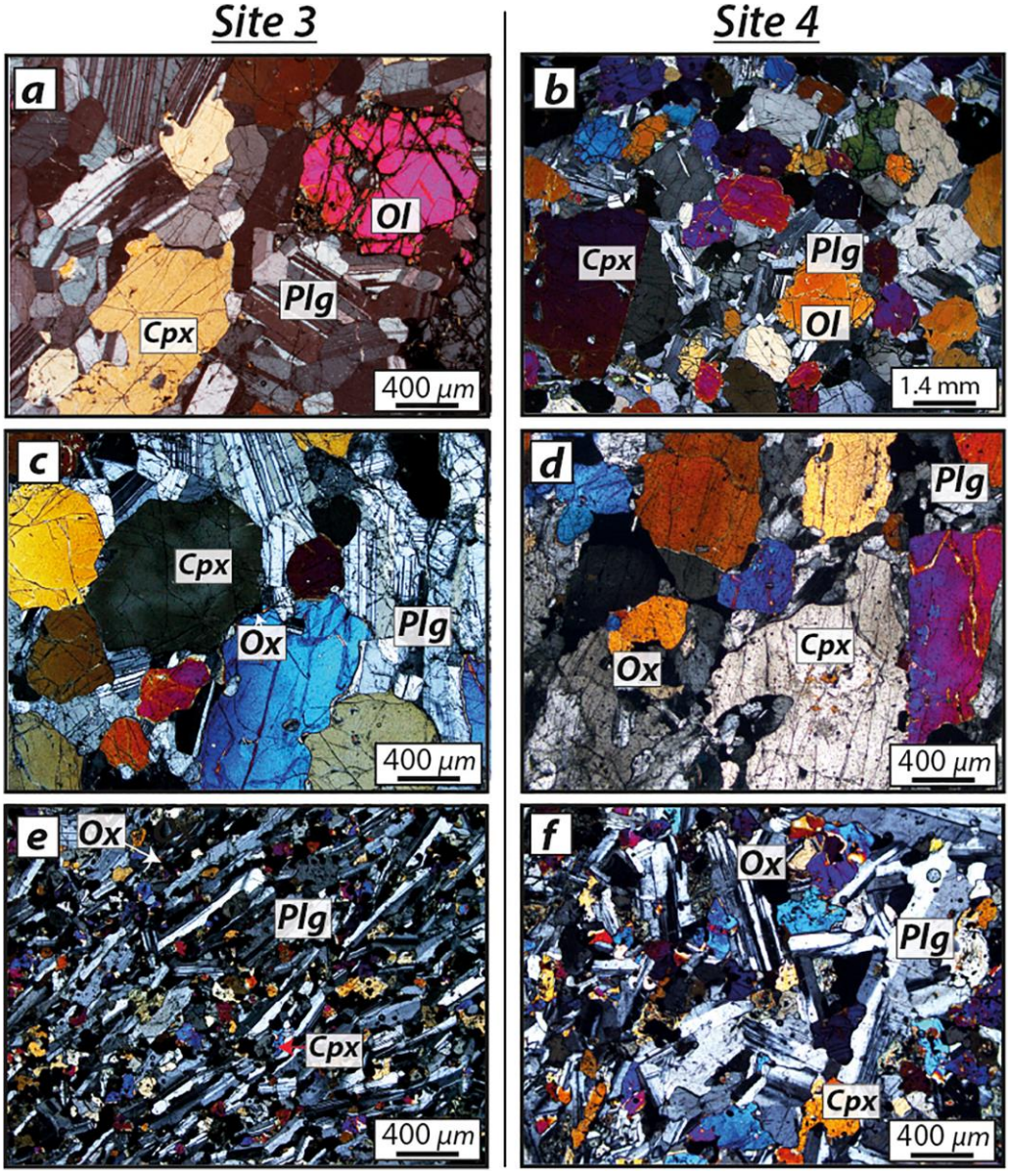

Fig. 7.1.3 – Representative parageneses and textures of samples collected at Sites 3 and 4; from Berthod et al. (2020). a) and b) Olivine gabbros. c) and d) Gabbros made of euhedral crystals of plagioclase and clinopyroxene. e) and f) Strong magmatic fabrics, marked by elongated plagioclases in ferrogabbros.

Samples of the Bellecombe Ash Member studied in the present thesis were subdivided in ultramafic (dunite and wherlite) and mafic (ophitic gabbros, sub-ophitic gabbros, poikilitic gabbros, dolerites, micro-monzogabbros and porphyrogabbros) ejecta. Among the samples sent to Urbino by Andrea Di Muro (Institute de Physique du Globe de Paris – Observatoire Volcanologique du Piton de la Fournaise) some of them (both from Bellecombe and Langevin caldera) are represented by lava lithic clasts and therefore considered as "volcanic" samples in Table 7.1.1. Samples sent to Urbino from La

Réunion Island also comprise several quartz xenocrysts (or supposed to be quartz) from the Langevin caldera and a sedimentary (carbonatic) clast from the Bellecombe Ash Member.

The modal mineralogy of the Bellecombe Ash Member mafic and ultramafic subvolcanic samples is reported in Fig. 7.1.4. Comparing these mineralogical data with literature (Berthod et al., 2020; Fig. 7.1.5), Upton et al. (2000; Fig. 7.1.6) and Brugier et al. (2016; Fig. 7.1.7) the widespread presence of plagioclase in the Bellecombe Ash Member intrusives (gabbroic rocks), can be emphasized if compared to the gabbroic rocks described by Berthod et al. (2020) from Piton des Neiges. The presence of opaque minerals is reported in several samples from Berthod et al. (2020) and Brugier et al. (2016), but are absent in Upton et al. (2000) samples. Only one dunite from Berthod et al. (2020) show amphibole, whereas the samples here investigated show biotite (< 0.1 vol%) in three samples (two porphyrogabbros and one sub-ophitic gabbro).

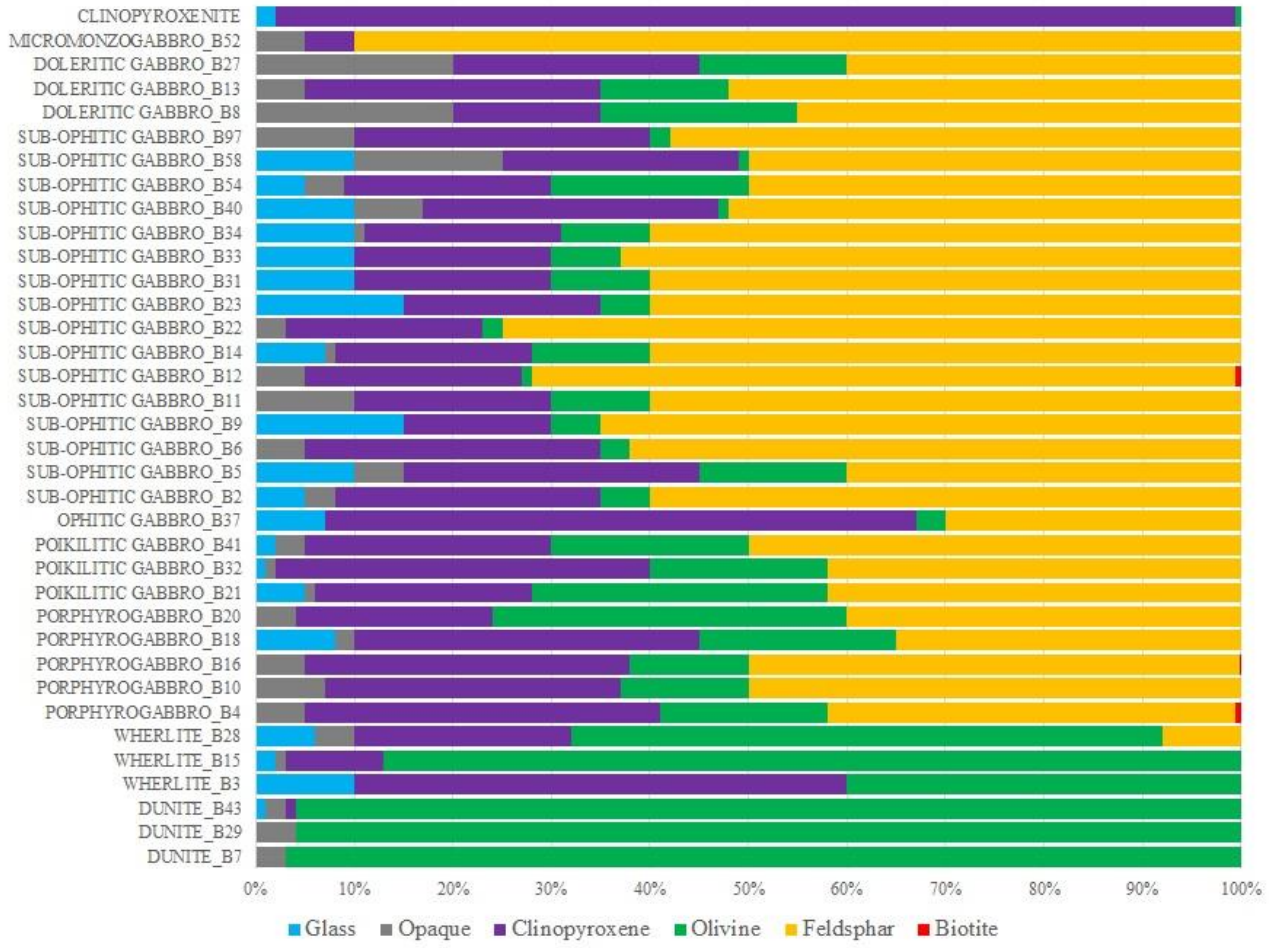

Fig. 7.1.4 – Modal mineralogy of the subvolcanic ejecta of the Bellecombe Ash Member. Biotite is present with low vol% in only three samples, two porphyrogabbros and one sub-ophitic gabbro.

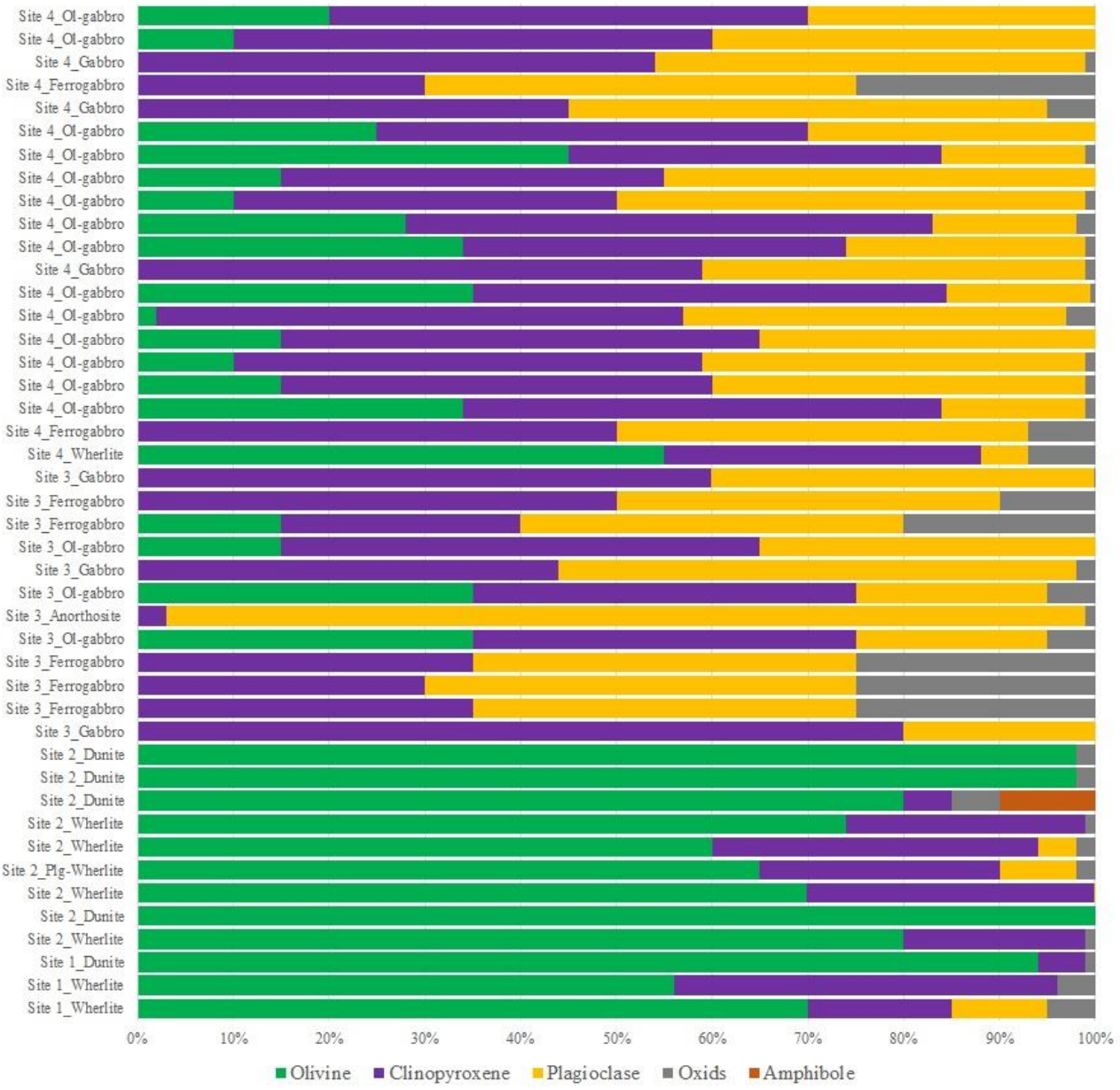

Fig. 7.1.5 – Modal mineralogy of Berthod et al. (2020) samples. Dunites and wherlites containing less than 10 vol% of plagioclase. Gabbroic rocks, including olivine gabbros, gabbros and ferrogabbros containing more than 10 vol% of plagioclase.

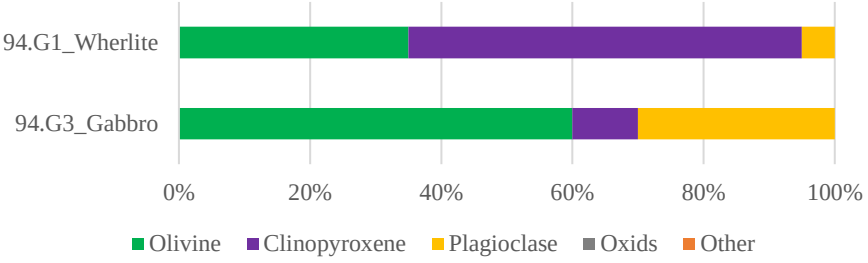

Fig. 7.1.6 – Modal mineralogy of Upton et al. (2000) samples.

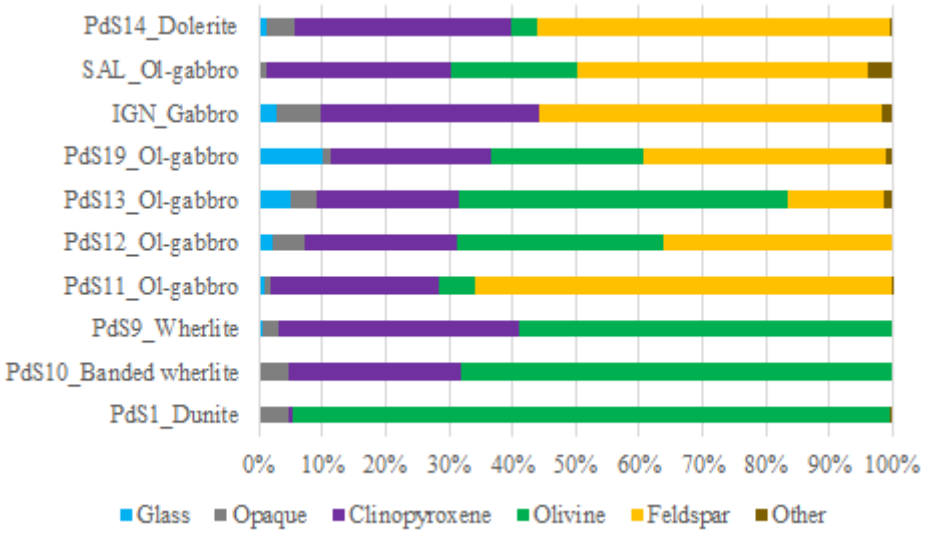

Fig. 7.1.7 – Modal mineralogy of Brugier (thesis, 2016) samples.

7.2 The ultramafic lithotypes

The investigated samples representative of the ultramafic group, includes dunites and wherlites (Table 7.2.1).

Table 7.2.1 – The analysed representative samples of ultramafic ejecta.

ROCK TYPE	SAMPLE NUMBER
DUNITES	B7
	B29
	B43
WHERLITES	B3
	B15
	B28

7.3 Dunites

Dunites show a cumulitic texture including olivine (> 95 vol%), oxides (2-4 vol%) and minor clinopyroxenes (≤ 1 vol%). Olivine crystals are euhedral to subhedral in shape and 2-8 mm in diameter and form a cumulus framework. Oxide crystals are interstitial in the olivine fabric and include magnetite, ilmenite and Cr-spinel compositions. Samples of dunite differ in grain size (e.g. B7 coarser grained, B29 and B43 finer grained; Fig. 7.3.1) and in oxides content. Furthermore, all dunite samples show the presence of rounded sulphide trails crossing the olivine crystals. Melt and fluid inclusions are evident in some olivine.

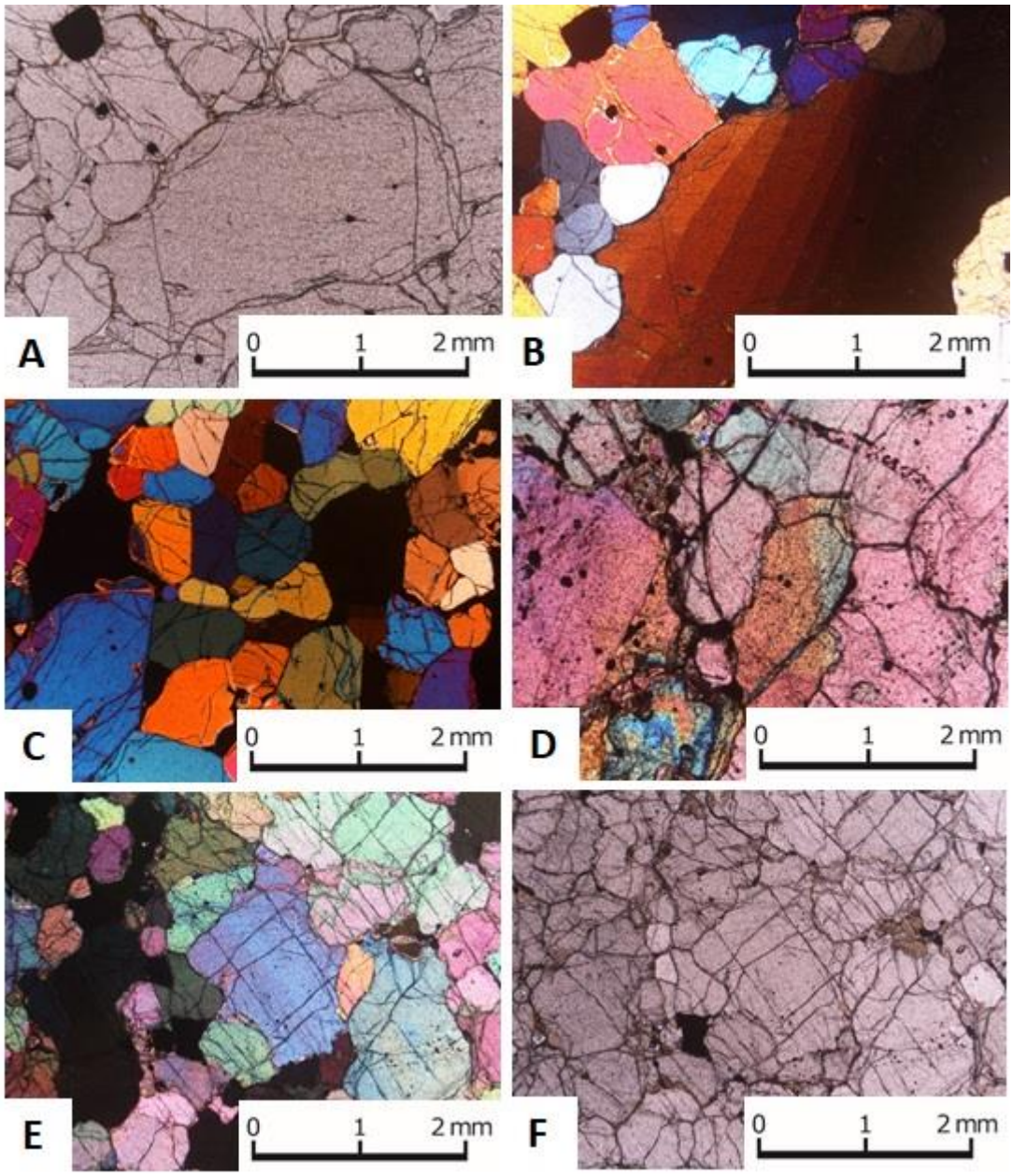

Fig. 7.3.1 – Plane-polarized (A and F) and crossed polars images (B, C, D and E). Dunites showing the presence of oxides (A and F, sample B29) and some sulphides trails (D, sample B7). Dunites samples have both finer (C, sample B43, E, sample 29 F) and coarser grain size (A, B, sample B43, D). Kink banding of the crystals (B) is also present.

7.4 Wherlites

The wherlite samples in the Bellecombe Ash Member shows different modal mineralogy, with olivine ranging from 40 to 87 vol% and clinopyroxene from 10 to 50 vol%. Feldspars are only present in one sample (B28; Fig. 7.4.1) with a small percentage (8 vol%). Interstitial glass is shown in all the samples (2-10 vol%). Oxides are also present but in small amount (0-4 vol%). Melt inclusions are shown in some olivine crystal. Samples of wherlite differ in grain size (e.g. B3 and B15 coarser grained, B28 finer grained). Despite

other wherlite samples, B28 show a poikilitic texture (with clinopyroxene as oikocrysts and olivine as cadacrysts), with small olivines (< 0.5 mm) with rounded margin and larger olivines (2-3 mm) with fritted margin and rounded contours. Poikilitic texture is maybe related to resorbed processes on samples due to a late-stage interactions with successive batches of basaltic magmas. Sample B3 evidence melt inclusions in some olivine crystals, respect other wherlites from Bellecombe.

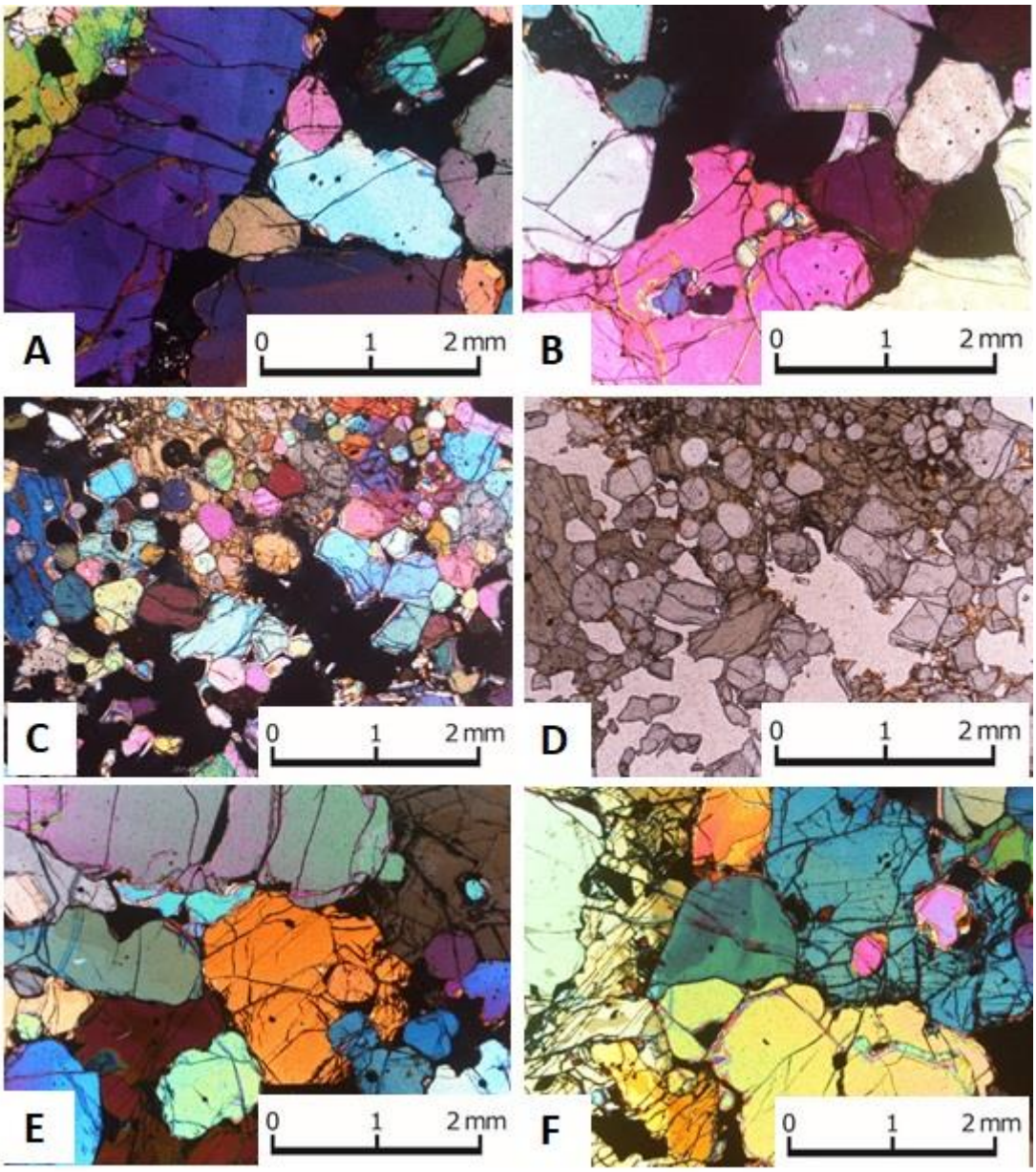

Fig. 7.4.1 – Plane-polarized (D) and crossed polars images (A, B, C, E and F). Wherlite samples of Bellecombe Ash Member show different grain size. Wherlite with finer grain size (C and D, sample B28) show a major olivine content respect to other samples. Some oxides are evident in the framework of the olivine and clinopyroxene (A, B and E, sample B15). Small melt inclusions in single crystals are evident (F, sample B15).

7.5 The mafic lithotypes

The mafic lithotypes include ophitic gabbros, sub-ophitic gabbros, poikilitic gabbros, doleritic gabbros, micro-monzogabbros and porphyrogabbros (Table 7.5.1).

Table 7.5.1 – Subdivision of the representative mafic samples analysed.

ROCK TYPE	**SAMPLE NUMBER**
OPHITIC GABBROS	B37
SUB-OPHITIC GABBROS	B2
	B5
	B6
	B9
	B11
	B12
	B14
	B22
	B23
	B31
	B33
	B34
	B40
	B54
	B58
	B97
POIKILITIC GABBROS	B21
	B32
	B41
DOLERITIC GABBROS	B8
	B13
	B27
MICRO-MONZOGABBRO	B52
PORPHYROGABBROS	B4
	B10
	B16
	B18
	B20

7.6 Ophitic gabbros

This group includes only one sample, with an evident ophitic texture, were random feldspar laths (30 vol%) are enclosed by clinopyroxene (60 vol%) or olivine (3 vol%). A small amount of interstitial glass is present (Fig. 7.6.1).

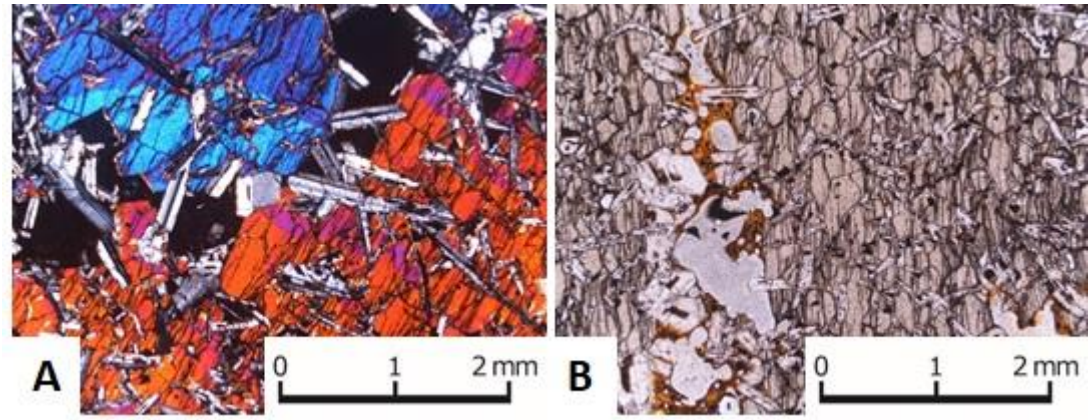

Fig. 7.6.1 – Crossed polars of ophitic texture (A) and plane-polarized of the sample with a small amount of interstitial glass (B).

7.7 Sub-ophitic gabbros

The sub-ophitic gabbros is the most represented group in terms of number of samples of mafic igneous subvolcanic clasts in the Bellecombe Ash Member. Clasts have an evident sub-ophitic texture, with a high content of feldspar (from 40 to 75 vol%) often zoned and some sieved plagioclase, a relatively low content in olivine (2-15 vol%) and clinopyroxene (some hourglass zoned) in the range 15-30 vol%. Oxides are not present in all the samples analysed in thin section (0-15 vol%). Interstitial glass is also present (0-15 vol%). The crystals surrounded by the interstitial glass are euhedral to subhedral in shape (Figg. 7.7.1 and 7.7.2).

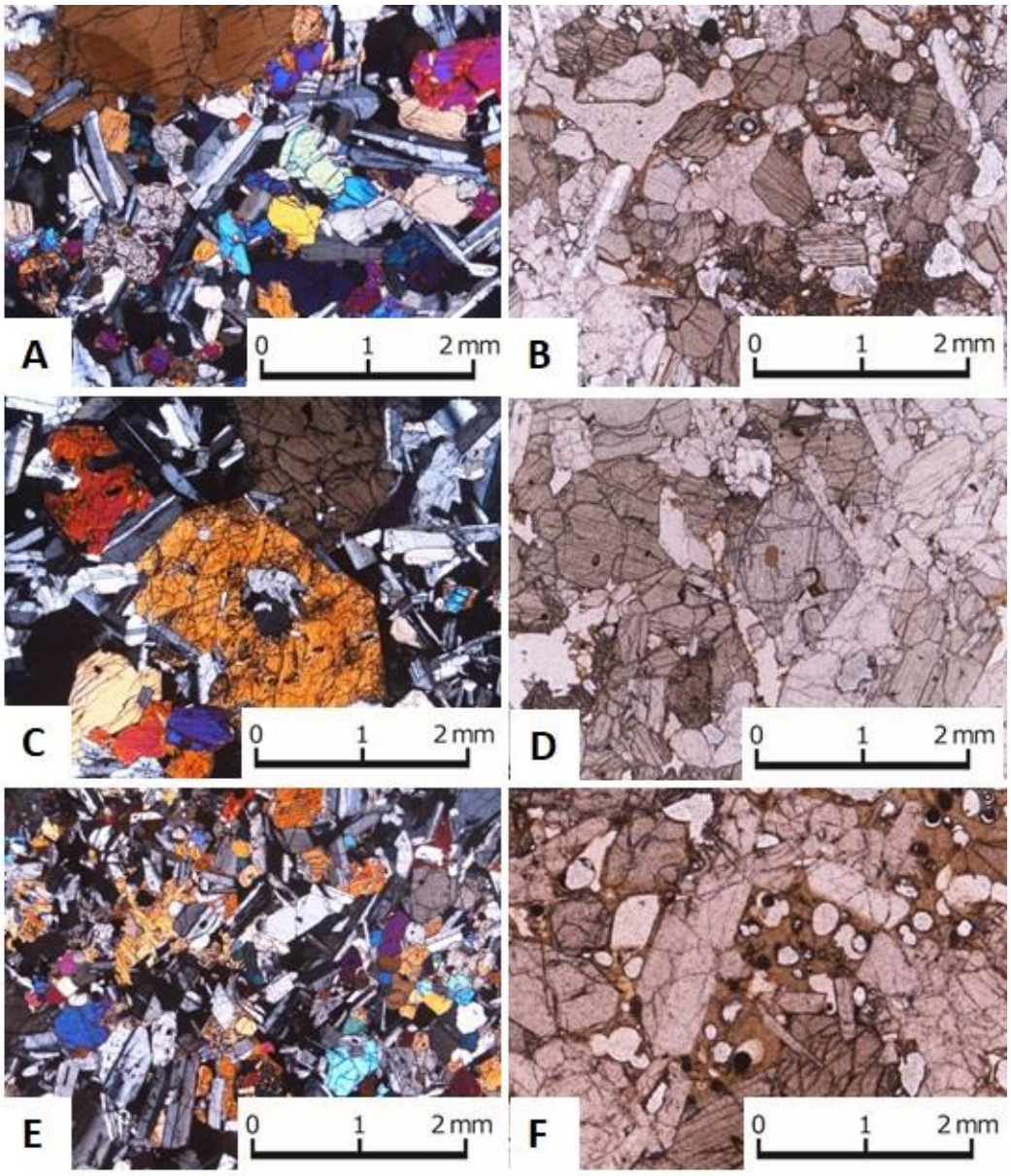

Fig. 7.7.1 – Crossed polars images (A, C and D) and plane-polarized (B, D and F). The sub-ophitic texture is evident in the Bellecombe Ash Member gabbros (A and C, sample B9, E, sample B54). The interstitial glass in these samples is enclosed (entrapped) between euhedral to subhedral crystals (B, sample B14, D, sample B33, F, and sample B9). Melt inclusions occurred in some olivine and clinopyroxene crystals (D).

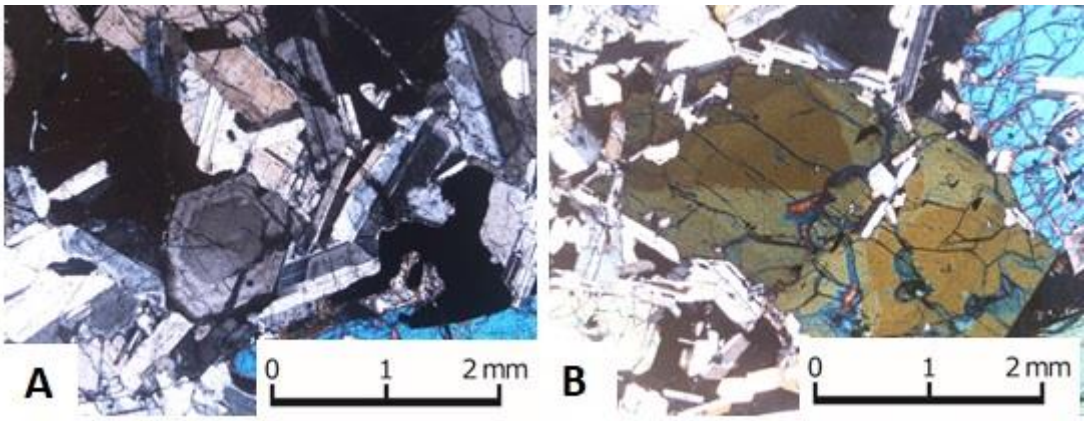

Fig. 7.7.2 - Plane-polarized light A) of sub-ophitic texture showing zoned plagioclase (sample B12), and crossed polars B) of a clinopyroxene with hourglass zoning (sample B23).

7.8 Poikilitic gabbros

The samples of this group show a poikilitic texture (olivines as cadacrystals and feldspars and clinopyroxenes as oikocrystals), with feldspar content ranging from 42 to 50 vol%, sometimes zoned and showing a sieved texture. Olivine is present (18-30 vol%) both as small (< 0,5 mm) and slightly larger crystals (> 1 mm). Clinopyroxene (22-38 vol%) show sizes > 3 mm. Interstitial glass is not abundant (1-5 vol%), as well as opaque minerals (1-3 vol%), including titano-magnetite (Fig. 7.8.1).

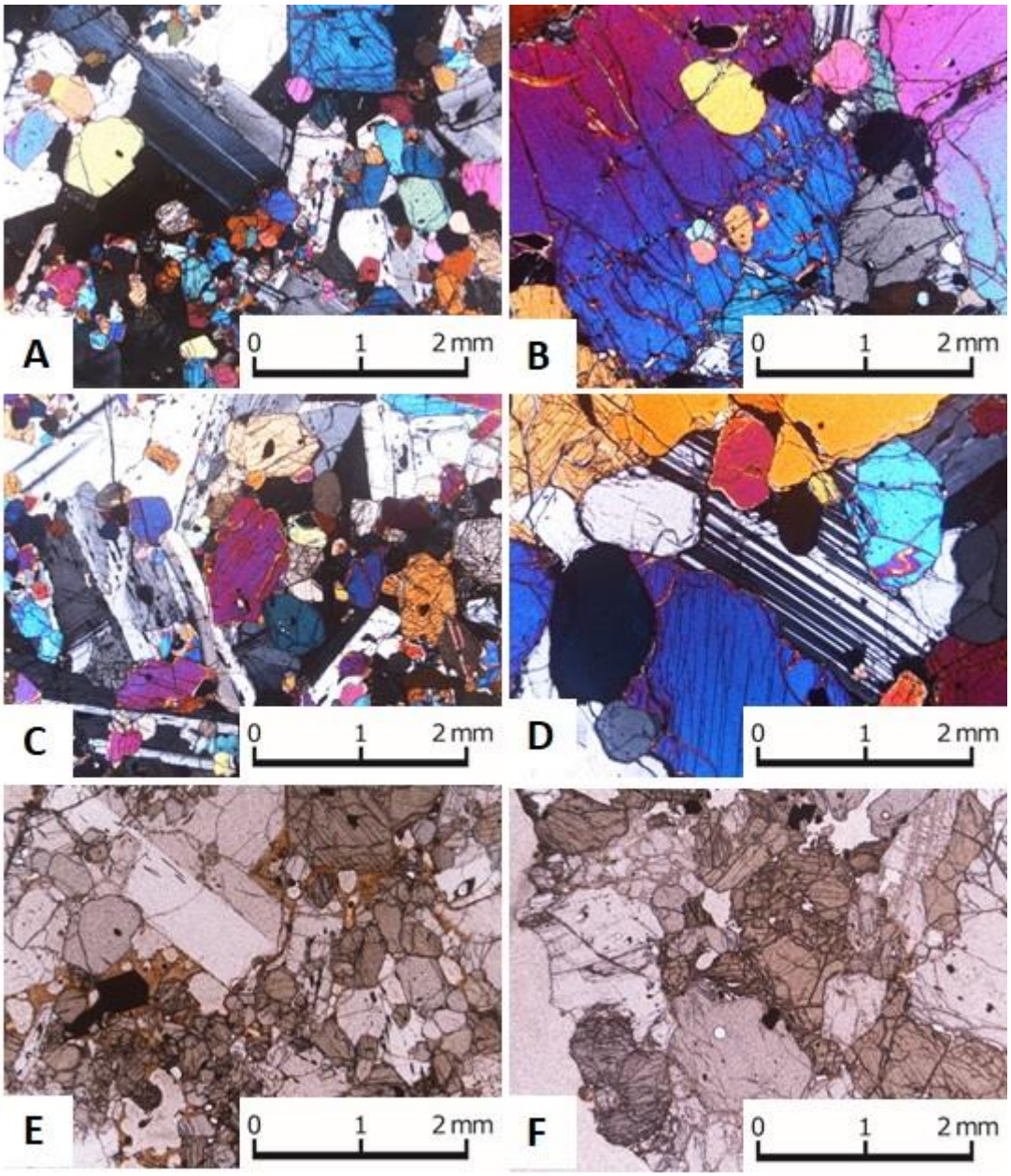

Fig. 7.8.1 – Crossed polars (A, B, C and D) and plane-polarized light of poikilitic gabbros. Different olivine size in the samples (A and C, sample B21, B, sample B41); plagioclase are often zoned (D, sample B32, E, sample B21). Crystal rim are euhedral to subhedral in shape, without resorbed margins (E). Some opaque mineral occurs as titano-magnetite (F, sample B41).

7.9 Doleritic gabbros

Doleritic gabbros are fine-grained (< 2 mm). Feldspar are present in high percentage (40-52 vol%). Also clinopyroxene (15-30 vol%) abundantly occurs. Olivine is present both as subhedral microcrystals and altered crystals (as celadonite, clay minerals or/and serpentine) in all the samples. Opaque minerals are present (5-20 vol%) often as crescumulate crystals (Fig. 7.9.1).

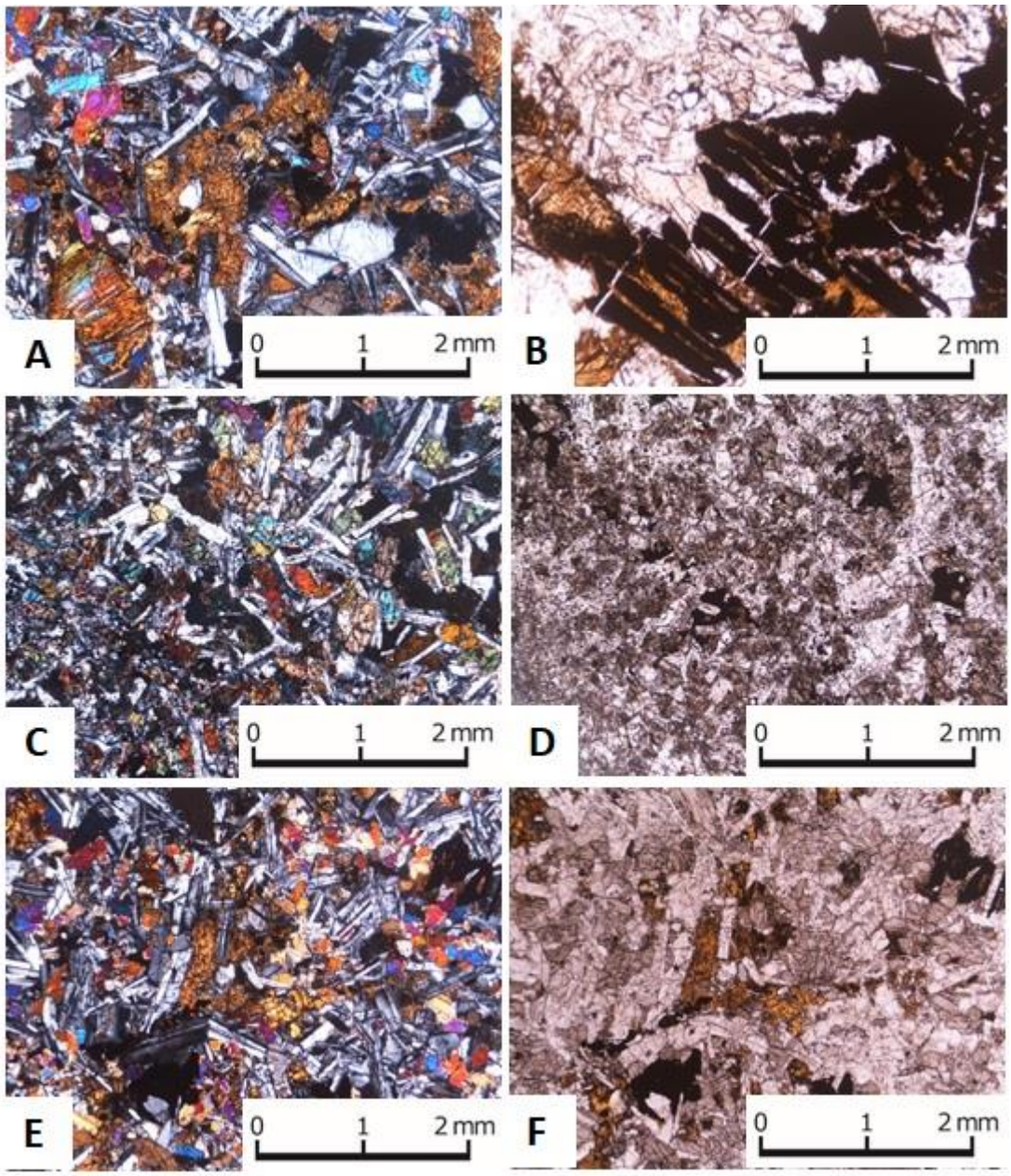

Fig. 7.9.1 – Crossed polars (A, C and D) and plane-polarized light (B, D and F) of doleritic gabbros. Altered olivine is present in all samples. As well as crescumulate opaque crystals (A and B, sample B8; C and D, sample B13, E and F, sample B27).

7.10 Micro-monzogabbros

A sample in the Bellecombe Ash Member consists of a micro-monzogabbro (Fig. 7.10.1) included in an aphiric lava. The subvolcanic crystalline part mostly consist of feldspar (90 vol%), and minor part of clinopyroxene (5 vol%) and opaque minerals (5 vol%).

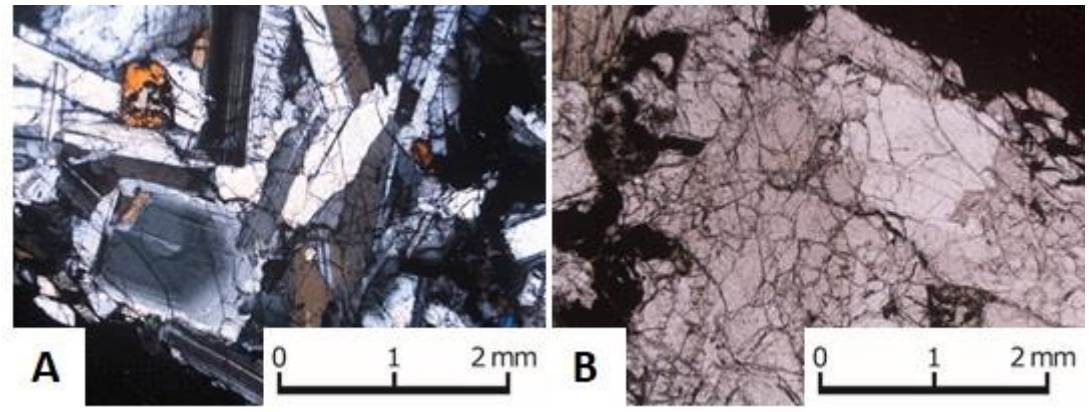

Fig. 7.10.1 – A) Crossed polars of zoned plagioclase on the micromonzogabbro; B) plane-polarized light of the contact between intrusive and aphiric portions of the sample (sample B52).

7.11 Porphyrogabbros

Samples of this group display a porphyritic-like texture. Feldspar and mafic minerals in the pseudo-groundmass are very small in size (<< 0.1 mm; 35-50 vol%), surrounding larger crystals (> 0.5 mm)of clinopyroxene (20-36 vol%) and olivine (12-36 vol%). Opaque minerals are also present (2-7 vol%) both as cromite and titano-magnetite. Only one sample show interstitial glass, altered and in small percentage (8 vol%). These samples also show rare biotite (phlogopite; < 1 vol%), never found in other samples of the Bellecombe Ash Member (Fig. 7.11.1).

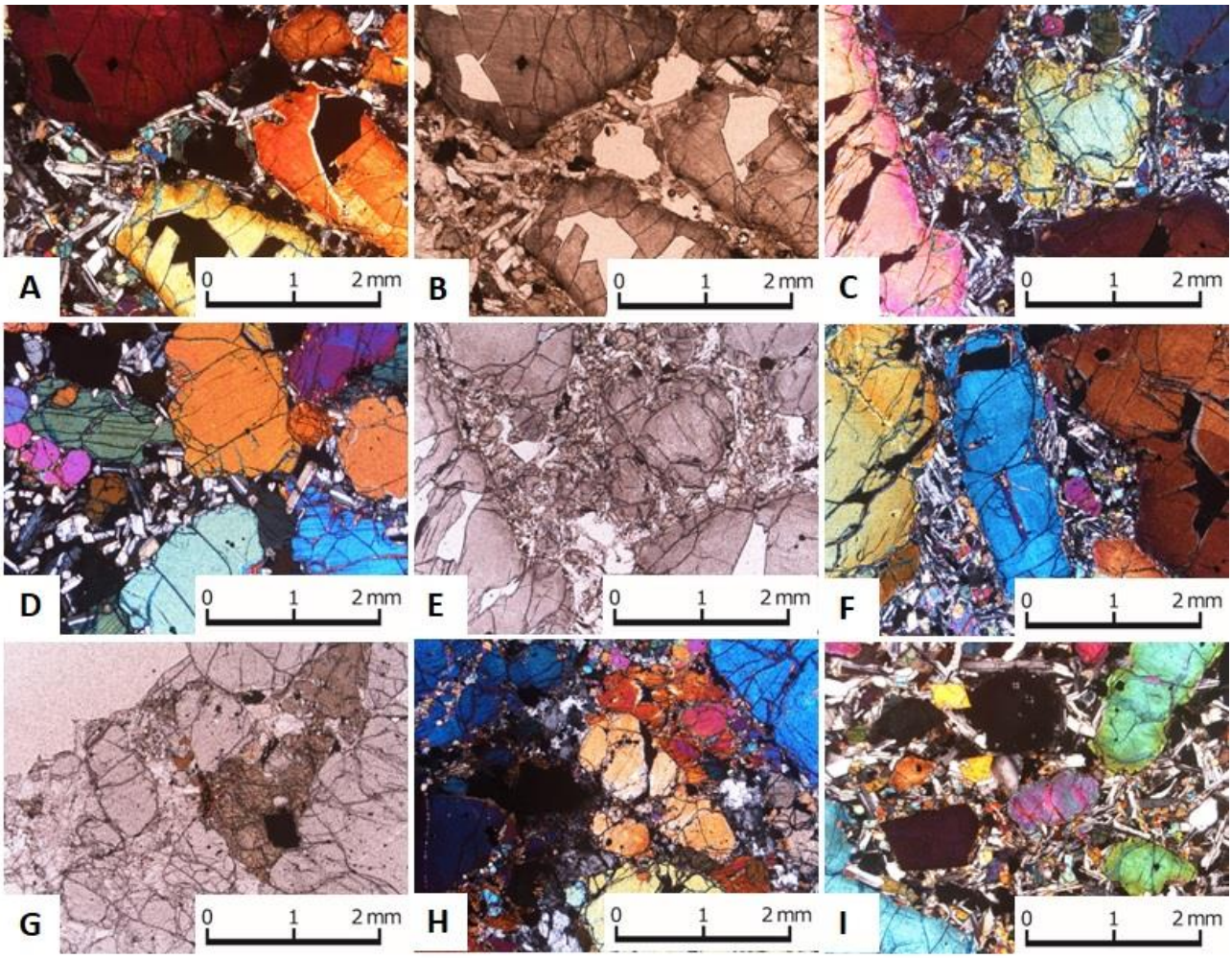

Fig. 7.11.1 – Crossed polars (A, B, C, D, F, H and I) and plane-polarized light (E and G) of porphyrogabbros. Porphyrogabbro samples showing a difference in crystal size (A, B and C, sample B10, E and F, sample B16, D, sample B18, I, sample B10, H, sample B20). Interstitial biotite is present in all the samples in small percentage (G, sample B20).

7.12 Samples with an evident magmatic layering: B108a and B108b

These samples show at the macroscopic scale an evident magmatic layering, furtherly investigated at the microscopic scale. In thin section, the samples show a gradual transition from fine grained to coarse grained subvolcanic igneous rock and a gradual transition from ultramafic to mafic lithotypes. It is not evident a crystal orientation. Resorbed margin at the mafic-ultramafic contacts are absent. Rounded crystals of olivine, some of them with fritted margin are evident, both in mafic and ultra-mafic portions. The transition between mafic lithotypes is gradual, whereas wherlites and plg-wherlites are surrounded by mafic lithotypes (fine-grained gabbro and gabbro). In this way, the samples emphasize a transition from wherlite to plg-wherlite to gabbro. Sample B108a also shows a small troctolite portion within the wherlitic domain of the sample (Figg. 7.12.1, 7.12.2, 7.12.3, 7.12.4 and 7.12.5) and rare phlogopite micro crystals (< 0.1 mm).

Fig.7.12.1 – Large (3.5 x 5 cm) thin section of the sample B108a. Ultramafic and mafic portions are evident in the whole sample, with different modal mineralogy and texture. Troctolite portion coexist with wherlite and plg-wherlite.

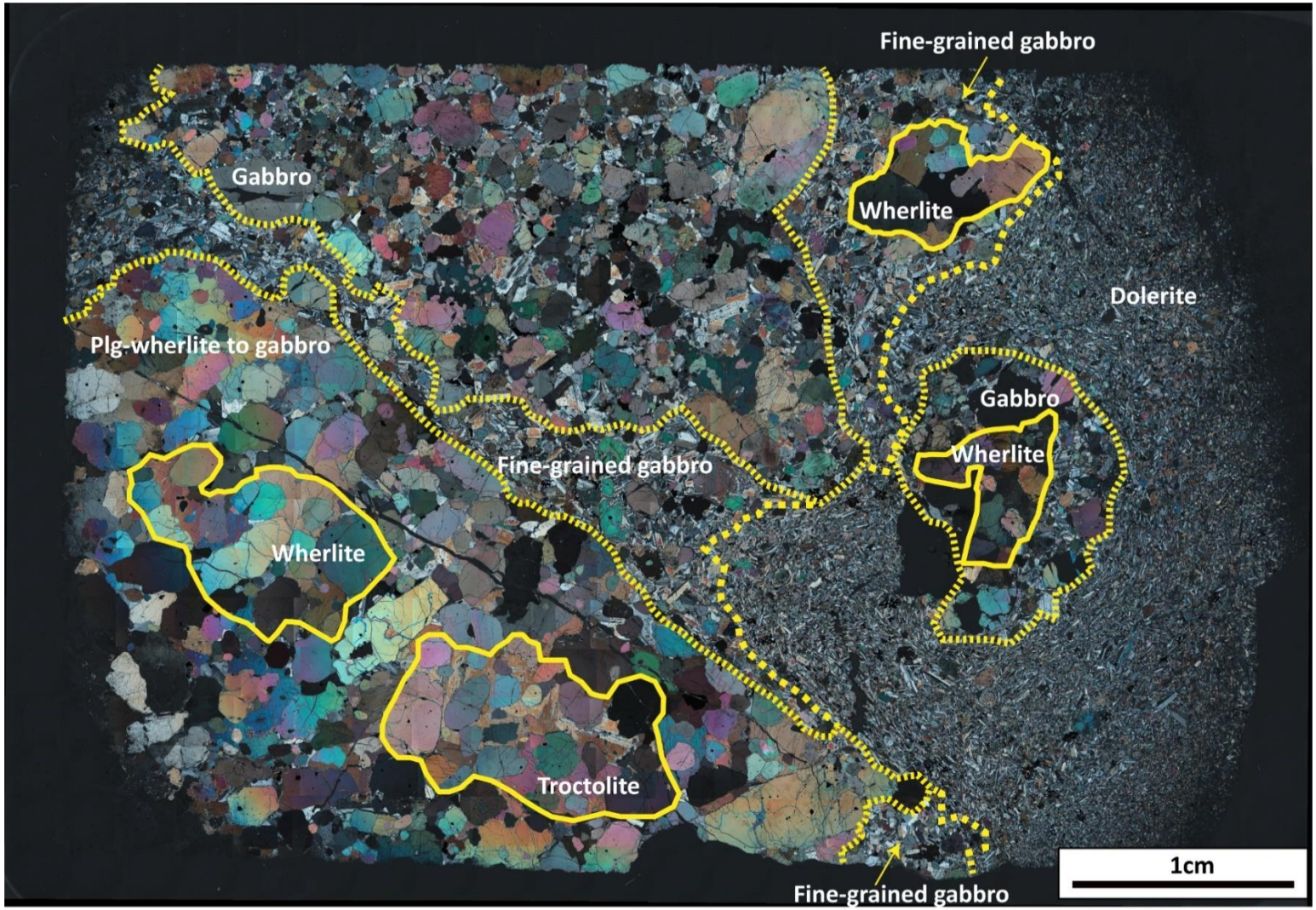

Fig.7.12.2 – Large (3.5 x 5 cm) thin section of the sample B108b. Ultramafic and mafic portions are evident in the whole sample, with different modal mineralogy and texture.

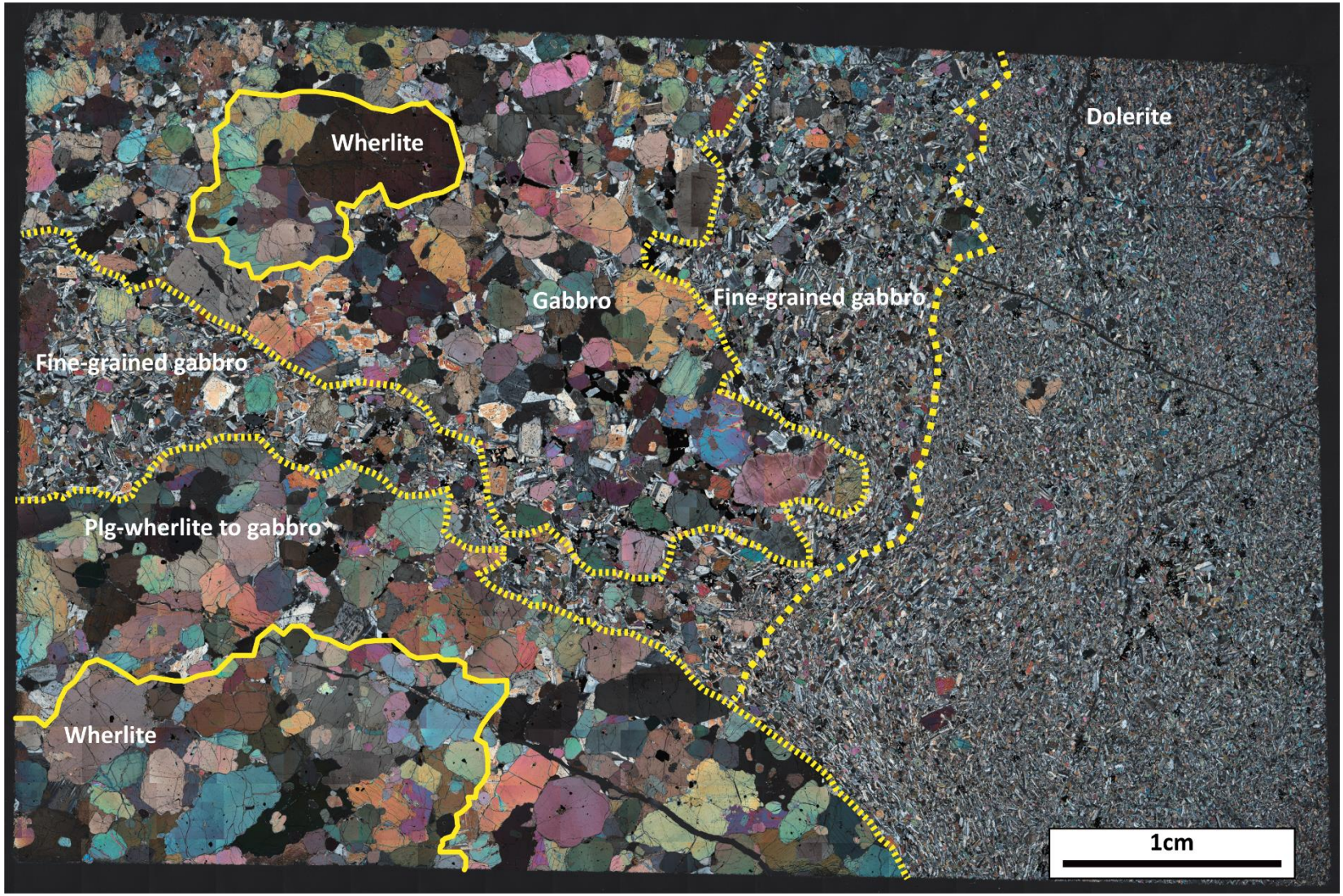

Fig. 7.12.3 – Detail of sample B108a.

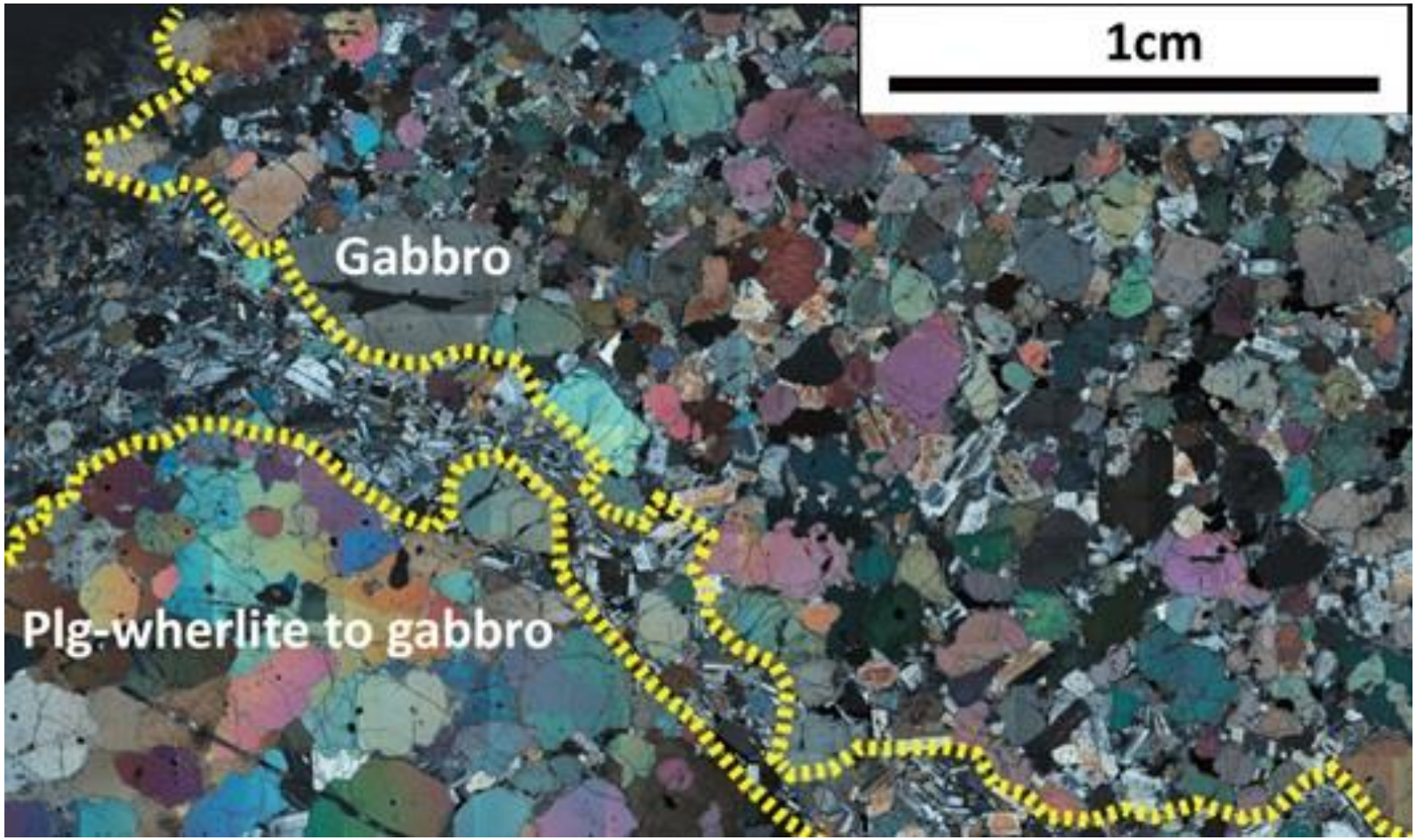

Fig. 7.12.4 – Detail of sample B108a.

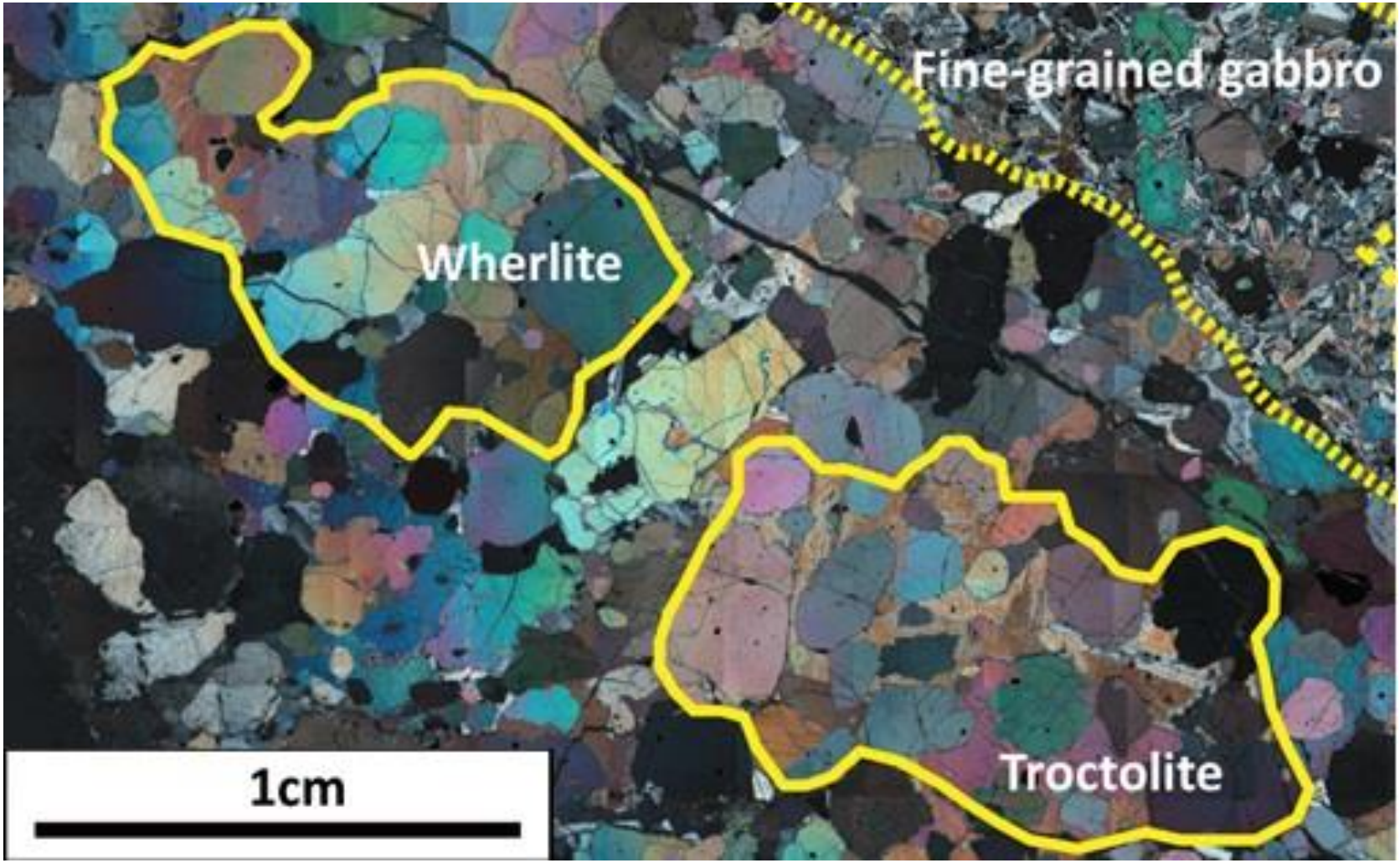

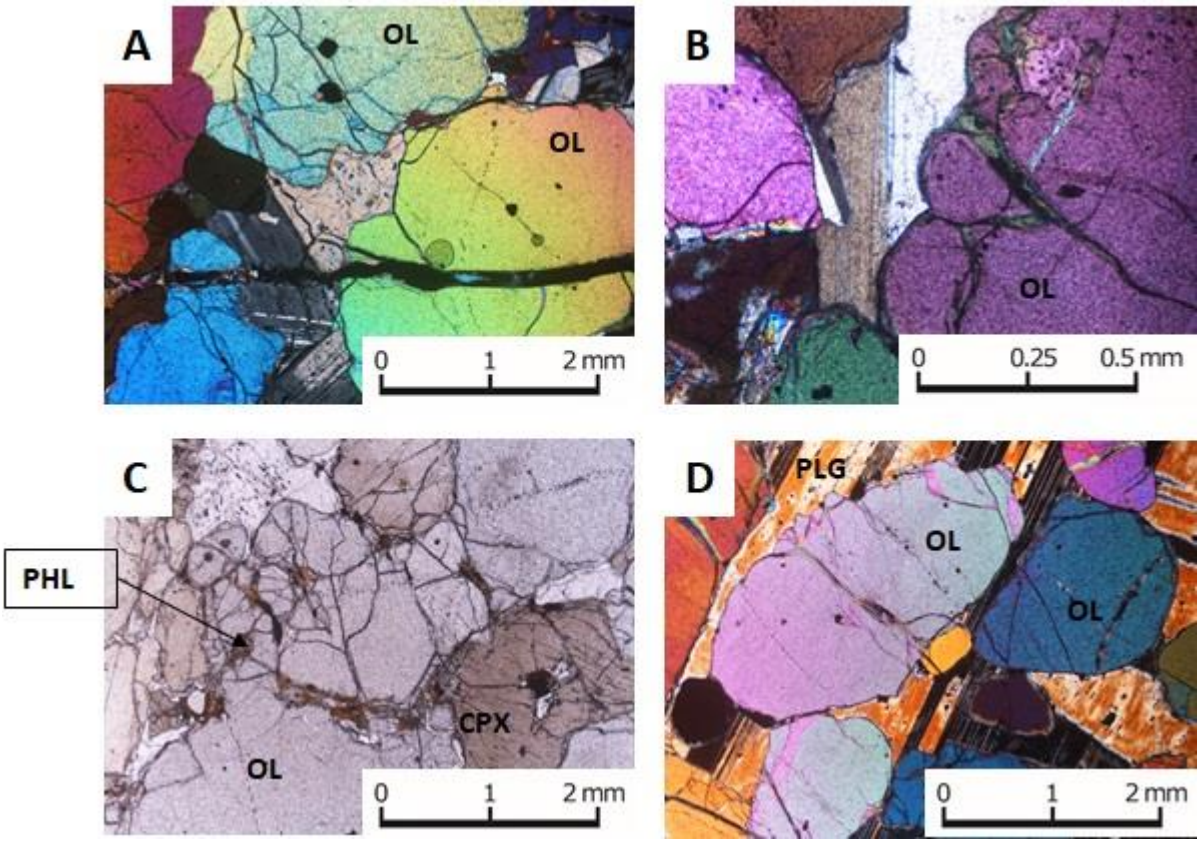

Fig. 7.12.5 – Crossed polars and plane-polarized light images of samples 108a and b. A) Fritted margin olivine on gabbro portions and B) a detailed of fritted margin olivine; C) plagioclase wherlite with phlogopite micro crystals; D) troctolite portion on sample B108a. [OL = olivine, CPX = clinopyroxene, PLG = plagioclase, PHL = phlogopite].

7.13 SEM-BSD-EDS analyses on sample B108a

The analyses with SEM-BSD-EDS on sample B108a permitted to investigate in detail the overall composite texture and the composition of single mineral phases (Table 7.13.1). Rounded olivines, often with fritted margins are widespread in the whole sample, in both ultra-mafic and mafic portions. Troctolite portion show olivine with a Fo content of about 79% and plagioclase with An_{82} Ab_{17} Or_1. Pyroxene near troctolite show a Fs_9 content (Fig. 7.13.1). Near the troctolite portion, olivine crystals with fritted margins are always characterized by Fo_{79} (Fig. 7.13.2).

Plagioclase in gabbro and fine-grained gabbro portions are often zoned, with a higher Ca-content on the core of the crystal. Mafic portions emphasize a high content in opaque minerals which are evident as both inclusions and interstial crystals (Fig. 7.13.3). Opaque crystals in B108a sample are both Cr-Fe spinel and Ilmenite. In mafic portion, plagioclase appears to be crystallized after rounded olivine and clinopyroxene crystals. Opaque minerals crystallized from late interstitial liquid (Fig. 7.13.4). Rounded olivine crystals in contact with plagioclase show a Fo_{67} composition, less forsteritic than other gabbro clasts in the Bellecombe Ash

Member. The presence of ilmenite suggests a relatively low oxygen fugacity environment of crystallization.

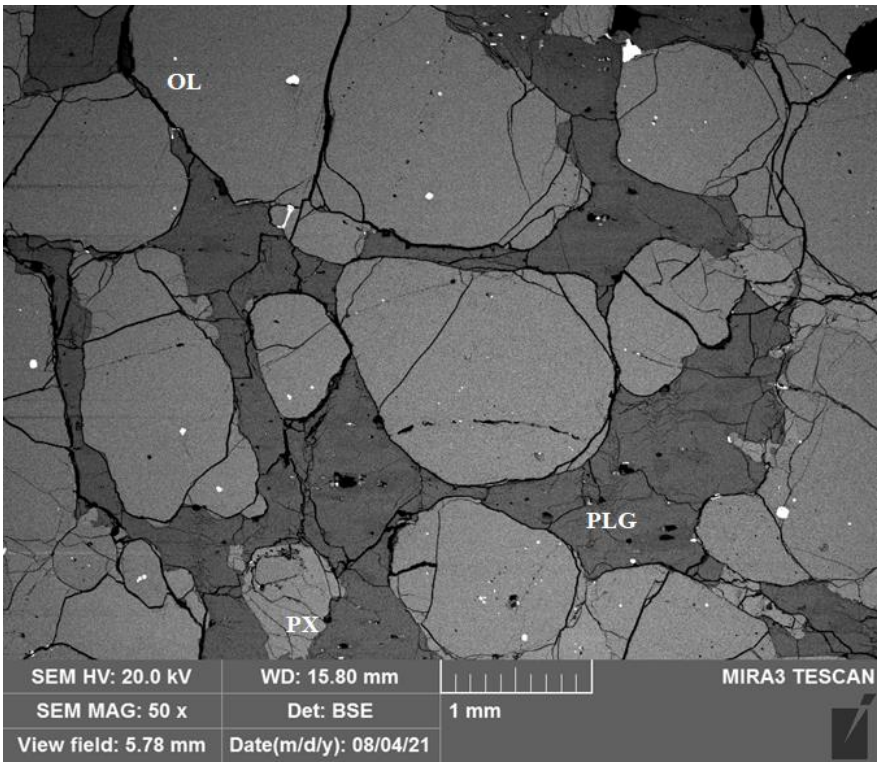

Fig. 7.13.1 – Troctolite portion in the composite sample B108a. Rounded Fo_{79} olivine are enclosed by plagioclase (An_{82}).

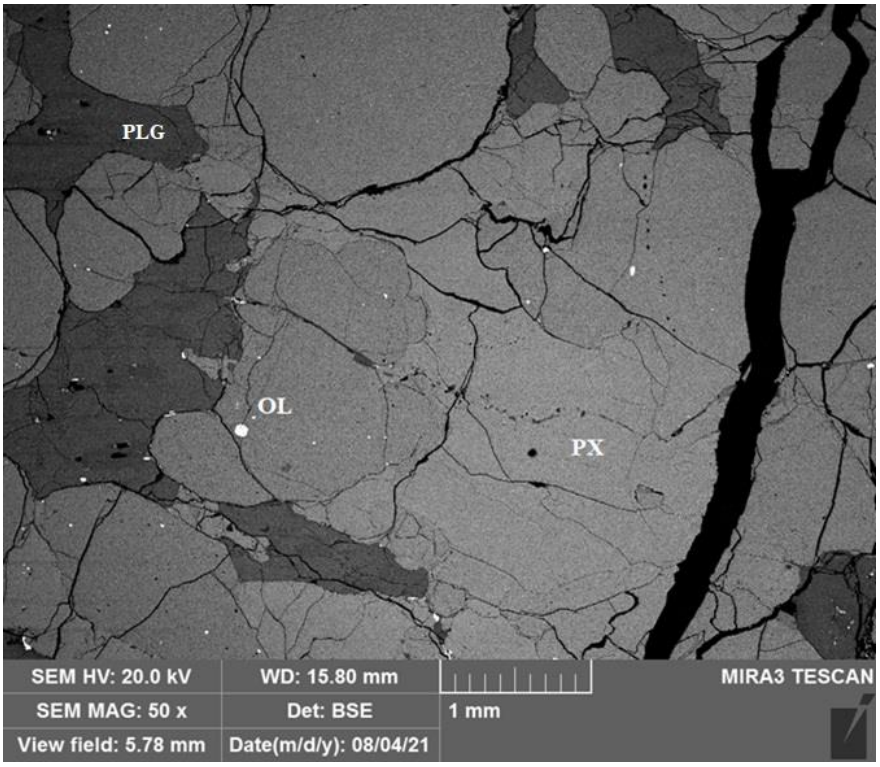

Fig. 7.13.2 – Ultramafic portion (plagioclase wherlite) near troctolite showing crystals of fritted margin olivine and clinopyroxene with rounded margin.

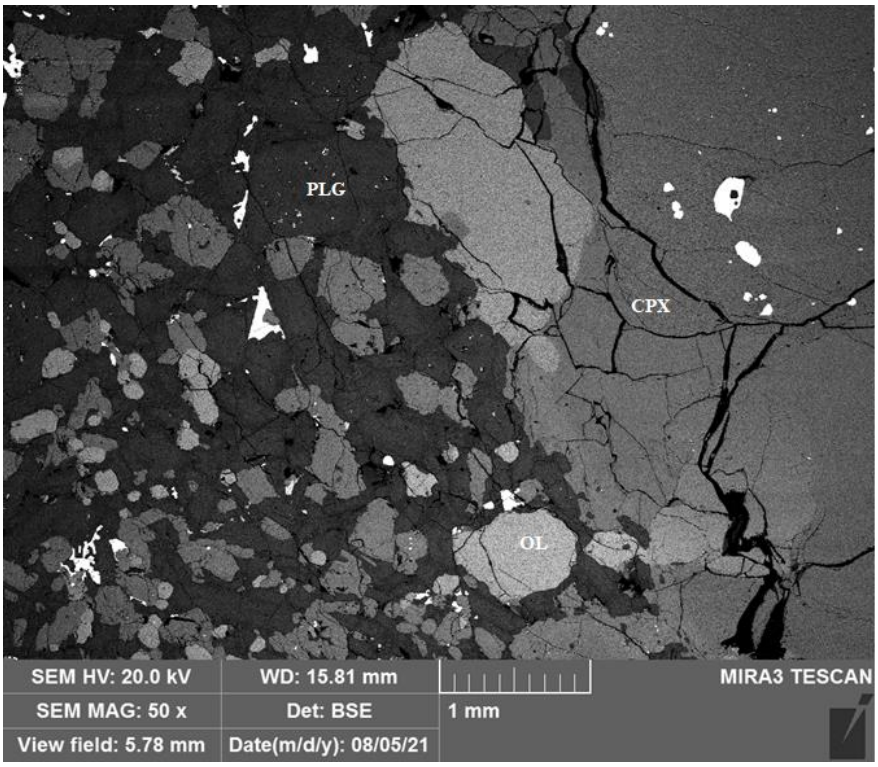

Fig. 7.13.3 – Contact between ultramafic portion and fine-grained gabbro on sample B108a. The massive presence of opaque minerals is evident both on single crystals and interstitially.

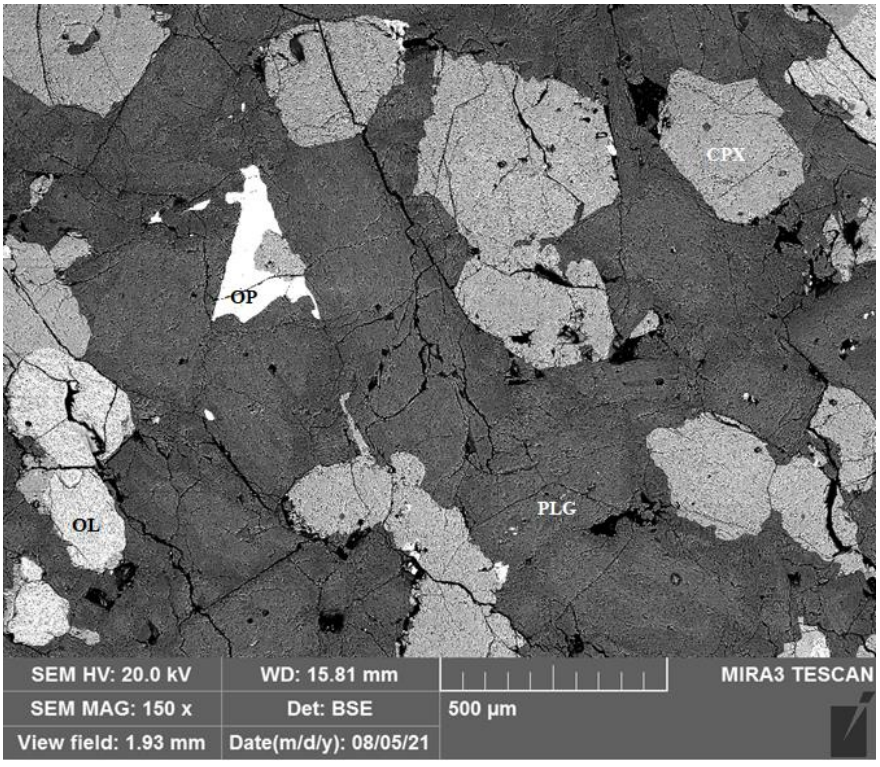

Fig. 7.13.4 – Detail of a portion of fine-grained gabbro. Olivine and clinopyroxene crystals show rounded margin and plagioclase are zoned. Ilmenite crystal (OP) is evident between plagioclase crystals.

The EDS map furtherly permit to investigate the composite B108a sample. Troctolite portion emphasizes the presence of fritted margin olivines surrounded by patchy zoned plagioclase (different Ca and Na contents). Ti is poorly present in troctolite portion (Fig. 7.13.5). On the mafic portion, gabbro displays small rounded olivine, surrounded by large anhedral clinopyroxene crystals, and fritted margin olivine. Clinopyroxene crystals are also zoned, with higher concentration of Ca on the core and higher Fe-content on the rim. In addition, also plagioclase is normally zoned, with a more albitic rim. Opaque minerals (both ilmenite and spinel) are present, mainly near the rim of other large crystals (olivine and clinopyroxene; Figg. 7.13.6, 7.13.7 and 7.13.8).

Also on the ultra-mafic portion (wherlite and plagioclase wherlite), single mineral phases show rounded margins, with subhedral crystals, also on plagioclase. Fe-Ti oxides are also present as crescumulates, interstitially and surrounding other crystals. Zoned plagioclase crystals present in sample B108a show a high Ca concentration on the core and high Na concentration on the rim of the crystals. Opaque minerals in the interstice, with regular margins despite the contact with other single mineral phases (olivine, clinopyroxene and plagioclase), suggests that oxides were formed last, as crystallization of an interstitial residual liquid.

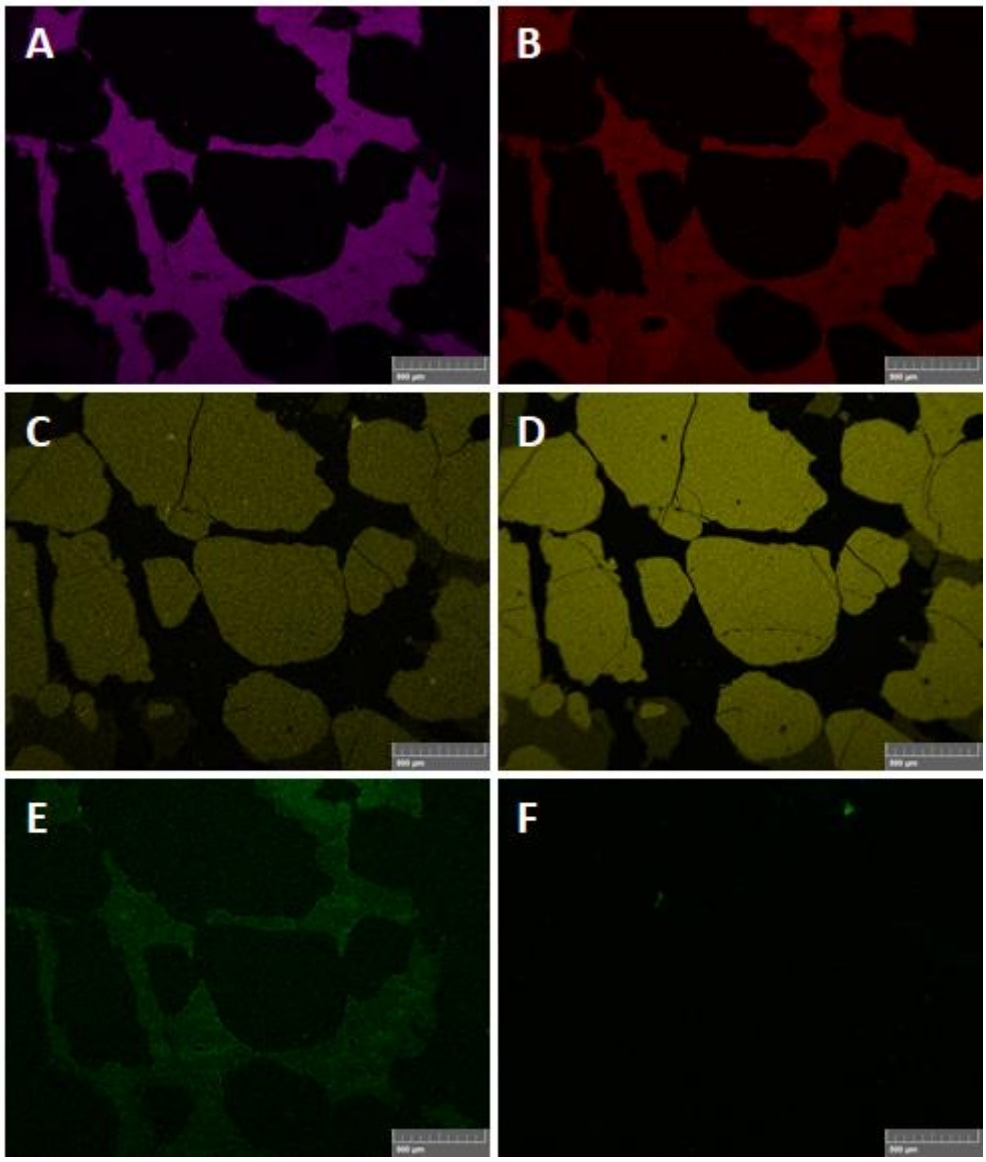

Fig. 7.13.5 – Different element contents in troctolite portion on sample B108a. Rounded margin of olivine is evident (A, B and D). Plagioclase is zoned (E) with lesser Na contents between olivine crystals. Some little clinopyroxene crystals occurs (C and D). Troctolite shows poor content of oxides (F). A) Al, B) Ca, C) Fe, D) Mg, E) Na, F) Ti.

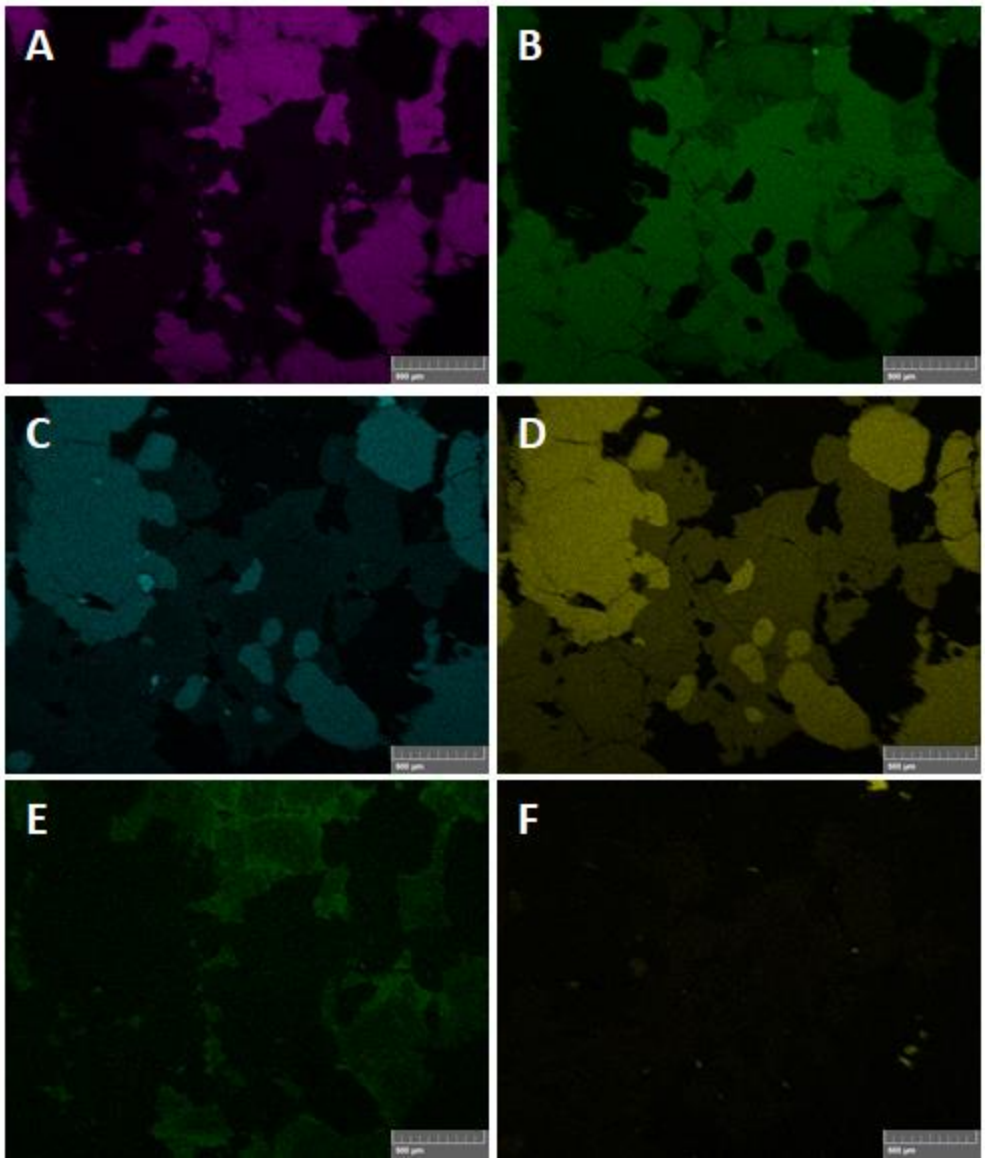

Fig. 7.13.6 – Different element contents in gabbro portions. Plagioclase are interstitial (A), and zoned (E), with higher contents of Na close to olivine crystals. Large clinopyroxene crystals surrounding rounded olivines (C and D). Few oxids crystals occurs, mostly spinels. A) Al, B) Ca, C) Fe, D) Mg, E) Na, F) Ti.

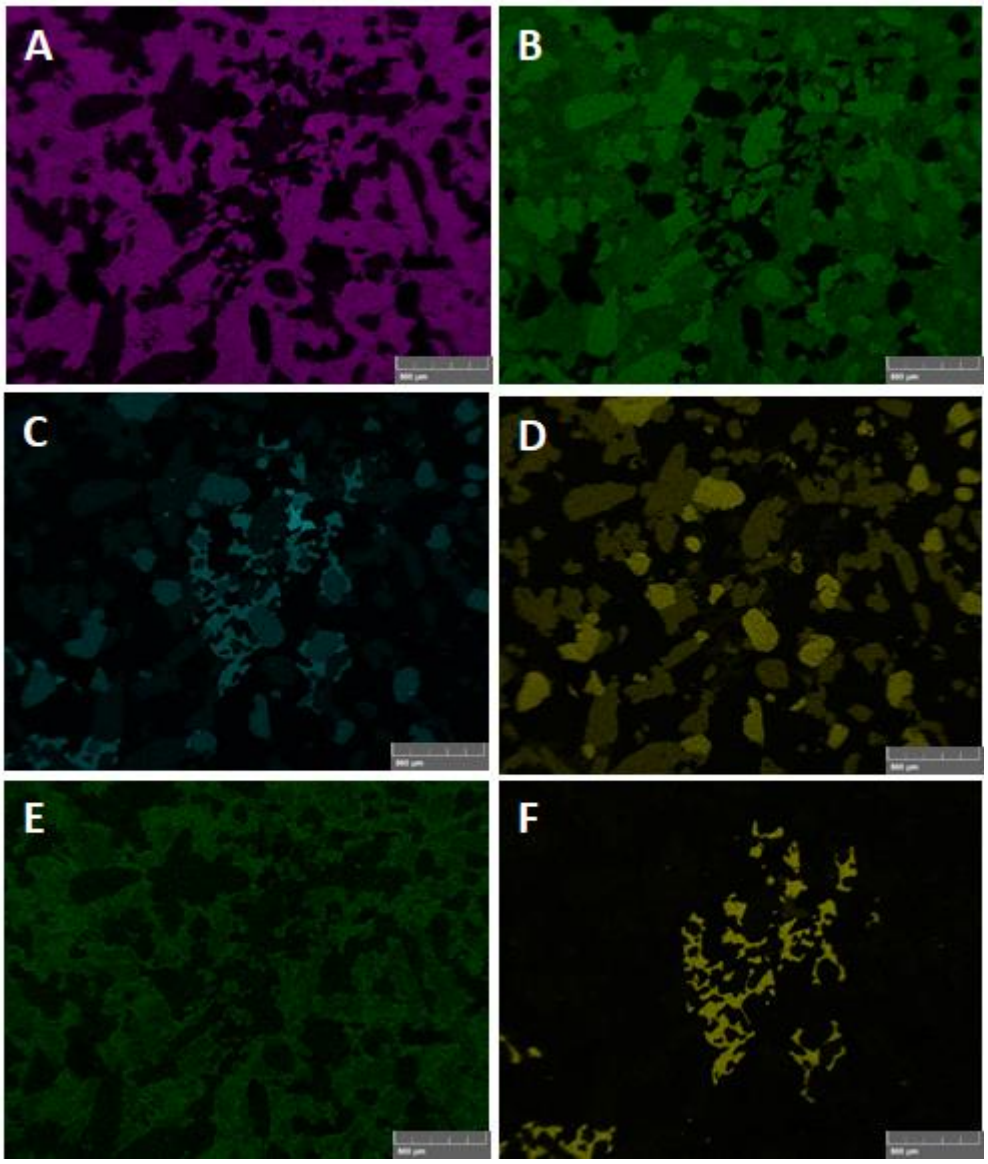

Fig. 7.13.7 - Different element contents in fine-grained gabbro portions. All single mineral phases show rounded margins with sub-hedral aspect (A, B, C and D). Plagioclase are zoned, with higher content of Na close to olivine and clinopyroxene (E). Fe-Ti oxides are massive evident and dentritic, in the interstices and surrounding other crystals. A) Al, B) Ca, C) Fe, D) Mg, E) Na, F) Ti.

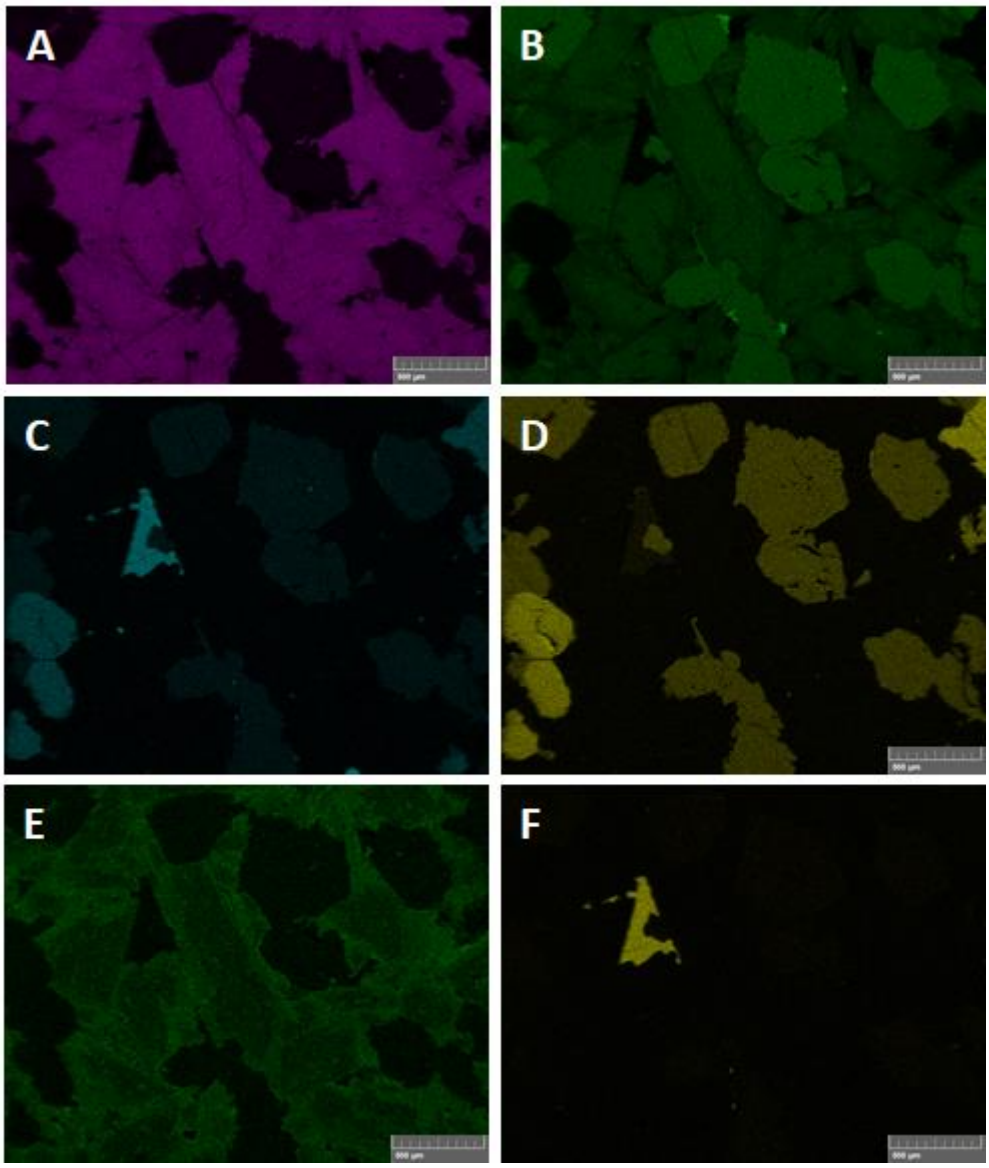

Fig. 7.13.8 – Detail of a portion of fine-grained gabbro. Fe-Ti oxides are interstitial (A, B, C, D, E and F) between plagioclase crystals. Plagioclase are subhedral and zoned, with higher contents of Na next to other single mineral phases and higher contents of Ca at the core of the crystals (B and E). A) Al, B) Ca, C) Fe, D) Mg, E) Na, F) Ti.

7.14 SEM-BSD-EDS analyses on sample B28

The SEM-BSD-EDS analyses on sample B28 permit to improve the study on single mineral phases (Table 7.14.1). This wherlite sample show fritted margin olivine and small rounded olivine surrounded by subhedral clinopyroxene crystals (Figg. 7.14.1 and 7.14.2). The composition of olivine in sample B28 is Fo_{79} therefore characterized by a less forsteritic composition with respect olivines in other wherlite samples analysed with EMPA (Fo_{80-85}). Zoned clinopyroxene crystal are also evident, showing an increase of Fs from rim (Fs_6) to the core (Fs_{10}).

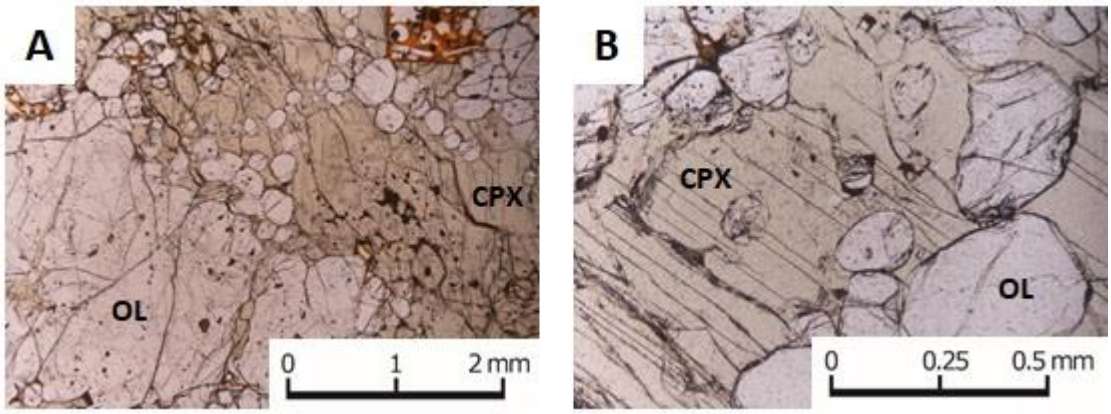

Fig. 7.14.1 – Plane-polarized light images of wherlite B28. A) and B) evidence the presence of rounded olivine and fritted margin olivine. [OL = olivine, CPX = clinopyroxene].

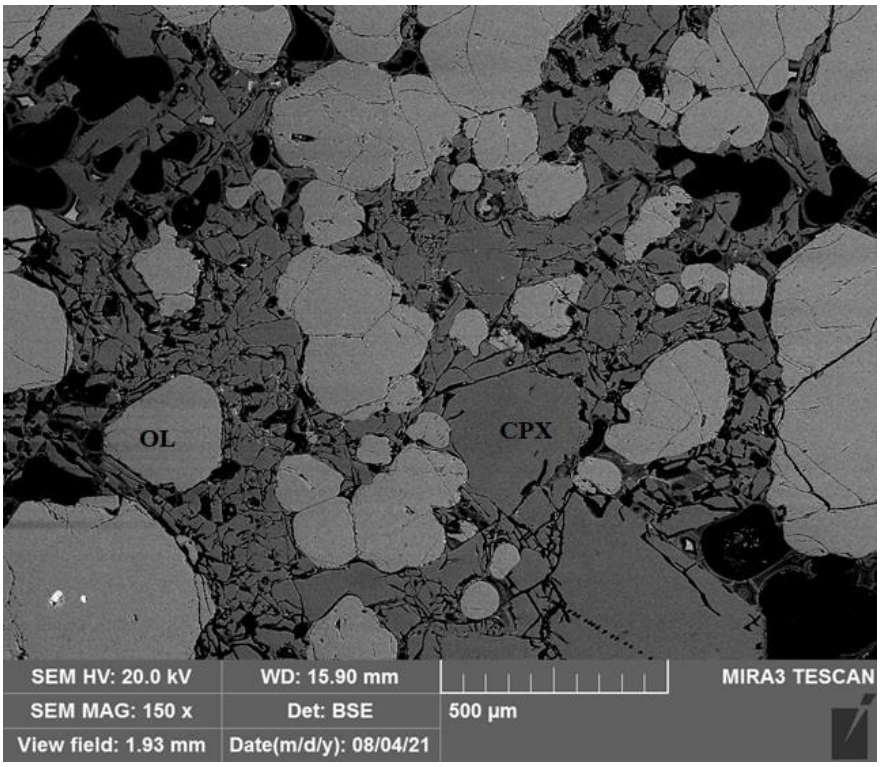

Fig. 7.14.2 – Rounded olivine and fritted margin olivine surrounded by clinopyroxene crystals in wherlitic sample B28. Some olivine crystals show fritted margin.

An EDS map of the sample displays the concentration of several elements, denoted the presence of single mineral phases (olivine, clinopyroxene) and interstitial glass on a particular structure. Al, Ca and Na concentration well evidence subhedral clinopyoxene crystals, surrounded rounded olivines, confirmed by high concentration of Mg and Fe. Interstitial glass is individuated by the presence of Ti (Figg. 7.14.3). The texture of this wherlitic sample suggest a changing on the conditions after the crystallization of the olivine, with consequent rounding of the crystals, and a rapid ascent of the sample, which led to a quenching of interstitial residual liquids forming Ti-rich interstitial glass.

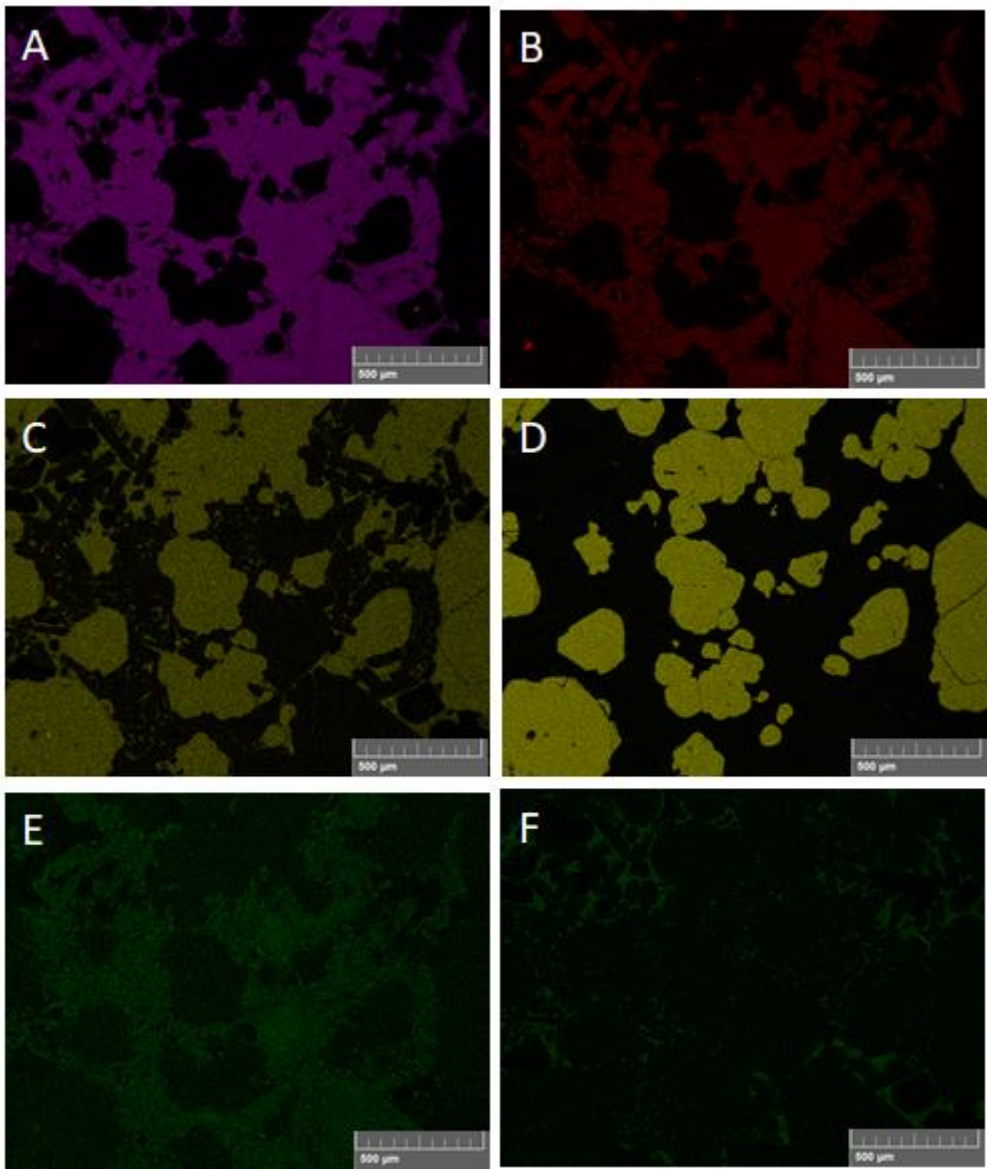

Fig. 7.14.3 – Different element contents on single mineral phase of wherlitic sample B28. Rounded olivine crystals are separated each other from clinopyroxene subhedral crystals (A, B, C and D). Clinopyroxene shows a little zoning (E). B28 sample display a Ti-rich intertitial glass. A) Al, B) Ca, C) Fe, D) Mg, E) Na, F) Ti.

8 Geochemistry: major and trace elements

The whole-rock composition of representative subvolcanic ejecta of the Bellecombe Ash Member are reported in Table 8.1. All the samples analysed were compared with literature data. In the legend, recent, Langevin-Bellecombe period and ancient samples are from Observatoire Volcanologique du Piton de la Fournaise (OVPF) database (> 50 ky, 50-3 ky and < 3 ky respectively). Site 1, Site 2, Site 3 and Site 4 are Piton des Neiges samples (Berthod et al., 2020). Other Piton de la Fournaise literature data (Upton et al., 2000) were subdivided in dunite, wherlite and gabbro. Finally, doleritic samples and ballistic block from Plan des Sables (Piton de la Fournaise; Brugier,

thesis, 2016) were compared with other literature data and samples of this PhD thesis.

Whole rock major data were plotted in Fig. 8.1. In addition to the bulk-rock analyses from this study from the Bellecombe Ash Member, data from previous studies (Upton et al., 2000; Berthod et al., 2020; Brugier, thesis, 2016; OVPF literature data subdived in three cathegories: Ancient > 50 ky, Langevin-Bellecombe period 50-3 ky, Recent < 3 ky) have been used to provide a comprehensive picture of the whole compositional range. The dunite samples from the Bellecombe Ash Member point out the highest MgO content (46.01 wt%) with respect other dunites from literature (Upton et al., 2000; Berthod et al., 2020). Wherlites and dunites from Cirque of Salazie (Piton des Neiges) show a depletion in Fe_2O_3 wt% content, indicating a differentiation from a tholeiitic magma, with MgO wt% values ranging between dunites and wherlites from the Bellecombe Ash Member. Wherlites from Bellecombe show a different content in major and trace elements, with sample B3 showing a depletion in MgO wt% and the highest CaO content with respect the other wherlites from Bellecombe. Gabbros from Cirque of Salazie are similar in composition to sub-ophitic gabbros from the Bellecombe Ash Member. Gabbros of Piton de la Fournaise from Upton et al. (2000) can be subdivided in two groups, i) a group with minor MgO wt% content and major and trace elements comparable to mafic ejecta (sub-ophitic, poikilitic and doleritic gabbros) from Bellecombe and ii) a second group showing a higher MgO wt% and major and trace elements comparable to wherlites and porphyrogabbros from the Bellecombe Ash Member. Despite the different textures, porphyrogabbros from Bellecombe are similar in composition to wherlites, with similar MgO wt% content and both major and trace elements. Poikilitic gabbros show some differences in major and trace elements content. In fact, sample B32 show the highest MgO wt% content (25.4 wt%) with respect to other poikilitic samples (MgO 13.6-17.9 wt%), while B21 show the lowest Fe_2O_3 wt% content. The highest CaO content in mafic and ultramafic samples of the Bellecombe Ash Member compared to other Bellecombe lavas should be the result of higher contribution of pyroxene accumulations (± plagioclase).

Bellecombe Ash Member subvolcanic samples were compared with literature data of intrusive clasts from Piton de la Fournaise (Upton et al., 2000; Brugier et al., 2016; OVPF data) and Piton des Neiges samples (Berthod et al., 2020).

Total alkali vs. silica diagram (Fig. 8.2) displays a $Na_2O + K_2O$ wt% content for the investigated Bellecombe Ash Member subvolcanic clasts ranging from 0.04 to 3.5 wt% with a SiO_2 wt% content < 49 wt% (picro-basalt to basalt fields in the TAS diagram). Ancient (> 50 ky) samples are more alkaline (basaltic trachyandesite). Dolerites and some sub-ophitic gabbros are quite close to typical SSB composition.

CaO/Al_2O_3 vs. MgO variation diagram (Fig. 8.3) of Bellecombe Ash Member ejecta, compared with literature data (Upton et al., 2000;

Berthod et al., 2020; data from OVPF), points out three different trend, interpreted as "fractionation trends": 1) a steep decrease of CaO/Al_2O_3 ratio correlated with decrease of MgO in the range of ca.13-6 wt.%: gabbro fractionation; 2) a much less steep decrease of CaO/Al_2O_3 ratio correlated with decrease of MgO from ca.36 wt.% downward: wherlite fractionation; 3) a constant CaO/Al_2O_3 ratio with a marked decrease of MgO wt% from concentration of ca. 46 wt.%: dunite fractionation (or oceanitic trend). Bellecombe Ash Member porphyrogabbro clasts mainly reflect the oceanitic trend, representing a compositional *trait d'union* between ultramafic clasts (dunite and wherlite) and other mafic ejecta. Doleritic gabbros of the Bellecombe Ash Member are similar in compositions to Steady State Basalts (SSB) group.

The trace element composition of the analysed samples is given from Fig.8.4 to Fig.8.7. Bellecombe Ash member subvolcanic samples show a REE and incompatible elements depletion with respect the volcanic samples, especially in comparison with ancient and recent products of Piton de la Fournaise (OVPF data).

CaO/Al_2O_3 vs. Sc and Th (Fig. 8.8) bulk rock composition (trace element) of Piton de la Fournaise lavas erupted from both peripheral (Boudoire et al., 2019) and central areas (Vlastelic et al., 2007; Peltier, 2007; Boivin and Bachelery, 2009; Salaun et al., 2010; Di Muro et al., 2014, 2015) were compared with Bellecombe Ash Member ejecta. Olivine-bearing basalts from peripheral vents are preferentially depleted in trace elements that are compatible in clinopyroxene (such as Sc). Sub-ophitic gabbros and doleritic gabbros are more similar in composition to peripheral products. Instead, porphyrogabbros of Bellecombe Ash Member show very low Sc content respect other samples. Olivine-bearing basalts from peripheral vents are preferentially enriched in incompatible trace elements such as Th (Boudoire et al., 2019). Samples of Bellecombe Ash Member reflect peripheral products composition; doleritic gabbros follow a plagioclase-fractionation trend, whereas sub-ophitic gabbros reflect a clinopyroxene fractionation trend.

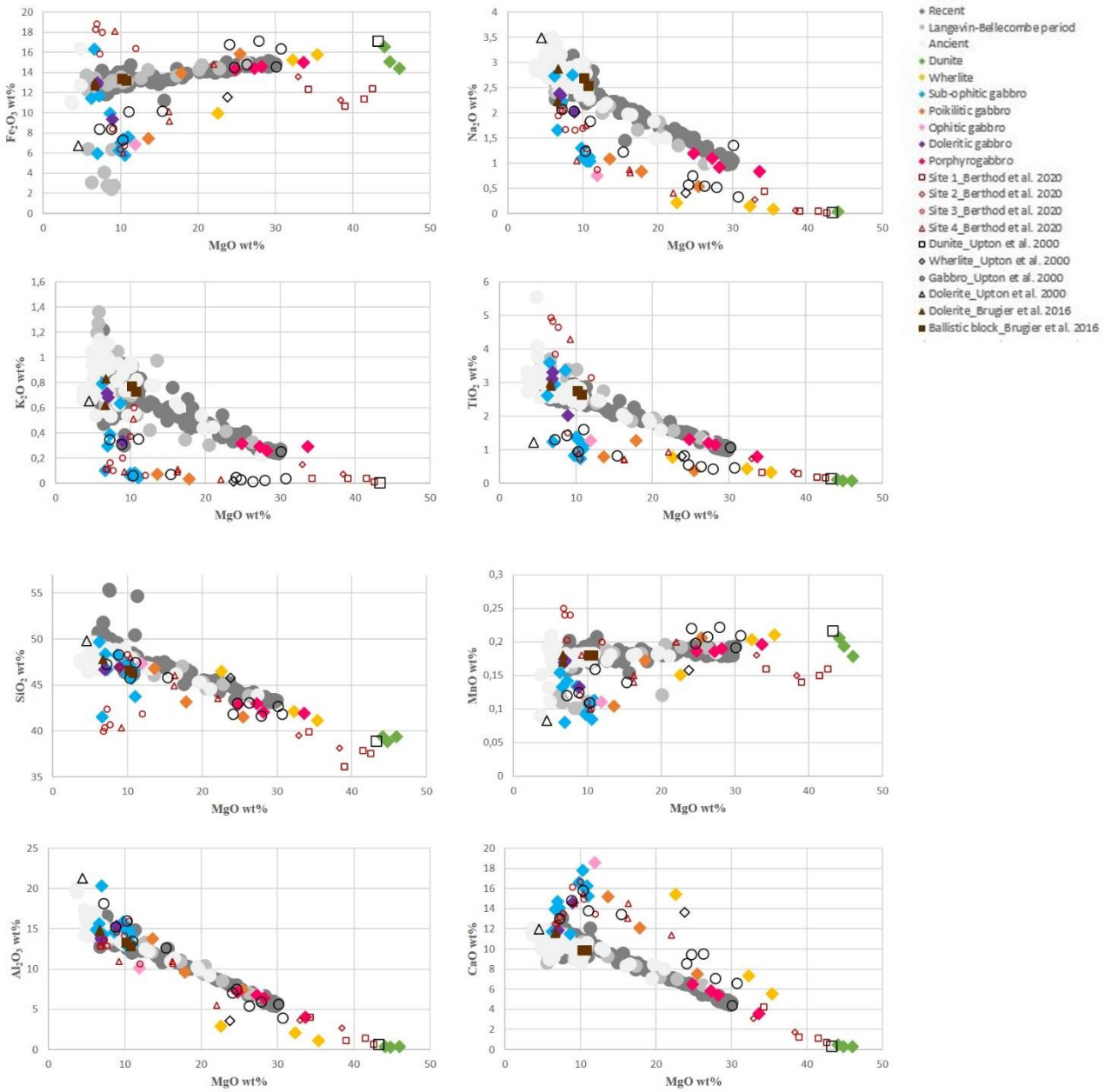

Fig. 8.1 – Major element vs. MgO wt% variation diagrams. All the samples of the Bellecombe Ash Member were compared with literature data.

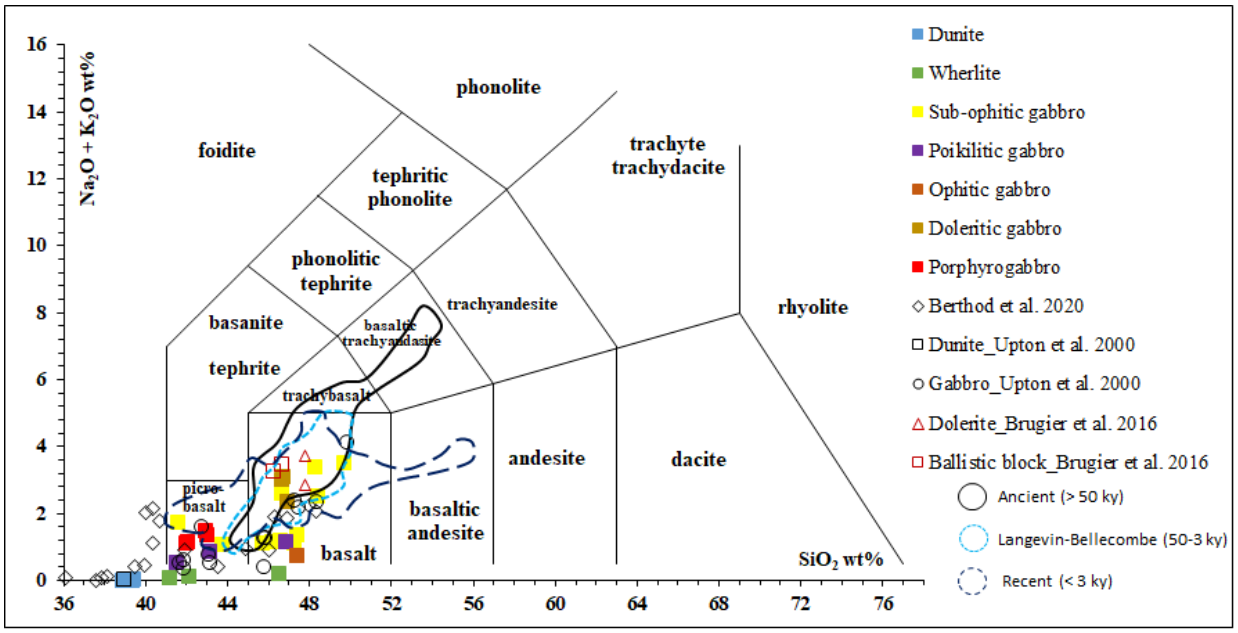

Fig. 8.2 – Total alkali vs. silica graph with analysed representative samples of the Bellecombe Ash Member compared with literature data, from OVPF database, Berthod et al. (2020), Upton et al. (2000) and Brugier (thesis, 2016).

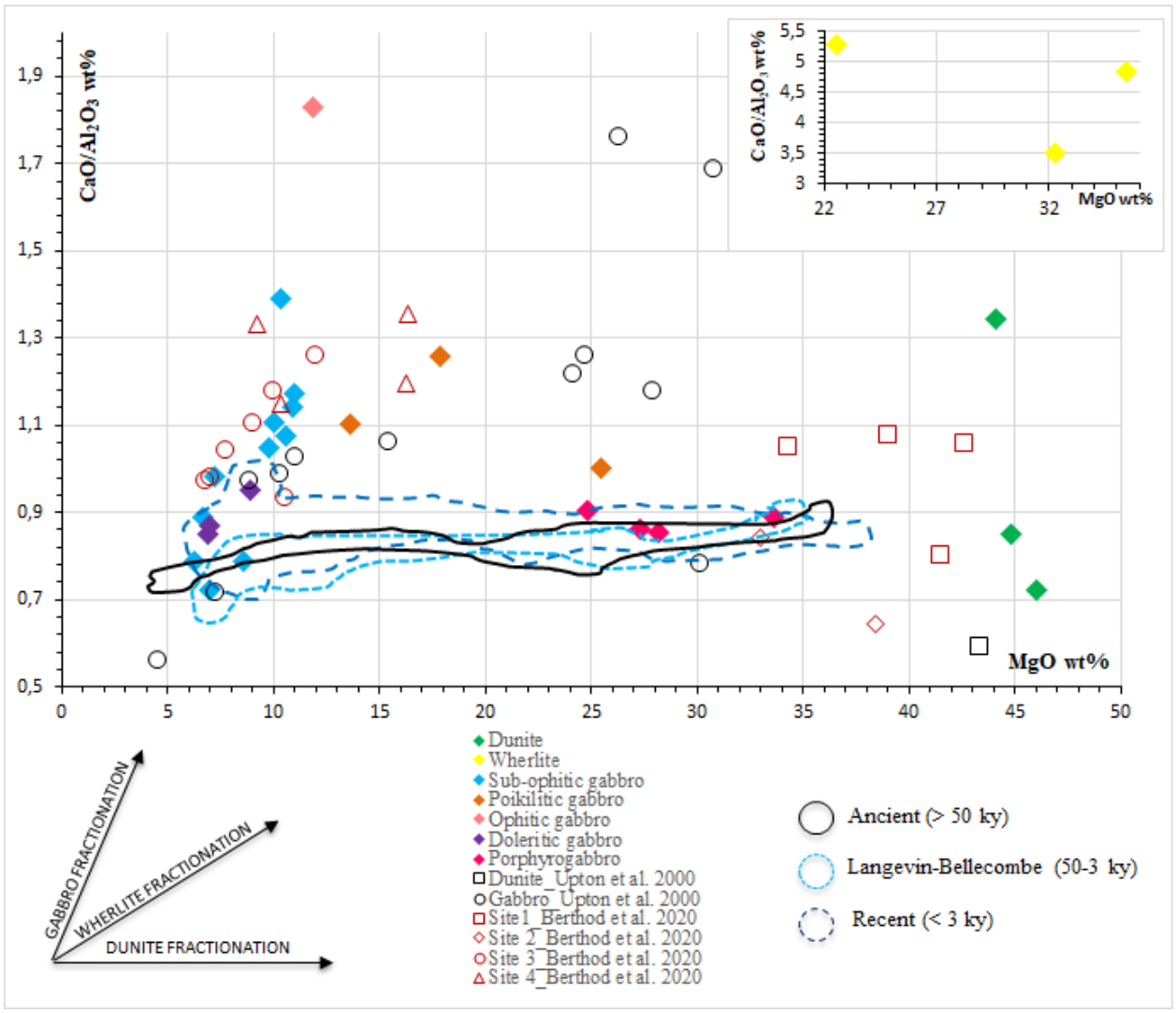

Fig. 8.3 – CaO/Al_2O_3 vs. MgO graph. Bellecombe Ash Member data were compared with literature data (OVPF data; Upton et al., 2000; Berthod et al., 2020).

Fig. 8.4 – Trace element vs. MgO wt% variation diagrams.

Fig. 8.5 - Trace element vs. MgO wt% variation diagrams.

Fig. 8.6 - Trace element vs. MgO wt% variation diagrams.

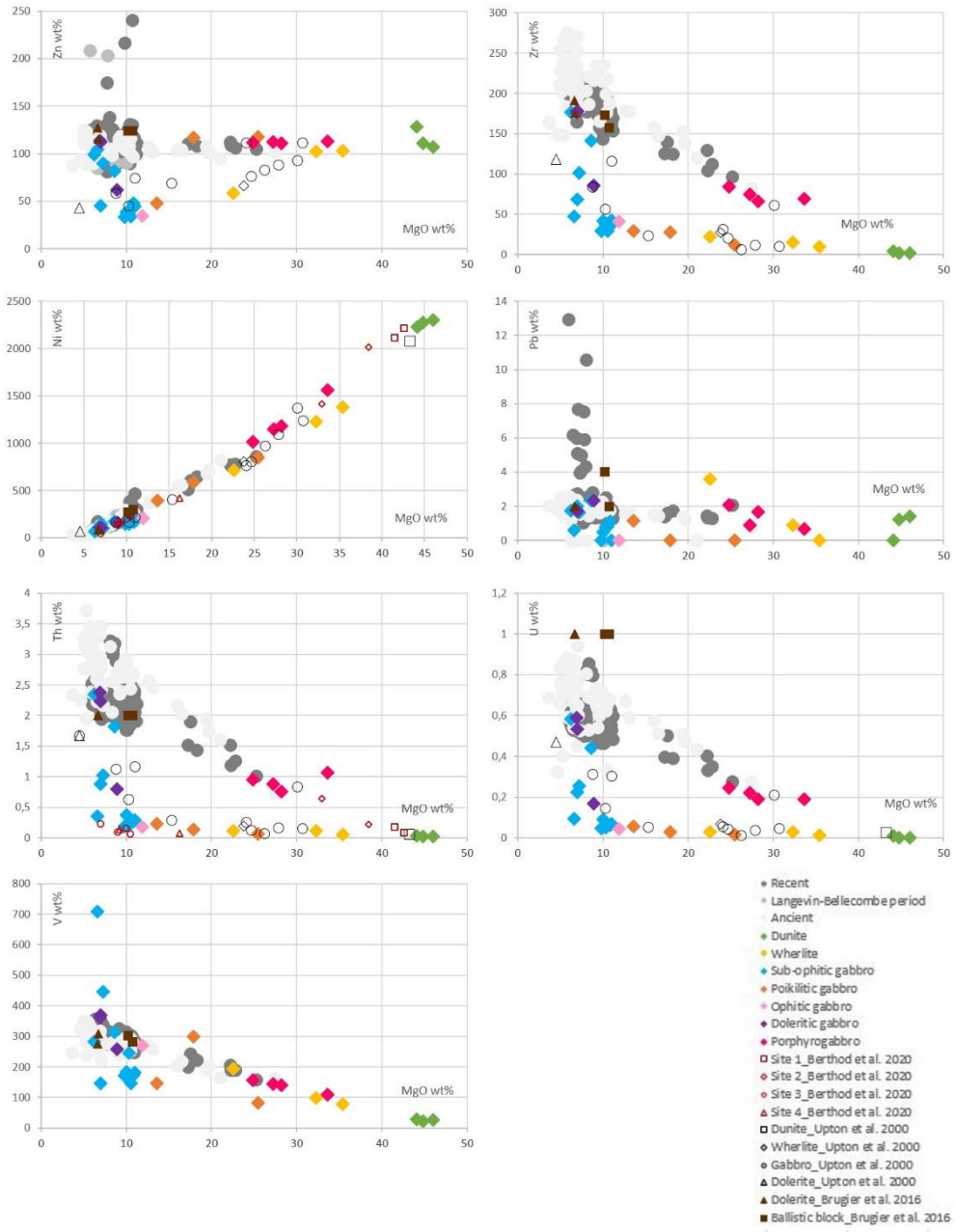

Fig. 8.7 - Trace element vs. MgO wt% variation diagrams.

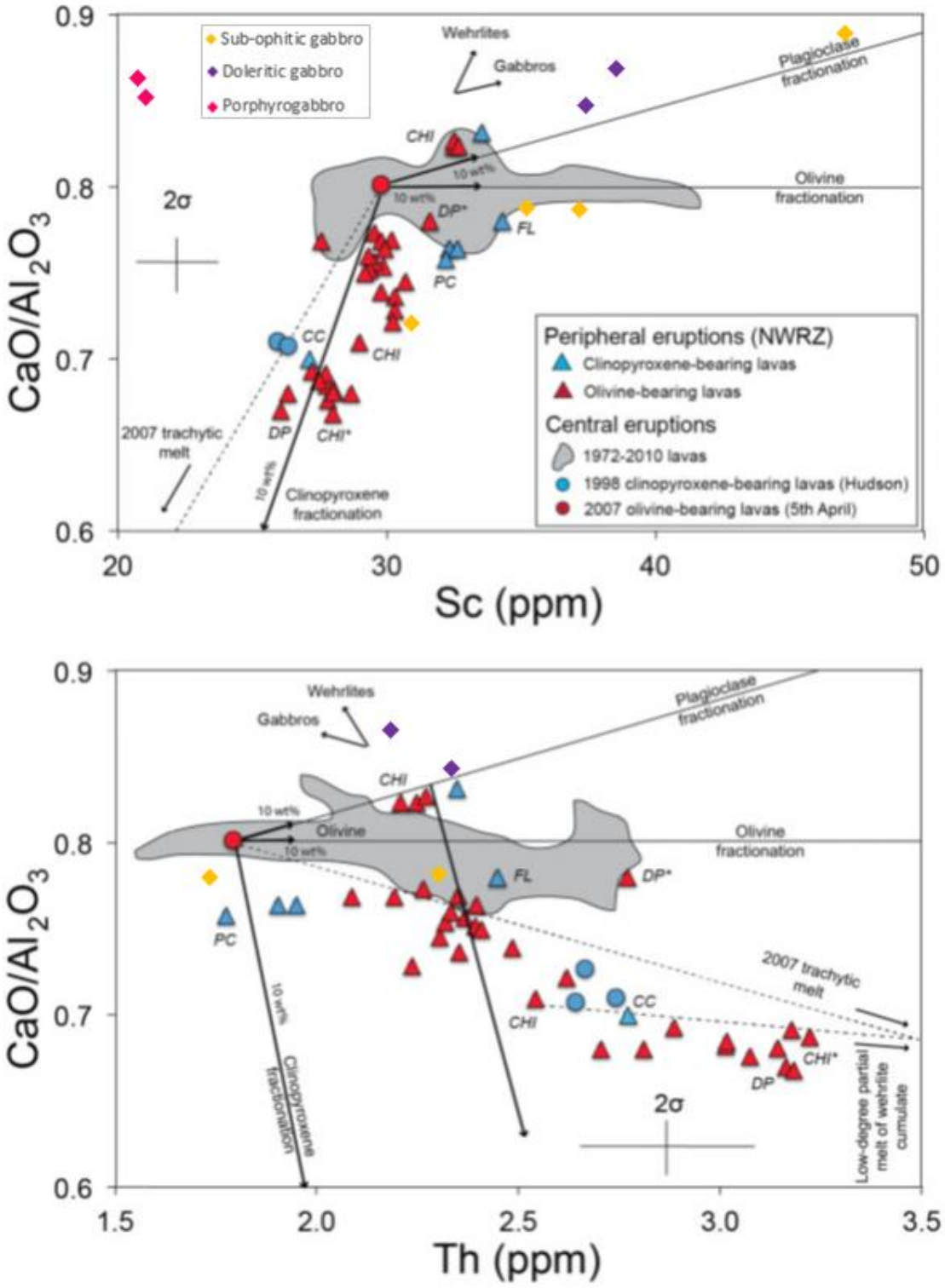

Fig. 8.8 – Bulk-rock composition (trace elements) of Piton de la Fournaise lavas emitted in both peripheral and central areas compared with Bellecombe Ash Member ejecta (Boudoire et al., 2019).

9 Mineral phases and glass composition

Representative chemical compositions of the mineral phases, interstitial glass, melt inclusions and trachitic glass of the pumices are given in Table 9.1 (see appendix on chapter 17).

9.1 Olivine

Olivine is present in almost all samples analysed. Fo content ranges from 83 to 89 % in the dunites (Fig. 9.1.1) to 29-44 % in the most evolved thrachite samples (pumices of Bellecombe Ash Member; Fig. 9.1.3). Wherlite samples show a Fo content 80-85 %, similar to dunites (Fig. 9.1.2)Sub-ophitic gabbros show a Fo content ranging from 68 to 80 Fo% (Fig. 9.1.4) whereas poikilitic gabbros and porphyrogabbros have a Fo content range from 72-81% and 79-84% respectively (Figg. 9.1.5 and 9.1.6).

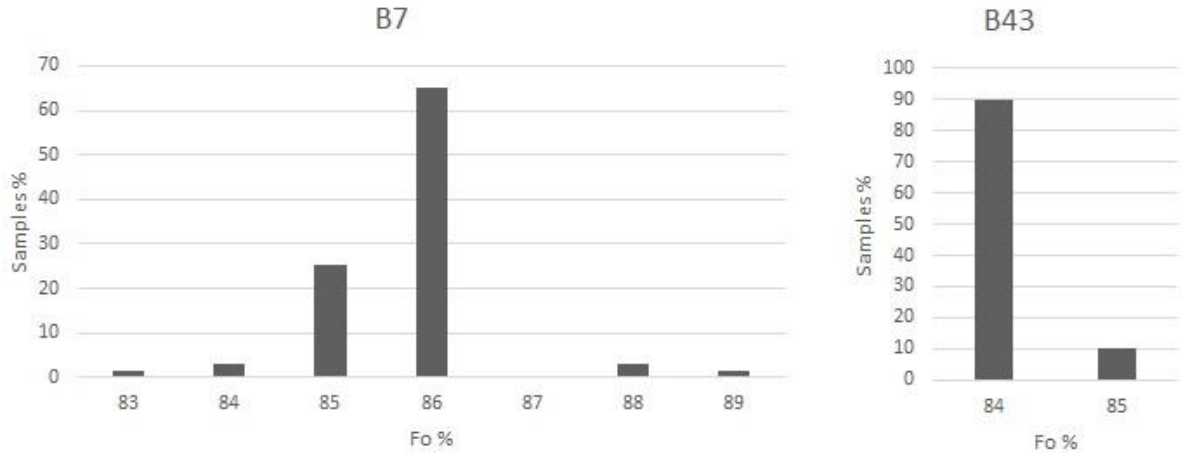

Fig. 9.1.1 – Fo content in different dunite samples showing a compositional range from 83 to 89 %.

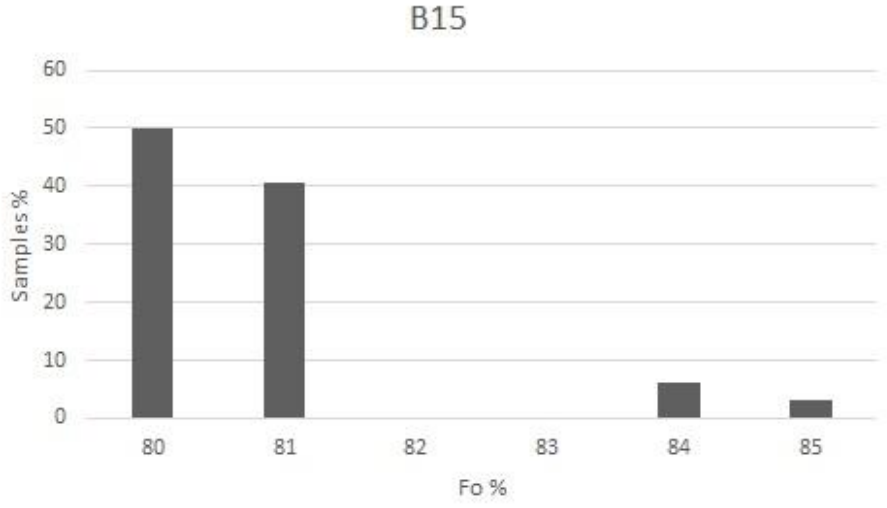

Fig. 9.1.2 – Wherlite sample showing a compositional range of Fo content from 80 to 85%.

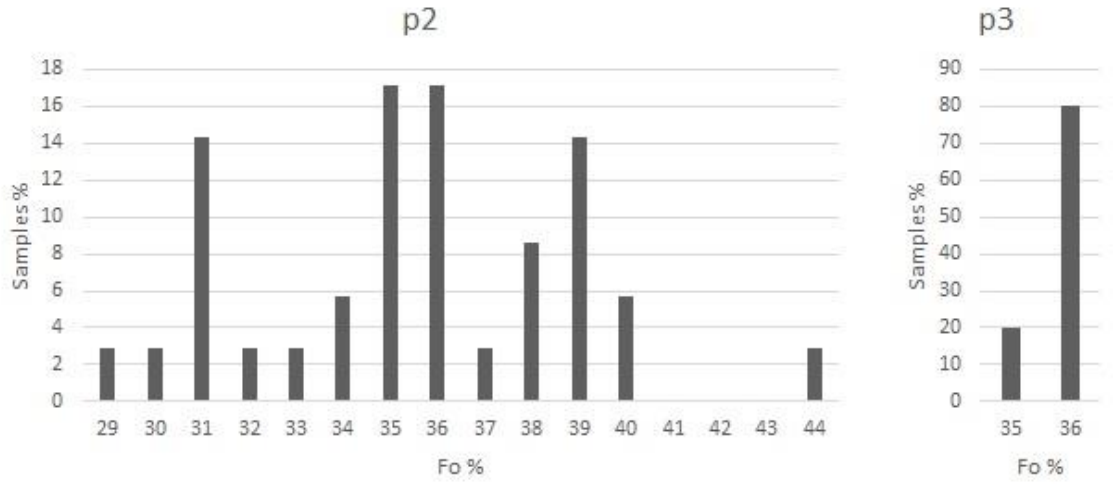

Fig. 9.1.3 – More differentiated samples (trachyte pumices of the Bellecombe Ash Member) showing lower Fo content (29 to 44%).

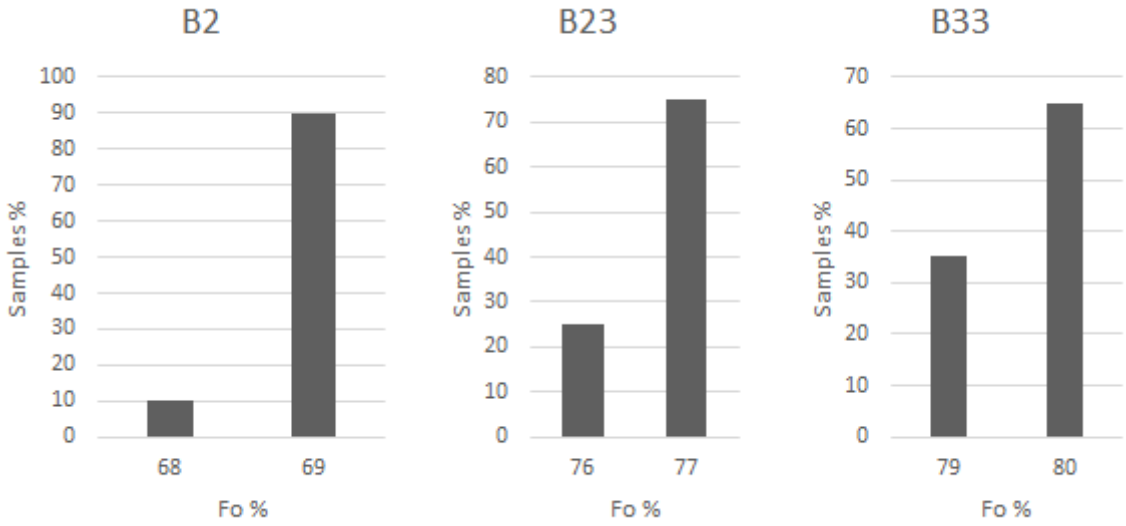

Fig. 9.1.4 – Sub-ophitic gabbro samples showing a wide range of Fo content (from 68 to 80%).

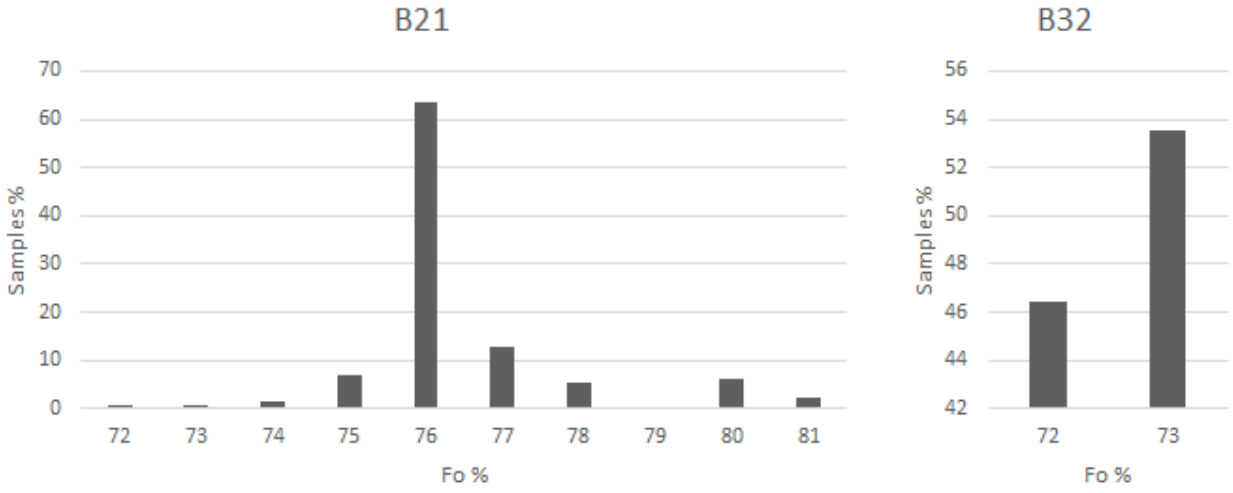

Fig. 9.1.5 – Poikilitic gabbros showing a Fo content from 72 to 81%.

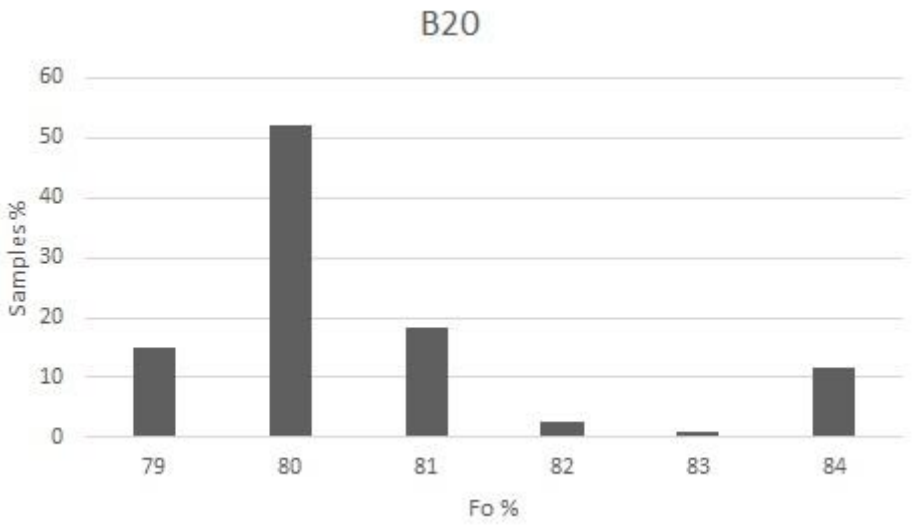

Fig. 9.1.6 – A representative porphyrogabbro sample showing a range of Fo content from 79 to 84%.

To better understand the shallow magmatic system of Piton de la Fournaise, olivine compositions of the Bellecombe Ash Member intrusive ejecta were compared to Boudoire et al. (2018) data from central and peripheral vents in a CaO vs. Fo% diagram (Fig. 9.1.7). Olivines in dunites have a Fo% content comparable to peripheral vents products (Pas des Sables and Chysny enclaves). Olivine found in poikilitic gabbros show Fo% intermediate between olivines in sub-ophitic gabbros and porphyrogabbros at the same range of CaO content (0.15-0.38 wt%). Olivine compositions in wherlitic samples range between those in sub-ophitic gabbros and dunitic samples. Finally, olivines in pumices of the Bellecombe Ash Member have the lowest Fo% in the range 0.15-0.30 wt% CaO. In Fig. 9.1.7 is evident that poikilitic gabbro samples show a disequilibrium between crystals and bulk rock. Indeed, these samples are relatively rich in MgO (13.6-25.4 wt%) but show olivine with a Fo% content ranging from 72 to 81

wt%. The same inference can be done for the porphyrogabbro samples, with a MgO from ca. 25 to 34 wt.% and a mean olivine value of 80 Fo% in B20 sample.

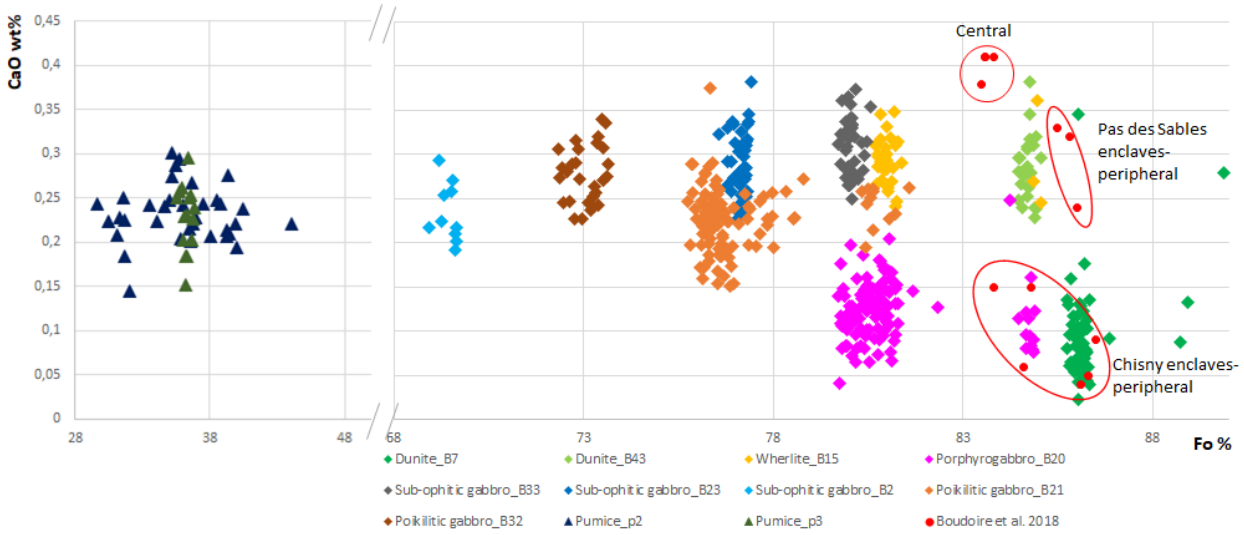

Fig. 9.1.7 – Evolution trend of Bellecombe Ash Member products. Dunites are the most primitive ejecta with the highest Fo%, comparable to products of Piton de la Fournaise peripheral vents.

In Fig. 9.1.8 the olivine compositions in the subvolcanic ejecta of the Bellecombe Ash Member were compared with peripheral-central extrusives and intrusive clasts respectively reported by Boudoire et al. (2018) and Berthod et al. (2020). Berthod et al. (2020) classified the CaO content of olivine into three populations. 1) A low CaO (0.05-0.20 wt%), high Fo_{84-89} population in dunites and wherlites from Site 1 and 2; 2) a high CaO (0.20-0.40 wt%), high Fo_{80-89} population only found in the dunites and wherlites of Site 2; 3) a low CaO (~0.01-0.12 wt%), low Fo_{70-79} population in the wherlite and olivine gabbros of Site 3 and 4. It can be seen that no one Bellecombe Ash Member samples can be included in population 3. A fourth group was recognized, with high CaO content (0.15-0.34 wt%) and Fo_{69-79}.

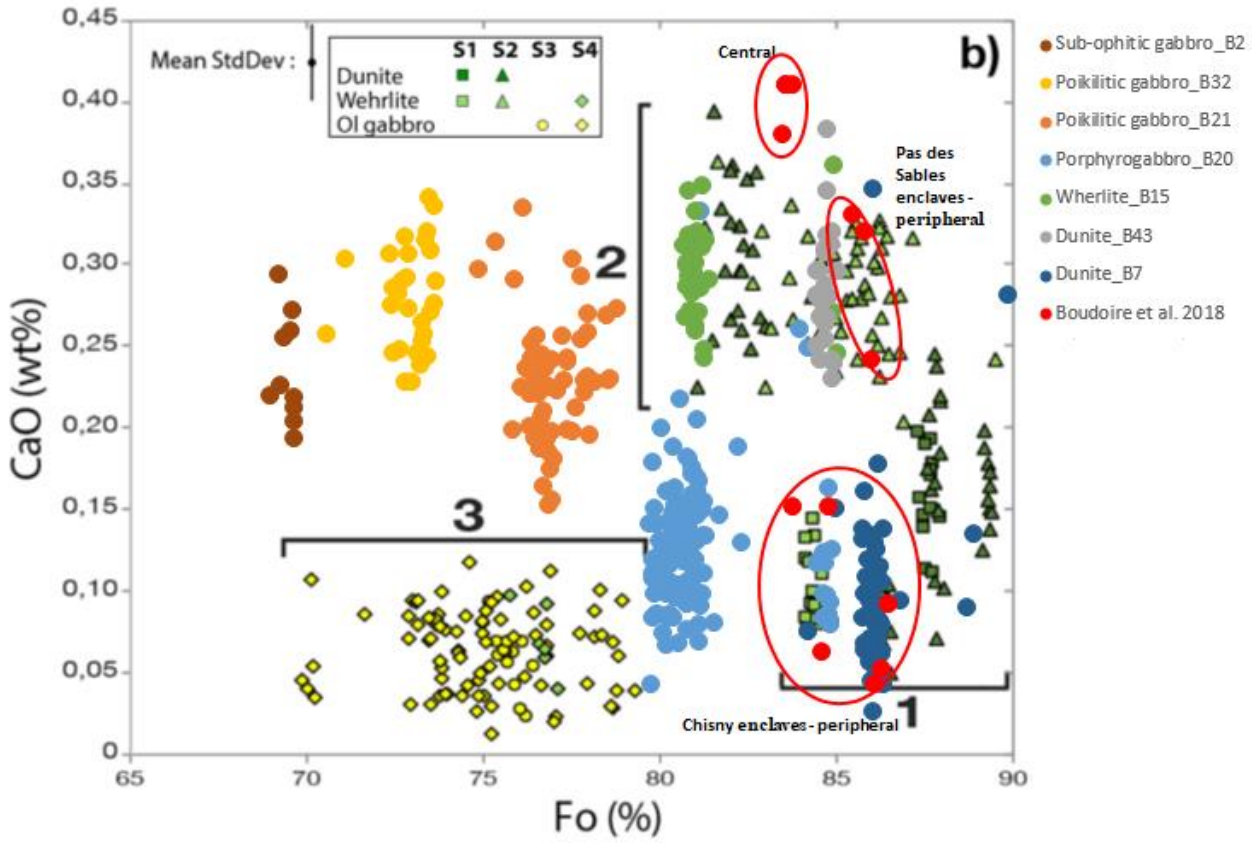

Fig. 9.1.8 – CaO vs. Fo wt%. Bellecombe Ash Member samples were plotted with Boudoire et al. (2018) and Berthod et al. (2020) data. Berthod et al. (2020) subdivided samples in four Site (1-2-3-4) and analysed three lithotypes: dunite, wherlite, ol-gabbro. Boudoire et al. (2018) distinguished samples in peripheral and central origin.

9.2 Plagioclase and Na-K feldspar (sanidine and anorthoclase)

Feldspar are present in all mafic samples in different percentages (see chapter 7.5). Triangular phase diagram Ab-An-Or with EMPA analyses on mineral phases (Fig.9.2.1) show the complete miscibility of feldspar on Bellecombe Ash Member samples. Sub-ophitic gabbros and poikilitic gabbros show the presence of plagioclase ranging from Ab_{13-42} and An_{57-87}. Porphyrogabbros have some sanidine microcrolites (Ab_{34-45} An_{4-8} Or_{49-60}) as well as plagioclase (ranging from Ab_{32-58} and An_{32-66}). Plagioclases in the pumices of Bellecombe Ash Member show a more albitic content (pumice p2 ranging from Ab_{53-76} and An_{17-45}, p3 from Ab_{41-67} and An_{29-57}). It is worth to note that pumices of Piton des Neiges (PDN1; Fig.9.2.1) have some anorthoclase (Ab_{66-68} An_{11-12} Or_{20-23}) as well as plagioclase (ranging from Ab_{58-68} and An_{26-38}).

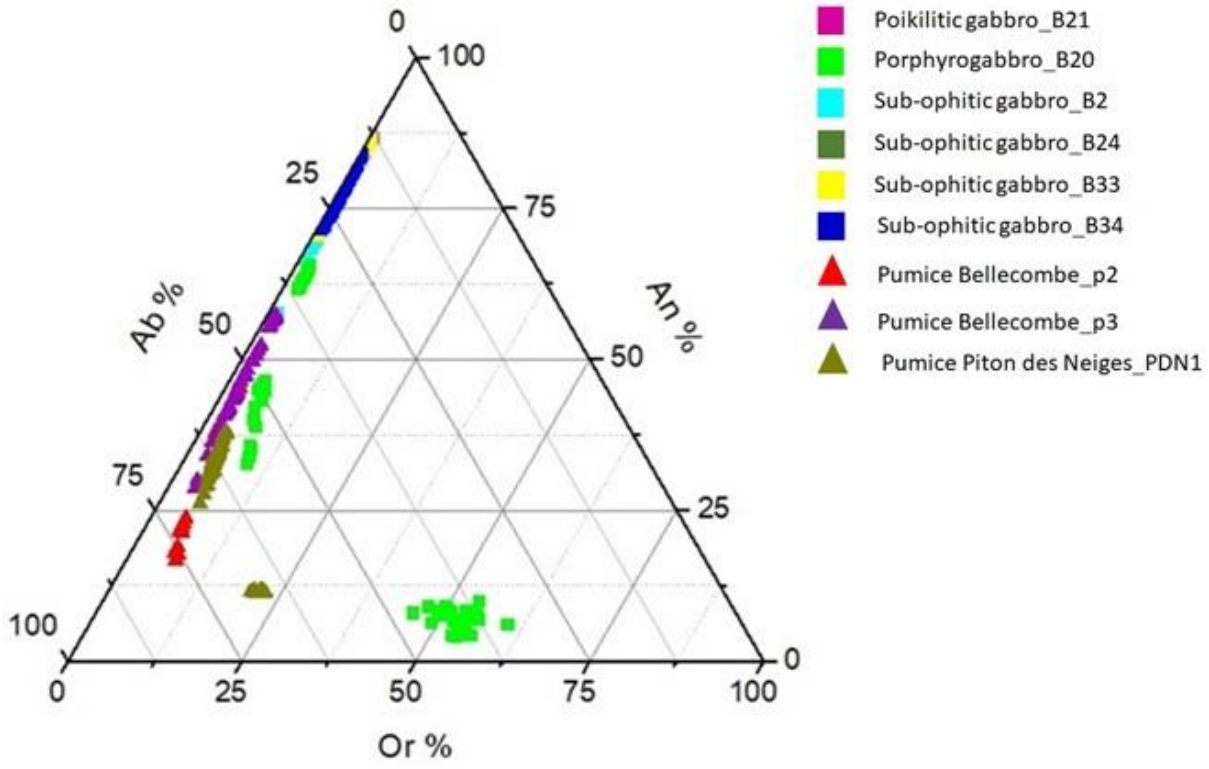

Fig. 9.2.1 – Ternary feldspar diagram (Ab-An-Or, EMPA data).

9.3 Clinopyroxene

In almost all samples, analysed clinopyroxene is present with different modal content and composition. Fs content range from 6-11% in few crystals of dunite samples (Fig. 9.3.1) to 17-23% in the trachyte pumices of Bellecombe Ash Member and Piton des Neiges; Fig. 9.3.2). Clinopyroxene compositions of wherlitic samples (Fs 8%; Fig. 9.3.3) are similar to those in the dunites. Clinopyroxene of porphyrogabbros and sub-ophitic gabbros are very similar, in the range Fs_{8-13} and Fs_{9-14} respectively (Figg. 9.3.4 and 9.3.5). Clinopyroxene compositions of poikilitic gabbros are also comparable (Fs_{8-15}; Fig. 9.3.6).

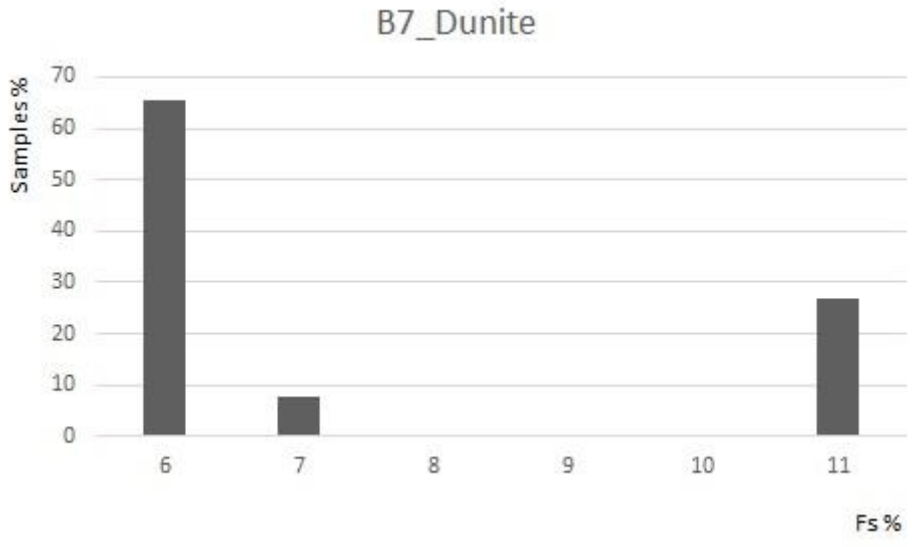

Fig. 9.3.1 – Dunite samples of Bellecombe Ash Member show a limited range of composition for Fs% content of clinopyroxene.

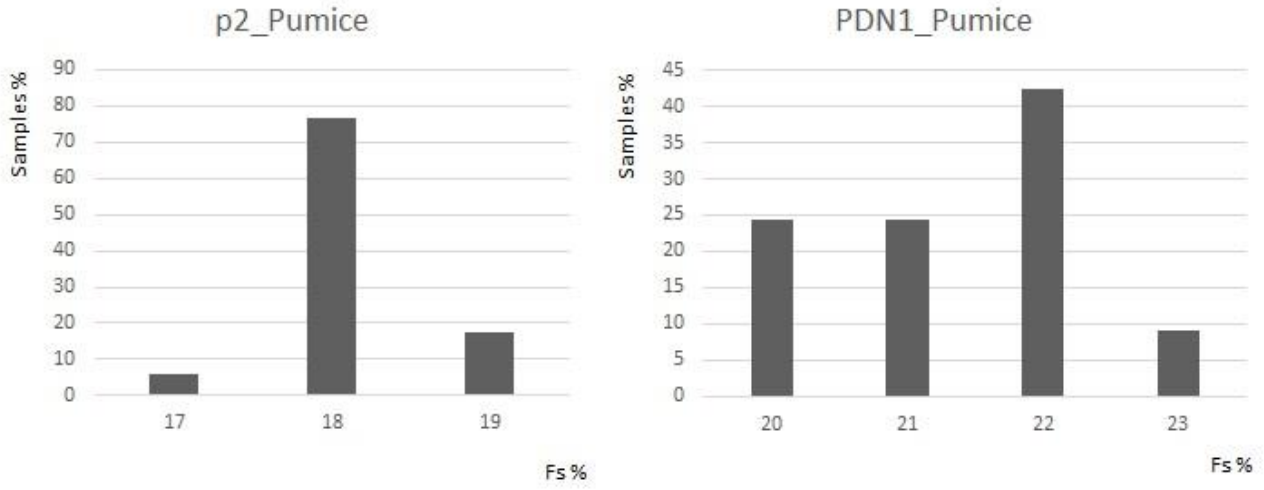

Fig. 9.3.2 – Both pumices of Piton de la Fournaise (p2) and Piton des Neiges (PDN1) show the highest content of Fs% of clinopyroxene.

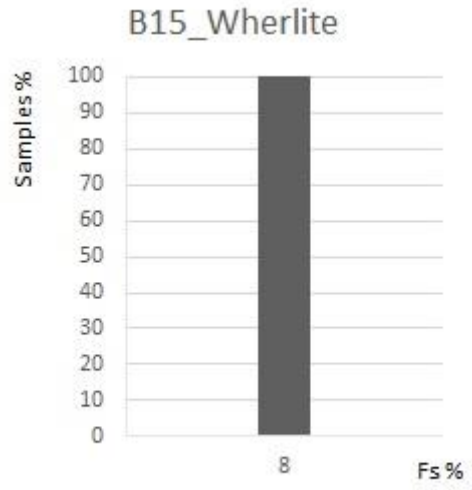

Fig. 9.3.3 – Fs% of clinopyroxene in the wherlite B15 sample.

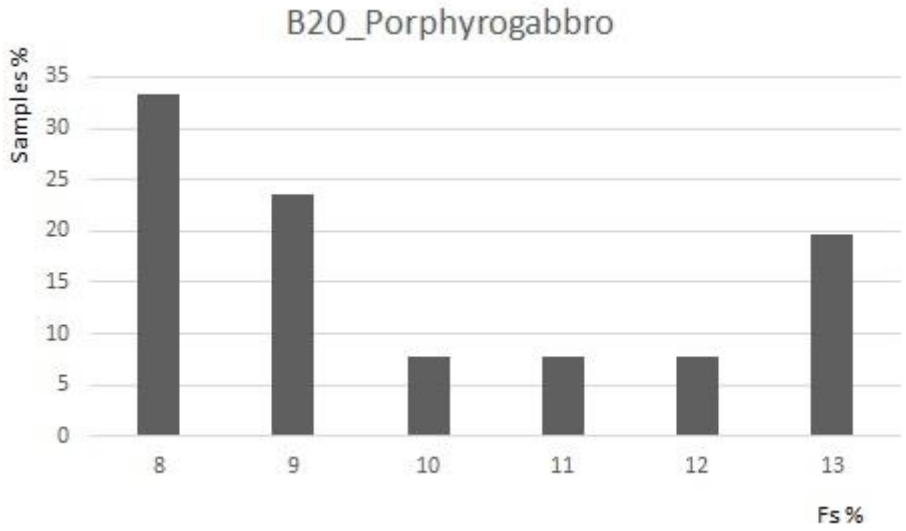

Fig. 9.3.4 – Fs% compositional variation of clinopyroxenes in the porphyrogabbro sample B20.

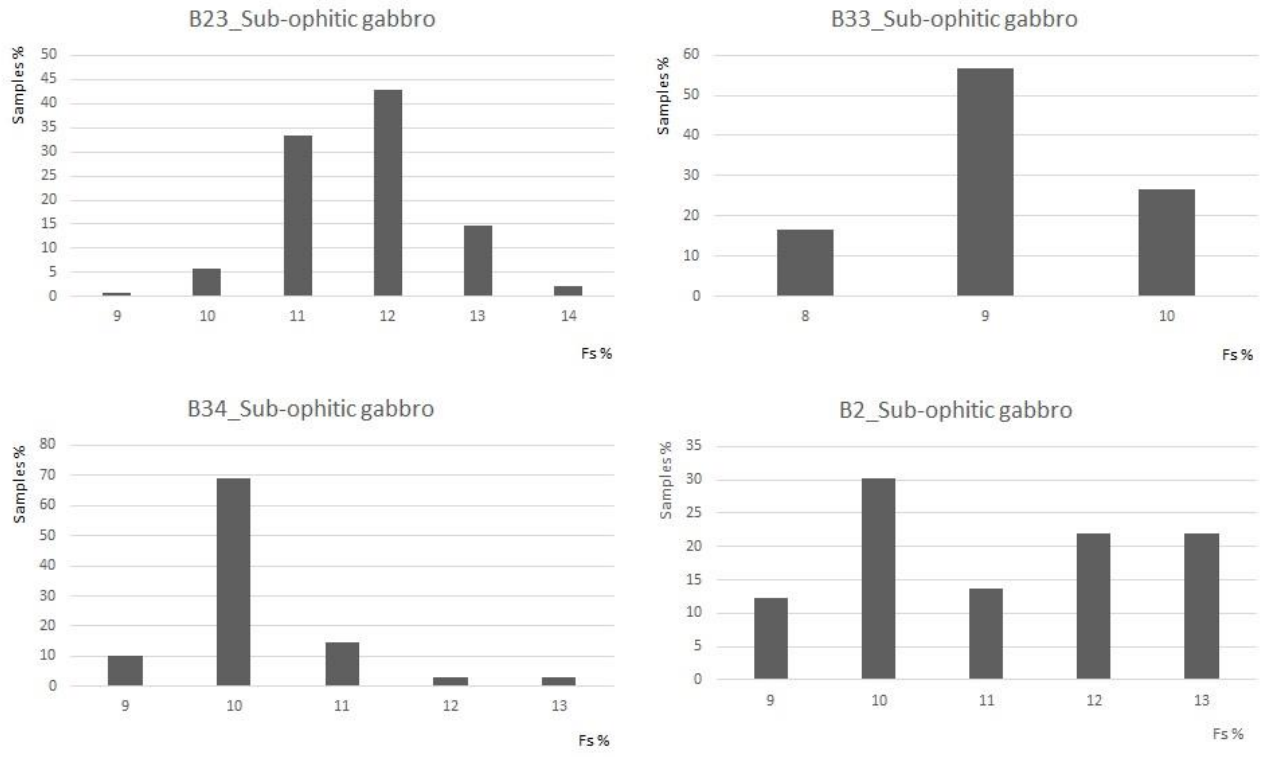

Fig. 9.3.5 – Fs% compositional variation of clinopyroxene in sub-ophitic gabbros.

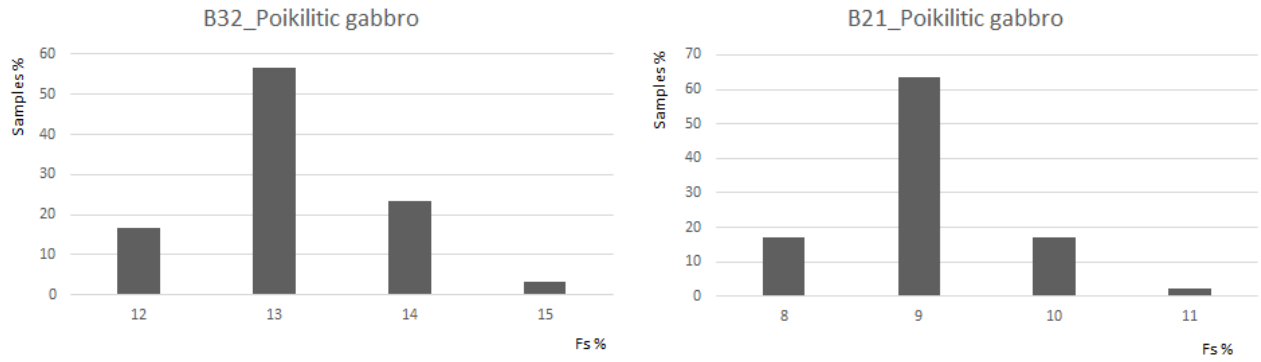

Fig. 9.3.6 – Composition of clinopyroxenes (Fs% content) in the poikilitic gabbros

Clinopyroxene of porphyrogabbros show a wide range of Al_2O_3 content (1.7-7.5 wt%; Fig. 9.3.7), whereas some clinopyroxenes of the poikilitic gabbros have the highest Mg# 84.7 among the Mg values of the whole suite of the mafic intrusive clasts, whereas dunites show the highest Mg# (86-88) on clinopyroxene between the ultra-mafic intrusive clasts. A_2O_3 vs. Mg# show three range of composition for Mg# content: evolved samples (pumices of Bellecombe and Piton des Neiges), mafic rocks + wherlite and dunite. Clinopyroxene of pumices of Bellecombe and Piton des Neiges show the lowest Al_2O_3 content (1.6-3.3 wt%) with the lowest Mg# (55.5-68.0 Mg#). Comparing Bellecombe Ash Member samples with Piton des Neiges data (Fig. 9.3.8; Berthod et al., 2020), it can be noticed that their composition are similar. Comparing all clinopyroxene crystals both mafic and ultramafic rocks, Mg# increases whereas TiO_2 decrease from mafic to ultramafic rocks (Fig. 9.3.9).

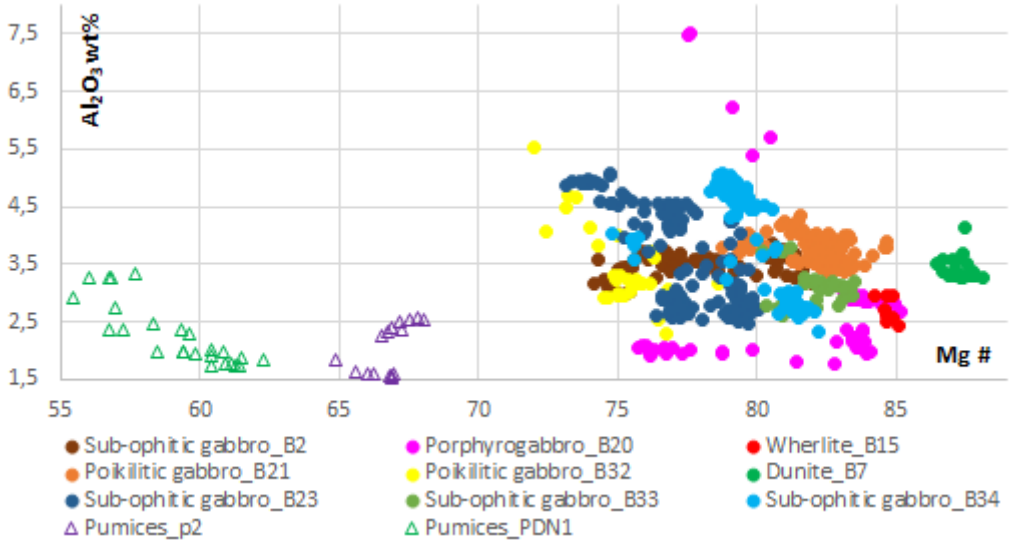

Fig. 9.3.7 – A_2O_3 vs. Mg# of Bellecombe Ash Member and Piton des Neiges samples (pumices PDN1).

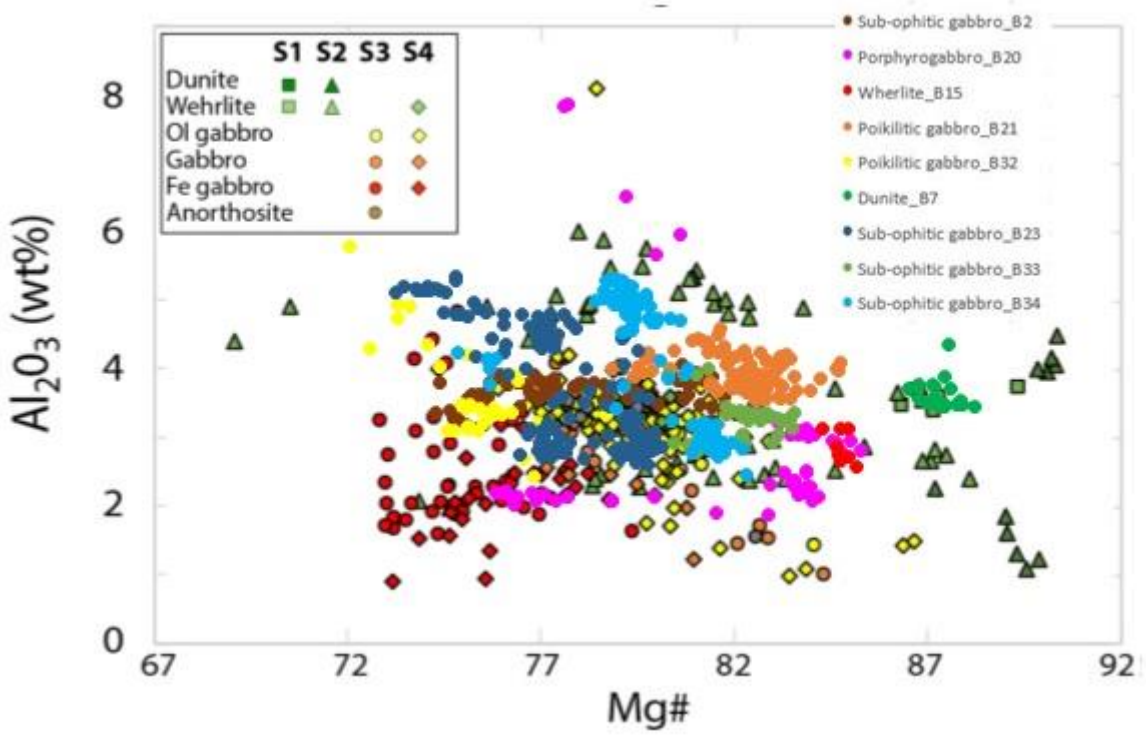

Fig. 9.3.8 – Chemical composition of Bellecombe Ash Member samples compared with samples investigated by Berthod et al. (2020).

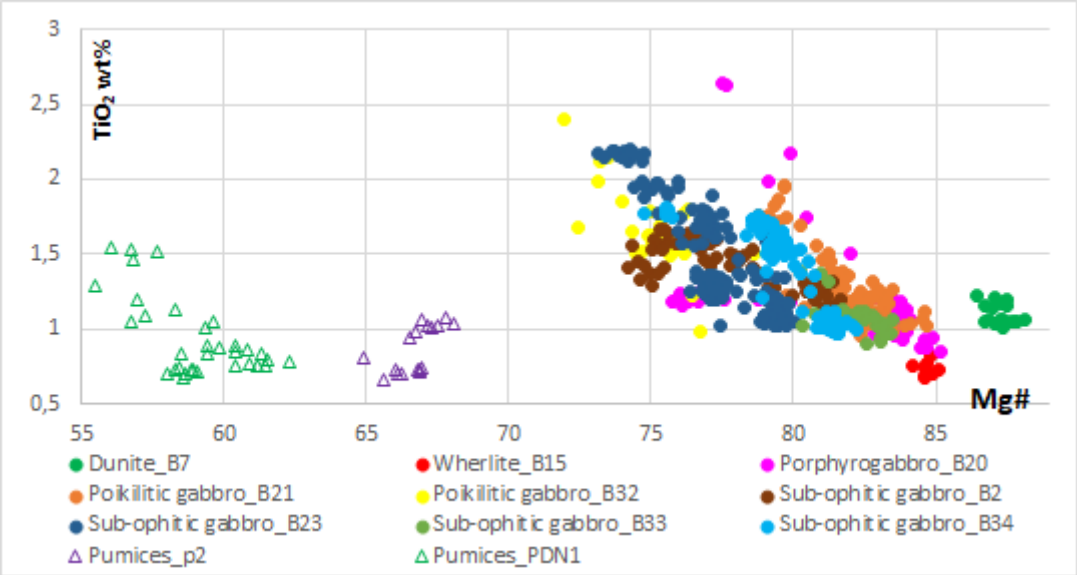

Fig. 9.3.9 – TiO_2 of clinopyroxene decreasing from more evolved samples (mafic rocks) to more primitive one (ultramafic rocks). Pumices show moderate TiO_2 content and the lowest Mg#.

9.4 Opaque minerals (Cr-spinel, magnetite and ilmenite)

Opaque minerals includes Cr-spinel, Ti-magnetite and ilmenite. Not all the mafic and ultramafic groups contain oxides and if present in small percentages. Cr-spinels in dunites show MgO content ranging from 10.5 to 11.5 wt%, high Cr_2O_3 contents (34.9-29.3 wt%), moderate Al_2O_3 content (15.6-18.7 wt%), FeO 28.6-31.2 wt% and TiO_2 2.5-3.4%. Wherlite show Cr-spinels with Al_2O_3 content ranging from 15.0 to 15.5 wt%, MgO 9.5-10.0 wt%, Cr_2O_3 26.7-31.3 wt%, FeO 37.7-39.4 wt% and low TiO_2 (3.6-4.8 wt%). In poikilitic gabbros oxides show low Al_2O_3 (0.5-10.7 wt%) and Cr_2O_3 (0.2-16.2 wt%), with high FeO (40.5-69.5 wt%). MgO ranging from 4.5 to 7.8 wt% and TiO_2 show a wide range of content 4.6-50.0 wt%, therefore implying bot magnetite and ilmenite. Opaque minerals in the sub-ophitic gabbros are ilmenites having moderate FeO (43.0-45.9 wt%) and high TiO_2 (47.2-49.4 wt%), with low Al_2O_3 (0.4-0.5 wt%) and MgO (5.2-5.7 wt%) contents. Oxides in porphyrogabbros show a wide range in composition for each major element: MgO 6.3-8.1%, Cr_2O_3 0.4-27.0 wt%, Al_2O_3 0.9-8.2 wt%, FeO 23.3-50.6 wt% and TiO_2 2.6-62.1 wt% therefore emphasizing the presence of magnetite, ilmenite and Cr-spinels.

9.5 Phlogopite

Phlogopite is evident only in porphyrogabbros as intertitial phase, often in association with opaque minerals. The composition is SiO_2 35.1-40.7 wt%, Al_2O_3 11.9-13.8 wt%, MgO 16.5-19.3 wt%, FeO 6.6-7.5 wt% and K_2O 8.0-9.4 wt%.

9.6 Interstitial glass

Not all the representative samples analysed show interstial glass. Glass is common in sub-ophitic gabbros and poikilitic gabbros, with a pale yellow (sideromelane) to pale-brown colour appearance in thin section. They can be also partially oxidised (yellow-orange to tachylite). The composition of the interstitial glass in the sub-ophitic gabbros is SiO_2 48.5-57.7 wt%, TiO_2 2.3-3.3 wt%, Al_2O_3 14.3-16.3 wt%, Cr_2O_3 0-0.1 wt%, FeO_{tot} 6.9-12.1 wt%, MnO 0.1-0.2 wt%, MgO 2.3-6.3 wt%, CaO 5.1-12.3 wt%, Na_2O 1.2-5.8 wt%, K_2O 0.9-3.0 wt%, P_2O_5 0.3-1.0 wt%. In the poikilitic samples the composition of the interstitial glass is SiO_2 53.2-56.0 wt%, TiO_2 3.1-3.4 wt%, Al_2O_3 15.8-16.4 wt%, Cr_2O_3 0-0.7 wt%, FeO_{tot} 7.4-9.0 wt%, MnO 0.1-0.2 wt%, MgO 3.3-4.1 wt%, CaO 6.5-7.7 wt%, Na_2O 3.4-4.7 wt%, K_2O 1.8-2.2 wt%, P_2O_5 0.7-0.9 wt%.

9.7 Melt inclusions

Melt inclusions are present in representative analysed samples of the Bellecombe Ash Member. Crystals of clinopyroxene, olivine, plagioclase and oxides show small melt inclusions in sub-ophitic gabbros. The composition of those melt inclusions is SiO_2 45.2-51.4 wt%, TiO_2 1.9-4.3 wt%, Al_2O_3 13.1-14.9 wt%, Cr_2O_3 0-0.1 wt% FeO_{tot} 9.5-14.9 wt%, MnO 0.10-0.3 wt%, MgO 3.5-6.2 wt%, CaO 6.4-11.5 wt%, Na_2O 2.2-4.6 wt%, K_2O 0.7-1.9 wt%, P_2O_5 0.2-0.8 wt%. In addition, samples of pumices from Bellecombe Ash Member (p2 and p3) and Piton des Neiges (PDN1) show some melt inclusions on few crystals too. The composition of those melt inclusions is more evolved than other samples, as evidenced in total alkali vs. silica graph (Fig. 9.8.1), SiO_2 ranging from 61.3 wt% to 67.8 wt%, with $Na_2O + K_2O$ 8.5-11.5 wt%.

9.8 Trachitic glass of the pumices

Some pumice samples from the Bellecombe Ash Member and Piton des Neiges were also investigated. They show a vesiculated-quenched texture, with a porphyritic index variable from 1 to 3 vol%. Bellecombe Ash Member (p2, p3) pumices also show the presence of few crystals of olivine, feldspar and clinopyroxene, whereas pumice from Piton des Neiges (PDN1) only display feldspars, clinopyroxene and opaque minerals.

Pumices from the Bellecombe Ash Member (p2 and p3) and Piton des Neiges (PDN1) show a more evolved groundmass glass composition than other interstitial glass in the subvolcanic samples of the Bellecombe Ash Member analysed. It is trachytic in composition (PDN1 59.4 wt% SiO_2 and 11.1 wt% alkali; p2 70.4 wt% SiO_2 and 10.6 wt% alkali; Fig. 9.8.1). Comparing all melt inclusions and interstitial glass data with whole rock literature data it is evident the different composition between intrusive ejecta of the Bellecombe Ash Member and the pumices (both Bellecombe Ash Member and Piton des Neiges). Dunites of Bellecombe Ash Member show different composition of interstitial glass. Sample B7 show a basaltic trachyandesite

composition, whereas interstitial glass of dunite B43, the sample with large crystals of olivine presenting kink-banding and rounded olivines, is basaltic. Interstitial glass of the sub-ophitic and poikilitic gabbros has a composition basaltic trachyandesitic, but melt inclusions are less evolved, basaltic with composition similar to the interstitial glass of dunite sample B43.

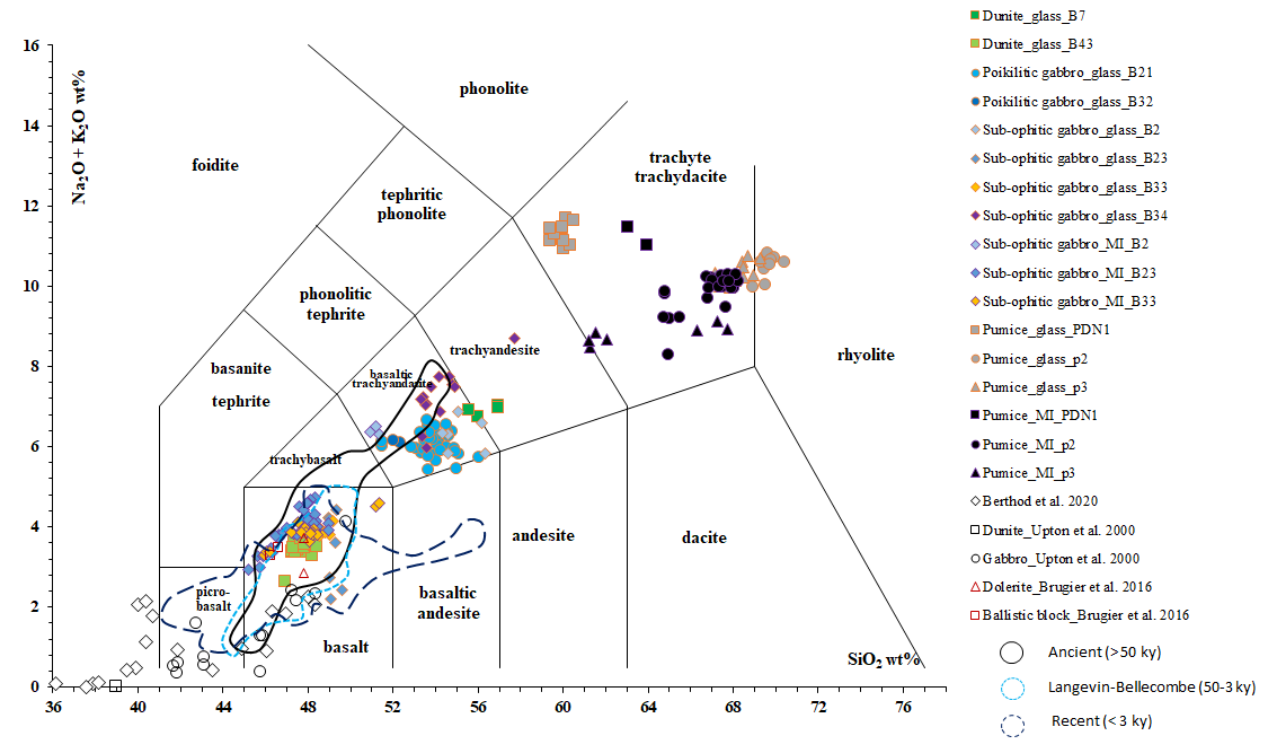

Fig. 9.8.1 – Total alkali vs. silica diagram of interstitial glass and melt inclusions of analysed representative subvolcanic samples of Bellecombe Ash Member (dunites and sub-ophitic gabbros) and some trachyte pumice samples (p2, p3: Bellecombe Ash Member; PDN1: Piton de Neiges) compared with whole rock literature data, from OVPF database, Berthod et al. (2020), Upton et al. (2000) and Brugier (thesis, 2016).

10 Fluid inclusions

Fluid inclusions in single mineral phases were analysed using both thin section and single hand-picked mineral phase (olivine, clinopyroxene, feldspar).

10.1 Thermobarometric evaluation

A Raman spectroscopy analyses were conducted on single hand-picked mineral phases of representative samples, both mafic and ultramafic, for a thermobarometric evaluation. Ultramafic lithotypes provided valuable results whereas no reliable results were obtained from mafic samples, due to the low CO_2 content. Dunite (B7) had a density > to wherlite (B3). Wherlite had ~86% of the density range from 0.34 to 0.42 g/cm^3, with only a little percentage (~14%) about 0.26 g/cm^3.

Dunite show a wider range of CO_2 density, with ~32% from 0.54 to 0.64 g/cm^3 and ~ 68% from 0.34 to 0.5 g/cm^3 (Fig. 10.1.1). Minor pressure registered on fluid inclusions of wherlite could be at least partly related to the fact that fluid inclusions analised were in clinopyroxene, which conserve worse the barometric data than olivine. Lamadrid (2017) equation for CO_2 Dyad splitting Raman spectroscopy have provided an indicative provenance of both dunite and wherlite samples of Bellecombe. Assuming a temperature of formation range of 1108-1225°C, dunite show a pressure of 309-338 MPa, corresponding to 13 km depth, ~ underplating level; wherlite sample pressure is about 151-166 MPa, and it correspond to 6 km depth, rather close to submarine base of the edifice (Fig. 10.1.2).

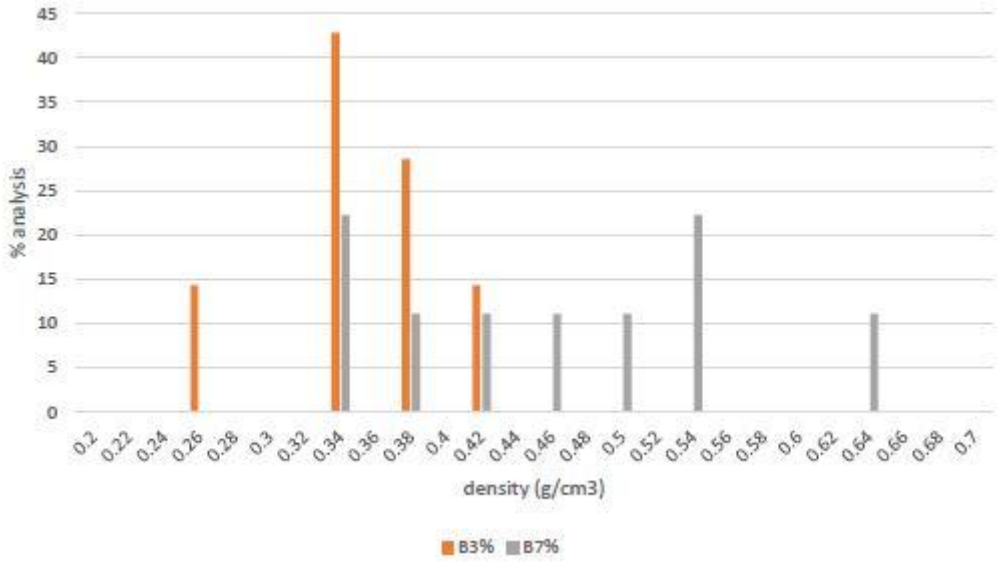

Fig. 10.1.1 – Density content of CO_2 on samples B3 (wherlite) and B7 (dunite).

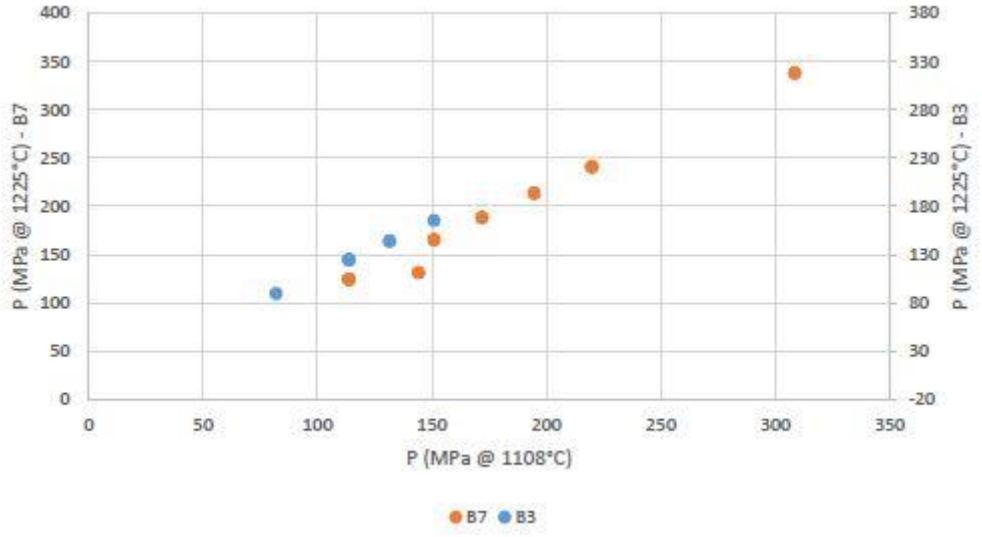

Fig. 10.1.2 – P vs. T°C diagram for samples B7 (dunite) and B3 (wherlite) of Bellecombe Ash Member.

Since dunite (B7) is the deepest sample analysed and wherlite (B3) is most superficial, it has been assuming that also other analysed

samples can be considered close to submarine base (or shallower depths) of the Piton de la Fournaise.

10.2 Noble gases and CO_2 analyses

Samples of the Bellecombe Ash Member show single mineral phase with both primary and secondary (along crystal fractures) fluid inclusions. Representative samples were chosen for this analyses, for both ultramafic (dunite and wherlite) and mafic (sub-ophitic gabbros, poikilitic gabbros and porphyrogabbros) samples. Single hand-picked mineral phase of olivine, clinopyroxene and feldspar were analysed for noble gases and CO_2 content.

In the investigated products, noble gases and CO_2 are expected to vary in function of magmatic degassing. Assuming that the various mineral phases containing a comparable amount of fluid inclusions and that the moles of gas mostly depend on the entrapment pressure, high content of gases (both noble gases and CO_2) indicate a deep provenance of the samples. Noble gases and CO_2 solubility in silicatic melts could be described with the ratio N_2 ~ Ar < CO_2 < Ne < He. Therefore, high content of CO_2 and Ar could indicate samples formed at high pressure. However, further and more independent information arise from noble gases and CO_2 ratios (e.g. He/CO_2, He/Ar*) that are generally considered as tracer of magmatic degassing and depressurization noble gases and CO_2 content in the subvolcanic ejecta of the Bellecombe Ash Member are reported in from Fig. 10.2.1 to Fig. 10.2.9.

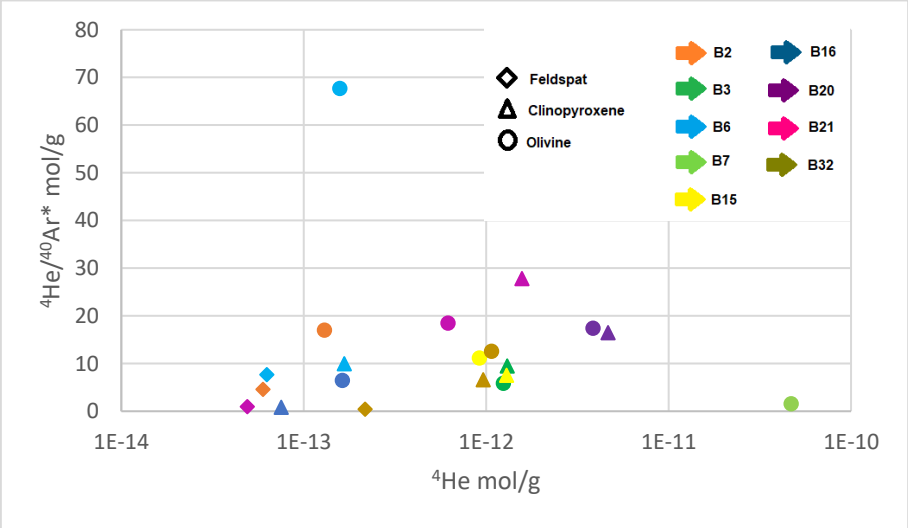

Fig. 10.2.1 – $^4He/^{40}Ar^*$ vs. ^4He. B2: sub-ophitic gabbro; B3: wherlite; B6: sub-ophitic gabbro; B7: dunite; B15: wherlite; B16: porphyrogabbro; B20: porphyrogabbro; B21: poikilitic gabbro; B32: poikilitic gabbro.

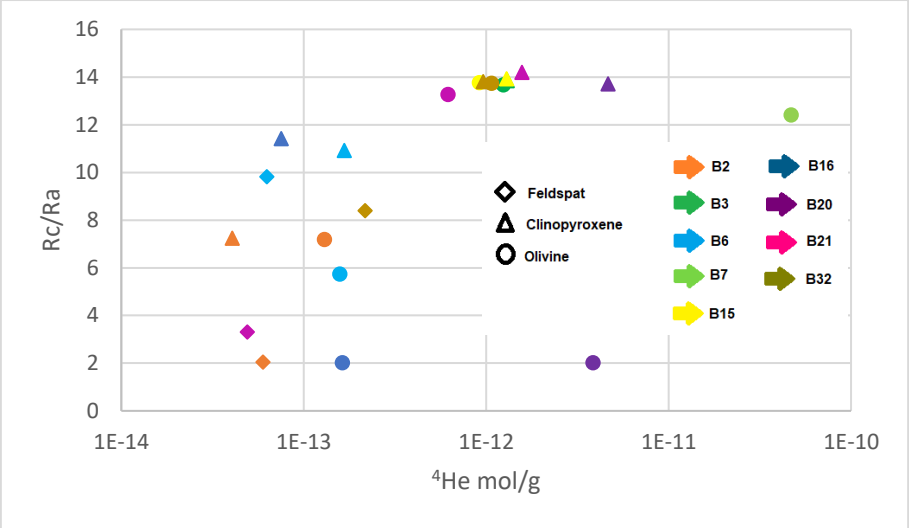

Fig. 10.2.2 – Rc/Ra vs ^{4}He. B2: sub-ophitic gabbro; B3: wherlite; B6: sub-ophitic gabbro; B7: dunite; B15: wherlite; B16: porphyrogabbro; B20: porphyrogabbro; B21: poikilitic gabbro; B32: poikilitic gabbro.

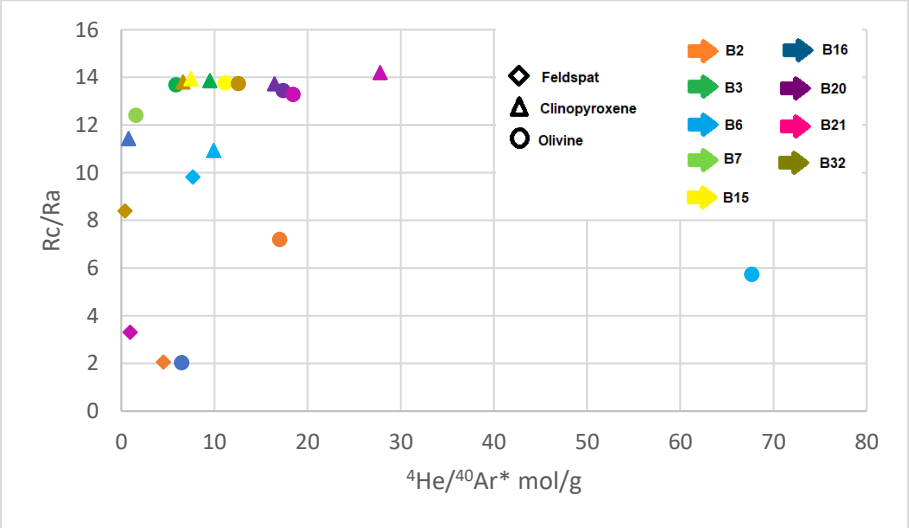

Fig. 10.2.3 – Rc/Ra vs. $^{4}He/^{40}Ar^{*}$. B2: sub-ophitic gabbro; B3: wherlite; B6: sub-ophitic gabbro; B7: dunite; B15: wherlite; B16: porphyrogabbro; B20: porphyrogabbro; B21: poikilitic gabbro; B32: poikilitic gabbro.

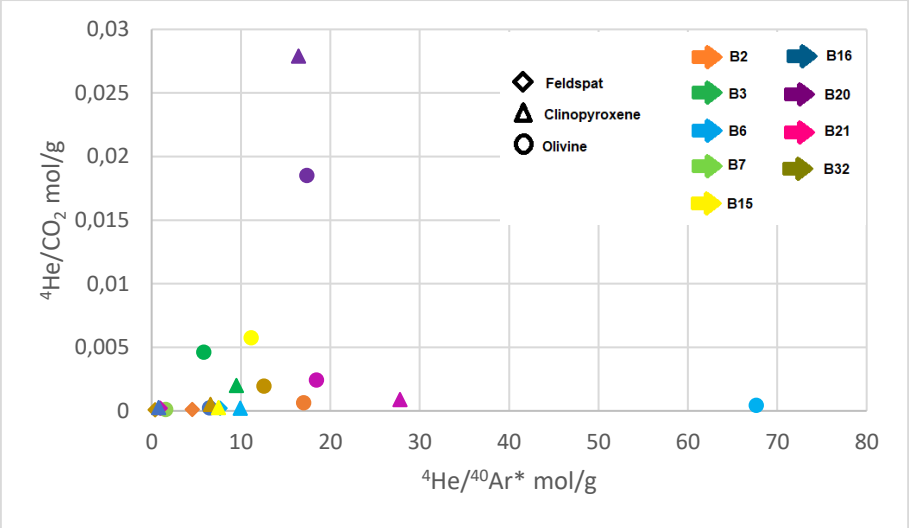

Fig. 10.2.4 – $^4He/CO_2$ vs. $^4He/^{40}Ar^*$. B2: sub-ophitic gabbro; B3: wherlite; B6: sub-ophitic gabbro; B7: dunite; B15: wherlite; B16: porphyrogabbro; B20: porphyrogabbro; B21: poikilitic gabbro; B32: poikilitic gabbro.

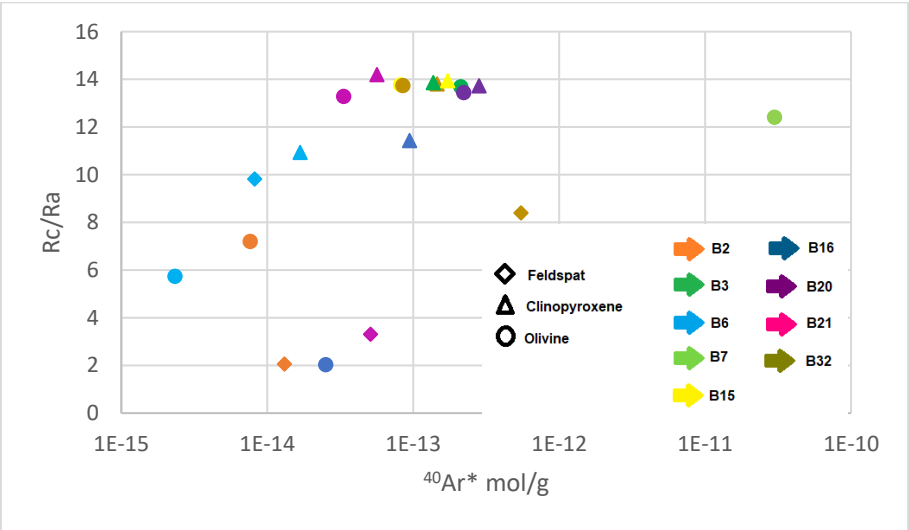

Fig. 10.2.5 – Rc/Ra vs. $^{40}Ar^*$. B2: sub-ophitic gabbro; B3: wherlite; B6: sub-ophitic gabbro; B7: dunite; B15: wherlite; B16: porphyrogabbro; B20: porphyrogabbro; B21: poikilitic gabbro; B32: poikilitic gabbro.

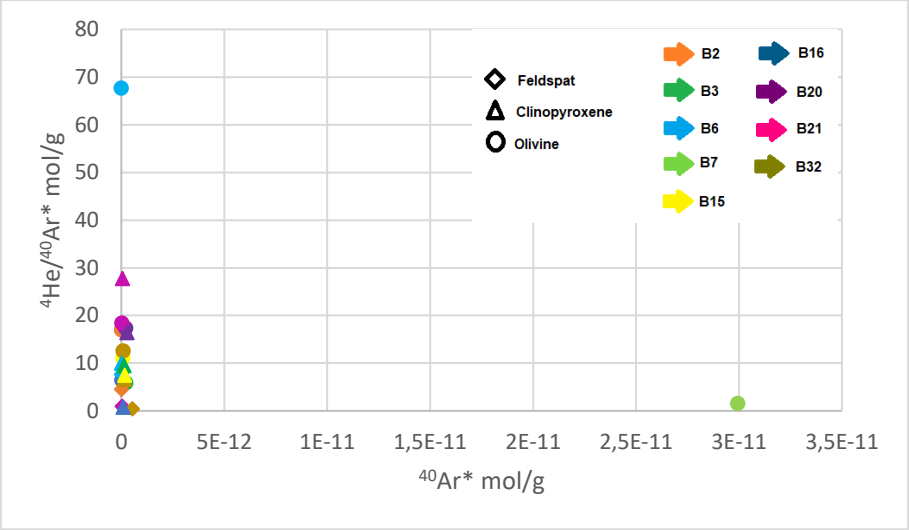

Fig. 10.2.6 – $^4He/^{40}Ar^*$ vs. $^{40}Ar^*$. B2: sub-ophitic gabbro; B3: wherlite; B6: sub-ophitic gabbro; B7: dunite; B15: wherlite; B16: porphyrogabbro; B20: porphyrogabbro; B21: poikilitic gabbro; B32: poikilitic gabbro.

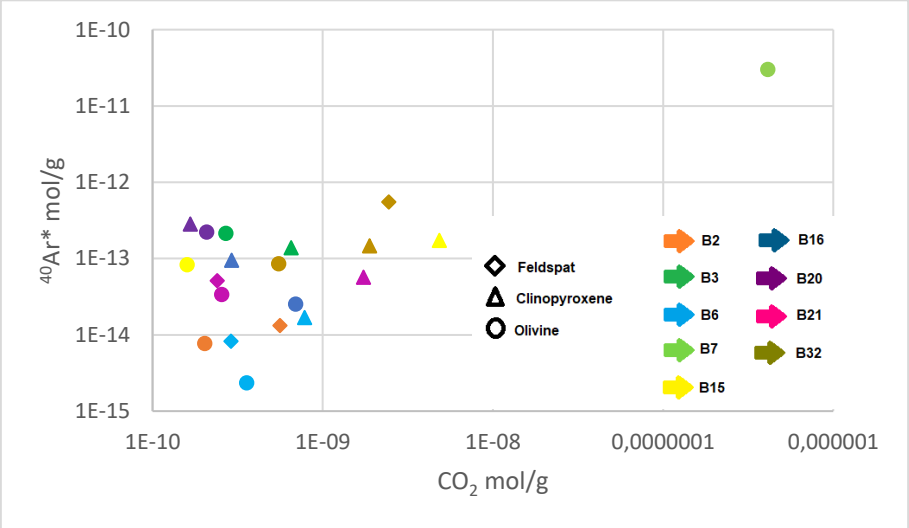

Fig. 10.2.7 – $^{40}Ar^*$ vs. CO_2. B2: sub-ophitic gabbro; B3: wherlite; B6: sub-ophitic gabbro; B7: dunite; B15: wherlite; B16: porphyrogabbro; B20: porphyrogabbro; B21: poikilitic gabbro; B32: poikilitic gabbro.

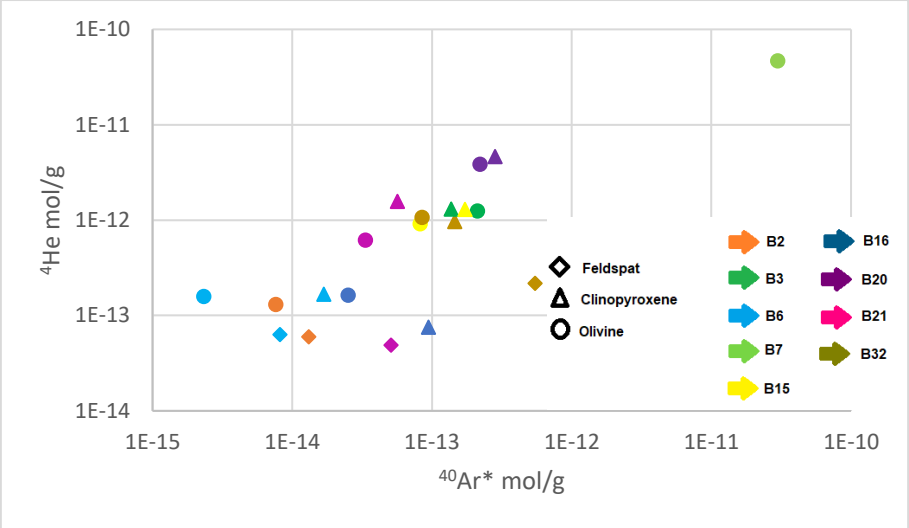

Fig. 10.2.8 – ^{4}He vs. $^{40}Ar^{*}$. B2: sub-ophitic gabbro; B3: wherlite; B6: sub-ophitic gabbro; B7: dunite; B15: wherlite; B16: porphyrogabbro; B20: porphyrogabbro; B21: poikilitic gabbro; B32: poikilitic gabbro.

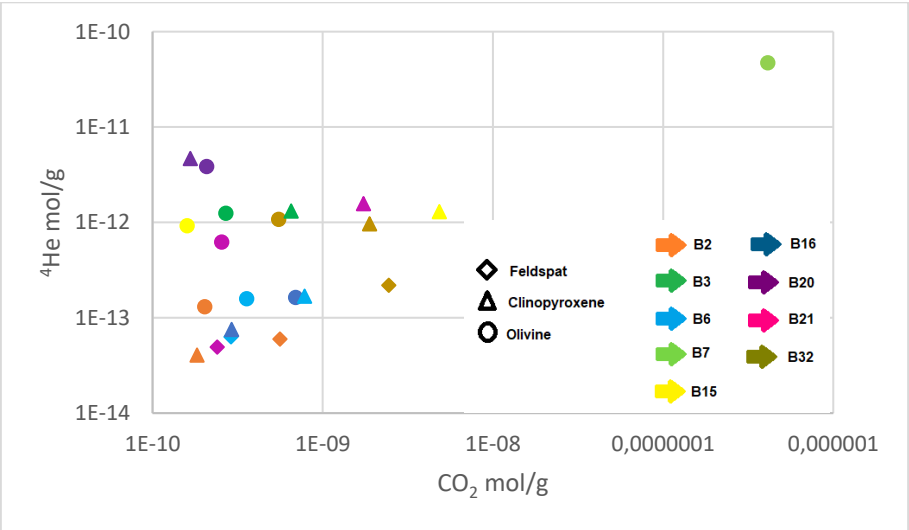

Fig. 10.2.9 – ^{4}He vs. CO_2. B2: sub-ophitic gabbro; B3: wherlite; B6: sub-ophitic gabbro; B7: dunite; B15: wherlite; B16: porphyrogabbro; B20: porphyrogabbro; B21: poikilitic gabbro; B32: poikilitic gabbro.

11 Quartz xenocrysts

Among the Bellecombe Ash Member deposits, loose quartz xenocrysts coming from sites near Langevin Caldera were sampled, from few millimetres to about one centimeter in size. The presence of these quartz xenocrysts might derive from the involvement of the shallow hydrothermal system or circulating hydrothermal fluids when the eruption of ther Bellecombe Ash Member occurred. The total number of the quartz xenocrysts is 52. These samples were investigate with a stereomicroscope and were subdivided on the bases of the presence of fluid inclusions. Subsequently, representative samples were prepared for different analyses, in order to try to understand their origin.

11.1 X-ray diffraction analyses

The samples analysed by X-ray diffractometric analyses (Q3, Q4, Q5, Q8, Q9; Fig. 11.1.1) were chosen among not containing fluid inclusions (at naked eye). For all the analyses was used the "side loaded" technique, with the exception of smaller samples (Q8 and Q9) where "scratch" technique was used.

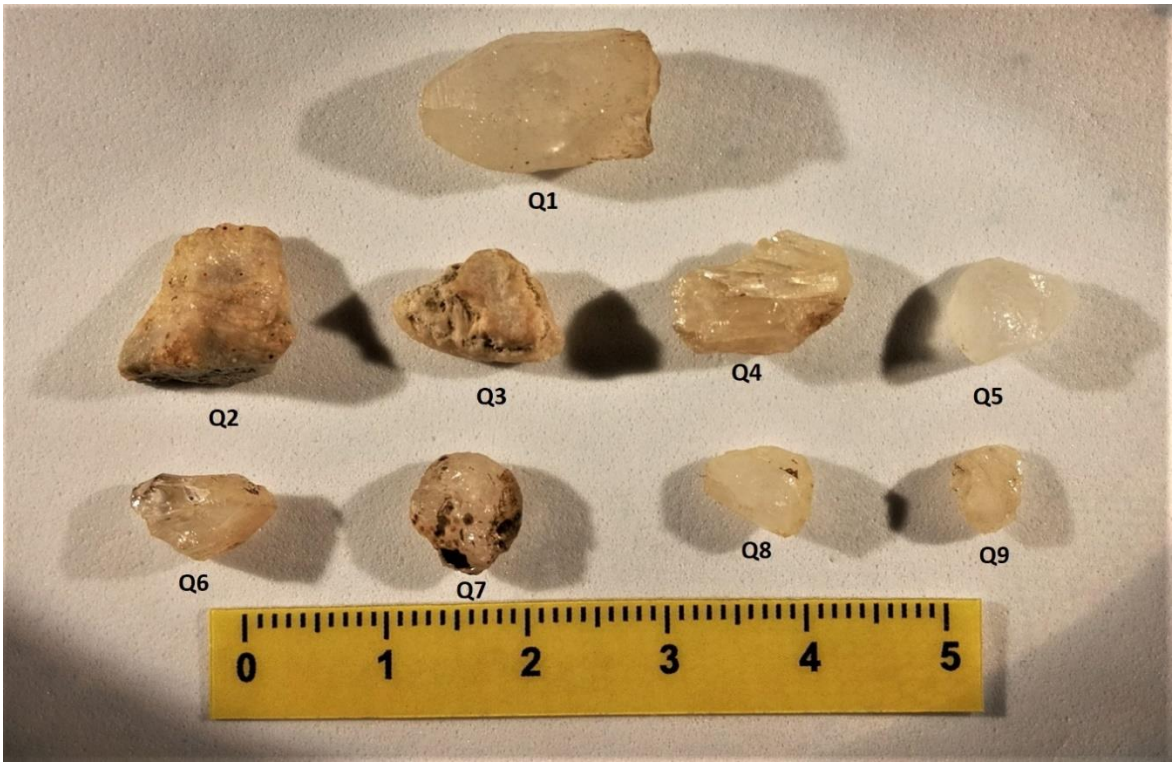

Fig. 11.1.1 - Some of the quartz crystals sampled on Langevin caldera.

All the analysed samples resulted in quartz xenocrysts (Figg. from 11.1.3 to 11.1.8), with the exception of a calcium carbonate crystal (Q3; Fig. 11.1.2).

Details on the diffractometric spectra were reported below.

Q3: concretionary aspect with evident lateral depositional bands. The sample, as evidenced by its spectrums, is a calcium carbonate concretion. Only two other samples found in the Langevin caldera were identified as calcium carbonate concretion.

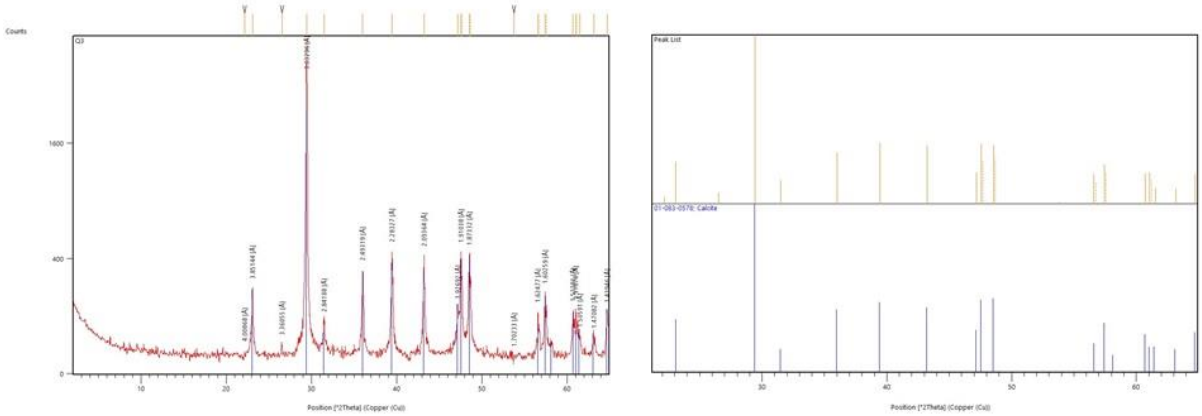

Fig. 11.1.2 - Q3 XRD analyses. Spectrum of analyses and pattern.

Q4: twinned sample.

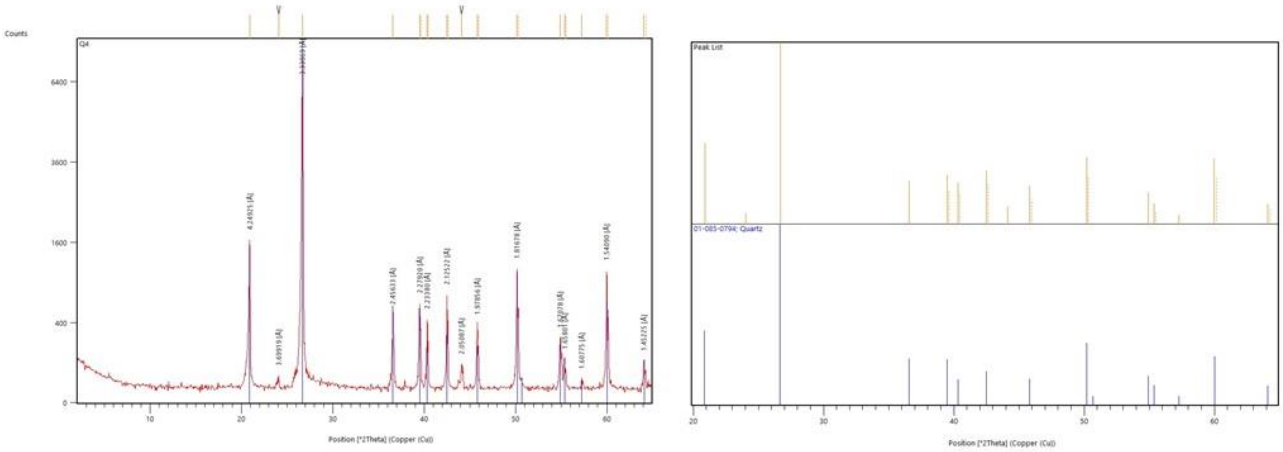

Fig. 11.1.3 - Q4 XRD analyses. Spectrum of analyses and pattern.

Q5: very transparent sample.

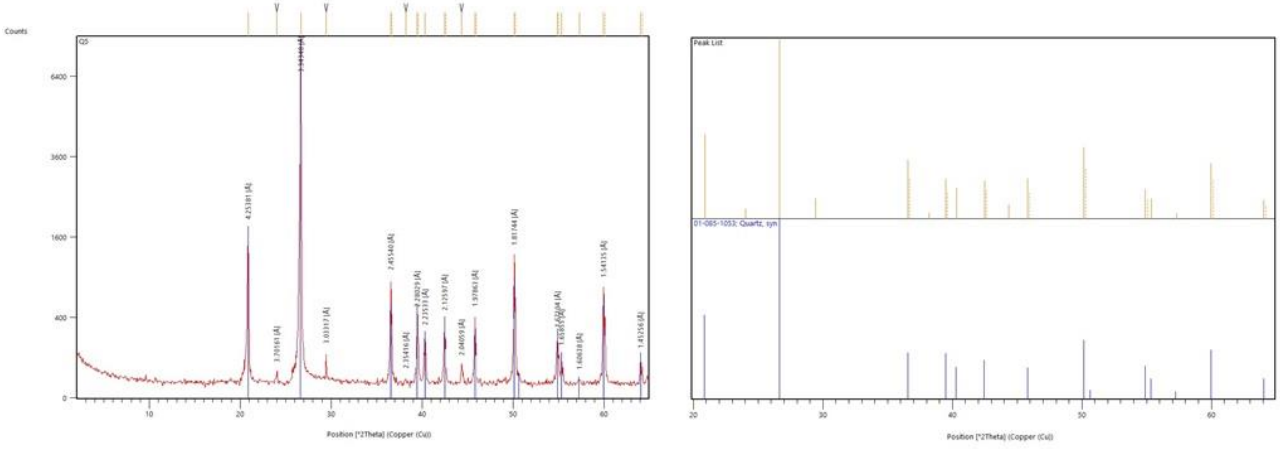

Fig. 11.1.4 - Q5 XRD analyses. Spectrum of analyses and pattern.

Q8: The analyses was also replicated with the "suspension in acetone" technique.

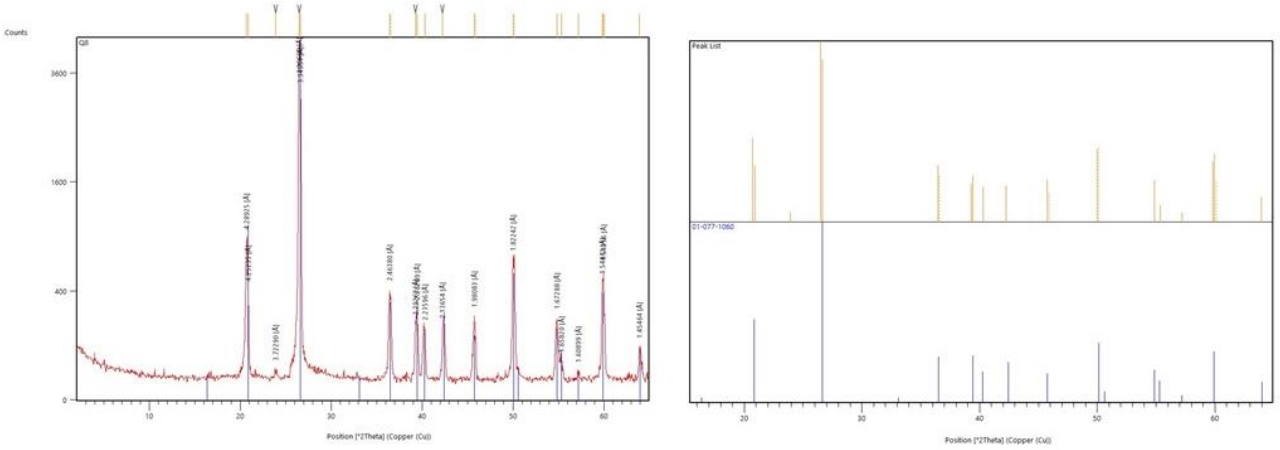

Fig. 11.1.5 - Q8 XRD analyses. Spectrum of analyses and pattern.

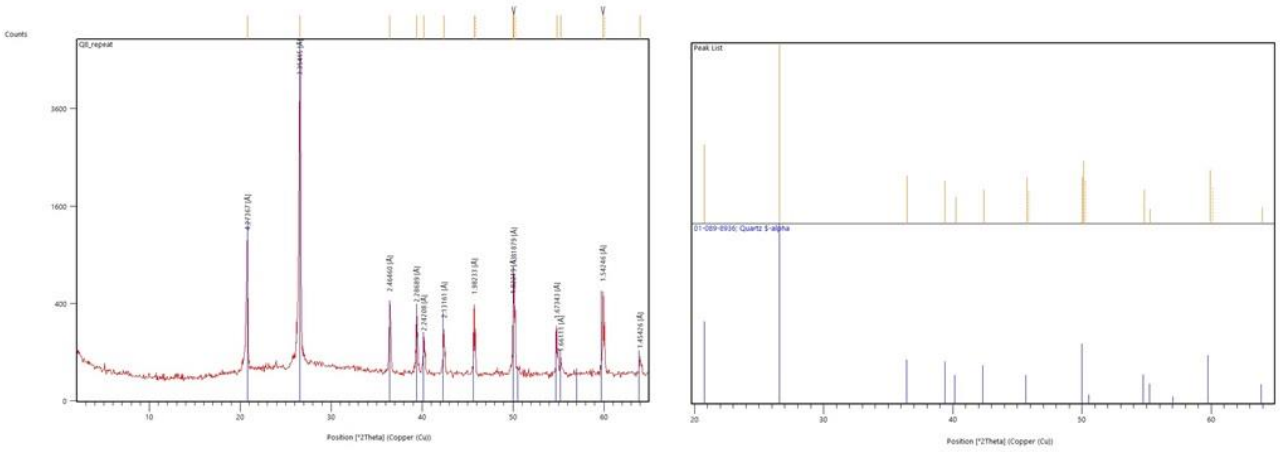

Fig. 11.1.6 - Q8 repetition of the XRD analyses. Spectrum of analyses and pattern.

Q9: The result of the analyses was good but also for this sample the analyses were replicated twice with the "suspension in acetone" technique to try to improve the result.

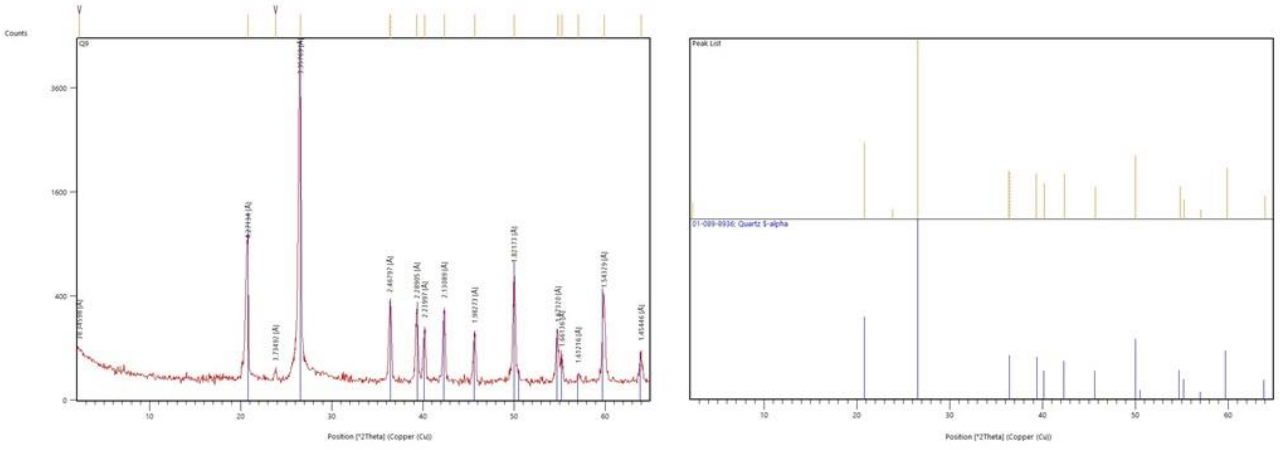

Fig. 11.1.7 - Q9 XRD analyses. Spectrum of analyses and pattern.

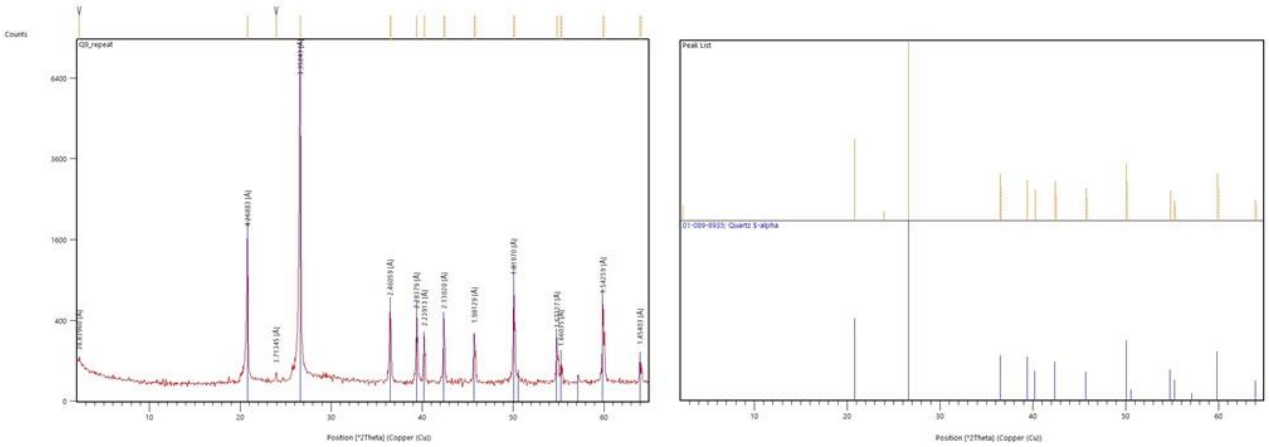

Fig. 11.1.8 – Q9 replication of the XRD analyses. Spectrum of analyses and pattern.

11.2 Laser Ablation Inductively Coupled Plasma Mass Spectrometry analyses

Some quartz samples were studied on thin section and display different accretions/layers on the crystal rim (Figg. from 11.2.1 to 11.2.4).

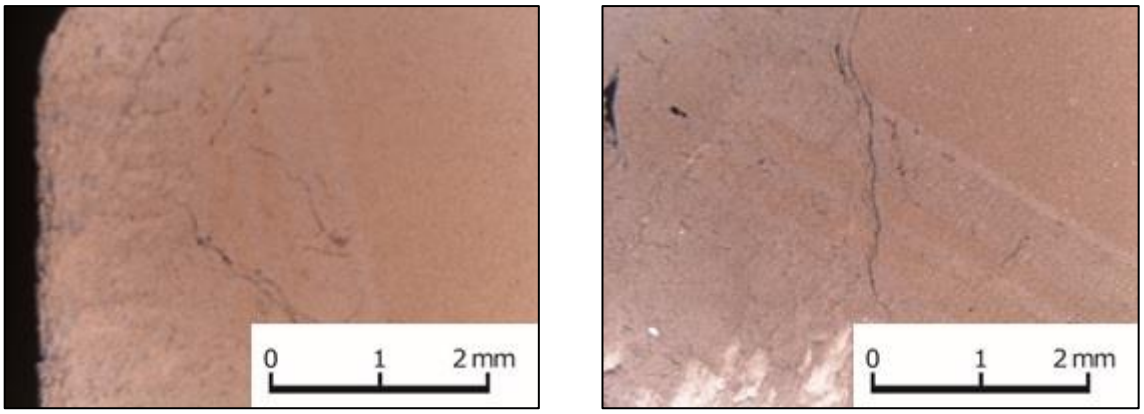

Fig. 11.2.1 – Plane-polarized light of quartz xenocryst Q1.

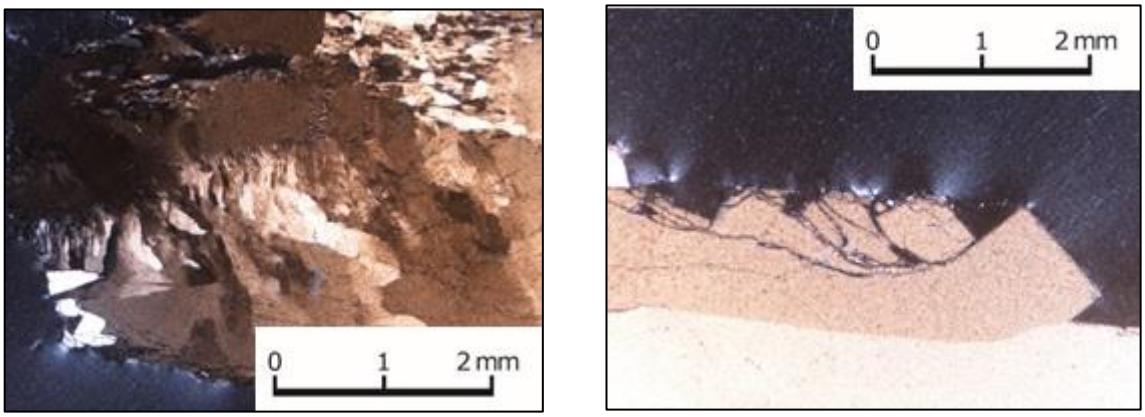

Fig. 11.2.2 – Crossed polars of quartz xenocryst Q13.

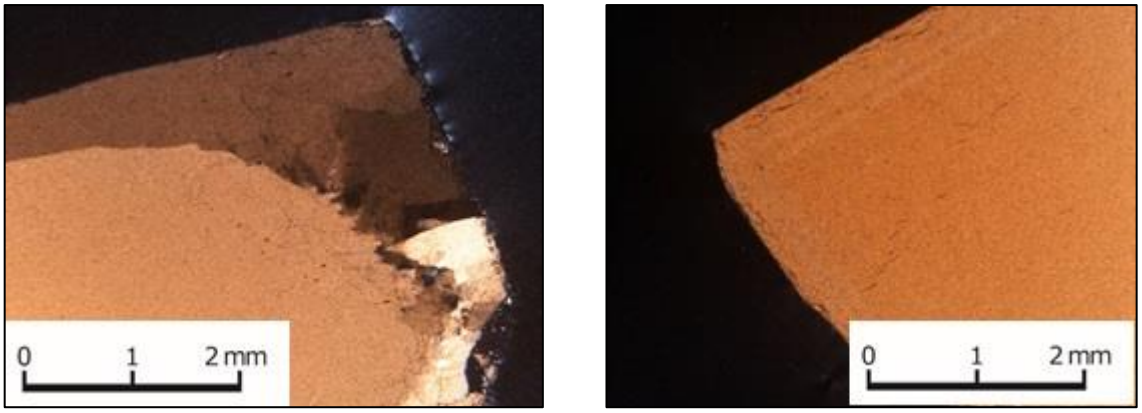

Fig. 11.2.3 – Crossed polars of quartz xenocryst Q16.

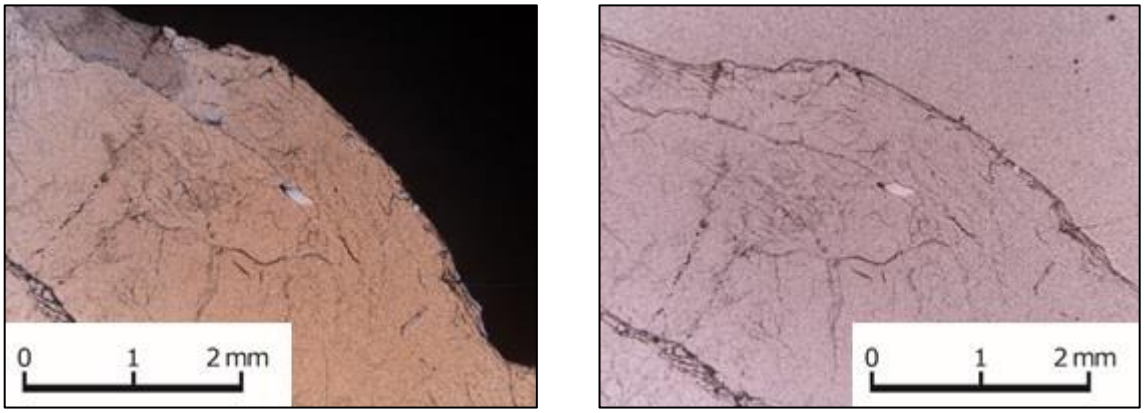

Fig. 11.2.4 – (On the left) Crossed polars and (on the right) plane-polarized light of quartz xenocryst Q19.

To better understand the nature of these rims, some quartz samples without trace of fluid inclusions were analysed with a transect rim-core and analysed through LA-ICP-MS (Figg. 11.2.5, 11.2.6, 11.2.7 and 11.2.8). The analyses were made on samples Q1, Q13, Q16 and Q19.

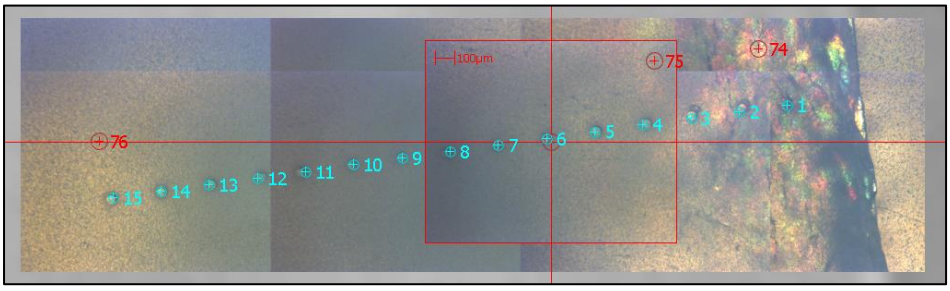

Fig. 11.2.5 – Q1 transect rim-core. The image was take with the LA-ICP-MS integrated camera. The laser spots of the ablation analyses are shown.

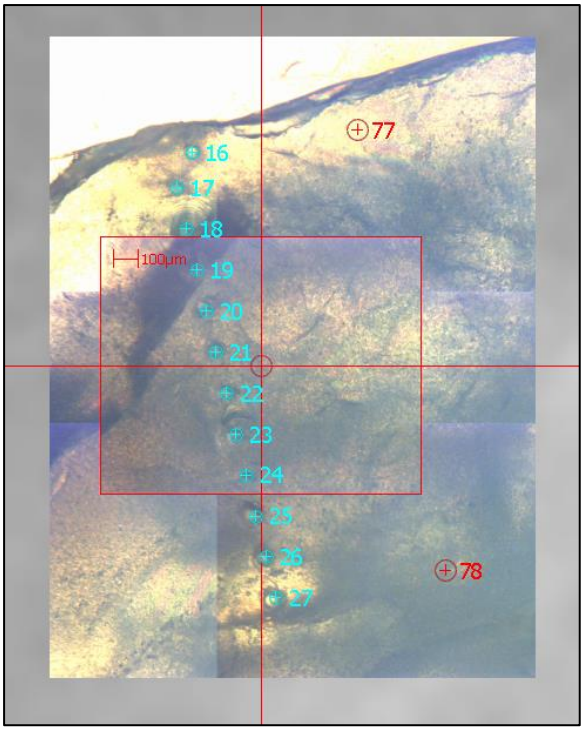

Fig. 11.2.6 – Q13 transect rim-core. The image was taken with the LA-ICP-MS integrated camera. The laser spots of the ablation are shown.

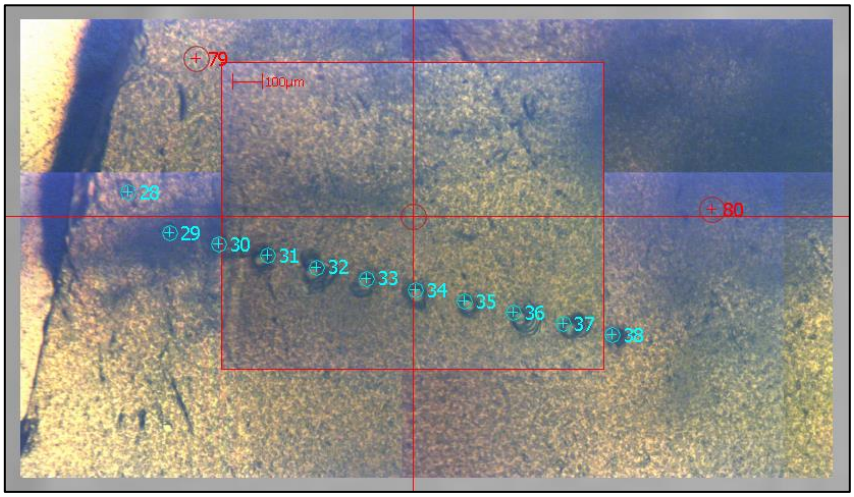

Fig. 11.2.7 – Q16 transect rim-core. The image was taken with the LA-ICP-MS integrated camera. The laser spots of the ablation are shown.

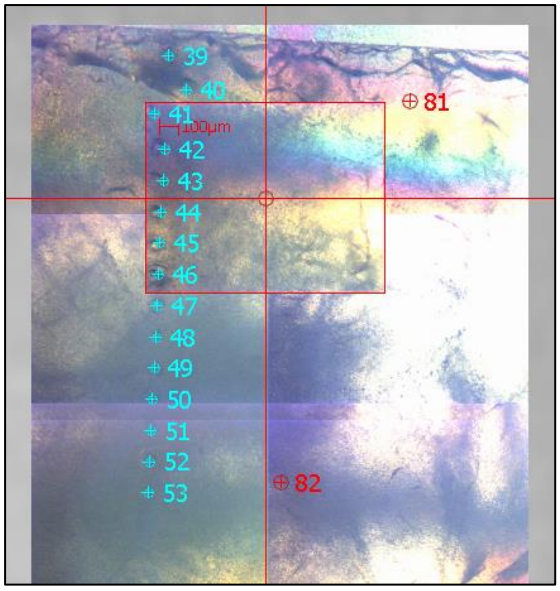

Fig. 11.2.8 – Q19 transect rim-core. The image was take with the LA-ICP-MS integrated camera. The laser spots of the ablation are shown.

Some enrichments in trace elements in quartz xenocrysts are shown from the core to the rim of the crystal (Figg.11.2.9 and 11.2.10).

Fig. 11.2.9 – Transect of quartz xenocrysts samples from the core (right) to the rim (left). Samples shows different content of trace elements through the core-rim transect. Some of them show an enrichment from the core to the rim.

Common trace elements in quartz can be very useful proxy of interaction between the hydrothermal system and the magmatic plumbing system during phreatomagmatic eruptions (e.g. Ti was found to be universally present in magmatic quartz, but at much lower abundance in hydrothermal quartz; Muller et al., 2003). As a matter of fact, in the investigated quartz xenocrysts Ti is very low, around 1 ppm (Limit Of Detection LOD are: Li 0.16-0.22 ppm; B 0.55-0.77

ppm; Al 0.37-0.46 ppm; P 4.4-6.7 ppm; Ti 0.45-0.57 ppm; K 1-1.5 ppm; Fe 2.9-4.3 ppm; Sr 0.0016-0.0041 ppm).

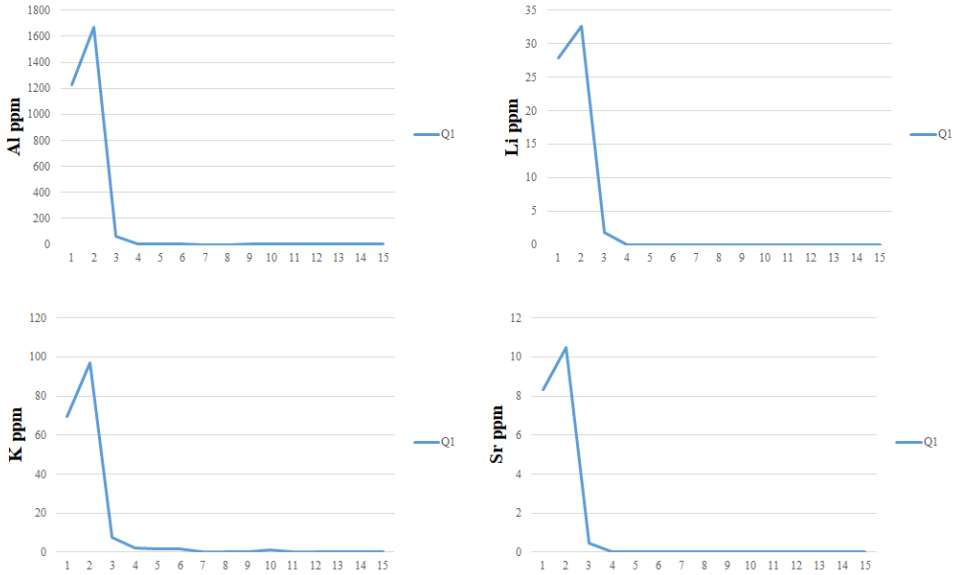

Fig. 11.2.10 - Transect of Q1 quartz sample from the core (right) to the rim (left). Q1 sample show the maximum concentration on the rim respect the other samples analyzed.

The enrichment of different elements is clearly visible in Q1 sample especially for Al, Li, K and Sr. This enrichment on the rim of Al^{3+} and Li^{+} can be interpreted as a substitution of Si^{4+} in the quartz structural lattice.

Sample Q1 is that better emphasizes this evidence of enrichments of different elements at the rims and therefore was mapped in detail (Fig. 11.2.11).

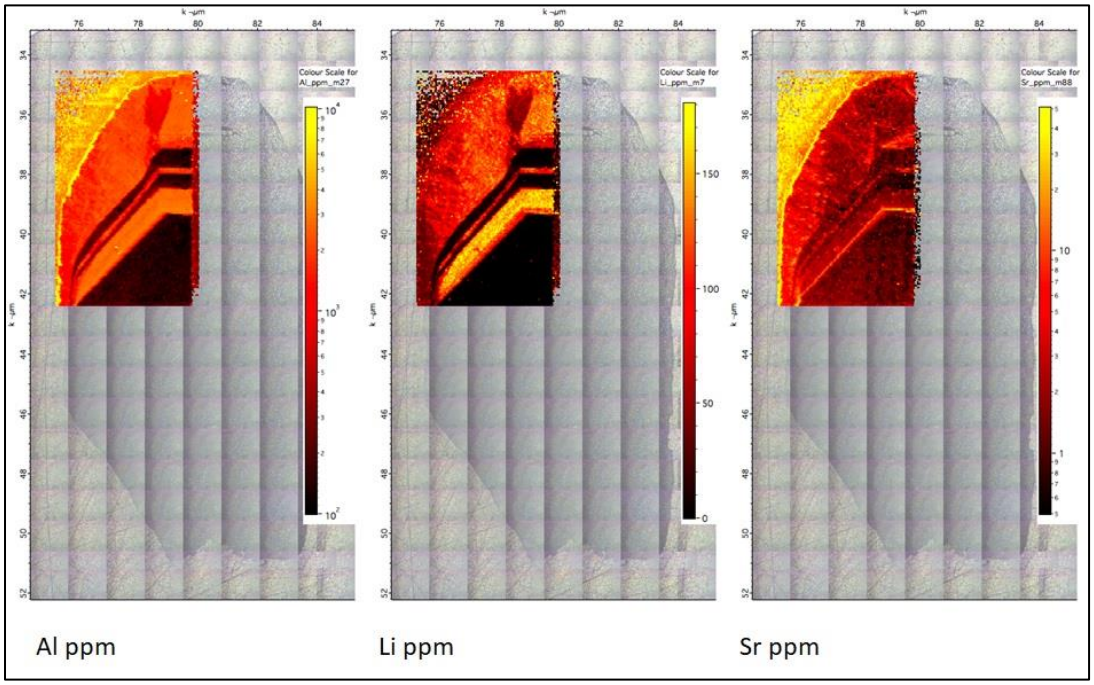

Fig. 11.2.11 -LA-ICP-MS map showing the enrichment in Al, Li and Sr toward the rim of the Q1 xenocryst.

11.3 Raman analyses

The analysed samples were both doubled-polished in thin sections (Q1, Q13, Q16 and Q19) or bulk crystals (Q14, Q15, Q17 and Q18). The fluid inclusions occur in different generations and are both biphase (liquid + vapour; Fig. 11.3.1) and monophase (vapour; Fig. 11.3.2). Raman analyses reveal the dominant presence of low-salinity aqueous inclusions (Fig. 11.3.3) with, locally, trace of CO_2 (Fig. 11.3.4). Characterization of true salinity, kind of dissolved salts and density of the inclusions, such as of immiscibility/boiling processes, would require a more detailed fluid inclusion study.

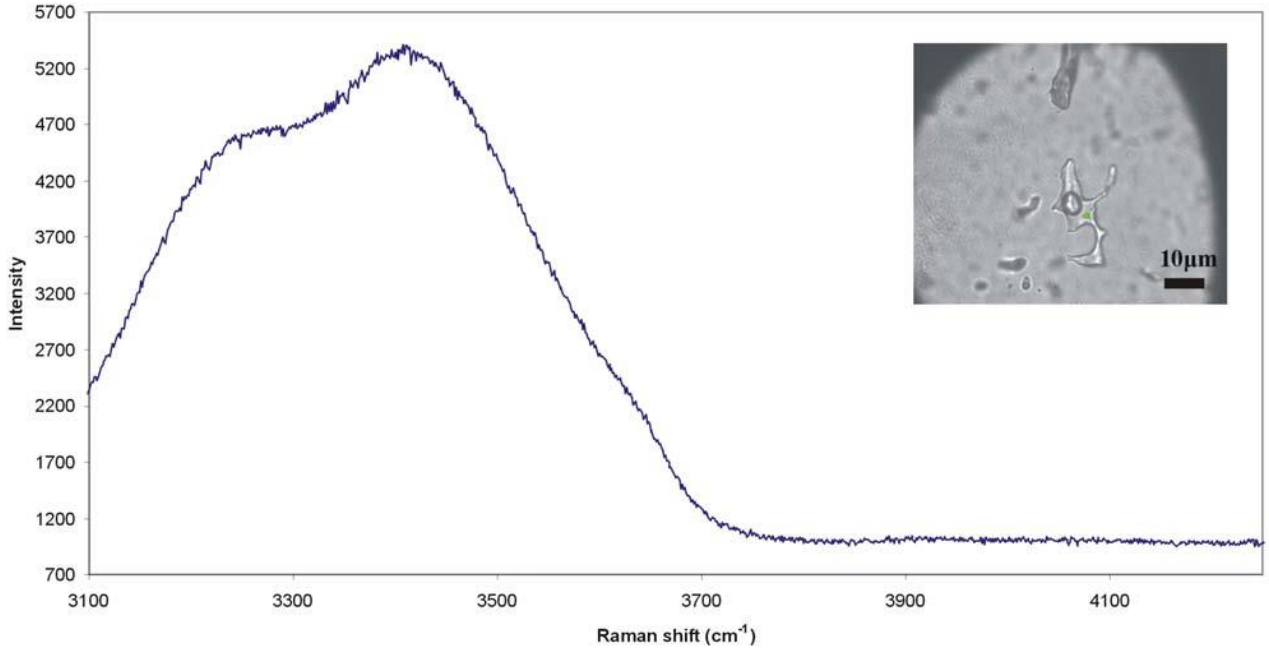

Fig. 11.3.1 - Typical Raman spectrum of the liquid water present in a biphase (liquid + vapour) fluid inclusion. The evident band at about 3200 cm^{-1} is typical of low-salinity water (e.g., Frezzotti et al., 2012). The green dot in the photomicrograph represents the analysed site.

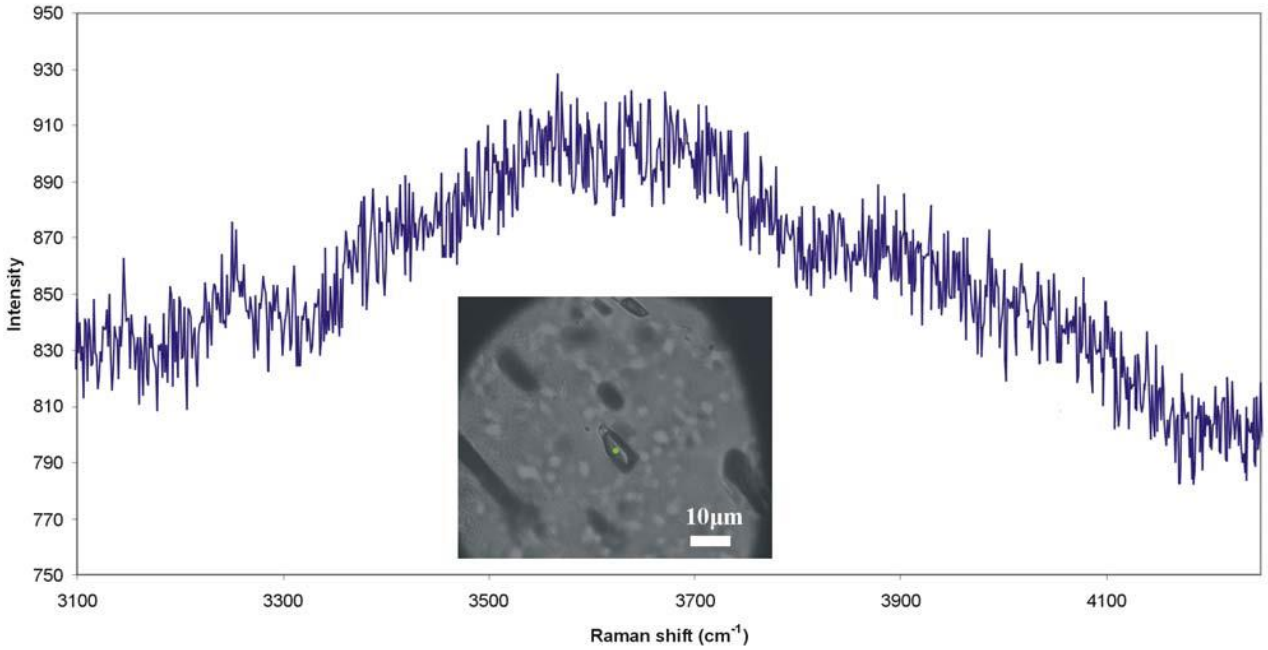

Fig. 11.3.2 – Raman spectrum of the vapour water present in a biphase (liquid + vapour) fluid inclusion. The two large bands at about 3550 and 3650 cm-1 are typical of low-salinity water (e.g., Frezzotti et al., 2012). The green dot in the photomicrograph represent the analysed site.

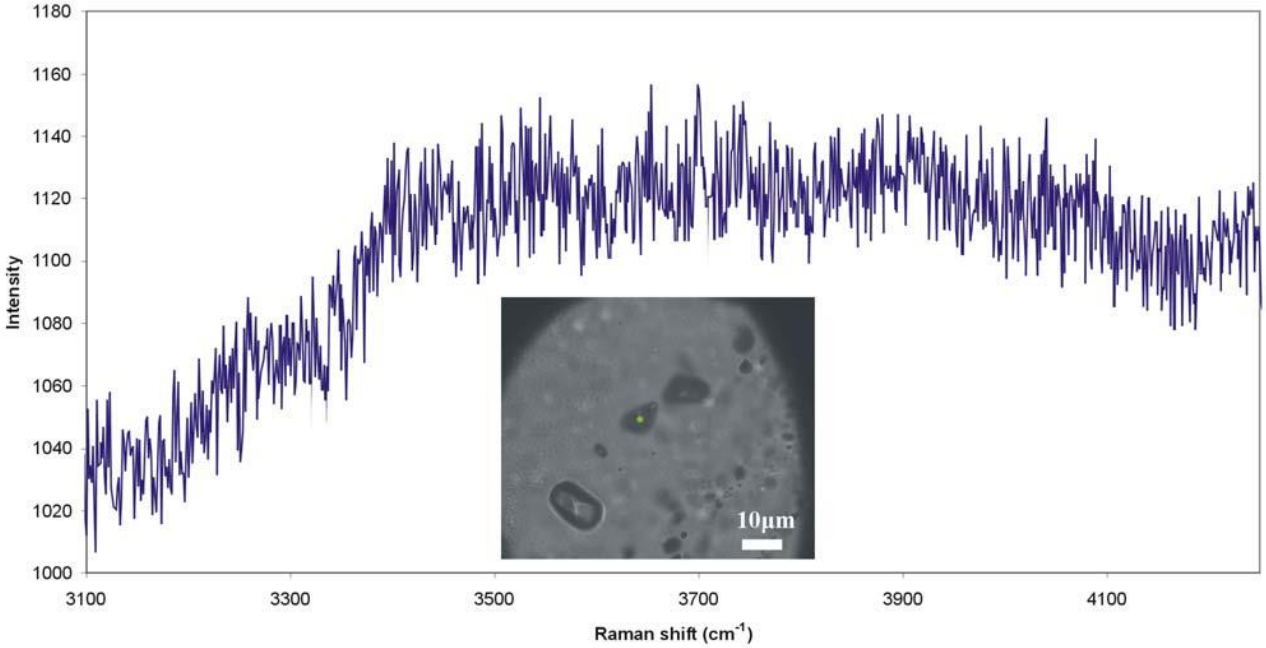

Fig. 11.3.3 – Raman spectrum of the vapour water present in a monophase (vapour) fluid inclusion also containing trace of CO_2 (Fig. 12.3.4). The green dot in the photomicrograph represents the analysed site.

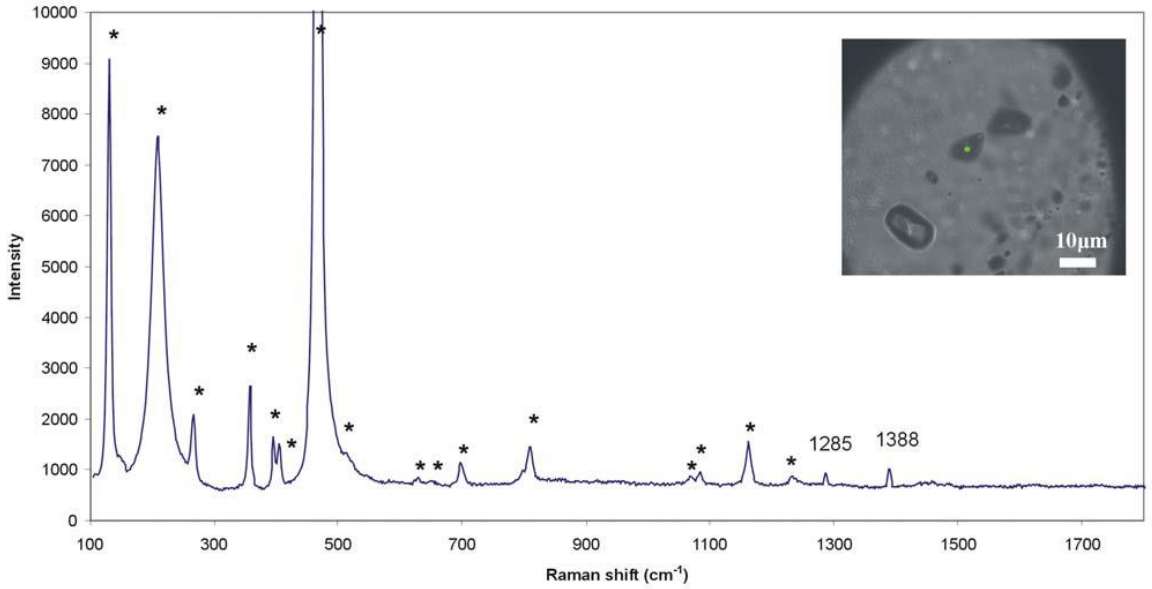

Fig. 11.3.4 – Raman spectrum of CO_2 in a monophase vapour inclusion of water (Fig. 12.3.3). The two peaks at 1285 and 1388 cm^{-1} and their low intensity are typical of low-density vapour CO_2 (e.g., Frezzotti et al., 2012). The green dot in the photomicrograph represents the analysed site.

12 Sedimentary clasts of Langevin Caldera

Some sub-centimeter to centimeter size carbonatic xenoliths (calcite, see XRD analyses in Fig. 11.1.2) from Langevin Caldera were detected. One of these carbonatic samples (≈ 4 cm in size) was used for a thin section investigation. The sample was identify as a sedimentary rock, probably a carbonatic biomicrite. Radiolaria, microforaminifera and broken sponge spicols were recognized, also suggesting an apparent reworking of the deposits (Fig. 12.1). Microforaminifera detected are mainly genera Hedbergella (Barremian-Albian L., 110-120 Ma) and Hedbergella similis. Some crystals of ematite and glauconite, typically sedimentary minerals, also occurred. Since the oldest sediments of the oceanic crust below the Réunion Island should be not older than 70-80 Ma, the hypothesis of a reworked older sedimentary rocks (from the adjacent Mascarene basin) could be the most reliable. The sediments probably were also subjected to some directional current, as suggest by the orientation of sponge spicols (Fig. 12.2).

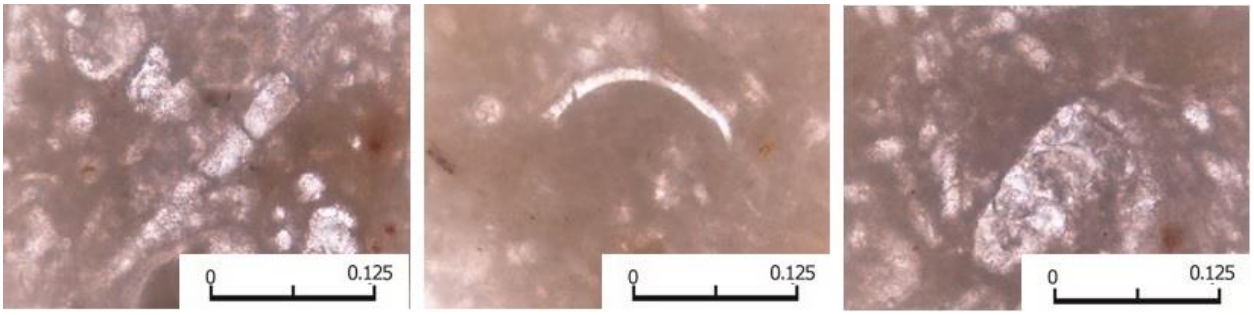

Fig. 12.1 – Plane-polarized light of sample B30. From the left: microforaminifer, a section of valve and a particular of microforaminifer (Hedbergella).

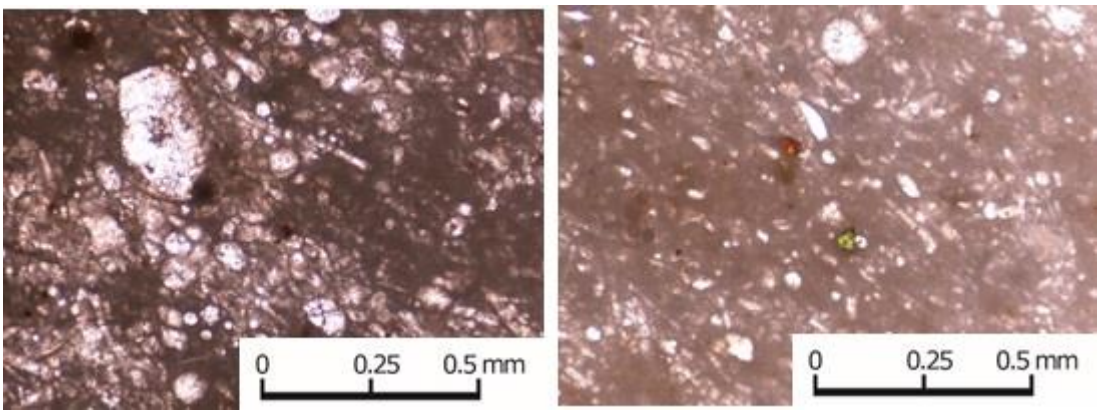

Fig. 12.2 – Plane-polarized light of sample B30. Glauconite and hematite were individuate.

13 Discussion

13.1 The subvolcanic crystallization below the Réunion Island: comparison between Piton de la Fournaise and Piton des Neiges mafic and ultramafic intrusive products

The detailed petrographic study by optical microscopy, together with phase and bulk rock chemistry, allowed the recognition of several petrographic groups among the mafic and ultramafic subvolcanic rocks of the Bellecombe Ash Member, unravelling an overall, much wider range of textures and igneous subvolcanic lithotypes than previously reported by the literature.

Comparing textures of Piton de la Fournaise subvolcanic ejecta with those of Piton des Neiges, a longer subsolidus strain history is pointed out for the latter, being an older and eroded magmatic plumbing system. Some differences in modal mineralogy and texture were also recognized. Some dunitic clasts of Piton des Neiges show the presence of amphibole, absent in other samples of Piton de la Fournaise. Wherlitic ejecta of the Bellecombe Ash Member are mainly made of olivine, clinopyroxene, interstitial glass and opaque minerals. Plagioclase are howewer detected in small amount in one wherlite sample (B28) and in a composite layered ejecta (B108) emphasizing the role of plagioclase crystallization in the transition wherlite-gabbro (through the presence of plagioclase-wherlite and troctolite patches) also at isobaric condition in the Piton de la Fournaise magmatic plumbing system.

The interstitial trapped liquid (as interstitial quenched glass) in the intrusive investigated ejecta range from basalt to basaltic trachyandesite.

Piton des Neiges dunitic samples has a homogeneous Fo% content close to 88, comparable with that found in the dunitic ejecta of the Bellecombe Ash Member which are however characterized by a wider compositional range from Fo_{89} down to Fo_{80}. Fo% content of Piton des Neiges wherlites is 77-85, whereas Bellecombe wherlitic ejecta are characterized by Fo_{80-85}. Wherlites of Piton des Neiges and Piton de la Fournaise are comparable in terms of Fs% content in clinopyroxene, respectively Fs_{7-9} and Fs_{8}. Also the ferrosilite contents in clinopyroxene of the gabbro samples are comparable in Piton des Neiges and ejecta of the Piton de la Fournaise being respectively Fs_{10-15} and Fs_{8-15}.

Most of the mafic and ultramafic subvolcanic ejecta of the Bellecombe Ash Member can be interpreted as cumulate cognates *sensu stricto*: dunites, wherlites, ophitic gabbros, poikilitic gabbros and some sub-ophitic gabbros (those with the higher CaO/Al_2O_3 ratios). By contrast, other subvolcanic clasts (doleritic gabbros and the sub-ophitic gabbros with the lower CaO/Al_2O_3 ratios) may simply represent slowly-cooled equivalents (with no crystal-liquid fractionation) of the erupted cotectic basalts (SSB). Finally, the porphyrogabbros may

represent oceanite (picritic) magmas, whose storing in the magmatic plumbing system allowed the fine-grained crystallization of an evolved groundmass represented by sanidine- and biotite-bearing (phlogopite) assemblage, which are instead absent in Piton des Neiges and other Piton de la Fournaise intrusive clasts analysed in previous works (Upton et al., 2000; Berthod et al., 2020; Brugier, thesis, 2016). The presence in the Bellecombe intrusive ejecta of such a hydrate interstitial phase could also indicate a vapor phase crystallization that can be either pneumatolytic within the magmatic plumbing system or linked to hydrothermal fluids.

13.2 Subvolcanic crystallization and relation between interstitial glass of Bellecombe Ash Member ejecta and trachitic pumices

The cumulitic mafic and ultramafic ejecta of the Bellecombe Ash Member can be interpreted as formed by solid-liquid crystal settling or *in situ* crystallization. By contrast, the subvolcanic samples reflecting the slowly-cooled equivalent of the basaltic melt (i.e. doleritic gabbros and some sub-ophitic gabbros) should have formed as an *in situ* crystallization front from the basaltic magma wall-rock inward without solid-liquid separation.

During the process of in *situ* crystallization, some residual liquids may have been interstitially entrapped and finally quenched as glass, so widespread in some of the investigated ejecta. The absence of resorbed margin on the crystal framework (clinopyroxene, feldspar and olivine) in contact with the interstitial glass, suggest a fast ascent of the magma carrying the subvolcanic clasts. The composition ranging from basalt to basaltic trachyandesite of the interstitial glass indicates that the melt was entrapped within the crystal frameworks, with no time to evolve and crystallize because involved in the explosive eruption. The quenched interstitial glass as well as the texture of the mafic and ultramafic ejecta represent a snapshot of the pre-eruptive plumbing system of Piton de la Fournaise. This suggest the clasts were disrupted from the wall rocks and transported very fast to the surface, mostly as cognates. Nevertheless, during the history of a magma plumbing system, liquid entrapped interstitially could also escape from the subvolcanic crystal frameworks and could also form small melt pockets (or larger body) of more evolved silicate magma. This is what happened in the mugearitic portion of a sill of Piton des Neiges studied by Upton et al. (1967).

The trachytic pumices of the Bellecombe Ash Member show a more evolved glass composition than the analysed interstitial glass in the subvolcanic ejecta. Therefore, these pumices likely represent a differentiated liquid, which can be considered akin with that quenched as interstitial glass in the intrusive suite found as ejecta in the Bellecombe Ash Member.

Porphyrogabbro samples show a modal mineralogy characterized by the presence of biotite (phlogopite) and sanidine. This mineral phase

association (also coupled with low-Ca plagioclase) is characteristic of a trachytic composition. Interstitial phlogopite and sanidine in porphyrogabbros can be thus related to the crystallization of the residual trachytic liquids otherwise erupted as quenched pumice glass. Trachytic pumices of the Piton de Neiges are similar to those found in the Bellecombe Ash Member but characterized by the feldspar pair albitic plagioclase-anorthoclase in the glassy groundmass. Different equilibrium of felspar pairs suggest different temperature of crystallization.

Vlastelic et al. (2021) consider the small volume of trachyte pumices erupted by Piton de la Fournaise in 2007 as a liquid remnant of Piton des Neiges or Les Alizés or a result from partial melting of an old syenite intrusion or remobilization of interstitial melts not fully solidified. Nevertheless, also the sanidine- and phlogopite-bearing microcrystalline groundmass in the porphyrogabbro ejecta seem to be representative of a trachyte liquid. In this way, as the porphyrogabbro ejecta were erupted during the Bellecombe Ash Member (about 5 ka), small fractions of evolved liquids in the Piton de la Furnaise plumbing system should have been not uncommon during the Holocene. The presence of trachyte pumices in the 2007 eruption of Piton de la Fournaise should therefore not be considered an exceptional event.

13.3 Thermobarometric evaluation and fluid inclusions of the subvolcanic ejecta in the Bellecombe Ash Member and some isobaric coexistence of ultramafic-mafic lithotypes

The presence in some Bellecombe Ash Member ejecta of fluid inclusions allowed a thermobarometric evaluation, to better understand the dynamic of the subvolcanic plumbing system of Piton de la Fournaise.

Both mafic and ultramafic analysed ejecta show different content in noble gases and CO_2. Ultramafic samples gave significant results for CO_2 content on Raman analyses, suggesting the deepest levels of crystallyzation. Dunite (B7) show a range of crystallization pressure of about 309-338 MPa, suggesting an underplating provenance (~ 13 km b.s.l.). By contrast, the wherlite (B15) pressure of crystallization ranges from 151 to 166 MPa, correspondent to an origin close to the submarine base of the edifice (~ 6 km b.s.l.). Fluid inclusion in mafic ejecta of Bellecombe Ash Member show a CO_2 content below the limit of detection, therefore indicating a possible even shallower depth (above 6 km b.s.l.).

High content of noble gases and CO_2 measured in fluid inclusions coupled to low He/Ar* and He/CO_2 ratios indicate the deepest provenance of the samples (Boudoire et al., 2018). Noble gases and CO_2 high content together with He/Ar* and He/CO_2 on the dunite sample (B7) agree with a deep provenance, close to the underplating, while the provenance of the wherlitic sample B15 is just shallower than the dunite one.

Noble gases and CO_2 from fluid inclusions of mafic intrusive ejecta (poikilitic gabbro and sub-ophitic gabbro), also suggest a shallower depth of crystallization than the wherlites, i.e. close to the submarine base of the edifice. Nevertheless, the presence of composite subvolcanic samples (B108a and B108b), displaying the coexistence of plagioclase-wherlite, troctolite and gabbro patchy portions (with modal and grain size variations) surrounding wherlite, could be explained by dissolution process due to percolation of basaltic melt. Also in the B28 wherlite sample, the dissolution of olivine and its progressive rounding, can involve basaltic melt percolation coupled by reaction, thus producing clinopyroxene. In a strongly active basaltic volcano such as Piton de la Fournaise, the transition from ultramafic to mafic intrusive domains (B108) or textural changes in the ultramafic lithotypes, could be therefore driven by the interaction of the persistently rising batches of basaltic magmas interacting with the already crystallized cumulates.

Fluid inclusion and thermobarometric studies should be deepened, together with a detailed petrologic investigation of the composite ejecta (B108a-b), aimed at a more exhaustive and consistent information about the petrogenetic history of the mafic and ultramafic samples of the Bellecombe Ash Member.

13.4 The involvement of the hydrothermal system in the Piton de la Fournaise explosive eruptions

As already documented by Ort et al. (2016), in the Bellecombe Ash Member deposits, quartz crystals and hydrothermally altered grains were found. This could indicate the involvement of a shallow hydrothermal system, from 0.5 to 2 km depth, in the magma plumbing system of this explosive eruption of the Piton de la Fournaise.

In the deposit at the Langevin Caldera, several loose quartz xenocrysts were found and collected. The analyses of these quartz xenocrysts pointed out the presence of a low-salinity aqueous inclusions (Raman analyses) coupled with trace of CO_2. A hydrothermal origin for these quartz xenocrysts is very likely. The enrichment, on the rim of some quartz crystals, of some trace element was also considered a very useful proxy of interaction between the hydrothermal system and the magmatic plumbing system during phreatomagmatic eruptions. Some quartz xenocrysts show a Li and Al enrichment on the rim. These enrichments can be interpreted as a substitution of Si in the quartz lattice by circulating fluids. The interaction between shallow hydrothermal and magmatic plumbing systems during the Bellecombe Ash Member eruption is thus strongly suggested. During the interaction, the eruption could have disrupted and transported to the surface not only the subvolcanic mafic and ultramafic suite but also quartz xenocrysts of hydrothermal origin.

14 Conclusions

The textural and petrologic studies of the subvolcanic ejecta of Piton de la Fournaise provides new insights on the magmatic plumbing system and the subvolcanic crystallization processes at La Réunion Island. With respect to the available literature data, a wider spectrum of subvolcanic lithotypes, mainly in terms of a great variety of textures, was emphasized. Several mafic and ultramafic lithotypes have been recognized. Based on the texture and modal mineralogy, mafic ejecta can be grouped into doleritic gabbros, poikilitic gabbros, sub-ophitic gabbros, ophitic gabbros, micro-monzogabbros and porphyrogabbros. Ultramafic samples consist of dunites and wherlites, these latter being also represented by composite samples making transition to plagioclase wherlite and troctolite-gabbro patchy microdomains.

A wide spectrum of crystallization processes can be envisaged in this mafic-ultramafic subvolcanic suite: (i) cumulitic dunites, wherlites, poikilitic to ophitic and sub-ophitic gabbros, and (ii) doleritic gabbros and some sub-ophitic gabbros instead representing *in situ* crystallization of cotectic basalt (SSB) in subvolcanic environment and thus retaining a liquid composition (e.g. slowly cooled equivalents of basalts).

Samples of the Bellecombe Ash Member defined as porphyrogabbros could represent oceanite (picritic) magmas stored at crustal levels where the basaltic melts may have evolved to a sanidine- and phlogopite-bearing micro-cryptocrystalline groundmass finally supporting the abundant olivine crystals. This groundmass in the porphyrogabbros could be really considered a trachytic liquid, which may be erupted as glassy pumice if the undercooling would be high enough to preclude groundmass crystallization.

The compositional range from basalt to basaltic trachyandesite of the interstitial glass found in the intrusive clasts indicate that the melt was entrapped within the crystal frameworks and quenched during the eruption. This likely suggests the clast were disrupted from the wall rocks and transported very fast to the surface, mostly as cognates. If not entrapped interstitially during *in situ* crystallization, silicate liquid could be also expelled from the crystal frameworks, forming separated melt pockets or larger body, like a differentiated sill. Trachytic pumices from the Bellecombe Ash Member show a more evolved composition than the quenched interstitial glass in the subvolcanic ejecta, therefore suggesting the liquid may really evolve and escape if not entrapped in the crystal framework of some crystallization front of the magma reservoirs.

Fluid inclusion barometry (Raman analyses) and noble gases and CO_2 from fluid inclusion crushing extraction and mass spectrometer analyses indicate the dunites are the intrusive ejecta from the deepest levels, approximately at the underplating levels of formation (~13 km b.s.l.). Wherlites should have crystallized close

to the submarine base of the edifice (~6 km b.s.l.), whereas the mafic subvolcanic samples are even shallower. Nevertheless, a large composite intrusive ejecta (B108) emphasizes the coexistence of ultramafic-mafic portions (wherlite to plagioclase-wherlite to troctolite and gabbro) at intermediate crustal level of crystallization. In fact, according to the liquidus curves of the La Reunion magmas (Fisk et al., 1988) the presence of troctolite patchy microdomains suggest a pression of crystallization below 0.3 GPa. Textures present in these composite ejecta can be the result of basaltic melts interacting with wherlite cumulates at relatively low pressure, leading to the instability of clinopyroxene and high dissolution of olivines (highly rounded crystals) with a high loss of temperature of the system. In this way at the same pressure, but lower temperature, plagioclase is the *liquidus phase,* and therefore wherlitic cumulates interacting with basaltic melts at relatively low pressure can produce troctolite patchy microdomains at the mesoscale (Fig. 14.1).

The presence of highly rounded olivines often with fritted margin, surrounded by clinopyroxene in the wherlite sample B28 can be also explained by processes of interaction with rising basaltic magmas and phase relations in the system forsterite-diopside-SiO_2 (Kushiro, 1969, 1972), where the ferromagnesian minerals (olivine, clinopyroxene) are not sensitive to water pressure. The peritectic between forsterite, diopside and enstatite in the anhydrous system at atmospheric pressure changes composition only slightly in the water-saturated system up to 2 GPa (whereas silica strongly reduce its stability). In particular the texture characterizing the wherlite sample B28 should reflect processes occurring in the forsterite-diopside-SiO_2 system along the upper part of the cotectic line Fo-Di that can be also considered a reaction curve towards the reaction point defined by the reaction basaltic liquid + forsterite = diopside + pigeonite. As a matter of fact, it can be predicted that at 0.3 GPa (pressure inferred for the wherlite lithotypes by fluid inclusions) textural and modal modifications of ultramafic cumulate assemblages may occur during percolation and rising of basaltic melts. It is worth to note that at this pressure (about 0.3 GPa) clinopyroxene can be out of its stability curve whereas plagioclase is on the liquidus (Fisk et al., 1988; Albarede et al., 1997). B28 wherlite has got, in fact, a plagioclase modal content of about 8 vol%.

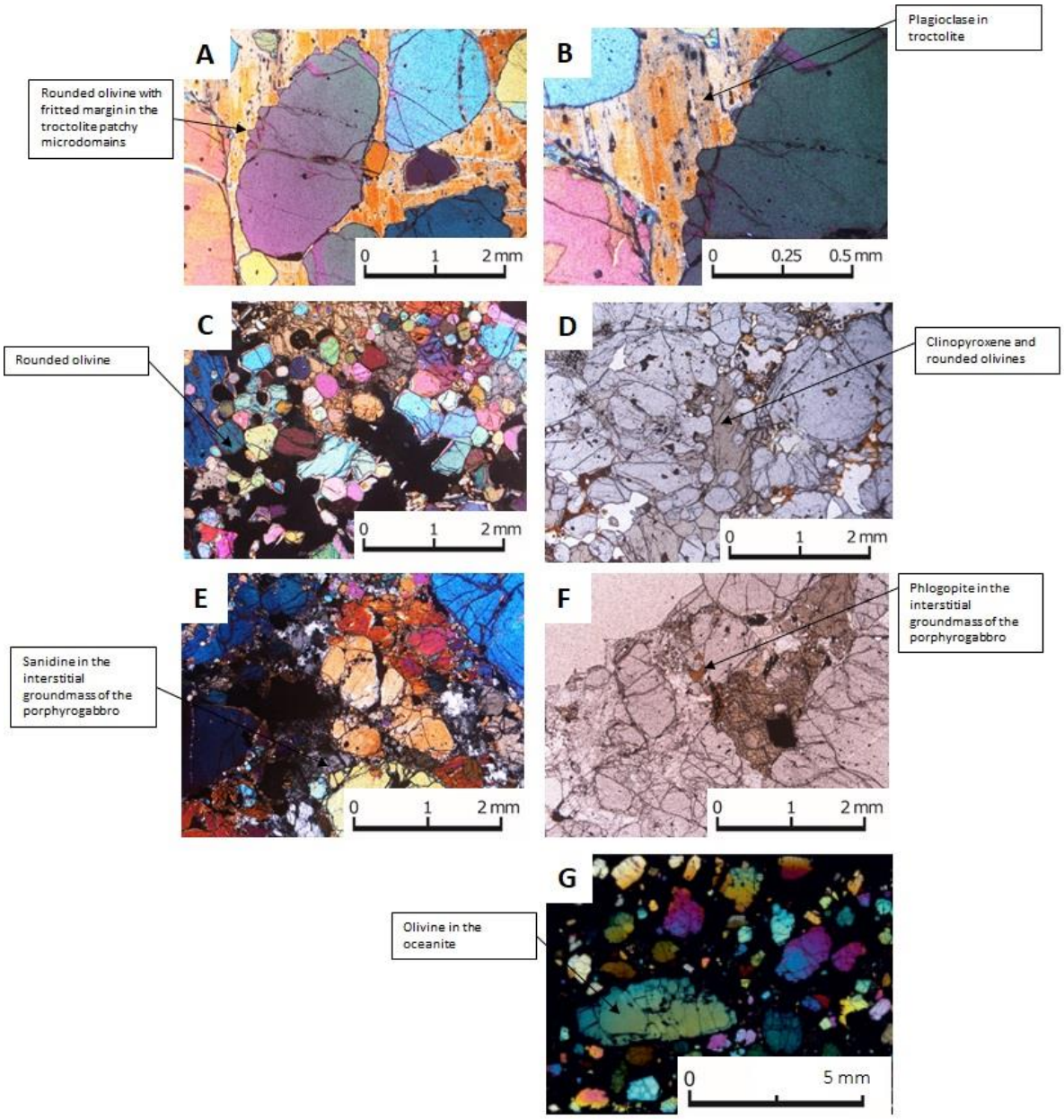

Fig. 14.1 – Thin section photos of some key-samples of the investigated subvolcanic ejecta. A-B: troctolite portions in the composite wherlite-plagioclase wherlite-troctolite-gabbro sample (B108a); B is a close up of A. C-D: wherlite B28 sample; E-F: porphyrogabbro B20 sample. G: oceanite sample (from Di Muro et al., 2014) for comparison.

The overall textural and geochemical data of the investigated mafic-ultramafic ejecta do not only reflect different mode of subvolcanic crystallization (i.e. cumulate *sensu stricto* vs. slowly-cooled equivalents of the steady state basalts) but also (i) the interaction between basaltic liquids and cumulates already formed at crustal level of the Piton de la Fournaise plumbing system and (ii) the possibility that small pockets of liquids may also evolve to trachytic compositions.

1. Some textures and modal mineralogy of composite ultramafic-mafic ejecta or plagioclase-bearing wherlites can be the result

of complex processes of modification of the pristine ultramafic cumulates by the interactions with high-temperature basalts persistently rising in the plumbing system of the Piton de la Fournaise. These destabilization/disequilibrium processes of cumulate assemblages occur at low-intermediate crustal levels where the liquidus curves of plagioclase and clinopyroxene straddled with stability-in (crystallization) and out of one or the other mineral phase as soon as the melt temperature rapidly decrease for loss of energy due to olivine dissolution. The presence of textures with rounded olivines, even with fritted margins, indicate an interaction of ultramafic cumulates with basaltic melts at crustal levels leading to the transition of wherlite to plagioclase wherlite and troctolite. It is worth to note that similar processes of basaltic percolation into peridotites in mantle environments give rise to dunitization processes (Renna et al., 2011; Drouin et al., 2009, 2010; Basch et al., 2018) rather than ultramafic (wherlite) to mafic (troctolite-gabbro) transition. In addition, the behaviour of part of the olivine-diopside curve not as cotectic but as reaction curve, in the Forsterite-Diopside-Quartz system, may also explain some textures in heterogranular wherlite ejecta.

2. Some ejecta, namely porphyrogabbros, may represent, for texture and modal mineralogy, the “unerupted” counterpart of the oceanite (picritic) magmas. The micro-criptocrystalline groundmass of the porphyrogabbros, otherwise erupted as basaltic glass in the oceanites, shows a modal mineralogy with sanidine and phlogopite microlites. In this way, an evolution of the basaltic interstitial melt towards trachytic terms may finally support, as groundmass, the olivine phyric magmas of the porphyrogabbros. In these subvolcanic lithotypes, if the sustained heat flux would prevent the crystallization of the evolved interstitial melt, then small pockets of trachyte could have the opportunity to survive and be erupted as very small volumes of pumices.
3. Trachytic melts effectively erupted as pumices in the Bellecombe Ash Member, formed when interstitial basaltic melt differentiated and quenched to form glass. It is worth to note that in April 2007, Piton de la Fournaise emitted a very small volume of trachytic pumice during its largest historical eruption. The trachyte, genetically related to the evolution of basic magmas of the La Réunion mantle plume, was interpreted by Vlastelic et al. (2021) as a liquid remnant of an extinct volcano, such as Piton des Neiges or Les Alizés or partial melting of old syenite intrusions or remobilization of interstitial melts not fully crystallized. The few trachitic pumices in the Bellecombe Ash Member and the sanidine- and phlogopite-bearing micro-cryptocrystalline groundmass in the porphyrogabbro ejecta agree with the hypothesis that small pockets of trachyte melt could generally form in the Piton de la Fournaise plumbing systems. Solidification and trapping of

these very small volumes of trachytic melts in the subvolcanic crystallization processes could be locally and temporarily prevented by very high heat flux which is not unlikely for La Reunion mantle plume.

4. Finally, the preliminary investigation of some loose quartz xenocrysts on the pyroclastic products highlighted the possible hydrothermal origin of these crystals with implications on the involvement of the hydrothermal system of the Piton de la Fournaise during the most violent and explosive eruptions of the volcano.

15 Acknowledgments

Thanks to my Supervisor Alberto Renzulli for his great help in this Ph.D. work. Thanks are due to the Institute de Physique du Globe de Paris – Observatoire Volcanologique du Piton de la Fournaise for providing the samples for this Ph.D. study, and in particular thanks to Andrea Di Muro for his assistance. Thanks to Istituto Nazionale di Geofisica e Vulcanologia – sezione Palermo for noble gases and CO_2 analyses, in particular thanks to Andrea Luca Rizzo for his support and help and Mariano Tantillo for the analyses. Thanks to Michele Mattioli, Fabrizio Frontalini and Rodolfo Coccioni of Università degli Studi di Urbino for the XRD analyses and the consulting about sedimentary samples. Thanks to Università degli Studi di Perugia and Maurizio Petrelli for the LA-ICP-MS analyses. Thanks to Filippo Ridolfi and University of Hannover for EMPA analyses. Thanks to Mattia Gilio, Maria Pia Riccardi and Università degli Studi di Pavia. Thanks to University of Nancy for ICP-OES-MS analyses. Thanks to Ilenia Arienzo and Istituto Nazionale di Vulcanologia e Geofisica – Sezione di Napoli, Osservatorio Vesuviano for providing pumice samples. Thanks to Università degli Studi di Torino, Simona Ferrando and Luca Martire. Thanks to Federico Bastianelli for his informatic help in these years of study. Thanks to my friend Alberto Caracciolo for his help (and his patience) with some translations. Furthermore, I acknowledge the two rewiewers of this thesis for their valuable comments and suggestions which significantly improved the quality of the thesis.

Thanks are also due to all my family, because they support me during these three (now four) years of hard work, because they love geology as much as I do and because they animated me to fall in love with geology every single moment.

16 References

Albarède, F., Luais, B., Fitton, G., Semet, M., Kaminski, E., Upton, B. G. J., & Cheminée, J. L. (1997). The geochemical regimes of Piton de la Fournaise volcano (Réunion) during the last 530 000 years. *Journal of Petrology*, *38*(2), 171-201.

Bachelery, P. (1981).”*Le Piton de la Fournaise, Ile de la Réunion: étude volcanologique, structurale et pétrologique. _ 63*”(Doctoral dissertation, Impr. UER Sci.).

Bachèlery, P., & Mairine, P. (1990). Evolution volcano-structurale du Piton de la Fournaise depuis 0, 53 Ma. In *Le volcanisme de la Réunion-Monographie* (pp. 213-242).

Bachelery, P., Lenat, J. F., Di Muro, A., & Michon, L. (Eds.). (2015). *Active Volcanoes of the Southwest Indian Ocean: Piton de la Fournaise and Karthala*. Springer.

Bambauer, H.U. (1961): Spurenelementgehalt und -Farbzentren in Quarzen aus Zerrklüften der SchweizerAlpen. *Schweiz. Mineral. Petrogr. Mitt.*, 41, 335 369.

Basch, V., Rampone, E., Crispini, L., Ferrando, C., Ildefonse, B., & Godard, M. (2018). From mantle peridotites to hybrid troctolites: Textural and chemical evolution during melt-rock interaction history (Mt. Maggiore, Corsica, France). *Lithos*, *323*, 4-23.

Bernard A, Munschy M (2000) Were the Mascarene and Laxmi Basins (western Indian Ocean) formed at the same spreading centre? C R Acad Sci Paris Sci de la Terre et des Planètes Earth Planet Sci 330:777–783

Berthod, C., Michon, L., Famin, V., Welsch, B., Bachèlery, P., & Bascou, J. (2020). Layered gabbros and peridotites from Piton des Neiges volcano, La Réunion Island. *Journal of Volcanology and Geothermal Research*, 107039.

Boivin, P., & Bachèlery, P. (2009). Petrology of 1977 to 1998 eruptions of Piton de la Fournaise, La Réunion Island. *Journal of volcanology and geothermal research*, *184*(1-2), 109-125.

Boudoire, G., Brugier, Y. A., Di Muro, A., Wörner, G., Arienzo, I., Metrich, M., & Michon, L. (2019). Eruptive activity on the western flank of Piton de la Fournaise (La Réunion Island, Indian Ocean): insights on magma transfer, storage and evolution at an oceanic volcanic island. *J Petrol. https://doi. org/10.1093/petrology/egz04*, *5*.

Boudoire, G., Rizzo, A. L., Di Muro, A., Grassa, F., & Liuzzo, M. (2018). Extensive CO2 degassing in the upper mantle beneath oceanic basaltic volcanoes: First insights from Piton de la Fournaise volcano (La Réunion Island). *Geochimica et Cosmochimica Acta*, *235*, 376-401.

Brugier, Y. (2012). Pétrologie naturelle et expérimentale de laves du Piton de la Fournaise, La Réunion (Doctoral dissertation, Msc thesis, Université d’Orléans).

Brugier, Y. (2016). Magmatologie du Piton de la Fournaise (Ile de La Réunion). Approche volcanologique, petrologique et experimentale. (Doctoral dissertation, Université d’Orléans).

Bureau, H., Métrich, N., Pineau, F., & Semet, M. P. (1998). Magma–conduit interaction at Piton de la Fournaise volcano (Réunion

Island): a melt and fluid inclusion study. *Journal of Volcanology and Geothermal Research*, *84*(1-2), 39-60.

Bureau, H., Métrich, N., Pineau, F., & Semet, M. P. (1998). Magma–conduit interaction at Piton de la Fournaise volcano (Réunion Island): a melt and fluid inclusion study. *Journal of Volcanology and Geothermal Research*, *84*(1-2), 39-60.

Bureau, H., Métrich, N., Semet, M. P., & Staudacher, T. (1999). Fluid-magma decoupling in a hot-spot volcano. *Geophysical Research Letters*, *26*(23), 3501-3504.

Bureau, H., Pineau, F., Métrich, N., Semet, M. P., & Javoy, M. (1998). A melt and fluid inclusion study of the gas phase at Piton de la Fournaise volcano (Réunion Island). *Chemical geology*, *147*(1-2), 115-130.

Burnard, P., Zimmermann, L., & Sano, Y. (2013). The noble gases as geochemical tracers: History and background. In *The Noble Gases as Geochemical Tracers* (pp. 1-15). Springer, Berlin, Heidelberg.

Carignan, J., Hild, P., Mevelle, G., Morel, J., & Yeghicheyan, D. (2001). Routine analyses of trace elements in geological samples using flow injection and low pressure on-line liquid chromatography coupled to ICP-MS: A study of geochemical reference materials BR, DR-N, UB-N, AN-G and GH. *Geostandards Newsletter*, *25*(2-3), 187-198.

Charvis, P., Laesanpura, A., Gallart, J., Hirn, A., Lépine, J. C., de Voogd, B., ... & Pontoise, B. (1999). Spatial distribution of hotspot material added to the lithosphere under La Réunion, from wide-angle seismic data. *Journal of Geophysical Research: Solid Earth*, *104*(B2), 2875-2893.

Chevallier, L., & Bachelery, P. (1981). Evolution structurale du volcan actif du Piton de la Fournaise, Ile de la Réunion—Océan indien occidental. *Bulletin volcanologique*, *44*(4), 723-741.

Chevallier, L., & Vatin-Perignon, N. (1982). Volcano-structural evolution of Piton des Neiges, Reunion Island, Indian Ocean. *Bulletin volcanologique*, *45*(4), 285-298.

Coffin MF, Rabinowitz PD (1987) Reconstruction of Madagascar and Africa: evidence fron the Davie fracture zone and western Somali basin. J Geophys Res 92(B9):9385–9406

D'Lemos, R.S., Kearsley, A.T., Pembroke, J.W.,Watt, G.R.,Wright, P. (1997): Complex quartz growth histories in granite revealed by scanning cathodoluminescence techniques. *Geol. Mag.*, 134, 459-552.

Dennen, W. H. (1967). Trace elements in quartz as indicators of provenance. *Geological Society of America Bulletin*, *78*(1), 125-130.

Dennen,W.H. (1966): Stoichiometric substitution in natural quartz. *Geochim. Cosmochim. Acta*, 30, 1235-1241.

Dennen,W.H., Blackburn,W.H., Quesada, A. (1970): Aluminium in quartz as a geothermometer. *Contrib. Mineral. Petrol.*, 27, 332- 342.

Di Muro, A., Métrich, N., Vergani, D., Rosi, M., Armienti, P., Fougeroux, T., Civetta, L. (2014). The shallow plumbing system of Piton de la Fournaise Volcano (La Reunion Island, Indian Ocean) revealed by the major 2007 caldera-forming eruption. *Journal of Petrology*, *55*(7), 1287-1315.

Di Muro, A., Métrich, N., Allard, P., Aiuppa, A., Burton, M., Galle, B., & Staudacher, T. (2016). Magma degassing at Piton de la Fournaise volcano. In *Active Volcanoes of the Southwest Indian Ocean* (pp. 203-222). Springer, Berlin, Heidelberg.

Drouin, M., Godard, M., Ildefonse, B., Bruguier, O., & Garrido, C. J. (2009). Geochemical and petrographic evidence for magmatic impregnation in the oceanic lithosphere at Atlantis Massif, Mid-Atlantic Ridge (IODP Hole U1309D, 30 N). *Chemical Geology*, *264*(1-4), 71-88.

Drouin, M., Ildefonse, B., & Godard, M. (2010). A microstructural imprint of melt impregnation in slow spreading lithosphere: Olivine-rich troctolites from the Atlantis Massif, Mid-Atlantic Ridge, 30 N, IODP Hole U1309D. *Geochemistry, Geophysics, Geosystems*, *11*(6).

Duffield, W. A., Stieltjes, L., & Varet, J. (1982). Huge landslide blocks in the growth of Piton de la Fournaise, La Reunion, and Kilauea Volcano, Hawaii. *Journal of Volcanology and Geothermal Research*, *12*(1-2), 147-160.

Duncan RA (1990) The volcanic record of the Reunion hotspot. In: Duncan RA, Backman J, Dunbar RB, Peterson LC (eds) Proceedings of ocean drilling program science results, vol 115, pp 3–10

Duncan RA, Backman J, Peterson L (1989) Reunion hotspot activity through tertiary time: initial results from the ocean drilling program, Leg 115. J Volcanol Geoth Res 36:193–198

Dyment J (1991a) Structure et évolution de la lithosphere océanique dans l'Océan Indien: apport des anomalies magnétiques. Thesis Thesis, IPGS, Université Louis-Pasteur, Strasbourg, 374 pp

Eggins, S. M., Kinsley, L. P. J., & Shelley, J. M. G. (1998). Deposition and element fractionation processes during atmospheric pressure laser sampling for analysis by ICP-MS. *Applied Surface Science*, *127*, 278-286.

Famin, V., Welsch, B., Okumura, S., Bachèlery, P., & Nakashima, S. (2009). Three differentiation stages of a single magma at Piton de la Fournaise volcano (Reunion hot spot). *Geochemistry, Geophysics, Geosystems*, *10*(1).

Fisk, M. R., Upton, B. G. J., Ford, C. E., & White, W. M. (1988). Geochemical and experimental study of the genesis of magmas of Reunion Island, Indian Ocean. *Journal of Geophysical Research: Solid Earth*, *93*(B5), 4933-4950.

Fontaine, F. J., Rabinowicz, M., Boulègue, J., & Jouniaux, L. (2002). Constraints on hydrothermal processes on basaltic edifices:

inferences on the conditions leading to hydrovolcanic eruptions at Piton de la Fournaise, Réunion Island, Indian Ocean. *Earth and Planetary Science Letters*, *200*(1-2), 1-14.

Frezzotti M.L., Tecce F., Casagli A. (2012): Raman spectroscopy for fluid inclusion analysis. J. Geochem. Explor. 112, 1–20.

Gailler, L. S., & Lénat, J. F. (2010). Three-dimensional structure of the submarine flanks of La Réunion inferred from geophysical data. *Journal of Geophysical Research: Solid Earth*, *115*(B12).

Gallart, J., Driad, L., Charvis, P., Sapin, M., Hirn, A., Diaz, J., ... & Sachpazi, M. (1999). Perturbation to the lithosphere along the hotspot track of La Réunion from an offshore-onshore seismic transect. *Journal of Geophysical Research: Solid Earth*, *104*(B2), 2895-2908.

Georgen JE, Lin J, Dick HJB (2001) Evidence from gravity anomalies for interactions of the Marion and Bouvet hotpots with the Southwest Indian Ridge: effects of transform offsets. Earth Planet Sci Lett 187:283–300

Gillot P.-Y., Lefèvre J.-C., Nativel P. E., (1994). Model for the structural evolution of the volcanoes of Réunion island. *Earth Planet. Sci. Lett.* 122, 291-302.

Gillot, P. Y., & Nativel, P. (1989). Eruptive history of the Piton de la Fournaise volcano, Réunion island, Indian Ocean. *Journal of volcanology and geothermal research*, *36*(1-3), 53-65.

Götze, J., Plötze, M., & Habermann, D. (2001). Origin, spectral characteristics and practical applications of the cathodoluminescence (CL) of quartz–a review. *Mineralogy and petrology*, *71*(3-4), 225-250.

Helz, R. T., & Thornber, C. R. (1987). Geothermometry of Kilauea Iki lava lake, Hawaii. *Bulletin of volcanology*, *49*(5), 651-668.

Hilton, D. R., Hammerschmidt, K., Loock, G., & Friedrichsen, H. (1993). Helium and argon isotope systematics of the central Lau Basin and Valu Fa Ridge: Evidence of crust/mantle interactions in a back-arc basin. *Geochimica et Cosmochimica Acta*, *57*(12), 2819-2841.

Jenkins, R., & Snyder, R. L. (1996). *Introduction to X-ray powder diffractometry* (Vol. 138, pp. 1-202). New York: Wiley. pp. 47; 244-247.

Kent R.W., Pringle M.S., Müller R.D., Saunders A.D., Ghose N.C., (2002). 40ar/39ar geochronology of the rajmahal basalts, India, and their relationship to the kerguelen plateau. *J. Petrol.* 43, 1141-1153.

Kluska, J. M. (1997). *Evolution magmatique et morpho-structurale du Piton des Neiges au cours des derniers 500 000 ans* (Doctoral dissertation, Paris 11).

Kurz, M. D. (1986). Cosmogenic helium in a terrestrial igneous rock. *Nature*, *320*(6061), 435.

Kushiro, I. (1969). The system forsterite-diopside-silica with and without water at high pressures. *American Journal of Science*, *267*(A), 269-294.

Kushiro, I. (1972). Effect of water on the composition of magmas formed at high pressures. *Journal of Petrology*, *13*(2), 311-334.

Labazuy, P. (1996). Recurrent landslides events on the submarine flank of Piton de la Fournaise volcano (Reunion Island). *Geological Society, London, Special Publications*, *110*(1), 295-306.

Lacroix, A. F. A. (1936). *Le volcan actif de l'île de la Réunion et ses produits*. Gauthier.

Lamadrid, H. M., Moore, L. R., Moncada, D., Rimstidt, J. D., Burruss, R. C., & Bodnar, R. J. (2017). Reassessment of the Raman CO2 densimeter. *Chemical Geology*, *450*, 210-222.

Le Friant, A., Lebas, E., Clément, V., Boudon, G., Deplus, C., De Voogd, B., & Bachèlery, P. (2011). A new model for the evolution of La Réunion volcanic complex from complete marine geophysical surveys. *Geophysical Research Letters*, *38*(9).

Lehmann, G. (1975): On the colour centres of iron in amethyst and synthetic quartz: a discussion. *Am. Mineral.*, 60, 335-337.

Lehmann, G.& Bambauer, H.V. (1973): Quarzkristalle und ihre Farben. *Angew. Chem.*, 7, 281-289.

Lenat, J. F., Bachelery, P., & Desmulier, F. (2001). Genese du champ de lave de l'Enclos Fouqué; une eruption d'envergure exceptionnelle du Piton de la Fournaise (Reunion) au 18 e siecle. *Bulletin de la Société Géologique de France*, *172*(2), 177-188.

Lénat, J. F., Bachèlery, P., & Merle, O. (2012). Anatomy of Piton de la Fournaise volcano (La Réunion, Indian Ocean). *Bulletin of volcanology*, *74*(9), 1945-1961.

Lénat, J. F., Boivin, P., Deniel, C., Gillot, P. Y., & Bachèlery, P. (2009). Age and nature of deposits on the submarine flanks of Piton de la Fournaise (Reunion Island). *Journal of volcanology and geothermal research*, *184*(1-2), 199-207.

Lénat, J. F., Vincent, P., & Bachélery, P. (1989). The off-shore continuation of an active basaltic volcano: Piton de la Fournaise (Réunion Island, Indian Ocean); structural and geomorphological interpretation from sea beam mapping. *J. Volcanol. Geotherm. Res*, *36*(1-3), 1-36.

Letourneur, L., Peltier, A., Staudacher, T., & Gudmundsson, A. (2008). The effects of rock heterogeneities on dyke paths and asymmetric ground deformation: the example of Piton de la Fournaise (Réunion Island). *Journal of Volcanology and Geothermal Research*, *173*(3-4), 289-302.

Luais, B. (2004). Temporal changes in Nd isotopic composition of Piton de la Fournaise magmatism (Réunion Island, Indian Ocean). *Geochemistry, Geophysics, Geosystems*, *5*(1).

Mairine, P., & Bachèlery, P. (1997). Un grand épisode érosionnel dans l'histoire ancienne du Piton de la Fournaise (île de la Réunion). *Comptes Rendus de l'Académie des Sciences-Series IIA-Earth and Planetary Science*, *325*(4), 243-249.

Maschmeyer, D. & Lehmann, G. (1983): A trapped-hole centre causing rose coloration of natural quartz. *Z. Kristallogr.,* 163, 181-196.

McNaught, A. D., & Wilkinson, A. (1997). Compendium of chemical terminology. IUPAC recommendations.

Merle, O., & Lénat, J. F. (2003). Hybrid collapse mechanism at Piton de la Fournaise volcano, Reunion Island, Indian Ocean. *Journal of Geophysical Research: Solid Earth*, *108*(B3).

Merle, O., Mairine, P., Michon, L., Bachèlery, P., & Smietana, M. (2010). Calderas, landslides and paleo-canyons on Piton de la Fournaise volcano (La Réunion Island, Indian Ocean). *Journal of Volcanology and Geothermal Research*, *189*(1-2), 131-142.

Michon L, Di Muro A, Villeneuve N, Saint-Marc C, Fadda P, Manta F (2013) Explosive activity of the summit cone of Piton de la Fournaise volcano (La Réunion island): a historical and geological review. J Volcanol Geotherm Res 264:117–133. doi:10.1016/ j.jvolgeores.2013.06.012

Michon, L., & Saint-Ange, F. (2008). Morphology of Piton de la Fournaise basaltic shield volcano (La Réunion Island): Characterization and implication in the volcano evolution. *Journal of Geophysical Research: Solid Earth*, *113*(B3).

Mohamed-Abchir A (1996) Les Cendres de Bellecombe: un évènement majeur dans le passé récent du Piton de la Fournaise, Ile de la Réunion. PhD thesis, Univ Paris VII 248 pp

Morandi, A., Di Muro, A., Principe, C., Michon, L., Leroi, G., Norelli, F., & Bachèlery, P. (2016). Pre-historic (< 5 kiloyear) explosive activity at Piton de la Fournaise volcano. In *Active Volcanoes of the Southwest Indian Ocean* (pp. 107-138). Springer, Berlin, Heidelberg.

Müller, A. (2000): Cathodoluminescence and characterisation of defect structures in quartz with applications to the study of granitic rocks. Unpubl. Ph.D. Thesis, University Göttingen, 230 pp.

Müller, A., Seltmann, R., Behr, H.-J. (2000): Application of cathodoluminescence to magmatic quartz in a tin granite – case study from the Schellerhau Granite Complex, Eastern Erzgebirge, Germany. *Mineralium Deposita*, 35, 169-189.

Müller, A., Wiedenbeck, M., KERKHOF, A. M. V. D., Kronz, A., & Simon, K. (2003). Trace elements in quartz-a combined electron microprobe, secondary ion mass spectrometry, laser-ablation ICP-MS, and

cathodoluminescence study. *European Journal of Mineralogy*, *15*(4), 747-763.

Oehler, J. F., Labazuy, P., & Lénat, J. F. (2004). Recurrence of major flank landslides during the last 2-Ma-history of Reunion Island. *Bulletin of Volcanology*, *66*(7), 585-598.

Oehler, J. F., Lénat, J. F., & Labazuy, P. (2008). Growth and collapse of the Reunion Island volcanoes. *Bulletin of Volcanology*, *70*(6), 717-742.

Ort, M., Di Muro, A., Michon, L., & Bachèlery, P. (2014). The Bellecombe ash: indications of explosive eruptions at Piton de la Fournaise, Reunion Island. In *IAVCEI-5IMC conference. Queretaro, Mexico*.

Ort, M. H., Di Muro, A., Michon, L., & Bachèlery, P. (2016). Explosive eruptions from the interaction of magmatic and hydrothermal systems during flank extension: the Bellecombe Tephra of Piton de La Fournaise (La Réunion Island). *Bulletin of Volcanology*, *78*(1), 5.

Peltier, A., Staudacher, T., & Bachèlery, P. (2007). Constraints on magma transfers and structures involved in the 2003 activity at Piton de La Fournaise from displacement data. *Journal of Geophysical Research: Solid Earth*, *112*(B3).

Perny, B., Eberhardt, P., Ramseyer, K., Mullis, J., Pankrath, R. (1992): Microdistribution of aluminium, lithium and sodium in a quartz: possible causes and correlation with short lived cathodoluminescence. *Am. Mineral.*, 77, 534 544.

Petrelli, M., Perugini, D., Alagna, K. E., Poli, G., & Peccerillo, A. (2008). Spatially resolved and bulk trace element analysis by laser ablation-inductively coupled plasma-mass spectrometry (LA-ICP-MS). *Periodico di Mineralogia*, 77(3).

Pichavant, M., Brugier, Y., & Di Muro, A. (2016). Petrological and experimental constraints on the evolution of Piton de la Fournaise magmas. In *Active Volcanoes of the Southwest Indian Ocean* (pp. 171-184). Springer, Berlin, Heidelberg.

Putirka, K. D. (2008). Thermometers and barometers for volcanic systems. *Reviews in mineralogy and geochemistry*, *69*(1), 61-120.

Ramseyer, K., & Mullis, J. (1990). Factors influencing short-lived blue cathodoluminescence of alpha-quartz. *American Mineralogist*, *75*(7-8), 791-800.

Ramseyer, K., Baumann, J., Matter, A., & Mullis, J. (1988). Cathodoluminescence colours of α-quartz. *Mineralogical Magazine*, *52*(368), 669-677.

Rançon, J. P., Lerebour, P., & Augé, T. (1989). The Grand Brule exploration drilling: New data on the deep framework of the Piton de la Fournaise volcano. Part 1: Lithostratigraphic units and

volcanostructural implications. *Journal of Volcanology and Geothermal Research*, *36*(1-3), 113-127.

Reed, S. J. B. (2005). *Electron microprobe analysis and scanning electron microscopy in geology*. Cambridge university press.

Renna, M. R., & Tribuzio, R. (2011). Olivine-rich troctolites from Ligurian ophiolites (Italy): evidence for impregnation of replacive mantle conduits by MORB-type melts. *Journal of Petrology*, *52*(9), 1763-1790.

Rizzo, A. L., Pelorosso, B., Coltorti, M., Ntaflos, T., Bonadiman, C., Matusiak-Małek, M., ... & Bergonzoni, G. (2018). Geochemistry of noble gases and CO2 in fluid inclusions from lithospheric mantle beneath Wilcza Góra (Lower Silesia, southwest Poland). *Frontiers in Earth Science*.

Saint-Ange, F., Bachèlery, P., Babonneau, N., Michon, L., & Jorry, S. J. (2013). Volcaniclastic sedimentation on the submarine slopes of a basaltic hotspot volcano: Piton de la Fournaise volcano (La Réunion Island, Indian Ocean). *Marine Geology*, *337*, 35-52.

Salaün, A., Villemant, B., Semet, M. P., & Staudacher, T. (2010). Cannibalism of olivine-rich cumulate xenoliths during the 1998 eruption of Piton de la Fournaise (La Réunion hotspot): Implications for the generation of magma diversity. *Journal of Volcanology and Geothermal Research*, *198*(1-2), 187-204.

Sano, Y., & Wakita, H. (1985). Distribution of 3He/4He ratios and its implications for geotectonic structure of the Japanese Islands. *J. Geophys. Res*, *23*, 109-123.

Schettino A, Scotese CR (2005) Apparent polar wander paths for the major continents (200 Ma to the present day): a palaeomagnetic reference frame for global plate tectonic reconstructions. Geophys J Int 163:727– 759. doi:10.1111/j.1365-246X.2005.02638.x

Schneider, N. (1993): Das lumineszenzaktive Strukturinventar von Quarzphänokristen in Rhyolithen. *Göttinger Arb.Geol. Paläont.,* 60, 81 pp.

Smietana, M. (2011). *Pétrologie, géochronologie (K-Ar) et géochimie élémentaire et isotopique (Sr, Nd, Hf, Pb) de laves anciennes de La Réunion: Implications sur la construction de l'édifice volcanique* (Doctoral dissertation, La Réunion).

Smith W, Sandwell D (1997) Global sea floor topography from satellite altimetry and ship depth soundings. Science 277:1956–1962

Smith, J.V. & Steele, I.M. (1984): Chemical substitution in silica polymorphs. *N. Jb. Miner. Mh.*, 1984, 137-144.

Sobolev, A. V., & Nikogosian, I. K. (1994). Petrology of long-lived mantle plume magmatism: Hawaii, Pacific and Reunion Island, Indian Ocean. *Petrology*, *2*(2), 111-144.

Staudacher, T., & Allègre, C. J. (1993). Ages of the second caldera of Piton de la Fournaise volcano (Réunion) determined by cosmic ray produced3He and21Ne. *Earth and Planetary Science Letters*, *119*(3), 395-404.

Storey, B. C. (1995). The role of mantle plumes in continental breakup: case histories from Gondwanaland. *Nature*, *377*(6547), 301-308.

Upton, B. G. J., & Wadsworth, W. J. (1966). The basalts of Reunion Island, Indian Ocean. *Bulletin Volcanologique*, *29*(1), 7-23.

Upton, B. G. J., & Wadsworth, W. J. (1967). A complex basalt-mugearite sill in Piton des Neiges volcano, Reunion. *American Mineralogist: Journal of Earth and Planetary Materials*, *52*(9-10), 1475-1492.

Upton, B. G. J., Semet, M. P., & Joron, J. L. (2000). Cumulate clasts in the Bellecombe Ash Member, Piton de la Fournaise, Réunion Island, and their bearing on cumulative processes in the petrogenesis of the Réunion lavas. *Journal of volcanology and geothermal research*, *104*(1-4), 297-318.

Villemant, B., Salaün, A., & Staudacher, T. (2009). Evidence for a homogeneous primary magma at Piton de la Fournaise (La Réunion): a geochemical study of matrix glass, melt inclusions and Pélé's hairs of the 1998–2008 eruptive activity. *Journal of volcanology and geothermal research*, *184*(1-2), 79-92.

Vlastélic, I., Peltier, A., & Staudacher, T. (2007). Short-term (1998–2006) fluctuations of Pb isotopes at Piton de la Fournaise volcano (Réunion Island): origins and constraints on the size and shape of the magma reservoir. *Chemical Geology*, *244*(1-2), 202-220.

Vlastélic, I., Staudacher, T., Bachèlery, P., Télouk, P., Neuville, D., & Benbakkar, M. (2011). Lithium isotope fractionation during magma degassing: constraints from silicic differentiates and natural gas condensates from Piton de la Fournaise volcano (Réunion Island). *Chemical Geology*, *284*(1-2), 26-34.

Vlastélic, I., Bachèlery, P., Sigmarsson, O., Koga, K. T., Rose-Koga, E. R., Bindeman, I., ... & Staudacher, T. (2021). Prolonged trachyte storage and unusual remobilization at Piton de la Fournaise, La Réunion Island, Indian Ocean: Li, O, Sr, Nd, Pb and Th Isotope study. *Journal of Petrology*, *62*(7), egab048.

Wager, L. R., Brown, G. M., & Wadsworth, W. J. (1960). Types of igneous cumulates. *Journal of Petrology*, *1*(1), 73-85.

Watt,G.R., Wright, P., Galloway, S., McLean, C. (1997): Cathodoluminescence and trace element zoning in quartz phenocrysts and xenocrysts. *Geochim. Cosmochim. Acta*, 61, 4337-4348.

Weil, J.A. (1984): A review of electron spin spectroscopy and its application to the study of paramagnetic defects in crystalline quartz. *Phys. Chem. Minerals*, 10, 149-165.

Welsch, B., Faure, F., Bachèlery, P., & Famin, V. (2009). Microcrysts record transient convection at Piton de la Fournaise volcano (La Réunion hotspot). *Journal of Petrology*, *50*(12), 2287-2305.

17 Appendix

Table 7.1.1 – Subdivision of the representative analysed samples of the Bellecombe Ash Member.

ROCK TYPE	Sample	Thin section	WR EOS/MS	SEM-BSD-EDS	EMPA	Raman	Noble gas and CO_2	Thermobarometry
DUNITES	B7	X	X		X	X	X	X
	B29	X	X					
	B43	X	X		X			X
WHERLITES	B3	X	X			X	X	X
	B15	X	X		X		X	X
	B28	X	X	X				
OPHITIC GABBROS	B37	X	X					
SUB-OPHITIC GABBROS	B2	X	X		X		X	X
	B5	X	X					
	B6	X	X				X	
	B9	X	X					
	B11	X	X					
	B12	X	X					
	B14	X	X					
	B22	X	X					
	B23	X	X					
	B31	X						
	B33	X						
	B34	X	X					
	B40	X	X					
	B54	X						

	B58	X						
	B97	X						
POIKILITIC GABBROS	B21	X	X		X		X	X
	B32	X	X		X		X	X
	B41	X	X					
DOLERITIC GABBROS	B8	X	X					
	B13	X	X					
	B27	X	X					
MICRO-MONZOGABBROS	B52	X						
PORPHYROGABBROS	B4	X	X					
	B10	X	X					
	B16	X	X				X	
	B18	X						
	B20	X	X		X		X	X
SEDIMENTARY	B30	X						
VOLCANICS (lavas and sub-volcanic products)	B17	X						
	B19	X						
	B46	X						
	B56	X						
	R07-4	X						
	L4	X						
	L7	X						
	PDN1	X			X			

	p2	X			X			X
	p3	X			X			
Samples with an evident magmatic layering	B108a	X		X				
	B108b	X						

Table 7.13.1 – SEM-BSD-EDS analyses of sample B108a on single mineral phases.

Mineral phase	**Olivine**										
SiO2	37,48	37,81	36,28	36,21	36,36	37,06	36,2	35,86	36,36	37,63	53,74
TiO2	0,09	0,06	0,07	0,1	0,11	0,04	0,04	0,03	0	0,02	0,39
Al2O3	0,05	0	0,06	0,05	0	0,03	0,06	0,07	0,04	0,05	0,85
Cr2O3	0,04	0,06	0,04	0,05	0,06	0,12	0,04	0	0	0,02	0,06
FeO	20,71	18,93	26,78	26,88	25,37	21,11	26,72	29,26	28,32	19,48	13,68
MnO	0,33	0,3	0,34	0,35	0,39	0,3	0,32	0,38	0,31	0,24	0,26
MgO	40,04	41,62	35,31	35,04	36,45	40,02	35,68	33,49	34,19	41,32	28,99
CaO	0,2	0,21	0,24	0,31	0,32	0,21	0,26	0,18	0,16	0,25	1,19
Na2O	0,29	0,28	0,24	0,3	0,24	0,32	0,24	0,27	0,18	0,3	0,25
NiO	0,07	0,04	0,1	0,11	0,1	0,06	0,05	0,05	0,03	0,08	0,05
Total	99,3	99,31	99,46	99,4	99,4	99,27	99,61	99,59	99,59	99,39	99,46
Fo	77,23	79,41	69,88	69,64	71,61	76,91	70,17	66,82	68,04	78,88	78,75
Fa	22,41	20,26	29,73	29,97	27,96	22,76	29,48	32,75	31,61	20,86	20,85
N° Mg	77,51	79,67	70,15	69,91	71,92	77,17	70,42	67,11	68,27	79,08	79,07

Mineral phase	**Clinopyroxene**						
SiO2	51,4	50,22	51,79	50,09	51,06	50,19	51,62
TiO2	0,82	1,18	0,86	1,3	0,83	1,25	0,79
Al2O3	2,9	3,06	1,79	3,36	3,45	3,18	2,79
FeO	5,64	7,99	8,85	7,91	5,81	7,75	5,52
MnO	0,13	0,13	0,2	0,17	0,06	0,16	0,05

MgO	16,32	14,96	15,11	15,12	16,09	15,21	16,36
CaO	21,16	21,15	20,29	20,52	21,13	20,71	21,41
Na2O	0,42	0,42	0,56	0,44	0,37	0,41	0,31
K2O	0,11	0,05	0,07	0,12	0,04	0,1	0,09
Cr2O3	0,62	0,31	0,05	0,24	0,67	0,47	0,6
Totale	98,9	99,16	99,52	99,03	98,84	98,96	98,94
Wo	43,15	43,19	41,21	42,28	43,37	42,56	43,66
En	46,31	42,51	42,70	43,35	45,95	43,49	46,42
Fs	8,98	12,74	14,03	12,72	9,31	12,43	8,79
N° Mg	83,76	76,95	75,27	77,31	83,16	77,77	84,08
Mineral phase	**Clinopyroxene**						
SiO2	50,64	50,95	50,97	50,18	50,53	50,39	
TiO2	1,34	1,19	1,08	1,31	1,02	1,6	
Al2O3	2,98	2,29	2,85	3,01	3,83	2,99	
FeO	7,39	9,12	8,22	8,7	5,5	7,21	
MnO	0,17	0,2	0,15	0,17	0,03	0,18	
MgO	15,24	15,46	15,13	14,67	15,76	15,59	
CaO	20,82	19,58	20,49	20,61	21,32	20,8	
Na2O	0,56	0,43	0,45	0,51	0,41	0,51	
K2O	0,08	0,11	0,11	0,09	0,13	0,06	
Cr2O3	0,24	0,18	0,12	0,25	1,09	0,26	
Totale	99,22	99,33	99,45	99,25	98,53	99,33	

Wo	42,66	39,97	42,01	42,29	44,16	42,41	
En	43,45	43,91	43,16	41,88	45,42	44,23	
Fs	11,82	14,53	13,16	13,93	8,89	11,48	
N° Mg	78,61	75,14	76,64	75,04	83,63	79,40	

Mineral phase	**Feldspar**								
SiO2	48,08	56,25	49,19	46,86	47,76	55,57	47,68	46,69	62,64
TiO2	0	0,13	0	0,06	0,11	0	0,21	0	0,06
Al2O3	32,96	27,25	31,94	33,34	32,71	27,87	32,79	33,73	22,87
Cr2O3	0	0,05	0	0,06	0,05	0	0,04	0	0
FeO	0,66	0,6	0,73	0,74	0,72	0,54	0,85	0,51	0,61
MnO	0	0	0	0	0	0	0	0	0
MgO	0,24	0,21	0,27	0,26	0,27	0,24	0,2	0,37	0,2
CaO	15,43	8,94	14,61	15,97	15,23	9,69	15,34	16,59	4
Na2O	2,35	5,7	2,8	1,99	2,43	5,31	2,37	1,84	8,45
K2O	0,17	0,6	0,26	0,21	0,26	0,51	0,23	0,18	0,78
Totale	99,89	99,73	99,8	99,49	99,54	99,73	99,71	99,91	99,61
Ab %	21,39	51,65	25,35	18,17	22,06	48,27	21,55	16,54	75,62
An %	77,60	44,77	73,10	80,57	76,39	48,68	77,08	82,40	19,78
Or %	1,02	3,58	1,55	1,26	1,55	3,05	1,38	1,06	4,59

Mineral phase	**Oxides**			
SiO2	0,3	0,41	0,47	17,03
TiO2	4,3	46,25	6,08	0,05
Al2O3	12,78	0,31	3,97	5,94
Cr2O3	29,03	0,05	1,64	0,05
FeO	46,19	48,05	84,68	64,36

MnO	0	0,27	0,17	0,09
MgO	6,63	4,39	2,49	0,4
CaO	0,15	0,11	0,12	0,88
Totale	99,38	99,84	99,62	88,8

Table 7.14.1 – SEM-BSD-EDS analyses of sample B28 on single mineral phases.

Mineral phase	**Olivine**					**Mineral phase**	**Clinopyroxene**					
SiO2	37,55	37,86	37,81	37,64	37,71	SiO2	54,36	50,47	52,14	52,03	52,74	50,21
TiO2	0,06	0,08	0,03	0,05	0,05	TiO2	0,48	0,93	0,72	0,65	0,98	1,3
Al2O3	0	0	0,04	0,04	0,08	Al2O3	3,92	3,49	3,36	3,6	4,09	3,77
Cr2O3	0,02	0,03	0,04	0,1	0,06	FeO	3,79	6,49	5,29	5,53	5,03	6,85
FeO	19,44	19,31	19,33	19,37	19,08	MnO	0	0,14	0,05	0	0	0,12
MnO	0,28	0,25	0,25	0,26	0,25	MgO	18,94	15,82	16,78	16,39	17,6	15,71
MgO	41,23	41,28	41,25	41,12	41,37	CaO	16,9	20,78	19,69	20,48	18,56	20,84
CaO	0,31	0,29	0,28	0,29	0,34	Na2O	0,51	0,43	0,44	0,39	0,48	0,4
Na2O	0,28	0,3	0,3	0,28	0,29	K2O	0	0,05	0,07	0	0,02	0,08
NiO	0,09	0,07	0,04	0,05	0,06	Cr2O3	0,5	0,76	0,78	0,71	0,16	0,21
Totale	99,26	99,47	99,37	99,2	99,29	Totale	98,9	98,6	98,54	99,07	99,5	99,28
Fo	78,84	79,00	78,97	78,87	79,23	Wo	35,86	42,73	41,05	42,40	38,79	42,73
Fa	20,85	20,73	20,76	20,84	20,50	En	55,91	45,26	48,68	47,21	51,18	44,82
N° Mg	79,08	79,21	79,18	79,10	79,45	Fs	6,28	10,42	8,61	8,94	8,21	10,96
						N° Mg	89,91	81,29	84,97	84,08	86,18	80,35

Mineral phase	**Feldspar**		**Mineral phase**	**Oxids**
SiO2	47,77		SiO2	0,32
TiO2	0,05		TiO2	6,72
Al2O3	32,77		Al2O3	12,25

Cr2O3	0		Cr2O3	19,73
FeO	0,77		FeO	51,53
MnO	0		MnO	0
MgO	0,31		MgO	8,78
CaO	15,51		CaO	0,11
Na2O	2,31		Totale	99,44
K2O	0,18			
Totale	99,67			
Ab %	21,00			
An %	77,92			
Or %	1,08			

Table 8.1 – Whole rock ICP-OES compositions of representative analysed ejecta of the Bellecombe Ash Member.

Rock type	**Dunite**			**Wherlite**			**Sub-ophitic gabbro**							
Sample	**B7**	**B29**	**B43**	**B3**	**B15**	**B28**	**B2**	**B5**	**B6**	**B9**	**B11**	**B12**	**B14**	**B22**
SiO2	39.36	39.39	38.89	46.5	41.17	42.09	46.57	43.72	48.24	45.72	49.68	46.65	46.13	48.36
Al2O3	0.393	0.36	0.329	2.917	1.14	2.078	14.22	12.994	14.613	14.93	14.858	14.293	14.888	20.343
Fe2O3	14.465	16.6	15.1	9.922	15.86	15.32	7.593	7.556	9.919	5.765	11.445	11.675	7.009	5.941
MnO	0.1783	0.2059	0.1937	0.1507	0.2106	0.2034	0.1123	0.1122	0.134	0.0846	0.1545	0.1416	0.0962	0.0803
MgO	46.015	44.125	44.805	22.59	35.41	32.29	10.86	11	8.612	10.575	6.262	7.241	10.012	6.984
CaO	0.283	0.483	0.28	15.408	5.532	7.296	16.25	15.22	11.51	16.028	11.723	14.028	16.483	14.68
Na2O	< L.D.	0.031	< L.D.	0.219	0.081	0.139	1.124	1.031	2.766	1.039	2.733	2.243	1.104	2.232
K2O	< L.D.	< L.D.	< L.D.	< L.D.	< L.D.	< L.D.	0.067	0.042	0.634	0.082	0.792	0.387	0.076	0.296
TiO2	0.07	0.105	0.071	0.765	0.315	0.435	1.028	1.133	3.352	0.731	2.602	2.954	1.371	1.227
P2O5	< L.D.	< L.D.	< L.D.	< L.D.	< L.D.	< L.D.	< L.D.	< L.D.	0.22	< L.D.	0.29	< L.D.	< L.D.	< L.D.
Total	99.6543	100.4899	99.69869	99.1617	99.37861	99.94139	99.55431	99.7682	99.78	99.8446	100.33	99.1826	100.1692	100.1033

Rock type	**Sub-ophitic gabbro**			**Poikilitic gabbro**			**Ophitic gabbro**	**Doleritic gabbro**			**Porphyrogabbro**			
Sample	**B23**	**B34**	**B40**	**B21**	**B32**	**B41**	**B37**	**B8**	**B13**	**B27**	**B4**	**B10**	**B16**	**B20**
SiO2	47.38	47.22	41.55	46.83	41.5	43.15	47.36	46.65	46.94	46.7	42.91	42.97	42.04	41.94
Al2O3	15.843	12.816	15.625	13.756	7.475	9.582	10.153	13.646	15.343	13.816	7.158	6.756	6.375	4.047
Fe2O3	6.233	7.402	16.36	7.462	15.87	13.995	6.862	12.97	9.329	12.755	14.325	14.485	14.625	15.09
MnO	0.0922	0.1064	0.1325	0.1042	0.2059	0.1718	0.1109	0.1723	0.133	0.1691	0.1865	0.1855	0.1902	0.1961
MgO	9.819	10.315	6.625	13.615	25.445	17.865	11.885	7.009	8.915	6.905	24.83	27.275	28.21	33.63
CaO	16.583	17.808	13.905	15.178	7.49	12.065	18.553	11.863	14.575	11.718	6.487	5.834	5.438	3.595
Na2O	1.294	1.058	1.65	1.082	0.542	0.831	0.748	2.342	2.016	2.378	1.197	1.095	0.918	0.838
K2O	0.067	0.057	0.099	0.071	< L.D.	0.033	< L.D.	0.683	0.332	0.713	0.315	0.293	0.259	0.29
TiO2	0.829	1.293	3.584	0.784	0.384	1.269	1.274	3.297	2.021	3.116	1.302	1.198	1.137	0.781

P2O5	< L.D.	< L.D.	< L.D.	< L.D.	< L.D.	< L.D.	< L.D.	0.32	< L.D.	0.35	0.13	0.15	0.11	0.11
Total	99.89021	99.6854	99.77049	98.8022	99.5019	98.6718	99.7159	100.33	99.944	100.4	98.72	99.11	100.01	99.66

Table 8.1 – Continue. Whole rock ICP-MS compositions of representative analysed ejecta of the Bellecombe Ash Member.

Rock type	**Dunite**			**Wherlite**			**Sub-ophitic gabbro**							
Sample	**B7**	**B29**	**B43**	**B3**	**B15**	**B28**	**B2**	**B5**	**B6**	**B9**	**B11**	**B12**	**B14**	**B22**
As	< L.D.	< L.D.	< L.D.	< L.D.	< L.D.	< L.D.	< L.D.	< L.D.	< L.D.	< L.D.	< L.D.	< L.D.	< L.D.	< L.D.
Ba	< L.D.	< L.D.	< L.D.	< L.D.	< L.D.	< L.D.	24.533	20.5431	117.6989	24.6039	128.8332	78.2151	23.1044	66.7128
Be	< L.D.	< L.D.	< L.D.	0.1077	< L.D.	0.0701	0.2388	0.2838	0.9873	0.1724	1.0651	0.5794	0.2485	0.5178
Bi	< L.D.	0.0733	< L.D.	0.0974	< L.D.	< L.D.	< L.D.	< L.D.	< L.D.	< L.D.	0.0564	0.0634	< L.D.	< L.D.
Cd	0.0298	0.03	0.0299	0.2264	0.0935	0.0904	0.1351	0.3072	0.1358	0.0636	0.1288	0.1332	0.1271	0.0777
Co	168.5371	169.0781	165.3549	77.2169	151.9122	137.8273	42.4135	41.3554	42.3577	38.1329	38.426	44.5825	37.5853	28.7782
Cr	3556.6429	1625.2103	3511.8354	3921.1512	2441.6341	2309.9943	958.5664	723.8789	338.9905	212.223	174.5259	102.1788	927.61	336.09
Cs	< L.D.	< L.D.	< L.D.	< L.D.	< L.D.	< L.D.	0.0224	< L.D.	0.2082	0.0327	0.2222	0.12	0.0279	0.1607
Cu	5.0771	15.2647	4.9343	10.5433	7.2828	14.7801	20.3033	27.8878	31.3634	12.85	44.4919	84.6075	15.9179	18.827
Ga	1.6836	1.4296	1.1215	5.547	2.4023	3.723	14.386	14.3737	20.8135	13.8124	21.4588	21.3644	14.5171	20.6735
Ge	0.8494	0.8162	0.8345	1.8046	1.2388	1.3164	1.4463	1.4848	1.4916	1.2589	1.5667	1.529	1.3464	1.1161
Hf	0.0433	0.1046	0.0461	0.8492	0.3454	0.5293	1.2201	1.5371	3.7235	1.0034	4.4844	2.8001	1.3558	1.8496
In	< L.D.	< L.D.	< L.D.	0.0529	0.0309	0.0358	0.0477	0.0577	0.0856	0.0424	0.0829	0.0879	0.0552	0.0474
Mo	< L.D.	< L.D.	< L.D.	< L.D.	< L.D.	< L.D.	< L.D.	< L.D.	0.6414	< L.D.	0.9072	0.5656	< L.D.	< L.D.
Nb	0.0731	0.2214	0.1816	0.9714	0.4475	0.7722	2.6552	2.6761	18.4663	1.9308	18.0519	10.5604	3.466	6.5935
Ni	2303.6328	2227.5309	2274.3222	711.7977	1383.0793	1226.8081	168.9093	185.9505	176.1571	195.162	69.7067	102.5265	187.4529	144.1745
Pb	1.4199	< L.D.	1.2323	3.5929	< L.D.	0.8964	1.1208	< L.D.	2.3291	0.8238	1.7251	1.6438	0.4824	1.9972
Rb	< L.D.	0.2335	< L.D.	0.2734	< L.D.	0.3789	1.1177	0.3603	14.9476	1.5033	19.1467	9.1236	1.2523	6.6327
Sb	< L.D.	< L.D.	< L.D.	< L.D.	< L.D.	< L.D.	< L.D.	< L.D.	< L.D.	< L.D.	< L.D.	< L.D.	< L.D.	< L.D.
Sc	4.45	5.32	4.75	69.34	27.55	34.49	52.07	55.73	37.18	48.67	35.2	46.41	52.25	30.89
Sn	< L.D.	< L.D.	< L.D.	0.4907	0.4197	< L.D.	0.4941	0.6016	1.4912	0.424	2.2197	1.1784	0.9638	0.687
Sr	1.3262	3.4768	1.0796	26.8132	10.3074	23.316	360.6072	319.0316	405.2594	328.6908	352.5668	422.0717	338.3764	574.084
Ta	0.0076	0.02	0.0156	0.0862	0.0396	0.0686	0.2284	0.2304	1.5752	0.1638	1.478	0.8852	0.313	0.5593
Th	0.0257	0.0347	0.0231	0.1175	0.0538	0.1138	0.272	0.2864	1.8151	0.2375	2.3488	1.0192	0.3729	0.8835
U	< L.D.	0.0102	< L.D.	0.0295	0.0138	0.0284	0.0623	0.0697	0.4408	0.0614	0.5825	0.255	0.0909	0.2237
V	27.3713	27.6552	22.1252	193.5274	78.8363	97.9822	173.2096	182.4005	314.0072	146.1379	283.2509	446.232	183.4892	147.3704
W	< L.D.	< L.D.	< L.D.	< L.D.	< L.D.	< L.D.	< L.D.	< L.D.	< L.D.	< L.D.	< L.D.	< L.D.	< L.D.	< L.D.
Y	0.4204	0.7596	0.4726	8.0524	3.0918	4.6294	8.9766	10.2831	20.9458	7.6382	25.1473	15.8182	8.9554	9.9845
Zn	106.8647	127.9181	110.905	58.4987	102.8215	102.3621	48.2442	44.3361	81.5842	33.7325	98.9431	89.4978	38.6339	45.2235
Zr	1.9346	3.8184	1.7864	22.4099	9.6336	15.2991	35.6697	42.7871	141.5424	29.2465	176.3469	101.3952	41.7361	68.6569
La	0.118	0.2425	0.3062	1.7738	0.6993	1.1755	3.4898	3.4458	13.7537	3.1178	18.028	7.9136	3.7219	7.2301

Ce	0.3153	0.6476	0.4342	5.1102	1.9232	3.0795	8.4675	9.4019	29.7166	6.9687	38.9158	17.9211	8.7655	15.4561
Pr	0.047	0.1043	0.0792	0.8924	0.3404	0.5621	1.338	1.5763	4.0639	1.1279	5.2605	2.6098	1.373	2.1125
Nd	0.2224	0.5165	0.3434	4.8398	1.9071	2.9281	6.7305	7.978	17.9686	5.742	23.0552	12.4814	6.7644	9.4972
Sm	0.0667	0.1549	0.0867	1.6411	0.6179	0.9531	2.0575	2.4924	4.6287	1.6493	5.6444	3.4659	2.009	2.3503
Eu	0.0207	0.0476	0.0232	0.5749	0.217	0.3313	0.878	0.9664	1.6858	0.6906	1.8028	1.4566	0.8228	1.1289
Gd	0.0654	0.1447	0.0735	1.8387	0.6652	1.0353	2.0731	2.5669	4.5336	1.7523	5.4879	3.526	2.0656	2.292
Tb	0.0114	0.0245	0.0123	0.3018	0.1109	0.1675	0.3278	0.4039	0.7125	0.2782	0.8708	0.5718	0.3373	0.3608
Dy	0.0752	0.1476	0.0779	1.8188	0.663	1.0064	1.9616	2.3667	4.2844	1.6623	5.1057	3.3445	1.9381	2.0902
Ho	0.0169	0.031	0.0171	0.3466	0.1302	0.1917	0.3694	0.444	0.8247	0.3111	0.9961	0.6465	0.3673	0.3991
Er	0.049	0.0854	0.047	0.8137	0.3058	0.4545	0.8539	1.0259	2.0134	0.7247	2.4206	1.537	0.8711	0.9458
Tm	0.0085	0.013	0.0078	0.1054	0.0403	0.059	0.1145	0.1352	0.2805	0.0965	0.346	0.2123	0.1165	0.1315
Yb	0.0637	0.0915	0.0553	0.6093	0.2436	0.3567	0.6683	0.7803	1.6925	0.5488	2.0271	1.2219	0.6584	0.7572
Lu	0.0122	0.0167	0.0087	0.0846	0.0357	0.0513	0.0939	0.1101	0.2462	0.0773	0.2991	0.176	0.0932	0.114

Rock type	**Sub-ophitic gabbro**	**Sub-ophitic gabbro**	**Sub-ophitic gabbro**	**Poikilitic gabbro**	**Poikilitic gabbro**	**Poikilitic gabbro**	**Ophitic gabbro**	**Doleritic gabbro**	**Doleritic gabbro**	**Doleritic gabbro**	**Porphyro gabbro**	**Porphyro gabbro**	**Porphyro gabbro**	**Porphyro gabbro**
Sample	**B23**	**B34**	**B40**	**B21**	**B32**	**B41**	**B37**	**B8**	**B13**	**B27**	**B4**	**B10**	**B16**	**B20**
As	< L.D.	< L.D.	< L.D.	< L.D.	< L.D.	< L.D.	< L.D.	< L.D.	< L.D.	< L.D.	< L.D.	< L.D.	< L.D.	< L.D.
Ba	21.4485	20.1253	34.891	19.9142	11.3032	16.0676	12.216	141.1865	70.8336	148.2733	60.633	63.5944	48.7911	56.327
Be	0.1903	0.2092	0.2668	0.2011	0.1221	0.2039	0.2059	1.086	0.5954	1.1105	0.5041	0.4426	0.3574	0.3719
Bi	< L.D.	< L.D.	< L.D.	0.0803	< L.D.	< L.D.	< L.D.	< L.D.	0.082	< L.D.	< L.D.	< L.D.	0.2234	< L.D.
Cd	0.0857	0.1055	0.12	0.1128	0.0607	0.0962	0.2205	0.2159	0.1428	0.2342	0.1001	0.0919	0.1081	0.0653
Co	37.9905	36.8434	63.2784	51.2614	124.0875	84.2485	34.7331	45.5879	41.326	45.4957	108.372	118.0504	118.8594	139.3364
Cr	124.8525	550.0253	45.9679	1933.344 1	1205.414 5	4288.197 2	1381.99 75	379.5522	333.7561	382.6178	1611.674 5	1815.506 7	2029.951 1	2658.048 7
Cs	< L.D.	< L.D.	0.0362	0.0232	< L.D.	< L.D.	< L.D.	0.2928	0.2148	0.3042	0.1019	0.1172	0.0956	0.0779
Cu	54.6905	23.6939	54.4371	16.9442	16.0156	18.9535	58.0853	123.1429	44.934	118.0934	39.9928	36.7014	20.0561	9.5923
Ga	15.8037	14.4345	23.578	13.1601	7.6131	13.5117	12.9347	21.9058	18.8446	22.4384	10.5525	9.8751	9.1738	7.201
Ge	1.322	1.5031	1.2917	1.3542	1.1071	1.3342	1.7947	1.5565	1.5209	1.6344	1.1959	1.2277	1.2139	1.1097
Hf	1.1399	1.4268	1.5949	0.9735	0.4555	1.088	1.7036	4.3206	2.5495	4.4732	2.0695	1.8466	1.6529	1.6905
In	0.0483	0.0593	0.0723	0.0416	0.0333	0.0563	0.073	0.095	0.1652	0.0964	0.0525	0.0521	0.1644	0.0394
Mo	< L.D.	< L.D.	< L.D.	< L.D.	< L.D.	< L.D.	< L.D.	0.8822	0.8755	0.9005	0.5124	< L.D.	< L.D.	< L.D.
Nb	1.4813	2.0137	3.6804	1.9496	0.4893	0.7174	1.4959	21.5047	7.7691	21.382	8.4017	7.8089	7.2888	6.876

Ni	145.568	146.3144	108.5797	390.4179	850.4694	589.7472	203.3379	106.7598	160.7673	106.2346	1012.7243	1146.5742	1178.8159	1562.5295
Pb	< L.D.	0.7915	0.586	1.1608	< L.D.	< L.D.	< L.D.	1.7155	2.3388	1.7705	2.0904	0.8769	1.6641	0.6597
Rb	0.8414	0.83	1.1103	1.1441	0.2484	0.4561	0.3021	15.7455	6.9663	16.9948	7.4673	7.0625	6.3108	6.7803
Sb	< L.D.	< L.D.	< L.D.	< L.D.	< L.D.	< L.D.	< L.D.	< L.D.	< L.D.	< L.D.	< L.D.	0.0639	< L.D.	< L.D.
Sc	55.05	65.89	47.05	45.81	23.31	45.71	84.85	38.53	47.31	37.39	22.21	20.76	21.06	15.08
Sn	0.5012	0.5627	1.0357	0.8165	0.4221	0.558	0.6813	1.5402	1.6966	1.6554	0.8948	0.9372	0.8571	0.9436
Sr	367.4287	314.8451	401.5141	287.3118	181.1577	222.3178	172.9135	370.1421	426.9755	376.3446	196.661	176.9609	143.3316	103.856
Ta	0.1303	0.178	0.33	0.1663	0.0486	0.0869	0.1366	1.7607	0.6989	1.7781	0.6987	0.6353	0.6043	0.5536
Th	0.1818	0.2113	0.3556	0.2245	0.0596	0.1385	0.1798	2.237	0.7935	2.3793	0.9474	0.878	0.7534	1.0624
U	0.0459	0.0503	0.0937	0.0552	0.0153	0.0289	0.0444	0.5348	0.169	0.5877	0.2461	0.2217	0.1878	0.1906
V	171.0035	245.908	709.3181	146.016	83.0706	300.2687	270.4003	369.9093	257.906	361.7314	156.1557	145.2547	139.3597	108.6753
W	< L.D.	< L.D.	< L.D.	< L.D.	< L.D.	< L.D.	< L.D.	< L.D.	< L.D.	< L.D.	< L.D.	< L.D.	< L.D.	< L.D.
Y	8.7325	10.1781	10.2959	7.5554	3.8437	8.4996	13.418	24.943	14.9248	25.7504	11.1959	10.5551	8.5443	8.9211
Zn	33.0323	40.5406	104.4528	48.0994	117.5548	116.8877	34.807	112.4472	61.7997	113.6664	111.6817	112.375	111.001	112.7347
Zr	29.3896	37.3924	47.0865	29.1306	12.2737	27.8801	40.9554	177.9659	85.579	176.1766	83.867	74.5281	66.1044	69.1597
La	2.7139	2.9859	4.1226	2.8023	1.338	2.5132	2.7933	20.0214	7.5066	21.1138	8.1929	7.7927	5.5522	7.6034
Ce	6.7707	7.9051	10.079	6.8733	3.288	6.3066	8.207	42.0701	17.0843	44.6289	17.7312	16.9548	11.9997	15.8931
Pr	1.138	1.3468	1.5576	1.1008	0.5274	1.0873	1.4768	5.8426	2.5791	6.1966	2.4552	2.3912	1.7261	2.1214
Nd	6.0049	7.1889	7.8154	5.5885	2.6993	5.65	7.9265	25.3643	12.0345	27.1186	10.9067	10.5932	7.7049	9.118
Sm	1.9033	2.2377	2.3046	1.6631	0.8489	1.8184	2.7121	6.1512	3.3621	6.3703	2.6427	2.5686	1.9745	2.0869
Eu	0.7884	0.9106	0.9477	0.6905	0.3854	0.7136	0.9976	2.0327	1.401	2.1544	0.9401	0.8865	0.7334	0.6804
Gd	2.0176	2.3754	2.3766	1.7221	0.8681	1.9529	3.0084	5.8052	3.4866	6.1599	2.5334	2.4468	1.9085	2.0053
Tb	0.3272	0.3838	0.3816	0.2822	0.14	0.3095	0.498	0.8825	0.5498	0.9307	0.3926	0.3773	0.3081	0.3076
Dy	1.9189	2.2632	2.2314	1.6441	0.8468	1.8498	2.951	5.2029	3.292	5.4196	2.2698	2.1966	1.8092	1.7899
Ho	0.3712	0.4263	0.423	0.3128	0.1591	0.3459	0.5552	0.9812	0.6195	1.0306	0.4372	0.4228	0.3443	0.3465
Er	0.8481	0.9808	0.9795	0.7286	0.3854	0.8279	1.2901	2.4224	1.4648	2.5196	1.0746	1.0295	0.8533	0.8747
Tm	0.1112	0.1319	0.1326	0.0961	0.0534	0.1109	0.1698	0.3214	0.1969	0.3449	0.1484	0.1407	0.1178	0.1192
Yb	0.639	0.7156	0.7779	0.5508	0.3272	0.6473	0.9675	1.9211	1.1538	2.0119	0.8708	0.8357	0.717	0.7197
Lu	0.091	0.1018	0.1085	0.08	0.0483	0.0886	0.1359	0.2732	0.1654	0.285	0.129	0.1205	0.1017	0.104

Table 9.1 – Single mineral phase EMPA analyses. Sample: sub-ophitic gabbro B2. Clinopyroxenes.

Sample	B2_1_Cpx rim detail to glass	B2_1_Cpx rim detail to glass	B2_1_Cpx rim detail to glass	B2_1_Cpx rim detail to glass	B2_1_Cpx rim detail to glass	B2_1_Cpx rim detail1 to glass	B2_1_Cpx rim detail1 to glass	B2_1_C px c-r	B2_1_C px c-r	B2_1_C px c-r	B2_1_C px c-r	B2_1_C px c-r	B2_1_C px c-r	B2_1_C px c-r
SiO2	50.4226412	50.583884	50.6191558	50.8469113	51.333663	51.013193	51.3104844	51.2147465	50.6947 3841	51.0202 4733	51.1875 3674	51.2147 4647	51.1280 7846	50.8670 6666
TiO2	1.60106684	1.52628893	1.53755683	1.45663279	1.40439068	1.36648955	1.32756406	1.31629615	1.22615 2916	1.29068 728	1.27941 9375	1.30400 3894	1.24766 437	1.25688 3565
Al2O3	3.43137182	3.39515408	3.30098797	3.21510019	3.17577808	3.02883755	3.10023823	3.69834827	3.62901 7178	3.60935 6121	3.71387 0161	3.84942 7974	3.62591 2801	3.68386 1179
FeO	8.33908075	8.47288481	8.33805149	8.65094714	8.67770795	8.27114946	8.50993824	6.18586464	6.20850 8403	6.31555 1651	6.39377 5563	6.46170 6856	6.46479 4642	6.50699 4384
Mno	0.23222222	0.17444444	0.17777778	0.24444444	0.26555556	0.23111111	0.36111111	0.13777778	0.17888 8889	0.11888 8889	0.17333 3333	0.14888 8889	0.18777 7778	0.15111 1111
MgO	14.1274497	14.2825023	14.30998	14.2039947	13.9753412	13.9007589	14.0440354	15.1500117	14.9831 8299	14.9488 359	15.0283 2488	15.0037 9125	14.9184 1419	15.2550 1569
CaO	21.9667688	21.5686224	21.8465165	21.8738006	21.5797381	22.1153158	21.403907	22.2689154	22.8772 5084	22.7984 2998	22.6569 5663	22.4083 6775	22.4154 4141	22.7266 8278
Na2O	0.37333717	0.38893622	0.36501768	0.37957679	0.3712573	0.38789628	0.40349533	0.28494258	0.26622 3721	0.26622 3721	0.25062 4675	0.28390 264	0.25686 4293	0.25790 4229
K2O	0.02428978	0.01795332	0.02006547	0.02112155	0.03168232	0.02217763	0.04435525	0.01161685	0.00739 2542	0.03590 6633	0.01900 9394	0.01689 7239	0.01267 2929	0.00316 8232
Cr2O3	0	0.06043839	0	0.06043839	0	0.02253635	0	0.28375312	0.16185 1961	0.25302 1736	0.25507 0495	0.12394 9919	0.32575 268	0.21716 8454
Total	100.518228	100.41067	100.515109	100.892529	100.815114	100.336929	100.505129	100.26852	100.071 3559	100.404 1275	100.702 8508	100.691 733	100.257 6209	100.708 6878
Fe2O3	2.19200245	1.88770406	2.0651084	2.12597057	0.75374397	1.3774674	0.87728182	0.65865289	2.03216 3277	1.43108 1828	1.18500 2598	1.03735 2013	0.78430 2773	2.29625 0333
FeO	6.36669281	6.77430791	6.47984421	6.73797541	7.99948083	7.03168912	7.7205504	5.59320151	4.37994 5509	5.02784 8464	5.32749 7177	5.52828 6091	5.75907 037	4.44080 3049
Wo	45.0062278	44.2355709	44.6520263	44.5707876	44.5216949	45.4909678	44.2986407	45.7336957	46.6382 13	46.5183 611	46.2278 509	45.8792 9525	46.0429 4839	45.9141 8365
En	40.2736604	40.7572085	40.6957353	40.2705405	40.1179595	39.7851904	40.4427015	43.291347	42.5004 031	42.4402 3089	42.6641 9973	42.7423 5293	42.6372 6996	42.8819 3496
Fs	13.3359194	13.5637219	13.3021517	13.7590378	13.9742624	13.2799441	13.7474485	9.91598796	9.87924 3439	10.0584 0465	10.1825 8079	10.3264 7536	10.3649 9056	10.2609 9782
Mg#	75.1239994	75.0303946	75.3654219	74.5342491	74.1658561	74.9742572	74.6310935	81.3634944	81.1391 5597	80.8406 3606	80.7318 8056	80.5413 5413	80.4442 4811	80.6916 9825

Sample	B2_1_Cpx c-r	B2_1_Cpx c-r	B2_1_Cpx c-r	B2_1_Cpx c-r	B2_1_Cpx c-r	B2_1_Cpx c-r	B2_1_Cpx c-r	B2_1_Cpx c-r	B2_1_Cpx c-r	B2_1_Cpx c-r	B2_1_Cpx c-r	B2_1_Cpx c-r	B2_1_Cpx c-r
SiO2	50.9073774	51.0716435	51.2308707	51.0877678	51.0706357	51.1693969	51.0887755	50.8590045	50.6977 6172	51.1180 0078	51.6138 2241	50.7622 5884	51.3860 6695	50.8166 7829
TiO2	1.27532195	1.25278615	1.27122453	1.26098099	1.29376034	1.28044373	1.2333234	1.27737066	1.28249 244	1.29785 7765	1.25790 792	1.30502 8249	1.24868 8725	1.28351 6795
Al2O3	3.67040888	3.62694759	3.62384322	3.6952439	3.72835726	3.66006095	3.68386118	3.69524 39	3.74491 3935	3.65695 6575	3.69627 8689	3.63729 5518	3.64039 9895	3.65385 2198
FeO	6.23732774	6.52860889	6.40509745	6.38142442	6.35878066	6.52346258	6.3279028	6.31658091	6.37010 2537	6.33922 4677	6.33099 0581	6.30937 6079	6.48846 7668	6.20850 8403
MnO	0.13777778	0.14333333	0.19	0.14888889	0.12666667	0.14777778	0.11	0.15444444	0.09111 1111	0.14888 8889	0.14333 3333	0.16	0.11	0.11555 5556
MgO	14.8438319	15.1882842	15.0351943	14.9841643	15.0773922	15.1205714	15.0440264	15.0440264	15.1745 4536	15.0116 4201	15.0646 3467	14.8497 2	15.0793 5485	15.0391 1968
CaO	22.9318191	22.4720308	22.7701353	22.7620511	22.7398196	22.5326622	22.5346832	22.4619255	22.4780 939	22.4669 7813	22.8226 8255	22.8408 7198	22.4487 887	22.1476 5258
Na2O	0.29638188	0.30262149	0.24646493	0.26206398	0.30366143	0.24542499	0.25790423	0.27454321	0.29326 2067	0.31822 0541	0.29950 1686	0.26726 3657	0.30782 1177	0.30054 1622
K2O	0.01478508	0.00316823	0.01795332	0.00633646	0.02534586	0.02534586	0.00739254	0.00739254	0.01056 0774	0.01161 6852	0.02428 9781	0.02217 7626	0.01478 5084	0
Cr2O3	0.09321853	0.17414451	0.14136437	0.13316933	0.21204656	0.1946321	0.16390072	0.22536349	0.19872 9623	0.17414 4515	0.20487 59	0.10038 9191	0.21716 8454	0.14853 5027
Total	100.315032	100.589424	100.790784	100.588922	100.72442	100.705146	100.287869	100.090532	100.142 8438	100.369 3862	101.253 4416	100.153 992	100.724 3731	99.5654 2512
Sample	B2_1_Cpx c-r	B2_1_Cpx c-r	B2_1_Cpx c-r	B2_1_Cpx c-r	B2_1_Cpx c-r	B2_1_Cpx c-r	B2_1_Cpx c-r	B2_1_Cpx c-r	B2_1_Cpx c-r	B2_1_Cpx c-r	B2_1_Cpx c-r	B2_1_Cpx c-r	B2_1_Cpx c-r	B2_1_Cpx c-r
Fe2O3	1.72237896	1.81331137	1.40628758	1.46896191	1.77847722	1.37153895	1.14480783	1.37728173	1.98441 0571	1.25433 0192	1.15369 0114	1.74215 5927	1.10082 9558	0.97577 157
FeO	4.68751218	4.89697135	5.1397044	5.05963631	4.75848727	5.28933673	5.29779211	5.07728764	4.58450 8055	5.21056 4558	5.29288 7513	4.74176 4993	5.49792 911	5.33049 84
Wo	46.8088644	45.6299108	46.3414849	46.390495	46.189777	45.884491	46.108829	46.0084247	45.7851 241	45.9653 8392	46.3243 1682	46.6987 2667	45.7655 3293	45.7001 9948
En	42.1586333	42.9108298	42.5759432	42.4913998	42.6123985	42.8422738	42.8299553	42.8751217	43.0062 4265	42.7331 9124	42.5453 2404	42.2436 5842	42.7739 415	43.1781 1783
Fs	9.93771432	10.3472823	10.1748595	10.1515788	10.0816367	10.3688343	10.1062673	10.0988237	10.1276 7332	10.1232 6767	10.0302 6362	10.0687 8623	10.3249 0592	9.99944 77
Mg#	80.924355	80.5714437	80.7114603	80.7161771	80.8675942	80.5137787	80.9085975	80.936244	80.9393 4329	80.8476 2415	80.9222 035	80.7525 9854	80.5553 1066	81.1961 1607

Table 9.1 – Continue. Single mineral phase EMPA analyses. Sample: sub-ophitic gabbro B2. Clinopyroxenes.

Sample	B2_1_Cpx c-r	B2_1_Cpx c-r	B2_1_Cpx c-r	B2_4_Cpx c-r	B2_4_Cpx c-r	B2_4_Cpx c-r	B2_4_Cpx c-r	B2_4_Cpx c-r	B2_4_Cpx c-r	B2_4_Cpx c-r	B2_4_Cpx c-r	B2_4_Cpx c-r	B2_4_Cpx c-r	B2_4_Cpx c-r
SiO2	50.9829599	50.9184628	51.8254536	50.8852065	51.1532726	51.0424182	51.3800203	50.8771443	50.35209745	50.13341189	50.44581983	51.29032903	50.43271885	50.75621223
TiO2	1.30195518	1.24868873	1.15547242	1.13703403	1.19951969	1.22922598	1.27634631	1.41053681	1.595945065	1.57033619	1.58262845	1.550873446	1.581604095	1.565214415
Al2O3	3.66213054	3.60521695	3.26787461	3.28857046	3.43240661	3.29477921	3.38687574	3.35479717	3.668339292	3.724218085	3.666269707	3.594869027	3.280292117	3.42412827
FeO	6.48846767	6.430829	6.25379593	6.28467379	6.42671195	6.79724627	6.97839638	7.27070679	7.715347975	8.128082039	8.081765249	8.162047685	7.999424288	8.298939531
Mno	0.13	0.12666667	0.19555556	0.14111111	0.07222222	0.14222222	0.14333333	0.16	0.15	0.184444444	0.113333333	0.174444444	0.223333333	0.24
MgO	14.9439292	15.0381383	15.3138964	15.0783735	15.1029071	15.2137992	14.8664029	14.9243023	14.70546222	14.33451362	14.42283472	13.23933205	14.48956621	14.37180475
CaO	22.0263897	22.5791463	22.3002417	22.8065142	22.2153577	22.5367043	22.0647896	22.5306411	22.32449426	22.35683103	21.93948465	21.58782233	22.13249472	21.80205342
Na2O	0.26726366	0.32134035	0.32861991	0.28182277	0.28806239	0.31302086	0.37437711	0.36397774	0.218386646	0.323420223	0.381656662	0.297421813	0.415974563	0.395175835
K2O	0.01056077	0.00211215	0.01267293	0.01795332	0	0	0.01161685	0	0	0.011616852	0.011616852	0.012672929	0.012672929	0.010560774
Cr2O3	0.17619327	0.16697386	0.20692466	0.11575488	0.10141357	0.0348289	0.11882802	0.00204876	0.146486268	0.037902041	0.052243354	0.027658246	0.020487592	
Total	99.8136566	100.270601	100.653583	99.9212596	99.8904603	100.569416	100.482159	100.892106	100.7300729	100.7668744	100.6454095	99.90981276	100.5680811	100.8640892
Fe2O3	0.54505217	1.84713333	0.80683677	2.15063686	1.00174937	2.4682552	1.10432427	2.75910831	2.163289334	2.984192564	2.276213279	0	2.922457881	2.048107087
FeO	5.99802373	4.76875808	5.52779532	4.34950707	5.52532683	4.57628306	5.98471324	4.78803075	5.768796416	5.442872709	6.033603476	8.162047685	5.369764507	6.456030222
Wo	45.5396368	45.9820886	45.4328163	46.3528392	45.5539696	45.4578521	45.1460054	45.3971803	45.37221945	45.41170171	44.76878565	46.01175805	44.90269687	44.50147552
En	42.9894553	42.611434	43.4106904	42.6405527	43.0907812	42.6979557	42.3229893	41.8408273	41.58512129	40.51271901	40.94967096	39.26241101	40.9023573	40.81682491
Fs	10.4709657	10.2222497	9.9449394	9.9700771	10.2863216	10.7016281	11.1448318	11.4348456	12.23946006	12.88676643	12.87222047	13.57867727	12.66773983	13.22202453
Mg#	80.4136117	80.6520217	81.3610308	81.0493105	80.7289623	79.9593417	79.1560015	78.5364595	77.26046398	75.86724606	76.08367129	74.30280542	76.3529646	75.53237223

Sample	B2_4_Cpx c-r	B2_4_Cpx c-r	B2_6_Cpx c-r	B2_6_Cpx c-r	B2_6_Cpx c-r	B2_6_Cpx c-r	B2_6_Cpx c-r	B2_6_Cpx c-r	B2_6_Cpx c-r	B2_6_Cpx c-r	B2_6_Cpx c-r	B2_6_Cpx c-r	B2_6_Cpx c-r	B2_6_Cpx c-r

SiO2	50.8338103	50.9940454	50.4307033	50.497216	50.1787614	50.0729458	49.8955788	50.9194706	50.47101402	50.56876747	50.12837306	50.4528742	49.97418462	50.30372461
TiO2	1.41975601	1.28863857	1.42282907	1.4996557	1.48941215	1.47814424	1.42282907	1.53243506	1.467900692	1.444340527	1.487363437	1.591847645	1.621553939	1.638967974
Al2O3	3.10541219	2.98744585	3.56382525	3.55658171	3.58969506	3.55554691	3.60107778	3.70973099	3.624878008	3.565894838	3.597973404	3.478972271	3.578312347	3.599008197
FeO	8.51302603	8.37613418	7.35201849	7.50537853	7.43127166	7.51258336	7.61756809	7.75240141	7.665943399	7.274823838	7.213068118	7.695791997	7.890322516	7.905761446
Mno	0.18777778	0.16	0.16888889	0.20555556	0.16777778	0.13333333	0.16777778	0.20777778	0.124444444	0.1	0.167777778	0.176666667	0.173333333	0.263333333
MgO	14.1578714	14.1215616	14.4375549	14.7653243	14.7103689	14.3404017	14.3698421	14.3305882	14.30899864	14.51017446	14.58377538	14.14707663	14.40418915	14.26876347
CaO	22.2759891	21.8202428	22.0779264	22.4467677	22.4538413	22.0152739	22.1324947	21.8303481	22.16382096	22.72061964	22.52558852	22.14967363	22.4275677	22.08803167
Na2O	0.37229723	0.359818	0.39309596	0.29950169	0.32965984	0.359818	0.32757997	0.37333717	0.297421813	0.317180605	0.284942576	0.381656662	0.360857934	0.489810049
K2O	0	0.00316823	0.01372901	0.01795332	0.01584116	0.00739254	0.01795332	0.02640194	0.014785084	0.003168232	0.013729007	0.015841161	0.017953316	0.017953316
Cr2O3	0	0.03790204	0.02560949	0.08092598	0.03073138	0	0.05531649	0.07785284	0.050194595	0.072730944	0.14341313	0.025609487	0.077852842	0.070682185
Total	100.86594	100.111055	99.8605713	100.793934	100.366629	99.4754399	99.5527015	100.682491	100.1392071	100.5049696	100.0025913	100.0904009	100.4482749	100.5753541
Sample	B2_4_Cpx c-r	B2_4_Cpx c-r	B2_6_Cpx c-r	B2_6_Cpx c-r	B2_6_Cpx c-r	B2_6_Cpx c-r	B2_6_Cpx c-r	B2_6_Cpx c-r	B2_6_Cpx c-r	B2_6_Cpx c-r	B2_6_Cpx c-r	B2_6_Cpx c-r	B2_6_Cpx c-r	B2_6_Cpx c-r
Fe2O3	2.38294325	1.31341262	2.00963999	2.71908949	3.11664416	2.11373195	2.61148728	1.07486135	1.568676285	2.236128259	2.468128082	1.676940965	3.259658289	2.841218918
FeO	6.36882745	7.19431104	5.54372229	5.05871186	4.62688093	5.61062408	5.26772308	6.78522933	6.254431205	5.262731008	4.992219292	6.186862052	4.957246094	5.349201378
Wo	45.1903129	44.8440778	45.4126642	45.446653	45.5279509	45.407757	45.4790064	45.014199	45.60911887	46.21550046	46.00516683	45.63984483	45.50930343	45.0787932
En	39.96292	40.3811927	41.3202791	41.5950816	41.5013207	41.1545797	41.0850189	41.1153301	40.97011559	41.06681496	41.44301358	40.55967176	40.66845986	40.51842
Fs	13.4800238	13.4365413	11.8038488	11.8609381	11.761127	12.0946584	12.2178641	12.4773818	12.31320199	11.55016842	11.49870265	12.37737346	12.49715377	12.59381522
Mg#	74.776794	75.033246	77.7806258	77.8117822	77.9185383	77.2867015	77.0784179	76.7181369	76.89107483	78.04859254	78.28044977	76.61869224	76.49391605	76.28829747

Table 9.1 – Continue. Single mineral phase EMPA analyses. Sample: sub-ophitic gabbro B2. Clinopyroxenes.

Sample	B2_6_Cpx c-r	B2_6_Cpx c-r	B2_6_Cpx c-r	B2_6_Cpx c-r	B2_6_Cpx c-r	B2_6_Cpx c-r	B2_6_Cpx c-r	B2_Cpx_ c-r	B2_Cpx_c -r	B2_Cpx_c -r	B2_Cpx_c -r	B2_Cpx_c -r	B2_Cpx_c -r	B2_Cpx_c -r	B2_Cpx_c -r	B2_Cpx_c -r	B2_Cpx_c -r
SiO2	49.85627 58	50.00441 76	49.87139 23	50.11325 65	50.22914 98	50.54558 88	50.10620 22	50.767	50.617	50.501	50.327	50.21	49.917	49.773	48.81	49.688	49.539
TiO2	1.637943 62	1.662528 14	1.614383 45	1.665601 2	1.530386 35	1.410536 81	1.373660 03	1.067	1.16	1.2	1.287	1.28	1.391	1.536	1.573	1.628	1.567
Al2O3	3.595903 82	3.472763 52	3.572103 59	3.452067 67	3.257526 68	3.010211 28	2.972958 75	3.157	3.244	3.399	3.37	3.484	3.381	3.57	3.448	3.471	3.38
FeO	8.128082 04	8.172340 3	7.938697 83	8.276295 77	8.358636 73	8.299968 79	8.375104 92	6.175	6.266	6.258	6.547	7.019	7.25	7.33	7.811	7.814	7.852
Mno	0.208888 89	0.137777 78	0.198888 89	0.132222 22	0.226666 67	0.211111 11	0.265555 56	0.111	0.093	0.16	0.091	0.133	0.138	0.13	0.159	0.169	0.159
MgO	14.13530 05	14.10684 15	14.15492 74	14.16179 68	14.34236 44	14.29231 58	14.30114 79	15.76	15.593	15.602	15.295	15.104	14.969	15.046	14.746	14.668	14.627
CaO	21.88794 79	22.57106 21	21.68382 21	22.19211 56	21.83540 07	21.70504 31	22.02032 66	22.012	21.847	22.301	22.053	21.891	21.507	21.709	21.539	21.447	21.422
Na2O	0.397255 71	0.385816 41	0.388936 22	0.381656 66	0.353578 38	0.413894 69	0.325500 1	0.254	0.289	0.236	0.27	0.271	0.33	0.294	0.272	0.316	0.347
K2O	0.019009 39	0.019009 39	0.010560 77	0.020065 47	0.008448 62	0.004224 31	0.024289 78	0.01	0.003	0.015	0.008	0.008	0.009	0	0.015	0	0
Cr2O3	0.005121 9	0.037902 04	0.017414 45	0.032780 14	0.053267 73	0.067609 05	0	0.064	0.094	0.051	0	0	0.048	0.119	0	0.043	0.081
Total	99.86660 77	100.5325 57	99.43371 26	100.3950 78	100.1421 58	99.89289 47	99.76474 57	99.313	99.112	99.672	99.248	99.4	98.892	99.388	98.373	99.201	98.893
Fe2O3	2.651670 75	3.230837 62	2.100449 09	2.747913 07	2.576478 93	2.193492 22	3.091242 69	2.31151 304	2.065974 698	2.712361 224	2.330504 287	2.460923 215	2.457098 631	2.751598 056	3.756437 928	2.405753 975	2.708693 364
FeO	5.742079 49	5.265197 04	6.048690 61	5.803693 33	6.040292 62	6.326240 34	5.593570 71	4.09507 512	4.407013 218	3.817387 503	4.449986 581	4.804634 192	5.039075 596	4.854081 77	4.430915 789	5.649276 083	5.414687 885
Wo	45.01934 92	45.80507	44.91330 52	45.24619 59	44.60258 63	44.46040 05	44.89813 66	44.7217 276	44.62494 184	45.21576 368	45.06752 386	44.78911 795	44.26133 142	44.39706 045	44.27739 199	44.19598 774	44.14109 366
En	40.45294 17	39.83292 87	40.79413 47	40.17469 82	40.76341 19	40.73485 91	40.57199 44	44.5518 948	44.31659 978	44.01459 441	43.49070 015	42.99815 133	42.86356 858	42.81405 406	42.17757 668	42.05698 078	41.93621 535
Fs	13.04910 09	12.94512 79	12.83473 18	13.17096 86	13.32700 85	13.27050 73	13.32886 49	9.79251 796	9.990209 404	9.903744 733	10.44327 483	11.20935 176	11.64611 279	11.70083 132	12.53318 587	12.56863 303	12.62878 913
Mg#	75.61008 83	75.47251 89	76.06749 37	75.31014 34	75.36161 04	75.42742 85	75.27151 69	81.9806 352	81.60413 113	81.63195 512	80.63692 721	79.32140 18	78.63478 102	78.53644 699	77.09191 888	76.99131 936	76.85551 526

Table 9.1 – Continue. Single mineral phase EMPA analyses. Sample: sub-ophitic gabbro B2. Olivines.

Sample	B2_Ol_c-r	B2_Ol_c-r	B2_Ol_c-r	B2_Ol_c-r	B2_Ol_c-r	B2_Ol_c-r	B2_Ol_c-r	B2_Ol_c-r	B2_Ol_c-r	B2_Ol_c-r
SiO2	37.907	37.303	37.77	38.015	37.282	37.171	37.433	37.614	37.452	37.394
TiO2	0.005	0.031	0.021	0.025	0.031	0.023	0.017	0.035	0	0.037
Al2O3	0.01	0.026	0	0.024	0.036	0.06	0.015	0.05	0.016	0.034
Cr2O3	0.016	0.054	0	0.014	0.061	0	0.028	0	0	0
FeO	27.305	26.751	27.245	26.69	26.509	26.964	27.222	26.879	26.681	27.153
Mno	0.442	0.474	0.419	0.413	0.512	0.404	0.427	0.504	0.471	0.465
MgO	34.526	34.896	34.872	34.706	34.733	35.227	34.926	35.211	34.953	35.003
CaO	0.218	0.271	0.293	0.258	0.211	0.202	0.225	0.192	0.217	0.254
Na2O	0.013	0	0	0.002	0	0	0.025	0	0.003	0.003
NiO										
Total	100.442	99.806	100.62	100.147	99.375	100.051	100.318	100.485	99.793	100.343
Fo	68.92147	69.55261	69.19876	69.53269	69.61229	69.64224	69.2432	69.62006	69.64398	69.31357
Fa	30.57721	29.91061	30.32884	29.99719	29.80468	29.90397	30.27581	29.81375	29.82282	30.16326

Table 9.1 – Continue. Single mineral phase EMPA analyses. Sample: sub-ophitic gabbro B2. Feldspars.

Sample	B2_2_small Pl r-r	B2_2_small Pl r-r	B2_2_small Pl r-r	B2_2_small Pl r-r	B2_2_small Pl r-r	B2_2_small Pl r-r	B2_5_Pl c-r	B2_5_Pl c-r	B2_5_Pl c-r	B2_5_Pl c-r	B2_5_Pl c-r	B2_5_Pl c-r	B2_5_Pl c-r
SiO2	49.7665845	49.7182117	49.1206055	48.8797491	49.2334755	49.6446446	48.00097 58	48.68827 32	48.640908 16	47.561589 13	47.837717 43	48.181366 16	46.847081 94	47.549495 92
TiO2	0.13521486	0.06453436	0.10448421	0.0932163	0.06043694	0.1024355	0.080924 04	0.035852 42	0.0645343 64	0.0696561 39	0.0419985 54	0.0727292 04	0.0501933 94	0.0573638 79
Al2O3	32.2244722	32.5669885	32.63425	32.803956	32.1365148	32.5038662	33.09162 83	33.49623 21	33.302725 93	33.246847 14	33.574876 35	33.903940 36	33.378265 78	33.435179 37
Cr2O3	0	0	0	0.00819504	0	0.03892642	0.018438 83	0.059414 01	0.0286826 26	0.0133169 33	0	0	0.0542921 13	0
FeO	0.7719465	0.82546813	0.73077602	0.70607373	0.85737525	0.87898975	0.704015 21	0.707103	0.8131169 82	0.6381424 42	0.8059121 48	0.6350546 56	0.7637124 06	0.6793129 22
Mno	0.07888889	0.01555556	0	0.03222222	0.00333333	0.01666667	0.018888 89	0	0	0	0.0355555 56	0	0	0
MgO	0.06280611	0.07752629	0.07458226	0.03140306	0.06182477	0.0863584	0.028459 02	0.065750 15	0.1118733 86	0.0618247 66	0.0716382 21	0.0834143 67	0.0618247 66	0.0765449 48
CaO	15.4084686	15.7035416	16.0137724	16.2461929	16.0026567	15.7530573	16.53823 43	16.47659 24	16.532171 2	16.941433 38	17.163748 64	16.969728 05	17.177895 98	17.262779 99
Na2O	2.93470055	2.82446729	2.58424198	2.74335225	2.77247047	2.86606474	2.385614 12	2.119390 4	2.3190581 91	2.1401891 29	2.0892322 45	1.9457210 21	1.9488408 3	1.9717194 31
K2O	0.12039283	0.10983205	0.11088813	0.11405636	0.09293481	0.11088813	0.107719 9	0.090822 66	0.0834301 17	0.0844861 94	0.0823740 39	0.0876544 26	0.0908226 59	0.0707571 88
SrO														
BaO														
Total	101.503475	101.906125	101.373601	101.658417	101.221023	102.001898	100.9748 98	101.7394 3	101.89650 1	100.75748 53	101.70305 32	101.87960 82	100.37292 99	101.10315 36
Ab %	25.4557333	24.402461	22.4591285	23.256529	23.7436244	24.6137254	20.57357 26	18.78205 91	20.148836 55	18.517555 25	17.967056 79	17.096410 25	16.944802 37	17.059797 12
An %	73.8571436	74.9731743	76.9067727	76.1072692	75.73269	74.7596773	78.81517 93	80.68835 24	79.374212 98	81.001462 17	81.566828 63	82.396820 43	82.535600 85	82.537382 52
Or %	0.68712308	0.62436462	0.63409873	0.63620187	0.52368559	0.6265973	0.611248 14	0.529588 51	0.4769504 71	0.4809825 78	0.4661145 79	0.5067693 21	0.5195967 82	0.4028203 59

Sample	B2_5_Pl c-r	B2_5_Pl c-r	B2_5_Pl c-r	B2_5_Pl c-r	B2_5_Pl c-r	B2_5_Pl c-r	B2_5_Pl c-r	B2_5_Pl c-r	B2_5_Pl c-r	B2_1_pl r-r	B2_1_pl r-r	B2_1_pl r-r	B2_1_pl r-r	B2_1_pl r-r
SiO2	47.9515952	47.9949292	49.6103805	48.8001354	48.389974	49.3030114	49.15083 85	49.64262 91	53.502378 78	47.332825 89	47.530348 33	49.731312 64	48.505867 31	51.103892 04
TiO2	0.05326646	0.05736388	0.06453436	0.04814468	0.0727292	0.05326646	0.087070 17	0.083997 11	0.1188251 78	0.0542908 14	0.0758022 69	0.0573638 79	0.0542908 14	0.0778509 79

Al2O3	33.6545554	33.4610492	32.2575855	32.2824206	32.3807258	32.0371747	32.2265418	32.3983173	29.479167 77	34.277500 44	33.833574 47	34.059159 23	33.211664 2	31.551857 08
Cr2O3	0	0.10551109	0.02868263	0.0747797	0.05429211	0	0	0	0.0102437 95	0.0133169 33	0.0133169 33	0	0.0030731 38	0
FeO	0.57124041	0.69578111	0.6906348	0.68240071	0.65872768	0.67210809	0.793561	0.755478 31	0.7390101 18	0.750332	0.8522289 39	0.8048828 86	0.7523905 24	0.7441564 28
Mno	0.01333333	0.04888889	0.02444444	0.03555556	0.02222222	0	0.011111 11	0.018888 89	0.0433333 33	0.0333333 33	0.0155555 56	0.0144444 44	0.0077777 78	0
MgO	0.0647688	0.06182477	0.08733975	0.07752629	0.09519051	0.10009724	0.092246 48	0.080470 33	0.0971532 04	0.0441605 47	0.0824330 21	0.0804703 3	0.0510299 66	0.0951905 13
CaO	17.3173483	16.8171389	15.9784041	15.5620682	16.1986983	15.8935201	15.65099 43	15.68737 32	12.498159 74	17.827662 85	17.390106	16.599876 3	16.796928 46	14.502028 66
Na2O	1.93324178	2.08923225	2.81302799	2.77663021	2.60712058	2.42305183	2.671596 63	2.907662 2	4.8939407 4	1.8178088 42	2.0653137 08	2.3408968 56	2.3388169 83	3.6189787 02
K2O	0.08131796	0.08448619	0.1077199	0.12356106	0.13940222	0.13200968	0.109832 05	0.120392 83	0.2376174 21	0.0665328 78	0.0749814 97	0.0813179 62	0.0792058 07	0.1594676 91
SrO														
BaO														
Total	101.640668	101.416205	101.662754	100.463222	100.619083	100.61424	100.793792	101.695209	101.61983 01	102.21776 45	101.93366 07	103.76972 45	101.80104 5	101.85342 21
Ab %	16.7288685	18.2657442	24.0151039	24.2340949	22.3782337	21.4568411	23.45026	24.946210 1	40.930269 09	15.519371 64	17.615472 43	20.236841 62	20.036259 03	30.832009 35
An %	82.8081336	81.2482421	75.3798082	75.0563233	76.834455	77.7739913	75.91540 61	74.374158 6	57.762126 81	84.106884 26	81.963728 78	79.300607 99	79.517273 81	68.274066 62
Or %	0.46299786	0.48601369	0.60508788	0.70958183	0.7873113	0.76916756	0.634333 98	0.679631 25	1.3076041 05	0.3737440 91	0.4207987 88	0.4625503 81	0.4464671 66	0.8939240 32

Sample	B2_1_pl r-r	B2_1_pl r-r	B2_1_pl r-r	B2_1_pl r-r	B2_1_pl r-r	B2_1_pl r-r	B2_1_pl1 r-r	B2_1_pl1 r-r	B2_1_pl1 r-r	B2_1_pl1 r-r	B2_1_pl1 r-r	B2_1_pl1 r-r	B2_1_pl1 r-r	B2_1_pl1 r-r
SiO2	51.1643581	49.3402988	50.6292335	47.7308941	48.5401314	47.8377174	47.2290258	46.4994021	48.62377612	48.90796656	48.41113716	48.19043607	48.53307704	48.72556064
TiO2	0.09628937	0.09526501	0.0727292	0.05838823	0.08297275	0.03994984	0.07068049	0.05019339	0.060436944	0.066583074	0.058388234	0.055315169	0.090143239	0.053266459
Al2O3	31.2890198	30.53983	31.2196887	33.2561603	33.2416732	33.5945374	33.8687574	32.968488	33.02747114	32.91364397	33.06161929	32.64252834	32.97987068	33.23649922
Cr2O3	0	0	0.01229255	0.02765825	0.00819504	0	0.01741445	0.03585328	0	0.007170656	0	0.038926421	0.071706565	0.028682626
FeO	0.66078621	0.77606355	0.70401521	0.8532582	0.69475185	0.80591215	0.64946432	0.76474167	0.624762036	0.711220044	0.681371446	0.705044472	0.692693328	0.665932516
Mno	0.04555556	0.04666667	0.00333333	0.01888889	0.03333333	0.02666667	0.00777778	0	0	0	0.015555556	0.002222222	0.013333333	0.041111111
MgO	0.08537706	0.10500397	0.08733975	0.04023517	0.053974	0.05004862	0.04514189	0.04121651	0.101078586	0.082433021	0.077526294	0.078507639	0.048085929	0.067712839
CaO	14.7890175	14.6687651	14.8102385	16.8949493	16.7534759	17.2233696	17.2557063	17.0394542	16.20577198	16.32299275	16.62008678	16.56349744	16.71103393	16.38362418
Na2O	3.48586684	3.37979333	3.31635721	2.16826741	2.32425787	2.10899104	1.96963956	1.96859962	2.378334567	2.418892087	2.453209988	2.338816983	2.362735521	2.294099718

K2O	0.16263592	0.16580416	0.14362653	0.09399089	0.0982152	0.06442072	0.06442072	0.05914034	0.088710504	0.108775975	0.081317962	0.097159123	0.087654426	0.095046968
SrO														
BaO														
Total	101.778906	99.1174907	100.998854	101.142691	101.830981	101.751613	101.178029	99.4270891	101.1103419	101.5396781	101.4602127	100.7124539	101.590334	101.5915363
Ab %	29.6283842	29.1490786	28.6016036	18.7464747	19.9560913	18.0734207	17.0567928	17.2328602	20.87719681	21.01455277	20.98377959	20.23943702	20.27240467	20.10562857
An %	69.4620675	69.9100241	70.5833622	80.7188322	79.4890505	81.5633312	82.5761377	82.4264997	78.61043001	78.36365005	78.55855554	79.20734297	79.23274244	79.34627657
Or %	0.90954828	0.94089726	0.81503424	0.53469317	0.55485817	0.36324808	0.36706951	0.34064017	0.512373178	0.621797178	0.457664873	0.55322001	0.494852892	0.548094869

Sample	B2_1_pl1 r-r	B2_1_pl1 r-r	B2_1_pl1 r-r	B2_1_pl1 r-r	B2_1_pl1 r-r	B2_2_Pl C-r	B2_2_Pl C-r	B2_2_Pl C-r	B2_2_Pl C-r	B2_2_Pl C-r	B2_2_Pl C-r	B2_2_Pl C-r	B2_2_Pl C-r	B2_2_Pl C-r
SiO2	48.8283529	48.4716032	47.6674047	47.0889461	48.186405	48.5925353	47.47996	48.1914438	48.27811185	48.88680344	48.67920333	48.27307301	47.71476979	48.83439953
TiO2	0.05531517	0.08502146	0.06453436	0.05531517	0.0819484	0.07068049	0.06658307	0.06760743	0.072729204	0.071704849	0.074777914	0.089118884	0.061461299	0.074777914
Al2O3	33.1557854	33.3751614	33.2892736	34.2930223	33.217873	34.085029	33.4175879	33.1516462	33.64938141	33.0605845	32.60320623	32.92916585	32.93020065	32.79671242
Cr2O3	0	0	0.06863343	0.04609708	0	0.04917022	0.01843883	0	0	0	0.003073138	0	0	0
FeO	0.74415643	0.70092742	0.75239052	0.74827348	0.72562971	0.7420979	0.70916152	0.69681038	0.726658974	0.685488494	0.728717498	0.76577093	0.699898162	0.727688236
Mno	0	0	0.00222222	0.02111111	0	0.00555556	0.02666667	0.02444444	0.008888889	0.018888889	0.003333333	0.008888889	0.007777778	0.013333333
MgO	0.09420917	0.07458226	0.05986208	0.07850764	0.07065688	0.06575015	0.06673149	0.08243302	0.066731494	0.099115895	0.073600912	0.093227822	0.087339749	0.068694185
CaO	16.4260662	16.9363808	16.8757493	17.7983577	16.3846347	17.1657697	16.6291815	16.6221078	17.03339106	16.68577083	16.52610806	17.01621215	16.60492892	16.63928673
Na2O	2.30449908	2.207785	2.16410767	1.87916509	2.20882493	1.96132007	2.09859167	2.28890004	2.160987857	2.302419209	2.378334567	2.437610942	2.361695584	2.534325028
K2O	0.06864503	0.08659835	0.0559721	0.06758896	0.10243951	0.0749815	0.06864503	0.07286934	0.092934814	0.087654426	0.098215201	0.074981497	0.096103046	0.099271278
SrO														
BaO														
Total	101.677029	101.93806	101.00015	102.076385	100.978412	102.81289	100.581548	101.198263	102.0898155	101.8984305	101.1685702	101.68805	100.564175	101.7884887
Ab %	20.1676391	18.9936333	18.7750921	15.9806306	19.4947049	17.060197	18.5174461	19.865078	18.57349147	19.88159236	20.5466479	20.50115843	20.35800545	21.48730906
An %	79.4370855	80.516167	80.9053961	83.6411735	79.9104074	82.5106602	81.0840117	79.7188003	80.90093709	79.62038083	78.89506339	79.08390642	79.09691415	77.95888777
Or %	0.39527536	0.49019964	0.31951183	0.3781959	0.59488767	0.42914275	0.39854225	0.41612174	0.525571443	0.498026808	0.558288707	0.414935147	0.545080399	0.553803167

Sample	B2_2_Pl C-r	B2_2_Pl C-r	B2_2_Pl C-r	B2_4_Pl r-r	B2_4_Pl r-r	B2_4_Pl r-r	B2_4_Pl r-r	B2_4_Pl r-r	B2_4_Pl r-r	B2_4_Pl r-r	B2_4_Pl r-r	B2_4_Pl r-r	B2_4_Pl r-r	B2_4_Pl r-r
SiO2	49.1377376	50.8660589	51.5211078	49.2929338	48.8726947	49.0419996	49.309058	47.7772514	47.75508049	48.54920132	48.81222865	48.82331409	48.24787882	48.29625166

TiO2	0.06248565	0.0932163	0.10653292	0.30013601	0.15570196	0.11575211	0.09628937	0.04916904	0.061461299	0.051217749	0.044047264	0.050193394	0.035852424	0.055315169
Al2O3	32.0702881	31.721563	30.7126404	32.3765867	32.2358549	32.3631344	32.1292713	33.8077047	32.50800532	32.91674834	32.77912095	32.88466978	32.73565966	32.95400087
Cr2O3	0.07170656	0.00307314	0.02048759	0.08399912	0.01024379	0.01024379	0	0	0.007170656	0	0.04097518	0.037902041	0.054292113	0
FeO	0.68960554	0.6690203	0.61446942	1.00867676	0.82135108	0.80591215	0.79047322	0.75959536	0.692693328	0.697839638	0.71945414	0.751361262	0.751361262	0.757536834
Mno	0	0.02444444	0	0.03888889	0	0.01333333	0	0.00555556	0.026666667	0	0	0	0	0
MgO	0.06575015	0.07752629	0.07458226	0.06967553	0.09224648	0.05593669	0.07360091	0.05888073	0.104022622	0.052992657	0.062806112	0.051029966	0.068694185	0.10892935
CaO	15.8632044	14.8840067	14.1907873	15.7742783	15.6075418	16.2472035	15.5671209	17.24358	16.51903439	16.20071936	16.56753954	16.65343407	16.57663425	16.73730755
Na2O	2.71527396	3.24148179	3.80928707	2.75791136	2.78806951	2.67575638	2.25666201	2.1308297	2.340896856	2.48752789	2.550964011	2.390813804	2.408492723	2.461529479
K2O	0.12567321	0.14151438	0.15629946	0.11933675	0.11405636	0.12250498	0.11194421	0.07920581	0.089766581	0.080261884	0.103495588	0.089766581	0.080261884	0.083430117
SrO														
BaO														
Total	100.801725	101.721905	101.206194	101.822423	100.697761	101.451777	100.33442	101.911772	100.1047982	101.0365088	101.6806314	101.732485	100.9591273	101.454301
Ab %	23.4804496	28.0417039	32.4085314	23.8711892	24.2697234	22.8023317	20.6413658	18.1939401	20.3055025	21.6441101	21.66554195	20.51747544	20.72435242	20.92164538
An %	75.804482	71.1527814	66.7165146	75.449169	75.0770064	76.5107604	78.6849045	81.361073	79.18215752	77.89638174	77.75609683	78.97564479	78.82122795	78.61177502
Or %	0.71506839	0.80551471	0.87495401	0.67964177	0.6532702	0.68690795	0.67372962	0.44498682	0.512339986	0.459508164	0.57836122	0.506879768	0.454419633	0.466579604
Sample	B2_4_Pl r-r	B2_5_Pl c-r	B2_5_Pl c-r	B2_5_Pl c-r	B2_5_Pl c-r	B2_5_Pl c-r	B2_5_Pl c-r	B2_5_Pl c-r	B2_5_Pl c-r	B2_5_Pl c-r	B2_5_Pl c-r	B2_5_Pl c-r	B2_5_Pl c-r	B2_5_Pl c-r
SiO2	49.1649473	47.7913601	47.4880221	47.4789522	46.6253731	47.267321	47.3308104	47.9919059	48.57439551	48.62176058	48.65400914	48.73563831	49.16091622	48.46152554
TiO2	0.10038679	0.0522421	0.03790113	0.05531517	0.06965614	0.07887533	0.06453436	0.0522421	0.064534364	0.101411143	0.069656139	0.065558719	0.080924044	0.064534364
Al2O3	33.1650985	33.8480616	33.566598	32.8525912	33.0460974	33.0088449	33.0336799	33.4031008	32.96124442	33.14854186	33.02126238	32.96641838	32.82465181	33.17130729
Cr2O3	0.01331693	0	0	0	0	0.06863343	0	0.02868263	0	0.02048759	0.076828462	0	0	0
FeO	0.80694141	0.72974676	0.77812207	0.67313735	0.71533709	0.73695159	0.73901012	0.70813226	0.710190782	0.674166612	0.706073734	0.71430783	0.66799104	0.701956686
Mno	0	0	0.01333333	0.06555556	0.00888889	0.06	0.05777778	0.00777778	0.015555556	0.007777778	0	0	0.018888889	0.044444444
MgO	0.04416055	0.08145168	0.08047033	0.07065688	0.06280611	0.07654495	0.08537706	0.08733975	0.401370307	0.099115895	0.086358403	0.059862075	0.096171858	0.118742805
CaO	16.6372657	17.3547377	17.5012636	16.9343597	17.5305688	16.8232021	16.8787809	16.8757493	16.69789712	16.24417188	16.47153976	16.42707671	16.14918264	16.47760291
Na2O	2.53432503	2.00707727	1.93844147	1.98107886	1.95508045	2.0965118	2.16826741	2.14538881	2.193225886	2.379374503	2.494807445	2.505206809	2.593601403	2.461529479
K2O	0.10138343	0.08659835	0.09610305	0.09504697	0.09293481	0.09504697	0.09187874	0.08765443	0.117224594	0.086598349	0.100327356	0.105607743	0.145738685	0.100327356
SrO														

BaO														
Total	102.567826	101.951276	101.500255	100.206694	100.106743	100.311932	100.450117	101.387974	101.7356385	101.3834062	101.6808628	101.5796766	101.7380666	101.6019709
Ab %	21.4868119	17.2217856	16.6063672	17.3755191	16.7049075	18.301261	18.7632233	18.6092587	19.07547361	20.84813202	21.39078563	21.49966917	22.33256621	21.15975258
An %	77.947615	82.2892966	82.8519174	82.0759686	82.7726121	81.1528126	80.7136321	80.8904661	80.25368042	78.65260879	78.04320819	77.90398792	76.84173367	78.27278512
Or %	0.56557313	0.48891775	0.54171542	0.54851233	0.52248037	0.54592638	0.52314457	0.50027525	0.67084596	0.499259182	0.56600618	0.596342906	0.82570012	0.567462298

Sample	B2_5_Pl c-r	B2_5_Pl c-r	B2_5_Pl c-r	B2_5_Pl c-r	B2_5_Pl c-r	B2_5_Pl c-r	B2_5_Pl c-r	B2_5_Pl c-r	B2_5_Pl c-r	B2_5_Pl c-r	B2_5_Pl c-r	B2_5_Pl c-r	B2_5_Pl c-r	B2_6_Pl r-r
SiO2	49.0147899	49.6607689	49.1447919	48.9795181	49.0863414	48.5794343	48.8011432	49.0520773	49.32719786	49.44611443	49.42293578	50.2916314	51.07063571	48.54113918
TiO2	0.10550856	0.08911888	0.0932163	0.06248565	0.07170485	0.09833808	0.06658307	0.05633952	0.104484208	0.087070174	0.061461299	0.074777914	0.075802269	0.085021464
Al2O3	32.6249369	32.3972825	32.5576754	32.4065957	32.4624745	32.8370693	32.8691479	32.1965328	32.44281339	32.43867422	32.12306252	31.85815565	31.36352485	32.11064501
Cr2O3	0.02356073	0	0.02048759	0.03278014	0.01024379	0	0	0.02253635	0	0	0	0	0	0
FeO	0.59903049	0.76268314	0.80385362	0.73077602	0.78944396	0.75959536	0.72562971	0.75753683	0.72974676	0.720483402	0.71430783	0.629908346	0.655639896	0.754449048
Mno	0.04333333	0.02444444	0.05111111	0	0.02222222	0.10444444	0	0.03555556	0.003333333	0.037777778	0	0	0	0.011111111
MgO	0.10892935	0.06182477	0.09224648	0.05888073	0.11481742	0.07163822	0.10402262	0.09813455	0.063787457	0.084395712	0.075563603	0.08047033	0.052992657	0.074582257
CaO	15.8935201	15.8632044	15.9359621	15.910699	16.1037091	16.4311188	16.0511618	16.0673302	15.63684701	15.63078387	15.70253107	14.97596437	14.5333549	16.05924601
Na2O	2.64871803	2.67575638	2.56344325	2.41785215	2.4792084	2.40537291	2.60920045	2.60712058	2.236903215	2.858785188	2.706954472	3.168686237	3.530584108	2.665357016
K2O	0.10666382	0.1214489	0.12778537	0.12356106	0.10455167	0.10032736	0.0887105	0.10560774	0.101383433	0.122504981	0.100327356	0.124617136	0.158411614	0.122504981
SrO														
BaO														
Total	101.168991	101.656532	101.390573	100.723148	101.244717	101.387339	101.315599	100.998771	100.6464967	101.4265898	100.9071439	101.2042114	101.440946	100.4240561
Ab %	23.0289936	23.2236639	22.3808349	21.4131963	21.6583056	20.8235231	22.6150554	22.5618818	20.43853183	24.69372836	23.6411252	27.49067021	30.26399906	22.93705835
An %	76.3608117	76.0827668	76.885081	77.8667822	77.740722	78.604994	76.8790299	76.8367755	78.9519571	74.61001236	75.78234912	71.79795911	68.8425332	76.3692792
Or %	0.61019475	0.69356932	0.73408409	0.72002153	0.60097236	0.57148293	0.50591477	0.60134273	0.609511071	0.696259279	0.576525685	0.71137068	0.893467739	0.693662446

Sample	B2_6_Pl r-r	B2_6_Pl r-r	B2_6_Pl r-r	B2_6_Pl r-r	B2_6_Pl r-r	B2_6_Pl r-r	B2_6_Pl r-r	B2_6_Pl r-r	B2_6_Pl r-r	B2_6_Pl r-r	B2_6_Pl r-r	B2_6_Pl r-r	B2_6_Pl r-r	B2_6_Pl r-r
SiO2	49.2929338	47.0516588	47.4829833	47.1030549	47.5454648	47.9012068	48.3758653	48.5250149	48.7981199	48.81928302	48.89990442	48.79106553	49.12866765	48.77594901
TiO2	0.09219195	0.04507162	0.05941259	0.07887533	0.0727292	0.03994984	0.06453436	0.06453436	0.077850979	0.061461299	0.060436944	0.055315169	0.058388234	0.110630338
Al2O3	32.7056507	32.2141243	33.0222972	32.7584251	33.297552	33.1847596	32.4169436	32.549397	32.5928583	32.52145762	32.74600759	32.18411528	32.37865626	32.0164789

Cr2O3	0.0747797	0	0.02253635	0.01843883	0	0	0	0	0	0	0	0	0	0
FeO	0.65975694	0.73592233	0.69269333	0.68857628	0.69681038	0.6175572	0.64123023	0.6690203	0.686517756	0.70916152	0.73489307	0.632996132	0.71945414	0.680342184
Mno	0.01888889	0	0.06888889	0.00333333	0.03555556	0.01111111	0.00333333	0.08222222	0.048888889	0	0	0.03	0.06	0.011111111
MgO	0.07065688	0.08733975	0.0755636	0.08047033	0.05691804	0.07948898	0.09813455	0.08439571	0.067712839	0.06967553	0.091265131	0.084395712	0.065750148	0.057899384
CaO	16.2593297	16.4250557	17.1061488	17.0162122	17.0384437	16.693855	16.5503606	16.3260243	16.43415038	16.40888728	16.15423526	16.03297239	16.08046701	15.98143567
Na2O	2.48024833	2.77975002	2.05907409	2.13602938	1.94884083	2.28058054	2.37001508	2.54368446	2.459449607	2.583202039	2.636238796	2.608160513	2.662237206	2.572802675
K2O	0.11722459	0.10877597	0.08448619	0.10877597	0.07920581	0.11616852	0.11088813	0.10032736	0.109832052	0.099271278	0.105607743	0.103495588	0.126729291	0.129897523
SrO														
BaO														
Total	101.771661	99.4476984	100.674084	99.9921916	100.77152	100.924678	100.631305	100.944621	101.2753807	101.2723996	101.4285889	100.5225163	101.2803499	100.3365468
Ab %	21.4883518	23.3047714	17.8004658	18.3969694	17.0705258	19.6906496	20.451063	21.8689934	21.17798842	22.04835044	22.66257783	22.608713	22.88778331	22.3924076
An %	77.8433985	76.0951831	81.7189635	80.9866	82.4729754	79.6493941	78.919341	77.5634659	78.19972852	77.39413855	76.74006728	76.80098335	76.3953373	76.86370486
Or %	0.66824971	0.60004551	0.48057065	0.61643055	0.45649882	0.6599563	0.62959597	0.56754072	0.622283063	0.557511006	0.597354893	0.590303645	0.716879389	0.743887545

Sample	B2_6_Pl r-r	B2_6_Pl r-r	B2_6_Pl r-r	B2_6_Pl r-r	B2_6_Pl r-r	B2_6_Pl r-r	B2_6_Pl r-r	B2_6_Pl r-r	B2_6_Pl r-r	B2_6_Pl r-r	B2_6_Pl r-r	B2_6_Pl r-r	B2_6_Pl r-r	B2_6_Pl r-r
SiO2	49.0530851	49.6587534	48.7537781	49.3292134	49.4249513	49.4461144	48.3980362	48.2257079	49.33324446	48.70338975	48.88378014	48.10175253	48.59958969	48.81122088
TiO2	0.0727292	0.07477791	0.07170485	0.0409742	0.06965614	0.07580227	0.09116759	0.06863178	0.081948399	0.074777914	0.050193394	0.061461299	0.077850979	0.089118884
Al2O3	32.5173185	32.7884341	32.3258818	32.0692533	32.5287012	32.3465777	32.1520367	31.7257022	32.4562657	32.195498	32.2906989	32.07442728	32.32174268	32.63942396
Cr2O3	0.0901454	0.04097518	0.03892642	0	0.00819504	0.0051219	0.02765825	0.03278014	0.003073138	0	0.002048759	0	0.043023939	0
FeO	0.6906348	0.69372259	0.67931292	0.67622514	0.74724421	0.64431801	0.64843506	0.73901012	0.681371446	0.64225949	0.821351078	0.712249306	0.816204768	0.869726393
Mno	0.01333333	0	0.02222222	0.02444444	0	0.04111111	0	0	0.037777778	0.035555556	0.014444444	0	0.035555556	0.035555556
MgO	0.07360091	0.06967553	0.06967553	0.08439571	0.08341437	0.08341437	0.09911589	0.09028379	0.093227822	0.103041277	0.102059931	0.10892935	0.06967553	0.079488985
CaO	16.1299827	15.9986146	15.8338992	16.0349934	16.0521723	15.5741945	15.7672046	15.910699	16.12695111	15.40038442	16.09461435	15.83187813	16.19263516	16.39473995
Na2O	2.59672121	2.46880903	2.66951676	2.68927555	2.74751199	2.72151358	2.84734589	2.70175479	2.662237206	2.739192501	2.696555108	2.678876189	2.633118987	2.624799496
K2O	0.12989752	0.14151438	0.12250498	0.11933675	0.11300028	0.12250498	0.13200968	0.14151438	0.108775975	0.133065756	0.124617136	0.114056362	0.138346143	0.103495588
SrO														
BaO														
Total	101.367449	101.935277	100.587423	101.068112	101.774847	101.060673	100.16301	99.6360841	101.584873	100.0271647	101.0803632	99.68363044	100.9277434	101.6475697
Ab %	22.3939712	21.6509708	23.2133067	23.1261115	23.4984713	23.8552947	24.4466771	23.3168648	22.86051541	24.16151608	23.10189492	23.28925873	22.55888258	22.33370569

An %	76.8689417	77.532442	76.0857705	76.1986556	75.8656246	75.4381598	74.8075657	75.8795409	76.52489619	75.06619458	76.19563444	76.05831019	76.66124016	77.08686749
Or %	0.73708702	0.81658714	0.70092284	0.67523294	0.63590414	0.7065455	0.74575725	0.80359437	0.614588398	0.772289333	0.702470636	0.652431082	0.779877262	0.579426821

Sample	B2_Pl_c-r	B2_Pl_c-r	B2_Pl_c-r	B2_Pl_c-r	B2_Pl1_c-r	B2_Pl1_c-r	B2_Pl1_c-r	B2_Pl1_c-r	B2_Pl1_c-r	B2_Pl1_c-r	B2_Pl1_c-r	B2_Pl1_c-r	B2_Pl1_c-r	B2_Pl1_c-r
SiO2	47.371	47.879	47.755	48.581	46.881	47.486	47.095	47.666	47.662	47.464	46.356	46.403	46.361	46.814
TiO2	0.069	0.086	0.046	0.076	0.052	0.068	0.061	0.054	0.052	0.051	0.065	0.051	0.036	0.056
Al2O3	32.043	32.278	32.368	31.918	32.326	32.101	32.075	32.127	32.226	31.825	32.555	32.69	33.009	32.713
Cr2O3	0.008	0	0.013	0.003	0.091	0	0.057	0	0.031	0	0.026	0.01	0	0.05
FeO	0.72	0.631	0.747	0.708	0.601	0.682	0.772	0.68	0.718	0.722	0.651	0.689	0.67	0.748
Mno	0	0	0	0	0	0.046	0.01	0	0	0.022	0	0.014	0.012	0.026
MgO	0.076	0.057	0.071	0.076	0.059	0.092	0.051	0.097	0.083	0.05	0.08	0.07	0.088	0.073
CaO	16.474	15.961	16.15	15.832	16.291	16.373	16.013	16.021	16.242	16.618	16.675	16.586	17.084	16.853
Na2O	2.33	2.343	2.258	2.493	2.149	2.274	2.222	2.186	2.226	2.149	1.791	1.79	1.79	1.763
K2O	0.054	0.079	0.074	0.084	0.064	0.077	0.082	0.073	0.08	0.071	0.061	0.052	0.068	0.074
SrO														
BaO														
Total	99.145	99.314	99.482	99.771	98.514	99.199	98.438	98.904	99.32	98.972	98.26	98.355	99.118	99.17
Ab %	20.3155091	20.8915965	20.1047312	22.0677273	19.1986007	19.995795	19.9734919	19.7163519	19.77967899	18.88594824	16.21438296	16.28805955	15.87531312	15.84766775
An %	79.3746936	78.6449154	79.4617398	77.4430273	80.4251937	79.5587016	79.5415147	79.8504253	79.75259	80.70349536	83.42224896	83.40060272	83.72786987	83.71465209
Or %	0.30979732	0.46348804	0.433529	0.48924536	0.37620559	0.44550342	0.48499348	0.43322286	0.467731016	0.410556405	0.363368084	0.311337737	0.396817015	0.437680168

Sample	B2_Pl1_c-r	B2_Pl1_c-r	B2_Pl1_c-r	B2_Pl1_c-r	B2_Pl1_c-r
SiO2	46.247	47.267	47.413	47.788	52.964
TiO2	0.064	0.056	0.064	0.069	0.109
Al2O3	32.721	32.468	32.317	31.737	28.415
Cr2O3	0.01	0	0	0.016	0
FeO	0.686	0.748	0.697	0.67	0.67
Mno	0.024	0.005	0.026	0.01	0.033

MgO	0.059	0.052	0.077	0.059	0.088
CaO	16.426	16.451	16.061	15.563	11.506
Na2O	2.003	2.176	2.237	2.468	4.657
K2O	0.075	0.064	0.066	0.085	0.242
SrO					
BaO					
Total	98.315	99.287	98.958	98.465	98.684
Ab %	17.9974363	19.241414	20.0524538	22.1861671	41.6754241
An %	81.5591562	80.3862199	79.5582703	77.3110643	56.8996206
Or %	0.44340753	0.37236613	0.38927596	0.50276861	1.42495536

Table 9.1 – Continue. Single mineral phase EMPA analyses. Sample: sub-ophitic gabbro B2. Opaque minerals.

Sample	B2_2_Oxide of MI	B2_2_Oxide of MI	B2_2_Oxide of MI	B2_3_Ox C-r	B2_3_Ox C-r	B2_3_Ox C-r	B2_3_Ox C-r	B2_3_Ox C-r	B2_3_Ox C-r	B2_3_Ox C-r	B2_3_Ox C-r	B2_3_Ox C-r	B2_3_Ox C-r
SiO2	0.03527186	0.06046605	0.00100777	0.04736507	0	0	0	0	0	0	0	0	0.00403107	0.01813 9816
TiO2	49.3862025	48.8801711	49.2069404	48.8945121	49.1086023	49.4241036	49.3800564	49.4363959	48.5339 3913	49.3841 5377	48.9867 0404	49.2878 644	49.4404933	49.1526 4954
Al2O3	0.51739623	0.4532391	0.49152642	0.47186536	0.51843103	0.50083955	0.45427389	0.39736031	0.47496 9742	0.44806 5138	0.44909 993	0.43771 7213	0.45013 4723	0.47600 4534
Cr2O3	0	0.00409752	0.00921942	0	0.03380452	0.00717066	0.01536569	0.01126817	0.01536 5692	0	0.02868 2626	0.10243 795	0.02458 5108	0
FeO	45.0734416	45.337962	45.1475485	45.4079518	45.8772953	45.2864989	45.0260956	45.2690014	44.7461 3632	45.6735 0139	44.6555 6127	45.4182 4441	45.7373 1563	44.6977 6101
Mno	0.48444444	0.39777778	0.37	0.54	0.49222222	0.56111111	0.47555556	0.51222222	0.32222 2222	0.53777 7778	0.47111 1111	0.41	0.48555 5556	0.46
MgO	5.26295588	5.36010908	5.16482133	5.40034425	5.55147146	5.33950083	5.45333691	5.62310968	5.35912 7739	5.61427 7567	5.54656 4728	5.50829 2254	5.54165 8001	5.37090 3885
CaO	0.08993663	0.08993663	0.07073667	0.00909472	0.00505262	0.06467353	0.0505262	0.00808419	0.02223 1526	0.00606 3143	0.02526 3098	0.04749 4624	0.04951 5672	0.01616 8383
Total	100.849649	100.583759	100.4618	100.771133	101.586879	101.183898	100.85521	101.257442	99.4739 9238	101.663 8388	100.162 9868	101.212 0509	101.733 2891	100.191 6272

Sample	B2_3_Ox C-r	B2_3_Ox C-r	B2_3_Ox C-r	B2_3_Ox C-r	B2_Opq_core zone	B2_Opq_core zone	B2_Opq_core zone	B2_Opq_core zone	B2_Opq_rim zone	B2_Opq_rim zone	B2_Opq_rim zone
SiO2	0	0	0	0.013100 98	0.023	0.011	0.044	0.027	0.017	0.025	0.024
TiO2	49.15162 52	49.08401 78	49.20796 47	49.31142 46	47.315	47.232	47.693	47.475	47.405	47.048	47.33
Al2O3	0.412882 19	0.490491 63	0.490491 63	0.477039 33	0.43	0.482	0.431	0.417	0.415	0.481	0.421
Cr2O3	0.033804 52	0.028682 63	0	0	0	0.036	0	0.009	0	0	0.038

FeO	45.64262 35	45.09917 32	44.85523 81	44.81715 54	43.967	43.574	44.001	43.816	43.995	43.973	43.041
Mno	0.558888 89	0.551111 11	0.526666 67	0.51	0.412	0.36	0.481	0.426	0.491	0.43	0.484
MgO	5.615258 91	5.548527 42	5.669232 91	5.650587 35	5.642	5.56	5.595	5.73	5.508	5.505	5.558
CaO	0.036378 86	0.039410 43	0.028294 67	0.066694 58	0.035	0.013	0.044	0.044	0.145	0.21	0.232
Total	101.4514 62	100.8414 14	100.7778 89	100.8460 02	97.824	97.268	98.289	97.944	97.976	97.672	97.128

Table 9.1 – Continue. Single mineral phase EMPA analyses. Sample: sub-ophitic gabbro B2. Glass.

Sample	B2_1_Glass	B2_1_Glass	B2_1_Glass	B2_1_Glass	B2_1_glass of Cpx rim detail1 to glass	B2_2_Glass	B2_2_Glass	B2_3_Glass	B2_3_Glass	B2_5_Glass	B2_5_Glass
SiO2	54.6738168	54.8487131	54.8719652	55.1803085	55.5503205	54.6343893	54.6738168	52.9632697	53.06840966	56.22058808	55.66557013
TiO2	2.61247924	2.58858778	2.50237077	2.52626223	2.40368865	2.79322333	2.83581246	2.97188991	3.083037134	2.560541285	2.493021941
Al2O3	15.0303952	15.0529679	15.2130295	14.853917	15.0468117	15.3115289	14.9493383	14.8580212	14.86417739	15.14325907	15.69834432
Cr2O3	0.011	0	0.011	0.037	0	0.081	0	0.029	0.022	0.088	0.004
FeOtot	10.1942058	9.99472267	10.3268518	10.4502435	10.0451076	10.6528114	10.8913686	12.4265662	11.4137265	9.594728109	9.463110362
MnO	0.19638682	0.17357421	0.2638328	0.16266383	0.18250089	0.14976975	0.26680836	0.27871059	0.194403117	0.147786043	0.182500886
MgO	3.12260676	3.26692892	3.20940191	3.21747587	3.32041895	3.18518001	3.32849292	3.46575036	3.309317249	3.031774632	2.92176683
CaO	6.33021533	6.44312887	6.05498858	6.13261664	6.6981925	6.34332137	6.36852529	6.91091354	6.772796085	6.223350734	6.027768352
Na2O	4.50207189	4.28819674	4.30102925	4.14596976	4.13634538	3.68399944	3.82836517	3.85082206	4.087154098	4.193022297	3.948135251
K2O	2.13767372	2.11790934	2.16888063	2.10750703	2.07525989	2.0825415	2.05965643	1.8370471	1.955633376	2.24585769	2.234415155
P2O5	0.94774347	0.81793133	0.78691427	1.02586051	0.78117037	0.83516303	0.88226301	0.76049233	0.845502051	0.908684949	0.860436191
F											
Cl											
Total	99.758595	99.5926609	99.7102648	99.8398249	100.239816	99.752928	100.084447	100.352483	99.61615667	100.3575929	99.49906942

Table 9.1 – Continue. Single mineral phase EMPA analyses. Sample: sub-ophitic gabbro B2. Melt Inclusions (MI).

Sample	B2_2_MI in Oxide	B2_2_MI in Oxide	B2_2_MI in Oxide
SiO2	50.9352806	51.3710051	51.1940868
TiO2	3.65435466	3.50788962	3.66162598
Al2O3	14.4989087	14.7903028	14.6876993
Cr2O3	0	0.011	0.007
FeOtot	12.6435298	12.7124235	12.9550937
MnO	0.25490613	0.19539497	0.22118314
MgO	3.80889396	3.58080439	3.54951777
CaO	6.4471615	6.43607178	6.43909625
Na2O	4.57692819	4.43470122	4.64857636
K2O	1.78503557	1.88281724	1.85681148
P2O5	0.74785575	0.76508745	0.79725329
F			
Cl			
Total	99.3528549	99.6874981	100.017944

Table 9.1 – Continue. Single mineral phase EMPA analyses. Sample: sub-ophitic gabbro B23. Clinopyroxenes.

Data set	B23_1_Cpx rim to MI	B23_1_Cpx rim to MI	B23_1_Cpx rim to MI	B23_1_Cpx rim to MI	B23_1_Cpx rim to MI	B23_1_Cpx rim to MI	B23_1_Cpx rim to MI	B23_1_Cpx rim to MI	B23_1_Cpx rim to MI	B23_1_Cpx rim to MI	B23_1_Cpx rim to MI	B23_1_Cpx rim to MI	B23_1_Cpx rim to MI	B23_1_Cpx rim to MI
SiO2	49.7731561	50.2470724	49.6586595	49.3669422	49.48343	49.4864169	49.5043381	49.5700491	49.37092466	49.9762631	49.46550879	49.29824423	50.39243327	51.13715884
TiO2	1.67753044	1.66329685	1.61347928	1.74564834	1.61754602	1.78834912	1.73853155	1.6734637	1.713114418	1.75988193	1.68363055	1.73141475	1.370491534	1.350157832
Al2O3	4.08849365	4.16309001	4.37155107	4.37870414	4.18659297	4.46249731	4.54935609	4.22848955	4.221336479	4.31534833	4.38687908	4.37461667	3.339464443	3.491722766
FeO	7.61632184	7.6112239	7.41138466	7.66832082	7.50314758	7.68769299	7.64690948	7.64690948	7.715221867	7.65506617	7.87631676	7.77741673	7.392012493	7.356326915
MnO	0.26606335	0.12986425	0.14781297	0.13303167	0.24494721	0.19215686	0.17737557	0.19215686	0.200603318	0.12880844	0.07496229	0.10452488	0.111915535	0.173152338
MgO	14.5213046	14.3643282	14.5811519	14.3015376	14.2760289	14.4133833	14.458514	14.3456872	14.33293286	14.36138484	14.46341955	14.3810069	14.74205278	14.76658036
CaO	22.2545501	21.7674217	21.5158389	21.6962569	21.6060479	21.5218529	21.5890084	21.4206184	21.63110595	22.11322272	21.75840082	21.57196897	21.78847077	21.70728241
Na2O	0.31877482	0.32498472	0.34257944	0.37776887	0.34154445	0.4067484	0.31359991	0.34878934	0.323949743	0.376733883	0.312564925	0.184227009	0.349824327	0.378803853
K2O	0.025	0.0125	0.021875	0.02708333	0.0125	0.009375	0.003125	0	0.01875	0.010416667	0.008333333	0.008333333	0.034375	0.017708333
Cr2O3	0.07798954	0	0.09014376	0	0.05469397	0.01215421	0	0.13470921	0.165094751	0.042539752	0	0.064822479	0.069886735	0.027346983
Totale	100.541195	100.283782	99.6643328	99.6952938	99.271785	99.9684727	99.9807581	99.4261637	99.52793929	100.6971261	100.0300161	99.43175348	99.52103985	100.3788936
Fe2O3	3.06331585	1.335302	2.08791495	2.58534122	2.04280765	2.52493974	2.1823651	1.77803478	2.274498062	2.358776381	2.69174554	1.648494494	2.096365828	1.215633401
FeO	4.8599165	6.40970446	5.5326558	5.34200232	5.66500676	5.41572441	5.68319333	6.0470142	5.668603465	5.532613218	5.45425448	6.294083232	5.505679436	6.262486595
Wo	45.4348881	45.083081	44.6304593	44.9528626	45.0649112	44.5464888	44.7507416	44.643869	44.89438368	45.35814993	44.77387044	44.95502995	44.73709408	44.59097007
En	41.2503063	41.3945164	42.0838829	41.2293196	41.4306266	41.5098013	41.7005804	41.6008377	41.39036476	40.98741324	41.41136517	41.69929354	42.11626858	42.20581542
Fs	12.1370818	12.3043717	11.9997106	12.4014127	12.2153248	12.4201888	12.3723397	12.4398206	12.49856219	12.25605181	12.65083483	12.65092325	11.84682752	11.79507839
N° Mg	77.2660132	77.0863567	77.8126603	76.8762943	77.2297359	76.9697921	77.1191574	76.9806272	76.80680822	76.98111533	76.59948202	76.72332513	78.04642733	78.15762377

Data set	B23_4_Cpx of MI	B23_4_Cpx of MI	B23_4_Cpx of MI	B23_6_Cpx of MI	B23_6_Cpx of MI	B23_6_Cpx of MI	B23_6_Cpx of MI1	B23_6_Cpx of MI1	B23_6_Cpx of MI1	B23_8_ Cpx of MI	B23_8_ Cpx of MI	B23_8_ Cpx of MI	B23_8_ Cpx of Mi1	B23_8_ Cpx of Mi1

SiO2	50.3326959	50.2211862	51.1112727	48.7397	48.9019865	48.9557501	50.772761	50.511908	50.3625646	48.87311345	48.66303712	48.46689951	50.85639332	50.76877855
TiO2	1.34914115	1.33490756	1.39895872	1.97541918	1.97033575	1.98151929	1.35727463	1.34100767	1.46910999 1	1.92763497 7	1.91441807 1	1.87680072 2	1.58806214 9	1.33694092 6
Al2O3	3.39566718	3.28326171	3.28939291	4.72205177	4.64438981	4.54833422	3.58777835	3.54690364	3.80645809 3	4.52278752 2	4.57899025 9	4.56059663 6	3.86368269 8	3.41917014 2
FeO	6.78739685	7.15037015	7.18707532	8.20666325	8.01600031	8.40752207	7.01680413	7.10041034	7.41240425 1	8.26274058 5	8.10062610 4	8.30250451 4	6.95766803 5	6.93727627 6
MnO	0.21644042	0.10241327	0.12880845	0.13936652	0.10769231	0.15837104	0.12669683	0.16470588	0.09185520 4	0.12141779 8	0.21855203 6	0.15520362	0.16681749 6	0.11825037 7
MgO	14.9108025	14.8117111	14.7911079	13.9287184	13.6903104	13.9414728	14.8313332	14.7842402	14.78620242	13.92871845	14.00622558	13.8119672	14.72341183	15.02559153
CaO	22.3237103	22.3317289	22.1342715	21.8035053	21.709287	22.2515431	22.2755988	21.9087491	22.19641543	22.07914378	22.02100912	21.82756102	21.97790928	22.40088907
Na2O	0.29600519	0.28669035	0.26185075	0.28979529	0.34050947	0.36534907	0.26288573	0.29497021	0.38811869 8	0.36431408 5	0.39639856 4	0.32394974	0.25046593 3	0.34464940 4
K2O	0	0	0.00833333	0	0.02604167	0.01875	0.02083333	0	0.01041666 7	0.00416666 7	0.00625	0	0.01041666 7	0.01666666 7
Cr2O3	0.06786103	0.05773252	0.04253975	0.04253975	0.04760401	0	0.01519277	0.12154215	0.09824656 9	0.05064256 2	0	0.03038553 7	0.12660640 4	0.07089958 6
Totale	99.6118595	99.5222692	100.311072	99.8052198	99.4065533	100.628612	100.251966	99.652895	100.5235453	100.0840373	99.90550685	99.32548295	100.3948274	100.3682129
Fe2O3	2.34689829	2.55944269	0.97335194	2.63005065	1.91111494	3.73107664	1.62343843	1.51731994	2.79961386 6	3.32684165 1	3.83147205 1	3.20402896 6	0.43627860 5	2.47770756 4
FeO	4.67563192	4.84735543	6.31124253	5.84011471	6.29635804	5.05025823	5.55601636	5.73510915	4.89328086 7	5.26921183 5	4.65302536 3	5.41948396 9	6.56509974 1	4.70780772 7
Wo	45.6479502	45.5371475	45.3587313	45.3163695	45.578076	45.5290752	45.5864433	45.1210736	45.06158501	45.46005208	45.35788299	45.36804178	45.45770458	45.3955594
En	42.4235315	42.0242147	42.1742405	40.2801285	39.9921379	39.6906533	42.2315877	42.365443	41.76679633	39.9033869	40.14094332	39.94397301	42.37214828	42.36728102
Fs	10.8331933	11.380736	11.4959856	13.3135462	13.1361016	13.4274968	11.2084103	11.4141516	11.74575837	13.27914661	13.02364331	13.4695253	11.23267454	10.97325456
N° Mg	79.6585439	78.689736	78.5803296	75.1583629	75.2747282	74.7214525	79.0261775	78.7760549	78.0504623	75.03100034	75.50316078	74.78254426	79.0454031	79.4279258

Dataset	B23_1Cpx r-r with Pl inc	B23_1Cpx r-r with Pl inc	B23_1Cpx r-r with Pl inc	B23_1Cpx r-r with Pl inc	B23_1Cpx r-r with Pl inc	B23_1Cpx r-r with Pl inc	B23_1Cpx r-r with Pl inc	B23_1Cpx r-r with Pl inc	B23_1Cpx r-r with Pl inc	B23_1Cpx r-r with Pl inc	B23_1Cpx r-r with Pl inc	B23_1Cpx r-r with Pl inc	B23_1Cpx r-r with Pl inc	B23_1Cpx r-r with Pl inc
SiO2	49.6218215	49.4864169	48.8999953	49.3470297	49.4455963	49.5033424	49.7363181	48.4768557	49.33209539	48.61425162	48.54754492	44.86971569	51.01768415	50.95197307
TiO2	1.60026237	1.67854712	1.79444923	1.7212479	1.60737917	1.56671176	1.55654491	1.95101873	1.635846349	1.983552659	1.939835199	1.887984258	1.231205674	1.296273521

Al2O3	4.25914559	4.44716929	4.54015928	4.43286314	4.26936427	4.13856518	3.80850183	4.55037796	4.232577026	4.430819407	4.590230807	4.220314611	2.872470792	2.754955978
FeO	6.84959171	7.34409186	7.64385071	7.66424247	7.59185173	7.79067137	7.93647245	7.87427758	6.847552538	7.760083736	8.346346795	8.066979702	7.928315744	7.777416733
MnO	0.18159879	0.15309201	0.15098039	0.23016591	0.15625943	0.1066365	0.1361991	0.11719457	0.122473605	0.095022624	0.156259427	0.131975867	0.201659125	0.168929117
MgO	14.5262101	14.3221407	14.2171627	14.3986668	14.5242479	14.4732306	14.4889282	13.9296995	14.477154999	13.735441117	13.588275722	14.030753145	14.81367335	15.152153841
CaO	22.1843876	21.2983351	21.6862336	21.6070502	21.7253242	22.0911716	21.914763	21.6792174	22.122243625	22.087162355	21.610057109	21.252228343	21.810521555	21.632108277
Na2O	0.35603422	0.38294378	0.32187977	0.32084479	0.37466392	0.30325008	0.33947449	0.33843951	0.337404522	0.327054691	0.340509471	0.492652001	0.326019707	0.307390009
K2O	0.01770833	0.02395833	0.01770833	0.01145833	0.02708333	0.01041667	0.01666667	0.01666667	0.0125	0.033333333	0.0125	0.052083333	0.013541667	0.023958333
Cr2O3	0.09419516	0.04557831	0.00506426	0.05064256	0.08913091	0	0.02734698	0.08609235	0.025321281	0.101285123	0.032411239	0.005064256	0.015192768	0.050642562
Totale	99.5967602	99.1366951	99.2724193	99.7335693	99.7217703	99.9839962	99.9338688	98.9337477	99.119848083	99.066721594	99.131559544	95.004686944	100.2150917	100.0651588
Fe2O3	2.45881629	1.61030333	2.64489025	2.42018016	2.95654815	3.15111018	3.01321869	2.70722554	2.494397408	2.522118829	2.457050702	8.365418153	2.124805065	2.270460028
FeO	4.63712174	5.89512319	5.26394934	5.48653771	4.93151715	4.95526774	5.22514509	5.43828623	4.603066284	5.490653441	6.135465518	0.539684334	6.01639275	5.734431796
Wo	45.8480029	44.6960475	45.1638455	44.8239945	44.7593211	45.2142056	44.8304024	45.3353889	45.876678744	46.161529144	45.353891542	44.309879449	44.32978693	43.841475636
En	41.7711276	41.8198334	41.1974763	41.5612167	41.6353075	41.2166352	41.2404141	40.5309135	41.773120704	39.942364844	39.680203338	40.703146041	41.89317282	42.727903423
Fs	11.0493317	12.0298416	12.4255987	12.4103108	12.2085276	12.4459883	12.672483	12.8529498	11.084000044	12.659163744	13.672672556	13.128206722	12.57792141	12.303255118
N° Mg	79.0813412	77.6603264	76.8278885	77.0058189	77.3260438	76.8069702	76.4945241	75.92353	79.030261433	75.933848116	74.373129245	75.612341044	76.90899809	77.643110776

Data set	B23_1Cpx r-r with Pl inc	B23_1Cpx r-r with Pl inc	B23_1Cpx r-r with Pl inc	B23_1Cpx r-r with Pl inc	B23_1Cpx r-r with Pl inc	B23_1Cpx r-r with Pl inc	B23_1Cpx r-r with Pl inc	B23_1Cpx r-r with Pl inc	B23_1Cpx r-r with Pl inc	B23_1Cpx r-r with Pl inc	B23_1Cpx r-r with Pl inc	B23_1Cpx r-r with Pl inc	B23_1Cpx r-r with Pl inc	B23_1Cpx r-r with Pl inc
SiO2	51.0724434	50.2779367	50.6174439	50.4999605	50.4581443	50.488013	50.9041832	50.532816	50.488013002	50.110672122	50.225168799	51.196896199	55.175403399	51.543372799
TiO2	1.2637396	1.32779076	1.35829131	1.3796417	1.33389087	1.36032468	1.34812446	1.31864059	1.318640594	1.271873078	1.310507113	1.144787439	1.02176854	1.038035502
Al2O3	2.95728583	2.76824026	2.78867762	2.89188628	3.05845076	2.93173913	2.94911089	2.94502342	2.947067152	3.004291757	3.112609759	2.767218394	2.83874915	2.610872598
FeO	7.75906415	7.855925	7.9323941	8.02415701	7.94258998	7.95176627	8.12407663	7.83247448	7.929296156	7.701967224	7.623458953	7.469501175	7.17789902	7.345111448

MnO	0.16365008	0.21221719	0.19638009	0.24072398	0.22594268	0.20482655	0.15942685	0.15942685	0.14253393 7	0.18159879 3	0.19004524 9	0.14992458 5	0.11508295 6	0.14781297 1
MgO	14.7793347	14.6684701	14.9068781	14.7224307	15.0040073	15.0187238	14.925519	14.6822055	14.8519363 1	14.6076416 8	14.8803883	15.1276262 4	13.7894018 3	15.4621823 4
CaO	21.8816864	21.4957925	21.7694264	22.0661136	21.8887026	21.2903166	21.2341865	21.4647205	21.5429016 4	21.3394303 2	21.7303358 1	21.6551616 7	21.3083583 4	21.5198482 4
Na2O	0.31670486	0.33326459	0.34154445	0.36017415	0.36534907	0.30739001	0.31463489	0.34257944	0.33636953 9	0.39225863 1	0.30118011	0.30842499 2	0.37362893 4	0.30325007 6
K2O	0.01145833	0.01875	0.025	0.01666667	0.01770833	0.00416667	0.01145833	0.015625	0.02083333 3	0.02291666 7	0.02291666 7	0.00520833 3	0.04791666 7	0.00208333 3
Cr2O3	0.04557831	0.05874537	0.06380963	0	0.06279678	0.0810281	0.05064256	0.06786103	0.00506425 6	0.05874537 1	0.02228272 7	0.03848834 7	0.02532128 1	0.06583533
Totale	100.205367	98.9583871	99.9360359	100.201755	100.294786	99.5572667	99.9707208	99.2935118	99.5755916 8	98.6326502 7	99.3966106 6	99.8247490 2	101.848208 8	99.9725693
Fe2O3	1.7429248	2.22764598	2.73491725	3.19664071	3.47659641	2.21513025	1.6361084	1.8257933	2.45440503 2	2.27525048	2.66303542	1.66838306 9	0	1.58535062 9
FeO	6.19076122	5.85146462	5.47148544	5.1477845	4.81431024	5.95856768	6.65188827	6.18960556	5.71879548 2	5.65467178 8	5.22723035 8	5.96827171 9	7.17789902 7	5.91859549 5
Wo	44.5882354	44.19325	44.1387264	44.6087795	44.1073946	43.4937461	43.4129647	44.1415372	43.9613789 5	44.1024613 3	44.4107624 6	44.1112886 5	45.5562907	43.6367885 3
En	41.9030155	41.9602625	42.0543001	41.4118764	42.0677755	42.6902428	42.4584522	42.0111347	42.1697556 5	42.0059694 3	42.3142798 4	42.8755790 8	41.0199086 8	43.6249824 5
Fs	12.34091	12.6066053	12.5538068	12.6617069	12.4925724	12.679632	12.964512	12.5724394	12.6267196 5	12.4245314 4	12.1610816 5	11.8762207 5	11.9782688 1	11.6254644 7
N° Mg	77.2492314	76.89696	77.0110932	76.5843021	77.1032025	77.1001252	76.6080501	76.9666249	76.9570586 7	77.1735860 6	77.6759964 1	78.3089856 7	77.3987156 2	78.9586055 6

Dataset	B23_1Cpx r-r with Pl inc	B23_1Cpx r-r with Pl inc	B23_3Cpxr-r	B23_3Cpxr-r	B23_3Cpxr-r	B23_3Cpxr-r	B23_3Cpxr-r	B23_3Cpxr-r	B23_3Cpxr-r	B23_3Cpxr-r	B23_3Cpxr-r	B23_3Cpxr-r	B23_3Cpxr-r	B23_3Cpxr-r
SiO2	51.1431326	51.6728037	51.3591826	50.8155728	50.6712075	50.9878155	51.0316229	51.1700144	51.2038655 4	51.5831976 9	51.1411413 3	50.9629249 2	51.4687011 1	50.8763057 7
TiO2	1.05430246	1.08785307	1.0858197	1.03295208	1.05430246	1.07463617	1.04718567	1.04921904	1.05735251 9	1.1132702	1.06040257 5	1.08378633 2	1.07666953 6	1.07971959 2
Al2O3	2.65685666	2.64050677	2.64970358	2.62926622	2.58430403	2.57715096	2.73860609	2.7191906	2.62926622 1	2.64663797 6	2.70079697 7	2.67525027 9	2.71305939 3	2.70795005 3
FeO	7.25334853	7.281897	7.13099798	7.15444851	7.14221345	6.99233402	7.08205776	6.8842577	7.19727119 8	7.12691963 1	7.19421243 4	7.07492064 7	7.30432793 1	7.11162581 2
MnO	0.16892911	0.14253394	0.15309201	0.13831071	0.14570136	0.08763198	0.2280543	0.10030166	0.15731523 4	0.15837104 1	0.16892911	0.21644042 2	0.15309200 6	0.16259426 8
MgO	15.1433239	15.3248279	15.4298059	15.5249729	15.2620373	15.3012815	15.3856563	15.5102564	15.6858738 1	15.4062594 7	15.5377272 7	15.5249729 3	15.4072405 8	15.2551696 2

CaO	21.3795232	21.8756725	21.8606376	21.8075146	21.8726655	21.5759783	21.4757461	21.5068181	21.98893482	21.68021972	22.06711592	21.79247976	21.62208506	21.62108273
Na2O	0.31566987	0.2835854	0.24218607	0.31980981	0.25771082	0.32394974	0.26702566	0.30842499	0.33947448	0.26288573	0.30842499	0.31877482	0.24736098	0.29600519
K2O	0.01458333	0.01875	0	0.0125	0.00625	0.009375	0.01875	0	0.00833333	0	0.00833333	0.009375	0.01145833	0.00520833
Cr2O3	0.04051405	0	0	0.04557831	0	0.04760401	0.02025702	0.09925942	0	0.04355260	0.04051404	0.05368111	0.02025702	0.11445218
Totale	99.1296696	100.32843	99.9114256	99.4353476	98.9963925	98.9301531	99.2747047	99.2484828	100.2676872	99.97776146	100.1870839	99.65892511	100.0039949	99.11566137
Fe2O3	1.31761624	1.52892707	1.70156748	3.00560789	2.43742325	1.73416822	1.74560606	1.57463344	3.232383124	1.146664581	2.95025995	2.71481601	1.42300329	1.856286245
FeO	6.06774293	5.90615159	5.59990883	4.44996943	4.94899317	5.43191037	5.5113422	5.4673852	4.286937648	6.095138214	4.539536038	4.632099302	6.023893896	5.441319009
Wo	43.9160542	44.2866635	44.3115482	43.9915818	44.5024107	44.113461	43.9227287	43.8741434	43.93716155	44.10578644	44.25833185	44.03140759	43.93959507	44.18446125
En	43.281012	43.1676151	43.5176526	43.5757786	43.2061169	43.529065	43.7832482	44.025304	43.61013392	43.60938852	43.35985853	43.64531855	43.56465117	43.37705512
Fs	11.6295307	11.5067964	11.2824329	11.2651743	11.34261	11.1588939	11.3057366	10.9619535	11.22519823	11.31702041	11.26240314	11.15772973	11.58609508	11.34382112
N° Mg	78.820951	78.9539639	79.4116509	79.4584636	79.2064625	79.5953366	79.477319	80.0645568	79.52926007	79.39603075	79.38129475	79.64031184	78.9919523	79.26966471

Dataset	B23_3Cpxr-r	B23_3Cpxr-r	B23_3Cpxr-r	B23_3Cpxr-r	B23_3Cpxr-r	B23_3Cpxr-r	B23_3Cpxr-r	B23_3Cpxr-r	B23_3Cpxr-r	B23_3Cpxr-r	B23_3Cpxr-r	B23_3Cpxr-r	B23_3Cpxr-r	B23_3Cpxr-r
SiO2	51.4886136	51.3243359	51.3223446	50.9410212	50.8663495	50.8962182	50.4850262	51.1152551	50.92907376	51.07045214	50.38247705	50.20326501	50.70207184	50.67519004
TiO2	1.01566843	1.04413561	1.02075186	1.120387	1.06853606	1.1061534	1.09496987	1.16308777	1.114286886	1.176304678	1.164104456	1.177321363	1.187488214	1.175287992
Al2O3	2.82137739	2.76313092	2.65992226	2.70284071	2.6905783	2.65379105	2.86940519	2.79991817	2.934804737	2.886776943	2.905170566	2.98794187	2.915389246	3.072756909
FeO	6.97296185	7.15444851	7.11672375	6.96276597	7.20134955	7.01680413	7.12182169	6.92096287	7.103469109	6.9352371	6.904649462	7.141193862	7.038215481	7.054528888
MnO	0.16259427	0.18582202	0.13514329	0.17104072	0.13831071	0.15309201	0.10769231	0.11508296	0.137254902	0.191101056	0.19638009	0.155203629	0.165761689	0.150980392
MgO	15.4366737	15.6534974	15.4768989	15.2904893	15.4347115	15.5318406	15.2551696	15.3532799	15.21396337	15.11487197	15.33758227	15.16883256	15.11781521	15.23947197
CaO	22.1412877	21.5779829	22.1583272	21.4105952	21.6270967	21.9478396	21.8095192	21.889705	21.56595504	21.82956566	22.05809502	21.74336599	22.08114842	21.70327312
Na2O	0.30221509	0.27323556	0.30118011	0.28565536	0.34154445	0.2835854	0.31049496	0.34050947	0.224591353	0.321879774	0.344649404	0.32394974	0.359139169	0.346719371

K2O	0.00625	0.00416667	0.00104167	0.009375	0.01979167	0.00729167	0.00833333	0.01458333	0	0.01875	0.01354167	0.0125	0.0125	0.01458333
Cr2O3	0	0.09419516	0.02329558	0.02329558	0.06077107	0	0	0.0790024	0.04861685	0.09115661	0.06887388	0	0.05064256	0.02329557
Totale	100.347642	99.9807555	100.192334	98.8941705	99.3882684	99.5966162	99.0624323	99.7123846	99.22339908	99.54493925	99.30664998	98.91357401	99.57952927	99.43279202
Fe2O3	2.17847595	1.993052	2.5858203	1.37661138	2.64374206	2.73392308	2.7542972	2.0559285	1.222011512	1.55430234	3.33651820	2.93965132	2.68535828	2.40237265
FeO	5.01274521	5.36107837	4.78997418	5.7240759	4.82248133	4.55679004	4.64347474	5.07101577	6.005596105	5.53665873	3.90241364	4.49606322	4.62190052	4.89284751
Wo	44.6312052	43.6474074	44.5010835	44.0208332	43.8310538	44.2953046	44.367703	44.4275842	44.29635618	44.68135429	44.64132023	44.36563089	44.82609996	44.25515176
En	43.2952608	44.0564898	43.2482419	43.7423187	43.5244312	43.6153878	43.1806119	43.3575623	43.48030376	43.04637675	43.18936612	43.06485023	42.70209957	43.23738464
Fs	10.9711303	11.2959332	11.1560915	11.1740256	11.3918939	11.0535967	11.3086378	10.9642179	11.38854258	11.0800289	10.9070928	11.37336705	11.15244792	11.22806612
N° Mg	79.7828267	79.5927032	79.4941123	79.6526412	79.2559064	79.7808633	79.246112	79.8161661	79.24406409	79.5293466	79.83769544	79.10775257	79.29153908	79.38497531
Dataset	B23_3Cpxr-r	B23_3Cpxr-r	B23_5Cpx r-r	B23_5Cpx r-r	B23_5Cpx r-r	B23_5Cpx r-r	B23_5Cpx r-r	B23_5Cpx r-r	B23_5Cpx r-r	B23_5Cpx r-r	B23_5Cpx r-r	B23_5Cpx r-r	B23_5Cpx r-r	B23_5Cpx r-r
SiO2	50.8663495	50.7379143	49.4983643	49.1220191	48.2408932	47.9531583	48.0756199	47.54794	47.66641908	47.6853359	48.19609021	47.44041279	47.40257914	47.69429651
TiO2	1.21392203	1.21697208	1.63584635	1.89306768	1.9601689	2.18688968	2.16655598	2.18993974	2.142155536	2.191973107	2.169606035	2.202139958	2.148255647	2.159439183
Al2O3	3.11567536	3.16268129	4.04761893	4.43490688	4.5554873	4.90905361	4.86920076	4.93664404	4.955037663	4.892703718	5.031677759	4.889638114	4.964234474	4.894747454
FeO	7.06676394	7.01884331	6.75477004	7.40220837	8.14854674	8.48297158	8.6165376	8.51865716	8.618576773	8.459521056	8.445246825	8.256623057	8.355523087	8.734809797
MnO	0.11930618	0.17843137	0.14464555	0.1372549	0.17209653	0.22699849	0.16892911	0.18793363	0.069683258	0.163650075	0.179487179	0.150980392	0.128808456	0.146757164
MgO	15.2993193	15.049138	14.6321693	14.0121122	13.5480505	13.5735592	13.1673826	13.3547732	13.31847242	13.30277477	14.00720668	13.36556536	13.31356693	13.84434359
CaO	21.5238575	21.9779093	22.1052041	21.8476075	21.942828	21.5629481	21.8435982	21.8546237	21.85061442	22.07914378	21.78546355	21.53989467	21.53889235	21.82054476
Na2O	0.30325008	0.31463489	0.28772533	0.35499924	0.34878934	0.42434311	0.35396425	0.34775435	0.363279102	0.360174152	0.425378093	0.401573485	0.341544455	0.429518026
K2O	0.00625	0	0.01458333	0.01666667	0.009375	0.02291667	0.00729167	0.00520833	0	0.009375	0.009375	0.00729167	0.01354167	0.01041667
Cr2O3	0.00303855	0.01316707	0.04861686	0.05874537	0.13167066	0.11647789	0.06583533	0.05773252	0.062796776	0.050642562	0.025321281	0.06583533	0.098246569	0.070899586

Totale	99.5146939	99.6565245	99.1209273	99.2208424	98.9262355	99.3428387	99.26908	98.9434742	98.98423824	99.14465156	100.2495313	98.25411949	98.20694616	99.73487315
Fe2O3	1.71448242	2.07575263	2.21082434	1.91564655	2.99020281	3.53628751	2.69613145	3.64085845	3.489847667	3.663561437	4.342486162	3.290034008	3.061004264	5.020700982
FeO	5.52405378	5.15105823	4.76544595	5.67848852	5.45792933	5.30098114	6.19052883	5.24257263	5.478373414	5.163008134	4.537829959	5.296214229	5.601197744	4.217127768
Wo	44.0377021	44.8848209	45.8068362	45.74056	45.9198799	45.0745596	45.9567307	45.8024998	45.74465883	46.14877555	44.79221556	45.53112626	45.63007776	44.82565136
En	43.5539497	42.7637364	42.188626	40.8180354	39.4489864	39.4791683	38.5456434	38.9433461	38.79556253	38.68753783	40.07173757	39.31000055	39.24399084	39.57166168
Fs	11.2855693	11.1886326	10.9255845	12.0964308	13.3102635	13.8410716	14.1499883	13.9352683	14.083501388	13.80136613	13.55334312	13.62277622	13.81655699	14.00595799
N° Mg	79.4207362	79.2620179	79.4300161	77.1396525	74.7716969	74.041618	73.1477015	73.6466841	73.3665834	73.70612627	74.72573851	74.26400607	73.96077207	73.85856619

Data set	B23_5Cpx r-r	B23_5Cpx r-r	B23_5Cpx r-r	B23_5Cpx r-r	B23_5Cpx r-r	B23_5Cpx r-r	B23_5Cpx r-r	B23_5Cpx r-r	B23_5Cpx r-r	B23_7Cpx cless c-r	B23_7Cpx cless c-r	B23_7Cpx cless c-r	B23_7Cpx cless c-r	B23_7Cpx cless c-r
SiO2	48.3414511	47.7719551	47.4832246	49.9354426	50.263998	49.8826746	48.8731135	48.8253236	48.92687706	49.53719361	48.49079444	48.4798426	48.7775337	48.54953617
TiO2	2.11267167	2.17773952	2.18078957	2.12182183	1.35015783	1.34812446	1.6460132	1.79546591	1.770048784	1.247472636	1.740564916	1.649063256	1.576878613	1.766998729
Al2O3	4.93051283	4.8773757	4.89883493	5.08685863	3.33742071	3.41508267	4.07214376	4.56366224	4.571837184	3.117719099	4.147761987	4.041487721	3.707336903	3.978131908
FeO	8.29128905	8.29842616	8.43097259	8.28109317	7.58063626	7.62345895	7.57961667	7.83451365	7.31962175	7.033117541	7.936472447	8.028235361	7.985412668	8.151605501
Mno	0.21538462	0.15942685	0.19004525	0.16470588	0.1372549	0.18898944	0.20165913	0.15942685	0.181598793	0.127752641	0.158371041	0.142533937	0.115082956	0.171040724
MgO	13.352811	13.5519749	13.266474	13.7315168	14.438892	14.6851488	14.1661454	14.248558	14.13769337	14.89216153	14.10139256	14.22206822	14.23874697	13.89339874
CaO	22.0791438	21.9338071	22.1603318	21.42563	21.4426695	21.914763	21.8155332	21.9368141	21.84059127	22.40088907	21.58199219	21.72331955	21.92679087	21.98392321
Na2O	0.44607776	0.39329361	0.36534907	0.40260846	0.32291476	0.32808967	0.30739001	0.35499924	0.369489001	0.336369539	0.361209135	0.359139169	0.024839597	0.358104186
K2O	0	0.01875	0	0.0125	0.00729167	0	0.0125	0.01666667	0	0.013541667	0.011458333	0.025	0.019791667	0.013541667
Cr2O3	0.02532128	0.08609235	0.06077107	0.08609235	0	0	0.02025702	0.04557831	0	0.131670663	0.101285123	0	0.075963842	0.124580701
Totale	99.7693418	99.1827489	98.9760218	101.162177	98.8812355	99.3863316	98.6741147	99.7354302	99.11775715	98.70621733	98.53001705	98.67068982	98.37241395	98.86628083
Fe2O3	3.27214826	3.84016966	3.97188886	0.66663248	1.25715241	3.03371451	2.79337495	3.51868963	2.559314702	3.955516467	3.303947673	4.049471619	2.170079829	3.585736627

FeO	5.34697401	4.84299922	4.85702326	7.68124992	6.44943668	4.89368923	5.06610713	4.66835798	5.0167222	3.47390026 9	4.96354395	4.38447620 8	6.03275094 2	4.9251202
Wo	46.0585126	45.7154391	46.3012829	44.8949156	44.6403466	44.822978	45.4502052	45.2120688	45.6022557 1	45.5116109 9	44.9147122	44.8567863	45.6651518 9	45.4909897 7
En	38.7571008	39.300888	38.5676495	40.0343672	41.8247614	41.7920022	41.0650739	40.8604023	41.0725239 7	42.0983999 4	40.8328780 1	40.8616237 9	41.2603115 3	40.0018047 6
Fs	13.500445	13.5002856	13.7496863	13.5440821	12.3183549	12.1706659	12.3258139	12.6035014	11.9291341 1	11.1532946 5	12.8920787 5	12.9395867 9	12.9809220 8	13.1662375 9
N° Mg	74.1655587	74.4318456	73.7186803	74.7210264	77.2485299	77.4461376	76.9140121	76.4261483	77.4929039 2	79.0555122 6	76.0035567 7	75.9492646 2	76.0681658 3	75.2365575 1

Data set	B23_7Cpx class c-r	B23_7Cpx class c-r	B23_7Cpx class c-r	B23_7Cpx class c-r	B23_7Cpx class c-r	B23_7Cpx class c-r	B23_7Cpx class c-r	B23_7Cpx class c-r	B23_7Cpx class c-r	B23_7Cpx class c-r	B23_7Cpx class c-r	B23_7Cpx class c-r	B23_7Cpx class c-r	B23_7Cpx class c-r
SiO2	50.0638779	50.1972913	50.1106721	49.9284732	50.3565909	49.9434076	49.9961755	49.7771386	49.9205082 4	49.8617665 2	50.2460767 7	50.0091186 4	51.3542045 3	50.1763832
TiO2	1.30644037	1.23120567	1.22612225	1.2362891	1.26068954	1.24645595	1.2362891	1.23933915	1.19155495 4	1.19663838	1.23323904 4	1.25865617 2	1.22408887 8	1.23832247
Al2O3	2.72327807	2.56386667	2.56693228	2.59656645	2.64459424	2.60678513	2.6650316	2.67933775	2.69262203 4	2.66196599 5	2.64663797 6	2.70590631 7	2.86531771 6	2.63335369 3
FeO	7.88039511	7.89874769	7.91404151	7.89874769	8.08023435	8.09348899	7.86510129	7.93443327	8.01090236 6	7.90078687 6	7.89263016 4	7.84470953 4	7.76620126 3	7.76212291 1
MnO	0.14253394	0.15625943	0.1984917	0.11719457	0.17104072	0.21749623	0.17420814	0.22383107	0.18687782 8	0.08657616 9	0.18371040 7	0.12352941 2	0.18371040 7	0.23227752 6
MgO	14.9716309	14.7812969	15.0412892	14.8941237	15.020686	14.6890732	14.8852938	14.792089	15.1992467 5	14.9117835 9	14.848993	14.8480119	16.0282787 4	15.0167616 1
CaO	21.4456764	21.3274025	21.5589388	21.2592446	21.3895464	21.2873096	21.478753	21.7503822	21.2923212	21.4316439 2	21.3614814	21.4887762 6	20.1256186 6	21.2812956 6
Na2O	0.37052398	0.35189429	0.33222961	0.34878934	0.37155897	0.32084479	0.32291476	0.32808967	0.29807516	0.35499923 6	0.31773984 1	0.34154445 5	0.48644210 2	0.33947448 8
K2O	0.01979167	0.00625	0.00104167	0.01354167	0.01354167	0.0125	0.00833333	0.00416667	0.00729166 7	0.01354166 7	0.00833333 3	0.025	0.059375	0.021875
Cr2O3	0.03848835	0.02835983	0.05570682	0.09115661	0.07596384	0.09318231	0.05064256	0	0.08102809 8	0.03848834 7	0.02228272 7	0	0.07292528 9	0.04861685 9
Totale	98.9241483	98.5142144	98.9497591	98.2929704	99.3084828	98.4173615	98.6321006	98.7288075	98.7994002	98.4197023 5	98.7388419 4	98.6452526 9	100.093237 3	98.7018665 6
Fe2O3	3.22293637	2.47729276	3.36619884	2.87118736	3.10573369	2.65511008	2.98397421	3.65945734	3.50658575 6	3.32122271 4	2.45301287 9	2.99754153	2.42818715 3	2.80553332 7
FeO	4.98036148	5.66965239	4.88509873	5.31522169	5.28566097	5.7043917	5.18008844	4.64161326	4.85563789	4.9123141	5.68538216 6	5.14748865 8	5.58129172 5	5.23767313 1
Wo	43.6787325	43.7968718	43.7604401	43.5824342	43.4141101	43.7798059	43.9116856	44.2810405	43.2482613 7	43.7477017 2	43.8113535 2	43.9537928 4	40.7653185 6	43.5658443 9

En	42.427778	42.2346176	42.4805627	42.4844021	42.4199346	42.0337706	42.3427785	41.9016702	42.95548312	42.3526167	42.37436509	42.25750757	45.17304699	42.77354595
Fs	12.5278521	12.6608166	12.5386556	12.6392191	12.801228	12.9923342	12.5508665	12.6085511	12.70063483	12.5883396	12.63500456	12.52448529	12.27859257	12.40300539
N° Mg	77.2036967	76.9364853	77.2104076	77.0711379	76.818257	76.3887809	77.1360301	76.8693819	77.18016401	77.0875127	77.0311773	77.1375873	78.6279509	77.52123848

Data set	B23_7Cpx cless c-r	B23_7Cpx cless c-r	B23_7Cpx cless c-r	B23_7Cpx cless c-r	B23_7Cpx cless c-r	B23_7Cpx cless c-r	B23_7Cpx cless c-r	B23_7Cpx cless c-r	B23_7Cpx cless c-r	B23_7Cpx cless c-r	B23_7Cpx cless c-r	B23_7Cpx cless c-r	B23_7Cpx cless c-r	B23_7Cpx cless c-r
SiO2	50.0638779	50.1972913	50.1106721	49.9284732	50.3565909	49.9434076	49.9961755	49.7771386	49.92050824	49.8617665	50.24607677	50.00911864	51.35420453	50.1763832
TiO2	1.30644037	1.23120567	1.22612225	1.2362891	1.26068954	1.24645595	1.2362891	1.23933915	1.191554954	1.19663838	1.233239044	1.258656172	1.224088878	1.23832247
Al2O3	2.72327807	2.56386667	2.56693228	2.59656645	2.64459424	2.60678513	2.6650316	2.67933775	2.692622034	2.66196599	2.646637976	2.705906317	2.865317716	2.633353693
FeO	7.88039511	7.89874769	7.91404151	7.89874769	8.08023435	8.09348899	7.86510129	7.93443327	8.010902366	7.90078687	7.892630166	7.844709534	7.766201263	7.762122911
Mno	0.14253394	0.15625943	0.1984917	0.11719457	0.17104072	0.21749623	0.17420814	0.22383107	0.186877828	0.08657616	0.183710407	0.123529412	0.183710407	0.232277526
MgO	14.9716309	14.7812969	15.0412892	14.8941237	15.020686	14.6890732	14.8852938	14.792089	15.19924675	14.9117835	14.848993	14.84801199	16.02827874	15.01676161
CaO	21.4456764	21.3274025	21.5589388	21.2592446	21.3895464	21.2873096	21.478753	21.7503822	21.29232122	21.43164392	21.36148146	21.48877626	20.12561866	21.28129566
Na2O	0.37052398	0.35189429	0.33222961	0.34878934	0.37155897	0.32084479	0.32291476	0.32808967	0.298075166	0.354999236	0.317739841	0.341544455	0.486442102	0.339474488
K2O	0.01979167	0.00625	0.00104167	0.01354167	0.01354167	0.0125	0.00833333	0.00416667	0.007291667	0.013541667	0.008333333	0.025	0.059375	0.021875
Cr2O3	0.03848835	0.02835983	0.05570682	0.09115661	0.07596384	0.09318231	0.05064256	0	0.081028098	0.038488347	0.022282727	0	0.072925289	0.048616859
Total e	98.9241483	98.5142144	98.9497591	98.2929704	99.3084828	98.4173615	98.6321006	98.7288075	98.79940025	98.41970235	98.73884194	98.64525269	100.0932373	98.70186656
Fe2O3	3.22293637	2.47729276	3.36619884	2.87118736	3.10573369	2.65511008	2.98397421	3.65945734	3.506585756	3.32122271	2.453012879	2.99754153	2.428187153	2.805533327
FeO	4.98036148	5.66965239	4.88509873	5.31522169	5.28566097	5.7043917	5.18008844	4.64161326	4.855637896	4.9123141	5.685382166	5.147488658	5.581291725	5.237673131
Wo	43.6787325	43.7968718	43.7604401	43.5824342	43.4141101	43.7798059	43.9116856	44.2810405	43.24826137	43.7477017	43.81135352	43.95379284	40.76531856	43.56584439
En	42.427778	42.2346176	42.4805627	42.4844021	42.4199346	42.0337706	42.3427785	41.9016702	42.95548312	42.3526167	42.37436509	42.25750757	45.17304699	42.77354595
Fs	12.5278521	12.6608166	12.5386556	12.6392191	12.801228	12.9923342	12.5508665	12.6085511	12.70063483	12.5883396	12.63500456	12.52448529	12.27859257	12.40300539
N° Mg	77.2036967	76.9364853	77.2104076	77.0711379	76.818257	76.3887809	77.1360301	76.8693819	77.18016401	77.0875127	77.0311773	77.1375873	78.6279509	77.52123848

Table 9.1 – Continue. Single mineral phase EMPA analyses. Sample: sub-ophitic gabbro B23. Olivines.

Data set	B23_2_Ol of MI	B23_2_Ol of MI	B23_2_Ol of MI	B23_4_Ol of MI1	B23_4_Ol of MI1	B23_4_Ol of MI1	B23_4_Ol of MI	B23_4_Ol of MI	B23_9_Ol of MI	B23_9_Ol of MI	B23_9_Ol of MI	B23_2Ol from Mi to r	B23_2Ol from Mi to r	B23_2Ol from Mi to r
SiO2	38.8740775	38.4648767	38.8641212	39.0254121	39.0144602	38.8810468	38.9626879	38.9945478	38.48180223	38.09649636	38.53556585	38.88901181	38.85615627	38.73469033
TiO2	0.02338376	0.03863403	0.054901	0.07015127	0.06710122	0.05388431	0.04575083	0.0477842	0.065067847	0.048800885	0.031517239	0.062017792	0.037617349	0.027450498
Al2O3	0.04087472	0.03065604	0	0.04087472	0.05518087	0.04291845	0.04189659	0.02145923	0.075618228	0.054159001	0.03985285	0.021459227	0.040874718	0.061312077
Cr2O3	0	0	0.05368112	0.07495099	0.03241124	0.03038554	0	0.02126988	0.033424091	0.01620562	0.026334132	0	0.005064256	0.014179917
FeO	20.5263442	20.4457968	20.1572534	20.4926978	20.5222659	20.4804628	20.4121504	20.8740237	20.385641067	20.23882041	20.4508947	20.46924728	20.40093489	20.55489267
MnO	0.2280543	0.31568627	0.3653092	0.22594268	0.28717949	0.22488688	0.26923077	0.28612368	0.284012066	0.246003017	0.342081448	0.263951735	0.233333333	0.329411765
MgO	39.8013841	39.7484045	39.4501492	39.2794373	39.2912106	39.7042549	39.6022202	39.3088704	39.498223285	39.12147975	39.46879019	39.54727843	39.371661	39.45799806
CaO	0.34580101	0.33477547	0.38188459	0.32575457	0.30370349	0.33778243	0.25759669	0.32976386	0.252585084	0.314729033	0.275638485	0.304705816	0.284659383	0.275638485
Na2O	0.01448976	0.02380461	0.01448976	0.03208448	0.00517492	0	0.03829438	0	0.023804614	0.010349832	0	0.013454782	0.025874578	0.010349832
NiO														
Totale	99.8544093	99.4026344	99.3417895	99.5673059	99.5786879	99.7556221	99.6298277	99.8838427	99.100178512	98.14704391	99.17067489	99.57112686	99.25617577	99.46592363
Fo	77.3656209	77.3353593	77.4055595	77.1640476	77.0915333	77.3642969	77.3390252	76.8031158	77.302699	77.292529	77.184421	77.270829	77.276988	77.102476
Fa	22.3825156	22.3156681	22.1871903	22.583764	22.5883252	22.3867344	22.3622432	22.8792559	22.381486	22.431323	22.435492	22.436148	22.462804	22.531803

Data set	B23_2Ol from Mi to r	B23_2Ol from Mi to r	B23_2Ol from Mi to r	B23_2Ol from Mi to r	B23_2Ol from Mi to r	B23_2Ol from Mi to r	B23_2Ol from Mi to r	B23_2Ol from Mi to r	B23_2Ol from Mi to r	B23_2Ol from Mi to r	B23_2Ol from Mi to r	B23_2Ol from Mi to r	B23_2Ol from Mi to r	B23_2Ol from Mi to r
SiO2	38.6998435	38.6430931	38.825292	38.6709705	38.5893295	38.7287166	38.8730818	38.7615721	38.689887322	38.78745832	38.89697678	41.66779399	38.76356338	38.52760087
TiO2	0.01728365	0.01525028	0.03050055	0.01423359	0	0.03050055	0.0203337	0.03456729	0.035583979	0.015250277	0.013216906	0.037617349	0.013216906	0.025417128
Al2O3	0.07459636	0.02759043	0.0510934	0.02350296	0.02759043	0.00102187	0.02656857	0.02656857	0.063355813	0.041896586	0	0.061312077	0.011240547	0.04496219
Cr2O3	0.03139839	0.02430843	0.03544979	0.01620562	0	0.01215421	0.06178393	0	0.040514049	0	0.038488347	0	0	0.021269876

FeO	20.5324617	20.7659474	20.9963742	20.3723864	20.5926174	20.7017133	20.8495536	20.4498751	20.37136684	20.59159784	20.96680619	20.49371739	20.91072886	20.53654009
MnO	0.23016591	0.37586727	0.33680241	0.34524887	0.23544495	0.32730015	0.31779789	0.27239819	0.307239819	0.274509804	0.282956259	0.290346908	0.293514329	0.314630468
MgO	39.7101415	39.2460798	39.8641747	39.4207161	39.5953525	39.7601778	39.5973147	39.248042	39.49429887	39.77881872	39.46780909	38.12173585	39.67580291	39.6061446
CaO	0.31673368	0.29167563	0.29167563	0.2856617	0.29768956	0.26561527	0.27062688	0.25458973	0.310719746	0.271629198	0.265615267	0.323749929	0.337782434	0.310719746
Na2O	0.00517492	0.02069966	0.0124198	0.02587458	0.03932936	0.00206997	0	0.00517492	0.045539261	0.023804614	0.018629698	0.050714177	0.002069966	0
NiO														
Totale	99.6177997	99.410512	100.443782	99.1748004	99.3773537	99.8292697	100.017061	99.052788	99.3585057	99.78496535	99.95049854	101.0469877	100.0079193	99.38728496
Fo	77.3184328	76.789102	76.9072631	77.2268068	77.2122593	77.1153013	76.926734	77.1463577	77.29310531	77.26103317	76.79976035	76.57539652	76.93123963	77.196687
Fa	22.4269429	22.7930532	22.723558	22.3889085	22.5268801	22.524024	22.722482	22.5494285	22.36526073	22.43603586	22.88740609	23.09323516	22.74540245	22.45488418

Dataset	B23_2Ol from Mi to r	B23_2Ol from Mi to r	B23_2Ol from Mi to r	B23_2Ol from Mi to r	B23_2Ol from Mi to r	B23_2Ol from Mi to r	B23_2Ol from Mi to r	B23_2Ol from Mi to r	B23_2Ol from Mi to r	B23_2Ol from Mi to r	B23_2Ol from Mi to r	B23_2Ol from Mi to r	B23_2Ol from Mi to r	B23_2Ol from Mi to r
SiO2	38.2896471	38.8322613	38.3623275	38.7824802	38.8890118	38.3862225	38.7307078	38.7974145	38.58435134	38.77451523	38.72075162	38.68092672	38.38622248	38.75958089	38.93580606
TiO2	0.0203337	0.04270077	0.02135039	0.02338376	0.02846718	0.02541713	0.0406674	0.02440044	0.018300332	0.035583979	0.016266962	0.023383758	0.022367073	0.028467183	0.020333702
Al2O3	0.08583691	0.07459636	0.03372164	0.01839362	0.00204374	0.03474351	0.04394032	0.03065604	0.029634171	0.014306155	0.091968115	0.004087472	0.008174944	0.026568567	0.066421416
Cr2O3	0	0.00506426	0.02633413	0.04557831	0.02633413	0	0	0.06887388	0.026334132	0	0.014179917	0.021269876	0	0.052668264	0.068873884
FeO	20.4498751	20.3254854	20.5977154	20.5732453	20.6405381	20.8464948	20.6293226	20.4294834	20.67826281	20.55693185	20.71394839	20.57630402	20.7384185	20.61708753	20.81692677
MnO	0.33574661	0.36003017	0.29351433	0.33046757	0.28506787	0.29984917	0.29984917	0.28612368	0.273453997	0.339969834	0.322021116	0.300904977	0.296681751	0.296681751	0.323076923
MgO	39.3402657	39.5080343	39.6826706	39.6463698	39.5835792	39.6316533	39.4629036	39.3795098	39.42365946	39.31868144	39.41188622	39.48841225	39.26864519	39.38735865	39.68855725
CaO	0.28065009	0.27664081	0.23354097	0.30671046	0.24356419	0.33377315	0.27664081	0.24556883	0.274636163	0.236547936	0.273633841	0.308715103	0.258599015	0.226524718	0.312724397
Na2O	0.0310495	0.00310495	0.00724488	0.02069966	0.02173465	0.05071418	0.06416896	0	0.020699664	0.013454782	0	0.016559731	0.016559731	0.008279866	0.047609227

NiO															
Totale	98.8334047	99.4279183	99.2584199	99.7473287	99.7203409	99.6088677	99.5482007	99.2620306	99.32933207	99.28999119	99.56465617	99.4205639	98.99566868	99.40321742	100.2803296
Fo	77.1332399	77.2927725	77.1971144	77.1700807	77.1241749	76.9599167	77.0670912	77.2107742	77.03074722	77.02919193	76.95385361	77.12238002	76.89022439	77.04626218	76.99041044
Fa	22.4927416	22.3070344	22.4784663	22.4644494	22.5602513	22.7092551	22.6002033	22.4704843	22.66567593	22.59238817	22.68890266	22.54371929	22.77971536	22.62400457	22.65350392

Table 9.1 – Continue. Single mineral phase EMPA analyses. Sample: sub-ophitic gabbro B23. Feldspars.

Data Set	B23_1_Pl_r-r	B23_1_Pl_r-r	B23_1_Pl_r-r	B23_1_Pl_r-r	B23_1_Pl_r-r	B23_1_Pl_r-r	B23_1_Pl_r-r	B23_1Pl r-r	B23_1Pl r-r	B23_1Pl r-r	B23_1Pl r-r	B23_1Pl r-r	B23_1Pl r-r	B23_1Pl r-r
SiO2	50.076821	50.480048	50.6761857	50.4601356	50.2948623	49.6606508	49.2843055	47.7022615	47.90138597	47.58079555	47.70923084	47.77295068	48.25383631	47.95216271
TiO2	0.06405116	0.08641823	0.09455172	0.09150166	0.0955684	0.0752347	0.06100111	0.0884516	0.046767515	0.074218013	0.084384865	0.04575083	0.070151273	0.064051162
Al2O3	31.7616995	31.3049245	31.6707532	31.7433058	31.3192306	31.9313295	32.2930708	32.6098498	32.79787355	32.57715007	32.18475278	32.37992956	32.54547216	32.62313413
Cr2O3	0	0.01012851	0.01316707	0	0.0435526	0.02025702	0.00303855	0	0.015192768	0.033424091	0.010128512	0	0.051655413	0.008102809
FeO	0.68006515	0.62398781	0.66681051	0.67904556	0.64641875	0.6331641	0.66477133	0.7432796	0.661712567	0.626026989	0.808533229	0.642340396	0.689241441	0.631124929
Mno	0.03800905	0.03800905	0.03273002	0.02533937	0	0	0.00739065	0.01794872	0	0.012669683	0	0.032730015	0	0
MgO	0.13735441	0.13735441	0.11773235	0.15501426	0.16874971	0.11577015	0.16090088	0.12656228	0.110864632	0.156976467	0.116751252	0.114789044	0.111845735	0.120675662
CaO	15.1761538	14.4895634	14.7862506	14.8704457	15.0999773	15.4989014	15.8126281	16.8490288	16.51325103	16.36991902	16.28171471	16.60746928	16.65056911	16.31178436
Na2O	2.88967308	3.1101245	3.17532844	3.08217996	3.21672777	2.77065002	2.75409028	2.09791094	2.1310304	2.238668653	2.370111518	2.217968979	2.262473266	2.301802628
K2O	0.128125	0.140625	0.1375	0.15208333	0.146875	0.12291667	0.115625	0.07604167	0.084375	0.104166667	0.086458333	0.084375	0.069791667	0.089583333
SrO														
BaO														
Totale	100.951952	100.421183	101.37101	101.259051	101.031962	100.828874	101.156822	100.311335	100.2624534	99.77401521	99.65206604	99.89830379	100.7050364	100.1024217
Ab %	25.4365339	27.7452079	27.7644035	27.0374676	27.5933436	24.269404	23.8073527	18.3084148	18.83904208	19.71833747	20.74626295	19.36958789	19.65743121	20.23625819
An %	73.8213784	71.4293534	71.4445273	72.0847199	71.577665	75.0221605	75.5349943	81.2549412	80.67016865	79.67796229	78.75578209	80.14558064	79.94358154	79.24553698
Or %	0.74208765	0.82543874	0.79106923	0.87781247	0.82899136	0.7084355	0.65765296	0.43664393	0.490789272	0.603700239	0.497954957	0.484831469	0.398987217	0.518204825

Data Set	B23_1Pl r-r	B23_1Pl r-r	B23_1Pl r-r	B23_1Pl r-r	B23_1Pl r-r	B23_1Pl r-r	B23_1Pl r-r	B23_1Pl r-r	B23_3Plr-r	B23_3Plr-r	B23_3Plr-r	B23_3Plr-r	B23_3Plr-r	B23_3Plr-r
SiO2	48.2797225	48.283705	48.2010683	48.2936612	48.6729933	47.9690883	48.1662215	47.9790445	45.9798347	46.0983137 6	45.8294957 1	46.6528754 5	46.9635096 5	47.7610032 1
TiO2	0.05795105	0.05286763	0.06303448	0.05591768	0.05896774	0.04371746	0.07930144	0.07320133	0.07116795 8	0.05286762 6	0.03253392 4	0.05693436 6	0.07320132 8	0.06303447 7
Al2O3	32.3615359	32.12855	32.2276712	32.4800726	31.8700175	32.0815441	32.3257706	32.4575915	32.2051901 4	32.2378899 1	32.6578776 4	32.0672379 7	32.1285500 4	31.4111987 5
Cr2O3	0.03139839	0	0	0.05165541	0	0.1266064	0.06178393	0.02532128	0	0	0	0	0.01316706 6	0.03139838 8
FeO	0.6250074	0.67394762	0.66579092	0.64641875	0.69128062	0.66375174	0.66273215	0.74226001	0.61990946 1	0.66477133	0.55771459 8	0.64030122	0.66783009 4	0.60665481 8
Mno	0	0.03589744	0.0158371	0	0.05806938	0.04751131	0.01794872	0	0.03800905	0	0.04012066 4	0.05490196 1	0	0.02956259 4
MgO	0.15010875	0.11478904	0.13539221	0.07358272	0.15991978	0.11675125	0.13048669	0.11184574	0.13343	0.11577014 7	0.10203470 6	0.11577014 7	0.10497801 5	0.12852448 5
CaO	16.4070049	16.4491024	16.2095475	16.2656776	16.2757008	16.4791721	16.4581233	16.0692225	17.4283708	17.2529644 9	17.2649923 6	16.6866527	16.8319893 5	15.8016025 8
Na2O	2.34216697	2.32250229	2.31939734	2.56054843	2.61022762	2.34009701	2.37528643	2.35769172	1.80708066 5	1.94783837	1.91057898 3	2.10929575	2.16932477 8	2.52949893 1
K2O	0.08541667	0.10104167	0.09583333	0.096875	0.09895833	0.09479167	0.084375	0.08229167	0.05520833	0.07604166 7	0.06979166 7	0.09479166 7	0.09791666 7	0.096875
SrO														
BaO														
Totale	100.340313	100.162403	99.9335725	100.524409	100.496135	99.9630313	100.36203	99.8984703	98.3382011	98.4464573 2	98.4651402 4	98.4787612 3	99.0504669 9	98.4593532 3
Ab %	20.4290451	20.2330302	20.4534983	22.0495331	22.3683322	20.3329949	20.6088426	20.8798705	15.7488969 3	16.8909186	16.6178594 8	18.5144208 5	18.8062670 9	22.3351115 5
An %	79.0807418	79.1877847	78.9904424	77.4015707	77.0736864	79.1250669	78.909472	78.6406072	83.9345187 9	82.6752069 4	82.9827242 4	80.9381159 7	80.6352026	77.1020581 8
Or %	0.49021313	0.5791851	0.55605934	0.5488962	0.55798137	0.54193819	0.48168542	0.47952223	0.31658427 8	0.43387445 6	0.39941627 8	0.54746318 1	0.55853031 1	0.56283026 8

Data Set	B23_3Plr-r	B23_3Plr-r	B23_3Plr-r	B23_3Plr-r	B23_3Plr-r	B23_3Plr-r	B23_3Plr-r	B23_5alt Pl r-r	B23_5alt Pl r-r	B23_5alt Pl r-r	B23_5alt Pl r-r	B23_5alt Pl r-r	B23_5alt Pl r-r	B23_5alt Pl r-r
SiO2	48.8312973	49.0503342	47.6355548	48.0377862	48.5664617	49.2604106	47.8068018	46.7663764	48.4390220 8	47.1467041 7	48.8611659 8	45.7000647 9	47.3089906 3	47.3697236

TiO2	0.06506785	0.09150166	0.0406674	0.04981757	0.05998442	0.08031812	0.05693437	0.05388431	0.062017792	0.055917681	0.050834256	0.056934366	0.064051162	0.051850941
Al2O3	31.2425905	30.8644994	31.9170234	31.6717751	30.9697518	31.107704	32.3492735	32.3605141	33.74718887	32.15614048	31.05865431	30.30860323	32.36766714	32.18168718
Cr2O3	0	0.03646264	0	0	0	0	0.01519277	0	0	0.046591157	0.025321281	0.010128512	0.003038554	0
FeO	0.64641875	0.66171257	0.7096332	0.65457545	0.74124043	0.58116512	0.70249608	0.69331979	0.658653803	0.584223884	0.690261029	0.696378556	0.714731139	0.605635233
Mno	0.0306184	0.0147813	0.0158371	0	0	0.01055807	0	0.04223228	0	0.002111614	0.005279035	0.012669683	0	0.040120664
MgO	0.1667875	0.15403316	0.15893868	0.13048669	0.1344111	0.17169301	0.12263787	0.10203471	0.115770147	0.069658309	0.15697647	0.1667875	0.118713456	0.136373309
CaO	15.4948921	14.9817034	16.1243502	15.4517923	15.5951243	15.503913	16.2446288	16.693669	16.93723314	16.87308455	15.31647885	16.04316213	16.9031542	16.35187723
Na2O	2.83378399	3.13082417	2.44773526	2.7344256	2.85344867	3.06458524	2.41668576	2.1310304	1.939558509	2.069966392	2.857588604	2.376321418	2.169324778	2.390811182
K2O	0.10520833	0.11979167	0.09583333	0.125	0.11875	0.12083333	0.09375	0.078125	0.070833333	0.0875	0.130208333	0.134375	0.088541667	0.116666667
SrO														
BaO														
Totale	99.4166648	99.1056442	99.1455733	98.8556589	99.0391725	99.9011805	99.808401	98.9211859	101.9702777	99.09189823	99.15276815	95.50542519	99.73821273	99.244746
Ab %	24.7157627	27.2517145	21.4316677	24.0805262	24.7063471	26.1671824	21.0969184	18.6811826	17.09511663	18.07576243	25.05084265	20.97334878	18.75236427	20.78310288
An %	74.6804701	72.0622069	78.0162292	75.1951679	74.6171274	73.1539515	78.3645859	80.8681908	82.49409425	81.42148594	74.19809928	78.2462945	80.74402932	78.54959271
Or %	0.60376721	0.68607859	0.55210315	0.72430583	0.67652554	0.67886609	0.53849568	0.45062663	0.410789151	0.502751631	0.751058071	0.780356726	0.503606411	0.667304421

Data Set	B23_5alt Plr-r	B23_5alt Plr-r	B23_5alt Plr-r	B23_5alt Plr-r	B23_5alt Plr-r	B23_5alt Plr-r	B23_5alt Plr-r	B23_5alt Plr-r	B23_5alt Plr-r	B23_5alt Plr-r	B23_5alt Plr-r	B23_5alt Pl r-r
SiO2	47.3508068	47.1705991	48.1273923	47.5917474	47.8824691	47.511102	47.5369882	47.2850957	47.744077633	48.240893225	48.672993355	47.682349044
TiO2	0.08133481	0.03355061	0.02643381	0.08336818	0.07015127	0.03761735	0.05591768	0.03965072	0.068117903	0.062017792	0.075234698	0.069134588
Al2O3	32.1418343	32.9378695	32.1837309	32.329858	31.7780493	31.9732261	32.2205182	32.647659	31.730021544	31.897607896	31.873083006	32.586346888
Cr2O3	0.04861686	0	0	0	0	0.02329558	0.00810281	0.01519277	0.033424091	0.028359834	0.020257025	0.036462644
FeO	0.65559504	0.60767441	0.60563523	0.67496721	0.67190845	0.69841773	0.62092905	0.61787029	0.747357953	0.625007401	0.606654818	0.732064134

Mno	0	0.05067873	0.03589744	0.00527903	0	0.02217195	0	0.0453997	0.054901961	0.02745098	0.040120664	0.025339367
MgO	0.0990914	0.1000725	0.12460007	0.11773235	0.10301581	0.14814654	0.13833551	0.14814654	0.144222132	0.125581176	0.118713456	0.120675662
CaO	16.6365366	16.9673028	16.344861	16.3739283	15.9389207	16.2917379	16.4450932	16.8319894	16.360898133	15.8026049	15.969992674	16.076238755
Na2O	2.25315842	2.15483501	2.43842041	2.30387259	2.58538802	2.42393064	2.20761916	2.1620799	2.386671258	2.677501528	2.680606477	2.284207913
K2O	0.09479167	0.09583333	0.10208333	0.09375	0.09583333	0.08333333	0.075	0.0875	0.117708333	0.108333333	0.115625	0.095833333
SrO												
BaO												
Totale	99.3617659	100.118416	99.9890544	99.5745031	99.125736	99.2129791	99.3085037	99.8805839	99.387400922	99.595358055	100.1732812	99.7086523
Ab %	19.5775536	18.5857292	21.1342506	20.1849782	22.5673938	21.1114665	19.4597624	18.7663972	20.744355053	23.320525533	23.145170177	20.338418711
An %	79.8805092	80.8704019	78.2835856	79.2745747	76.8821987	78.4109723	80.1052402	80.7338798	78.582472022	76.058630001	76.197942088	79.100132377
Or %	0.54193719	0.54386897	0.58216382	0.54044712	0.55040754	0.47756124	0.43499748	0.49972298	0.673172939	0.620844468	0.656887753	0.561448912

Table 9.1 – Continue. Single mineral phase EMPA analyses. Sample: sub-ophitic gabbro B23. Glass.

Data set	B23_1_Glass	B23_1_Glass	B23_1_Glass	B23_1_Glass	B23_5_Glass	B23_5_Glass	B23_5_Glass
SiO2	49.614913	49.2602139	49.051391	49.0304088	49.3231605	48.94648	49.0364037
TiO2	3.26352035	3.25846376	3.2311582	3.31610884	3.25441849	3.26958825	3.22205634
Al2O3	14.6177439	14.3343874	14.1180614	14.2978253	14.3770432	14.6279001	14.4339177
Cr2O3	0.051	0	0.044	0	0.066	0	0.015
FeOtot	11.716904	12.0686156	11.9909118	12.3119509	11.5134429	11.7250833	11.8109664
MnO	0.19176707	0.20883534	0.17570281	0.20180723	0.16666667	0.25502008	0.20180723
MgO	5.47619798	5.81068308	5.54986434	5.57176515	5.42542792	5.56280573	5.37863983
CaO	10.5526848	10.2742365	10.6519137	10.6620391	10.7531676	10.3025876	10.429155
Na2O	1.39121129	2.60204199	1.17040056	1.68147893	3.43448809	3.25514416	3.25618083
K2O	1.02739808	0.99525949	1.02739808	1.05020611	0.9776351	0.98281875	0.95171689
P2O5	0.41370031	0.43810398	0.40788991	0.50550459	0.34165138	0.40905199	0.42299694
F							
Cl							
Total	98.3170408	99.250841	97.4186919	98.6290949	99.6331018	99.3364799	99.1588408

Table 9.1 – Continue. Single mineral phase EMPA analyses. Sample: sub-ophitic gabbro B23. Melt inclusions (MI).

Data set	B23_1_MI in Cpx	B23_1_MI in Cpx	B23_1_MI in Cpx	B23_1_MI in Cpx	B23_1_MI in Cpx	B23_2_MI in Cpx	B23_2_MI in Cpx	B23_2_MI in Cpx	B23_2_MI in Cpx	B23_2_MI in Cpx	B23_4_MI in Ol	B23_4_MI in Ol	B23_4_MI1 in Ol
SiO2	46.639437	46.6334421	46.4695811	46.8282768	47.0251098	48.1791309	48.4059385	48.0622301	48.36697158	47.79645553	48.29803006	48.01626907	48.41093429	47.56964793
TiO2	3.85210691	3.87840116	3.97043101	3.94312545	4.0938117	3.20385264	3.22711293	3.13710571	3.194750783	3.20284132	3.18160366	3.207897905	3.254418493	3.764122321
Al2O3	14.2145449	14.0906398	14.1922013	13.924079	14.0500153	14.5212605	14.3638402	14.0266561	14.22876346	14.0530621	14.39430868	14.1972794	14.28157543	14.47962032
Cr2O3	0.058	0	0	0.094	0	0.011	0	0.029	0	0.08	0.007	0	0	0.084
FeOtot	13.6267798	13.6922145	13.4366101	13.5184035	13.3558391	11.6708952	11.5635414	11.4848152	11.37234929	11.36416995	11.59625871	11.19240382	11.53184641	11.29464556
MnO	0.19578313	0.16064257	0.18473896	0.24598394	0.21084337	0.19678715	0.22188755	0.19879518	0.257028112	0.128514056	0.146586345	0.261044177	0.159638554	0.206827309
MgO	5.16859115	5.30596896	5.14669034	5.06306907	5.04216375	5.34379763	5.50506723	5.3816263	5.414477517	5.345788613	5.359725492	5.381626302	5.381626302	5.142708375
CaO	10.1496942	9.81758127	9.8287192	10.0342647	10.1253932	10.3775155	10.2742365	10.2701863	10.26512365	10.47674436	10.28841205	10.20335875	10.82809551	9.598872772
Na2O	3.01256335	2.93584976	2.99286662	3.01671003	3.16599053	3.05506683	3.19087061	2.85395283	2.925483063	3.216787365	3.151477148	3.013600023	3.064396858	3.270694211
K2O	0.80553815	0.79828105	0.79413414	0.83352982	0.81072179	0.94549652	0.95690053	0.96415763	0.985928934	0.975561647	0.918541572	0.932019044	0.928908859	1.237853992
P2O5	0.33119266	0.33932722	0.3346789	0.35327217	0.30911315	0.33351682	0.44740061	0.40324159	0.373027523	0.373027523	0.42648318	0.392782875	0.350948012	0.399755352
F														
Cl														
Total	98.0542311	97.6523484	97.3506517	97.8547145	98.1890018	97.8383197	98.1567961	96.811767	97.38390391	97.01295247	97.7684269	96.79828136	98.19238872	97.04874814

Data set	B23_4_MI1 in Ol	B23_4_MI1 in Ol	B23_4_MI in Cpx	B23_4_MI in Cpx	B23_4_MI in Cpx	B23_6_MI in Cpx	B23_6_MI in Cpx	B23_6_MI in Cpx	B23_6_MI1 in Cpx	B23_6_MI1 in Cpx	B23_6_MI1 in Cpx	B23_8_MI in Cpx	B23_8_MI in Cpx	B23_8_ MI1 in Cpx
SiO2	48.3399945	47.9663114	45.1926643	45.7062286	45.6453056	46.3177099	46.2497675	45.9010633	48.31101904	47.98529535	48.26379253	47.30587168	47.50570217	48.96146729
TiO2	3.7509752	3.7985071	4.24348664	4.27281483	4.22839339	4.04729111	4.17673971	4.00178184	3.565904166	3.454659282	3.680400115	3.646809535	3.619503973	3.301950397
Al2O3	14.3181376	14.4257927	13.061822	13.2842417	13.4610664	13.6671285	13.8946262	13.7747836	14.44915188	14.5608695	14.81197586	13.94540693	13.9088448	14.44610503
Cr2O3	0	0.007	0.004	0.062	0	0	0	0	0.12	0	0.033424091	0	0.004	0

FeOtot	11.3549682	11.3641699	15.0980385	14.5275295	14.9022972	14.249432	14.2555665	13.8936307	13.13295214	13.1482884	13.7440453	13.33232354	13.25257498	12.42339443
MnO	0.18273092	0.20381526	0.31526104	0.23293173	0.29457014	0.22791165	0.17771084	0.20582329	0.240963855	0.16064257	0.249170437	0.170682731	0.213855422	0.201807229
MgO	5.21139728	5.22832063	5.42940989	5.29601404	5.35584095	5.09890675	5.30397798	5.37465786	4.492652516	4.84704744	4.201082791	4.950578542	5.215379244	4.967501895
CaO	9.89352171	10.0535029	10.1122302	10.3663776	10.454216	10.1010923	10.2438603	10.2570233	9.505719154	9.279922885	8.848496517	9.941111063	9.567484053	9.474330435
Na2O	3.52364172	3.09238695	2.17908058	2.30555433	2.5377788	2.65491216	2.76790921	2.59996865	3.383691254	3.282097582	3.129789184	2.970059878	2.972133218	3.116230364
K2O	1.21815615	1.18083392	0.75577518	0.67283689	0.728125	0.69460819	0.69046127	0.66661651	0.915431386	0.894696814	0.964583333	0.868778598	0.834566553	0.962084175
P2O5	0.53920489	0.53688073	0.30330275	0.33932722		0.20801223	0.24752294	0.22079511	0.327706422	0.231253823		0.296330275	0.314923547	0.413700306
F														
Cl														
Total	98.3327281	97.8575217	96.6950711	97.0658565	97.6075934	97.2670048	98.0081425	96.8961443	98.44519181	97.84477365	97.92676015	97.42795277	97.40896796	98.26857154

Dataset	B23_8_ MI1 in Cpx	B23_8_ MI1 in Cpx	B23_9_MI in Ol	B23_9_MI in Ol	B23_9_MI in Ol	B23_9_MI in Ol
SiO2	48.9684614	48.3539826	48.0902064	47.8014513	47.9952869	47.9703081
TiO2	3.28779196	3.19778473	3.70445461	3.65186612	3.74389598	3.63467373
Al2O3	14.1779827	14.2419665	14.2886847	14.2693881	14.3861838	14.441027
Cr2O3	0	0	0	0.033	0.022	0
FeOtot	12.0246516	12.1391624	11.263973	11.5001515	11.4899273	11.2118297
MnO	0.24297189	0.1686747	0.15863454	0.21485944	0.21987952	0.23493976
MgO	5.18252803	5.44931971	5.00035311	5.05211866	5.0939293	4.68577784
CaO	9.99072549	9.79733048	10.0757788	9.73759066	9.98768787	10.0443901
Na2O	2.97835324	3.02189338	3.38680126	3.26862087	3.2986843	3.40338799
K2O	0.93927614	0.86670514	1.27724968	1.16528299	1.28243332	1.17772373
P2O5	0.34281346	0.47993884	0.55431193	0.53688073	0.56012232	0.51828746
F						

Cl						
Total	98.1355559	97.7167584	97.8004481	97.2312103	98.0800305	97.3223453

Table 9.1 – Continue. Single mineral phase EMPA analyses. Sample: sub-ophitic gabbro B33. Clinopyroxenes.

Data Set	B33_5_Cpx of MI	B33_5_Cpx of MI	B33_5_Cpx of MI	B33_10Cpx c-r	B33_10Cpx c-r	B33_10Cpx c-r	B33_10Cpx c-r	B33_10Cpx c-r	B33_10Cpx c-r	B33_10Cpx c-r	B33_10Cpx c-r	B33_6Cpc r-r	B33_6Cpc r-r	B33_6Cpc r-r	B33_6Cpc r-r
SiO2	50.6572688	50.3814814	51.0226623	51.7146198	51.8092049	51.6509	51.3561958	51.8330989	50.0250486	51.7614141	51.8450461	50.5248505	50.7976516	50.8046209	50.8713276
TiO2	1.37455827	1.32067396	1.37760833	1.0258352	1.0227852	1.1000532	1.0136350		1.0614192	1.0583692	1.0492190	1.0675193	1.0258352	1.0878530	1.0705694
Al2O3	3.72266492	3.80237062	3.72164305	2.7794808	2.8377272	2.7283874	2.8254648	2.6190475	2.7723277	2.8745145	2.7610871	3.1810749	3.1350908	3.1310033	3.1902717
FeO	6.31634723	6.26128948	6.57838132	6.8128865	6.5977535	6.6436349	6.5426957	6.5121081	6.0736852	6.0685873	6.1267038	5.5832635	5.7178491	5.9350213	5.8728264
Mno	0.1668175	0.15098039	0.12352941	0.1815987	0.1868778	0.1499245	0.1604826	0.1562594	0.1171945	0.1699849	0.1921568	0.1657616	0.0971342	0.1076923	0.0918552
MgO	15.0422703	15.1953223	14.9706498	15.615234	15.751607	15.627988	15.667232		16.539433	15.666251	15.817341	15.839906	15.578933	15.303243	15.289508
CaO	22.5402118	22.3487683	22.1432924	22.089167	22.078141	21.974902	22.220471	22.258559	21.449685	22.014995	22.305668	23.080463	22.231496	22.814847	22.743683
Na2O	0.26806065	0.22355637	0.28048045	0.2846203	0.3115299	0.2701306			0.2794454	0.2287312	0.2763405	0.2494309	0.2825504	0.2421860	0.2245913
K2O	0.00416667	0.00833333	0	0.0041666	0.015625	0	0	0	0.0125	0	0	0	0.003125	0.009375	0.0020833
Cr2O3	0.0810281	0.04051405	0.05368112	0.0587453	0.0435526	0.1114136	0.0182313	0.0688738	0.0688738	0.0941951	0.0638096	0.1630690	0.1377477	0.0911566	0.0587453
Totale	100.092366	99.6927763	100.218247	100.50761	100.61125	100.14592	100.03250	100.18218		99.842848	100.37356	99.692271	98.869666	99.435843	99.356716
Fe2O3	1.73926725	1.92795705	0.8575335	1.8469754	1.9351449	1.3659952	2.1218647	1.1845372	4.0766992	0.5774230	1.5474362	3.5808681	1.8077817	2.1240840	1.7473816
FeO	4.7513354	4.52649249	5.80676324	5.1509577	4.8564887	5.4144974	4.6334184	5.4462484	2.4054263	5.5490157	4.7343037	2.3611588	4.0911872	4.0237471	4.3005132
Wo	46.1084003	45.8123694	45.5476219	44.490680	44.415247	44.488897	44.824248	45.071273	43.150441	44.961878	44.974635	46.226176	45.479623	46.391868	46.408210
En	42.8140536	43.3401066	42.8464714	43.761189	44.090533	44.022902	43.974706	43.688059	46.295186	44.518636	44.374840	44.141488	44.344196	43.297087	43.408865
Fs	10.0852439	10.0182367	10.5618721	10.710733	10.360101	10.498537	10.301840	10.292543	9.5370694	9.6741275	9.6422335	8.7283052	9.1301770	9.4198702	9.3536160
N° Mg	80.9350136	81.2246106	80.2243032	80.337148	80.973405	80.744204	81.019720	80.932884	82.918351	82.148672	82.149655	83.490941	82.926069	82.131233	82.272221

Data Set	B33_6Cpc r-r	B33_6Cpc r-r	B33_6Cpc r-r	B33_6Cpc r-r	B33_6Cpc r-r	B33_6Cpc r-r	B33_6Cpc r-r	B33_6Cpc r-r	B33_6Cpc r-r	B33_6Cpc r-r	B33_6Cpc r-r	B33_6Cpc r-r	B33_6Cpc r-r	B33_6Cpc r-r	B33_6Cpc r-r
SiO2	50.7289536	50.4840305	50.8972138	50.360573	50.286897	50.891240	50.826524	50.595540	50.802629	50.933056	51.078417	50.469096	50.765791	50.705058	50.746874

TiO2	1.09801992	1.06040257	1.120387	1.12343705	1.08886976	1.11123683	1.06751937	1.08988644	0.94145041	0.96991759	0.96890091	0.92010029	0.98415191	0.90688312	1.04210242
Al2O3	3.21377469	3.15450634	3.0666257	3.26384621	3.22705897	3.14326584	3.12282844	3.19129359	3.11158781	3.09421613	2.96648263	2.89188628	3.10239108	3.06253823	3.08195373
FeO	6.09305747	6.12772346	5.89219865	6.04003892	5.92176672	5.83510172	5.88098318	5.82082749	5.70255523	5.62302743	5.59142028	5.66279133	5.61690997	5.76678933	5.65055638
Mno	0.14042232	0.17420814	0.14464555	0.11508296	0.14253394	0.12458522	0.13197582	0.09607843	0.11719457	0.09607843	0.16365007	0.15625947	0.07707390	0.16259426	0.08974359
MgO	15.4062595	15.3670154	15.3218846	15.13253318	15.19139799	15.42686266	15.57206599	15.66527066	15.67017616	15.82322822	15.75847543	15.58972572	15.71923131	15.36309094	15.59463124
CaO	23.1646582	22.4008891	22.4991166	22.57228611	22.84892699	22.62741378	22.54722879	22.35678669	22.62440682	22.61638824	22.51515375	22.50913982	22.53319554	22.47806784	22.56727448
Na2O	0.26909563	0.27634051	0.27530553	0.29186526	0.29186526	0.25150092	0.19768179	0.23390629	0.24115108	0.29186526	0.24011615	0.24011615	0.23804613	0.23390629	0.25564089
K2O	0.00416667	0.00416667	0.00208333	0.01041667	0	0	0.003125	0.01770833	0	0.00520833	0.00208333	0.00729167	0	0	0.00208333
Cr2O3	0.03342409	0.06380963	0.13268351	0.14483773	0.0790024	0.02835983	0.13977347	0.07697669	0.13774767	0.01012850	0.09925941	0.05368110	0.08913088	0.06583533	0.11445211
Totale	100.118408	99.0492827	99.2194608	98.91007782	98.99931667	99.41120703	99.34993222	99.06729843	99.21115194	99.45298591	99.28469957	98.44640676	99.03679075	98.67892865	99.03086061
Fe2O3	3.2955942	2.58341557	1.66313062	2.33731853	2.89629745	1.93729727	1.94526155		2.40735473	2.76477485	1.99363231	2.63384786	2.26290921	1.89667343	2.16123189
FeO	3.12764552	3.80313769	4.39569541	3.93689394	3.31564636	4.09190031	4.13061541	3.73174176	3.53639131	3.13525261	3.79752701	3.29282648	3.58071891	4.06014165	3.70585603
Wo	46.4745535	45.655033	45.9961065	46.18811841	46.50086701	46.08248503	45.86288703	45.51454436	45.87702929	45.64359707	45.72503512	45.88531284	45.78065354	46.08168656	45.92564463
En	43.0068302	43.5776523	43.5831575	43.08411866	43.01737266	43.71489976	44.07226402	44.37410566	44.21226903	44.43268955	44.52913182	44.21851677	44.43665969	43.82267536	44.15726401
Fs	9.5416383	9.74812097	9.40223997	9.64701165	9.40686438	9.27572262	9.33719688	9.24961999	9.02580365	8.85778553	8.86338489	9.01039247	8.90748314	9.22787757	8.97564577
N° Mg	81.8422143	81.7196819	82.2550355	81.70528119	82.05626844	82.49553933	82.51771	82.75088116	83.04633668	83.37829505	83.39957462	83.07237071	83.30185352	82.60550172	83.10718202

Table 9.1 – Continue. Single mineral phase EMPA analyses. Sample: sub-ophitic gabbro B33. Olivines.

Data set	B33_3_Ol of MI	B33_3_Ol of MI	B33_3_Ol of MI	B33_4_Ol of MI	B33_4_Ol of MI	B33_4_Ol of MI	B33_8_Olof MI	B33_8_Olof MI	B33_8_Olof MI	B33_4Ol c-r	B33_4Ol c-r	B33_4Ol c-r	B33_4Ol c-r	B33_4Ol c-r
SiO2	39.4256523	39.6277636	39.5481138	39.7920413	39.4057398	39.7860676	39.3121513	39.4067355	39.43162603	38.95571851	39.1508605	39.403748	39.55010509	39.37587117
TiO2	0.0274505	0.02643381	0	0.02338376	0.04270077	0.03050055	0.01321691	0.01728365	0.04168409	0.01525027	0.0132169	0.0091501	0	0.0030050
Al2O3	0.01226242	0.0572246	0.04189659	0.00715308	0.0510934	0.04189659	0.06131208	0.00102187	0.04496219	0.01839362	0.0173717	0.0030656	0.0592683	0.0286123
Cr2O3	0.0435526	0.01924417	0	0	0.07495099	0	0	0	0	0.01215415	0	0.0020257	0.0557068	0.0698867
FeO	17.7602022	17.8244362	17.8927486	18.3230147	18.2618394	18.1507043	18.3230147	18.030393	17.95188468	18.14968474	18.308740	18.275094	18.400503	18.115018
Mno	0.22277526	0.2745098	0.20588235	0.31568627	0.32096531	0.29457014	0.28084465	0.30723982	0.291402715	0.22066365	0.1784313	0.2914027	0.2618401	0.3040723
MgO	41.5722749	41.0650447	41.2141723	41.6438954	41.6438954	41.5389174	41.5860103	41.3436779	41.41726063	41.38880864	41.403525	41.443750	41.295603	41.522238
CaO	0.31472903	0.37386602	0.2716292	0.27363384	0.28666402	0.26661759	0.3087151	0.28065009	0.276640806	0.33477546	0.3648451	0.3047058	0.3227476	0.2495781
Na2O	0.00310495	0.04967919	0.04243431	0.0186297	0.04346929	0.0248396	0.02173465	0.02276963	0.010349832	0.03622441	0.0186296	0.0082798	0.0186296	0.0103498
NiO														
Totale	99.3820041	99.3182021	99.2168772	100.397438	100.131318	100.134114	99.9069997	99.4097714	99.46581097	99.13167354	99.455621	99.741222	99.964404	99.678678
Fo	80.4697847	80.1735871	80.2321907	79.9274722	79.9755458	80.0542396	79.9355519	80.0723011	80.18291028	80.06223519	79.967032	79.912702	79.772541	80.070394
Fa	19.2852113	19.5219082	19.5400907	19.7282748	19.674234	19.6232119	19.7577324	19.5896123	19.49655784	19.695241	19.837163	19.768050	19.940073	19.596451

Data set	B33_4Ol c-r	B33_4Ol c-r	B33_4Ol c-r	B33_4Ol c-r	B33_4Ol c-r	B33_4Ol c-r	B33_4Ol c-r	B33_4Ol c-r	B33_4Ol c-r	B33_4Ol c-r	B33_4Ol c-r	B33_4Ol c-r	B33_4Ol c-r	B33_4Ol c-r
SiO2	39.3141426	39.1528517	39.3828405	39.3400288	39.2544052	39.1438911	39.3718887	37.9421749	39.49534586	38.42803862	39.151856	38.772523	39.217567	39.037359
TiO2	0.02338376	0.01525028	0.01728365	0.02135039	0.01423359	0.01931702	0.01525028	0.04473415	0.04575083	0.01525027	0.0294838	0.0264338	0.0284671	0.0162669
Al2O3	0.04904966	0.00510934	0.06335581	0.03167791	0.01941549	0.00919681	0.0255467	0.06233394	0.013284283	0.06233394	0.0694870	0.0143061	0.0194154	0.0408747
Cr2O3	0	0.08204095	0.06786103	0	0	0.03848835	0.05975822	0	0.045578305	0	0.0101285	0	0.0577325	0
FeO	18.0976858	18.0844311	18.3016033	18.2302322	18.2373693	18.5503828	18.2078013	18.1160383	18.05792183	18.39744461	18.474933	18.312818	18.214938	18.214938

Mno	0.34208145	0.17104072	0.28612368	0.27556561	0.24494721	0.29034691	0.25972851	0.27134238	0.294570136	0.22066365	0.28929101	0.23544947	0.28929101	0.26078414
MgO	41.5075221	41.8940767	41.6370277	41.7380813	41.6252545	41.5173331	41.4486559	42.7368441	42.11678703	41.53008747	41.64585762	41.09643997	41.32405585	41.63408438
CaO	0.35682655	0.28265474	0.26461295	0.3407894	0.32174529	0.31172207	0.27062688	0.35381958	0.313726712	0.33678012	0.36083584	0.28866868	0.28365709	0.33277082
Na2O	0.03829438	0	0.01345478	0.00206997	0.01448976	0.03622441	0.00310495	0.02690956	0.00310495	0.03829478	0.01655931	0	0.02483997	0.03932961
NiO														
Totale	99.7289862	99.6874555	100.034163	99.9797955	99.7318603	99.9169026	99.6623614	99.5541969	100.3860699	99.02889306	100.0484331	98.74663634	99.45996438	99.57640848
Fo	80.0464057	80.3549674	79.9690478	80.0785171	80.0559147	79.7050752	80.0005874	80.5538624	80.35363891	79.90233592	79.82064507	79.79373891	79.92021152	80.06482075
Fa	19.5787752	19.4586365	19.7187233	19.6210927	19.6764236	19.9782228	19.7145867	19.1555489	19.32704837	19.85644891	19.86432219	19.94652566	19.76190647	19.65024026

Data set	B33_4Ol c-r	B33_4Ol c-r	B33_4Ol c-r	B33_4Ol c-r	B33_4Ol c-r	B33_4Ol c-r	B33_4Ol c-r	B33_4Ol c-r	B33_4Ol c-r
SiO2	39.2802914	38.9606966	35.7627574	39.1767467	38.951736	38.5106753	38.9168892	38.8352482	38.68092672
TiO2	0	0.0071168	0.0406674	0.03151724	0.0203337	0.02846718	0.00813348	0.0274505	0.051850941
Al2O3	0.054159	0.03269977	0.01737176	0.02656857	0.02145923	0.00919681	0.06029021	0.04700593	0.00510934
Cr2O3	0.05064256	0.0020257	0.02835983	0.03848835	0	0.08204095	0	0	0
FeO	18.1884291	18.0966662	18.3933663	18.0915682	18.2587807	18.1517239	17.9692177	18.2394085	18.1027837
Mno	0.27662142	0.28717949	0.32518854	0.25972851	0.29562594	0.28401207	0.24600302	0.27134238	0.323076923
MgO	41.4879	41.5987647	42.2462926	41.5379363	41.2671519	41.468278	41.8911334	41.6066135	41.31130151
CaO	0.26561527	0.32074296	0.33076618	0.29267795	0.32074296	0.34179172	0.29969421	0.31873832	0.328761538
Na2O	0.01034983	0	0	0	0	0.03208448	0	0	0.008279866
NiO									
Totale	99.6140086	99.3058922	97.14477	99.4552318	99.1358304	98.9082704	99.3913612	99.3458073	98.81209054
Fo	80.0176836	80.1304553	80.0887199	80.1356701	79.8544991	80.035431	80.3878451	80.0239112	79.98290342
Fa	19.6791874	19.5552422	19.5610164	19.5796363	19.8204775	19.6531248	19.3439382	19.67957	19.66170149

Table 9.1 – Continue. Single mineral phase EMPA analyses. Sample: sub-ophitic gabbro B33. Feldspars.

Data Set	B33_10_Pl from Ml to r	B33_10_Pl from Ml to r	B33_10_Pl from Ml to r	B33_10_Pl from Ml to r	B33_10_Pl from Ml to r	B33_10_Pl from Ml to r	B33_10_Pl from Ml to r	B33_10_Pl from Ml to r	B33_10_Pl from Ml to r	B33_10_Pl from Ml to r	B33_10_Pl from Ml to r	B33_10_Pl from Ml to r	B33_10_Pl from Ml to r	B33_10_Pl from Ml to r
SiO2	47.0640675	50.7399055	48.2996349	48.3623592	48.6889233	48.6690109	46.5921425	46.7793195	46.90675917	46.20086287	46.75940705	46.32432005	46.80321444	46.43383852
TiO2	0.054901	0.0955684	0.07320133	0.06608453	0.06405116	0.06608453	0.07930144	0.04270077	0.029483868	0.055917681	0.057951052	0.0477842	0.04168409	0.059984422
Al2O3	33.4958094	31.2323719	32.1980371	32.0876753	31.8403833	32.3911701	33.6971173	33.30472	33.64602394	33.73083898	33.6439802	33.56938384	33.42019113	33.77069183
Cr2O3	0	0	0.02835983	0.05874537	0.02532128	0	0.00810281	0.03848835	0.056719669	0.036462644	0.00810281	0	0	0
FeO	0.60563523	0.55567542	0.70351567	0.57504759	0.59849811	0.57708677	0.53834243	0.59034141	0.611752758	0.670888858	0.595439351	0.55669501	0.545479543	0.523048608
MnO	0.04117647	0.02006033	0.00527903	0.0306184	0	0.02322775	0.01055807	0	0	0.054901961	0.096078431	0.030618401	0.048567119	0.009502262
MgO	0.14029772	0.18640956	0.15599537	0.18052294	0.15108985	0.1658064	0.10792132	0.12852449	0.140297726	0.102034706	0.103015809	0.111845735	0.146184338	0.134411103
CaO	17.469466	14.6779999	16.4681466	15.9920437	15.7474772	16.0561923	17.5386262	17.4494196	17.52760066	17.94957812	17.79121128	17.50755422	17.56769353	17.72505804
Na2O	1.84847999	3.30780629	2.3835663	2.56882829	2.50258937	2.63713718	1.70151237	1.69323251	1.835025206	1.515215399	1.805010694	1.750156584	1.740841735	1.588699206
K2O	0.07291667	0.1375	0.09166667	0.11770833	0.1	0.10208333	0.08020833	0.065625	0.063541667	0.047916667	0.048958333	0.055208333	0.066666667	0.066666667
SrO														
BaO														
Totale	100.79275	100.953297	100.407403	100.039634	99.7183336	100.687799	100.353833	100.092372	100.8172047	100.3646179	100.909155	99.95356638	100.3805226	100.3119007
Ab%	16.0040284	28.7401727	20.6473315	22.3697564	22.2048757	22.7791766	14.8653815	14.8803685	15.87035955	13.21521571	15.46888378	15.270321	15.14747253	13.90249561
An%	83.580584	70.4737521	78.8301999	76.9558002	77.2113152	76.6406308	84.6735425	84.7401606	83.76805126	86.50980588	84.25504704	84.41273101	84.47084542	85.71364521
Or%	0.41538755	0.78607522	0.52246865	0.67444338	0.58380909	0.58019268	0.46107603	0.37947093	0.361589189	0.274978402	0.276069181	0.316947989	0.381682043	0.383859182

Data Set	B33_10_Pl from Ml to r	B33_11_Pl r-r	B33_11_Pl r-r	B33_11_Pl r-r	B33_11_Pl r-r	B33_11_Pl r-r	B33_11_Pl r-r	B33_11_Pl r-r	B33_11_Pl r-r	B33_11_Pl r-r	B33_11_Pl r-r	B33_11_Pl r-r	B33_11_Pl r-r	B33_11_Pl r-r
SiO2	46.3502062	46.3044076	47.0809931	47.0103039	47.1725904	47.0541113	46.669801	46.2745389	47.40656163	47.28410007	47.23631019	48.86713972	49.36594655	49.40577145

TiO2	0.05998442	0.03660066	0.05693437	0.03456729	0.04473415	0.00610011	0.04676752	0.04168409	0.053884311	0.063034477	0.061001107	0.063034477	0.068117903	0.042700775
Al2O3	33.4620877	32.817289	33.3445729	33.7625169	33.4927437	33.4712845	33.7104016	33.6266084	33.746167	33.77784491	33.29450137	32.48416009	32.3053332	32.07643478
Cr2O3	0	0.03646264	0	0	0	0.03848835	0	0	0	0	0.010128512	0.003038554	0	0
FeO	0.58422388	0.57912594	0.53120531	0.55873419	0.56791048	0.49042179	0.53018572	0.51183314	0.514891905	0.510813553	0.561792949	0.627046577	0.598498115	0.582184708
MnO	0	0	0	0	0.03589744	0.02322775	0.02217195	0.00316742	0.014781297	0	0.009502262	0.040120664	0.005279035	0.025339367
MgO	0.10694022	0.13735441	0.12852449	0.12460007	0.11282684	0.13146779	0.11773235	0.0990914	0.151089853	0.121656765	0.129505588	0.167768603	0.146184338	0.161881985
CaO	17.7120279	17.4554335	17.0023841	17.210867	16.9302169	16.9061612	17.5476471	17.6779489	17.509558887	17.501540229	17.293057336	16.099292115	15.403680844	15.600135911
Na2O	1.67874274	1.75015658	1.96853804	1.75222655	1.89815918	1.86917965	1.66011305	1.70254736	1.721177055	1.67770776	1.909543996	2.495344485	2.757195234	2.583318057
K2O	0.05625	0.08020833	0.0625	0.09166667	0.08854167	0.06041667	0.05833333	0.0625	0.070833333	0.0625	0.058333333	0.097916667	0.1125	0.113541667
SrO														
BaO														
Totale	100.010463	99.1970387	100.175652	100.545483	100.343621	100.050859	100.363154	99.9999197	101.1889452	100.9991978	100.5636767	100.944862	100.7627352	100.5913087
Ab%	14.5934127	15.2867966	17.2600253	15.4745581	16.7799563	16.6130337	14.5683601	14.7886682	15.040555782	14.72940982	16.59884593	21.78151745	24.30682099	22.90446099
An%	85.0848456	84.252235	82.3794046	83.9927802	82.7050309	83.0336475	85.0948168	84.8541231	84.552168877	84.90954533	83.06751483	77.65610711	75.04061177	76.43315542
Or%	0.3217417	0.46096842	0.36057012	0.53266179	0.51501276	0.35331881	0.33682313	0.35720867	0.407275345	0.361044849	0.333639239	0.562375442	0.652567243	0.662383591

Data Set	B33_11_Pl r-r	B33_11_Pl r-r	B33_7Pl r-r	B33_7Pl r-r	B33_7Pl r-r	B33_7Pl r-r	B33_7Pl r-r	B33_7Pl r-r	B33_7Pl r-r	B33_7Pl r-r	B33_7Pl r-r	B33_7Pl r-r	B33_7Pl r-r	B33_7Pl r-r
SiO2	47.2721526	47.0132908	46.4726678	46.6837397	48.1393397	48.3484204	48.1224141	48.1562653	47.860565455	47.503137	47.597721173	47.474263945	47.540970645	47.992983243
TiO2	0.0681179	0.0477842	0.04981757	0.08031812	0.07015127	0.05693437	0.07218464	0.07625138	0.046767515	0.074218013	0.072184643	0.070151273	0.052867626	0.082351494
Al2O3	33.5182904	34.0527274	33.8943379	33.3445729	32.5219692	32.4116075	32.6466371	32.810136	32.836704533	32.787654877	32.588390621	32.422848001	32.953197417	32.740648904
Cr2O3	0.03848835	0	0	0	0	0	0.04659116	0.02329558	0.023295578	0	0.033424091	0.076976694	0	0.020257025

FeO	0.56994965	0.57708677	0.59441976	0.50163726	0.58218471	0.52508778	0.59238059	0.60971358	0.60257646 7	0.52712696	0.61583111	0.54242077 9	0.57810635 6	0.57096924 1
Mn o	0	0.02850679	0.05595777	0.03484163	0	0	0	0	0.05806938 2	0.06651583 7	0.04751131 2	0.01266968 3	0	0.03061840 1
Mg O	0.14029772	0.12460007	0.12460007	0.13735441	0.1667875	0.17365522	0.18052294	0.17267412	0.13441110 3	0.13931661 8	0.15207095 6	0.1667875	0.15108985 3	0.1667875
CaO	16.9151821	17.671935	17.4393963	17.295062	16.1363781	16.3739283	16.2736961	16.3689167	16.6646016 2	16.5473299 7	16.4942069 2	16.7708477 3	16.5463276 5	16.5322951 5
Na2 O	1.84020012	1.60525894	1.65390315	1.68805759	2.37218148	2.37011152	2.23763367	2.18691949	2.23142377	2.11757561 9	2.11861060 2	1.97992285 4	2.01925221 5	2.11447066 9
K2O	0.07291667	0.05625	0.07395833	0.059375	0.10520833	0.09479167	0.090625	0.09583333	0.08854166 7	0.07916666 7	0.08645833 3	0.08645833 3	0.08958333 3	0.10208333 3
SrO														
BaO														
Tota le	100.435596	101.17744	100.359059	99.8249587	100.0942	100.354537	100.262685	100.500005	100.546957 1	99.8420415 5	99.8064097 2	99.6033468	99.9313951 6	100.353465
Ab %	16.3784233	14.0716044	14.585219	14.9592361	20.8848655	20.6442721	19.8194066	19.3610724	19.4061348 7	18.7168701 8	18.7650337 6	17.5146397 2	17.9941678 5	18.6833729 4
An %	83.1945589	85.6039565	84.985638	84.6945553	78.5056733	78.8124612	79.6524379	80.080682	80.0872049 4	80.8227155 6	80.7310977 8	81.9821240 5	81.4805646 6	80.7231272 8
Or %	0.42701777	0.32443907	0.42914307	0.34620863	0.60946114	0.54326667	0.52815547	0.5582456	0.50666019 6	0.46041425 7	0.50386845 7	0.50323623 3	0.52526748 9	0.59349978 3
Data Set	B33_7Pl r-r	B33_7Pl r-r	B33_7Pl r-r	B33_7Pl r-r	B33_7Pl r-r	B33_7Pl r-r	B33_7Pl r-r	B33_7Pl r-r	B33_7Pl r-r	B33_7Pl r-r	B33_7Pl r-r	B33_7Pl r-r	B33_7Pl r-r	B33_7Pl r-r
SiO2	48.1921077	47.5728306	47.8784867	47.714209	47.592743	47.2512445	47.31596	46.3073945	46.3970004 9	47.7958499 9	48.2677750 2	48.4211008 7	48.6739889 7	47.0292207 3
TiO2	0.04676752	0.05388431	0.0681179	0.03863403	0.08031812	0.06100111	0.05998442	0.0406674	0.05083425 6	0.05490099 6	0.07523469 8	0.08438486 5	0.07930143 9	0.07726806 9
Al2 O3	32.2338024	32.8223984	32.6517464	33.0053127	32.5975874	32.7988954	32.7222553	33.7706918	33.5796025 2	32.5536471 1	32.5209473 3	32.4698539 4	32.5669313 9	33.4498253
Cr2 O3	0	0.02532128	0	0.02025702	0	0.01012851	0.05165541	0.02532128	0	0	0.04355260 3	0	0.00303855 4	0.02329557 8
FeO	0.60767441	0.54547954	0.5148919	0.60155688	0.64947751	0.56893006	0.52814655	0.51591149	0.66069297 9	0.58320429 6	0.54751871 8	0.58932182 4	0.57606718	0.54140119 1
Mn o	0	0.0453997	0.02533937	0.01055807	0.00950226	0	0.00211161	0.03800905	0.00527903 5	0	0.03061840 1	0	0.00316742 1	0.04856711 9
Mg O	0.25508676	0.15305206	0.17071191	0.15403316	0.16874971	0.1324489	0.18739066	0.11577015	0.13637330 9	0.13833551 5	0.13146779 4	0.15599536 8	0.17856073 5	0.14814654 4

CaO	16.5453253	16.5994507	16.7788663	16.749799	16.862059	16.9061612	16.3598958	17.5757121	17.7320743	16.4180304 7	15.8246559 8	15.880786	16.2696868 5	17.4213545 5
Na2O	2.19002444	2.25522838	2.16311488	2.14241522	2.06168653	2.10412084	1.91161396	1.58352429	1.56696455 9	2.26557821 6	2.47567980 4	2.43428047 7	2.61022762	1.77810113
K2O	0.12395833	0.09166667	0.07708333	0.090625	0.08958333	0.06979167	0.08125	0.06354167	0.06458333 3	0.10625	0.09270833 3	0.09583333 3	0.1	0.08541666 7
SrO														
BaO														
Total	100.194747	100.164712	100.328359	100.5274	100.111707	99.9027222	99.2202637	100.036544	100.193404 8	99.9157965 9	100.010158 7	100.131556 7	101.060970 2	100.602596 9
Ab %	19.1862695	19.6304716	18.8328792	18.6980013	18.0239232	18.3088121	17.3695292	13.9669173	13.7354103 4	19.8593842	21.9448089	21.5937750 6	22.3733898 6	15.5138872 8
An %	80.0991857	79.8445231	80.7255404	80.7815815	81.4607699	81.2916066	82.1447091	85.6643204	85.8920993 1	79.5278031	77.5144763 7	77.8468710 6	77.0626277 9	83.9957483 6
Or %	0.71454472	0.52500537	0.44158034	0.52041723	0.51530697	0.39958131	0.48576176	0.36876232	0.37249034 9	0.61281270 4	0.54071473 8	0.55935388	0.56398235 1	0.49036435 9
Data Set	B33_7Pl r-r	B33_7Pl r-r	B33_6Pl r-r	B33_6Pl r-r	B33_6Pl r-r	B33_6Pl r-r	B33_6Pl r-r	B33_6Pl r-r	B33_6Pl r-r	B33_6Pl r-r	B33_6Pl r-r	B33_6Pl r-r	B33_6Pl r-r	B33_6Pl r-r
SiO2	46.5692432	46.7842976	45.5108965	46.0684451	46.2546265	47.9372284	46.3790793	46.242679	45.5328002 3	46.2436746 4	46.9814308 5	46.7295383 8	46.4238823	46.6628316 8
TiO2	0.01321691	0.06100111	0.05185094	0.0681179	0.05083426	0.05185094	0.07320133	0.05185094	0.05185094 1	0.05998442 2	0.0477842	0.04676751 5	0.06811790 3	0.03558397 9
Al2O3	33.8279164	33.5908431	33.1524617	33.0676467	33.4794595	33.8085009	33.5520121	33.336398	33.6603300 9	33.1851615	33.6123023	33.2250143 5	33.2209268 8	32.8837104 5
Cr2O3	0.02025702	0	0.06684818	0	0.04659116	0	0.08811806	0	0.03848834 7	0.03342409 1	0	0.03342409 1	0	0
FeO	0.5995177	0.55159707	0.61073317	0.5403816	0.61787029	0.53426408	0.52712696	0.5322249	0.54853830 6	0.53732283 9	0.56281253 7	0.58218470 8	0.60359605 5	0.59645893 9
MnO	0.00950226	0.00316742	0	0.01794872	0	0.02956259	0	0.01266968	0.04012066 4	0.03061840 1	0	0.02850678 7	0.03589743 6	0
MgO	0.13048669	0.12263787	0.10497801	0.14716544	0.15108985	0.11773235	0.1344111	0.11577015	0.14324102 9	0.11969455 9	0.14324102 9	0.14127882 3	0.12754338 2	0.13833551 5
CaO	17.3712385	17.6939861	18.1129566	17.4043151	17.6258282	17.3993035	17.2659947	17.8683901	18.1881307	17.1366951 7	17.3722407 8	17.2970666 5	17.2379296 7	17.0244351 3
Na2O	1.6570081	1.64148335	1.66839291	1.79880079	1.68909258	1.89401925	1.83916514	1.66735793	1.52970516 3	1.79052092 9	1.85675985 3	1.83295524	1.83709517 3	2.04409181 2
K2O	0.05	0.071875	0.06041667	0.07291667	0.059375	0.05520833	0.078125	0.05625	0.0625	0.071875	0.08645833 3	0.07708333 3	0.08645833 3	0.07083333 3
SrO														

BaO													
Total	100.248387	100.520889	99.3395347	99.185738	99.9747673	101.82767	99.9372336	99.8835906	99.79570547	99.20897154	100.6630299	99.99381988	99.64144712	99.45628084
Ab%	14.6777379	14.3154951	14.2386257	15.6903038	14.7284888	16.405242	16.0881984	14.4005291	13.16260661	15.83472673	16.12672909	16.01947833	16.08711243	17.77717135
An%	85.030844	85.2720657	85.4221097	83.8912042	84.9308517	83.2801172	83.4621369	85.2798139	86.48353762	83.74703754	83.37917698	83.5372509	83.41473152	81.81749558
Or%	0.29141816	0.41243912	0.33926464	0.41849203	0.34065947	0.31464077	0.44966473	0.31965701	0.353855777	0.418235731	0.494093927	0.443270776	0.498156044	0.405333075
Data Set	B33_6Pl r-r	B33_6Pl r-r	B33_6Pl r-r	B33_6Pl r-r	B33_6Pl r-r	B33_6Pl r-r	B33_6Pl r-r	B33_6Pl r-r	B33_6Pl r-r	B33_6Pl r-r	B33_6Pl r-r			
SiO2	48.2697663	48.2030596	47.9690883	46.7594071	48.3962103	48.3404555	48.7247657	48.1632347	48.86216161	48.58836544	48.68593644			
TiO2	0.06506785	0.04676752	0.03660066	0.06405116	0.06303448	0.07625138	0.05896774	0.05795105	0.070151273	0.054900996	0.044734145			
Al2O3	31.9446138	32.0641724	32.3022676	33.1299806	31.6452065	31.8189241	31.7821368	31.9916197	31.88534547	31.55221652	31.88943294			
Cr2O3	0.03848835	0	0	0	0.03848835	0	0	0	0.003038554	0.013167066	0.028359834			
FeO	0.54445995	0.59238059	0.57606718	0.57300842	0.50571561	0.54344037	0.57096924	0.61277235	0.546499131	0.523048608	0.549557894			
MnO	0.04223228	0	0.00316742	0.00950226	0.0612368	0	0	0	0.017948718	0.052790347	0.045399698			
MgO	0.17954184	0.19720169	0.14127882	0.12263787	0.17267412	0.2011261	0.16090088	0.15893868	0.155995368	0.174636323	0.154033162			
CaO	15.9309021	15.9880344	16.1794779	17.6528909	16.1063084	15.7264285	15.6071522	16.1313664	15.76351436	15.62118467	16.00908319			
Na2O	2.34941185	2.44256034	2.23349374	1.84434005	2.53984876	2.71165597	2.58952796	2.55537351	2.551233578	2.703376108	2.498449435			
K2O	0.121875	0.12604167	0.103125	0.05625	0.10104167	0.11354167	0.11041667	0.10208333	0.127083333	0.102083333	0.113541667			
SrO														
BaO														
Total	99.4863593	99.6602182	99.5445666	100.212068	99.629765	99.5318235	99.6048372	99.7733398	99.98297139	99.38576941	100.0185284			
Ab%	20.9152174	21.5004885	19.8671686	15.849821	22.0728107	23.627293	22.9431833	22.1498712	22.48619653	23.70796503	21.87825556			
An%	78.3708948	77.7695008	79.5292619	83.8321125	77.3494095	75.7217584	76.4131222	77.2679133	76.77680521	75.70298146	77.46754601			

Or									0.73699829	0.58905351	0.65419842
%	0.7138878	0.73001077	0.60356953	0.31806655	0.57777984	0.65094867	0.64369451	0.5822155	1	7	7

Table 9.1 – Continue. Single mineral phase EMPA analyses. Sample: sub-ophitic gabbro B33. Glass.

Data set	B33_1_Glass	B33_1_Glass	B33_1_Glass	B33_1_Glass	B33_2_Glass	B33_2_Glass	B33_2_Glass	B33_2_Glass
SiO2	49.1622969	49.0304088	48.6876995	48.9344902	48.5498165	48.5707987	48.7176741	48.7896131
TiO2	3.03698531	2.94798941	2.9773176	3.00765712	2.99450999	3.02990609	2.97630628	3.01170238
Al2O3	14.7375865	14.3069658	14.4999326	14.6146971	14.5720413	14.3008721	14.3557153	14.5903223
Cr2O3	0.018	0.015	0.048	0.018	0	0	0.044	0.066
FeOtot	10.6771054	10.4276356	10.5401015	10.7210694	11.1024311	10.9286201	10.7875265	11.1433278
MnO	0.23493976	0.25301205	0.16465863	0.20481928	0.21686747	0.22188755	0.25803213	0.13353414
MgO	6.15512309	6.07150182	6.08046124	6.22978494	6.32336113	6.22381199	6.18001037	6.27159558
CaO	11.6847038	11.3212022	11.4184059	11.2766504	11.0022523	11.1298322	11.0913557	11.4771332
Na2O	3.22922741	2.89852964	2.99182995	2.99493996	2.83632943	2.99079328	2.93170308	2.97938991
K2O	0.91854157	0.89469681	0.88432953	0.88225607	0.94238633	0.95171689	0.9486067	0.89158663
P2O5	0.34629969	0.38232416	0.42648318	0.45437309	0.4253211	0.46948012	0.35559633	0.39510703
F								
Cl								
Total	100.200809	98.5492662	98.7192197	99.3387375	98.9653166	98.8177191	98.6465265	99.7493121

Table 9.1 – Continue. Single mineral phase EMPA analyses. Sample: sub-ophitic gabbro B33. Melt inclusions (MI).

Dataset	B33_3_MI in Ol	B33_3_MI in Ol	B33_3_MI in Ol	B33_3_MI in Ol	B33_3_MI1 in Ol	B33_3_MI1 in Ol	B33_4_MI in Ol	B33_4_MI in Ol	B33_4_MI in Ol	B33_5_MI in Cpx	B33_5_MI in Cpx	B33_5_MI in Cpx	B33_8_MI in Ol	B33_8_MI in Ol	B33_8_MI in Ol	B33_10_Mi in Pl	B33_10_Mi in Pl
SiO2	47.8703928	48.2810445	48.0952021	48.0792157	47.19196 83	47.89736 99	47.5376751	48.2290885	47.6825 5216	45.94502 605	46.06292 604	46.18482 264	48.2111038	48.4538 9784	48.1171 8347	51.20456 453	51.37242 214
TiO2	2.98540814	2.97124 97	2.96417048	2.91866 121	3.103732 24	3.200818 69	3.32217674	3.24228 269	3.33936 9131	3.786371 298	3.772212 858	3.796484 469	2.97731 7602	2.88832 1695	2.93079 7014	1.943751 505	1.945774 139
Al2O3	14.9244596	14.5893067	14.3943087	14.6959463	14.53547 91	14.59844 73	14.414621	14.5202449	14.7182 898	13.78595 541	13.80931 455	13.89868 865	14.4907 9208	14.5039 9508	14.4176 6782	14.49587 016	14.10282 723
Cr2O3	0	0	0.033	0.022	0	0	0.033	0	0	0.004	0.095	0	0	0	0.052	0.007	0.022
FeO tot	10.9173735	10.4552408	10.830468	10.7476522	11.08607 24	11.42347 02	10.8161542	10.8642078	10.7128 9003	14.00711 905	13.81490 457	13.98871 554	10.9562 2539	10.9286 2012	11.1310 5877	9.485989 094	9.904157 831
MnO	0.15963855	0.16767068	0.22289157	0.11947791	0.106425 7	0.236947 79	0.21184739	0.23493976	0.13453 8153	0.243975 904	0.168674 699	0.254016 064	0.20783 1325	0.16967 8715	0.23293 1727	0.172690 763	0.144578 313
MgO	5.84552528	6.08046124	5.95602482	6.00281291	5.862448 63	5.360720 98	5.72108886	5.80968759	5.83855 6837	5.719097 873	5.940096 956	6.030686 67	5.97493 9153	6.16308 7021	6.17403 7426	5.685251 167	5.888331 405
CaO	11.4295439	11.0518667	11.1379325	11.3232272	11.15717 08	11.67052 82	10.712666	10.8736598	11.3606 9119	10.65292 621	10.81088 234	10.80278 203	11.3485 4072	11.3991 6769	11.4943 4638	10.34815 187	9.994775 647
Na2O	3.03226008	2.98871994	2.99286662	2.77412923	2.914079 69	2.937923 1	3.14836714	2.85913618	2.83010 9413	2.607225 338	2.708819 009	2.719185 71	2.99493 9961	2.95139 9816	3.03433 3425	3.178430 571	3.294537 624
K2O	0.93823942	0.95068016	0.85011748	0.86048477	0.961047 45	0.923725 22	0.970378	1.00147986	1.02221 4436	0.693571 458	0.668689 971	0.673873 614	0.82005 2352	0.84804 4025	0.81175 8523	1.316645 369	1.303167 896
P2O5	0.3858104	0.33351682	0.41834862	0.46948012	0.496207 95	0.472966 36	0.43461774	0.46715596	0.50085 6269	0.389296 636	0.323058 104	0.392782 875	0.38697 2477	0.39626 9113	0.36024 4648	0.251009 174	0.241712 538
F																	
Cl																	
Total	98.4886517	97.8697573	97.895331	98.0130876	97.41463 23	98.72291 77	97.3225921	98.1018831	98.1400 6742	97.83456 523	98.17457 91	98.74203 826	98.3687 1486	98.7024 811	98.7563 592	98.08935 42	98.21428 476

Table 9.1 – Continue. Single mineral phase EMPA analyses. Sample: sub-ophitic gabbro B34. Clinopyroxenes.

Data Set	B34_1_Cpx rim detail to glass	B34_1_Cpx rim detail to glass	B34_1_Cpx rim detail to glass	B34_1_Cpx rim detail to glass	B34_1_Cpx rim detail to glass	B34_1_Cpx rim detail to glass	B34_1_Cpx rim datail to glass	B34_1_Cpx rim datail to glass	B34_1_Cpx rim datail to glass	B34_1_Cpx rim datail to glass	B34_1_Cpx rim datail to glass	B34_1_Cpx rim datail to glass	B34_1_Cpx rim datail to glass	B34_1_Cpx rim datail to glass
SiO2	49.8502292	49.1165744	49.7978253	49.4612309	48.8313762	48.1702807	51.8264614	50.9708667	51.35885722	51.41025337	51.7508788	51.71258363	52.00483622	51.56242627
TiO2	1.77930461	1.77418283	1.74959831	1.81105961	1.80081606	1.76393928	1.08069451	1.10937645	1.112449512	1.109376448	1.050988213	1.025379339	1.102205963	1.027428049
Al2O3	3.9280722	4.03982979	3.95187243	3.81424503	3.57831235	3.94359409	3.00503732	3.021594	3.060916114	3.035046303	2.858096791	2.781522149	2.753582752	2.756687129
FeO	8.08485303	8.29276396	8.017951	8.13631613	8.10132123	8.13631613	6.56977937	6.21777176	6.670647042	6.408185231	6.384512205	6.301141983	6.378336633	6.222918071
MnO	0.15222222	0.17666667	0.12888889	0.21777778	0.19888889	0.27888889	0.14333333	0.19555556	0.183333333	0.157777778	0.104444444	0.113333333	0.13	0.192222222
MgO	13.9939867	13.7908482	14.0302965	14.1146922	14.0577742	14.0734757	15.5611955	15.3060457	15.25403435	15.45717287	15.62694564	15.59357989	15.71624808	15.56315818
CaO	22.3214627	22.4972939	22.6064304	22.2456734	22.2992312	21.7828534	22.1678631	22.0344739	21.87885322	22.17190515	21.82529545	22.41544141	22.42655718	22.16281044
Na2O	0.30782118	0.39725571	0.37021736	0.33277965	0.40141545	0.3712573	0.26310391	0.26726366	0.288062385	0.227746074	0.267263657	0.229825946	0.307821177	0.226706137
K2O	0.02112155	0.01161685	0.00633646	0.01161685	0	0.01478508	0.00422431	0.01372901	0.003168232	0	0.010560774	0	0.011616852	0.007392542
Cr2O3	0.09116978	0.08809664	0.07580408	0	0	0.01741445	0.2048759	0.07068219	0.171071376	0.237656043	0.197705243	0.219217213	0.151608166	0.154681304
Totale	100.439073	100.097032	100.659417	100.145392	99.2691356	98.5353907	100.621693	99.1366767	99.81032141	99.97746322	99.87898597	100.1728077	100.8312048	99.72174903
Fe2O3	2.22235403	3.73998001	2.98225534	3.13798061	4.20287811	4.42409364	1.10942514	1.34935116	0.987872842	1.047847587	0.680970199	1.203283792	1.596087722	1.042521222
FeO	6.08515441	4.92748876	5.33448481	5.31272662	4.31952522	4.15546796	5.57150641	5.00361072	5.781748182	5.465320434	5.771767722	5.218413977	4.942159326	5.284845996
Wo	45.8720344	46.027823	46.0824667	45.5501325	45.5932785	45.0177625	44.8526181	45.2749324	44.80498447	45.16308889	44.50906085	45.33269597	45.00639368	45.15203019
En	40.0145288	39.2583489	39.7943553	40.212993	39.9924853	40.4689002	43.8084437	43.7591651	43.46477087	43.80882321	44.34179794	43.87943023	43.88452282	44.11650305
Fs	12.9686816	13.2430435	12.7574969	13.003799	12.9290059	13.1248787	10.3755971	9.97213725	10.66272196	10.18858865	10.16282313	9.946765153	9.99119396	9.895662625
N° Mg	75.5230355	74.7758243	75.7239824	75.5644816	75.5694604	75.5104437	80.8511935	81.4407304	80.30072814	81.13133889	81.35419909	81.52058662	81.45510713	81.67882642

Data Set	B34_1_Cpx rim datail to glass	B34_1_Cpx rim datail to glass	B34_1_Cpx rim datail to glass	B34_1_Cpx rim datail to glass	B34_1_Cpx rim datail to glass	B34_1_Cpx rim datail to glass	B34_1_Cpx rim datail to glass	B34_1_Cpx rim datail to glass	B34_1_Cpx rim datail to glass	B34_1_Cpx rim datail to glass	B34_1_Cpx rim datail to glass	B34_1_Cpx rim datail to glass	B34_1_Cpx rim datail to glass	B34_1_Cpx rim datail to glass

SiO2	51.9604944	51.9272381	51.8173915	49.6456524	49.5237125	49.465262	49.1387453	48.9442462	49.18510264	49.2979726	49.42092024	49.23851432	49.34432991	49.14176863
TiO2	1.05508563	1.10220596	1.05303692	1.61745652	1.70350234	1.71477024	1.71681895	1.71681895	1.637943619	1.707599758	1.702477983	1.720916373	1.623602649	1.736281698
Al2O3	2.74220003	2.69873875	2.69873875	4.75487138	4.86145501	5.0404741	4.86145501	5.03633493	4.830411231	4.730036362	4.805576212	4.677261946	4.751767004	4.898707534
FeO	6.35775139	6.46170686	6.39583409	6.75607579	6.90120173	6.80548036	6.75710505	6.95369409	6.955752617	6.63873992	6.785924387	6.734461286	7.083381106	6.919728447
MnO	0.10222222	0.15888889	0.12666667	0.19111111	0.18	0.14333333	0.18222222	0.20888889	0.178888889	0.138888889	0.141111111	0.122222222	0.083333333	0.118888889
MgO	15.7319496	15.6995652	15.6671808	14.551391	14.4611072	14.3884876	14.227547	14.4424616	14.54942828	14.23441638	14.44540566	14.23834176	14.38750628	14.22656562
CaO	22.3477363	22.2042419	22.4750623	22.0142634	22.3416732	22.2658839	22.6124936	22.6064304	22.31034693	22.45485185	22.16281044	22.17695777	21.92533732	22.42958875
Na2O	0.23918537	0.23502563	0.28390264	0.26726366	0.30262149	0.27350328	0.28806239	0.37957679	0.290142258	0.258944166	0.330699778	0.32446016	0.297421813	0.311980923
K2O	0.01478508	0	0.00422431	0.02006547	0.00422431	0.01689724	0.00316823	0.01161685	0.016897239	0.012672929	0	0.005280387	0.005280387	0.003168232
Cr2O3	0.22741225	0.30116757	0.18233955	0.20897342	0.27146057	0.22741225	0.28682626	0.30424071	0.214095315	0.345215891	0.226387869	0.231509766	0.314484506	0.229461007
Totale	100.55141	100.487611	100.522038	99.8181507	100.279498	100.114092	99.7876177	100.300069	99.9549137	99.47412285	99.79492581	99.23841622	99.50195979	99.78667872
Fe2O3	1.16417213	0.94242895	1.70934507	1.58450255	2.17587565	1.77049273	2.34868907	3.75928963	2.904995817	1.591311537	2.021728127	1.758890436	1.792075137	2.340754257
FeO	5.31021649	5.61369891	4.85774657	5.33032294	4.94332486	5.21237151	4.64372876	3.57104389	4.341805393	5.206860277	4.966751156	5.151792305	5.470852164	4.813491991
Wo	45.0264466	44.8411764	45.1484882	45.8457699	46.1632078	46.2976509	46.9098318	46.3092901	45.99246324	46.86784148	46.02173916	46.36442278	45.66714201	46.54396174
En	44.102944	44.1143181	43.7909192	42.1648461	41.5750451	41.6279536	41.0673184	41.1650124	41.73276622	41.33855788	41.73676992	41.41838865	41.69595963	41.0764597
Fs	9.99852701	10.1856007	10.0285431	10.9821652	11.1302099	11.0452652	10.9414388	11.1185988	11.19238964	10.81555375	10.99880639	10.98965592	11.5158634	11.20803386
N° Mg	81.5189369	81.2419596	81.3663261	79.3362507	78.8821629	79.0305862	78.9623144	78.734065	78.85242008	79.26231814	79.14347929	79.03059347	78.35844979	78.56336918

Data Set	B34_1_Cpx rim datail to glass	B34_1_Cpx rim datail to glass	B34_1_Cpx rim datail to glass	B34_1_Cpx rim datail to glass	B34_1_Cpx rim datail to glass	B34_1_inter stitial Cpx c-r	B34_1_inter stitial Cpx c-r	B34_1_inter stitial Cpx c-r	B34_1_inter stitial Cpx c-r	B34_1_inter stitial Cpx c-r	B34_1_inter stitial Cpx c-r	B34_2_Cpx c-r	B34_2_Cpx c-r	B34_2_Cpx c-r
SiO2	49.2556464	49.2838639	48.858586	49.0198288	48.7779645	49.5499145	49.9237962	49.6879786	49.89658652	50.17271483	50.16767599	51.87684974	51.88088081	51.96956435
TiO2	1.73320863	1.76189057	1.67891782	1.68711266	1.61848087	1.69735621	1.71169718	1.6953075	1.671747334	1.575457965	1.648187169	0.998746109	1.057134343	1.017184499
Al2O3	5.04461327	5.06220474	4.68864466	4.69174904	4.82627206	4.95458633	5.02081305	4.79212391	4.815924137	4.738314702	4.833515609	2.835331357	2.852922829	2.684251657

FeO	6.94237221	6.87958723	6.93310885	6.82503634	6.62124247	6.75916357	6.68402745	6.97427933	6.851797155	6.691232282	6.631535086	6.414360803	6.47920431	6.466853166
MnO	0.17444444	0.11333333	0.13333333	0.15777778	0.09333333	0.16666667	0.16222222	0.07777778	0.157777778	0.124444444	0.148888889	0.168888889	0.088888889	0.122222222
MgO	14.2883904	14.3335323	14.4709206	14.4012451	14.2677821	14.5121372	14.1460953	14.3296069	14.4483497	14.58671941	14.52783868	15.73783768	15.79769975	15.72704288
CaO	22.3487468	22.4407045	22.5559042	22.800451	22.5518621	21.9788951	22.3527889	22.2547681	22.10824215	22.50739909	22.28710488	21.85965326	21.91523208	21.74344301
Na2O	0.32342022	0.36813749	0.32446016	0.30366143	0.33381959	0.28806239	0.31510073	0.32134035	0.342139078	0.253744484	0.316140668	0.267263657	0.235025628	0.284942576
K2O	0.00528039	0.01056077	0.00528039	0.01056077	0	0.00739254	0.01372901	0.01372901	0	0	0.001056077	0.008448619	0	0.024289781
Cr2O3	0.2847775	0.2847775	0.26428991	0.26428991	0.31038699	0.35545969	0.31550889	0.3349721	0.314484506	0.338045234	0.315508885	0.186437069	0.231509766	0.289899398
Totale	100.116123	100.253815	99.6491561	99.8974229	99.0907571	99.9141744	100.33027	100.146912	100.2925638	100.6500272	100.561943	100.1673801	100.3069886	100.0397941
Fe2O3	2.31008764	2.57405367	3.51350273	3.31932407	2.87525181	1.42843343	0.82823405	1.62632008	1.429964853	1.311674825	1.119412301	0.941820037	0.827550425	0.68242848
FeO	4.86372992	4.56342539	3.7716204	3.838272	4.03405922	5.47384345	5.93877333	5.51089862	5.565099034	5.510972832	5.624275571	5.566900764	5.734565324	5.852796505
Wo	46.3343267	46.3456017	46.3260588	46.8037018	46.8111372	45.8197653	46.7406475	46.1543075	45.88780095	46.42107419	46.19146435	44.38726907	44.38193685	44.20359516
En	41.2177125	41.1885179	41.3534905	41.1327462	41.2072992	42.0948801	41.1576419	41.3498882	41.72652094	41.8599207	41.8947864	44.46426488	44.51485167	44.48639842
Fs	11.2345562	11.0900311	11.1145396	10.9355361	10.7276507	10.9986228	10.9093677	11.2898156	11.10058527	10.77194996	10.72804266	10.16639287	10.24189215	10.26173098
N° Mg	78.5813722	78.7866508	78.8165487	78.9977014	79.3440627	79.2844281	79.0474472	78.5526612	78.98695184	79.53340852	79.6133297	81.39068192	81.29565157	81.25647198

Data Set	B34_2_Cpx c-r	B34_2_Cpx c-r	B34_2_Cpx c-r	B34_2_Cpx c-r	B34_2_Cpx c-r	B34_2_Cpx c-r	B34_2_Cpx c-r	B34_2_Cpx c-r	B34_2_Cpx c-r	B34_2_Cpx c-r	B34_2_Cpx c-r	B34_2_Cpx c-r	B34_2_Cpx c-r	B34_2_Cpx c-r
SiO2	52.2194907	51.5271544	51.8234381	51.6511098	51.2993989	51.9967741	52.1318149	51.9917352	52.10561297	51.73878559	51.5241311	51.88289635	51.71157586	52.16003242
TiO2	1.01103837	1.01001401	1.04381773	1.0581587	1.04689079	1.04381773	1.03357418	1.03869595	1.015135789	1.000794819	0.969039815	1.047915148	1.002843529	1.028452404
Al2O3	2.62630328	2.85188804	2.93053226	2.92328872	2.96985438	2.77841777	2.89638411	2.81980947	2.759791507	2.82394864	2.763930677	2.742200035	2.808426753	2.804287583
FeO	6.6202132	6.47199948	6.60992058	6.49876029	6.41641933	6.46994095	6.42465342	6.56051601	6.559486746	6.456560546	6.406126707	6.450384974	6.46376538	6.464794642
MnO	0.15444444	0.16333333	0.14333333	0.14666667	0.16888889	0.11666667	0.18777778	0.19333333	0.118888889	0.135555556	0.105555556	0.147777778	0.213333333	0.14
MgO	15.6347964	15.5690463	15.840879	15.8310655	15.6701248	15.8654126	15.7486325	15.7662967	15.66031138	15.6779756	15.86050586	15.86246855	15.89387161	15.82910281

CaO	21.8869374	21.8515691	21.7778008	21.9293794	21.7778008	21.7596114	21.8768322	21.932411	22.18908406	21.65552743	21.66866424	22.09914743	22.15472625	21.98596875
Na2O	0.24958474	0.25374448	0.2599841	0.28182277	0.26726366	0.19862785	0.21110709	0.21318696	0.232945756	0.132071924	0.230865883	0.285982512	0.274543212	0.241265247
K2O	0	0.00422431	0.02112155	0.01161685	0.00528039	0	0.00316823	0.00739254	0	0	0	0.001056077	0.001056077	0.005280387
Cr2O3	0.31038699	0.19668086	0.30116757	0.28067998	0.21716845	0.27760684	0.15160817	0.19668086	0.212046556	0.199754002	0.332923337	0.177217653	0.286826259	0.219217213
Totale	100.402809	99.7029734	100.450827	100.331869	99.621922	100.229269	100.513944	100.523377	100.6412571	99.6212201	99.52881984	100.5198289	100.524142	100.6591842
Fe2O3	0.30400512	1.01511043	1.1589545	1.5466726	1.37771286	0.39650688	0.36688783	0.8088145	0.816228061	0	0.999248625	1.567464645	1.924869502	0.749442466
FeO	6.34666605	5.55859193	5.56708056	5.10704726	5.17673813	6.1131597	6.09452371	5.83273581	5.825035749	6.456560546	5.506991792	5.039963026	4.731746606	5.790438058
Wo	44.4313053	44.5721532	44.0413219	44.2666839	44.3782745	44.1871403	44.4775955	44.4190366	44.80804753	44.42300821	44.08234497	44.44498948	44.47714196	44.42220616
En	44.1618445	44.1869367	44.5734754	44.4643238	44.430351	44.8277591	44.5502979	44.4286741	44.00154604	44.74866476	44.89525902	44.38834581	44.39674013	44.50017458
Fs	10.4899737	10.3042837	10.4337617	10.239518	10.2058099	10.2551832	10.1954152	10.3709635	10.33915034	10.33805345	10.17247004	10.12584488	10.12871649	10.19547813
N° Mg	80.8058103	81.0900111	81.0320201	81.2819033	81.3204117	81.3822886	81.3767789	81.074759	80.97346735	81.23312881	81.52734784	81.42530458	81.4238759	81.35961887

Data Set	B34_2_Cpx c-r	B34_2_Cpx c-r	B34_2_Cpx c-r	B34_2_Cpx c-r	B34_2_Cpx c-r	B34_2_Cpx c-r	B34_2_Cpx c-r	B34_2_Cpx c-r	B34_2_Cpx c-r	B34_2_Cpx c-r	B34_2_Cpx c-r	B34_2_Cpx c-r	B34_2_Cpx c-r	B34_2_Cpx c-r
SiO2	51.702506	51.0262939	49.3231668	49.7524758	49.9933322	49.7988331	49.9852701	50.2603906	49.91774964	49.77867772	50.64334227	50.17170706	50.63225683	50.80861615
TiO2	1.00898966	1.24971308	1.46585198	1.45458408	1.53038635	1.52219151	1.5201428	1.50580183	1.539605541	1.526288926	1.427950847	1.360343419	1.375708743	1.381854873
Al2O3	2.64906871	3.73353122	4.34302398	4.46719908	4.51790391	4.45374677	4.50134723	4.31508458	4.435120509	4.447538019	3.929106993	3.796653558	3.652817405	3.554512121
FeO	6.33613689	6.50596512	6.74475391	6.4009804	6.46376538	6.53684298	6.59345239	6.91972845	6.527579624	6.574925676	6.588306082	6.361868441	6.62330099	7.022654647
MnO	0.14111111	0.16111111	0.16111111	0.12111111	0.15444444	0.17888889	0.21	0.11888889	0.173333333	0.13	0.133333333	0.196666667	0.128888889	0.174444444
MgO	15.8163453	15.17062	14.4866222	14.8457946	14.7339212	14.5739619	14.6210665	14.6171411	14.47386468	14.56316712	14.7849512	14.94196648	15.07150409	14.8732723
CaO	22.250726	22.0455897	22.54782	22.1789788	22.2497155	22.7014197	22.3699678	22.6236093	22.17998934	22.77619845	22.65897768	22.43059927	22.37603098	22.38613622
Na2O	0.26830359	0.30678124	0.2714234	0.32965984	0.29118219	0.31094099	0.30262149	0.32861991	0.355658252	0.357738125	0.322380287	0.32134035	0.237105501	0.281822767
K2O	0.00105608	0	0.01478508	0	0.0095047	0.00422431	0	0.00739254	0	0.002112155	0.001056077	0.006336465	0.009504697	0.005280387

Cr2O3	0.30526509	0.37902041	0.34931341	0.38311793	0.26019239	0.29809443	0.35238655	0.26736305	0.30526509	0.246875459	0.375947276	0.2847775	0.18438831	0.017414451
Totale	100.174243	100.199605	99.3585585	99.5507837	99.9441559	100.08105	100.103868	100.696657	99.60290092	100.1566462	100.4894048	99.58748171	100.1071181	100.4885939
Fe2O3	1.64406347	1.07858063	2.64255786	2.06595762	1.58730625	2.34299163	1.71663227	2.20480754	1.420752408	2.7124097	1.665254885	2.249508464	1.671083972	1.895034034
FeO	4.85679048	5.5354464	4.36695125	4.54200898	5.03548974	4.42859331	5.04880777	4.93581835	5.249170963	4.13426956	5.089891399	4.337735955	5.119641231	5.317482156
Wo	44.7802478	45.1871491	46.5285149	45.7976679	46.0440841	46.6679414	46.2115032	46.2105313	46.15296958	46.65462161	46.28383565	45.9944713	45.71637568	45.61872643
En	44.2893537	43.2660701	41.5941891	42.6536463	42.4246842	41.6863773	42.0256739	41.5424788	41.90576012	41.50688719	42.02036542	42.63079291	42.84461375	42.17173235
Fs	9.95325669	10.4088632	10.8637331	10.3168392	10.4407887	10.4889503	10.6315346	11.0323103	10.60202542	10.51241816	10.50415557	10.18234446	10.56237486	11.17027005
N° Mg	81.6504836	80.6075899	79.2905769	80.5234196	80.250269	79.8967237	79.8099161	79.0159686	79.80866016	79.79131385	80.00142528	80.72005381	80.22286009	79.05914749

Data Set	B34_4_Cpx c-r	B34_4_Cpx c-r	B34_4_Cpx c-r	B34_4_Cpx c-r	B34_4_Cpx c-r	B34_4_Cpx c-r	B34_4_Cpx c-r	B34_4_Cpx c-r	B34_4_Cpx c-r	B34_4_Cpx c-r	B34_4_Cpx c-r	B34_4_Cpx c-r	B34_4_Cpx c-r	B34_4_Cpx c-r
SiO2	52.0834421	51.6128146	51.7801041	51.9887119	51.1230396	51.9151449	52.2970888	51.5432787	51.76095647	49.45619211	49.68999417	49.62348152	49.47634746	49.79278646
TiO2	1.01616014	1.03664724	0.97006417	0.98440514	1.04279337	1.02230627	0.98235643	1.02128192	1.005916594	0.991575624	1.536532476	1.60106684	1.539605541	1.563165705
Al2O3	2.62423369	2.7339217	2.6780429	2.62837286	2.75875671	2.68735603	2.69563437	2.67390373	2.57663324	2.325178671	4.710375305	4.78384557	4.572747907	4.732105947
FeO	6.44318014	6.42979973	6.34745877	6.53169667	6.38759999	6.33716615	6.38451221	6.23423995	6.389658515	6.346429511	6.785924387	6.598598702	6.793129221	6.764309885
MnO	0.09555556	0.19555556	0.16777778	0.14444444	0.16444444	0.15222222	0.12111111	0.14111111	0.157777778	0.121111111	0.122222222	0.085555556	0.178888889	0.17
MgO	16.0665884	16.0420548	15.8026065	16.0332227	16.1755178	15.8055505	15.8565805	16.0391107	15.80751321	16.46599603	14.50919312	14.49349159	14.41792799	14.3708234
CaO	21.7373799	21.8788532	22.3406626	21.9869793	22.1264316	21.9991056	21.6818011	22.3588521	21.94857937	21.9374636	22.40129408	21.9415057	22.47607285	22.35784155
Na2O	0.21942658	0.23398569	0.25582436	0.24230518	0.27246334	0.25062467	0.2828627	0.27038347	0.317180605	0.236065565	0.308861113	0.322380287	0.28390264	0.32134035
K2O	0.00316823	0.01372901	0.00422431	0.01478508	0.01267293	0	0.00211215	0	0.010560774	0	0.002112155	0.00422431	0.00422431	0.014785084
Cr2O3	0.29604567	0.23253415	0.2345829	0.32780144	0.30321633	0.26531429	0.21716845	0.34111837	0.353410927	0.32575268	0.555213688	0.569555001	0.521409164	0.513214128
Totale	100.289135	100.177362	100.346765	100.554923	100.06372	100.169476	100.304059	100.282162	99.97477655	97.88001222	100.066509	99.45415007	99.7428468	100.0871584
Fe2O3	0.72575892	1.7420931	1.72541887	1.45833024	3.0607997	0.91898219	0.32949096	2.30428111	1.446162424	5.29065878	1.91020182	1.064399378	2.093688792	1.58111864

FeO	5.79013427	4.86224518	4.79490788	5.21947507	3.63345872	5.51025586	6.08803261	4.16082243	5.088385642	1.585836483	5.067103755	5.640840421	4.909204991	5.341601922
Wo	43.8973587	44.0733679	44.9096624	44.1219273	44.1540812	44.5408274	44.033018	44.6899817	44.33653709	43.67484302	46.24069076	45.86282283	46.4830823	46.3714081
En	45.144595	44.9637555	44.2001114	44.7672719	44.9126378	44.5260103	44.8067591	44.605854	44.42933422	45.61249659	41.67209793	42.15200875	41.48854816	41.47180716
Fs	10.1561666	10.1099144	9.95960181	10.2308864	9.94936884	10.0149019	10.1206677	9.7261852	10.07468205	9.862175956	10.93348386	10.76575317	10.96586032	10.95070933
N° Mg	81.6346714	81.6429259	81.6106821	81.3977655	81.8647376	81.6378174	81.5744733	82.0986193	81.51570702	82.22220069	79.21611454	79.65569067	79.09449245	79.11067598

Data Set	B34_4_Cpx c-r	B34_4_Cpx c-r	B34_4_Cpx c-r	B34_4_Cpx c-r	B34_4_Cpx c-r	B34_4_Cpx c-r	B34_4_Cpx c-r	B34_4_Cpx c-r	B34_4_Cpx c-r	B34_4_Cpx c-r	B34_4_Cpx c-r	B34_4_Cpx c-r	B34_4_Cpx c-r	
SiO2	49.8895321	49.5861941	49.7595301	49.721235	50.0860468	49.5942563	49.638598	49.8502292	49.90364089	49.85728359	50.18178473	49.98829337	51.53622431	
TiO2	1.52526457	1.5723849	1.56828748	1.56521442	1.51399667	1.57955539	1.54984909	1.50682618	1.540629896	1.490436501	1.498631341	1.56828748	1.215909366	
Al2O3	4.68243591	4.66898361	4.68967946	4.55722602	4.71347968	4.66380964	4.50238202	4.47961659	4.422703	4.512729944	4.508590774	4.331641263	3.249248343	
FeO	6.57904272	6.80856815	6.65932516	6.77769029	6.78077808	6.54404782	6.69637859	6.80856815	6.739607596	6.536842982	6.553311174	6.71078826	7.048386197	
MnO	0.21	0.18555556	0.14111111	0.16222222	0.15222222	0.12444444	0.13555556	0.15111111	0.18	0.193333333	0.11	0.141111111	0.14	
MgO	14.25895	14.5082118	14.3767115	14.6024209	14.4640512	14.4336295	14.4277414	14.6554136	14.44933104	14.38554359	14.66424571	14.32371882	14.7633616	
CaO	22.5043675	22.4053362	22.4073572	22.484157	22.3174206	22.3164101	22.6862618	22.3265153	22.30125221	22.98638742	22.53670428	22.24870497	22.45990447	
Na2O	0.28494258	0.31198092	0.36189787	0.29846175	0.34421895	0.28910232	0.27766302	0.33797933	0.354618315	0.314060795	0.272463339	0.342139078	0.328619905	
K2O	0.00105608	0.00422431	0.01689724	0	0.01161685	0	0.00422431	0.01478508	0.014785084	0.006336465	0.016897239	0.021121549	0.008448619	
Cr2O3	0.50911661	0.45380012	0.36058158	0.42921501	0.45584888	0.40155676	0.35853282	0.44662946	0.281704362	0.442531943	0.381069173	0.404629902	0.072730944	
Totale	99.9355915	100.05144	99.9807972	100.168628	100.383831	99.5452555	99.9186539	100.131045	99.90656804	100.2829546	100.3426286	99.6758059	100.7501028	
Fe2O3	1.08567835	2.21571996	1.88960169	2.21709739	1.51834254	1.46966219	2.12643908	2.24642854	1.869007155	2.255205011	1.522040597	1.189712496	1.179411997	
FeO	5.60213739	4.81483893	4.95904075	4.78272164	5.41455674	5.2216296	4.78298529	4.78720702	5.057854378	4.50758468	5.183762285	5.640271856	5.987138296	
Wo	46.8888823	46.2242293	46.4267724	46.2329562	46.1501679	46.4630878	46.7851872	45.8977586	46.16443297	47.22613826	46.42081953	46.31682989	45.74517962	
En	41.3372435	41.6469306	41.4465427	41.778305	41.6169392	41.8128901	41.3994604	41.9198298	41.61758694	41.123388	42.02744846	41.48974589	41.83825743	

Fs	10.6995157	10.9640839	10.7697698	10.8781519	10.9447832	10.6347809	10.7791317	10.9250811	10.88958211	10.48281959	10.53614003	10.90450541	11.20535116
N°													
Mg	79.4385433	79.1600979	79.3747024	79.3412763	79.1772744	79.7230636	79.3418503	79.3261434	79.26077085	79.68690187	79.95544	79.18759188	78.87520956

Table 9.1 – Continue. Single mineral phase EMPA analyses. Sample: sub-ophitic gabbro B34. Feldspars.

Data Set	B34_2_Pl (confuso per vetro)	B34_2_Pl (confuso per vetro)	B34_2_Pl (confuso per vetro)	B34_1_Plc-r	B34_1_Plc-r	B34_1_Plc-r	B34_1_Plc-r	B34_1_Plc-r	B34_1_Plc-r	B34_1_Plc-r	B34_1_Plc-r	B34_1_Plc-r	B34_1_Plc-r	B34_1_Plc-r
SiO2	47.7487295	47.5475481	47.0592536	49.0742482	49.4058037	49.2808406	49.318128	50.330934	49.650691	49.183087	49.842167	50.034650	49.212312	50.230157
TiO2	0.08102321	0.07582942	0.05609299	0.0901432 4	0.0676074 3	0.0891188	0.0737535 6	0.0839971 1	0.0676074 29	0.0758022 69	0.0717048 49	0.0839971 09	0.0850214 64	0.0880945 29
Al2O3	33.081439	33.2353444	33.3358959	32.0578706	32.5628493	32.7553207	32.468683 2	31.574622 5	32.378656 26	32.965383 59	32.216193 84	31.986469 92	32.847417 25	32.131340 86
Cr2O3	0	0	0	0	0	0	0.0409751 8	0.0225363 5	0	0.0307313 85	0	0.0430239 39	0.0276582 46	0
FeO	0.73520851	0.75268899	0.83392182	0.7225419 3	0.7451856 9	0.7101907 8	0.6782836 6	0.7719465	0.7369515 94	0.7019566 86	0.6988689	0.7420979 04	0.7565075 72	0.6813714 46
Mno	0	0	0.05058448	0	0	0.0033333 3	0.0377777 8	0.0711111 1	0	0.0211111 11	0.0166666 67	0.0277777 78	0.06	0.0244444 44
MgO	0.05853626	0.03633285	0.09587836	0.0922464 8	0.0745822 6	0.0991158 9	0.0912651 3	0.1010785 9	0.0863584 03	0.1079480 04	0.0873397 49	0.0932278 22	0.0893024 4	0.0883210 94
CaO	17.3382773	17.355416	17.4441338	15.762152 7	15.962235 7	16.140087 9	16.093603 8	14.972932 8	15.333689 84	16.170403 64	15.726783 64	15.563078 77	15.584299 77	15.542868 29
Na2O	1.88317069	2.05106268	2.01577328	2.8130279 9	2.6445582 9	2.6653570 2	2.5956812 8	3.1957245 8	2.9128618 81	2.5811221 66	2.7901493 85	3.0033363 48	2.7131940 9	2.8972628 35
K2O	0.06241383	0.07177591	0.05929314	0.1203928 3	0.1193367 5	0.1182806 7	0.1277853 7	0.1467947 6	0.0982152 01	0.0908226 59	0.1203928 27	0.1351779 11	0.1130002 85	0.1415143 75
SrO														
BaO														
Totale	100.988798	101.125998	100.950827	100.732623	101.582159	101.861646	101.525937	101.271679	101.265031 9	101.928366 86	101.570269 69	101.712838 2	101.488713 5	101.825375 5
Ab %	16.3677443	17.5470977	17.2370484	24.245192 1	22.908871 2	22.854662 3	22.428586 2	27.629471 9	25.437866 98	22.295926 74	24.136255 81	25.686128 85	23.801124 61	25.020898 06
An %	83.2753183	82.0488691	82.4293426	75.072053 9	76.410928 5	76.478000 6	76.844900 2	71.535452 3	73.997779 01	77.187866 98	75.178484 54	73.553172 72	75.546634 15	74.174969 36
Or %	0.35693743	0.40403329	0.33360901	0.6827540 6	0.6802003 5	0.6673371 5	0.7265136 3	0.8350758 1	0.5643540 06	0.5162062 79	0.6852596 48	0.7606984 26	0.6522412 43	0.8041325 83

Data Set	B34_1_Plc-r	B34_1_Plc-r	B34_3_sievePl c-r	B34_3_sievePl c-r	B34_3_sievePl c-r	B34_3_sievePl c-r	B34_3_sievePl c-r	B34_3_sievePl c-r	B34_3_sievePl c-r	B34_3_sievePl c-r	B34_3_sievePl c-r	B34_3_sievePl c-r	B34_3_sievePl c-r
SiO2	50.0336429	50.5062859	47.8185698	47.4557735	47.7319018	47.8044611	48.030201	48.90192	48.801143 2	48.380904 14	47.646241 6	47.927408 74	47.959657 31	48.105783 6
TiO2	0.09936243	0.08092404	0.08297275	0.0594125 9	0.0594125 9	0.0717048 5	0.0645343 6	0.1116546 9	0.0839971 09	0.0747779 14	0.0481446 84	0.0921919 49	0.0635100 09	0.0450716 19

Al2O3	31.7546764	31.8126248	33.3803354	33.5831547	33.5976418	33.3482568	33.6183376	32.4883443	32.4924833	33.3027259	33.6100593	33.2478819	33.3699874	33.2116642
Cr2O3	0	0.04097518	0.02765825	0	0	0	0.0020487 6	0.0460970 8	0.0122925 54	0.0122925 54	0.0338045 23	0.0307313 85	0	0
FeO	0.69269333	0.68445923	0.59079639	0.7369515 9	0.6268205 6	0.5918256 5	0.6556399	0.6402009 7	0.6607862 06	0.6741666 12	0.6082938 44	0.6618154 68	0.6926933 28	0.6649032 54
Mno	0	0.00777778	0.02666667	0	0.0488888 9	0.0333333 3	0.0322222 2	0.0433333 3	0	0.03	0.0322222 22	0.0322222 22	0	0.0355555 56
MgO	0.107948	0.08341437	0.07654495	0.0500486 2	0.0520113 1	0.0902837 9	0.0696755 3	0.0706568 8	0.0353284 38	0.0353284 38	0.0490672 75	0.0441605 47	0.0657501 48	0.0392538 2
CaO	15.25689	15.2013112	17.0091385	17.215285 4	16.972759 6	16.945475 5	16.898991 4	16.133014 3	16.099666 96	16.664549 83	17.061685 73	16.983875 39	16.683749 79	16.978822 77
Na2O	3.01685552	3.15932681	2.1537083	2.1339495 1	2.0715533 3	2.2088249 3	2.1672274 8	2.6653570 2	2.5676029 93	2.4448904 97	2.1360293 84	2.2857802 26	2.1682674 12	2.2712211 17
K2O	0.12989752	0.14890692	0.08554227	0.0781497 3	0.0929348 1	0.0707571 9	0.0834301 2	0.0887105	0.0918787 36	0.0887105 04	0.0792058 07	0.0813179 62	0.0770936 52	0.0887105 04
SrO														
BaO														
Total	101.091966	101.726006	101.251933	101.31272 6	101.25392 5	101.16492 3	101.62230 8	101.18928 9	100.84517 96	101.70834 64	101.30475 44	101.38738 58	101.08070 91	101.44098 64
Ab %	26.1578069	27.1011091	18.5516569	18.241154 2	17.994954 2	19.009706 2	18.746811 4	22.900544	22.279053 5	20.874916 04	18.387986 43	19.495621 63	18.955970 44	19.392098 89
An %	73.1011221	72.0584262	80.963514	81.319296 3	81.473861 5	80.589614 6	80.778337	76.597948 4	77.196385 52	78.626713 29	81.163375 55	80.048025 06	80.600559 91	80.109530 35
Or %	0.74107096	0.84046472	0.48482913	0.4395494 7	0.5311842 2	0.4006791 8	0.4748515 6	0.5015076 5	0.5245609 77	0.4983706 69	0.4486380 24	0.4563533 1	0.4434696 51	0.4983707 55

Data Set	B34_3_sievePl c-r	B34_3_sievePl c-r	B34_3_sievePl c-r	B34_3_sievePl c-r	B34_3_sievePl c-r	B34_3_sievePl c-r	B34_3_sievePl c-r	B34_3_sievePl c-r	B34_3_sievePl c-r	B34_3_sievePl c-r	B34_2_Plr-r	B34_2_Plr-r	B34_2_Plr-r	B34_2_Plr-r
SiO2	48.4333081	48.4282692	48.8948656	49.00572	49.369524 1	49.525728 1	49.232467 7	48.542146 9	48.210591 42	48.309352 64	47.602907 6	48.686257 7	48.945253 96	48.693312 08
TiO2	0.12702002	0.05019339	0.10550856	0.0512177 5	0.0942406 6	0.1085816 3	0.0839971 1	0.0409742	0.0778509 79	0.0686317 84	0.0409741 99	0.0655587 19	0.0635100 09	0.0921919 49
Al2O3	32.9291659	33.0460974	32.8815654	32.904330 8	32.367273 5	32.927096 3	32.942618 2	32.932270 2	33.834609 26	33.642137 86	32.90847	31.860225 24	31.693623 65	31.609805 46
Cr2O3	0.03585328	0	0.01536569	0	0.0327801 4	0.0071706 6	0.0133169 3	0	0.0542921 13	0.0071706 56	0	0.0542921 13	0.0081950 36	0.0122925 54
FeO	0.73180528	0.67931292	0.63711318	0.6093231 1	0.7091615 2	0.7266589 7	0.5753574 6	0.6844592 3	0.6093231 06	0.7462149 52	0.7390101 18	0.7184248 78	0.7019566 86	0.6710788 26
Mno	0	0.03888889	0	0.0388888 9	0.0133333 3	0	0.0055555 6	0.0055555 6	0	0.0433333 33	0.0466666 67	0.0433333 33	0.0033333 33	0.0144444 44

MgO	0.16094066	0.04121651	0.04612324	0.0745822 6	0.0893024 4	0.0912651 3	0.0736009 1	0.0667314 9	0.0618247 66	0.0392538 2	0.0559366 93	0.0736009 12	0.0794889 85	0.0726195 67
CaO	16.5402554	16.4826555	15.8369307	16.213856 2	15.739920 5	15.612594 4	15.930909 5	16.130993 2	16.773686 41	16.913138 71	16.945475 48	16.210824 6	15.708594 21	15.894530 61
Na2 O	2.23378341	2.43657101	2.56448318	2.6466381 6	2.7475119 9	2.8036685 6	2.5520039 5	2.5041668 7	2.2109048 05	1.9821187 95	2.2816204 81	2.7922292 57	2.7391925 01	2.7173538 36
K2O	0.12567321	0.09187874	0.10560774	0.1119442 1	0.1013834 3	0.0918787 4	0.0971591 2	0.1087759 7	0.0897665 81	0.0739254 2	0.0918787 36	0.1394022 2	0.1108881 3	0.1214489 04
SrO														
BaO														
Total e	101.317805	101.295084	101.087563	101.65650 1	101.26443 2	101.89464 2	101.50698 6	101.01607 4	101.92284 94	101.82527 8	100.71294	100.64414 9	100.05403 65	99.899078 23
Ab %	19.4977425	20.9952435	22.524184	22.659420 3	23.866283	24.397443 2	22.348047 3	21.794822 5	19.160089 05	17.422206 35	19.490781 87	23.578912	23.834131 85	23.464729 15
An %	79.7804887	78.4838389	76.8654968	76.709959 3	75.554255 9	75.076485 3	77.092125 6	77.582253 4	80.328047 33	82.150251 07	79.992786 34	75.646529 04	75.531014 03	75.845229 59
Or %	0.72176878	0.52091752	0.61031926	0.6306203 1	0.5794611	0.5260714 8	0.5598271 2	0.6229241 4	0.5118636 26	0.4275425 83	0.5164317 93	0.7745589 62	0.6348541 26	0.6900412 55

Data Set	B34_2_Pl r-r	B34_2_Pl r-r	B34_2_Pl r-r	B34_2_Pl r-r	B34_2_Pl r-r	B34_2_Pl r-r	B34_2_Pl r-r	B34_2_Pl r-r	B34_2_Pl r-r	B34_2_Pl r-r	B34_2_Pl r-r	B34_2_Pl r-r	B34_2_Pl r-r	B34_2_Pl r-r
SiO2	48.6207528	49.1125434	49.0853336	48.876725 8	48.379896 4	48.928121 9	48.585480 9	49.287894 9	49.032929 74	48.983549 13	48.743700 45	48.709436 36	49.060139 46	48.546178 01
TiO2	0.08297275	0.07887533	0.07375356	0.0645343 6	0.0798996 9	0.0921919 5	0.0737535 6	0.0747779 1	0.0850214 64	0.0880945 29	0.1044842 08	0.0778509 79	0.0747779 14	0.0727292 04
Al2O 3	31.7857202	31.8985126	31.9305911	32.034070 4	31.936799 9	31.806416	31.705006 4	31.833320 6	32.081670 82	31.905756 1	31.728806 59	31.723632 63	31.611875 04	32.046487 88
Cr2O 3	0	0	0	0	0	0.0081950 4	0	0	0.0153656 92	0.0440483 18	0	0	0.0122925 54	0
FeO	0.67004956	0.80076584	0.6988689	0.7544490 5	0.6515228 5	0.6926933 3	0.7246004 5	0.7575368 3	0.6175572 02	0.6206449 88	0.7081322 58	0.6751958 74	0.6782836 6	0.7287174 98
Mno	0.01111111	0	0.01888889	0	0	0	0.0277777 8	0	0.0155555 56	0.0322222 22	0.0111111 11	0.0133333 33	0.03	0.0277777 78
MgO	0.1099107	0.10304128	0.0863584	0.0794889 8	0.0608434 2	0.0932278 2	0.0755636 7	0.1050039 8	0.0765449 48	0.0863584 03	0.1177614 59	0.0961718 58	0.0755636 03	0.0951905 13
CaO	15.8419834	15.6287628	15.5954155	15.699499 5	15.971330 4	15.837941 3	16.020846 1	15.756088 8	15.613604 96	15.914741 09	15.704552 12	16.011751 38	15.666152 21	16.130993 21
Na2 O	2.79950881	2.73607269	2.80054875	2.8171877 3	2.7027947 3	2.8920631 5	2.7298330 7	2.8816637 9	2.8182276 68	2.8972628 35	2.8868634 71	2.9066222 62	2.8213474 77	2.6996749 17
K2O	0.12356106	0.11405636	0.10032736	0.1182806 7	0.1140563 6	0.1214489	0.1256732 1	0.1267292 9	0.1066638 2	0.0971591 23	0.1489069 17	0.1256732 14	0.1045516 65	0.1182806 72

SrO														
BaO														
Total				100.444236	99.8971437	100.472299	100.068535	100.823016	100.463141	100.669836	100.154386	100.339679	100.134936	100.466027
Ab %	24.0608998	23.9008823	24.385263	24.3478861	23.2927151	24.6678309	23.400609	24.6889634	24.4712272	24.6456336	24.7519352	24.5545328	24.4330416	23.0909304
An %	75.2403471	75.4435494	75.0399383	74.9794915	76.0605316	74.6505702	75.8905548	74.5966248	74.9193635	74.8105551	74.4080061	74.7469091	74.9712088	76.2434044
Or %	0.69875311	0.65556826	0.5747987	0.6726224	0.6467533	0.6815989	0.7088362	0.7144118	0.6094090	0.5438107	0.8400591	0.6985508	0.5957499	0.6656651
				5	2	2	1	6	76	43	73	4	53	91

Data Set	B34_2_Pl r-r	B34_2_Pl r-r	B34_2_Pl r-r	B34_2_Pl r-r	B34_2_Pl r-r	B34_2_Pl r-r	B34_2_Pl r-r	B34_2_Pl r-r	B34_2_Pl r-r	B34_2_Pl r-r	B34_4_Pl r-r	B34_4_Pl r-r	B34_4_Pl r-r
SiO2	46.9962315	47.2380957	46.6636682	47.0718141	47.0385578	47.3580201	47.7167853	47.6371717	46.9811502	47.3660822	47.8921368	48.4726109	46.4308739	48.3395857
TiO2	0.04916904	0.05121775	0.05429081	0.0522421	0.0542908 1	0.0542908 1	0.0706804 9	0.0665830 7	0.0635100 09	0.0901432 39	0.0942406 59	0.0696561 39	0.0973137 23	0.0932163 04
Al2O3	32.1478975	32.7294509	33.1361243	33.0191928	32.913644	32.6528763	32.2399941	32.6549459	33.1785508 4	33.0543757 4	32.5876843 4	32.6528763 27	32.8308605 7	32.5938930 9
Cr2O3	0.03380452	0.06146277	0	0.0307313 8	0	0.0235607 3	0.0102437 9	0	0.0614627 7	0.0235607 28	0	0	0	0.0256094 87
FeO	0.73592233	0.67931292	0.72974676	0.7513612 6	0.6865177 6	0.7390101 2	0.6906348 7	0.7781220 88	0.7235711 1	0.6525521 66	0.6916640 69	0.8676678 42	0.7410686 78	0.7184248 78
Mno	0.00222222	0	0.01111111	0.0111111 1	0.0711111 1	0	0.0466666 7	0.0188888 9	0	0.0266666 67	0.0077777 78	0.0033333 33	0.0566666 67	0.0188888 89
MgO	0.09126513	0.10598531	0.06673149	0.0529926 6	0.0834143 7	0.0696755 3	0.0686941 8	0.0843957 1	0.0716382 21	0.0686941 85	0.0598620 75	0.0736009 12	0.0736009 12	0.0686941 85
CaO	16.4533503	16.7312444	17.2102327	17.049559 4	17.26278	16.551371 2	16.111793 3	16.585729	17.053601 54	17.189011 74	16.333097 99	16.573602 68	17.318358 8	16.585728 97
Na2O	2.39289368	2.06947345	2.03619549	2.0580341 5	2.1589079 8	2.1713872 2	2.4230518 3	2.4001732 3	1.9935580 96	2.1495485 57	2.3492163 47	2.5166461 09	2.1765869 03	2.3991332 95
K2O	0.09927128	0.08343012	0.07814973	0.0876544 3	0.0855422 7	0.0728693 4	0.0844861 9	0.0813179 6	0.0781497 3	0.0739254 2	0.0992712 78	0.0982152 01	0.0538599 49	0.0823740 39
SrO														
BaO														
Total				100.184693	100.354766	99.6930613	99.4630306	100.307327	100.205157 4	100.694560 6	100.114951 4	101.328209 5	99.7791901 1	100.925548 8
Ab %	20.7170836	18.2010754	17.556439	17.8380876	18.3664752	19.1048585	21.2884059	20.6573852	17.3824374 8	18.3771653 6	20.5347281 4	21.4367834 7	18.4735844 5	20.6490481 1

An %	78.7174056	81.3161192	82.0002009	81.662014 1	81.154691 3	80.473286 2	78.223191 1	78.882113	82.169208 19	81.206984 2	78.894317 15	78.012753 34	81.225632 61	78.884455 68
Or %	0.56551084	0.48280543	0.44336004	0.4998983 1	0.4788335 4	0.4218552 9	0.4884029 6	0.4605018 2	0.4483543 25	0.4158504 42	0.5709547 11	0.5504631 92	0.3007829 39	0.4664962 15

Table 9.1 – Continue. Single mineral phase EMPA analyses. Sample: sub-ophitic gabbro B34. Glass.

Data set	B34_1_Glass	B34_1_Glass	B34_3_Glass	B34_3_Glass	B34_3_Glass	B34_3_Glass	B34_3_Glass	B34_1_Glass	B34_1_Glass	B34_1_Glass	B34_1_Glass	B34_1_Glass	B34_1_Dark zone in Glass
SiO2	53.3838297	53.559737	54.6424769	53.780126	54.145083	54.821417	54.881063	53.594109	54.207763	53.522331	53.429322	53.312051	57.74006343
TiO2	2.6571458	2.5698901	2.6664947	2.6893474	2.6426032	2.7423241	2.6072854	2.6561071	2.6301381	2.7173939	2.7641380	2.6374094	2.323704201
Al2O3	15.968191	16.011285	15.850197	15.591636	15.992816	15.733229	15.865588	15.967165	15.808130	15.700396	15.774270	16.098498	16.32319998
Cr2O3	0	0	0.092	0.004	0	0	0.037	0.015	0	0.114	0.059	0	0.026
FeOtot	9.5875302	9.9844400	9.0374092	9.4240363	9.1978183	9.1895922	9.0374092	10.239449	9.8271156	10.036881	10.318625	10.138679	6.875999021
MnO	0.2360609	0.188452	0.1805171	0.1299327	0.2231668	0.2092809	0.1785334	0.1854764	0.1973786	0.2023379	0.2271342	0.2380446	0.239036486
MgO	2.9580996	2.9480072	2.8975449	2.8450641	2.8904802	3.0125989	2.8571750	3.1649950	3.0751722	3.1599488	3.1892169	3.1559118	2.279886449
CaO	6.7042414	6.1668939	6.0328091	6.7052495	6.1426982	6.1043882	6.0025644	6.7183556	6.7929592	7.0329004	6.7203719	6.9270440	5.132525285
Na2O	4.0005346	3.8903889	5.4003475	5.1650848	5.3907231	5.1330035	5.0228578	4.9276834	4.7277101	4.9362384	5.1490442	5.0367597	5.760727139
K2O	2.2593806	2.0939840	2.3301163	2.3394784	2.3550818	2.4237371	2.4591049	2.1407944	2.1480760	2.1002254	2.0783805	2.1553576	2.936570755
P2O5	1.0189678	0.8029971	0.8512459	0.7731289	0.8558410	0.9086849	0.9109825	0.8707752	0.8305679	0.8788166	0.9672727	0.8523947	0.901792269
F													
Cl													
Total	98.7739827	98.216075	99.9811595	99.447085	99.836313	100.278257	99.859565	100.479912	100.24501	100.40147	100.67677	100.55215	100.539505

Table 9.1 – Continue. Single mineral phase EMPA analyses. Sample: Poikilitic gabbro B21. Clinopyroxenes.

Data Set	B21_3_small Cpx r-r	B21_3_small Cpx r-r	B21_3_small Cpx r-r	B21_3_small Cpx r-r	B21_3_small Cpx r-r	B21_3_small Cpx r-r	B21_4_Cpx rim detail to glass	B21_4_Cpx rim detail to glass	B21_4_Cpx rim detail to glass	B21_4_Cpx rim detail to glass	B21_4_Cpx rim detail to glass	B21_5_Cpx rim detail to glass	B21_5_Cpx rim detail to glass	B21_5_Cpx rim detail to glass
SiO2	51.03334	51.08071	51.12303	51.66622	51.28932	51.43947								
	83	34	96	63	13	86	51.2268397	50.8952842	50.72597921	50.80156177	50.82070936	50.58489175	50.24426632	50.96784342
TiO2	1.057134	1.059183	1.104254	1.116546	1.149326	1.162642								
	34	05	67	93	29	91	1.69633185	1.74959831	1.829498001	1.863301716	1.754720087	1.946274469	1.958566729	1.761890572
Al2O3	3.454137	3.513120	3.553477	3.414815	3.775957	3.733531								
	25	42	33	14	71	22	3.80803627	3.76871416	3.700417858	3.822523369	3.79768835	4.038794995	3.95290722	4.309910621
FeO	5.832827	5.683584	5.503463	5.580658	5.832827	5.892524								
	77	78	93	58	77	97	6.40921449	6.66241295	6.805480365	6.732402762	6.987659739	6.665500732	6.66447147	6.924874757
Mno	0.077777	0.134444		0.185555	0.104444	0.085555								
	78	44	0.18	56	44	56	0.14777778	0.12555556	0.164444444	0.203333333	0.208888889	0.112222222	0.187777778	0.121111111
MgO	15.20202	15.26581	15.27366	15.32076	15.14510	15.02538								
	3	05	13	58	5	08	14.6259732	14.7349026	14.64265611	14.60045825	14.53568945	14.64363745	14.633824	14.6985928
CaO	22.61855	22.69434	22.62967	22.44070	22.55792	22.58318								
	67	6	25	45	53	84	22.2608313	22.1042	22.11834738	22.059737	22.16483148	22.15068415	22.37603098	21.32811769
Na2O	0.280782	0.292222	0.268303	0.262063	0.322380	0.320300								
	83	13	59	98	29	41	0.37229723	0.36085793	0.399335581	0.446132719	0.366057616	0.379576789	0.365017679	0.544926678
K2O	0.008448	0.010560	0.020065	0.006336	0.008448	0.008448								
	62	77	47	46	62	62	0.02428978	0.03590663	0.017953316	0.031682323	0.04118702	0.012672929	0.017953316	0.093990891
Cr2O3	0.611554	0.718090	0.480433	0.500921	0.607457	0.500921								
	56	03	98	57	04	57	0.41794684	0.4896534	0.380044794	0.266338669	0.235607284	0.311411367	0.382093553	0.182339551
Totale	99.56503	99.73398	99.65593	99.99367	100.1857	100.2510								
	67	55	84	33	37	52	100.571592	100.437432	100.4041123	100.5611332	100.677432	100.5342555	100.4008155	100.7512585
Wo	46.31960	46.40946	46.50318		46.25658	46.40210								
	39	7	88	46.18554	67	25	46.1003578	45.6136402	45.57972507	45.54311105	45.69469725	45.75130996	46.04126131	44.27586179
En	43.31638	43.43698	43.67154	43.87336	43.21132	42.95649								
	77	5	12	16	82	01	42.1442753	42.3075715	41.98457753	41.94109342	41.69537694	42.08392665	41.89603113	42.45620302
Fs	9.323467	9.072136	8.827524	8.965062	9.335808	9.450443								
	2	95	61	85	36	27	10.3601507	10.7312379	10.94652211	10.84902724	11.24427519	10.74601682	10.70355926	11.22082436
N° Mg	82.28819	82.72274	83.18536	83.03306	82.23345	81.96718								
	74	11	82	17	94	89	80.2680432	79.7671968	79.31929965	79.4487546	78.76020196	79.6592309	79.65086956	79.09566735

Data Set	B21_7_Cpx c-r	B21_7_Cpx c-r	B21_7_Cpx c-r	B21_7_Cpx c-r	B21_7_Cpx c-r	B21_7_Cpx c-r	B21_7_Cpx c-r	B21_7_Cpx c-r	B21_7_Cpx c-r	B21_7_Cpx c-r	B21_7_Cpx c-r	B21_7_Cpx c-r	B21_6_cpx c-r	B21_6_cpx c-r
SiO2	51.94134	51.59568	51.73374	50.61411	51.11699	50.34705								
	69	26	67	7	3	86	51.0474571	51.5976981	52.78384053	50.7945074	51.37901257	51.01319296	51.55637966	51.9403391
TiO2	0.960844	1.053036	1.201568	1.212836	1.254834	1.213860								
	97	92	4	3	86	66	1.13396097	1.16366726	1.142155807	1.109376448	1.155472422	1.230250336	1.016160144	1.058158698

Al2O3	3.47793748	3.73353122	3.92600262	3.73663559	3.85770631	3.86598465	3.76871416	3.70352224	4.059490844	3.694209104	3.785270841	3.500702913	3.393084496	3.572103593
FeO	5.81738884	5.77415984	5.64653135	5.86885194	5.68873109	5.94604659	5.87193973	5.89046644	5.952222164	6.038680172	5.833857034	6.126167443	5.466410499	5.568307437
MnO	0.14888889	0.16	0.16888889	0.13777778	0.13333333	0.14666667	0.16777778	0.12666667	0.134444444	0.141111111	0.096666667	0.097777778	0.094444444	0.121111111
MgO	15.25207017	14.60438636	15.18632015	15.20398057	14.86345888	14.91939555	15.3943668	15.0263622	13.67210541	15.87228201	15.06267198	15.15491845	15.40025483	15.34628082
CaO	22.19312062	22.07489549	22.24971555	22.09712064	22.39219494	22.47809439	22.4892097	22.0486212	22.09106324	22.30125221	22.36491522	22.37603098	22.17695777	22.04255809
Na2O	0.27662308	0.26622372	0.28182277	0.26518378	0.29014226	0.25582436	0.28702245	0.25478442	0.266223721	0.292222131	0.258944166	0.328619905	0.25478442	0.327579969
K2O	0.00528039	0.01795332	0.00633646	0.0095047	0.00211215	0.00844862	0	0.00528039	0.020065471	0.006336465	0.005280387	0.006336465	0.024289781	0.012672929
Cr2O3	0.62589587	0.78672345	0.57877442	0.62282273	0.75804083	0.62487149	0.51833603	0.55521369	0.536774857	0.46916581	0.770333382	0.533701718	0.783650316	0.961892348
Totale	100.073508	99.2798661	100.400934	99.1460192	99.5995112	99.1813796	100.160449	99.817069	100.1216116	100.2499771	99.94209129	99.83399723	99.38276604	99.98911175
Wo	45.80045392	46.58709241	46.06825851	45.737728	46.61300141	46.49902955	45.8854855	45.92019	47.77259082	44.93668227	46.26083454	45.81594119	45.88399461	45.60425332
En	43.79565593	42.88457334	43.75027841	43.78719643	43.05078741	42.94242183	43.7032631	43.5438666	41.13850188	44.50020633	43.35100035	43.17556802	44.33411625	44.17711946
Fs	9.370823126	9.511611669	9.125515848	9.481789030	9.243236555	9.600880452	9.3514956	9.57569429	10.04707525	9.497561853	9.418903241	9.790858349	8.827949475	8.992178253
N° Mg	82.37456527	81.84674775	82.74160050	82.20016977	82.32448799	81.72767988	82.3738797	81.9733181	80.3712768	82.41119555	82.15099403	81.51497275	83.39426929	83.087649

Data Set	B21_6_cpx c-r	B21_6_cpx c-r	B21_6_cpx c-r	B21_6_cpx c-r	B21_6_cpx c-r	B21_6_cpx c-r	B21_6_cpx c-r	B21_6_cpx c-r	B21_6_cpx c-r	B21_6_cpx c-r	B21_6_cpx c-r	B21_6_cpx c-r	B21_6_cpx c-r	B21_6_cpx c-r
SiO2	53.01562712	52.06127123	51.54126316	51.08373673	50.57078	51.16536599	51.3054455	51.5231233	51.84258564	51.57451948	51.27722805	50.97086672	51.47475049	51.42133881
TiO2	1.021281922	1.020257561	1.065329181	1.011038371	1.052012571	0.986453851	1.03972031	1.11142516	1.037671599	1.105279028	1.222055496	1.084791928	1.068402248	1.024354984
Al2O3	3.8866805	3.4872506	3.7976883	3.9849857	3.7314616	3.4903549	3.57313839	3.38066699	3.358936345	3.602112574	3.715939745	3.664200122	3.531746687	3.472763516
FeO	5.284231125	5.259528848	5.323343085	5.352162423	5.570365965	5.571395222	5.67740921	5.60844866	5.727843047	5.727843047	5.611536441	5.651677659	5.725784523	5.83694482
MnO	0.091111111	0.08	0.098888889	0.194444444	0.088888889	0.132222222	0.18333333	0.07777778	0.091111111	0.123333333	0.155555556	0.073333333	0.086666667	0.115555556
MgO	16.37473094	15.34922496	16.34234655	14.78593251	14.83009319	15.83400955	15.2658105	15.0891683	15.11860867	15.33646737	15.11173925	15.39632944	15.33744871	15.17356402

CaO	19.99523 66	21.54335 93	20.78041 37	21.28163 36	22.47000 97	22.28306 28	22.5569148	22.6054199	22.08601062	22.48213599	22.53468324	22.50032542	22.41645194	22.46798866
Na2O	0.368137 49	0.261024 04	0.462771 7	0.396215 77	0.239185 37	0.265183 78	0.25166461	0.25062467	0.278702958	0.261024039	0.264143848	0.248544802	0.287022449	0.266223721
K2O	0.057028 18	0.020065 47	0.070757 19	0.085542 27	0.011616 85	0.010560 77	0.00105608	0.01689724	0.012672929	0	0.013729007	0.010560774	0.017953316	0.008448619
Cr2O3	0.871746 95	0.913746 51	0.745748 27	0.912722 13	0.867649 43	0.675066 09	0.74062638	0.48350712	0.502970333	0.648432222	0.686334263	0.574676898	0.514238508	0.436385666
Totale	100.0940 65	99.08198 19	99.48280 18	98.17569 19	98.56441 71	99.73860 9	99.8544927	99.663552	99.55414292	100.2127149	99.90661063	99.60063021	99.94622703	99.7871827
Wo	42.03350 81	45.37557 59	42.83592 15	45.52285 57	46.92464 05	45.34325 46	46.332746	46.6749172	45.91955335	46.10354421	46.5408329	46.12245049	45.98665023	46.21312344
En	47.89543 91	44.98275 72	46.87262 08	44.00724 24	43.09158 51	44.83112 17	43.6293865	43.349808	43.73640702	43.75956293	43.4258215	43.91285436	43.77931112	43.42497989
Fs	8.670601 78	8.646770 11	8.565184 6	8.936185 34	9.079872 9	8.849120 71	9.10242032	9.03882696	9.295437478	9.168244745	9.046130062	9.042724604	9.168499144	9.370981074
N° Mg	84.67171 88	83.87684 82	84.54992 12	83.12125 66	82.59609 13	83.51512 53	82.7382734	82.7465881	82.47197025	82.67783015	82.76006554	82.92394346	82.68389363	82.25057201

Data Set	B21_6_cpx c-r	B21_6_cpx c-r	B21_6_cpx c-r	B21_6_cpx c-r	B21_6_cpx c-r	B21_4_cpx c-r	B21_4_cpx c-r	B21_4_cpx c-r	B21_4_cpx c-r	B21_4_cpx c-r	B21_4_cpx c-r	B21_4_cpx c-r	B21_4_cpx c-r	B21_4_cpx c-r
SiO2	51.47978 93	51.51103 01	51.02226 29	51.50196 02	50.82272 49	50.85497 35	50.3500819	51.3669194	50.52845677	50.91140844	49.50154164	50.47504509	50.61915585	50.41760234
TiO2	1.003867 88	1.088889 35	1.064304 83	1.169813 39	1.278395 02	1.395171 49	1.55906829	1.3675139	1.509899246	1.289662925	1.351124224	1.369562613	1.190300491	1.214885011
Al2O3	3.443789 33	3.535885 86	3.391014 91	3.444824 12	3.591764 65	3.593834 23	4.18470073	3.54623378	4.1205436	3.900132804	4.356476282	4.286110394	4.04914292	4.117439222
FeO	5.781364 67	5.968690 36	5.814301 06	5.683584 78	5.946046 59	6.181747 59	6.28467379	6.40612671	6.166308661	6.061323936	6.008831574	6.091172535	5.77004279	5.984129286
Mno	0.073333 33	0.111111 11	0.171111 11	0.124444 44	0.17	0.16	0.21222222	0.22888889	0.145555556	0.143333333	0.145555556	0.112222222	0.158888889	0.072222222
MgO	15.24029 55	15.12940 35	15.46796 77	15.08033 62	15.00673 53	15.08131 75	14.8614962	15.6151695	14.96257474	15.23440744	14.91547015	15.06856005	14.90369401	14.92233957
CaO	22.78428 26	22.40028 36	22.54984 11	23.02478 73	22.59834 62	22.17493 67	21.8930006	22.2345576	22.13855786	21.78588502	21.88188479	22.4316098	22.26588388	22.58723048
Na2O	0.252704 55	0.238145 44	0.277663 02	0.306781 24	0.295341 94	0.310940 99	0.3057413	0.31198092	0.326540032	0.307821177	0.354618315	0.315100732	0.291182194	0.32134035
K2O	0.011616 85	0	0.013729 01	0	0.001056 08	0.010560 77	0.01161685	0.00633646	0.00422431	0.021121549	0.025345858	0.015841161	0.027458013	0.010560774
Cr2O3	0.416922 46	0.328825 82	0.527555 44	0.362630 34	0.297070 05	0.330874 58	0.30014319	0.2898994	0.479409605	0.685309884	0.967014246	0.822576737	1.030525775	1.159597591

Total	100.071044	99.98343	99.77219	100.3365	99.71041	99.76348								
		93	56	32	07	28	99.6626018	101.083727	99.90266077	99.65509661	98.5408484	100.1652246	99.27574903	99.64774926
Wo	46.5370039	46.14707	45.91447	46.99034	46.44677	45.67739								
		22	05	87	55	35	45.581942	44.8944517	45.77729946	45.13229364	45.61851666	46.03943113	46.35486358	46.47337943
En	43.311911	43.36739	43.82180	42.82279	42.91568	43.22441								
		54	36	03	32	33	43.0527569	43.8694085	43.04850488	43.91255053	43.26575413	43.03206214	43.17180343	42.71978789
Fs	9.217046	9.597719	9.240637	9.053859	9.539059	9.939133								
	33	04	98	06	66	85	10.2133596	10.0962024	9.952322676	9.801172644	9.77788241	9.758178427	9.376327064	9.610380557
N°	82.45339	81.87916	82.58535	82.54733	81.81468	81.30460								
Mg	94	87	1	26	61	74	80.8257852	81.2914146	81.22232589	81.75294493	81.56634227	81.51518477	82.15668764	81.63510487

Data Set	B21_4_cpx c-r	B21_4_cpx c-r	B21_4_cpx c-r	B21_4_cpx c-r	B21_4_cpx c-r	B21_4_cpx c-r	B21_4_cpx c-r	B21_4_cpx c-r	B21_Cpx to Pl	B21_Cpx to Pl	B21_Cpx to Pl	B21_Cpx to Pl	B21_Cpx to Pl	B21_Cpx to Pl
SiO2	50.7793909	51.10893	51.07769	50.34201	51.68537	50.55566								
		09	01	98	39	65	51.1845134	50.4367499	51.35422468	50.75172164	48.99204637	49.5894607	50.45047012	49.66782681
TiO2	1.10732774	1.068402	1.082743		1.106303	1.070450								
		25	22	1.11962	38	96	1.1718621	1.71681895	1.035758151	1.116386031	1.446133386	1.377909795	1.344831691	1.355168598
Al2O3	3.77078375	3.379632	3.611425	3.599008	3.585555	3.520363								
		19	71	2	89	97	3.57934714	3.7500879	3.654795007	3.896442917	4.071715436	3.99704312	4.034379278	3.984597734
FeO	5.5827171	5.595068	5.829739	5.891495	5.805037	5.855471								
		25	99	71	7	54	6.26203003	6.67785188	5.294769556	5.6664032	6.154172358	6.075402183	6.202646312	6.149122988
Mno	0.13	0.105555	0.094444	0.107777	0.132222	0.078888								
		56	44	78	22	89	0.17555556	0.20777778	0.110166254	0.103280863	0.15836399	0.100329981	0.129838799	0.101313609
MgO	15.2824934	15.46404	15.35903	15.34824	15.09309	15.01458								
		23	83	35	37	6	15.3129151	14.5337268	15.76640437	15.51093254	14.982026	15.20855767	15.05287952	15.661621
CaO	22.4811255	22.42049	22.55388	22.72769	22.10116	22.72769								
		4	32	33	85	33	22.376031	22.3588521	22.19276343	22.26363124	22.15530472	21.86170948	21.97914758	21.78274248
Na2O	0.29742181	0.313020	0.283902	0.303661	0.270383	0.263103								
		86	64	43	47	91	0.29846175	0.38685634	0.165320473	0.284462043	0	0.156084693	0.220735157	0.291850668
K2O	0.01689724	0.010560	0.016897	0.016897		0.015841								
		77	24	24	0	16	0.01584116	0.02534586	0.001049007	0	0.005245036	0.015735109	0	0.012588087
Cr2O3	0.84716184	0.782625	0.711943	0.789796	0.565457	0.623847								
		94	75	59	48	11	0.32267954	0.34624027	0.967965368	0.798268398	0.347186147	0.308225108	0.361038961	0.384415584
Total	99.4481574	99.46570	99.90976	99.45641	99.77913	99.10206								
		71	48	69	87	63	100.376557	100.094067	99.57525093	99.59326047	97.9650073	98.38223273	99.41492845	99.00683197
Wo	46.2185404	45.87710	46.03910	46.16514	45.92733	46.70184								
		87	89	76	45	17	45.5628327	46.1069412	45.69979748	45.63795832	46.3453019	45.50027093	45.63343643	44.543592
En	43.7162927	44.02757	43.62349	43.37789	43.64004	42.92822								
		73	98	24	32	27	43.3846836	41.7008299	45.17378193	44.24039688	43.6063195	44.04217833	43.48533432	44.56154981
Fs	8.9586419	8.936235	9.288661	9.340772	9.415847	9.391584								
	3	32	03	18	09	45	9.95270552	10.7486009	8.510367246	9.066424052	10.04837859	9.869683898	10.05188922	9.814862154

N° Mg	82.99259 03	83.12765 85	82.44513	82.28184 98	82.25296 56	82.04965 78	81.3400961	79.5067349	84.14733701	82.9920001	81.27213655	81.69292714	81.22448541	81.9501475
Data Set	B21_Cpx to Pl	B21_Cpx to Pl	B21_Cpx to Pl	B21_Cpx to Pl	B21_Cpx to Pl	B21_Cpx to Pl	B21_Cpx to Pl	B21_Cpx to Pl	B21_Cpx to Pl	B21_Cpx to Pl	B21_Cpx_c-r	B21_Cpx_c-r	B21_Cpx_c-r	B21_Cpx_c-r
SiO2	50.00877 03	50.13497 02	50.36090 89	50.52069 43	50.89522 32	50.32427 02	50.3436072	51.3847569	50.55122654	51.66972458	49.54875104	48.78951578	49.13249471	49.94567027
TiO2	1.462672 44	1.467840 89	1.366539 2	1.365505 51	1.313820 97	1.164969 5	1.1091502	1.08330793	1.215620345	1.229058325	1.217687726	1.256967975	1.261102738	1.220788798
Al2O3	4.232468 34	4.204466 22	4.181649 68	4.035416 39	3.920296 57	3.934816 19	3.82073349	3.9285935	4.0291937	3.961781193	3.74606117	3.689019818	3.86118099	4.013636968
FeO	6.271317 75	6.283436 23	6.146093 37	6.080451 55	5.789607 83	5.647215 59	5.59571202	5.52199121	5.617929246	6.265258502	5.813844809	5.768400477	5.721946272	5.71891665
MnO	0.129838 8	0.152462 23	0.201643 59	0.141642 33	0.102297 24	0.150494 97	0.07180479	0.09049371	0.060001263	0.126887918	0.154429481	0.156396736	0.0649194	0.213447117
MgO	14.99699 51	15.09179 91	14.94410 44	15.05088 36	15.59875 1	15.85821 46	15.3762111	15.2444834	14.94510234	13.83240275	15.89513823	16.34520775	15.67359624	15.9540165
CaO	22.17352 79	22.18871 38	21.93865 17	22.29299 08	22.04697 82	22.29096 6	22.1634039	22.191751	22.28894118	21.87689544	21.82627557	21.98117237	21.40005626	21.58228779
Na2O	0.136689 55	0.049873 22	0.254907 55	0.253060 39	0.253983 97	0.291850 67	0.15700827	0.10621148	0.247518921	0.336182415	0.241977452	0.268761216	0.255831123	0.245671765
K2O	0.002098 01	0	0.006294 04	0.006294 04	0.004196 03	0	0.01153908	0.01363709	0.014686102	0.014686102	0.022029153	0.007343051	0.001049007	0
Cr2O3	0.386147 19	0.425108 23	0.384415 58	0.394805 19	0.455411 26	0.514285 71	0.76277056	0.82337662	0.521212121	0.603463203	0.541125541	0.625974026	0.658874459	0.432900433
Totale	99.41437 81	99.57356 19	99.40079 24	99.74693 89	99.92515 5	99.66279 76	98.6491701	99.5652263	98.97021964	99.31287722	98.46619462	98.26278518	97.37217675	98.89443586
Wo	46.01968 63	46.05172 95	45.71464 82	46.02304 92	45.24341 53	45.22220 58	45.9729664	46.3242654	46.51624099	46.92403809	44.61756193	44.21641729	44.45615583	44.32673393
En	43.30758 87	43.58185 67	43.32776 03	43.23345 55	44.53967 37	44.76391 28	44.3778539	44.2772439	43.39752531	41.28176061	45.2107184	45.74820319	45.30399953	45.59205716
Fs	10.15935 2	10.17909 99	9.996384 43	9.798085 65	9.273716 21	8.942430 38	9.05982415	8.99727568	9.15144735	10.48931261	9.276581883	9.057043405	9.278101367	9.168121645
N° Mg	80.99881 55	81.06599 94	81.25354 95	81.52404 13	82.76689 83	83.34939 63	83.0459996	83.1114841	82.58491672	79.7390474	82.97478158	83.47413073	83.00156789	83.25768497
Data Set	B21_Cpx_c-r	B21_Cpx_c-r	B21_Cpx_c-r	B21_Cpx_c-r										

SiO2	50.83517 65	49.42865 75	49.78486 71	49.39100 11
TiO2	1.178407 48	1.112251 27	1.176340 1	1.120520 79
Al2O3	3.958669 85	3.782360 21	3.861180 99	3.575974 23
FeO	5.717906 78	5.724975 89	5.677511 81	5.925940 83
Mno	0.088526 45	0.118035 27	0.139675 07	0.168200 26
MgO	14.81836 44	17.69441 84	15.72948 07	15.72349 31
CaO	21.28970 49	20.79666 74	21.31602 73	21.99332 11
Na2O	0.271531 95	0.356501 13	0.324175 9	0.229047 36
K2O	0.014686 1	0.025176 17	0.030421 21	0.001049 01
Cr2O3	0.621645 02	0.460606 06	0.435497 84	0.405194 81
Total	98.17297 44	99.03904 33	98.03968 02	98.12854 78
Wo	45.43026 46	41.15677 84	44.20562 83	44.96610 13
En	43.99737 75	48.72308 92	45.38753 36	44.72953 17
Fs	9.523816 98	8.843407 45	9.190257 78	9.456927 86
N° Mg	82.20552 24	84.63792 66	83.16117 68	82.54743 36

Table 9.1 – Continue. Single mineral phase EMPA analyses. Sample: Poikilitic gabbro B21. Olivines.

Data set	B21_1_Ol rim detail to glass	B21_1_Ol rim detail to glass	B21_1_Ol rim detail to glass	B21_2_Ol rim detail to glass	B21_2_Ol rim detail to glass	B21_2_Ol rim detail to glass	B21_2_Ol rim detail to glass	B21_2_Ol rim detail to glass	B21_2_Ol rim detail to glass	B21_2_Ol rim detail to glass	B21_3_Ol rim detail to glass	B21_3_Ol rim detail to glass	B21_3_Ol rim detail to glass	B21_3_Ol rim detail to glass
SiO2	38.9139359	38.9109125	38.778895	39.7090644	39.4188274	39.3805322	39.4168119	39.4359594	39.58410127	39.85418297	39.01068154	39.21122728	38.97339414	39.281771
TiO2	0.06555872	0.07887533	0.07375356	0.05736388	0.02663323	0.06351001	0.05531517	0.06043694	0.044047264	0.136239213	0.033803714	0.037901134	0.057363879	0.059412589
Al2O3	0.07864423	0.08485298	0.16349721	0.03828732	0.01966106	0.01966106	0.01862626	0.05173962	0.039322114	0.710902424	0.046565661	0.039322114	0.066226718	0.037252529
Cr2O3	0	0	0	0.01946321	0.0399508	0.05429211	0	0.01639007	0	0.009219415	0	0.01946321	0	0.012292554
FeO	20.9578329	21.0875199	20.7890339	21.441586	21.2192655	21.5012832	20.9784181	21.2367629	20.85902376	20.62846907	21.09987106	21.30057715	21.0556128	20.73345379
MnO	0.32666667	0.32888889	0.30555556	0.35222222	0.34111111	0.40111111	0.33444444	0.35333333	0.315555556	0.301111111	0.334444444	0.332222222	0.291111111	0.26
MgO	39.0487185	38.7180051	38.5129039	39.0418491	39.0565693	39.2341928	38.8632442	39.1017112	38.63557207	37.90250699	38.47463141	38.66599378	38.7700164	38.280325
CaO	0.25970465	0.28698879	0.27082041	0.15966278	0.20412583	0.21018897	0.21827316	0.21423107	0.264757265	0.375914895	0.171789065	0.268799361	0.240504691	0.231409976
Na2O	0	0	0.01039936	0.02703835	0.00207987	0.02703835	0.04783707	0.02079873	0.04055752	0.219426582	0.007279555	0.062396185	0	0.015599046
NiO														
Totale	99.6510615	99.4960436	98.9048589	100.846537	100.328224	100.89181	99.9329703	100.491363	99.78293681	100.1379727	99.17906645	99.93790244	99.45422974	98.91151649
Fo	76.5792575	76.3148711	76.4922816	76.1490945	76.3510131	76.1475849	76.4697239	76.3468722	76.48130964	76.34592592	76.18548835	76.10824056	76.39834185	76.47025663
Fa	23.0567551	23.3168112	23.1629093	23.4605787	23.2701138	23.4100985	23.1563794	23.2611538	23.16377811	23.30946881	23.4382422	23.52021704	23.27572846	23.23464455

Data set	B21_3_Ol rim detail to glass	B21_3_Ol rim detail to glass	B21_7_Ol c-r	B21_7_Ol c-r	B21_7_Ol c-r	B21_7_Ol c-r	B21_7_Ol c-r	B21_7_Ol c-r	B21_7_Ol c-r	B21_7_Ol c-r	B21_7_Ol c-r	B21_4_ol c-r	B21_4_ol c-r	B21_4_ol c-r
SiO2	38.935099	39.0913029	39.5236352	39.4964255	38.9260291	39.221305	38.8504465	39.524643	39.82697324	41.26505753	39.06711652	39.60828769	39.25960012	39.28277877
TiO2	0.05633952	0.09526501	0.02560887	0.02356016	0.0204871	0.02253581	0.00614613	0.01946274	0.01638968	0.02253581	0.03073065	0.041998554	0.039949844	0.01229226
Al2O3	0.06208755	0.39115155	0.02586981	0.05691359	0.00827834	0.03104377	0.04346128	0.03311336	0.026904604	0.020695849	0.065191925	0.013452302	0.035182944	0.032078566
Cr2O3	0.05531649	0.01946321	0	0.02356073	0.04814584	0	0.01434131	0	0	0.014341313	0.002048759	0.007170656	0	0.016390072
FeO	20.8765212	20.9588622	21.3870352	21.2079436	20.8929894	21.1338367	21.1039881	21.1554512	20.8281459	20.68301995	20.73242453	21.71331122	20.97327184	21.71434048

MnO	0.36333333	0.40111111	0.30333333	0.27555556	0.32222222	0.36222222	0.28555556	0.29666667	0.316666667	0.386666667	0.372222222	0.377777778	0.313333333	0.382222222
MgO	38.7876806	37.607122	38.9083861	37.8985816	38.2744369	38.8190837	38.6561803	38.871095	38.81319561	37.92507793	38.6944528	39.19199497	38.96824819	38.73959469
CaO	0.24252574	0.28900984	0.22938893	0.25667307	0.21928369	0.17886273	0.1859364	0.21726264	0.240504691	0.240504691	0.229388928	0.22736788	0.153599635	0.247578358
Na2O	0.03743771	0.07799523	0.03223803	0.03119809	0.0114393	0.01871886	0.03223803	0.04055752	0.005199682	0.034317901	0	0.008319491	0.054076693	0
NiO														
Totale	99.4163412	98.9312831	100.435495	99.2704119	98.7233119	99.7876087	99.1782936	100.158252	100.0739801	100.5922176	99.19357633	101.1896805	99.7972626	100.4272754
Fo	76.4961113	75.8322386	76.1738076	75.8694247	76.2772284	76.2945463	76.3091379	76.3564148	76.5889316	76.23509402	76.56746661	75.97207157	76.54060654	75.75489579
Fa	23.0967635	23.7082189	23.488781	23.8171528	23.3579178	23.3009705	23.3705854	23.312481	23.0560375	23.32329244	23.01405305	23.61185479	23.10971827	23.82043697
Data set	B21_4_ol c-r	B21_4_ol c-r	B21_4_ol c-r	B21_4_ol c-r	B21_4_ol c-r	B21_2_ol c-r	B21_2_ol c-r	B21_2_ol c-r	B21_2_ol c-r	B21_2_ol c-r	B21_2_ol c-r	B21_2_ol c-r	B21_2_ol c-r	B21_2_ol c-r
SiO2	39.3049497	39.3140196	39.1356447	39.1316136	39.1487457	39.5347207	37.5272477	39.1487457	34.7800734	39.29991082	38.56323275	39.96100633	38.61462889	38.73757653
TiO2	0.02356016	0.02765758	0.02765758	0.05019339	0.02253581	0.03790113	0.01741403	0.03073065	0.019462745	0.01638968	0.00614613	0.009219195	0.045071619	0.01434097
Al2O3	0.06415713	0.05070483	0	0.0134523	0.03932211	0.04863525	0.03518294	0.04656566	0.198680153	0.025869812	0.070365888	0.024835019	0.014487095	0.047600453
Cr2O3	0	0.01946321	0	0	0.01946321	0.01946321	0	0.03585328	0	0.04097518	0.021511969	0	0.048145836	0.007170656
FeO	21.0597298	21.1883876	21.4858443	21.4014448	21.1791242	21.4210008	21.1111929	20.8312337	20.7602146	21.07413951	21.02988125	21.158539	20.94136472	21.31086977
MnO	0.37777778	0.39333333	0.37555556	0.30222222	0.28555556	0.31444444	0.36666667	0.38111111	0.324444444	0.346666667	0.268888889	0.4	0.296666667	0.412222222
MgO	38.7052476	38.2459779	38.9800243	38.9339011	39.3215326	39.0604947	39.5276151	38.4746314	42.81512253	38.69837818	38.15471278	38.5629525	38.6080944	39.03596103
CaO	0.21221002	0.23848364	0.17279959	0.24454679	0.26071517	0.22938893	0.23343102	0.22534683	0.257683598	0.229388928	0.219283689	0.246567835	0.291030887	0.25566255
Na2O	0	0	0	0.02703835	0	0.03119809	0.07903517	0.06967574	0.172629444	0	0.037437711	0.012479237	0.018718855	0
NiO														

Totale	99.7476322	99.4780277	100.177526	100.104413	100.276994	100.697247	98.8977856	99.2438941	99.32831091	99.73171878	98.37146105	100.3755991	98.87820896	99.82140419
Fo	76.2905827	75.951604	76.0637281	76.1745952	76.5533973	76.2068157	76.6352388	76.373295	78.35064189	76.30180113	76.14976739	76.1214985	76.41484201	76.20468418
Fa	23.2863449	23.6045941	23.5198948	23.4894461	23.1307374	23.4446246	22.9608587	23.1968759	21.31202194	23.30984172	23.54532347	23.42988604	23.2515432	23.33809565
Data set	B21_2_ol c-r	B21_2_ol c-r	B21_2_ol c-r	B21_2_ol c-r	B21_2_ol c-r	B21_2_ol c-r	B21_2_ol c-r	B21_2_ol c-r	B21_1_ol c-r	B21_1_ol c-r	B21_1_ol c-r	B21_1_ol c-r	B21_1_ol c-r	B21_1_ol c-r
SiO2	37.6774051	39.2364215	39.0701398	38.9875029	39.0308369	39.0368835	39.1366525	39.4359594	38.73354546	38.76377849	38.31431416	39.76751496	39.45006818	39.49541772
TiO2	0.03585242	0.02560887	0.031755	0.03073065	0.00819484	0.01536532	0.03380371	0.04814468	0.049169039	0.0204871	0.049169039	0.035852424	0.043022909	0.01434097
Al2O3	0.07967902	0.04449608	0.03518294	0.0134523	0.06105276	0.04863525	0.02069585	0.00931313	0.009313132	0.052774416	0.070365888	0.048635246	0.026904604	0.062087548
Cr2O3	0	0	0.01946321	0.05326773	0.03585328	0	0.03380452	0	0.023560728	0.064535908	0.016390072	0	0.053267734	0.048145836
FeO	20.9012235	21.138983	21.1286904	21.2470555	20.8734334	21.7452183	21.5414245	21.0412031	21.1369245	21.42511786	21.25117258	21.19250464	21.18118276	21.36747918
MnO	0.38111111	0.3	0.34111111	0.26888889	0.34333333	0.31333333	0.32444444	0.33888889	0.333333333	0.332222222	0.373333333	0.283333333	0.324444444	0.375555556
MgO	41.4775486	38.9162369	39.1929763	38.680714	38.3470565	39.3951335	39.0555879	38.7307626	39.26952126	39.07914023	40.12329184	37.80633513	38.38434763	38.53253079
CaO	0.24656783	0.23140998	0.24454679	0.27789408	0.21221002	0.19705216	0.22534683	0.22736788	0.167746969	0.279915124	0.233431024	0.195031115	0.214231069	0.260715169
Na2O	0.08631472	0.01351917	0.06447606	0.16119014	0.05511663	0.03743771	0.0343179	0.03743771	0.02599841	0.036397774	0	0.032238029	0.015599046	0
NiO												0.736	0.012	0.022
Totale	100.885702	99.9066755	100.128342	99.7206962	98.9670877	100.789059	100.406078	99.8690774	99.74911283	100.0543691	100.4314679	100.0974449	99.70506838	100.1782728
Fo	77.6453158	76.3883729	76.4896823	76.2141559	76.309956	76.0938154	76.095798	76.3513692	76.52445273	76.1970254	81.22166361	80.44960299	80.64564937	80.51113553
Fa	21.9493335	23.2770511	23.1320776	23.4848269	23.3018558	23.5623176	23.5450362	23.2690578	23.10648422	23.43493133	18.24010346	19.1210038	18.86887738	18.93000735
Data set	B21_1_ol c-r	B21_1_ol c-r	B21_1_ol c-r	B21_1_ol c-r	B21_1_ol c-r	B21_1_ol c-r	B21_1_ol c-r	B21_Ol_c-r	B21_Ol_c-r	B21_Ol_c-r	B21_Ol_c-r	B21_Ol_c-r	B21_Ol_c-r	B21_Ol_c-r

SiO2	38.9240135	38.5289687	39.3291361	38.6146289	37.9666344	38.908897	39.182002	38.5459463	39.02326715	38.86958816	39.01105425	38.71387369	39.16066227	39.21358483
TiO2	0.031755	0.02970629	0.03790113	0.02151145	0.02560887	0.00512177	0.04302291	0.0227412	0.037212868	0.022741197	0.034111795	0.020673815	0.018606434	0.031010723
Al2O3	0.03518294	0.00724355	0.03621774	0.01241751	0.07760943	0.03207857	0.05587879	0.06118981	0.031113465	0.05289289	0.046670197	0.120305397	0.044595966	0.021779425
Cr2O3	0.03892642	0.01639007	0.03892642	0.02356073	0	0.02868263	0	0.05108225	0.004329004	0	0	0	0.004329004	0
FeO	21.3407184	21.7472769	21.2892553	21.2491141	20.9732718	21.4261471	21.0556128	21.2881446	21.1528215	21.07809082	21.14070301	20.76502987	21.13767339	20.96296518
MnO	0.33222222	0.32666667	0.32222222	0.38888889	0.33888889	0.37555556	0.33	0.23016878	0.328531508	0.275415635	0.323613371	0.297055435	0.27738289	0.307875335
MgO	38.6767886	38.6571617	38.3470565	38.6630497	40.4981658	38.5688406	39.1821815	39.5242871	39.8715691	38.38164938	39.46940055	39.39156148	40.12504507	39.52428708
CaO	0.2576836	0.25869412	0.25060993	0.26172569	0.26273622	0.24454679	0.22736788	0.18526872	0.224752223	0.234876197	0.185268724	0.196405096	0.239938184	0.223739826
Na2O	0.02183866	0.02911822	0.03119809	0	0.01039936	0	0.01559905	0	0	0.013853671	0	0.055414684	0	0
NiO	0.021	0.003	0.007	0	0.002	0.038	0.001	0.01363709	0.004196029	0	0	0.02307816	0.004196029	0.001049007
Totale	99.6801293	99.6042261	99.6895234	99.234897	100.155315	99.62787	100.092665	99.9224659	100.6777928	98.92910795	100.2108219	99.58339763	101.0124292	100.2862914
Fo	80.6406063	80.3504029	80.5555391	80.6325078	81.5964679	80.4841096	81.0472684	76.601483	76.78752183	76.21073861	76.62059744	76.92296057	76.9556802	76.80730881
Fa	18.866072	19.1660252	18.9623832	18.7898781	17.9172464	18.9577468	18.466591	23.1450644	22.85299253	23.47854918	23.02246795	22.74745439	22.74205888	22.85276032
Dataset	B21_Ol_c-r	B21_Ol_c-r	B21_Ol_c-r	B21_Ol_c-r	B21_Ol_c-r	B21_Ol_c-r	B21_Ol_c-r	B21_Ol_c-r	B21_Ol_c-r	B21_Ol_c-r	B21_Ol_c-r	B21_Ol_c-r	B21_Ol_c-r	B21_Ol_c-r
SiO2	39.8496733	38.8889253	39.3408025	38.6843592	39.1881413	38.586656	38.7881688	38.9316704	37.44373214	38.75356562	38.90520912	38.98357522	38.45434958	39.55249279
TiO2	0.0113706	0.0330781	0.03101072	0.01447167	0.04134763	0.03101072	0.02687596	0.02480858	0.033078105	0.024808578	0.009303217	0.012404289	0.027909651	0.034111795
Al2O3	0.09645174	0.04978154	0	0.01763096	0.00103712	0.02489077	0.05081866	0.03941039	0	0	0	0.022816541	0.051855775	0.022816541
Cr2O3	0	0	0.00952381	0	0	0.00606061	0	0.00779221	0.051082251	0.055411255	0.064935065	0.012121212	0.035497835	0
FeO	20.8084545	21.1629202	21.1588807	21.3770135	21.1932165	21.2669373	21.116466	20.916511	21.21947318	20.80542483	21.1992757	21.05183409	21.02961687	21.02658724
MnO	0.29607181	0.26459574	0.29803906	0.32066249	0.22229976	0.26262848	0.34033503	0.26459574	0.283284653	0.273448381	0.302957199	0.283284653	0.337384153	0.214430744
MgO	37.6661287	39.3636192	39.0931784	39.6480312	39.3785883	39.3316853	40.2348181	39.9763525	39.4274872	39.20594522	39.66998586	39.64603537	39.66499618	39.56520249

CaO	0.22373983	0.18729352	0.23082661	0.22677702	0.19944229	0.23588859	0.1538844	0.22171503	0.193367904	0.18324393	0.208553865	0.192355506	0.192355506	0.150847213
Na2O	0.01200651	0.01200651	0.00461789	0.02031872	0	0	0	0	0	0	0	0.035095966	0.007388624	0.006465046
NiO	0.01783312	0	0.00734305	0.00629404	0.01888213	0.00314702	0.00839206	0	0.008392058	0.004196029	0	0	0	0.002098015
Totale	98.9817301	99.9622202	100.174223	100.315559	100.242955	99.7489047	100.719759	100.382856	98.6598975	99.30604384	100.36022	100.2395229	99.80135416	100.5750519
Fo	76.0816985	76.6038843	76.455069	76.5076633	76.6211855	76.5040723	76.968931	77.0844932	76.56990987	76.82508505	76.6799619	76.80861978	76.78995923	76.85170263
Fa	23.578517	23.1035551	23.2137575	23.1407692	23.133058	23.2056852	22.661158	22.625623	23.1175115	22.87047358	22.98731855	22.87955557	22.83893398	22.91164855

Dataset	B21_Ol_c-r	B21_Ol_c-r	B21_Ol_c-r	B21_Ol to Opq	B21_Ol to Opq	B21_Ol to Opq	B21_Ol to Opq	B21_Ol to Opq	B21_Ol to Opq	B21_Ol to Opq	B21_Ol to Opq	B21_Ol to Opq	B21_Ol to Opq	B21_Ol to Opq
SiO2	38.8156479	39.3886364	38.5774963	38.8675527	35.5548037	39.2451348	37.5200628	39.5362089	38.7556011	39.09247358	37.48851277	38.99477038	38.76577851	39.07720745
TiO2	0.02894334	0	0.0341118	0.02997703	0.00826953	0.03721287	0.00310107	0.0341118	0.005168454	0.018606434	0.037212868	0.04031394	0.012404289	0.021707506
Al2O3	0.026965	0.01763096	0.04252174	0.03733616	0.08919193	0.03629904	0	0.01451962	0.030076349	0.06222693	0.060152699	0.049781544	0.02074231	0.046670197
Cr2O3	0	0.02597403	0.04329004	0	0.02597403	0	0	0.05021645	0.038095238	0	0	0.025974026	0	0.025974026
FeO	21.3588358	20.9892219	20.9427677	20.1257796	20.611529	20.6478845	19.9490517	20.4085443	20.32270504	20.62970675	20.19243129	20.30755693	20.16617457	20.46711703
MnO	0.31869523	0.28820279	0.3786965	0.216398	0.23607054	0.32656425	0.2813174	0.29607181	0.265579362	0.291153671	0.30590808	0.30590808	0.254759462	0.243939563
MgO	39.6769714	39.620089	39.288774	40.5162363	42.7675819	40.0931111	42.196762	39.715891	39.47439024	40.20687589	37.75195122	39.9553958	42.03010652	39.4654088
CaO	0.21969024	0.22373983	0.20551667	0.1943803	0.22778942	0.22778942	0.2723349	0.24196298	0.197417493	0.238925787	0.243987774	0.196405096	0.228801813	0.255124145
Na2O	0	0.00461789	0	0	0.01570083	0.00277073	0	0	0	0	0	0.007388624	0	0.029554498
NiO	0.00839206	0.00629404	0.01678412	0.00734305	0.00419603	0.00314702	0	0.00104901	0.003147022	0	0.010490073	0.015735109	0.003147022	0.003147022
Totale	100.454141	100.564407	99.5299589	99.9950031	99.5411069	100.619914	100.22263	100.298576	99.0921803	100.539969	96.09064678	99.89922953	101.4819145	99.63585024
Fo	76.5374774	76.845112	76.6574129	78.021846	78.5239673	77.3077355	78.8023131	77.3692768	77.3614519	77.40255251	76.64855586	77.55116061	78.57904892	77.25341005
Fa	23.1132308	22.8372911	22.9227757	21.741389	21.2297655	22.3344985	20.8991943	22.3030216	22.3428281	22.27898784	22.99855953	22.11148917	21.15033488	22.47528327

Data set	B21_Ol to Opq	B21_Ol to Opq	B21_Ol to Opq	B21_Ol to Opq	B21_Ol to Opq	B21_Ol to Opq	B21_Ol to Opq	B21_Ol to Pl	B21_Ol to Pl	B21_Ol to Pl	B21_Ol to Pl	B21_Ol to Pl	B21_Ol to Pl	B21_Ol to Pl
SiO2	39.1749106	40.9824198	39.0568526	38.7749382	39.2512413	39.1240236	39.1148639	39.3652283	38.56630116	39.30619932	38.63550759	38.75458336	38.56223019	38.75356562
TiO2	0.01033691	0.01447167	0.01757274	0.03204441	0.02067382	0.02894334	0.01343798	0.01757274	0.022741197	0.042381322	0.022741197	0.019640125	0.04031394	0.029977032
Al2O3	0.03422481	0.06948674	0.06741251	0.05496712	0.05289289	0	0	0.03941039	0	0	0.026965003	0.012445386	0	0.068449623
Cr2O3	0	0.13333333	0.04155844	0.00779221	0.02424242	0	0.05800866	0.01385281	0.025974026	0.063203463	0	0.032034632	0.032034632	0.057142857
FeO	20.0530687	20.0399403	20.2358559	20.2005103	19.8965382	20.1277994	20.0480193	21.3204606	20.91348135	20.81148408	21.34065807	21.37499379	21.50728728	21.38812215
MnO	0.27148113	0.23016878	0.35508944	0.25082495	0.30590808	0.22623427	0.33246602	0.33443327	0.232136035	0.331482389	0.29902269	0.252792208	0.300989944	0.313777099
MgO	39.8745629	35.8089682	40.1250451	40.3545705	40.1440059	40.4553622	40.1799316	39.304741	39.48736341	37.17514372	39.2378792	39.57518186	39.56121074	39.22191221
CaO	0.25309935	0.28954566	0.21057866	0.22070263	0.22981421	0.25714894	0.22778942	0.24196298	0.173119956	0.197417493	0.251074555	0.255124145	0.232851402	0.199442288
Na2O	0	0	0.04156101	0	0	0	0	0	0	0	0.007388624	0.020318717	0	0.002770734
NiO	0	0.01049007	0.00629404	0	0	0.00209801	0	0	0.016784116	0.003147022	0.002098015	0	0.005245036	0.013637095
Totale	99.6716844	97.5788245	100.15782	99.8963503	99.9253168	100.22161	99.9745169	100.637662	99.43790125	97.9304588	99.82333494	100.2971142	100.2421632	100.0487967
Fo	77.7612645	75.8958027	77.6432822	77.8607376	77.9807561	77.9859455	77.8448999	76.3864686	76.89651773	75.80837076	76.36880598	76.53329781	76.37685128	76.30944735
Fa	21.9379311	23.8270252	21.9663237	21.8642997	21.6816187	21.766269	21.7891301	23.2442493	22.84663894	23.80756651	23.30052629	23.18894304	23.29299108	23.34369763

Data set	B21_Ol to Pl	B21_Ol to Pl	B21_Ol to Pl
SiO2	38.5459463	38.677235	39.2237622
TiO2	0.01964012	0.02480858	0.03721287
Al2O3	0.07674655	0.0331877	0.03629904

Cr_2O_3	0.03549784	0.01991342	0.02770563
FeO	21.2154337	21.2012955	21.00437
MnO	0.31180984	0.31476073	0.30000632
MgO	39.6250787	39.841631	39.3396688
CaO	0.18830592	0.2348762	0.16198358
Na_2O	0.02308945	0.00646505	0
NiO	0.01153908	0	0.00734305
Totale	100.053088	100.354173	100.138352
Fo	76.6388048	76.7454865	76.6957458
Fa	23.0185492	22.910026	22.9719406

Table 9.1 – Continue. Single mineral phase EMPA analyses. Sample: Poikilitic gabbro B21. Feldspars.

Data Set	B21_7_Pl c-r	B21_7_Pl c-r	B21_7_Pl c-r	B21_7_Pl c-r	B21_7_Pl c-r	B21_7_Pl c-r	B21_7_Pl c-r	B21_7_Pl c-r	B21_6_pl c-r	B21_6_pl c-r	B21_6_pl c-r	B21_5_pl c-r	B21_5_pl c-r	B21_5_pl c-r
SiO2	47.6371717	46.2101729	46.6021944	46.8561518	46.8652218	47.3781754	48.7013742	48.7719179	47.4305793 5	46.2907942 6	47.6573270 4	47.5686435	46.3885477 1	46.7835925 8
TiO2	0.05429081	0.01946274	0.031755	0.05121775	0.05121775	0.07989969	0.06965614	0.09014324	0.09526501 3	0.03994984 4	0.06760742 9	0.06351000 9	0.04404726 4	0.04916903 9
Al2O3	33.4807102	33.347222	33.3099695	33.8449572	33.6597293	33.0823151	33.0243668	32.3683083	33.4610491 8	34.2640481 3	33.4486316 7	33.6173028 4	33.3710222 4	34.0870986 2
Cr2O3	0	0	0.03892642	0.01536569	0	0.0051219	0	0	0	0	0	0.01843883 1	0.06965780 6	0.00512189 7
FeO	0.66696178	0.59491344	0.60520606	0.62887908	0.73798086	0.68754702	0.73489307	0.63814244	0.67107882 6	0.64123022 8	0.67004956 4	0.66696177 8	0.68754701 8	0.57638672 2
Mno	0.02111111	0	0	0	0	0.01333333	0.00222222	0.04	0.02111111 1	0	0	0.04333333 3	0.05111111 1	0.05
MgO	0.10598531	0.1422951	0.08930244	0.07261957	0.06575015	0.10107859	0.08930244	0.05495535	0.06084342 1	0.06280611 2	0.08537705 8	0.05004862	0.10500396 8	0.05299265 7
CaO	17.0040859	17.1122119	17.392127	17.6033265	17.4557901	16.7181076	16.8676651	16.1734352	16.6847603 1	17.8943574 3	16.9000019 3	16.7221496 9	17.7377262 3	17.5325898 7
Na2O	1.89060439	1.60982156	1.75853247	1.76789189	1.7023759	2.10275142	2.27122112	2.50312694	2.22442397 8	1.61294137	1.98731847 7	2.09547186 4	1.76789189 5	1.44759148 1
K2O	0.05491603	0.04541133	0.06336465	0.06442072	0.07286934	0.06653288	0.08659835	0.0982152	0.09715912 3	0.05174779 4	0.07181326 5	0.0654768	0.09399089 1	0.08871050 4
SrO														
BaO														
Totale	100.915837	99.081511	99.891378	100.90483	100.610935	100.234863	101.847299	100.738245	100.746270 3	100.857875 2	100.888126 4	100.911337 3	100.316546 1	100.673253 4
Ab %	16.6967279	14.5082339	15.4106888	15.3224953	14.93784	18.4695516	19.4966654	21.756488	19.3287690 4	13.9825112 7	17.4732077 8	18.4148970 4	15.1990288 3	12.9312999 1
An %	82.984161	85.2224805	84.223943	84.3101281	84.6414437	81.1459303	80.0142065	77.6818219	80.1157331 9	85.7223198 7	82.1113391 7	81.2064973 8	84.2692817 6	86.5472853 3
Or %	0.3191111	0.2692856	0.36536822	0.3673766	0.42071626	0.38451814	0.48912813	0.56169005	0.55549777	0.29516886 2	0.41545304 6	0.37860558 3	0.53168940 3	0.52141475 3

Data Set	B21_5_pl c-r	B21_5_pl c-r	B21_5_pl c-r	B21_5_pl c-r	B21_5_pl c-r	B21_5_pl c-r	B21_4_pl c-r	B21_4_pl c-r	B21_4_pl c-r	B21_3_pl c-r	B21_3_pl c-r	B21_3_pl c-r	B21_3_pl c-r	B21_3_pl c-r
SiO2	47.3146861	46.5376973	48.9250986	49.4541766	47.3298026	47.9022146	46.1990874	46.7563829	46.3028874 7	48.9744792 2	49.1478152 4	47.8346941 3	48.7527703 6	48.1722962 6
TiO2	0.04712033	0.05941259	0.0819484	0.07477791	0.04302291	0.05736388	0.02765758	0.03585242	0.04507161 9	0.05941258 9	0.06760742 9	0.05838823 4	0.06351000 9	0.06248565 4

Al2O3	33.6742164	33.536589	31.7205283	32.2182634	32.7429032	32.9208875	34.2661177	34.0250111	33.39792684	32.39107377	32.25344637	32.54318826	32.77808615	32.57733642
Cr2O3	0	0.03585328	0	0	0	0	0	0	0	0.10141357	0	0	0	0.023560728
FeO	0.65872768	0.56094779	0.67416661	0.65152285	0.68445923	0.60726458	0.64225949	0.59388418	0.665932516	0.6474058	0.6988689	0.65769842	0.651522848	0.64225949
Mno	0.00333333	0.00777778	0.02888889	0	0.01666667	0.04222222	0.03444444	0.01	0.016666667	0	0.03666666 7	0.01555555 6	0	0.061111111
MgO	0.08733975	0.06084342	0.09617186	0.10402262	0.10107859	0.10009724	0.0647688	0.07163822	0.08047033	0.116780114	0.10991069 5	0.09715320 4	0.06967553	0.060843421
CaO	17.2557063	17.2152854	15.3923002	15.3902792	16.398782	16.7019392	17.5113689	17.6690106	17.70336841	15.82985708	15.75608883	16.30278227	16.03701448	16.30682437
Na2O	1.87708522	1.67741743	2.84006633	2.7506318	1.99147822	2.03827536	1.58070334	1.59838226	1.884364773	2.690315489	2.69967491 7	2.43865087 8	2.526005537	2.321138064
K2O	0.07075719	0.08976658	0.13412183	0.11722459	0.08659835	0.08448619	0.05069172	0.05914034	0.079205807	0.11511244	0.11300028 5	0.08237403 9	0.10243951	0.105607743
SrO														
BaO														
Totale	100.988972	99.7815906	99.893291	100.760899	99.3947918	100.454751	100.377099	100.819302	100.1758944	100.9258501	100.8830793	100.030485	100.9810244	100.3334633
Ab %	16.3806635	14.9108332	24.838549	24.2721984	17.9243996	18.0006166	13.9998648	14.0194237	16.07906291	23.36632766	23.51459496	21.20238615	22.05065038	20.35767486
An %	83.2130521	84.5641326	74.389643	75.0471773	81.5627499	81.5084503	85.704727	85.6392691	83.47623939	75.97583031	75.83778889	78.32637881	77.36095769	79.03287937
Or %	0.40628442	0.52503415	0.77180808	0.68062437	0.51285049	0.49093317	0.29540822	0.34130716	0.446977702	0.657842022	0.647616152	0.47123504	0.588391924	0.609445766

Data Set	B21_3_pl c-r	B21_3_pl c-r	B21_3_pl c-r	B21_3_pl c-r	B21_2_pl c-r	B21_2_pl c-r	B21_2_pl c-r	B21_2_pl c-r	B21_2_pl c-r	B21_2_pl c-r	B21_2_pl c-r	B21_1_pl c-r	B21_1_pl c-r	B21_1_pl c-r
SiO2	47.8770204	48.0584185	47.0788685	47.3449191	48.3547022	48.4786576	48.4413702	48.2438478	47.85686502	47.01134805	47.1836763	47.44670363	48.97750252	47.71073872
TiO2	0.07989969	0.05531517	0.04916904	0.05531517	0.06658307	0.0614613	0.06248565	0.0819484	0.043022909	0.053266459	0.036876779	0.058388234	0.071704849	0.071704849
Al2O3	33.0512714	32.8619043	33.8273657	33.1599246	32.7698078	32.0816708	32.4428134	31.7991725	33.07714118	33.03057552	33.13095038	33.43724895	31.81469437	32.40970004
Cr2O3	0.05941401	0.03073138	0	0	0.02356073	0	0.01843883	0	0	0	0.10141357	0	0.038926421	0.003073138
FeO	0.62990835	0.66181547	0.73798086	0.61858646	0.67622514	0.65049359	0.68240071	0.64123023	0.6988689	0.670049564	0.728717498	0.60108901	0.764741668	0.69372259
Mno	0.02111111	0	0.02111111	0.00222222	0.02333333	0.04555556	0.00333333	0	0.045555556	0	0.03222222 2	0.04555556	0	0.037777778

MgO	0.08243302	0.09519051	0.05691804	0.07850764	0.10009724	0.08243302	0.08243302	0.06967553	0.09519051 3	0.08733974 9	0.09420916 7	0.06673149 4	0.11874280 5	0.08733974 9
CaO	16.8646336	16.6534341	16.9929701	17.0980646	16.0097303	15.6004682	16.2957086	15.9996251	16.3745294 7	17.2304432 2	17.0263173 9	16.8201705 1	15.1730165 4	15.7853940 3
Na2O	2.08091275	2.11315078	1.95716032	2.01019708	2.5249656	2.50104706	2.55408382	2.49272757	2.15058849 3	2.15474823 9	2.00083765	1.80012992 4	2.35025628 4	2.45113011 5
K2O	0.09504697	0.08976658	0.06970111	0.08765443	0.11300028	0.11828067	0.09927128	0.11194421	0.10243951	0.09293481 4	0.09610304 6	0.06336464 6	0.11405636 2	0.09821520 1
SrO														
BaO														
Totale	100.841651	100.619727	100.791245	100.455391	100.662006	99.6200678	100.682339	99.4401713	100.444201 5	100.330705 6	100.431324	100.339382	99.4236418 2	99.3487962 1
Ab %	18.153529	18.5772968	17.1781017	17.4552799	22.0592274	22.3313784	21.9717141	21.8511111	19.0882384 8	18.3578944 8	17.4398044 5	16.1640078 6	21.7416655 6	21.8095959 4
An %	81.3008921	80.9034505	82.4193662	82.0439088	77.2912018	76.973726	77.4663788	77.5032162	80.3135040 5	81.1211305 4	82.0090338 7	83.4616193 2	77.5640951 2	77.6153984 7
Or %	0.5455789	0.51925277	0.40253214	0.50081132	0.64957077	0.69489559	0.56190709	0.64567272	0.59825747 3	0.52097498 5	0.55116168 1	0.37437282 4	0.69423932	0.57500558 9

Data Set	B21_1_pl c-r	B21_1_pl c-r	B21_Ol to Pl	B21_Ol to Pl	B21_Ol to Pl	B21_Ol to Pl	B21_Ol to Pl	B21_Ol to Pl	B21_Ol to Pl	B21_Ol to Pl	B21_Ol to Pl	B21_Ol to Pl
SiO2	48.116869	47.0687908	46.9524922	46.2889246	46.5260584	46.9759002	46.791689	47.7900935	48.5544174 7	49.2291801 7	49.1518318	48.824119
TiO2	0.0409742	0.05736388	0.07545943	0.02894334	0.03928025	0.0330781	0.06305514	0.0444487	0.06925728 2	0.05168453 8	0.10336907 7	0.07029097 2
Al2O3	32.7046159	33.4558752	33.8327817	34.0287965	34.2268856	33.4915707	33.5973565	32.6743237	32.8361137 1	32.353855	32.3673375	31.8747076 4
Cr2O3	0.02868263	0	0.06060606	0.02770563	0	0	0.00865801	0.02337662	0.03030303	0	0	0.04761904 8
FeO	0.64637654	0.6690203	0.69782296	0.65843787	0.59683555	0.65035888	0.6766156	0.5756282	0.61501328 6	0.59481580 6	0.72811917 8	0.66449711 4
Mno	0.01	0	0.0432796	0.04032872	0.02852519	0	0	0	0	0.01868891 8	0	0.00983627 3
MgO	0.07850764	0.06967553	0.06087415	0.07484526	0.09380606	0.11077099	0.0838267	0.06985558	0.12374417	0.08582257	0.13771528 6	0.12574004 4
CaO	16.3896873	17.3244219	17.213793	17.9265208	17.7736488	17.0072639	16.9728424	16.5020776	15.8257961 7	16.1092674 4	15.5524488 7	15.1819114 3
Na2O	2.28474029	1.89580407	1.72801455	1.48326637	1.57377702	1.84992686	1.80097722	2.17317918	2.4881193	2.28862643 8	2.59987224 5	2.76149840 6
K2O	0.08026188	0.05914034	0.04930334	0.03986228	0.0430093	0.07343051	0.06084242	0.05664639	0.10699874 2	0.10385172 1	0.10909675 7	0.12902789 5

SrO												
BaO												
Totale	100.380715	100.600092	100.714427	100.597631	100.901826	100.1923	100.055863	99.9096295	100.6497632	100.8357926	100.7497907	99.68924782
Ab %	20.051257	16.4735064	15.3290565	12.9932168	13.7762981	16.3761589	16.0511898	19.1815875	22.01122849	20.32718075	23.07726649	24.57739785
An %	79.4852681	83.1883598	84.3831662	86.7770246	85.9759804	83.1961343	83.5920162	80.4894295	77.36594964	79.06590401	76.28556207	74.66701108
Or %	0.4634749	0.33813373	0.28777727	0.22975858	0.24772155	0.42770678	0.35679405	0.32898294	0.622821877	0.606915233	0.637171441	0.755591075

Table 9.1 – Continue. Single mineral phase EMPA analyses. Sample: Poikilitic gabbro B21. Opaque minerals.

Data set	B21_Opq in Ol_r-r	B21_Opq in Ol_r-r	B21_Opq in Ol_r-r	B21_Opq in Ol_r-r	B21_Opq in Ol_r-r	B21_Opq in Ol_r-r	B21_Opq in Ol_r-r	B21_Opq in Ol_r-r	B21_Opq in Ol_r-r	B21_Opq con Ml_c-r	B21_Opq con Ml_c-r	B21_Opq con Ml_c-r	B21_Opq con Ml_c-r
SiO2	0.04681611	0.0732774	0.07531288	0.04376289	0.05801127	0.26766605	0.0630999 8	0.0834548 1	0.0722596 55	0.0936322 3	0.04681611 5	0.01526612 4	0.01933709 1	0.03358547 4
TiO2	4.65574322	4.65781061	4.72189943	4.78081981	4.71052884	4.73947218	4.7187983 6	4.6960571 6	4.7094951 45	4.6578106 06	49.6750436 1	49.6502350 3	49.9613759 5	49.9427695 2
Al2 O3	10.7165144	10.5070171	10.6874752	10.6314709	10.5775409	10.252923 8	10.649101 9	10.708217 5	10.708217 49	10.753850 57	0.57352486 9	0.53204024 9	0.56626506 1	0.59737852 5
Cr2 O3	15.8692641	15.9350649	15.7852814	16.0909091	16.0060606	16.231168 8	15.907359 3	15.638095 2	15.903896 1	15.817316 02	0.76450216 5	0.86580086 6	0.87359307 4	0.73246753 2
FeO	55.3289785	56.0793149	55.6420395	55.5673088	55.8480538	55.455212 8	55.705661 5	55.530953 3	55.489548 5	55.172448 05	40.6858050 5	40.6777260 6	40.7443777 4	40.862533
Mno	0.32361337	0.32853151	0.31672798	0.32164612	0.27246475	0.2783665 2	0.3049244 5	0.2400050 5	0.2803337 71	0.3206624 89	0.34525317 1	0.35508944 4	0.29508818	0.34525317 1
Mg O	6.60235023	6.63628009	6.56642451	6.81091904	6.80293554	6.0245447 9	6.5275049 7	6.5295008 4	6.5195214 74	6.6292945 28	7.69908283 6	7.55737580 3	7.63621281 4	7.67712822 5
CaO	0.06074384	0	0.00202479	0	0.00506199	0.0192355 5	0	0.0344215 1	0.0425206 91	0	0.02024794 8	0.02733473	0.00809917 9	0.06074384 4
V	0	0	0	0	0	0	0	0	0	0	0	0	0	0
Ba	0	0	0	0	0	0	0	0	0	0	0	0	0	0
Ni	0	0	0	0	0	0	0	0	0	0	0	0	0	0
Zn	0	0	0	0	0	0	0	0	0	0	0	0	0	0
Tota l	93.6040238	94.2172966	93.7971856	94.2468367	94.2806577	93.268590 5	93.876450 5	93.460705 5	93.725792 83	93.445014 5	99.8102757 6	99.6808683	100.104349 1	100.251859 3

Data set	B21_Opq con Ml_c-r	B21_Opq con Ml_c-r	B21_Opq con Ml_c-r	B21_Opq con Ml_c-r	B21_Opq con Ml_c-r	B21_Opq con Ml_c-r
SiO2	0	0.0122129	0.01526612	0	0	0.0142483 8
TiO2	49.9438032	49.9148599	50.048206	49.9882519	49.877647	49.680212 1
Al2 O3	0.54655987	0.48951851	0.55589391	0.58285891	0.59115583	0.5755991
Cr2 O3	0.81298701	0.78874459	0.73506494	0.75411255	0.84242424	0.8138528 1

FeO	40.9998759	40.9473624	40.5424029	40.9362538	40.8988885	40.8726317
MnO	0.28623554	0.35312219	0.38558189	0.34426954	0.28721916	0.29508818
MgO	7.68311585	7.46556561	7.80686002	7.79488477	7.68211791	7.60827058
CaO	0.04454549	0.04150829	0.04150829	0.03138432	0.04454549	0.05568186
V	0	0	0	0	0	0
Ba	0	0	0	0	0	0
Ni	0	0	0	0	0	0
Zn	0	0	0	0	0	0
Total	100.317123	100.012894	100.130784	100.432016	100.223998	99.9155847

Table 9.1 – Continue. Single mineral phase EMPA analyses. Sample: Poikilitic gabbro B21. Glass.

Data set	B21_1_Glass	B21_1_Glass	B21_1_Glass	B21_2_Glass	B21_2_Glass	B21_2_Glass	B21_3_Glass	B21_3_Glass	B21_4_Glass
SiO2	54.9710395	56.0183957	53.4647066	54.0530863	53.849883	53.7053155	54.4665696	54.0854371	54.56362194
TiO2	3.24819984	3.10069604	3.34895947	3.33337809	3.18483553	3.3635021	3.27728509	3.16821538	3.319874218
Al2O3	16.005129	16.3857882	16.1128627	16.0092331	16.1313313	16.4145171	16.122097	16.1241491	16.2257266
Cr2O3	0	0.007	0	0.044	0.011	0.059	0	0.078	0
FeOtot	8.60965153	7.36853731	9.01581567	8.50065559	8.64358423	8.97776992	8.33818993	8.21582656	8.09037839
MnO	0.14282678	0.0753808	0.13489196	0.1676231	0.16068013	0.12794899	0.13885937	0.07835636	0.09025859
MgO	3.76448714	3.2972063	3.80384773	3.6272297	3.7503577	3.64337764	3.52529587	3.66659029	3.453639411
CaO	7.3161925	6.54898532	7.65190865	7.26880914	7.12867537	7.37668189	7.21739315	7.10952039	7.022818923
Na2O	3.41558613	3.47974867	4.17912041	4.18767542	4.32134739	4.49565563	4.64429886	4.36946929	4.273225478
K2O	2.03677136	2.25834046	1.99516214	1.8609724	1.96187476	1.8474494	1.90466208	1.94002992	1.994121905
P2O5	0.76508745	0.77198013	0.80184841	0.6938631	0.85813863	0.73981429	0.81908011	0.81793133	0.844353271
F									
Cl									
Total	100.274971	99.3120589	100.509124	99.7465259	100.001708	100.751033	100.453731	99.6535257	99.87801873

Data set	B21_4_Glass	B21_4_Glass	B21_5_glass	B21_5_Glass	B21_5_Glass	B21_6_glass	B21_6_glass	B21_6_glass	B21_7_glass	B21_7_glass
SiO2	53.638592	53.8266309	53.6547674	54.9134147	54.1905771	53.9388476	53.6780195	53.6982388	53.25745949	53.58905491
TiO2	3.23054093	3.25754867	3.3458432	3.29806028	3.34792072	3.29806028	3.18795181	3.23365721	3.246122319	3.298060276
Al2O3	15.8891869	16.1446698	16.0913159	16.2565077	16.0851597	16.1087585	16.0369361	16.1036284	15.7670887	15.75682834
Cr2O3	0.074	0.022	0.015	0	0.067	0.029	0	0	0.041	0.029
FeOtot	8.59628411	8.67031909	8.98496776	8.40811186	8.65283861	8.29294633	8.56235141	8.38240527	8.525333914	8.927385
MnO	0.11505491	0.11505491	0.1676231	0.0753808	0.1130712	0.11703861	0.10712009	0.12001417	0.124973433	0.249946865
MgO	3.61814649	3.57474892	4.14699133	3.75843167	3.616128	3.65750708	3.65447934	3.739256	3.557591736	3.307298758
CaO	7.20327896	7.14984666	7.49766069	7.26679282	7.03290049	6.99459054	7.2627602	7.28292333	7.197230016	7.727520392
Na2O	4.59938508	4.28284986	3.82943454	3.90215209	3.92995586	4.6336051	4.37909368	4.42186871	4.396203689	4.722363291
K2O	1.92546669	1.90570231	1.94002992	1.98892075	1.98580006	1.91402415	1.85681148	1.9327483	1.957713837	1.943150609
P2O5	0.78346793	0.89719715	0.84665083	0.90983373	0.76049233	0.70879724	0.80069963	0.75015331	0.731772835	0.869626431
F										
Cl										
Total	99.6734041	99.8465682	100.520285	100.777606	99.7818441	99.6931755	99.5262232	99.6648934	98.80248997	100.4202349

Table 9.1 – Continue. Single mineral phase EMPA analyses. Sample: Poikilitic gabbro B32. Clinopyroxenes.

Data Set	89 / 1 .	89 / 4 .	89 / 5 .	89 / 6 .	89 / 7 .	89 / 8 .	89 / 9 .	89 / 10 .	89 / 11 .	89 / 12 .	89 / 13 .	89 / 14 .	89 / 15 .	89 / 16 .
SiO2	48.264361	50.498304	48.922839	48.807835	49.352326	49.205772	50.011823	49.805221	50.5552975	51.5771101	51.5659149	49.9884154	50.1726266	50.4331685
TiO2	2.4033310	1.5019526	2.1469757	2.1242345	1.9836525	1.8451380	1.7800155	1.6477030	1.48437994	0.98200623	1.22905832	1.50402006	1.52986233	1.62806296
Al2O3	5.5164173	3.1787589	4.6670197	4.7012445	4.4958956	4.1422392	4.0094885	3.8207334	3.24409727	2.29513659	2.54404431	3.15801668	3.15594245	3.14764552
FeO	8.9060791	8.4122507	8.5697910	8.5485836	8.5344454	8.4607246	8.4778925	8.481932	8.14160445	7.98911347	8.09212062	7.89216556	8.21936475	8.32641140
Mno	0.2144307	0.1790201	0.1603312	0.2508249	0.1937745	0.2104962	0.2114798	0.2193488	0.19082369	0.17902016	0.21836525	0.18492192	0.10623174	0.20557809
MgO	12.829476	15.064854	13.326448	13.106902	13.058003	13.492106	14.260517	13.758555	14.207627	14.7834365	14.7435191	16.2623789	14.5279647	14.5429337
CaO	21.579250	21.660242	21.397019	21.771606	21.868796	21.789829	21.565077	21.525593	22.1178460	21.6845399	21.2330106	19.8672866	21.5691266	21.65923
Na2O	0.5365988	0	0.0840456	0.3999093	0.4460882	0	0.3906735	0.4008328	0	0.38236131	0.42761664	0.50704435	0.25767827	0.37127838
K2O	0	0	0	0	0	0.0073430	0.0041960	0.0073430	0.01049007	0	0	0	0	0
Cr2O3	0.0484848	0.0424242	0.0398268	0.0129870	0.0813852	0.0060606	0.0129870	0.0164502	0	0.05021645	0.06320346	0.03982684	0.09870129	0.01471861
Totale	100.24994	100.49538	99.274471	99.711140	99.932983	99.153648	100.71116	99.667264	99.9521659	99.8727243	100.053649	99.3642496	99.5387975	100.314308
Wo	45.571239	44.036004	45.739088	45.927055	46.033335	46.197504	44.252879	44.830890	45.8484738	44.0904340	43.4771366	40.0772658	44.3214800	44.1437391
En	37.697652	42.614798	39.636889	38.470612	38.245051	39.801124	40.717087	39.869975	40.9783529	41.8235084	42.0050407	45.6451359	41.5372145	41.2409849
Fs	14.680450	13.349197	14.298906	14.075720	14.022363	14.001372	13.579280	13.788447	13.1731731	12.6791779	12.9333208	12.4266499	13.1831227	13.2459257
N° Mg	71.972161	76.146812	73.489023	73.212744	73.171882	73.976352	74.990443	74.303293	75.6734960	76.7365999	76.4584883	78.6012265	75.9081844	75.6897104

Data Set	89 / 17 .	89 / 19 .	89 / 20 .	91 / 1 .	91 / 3 .	91 / 4 .	91 / 6 .	91 / 7 .	91 / 9 .	91 / 10 .	91 / 11 .	91 / 12 .	92 / 1 .	92 / 2 .	92 / 4 .
SiO2	48.207367	50.239797	49.909031	50.443345	51.062132	50.762916	50.393476	50.744597	50.1889105	50.1492186	50.2581169	50.8433183	49.9375283	49.7115897	51.2412553
TiO2	1.6725116	1.5722436	1.5608730	1.5877490	1.5143569	1.5381318	1.5029863	1.5277949	1.61979343	1.68491595	1.62806296	1.62909665	1.79241979	1.77794812	1.68388226
Al2O3	3.0605278	2.9868926	3.1839445	2.9422966	2.9298512	2.9692616	2.9308883	3.0335628	3.28869323	3.23165188	3.30736131	3.232689	3.62679288	3.72428174	4.07586389

FeO	8.42840868	8.61220575	8.25067085	8.42739881	8.56878117	8.53242571	8.60614651	8.38902359	8.57787003	8.54454419	8.46274439	8.65563033	7.84066199	7.87701745	7.90630380
Mno	0.1731184	0.14754409	0.16918389	0.16721664	0.18197104	0.19869271	0.15344585	0.16328213	0.21639799	0.18688918	0.17705290	0.22820152	0.20164359	0.11606801	0.11705164
MgO	15.695550	14.507008	14.380270	14.376278	14.162719	14.374282	14.103841	14.448129	14.3443443	14.6507109	14.2844681	14.5279647	14.1587281	14.0958580	11.6618900
CaO	20.602287	21.491172	21.224911	21.329188	21.287680	21.723011	20.925241	21.139870	21.0943122	21.0862130	21.2674322	21.1520189	21.7716061	21.8930938	21.3555107
Na2O	0.2207351	0	0.3306409	0.4386995	0.3417238	0	0.2872327	0.3666604	0.39898572	0.43869958	0.40360361	0.35095966	0.10713505	0.37497269	0.07111551
K2O	0.0010490	0.0167841	0	0.0010490	0.0073430	0.0199311	0.0199311	0.0041960	0	0	0.00209801	0.01468610	0.01468610	0.00839205	0.01993113
Cr2O3	0.0337662	0.0441558	0.0380952	0.0545454	0.0164502	0.0545454	0.0709956	0.0796536	0	0	0.06666666	0.09610389	0.02077922	0	0.01904761
Totale	98.061556	99.573647	99.009526	99.713222	100.05656	100.11865	98.923191	99.817117	99.7293075	99.9728434	99.7909405	100.634565	99.4512019	99.5792216	98.1328044
Wo	41.688808	44.404723	43.969468	43.793375	44.073546	44.897759	43.788976	43.628307	43.5199727	43.0907326	43.8696229	43.3821727	45.5607516	45.2964120	48.6660444
En	44.190763	41.705930	41.449879	41.070639	40.798784	41.337263	41.066020	41.488580	41.1770134	41.6576614	40.9981082	41.4586492	41.2264132	40.5787889	36.9773621
Fs	13.312143	13.889346	13.341139	13.505976	13.847362	13.764977	14.057282	13.513747	13.8134147	13.6292680	13.6256872	13.8565948	12.8071203	12.7208701	14.0633223
N° Mg	76.849617	75.017038	75.650863	75.253180	74.659947	75.019205	74.498475	75.430589	74.8803287	75.3481189	75.0554001	74.9497717	76.2978293	76.1332992	72.4468383

Table 9.1 – Continue. Single mineral phase EMPA analyses. Sample: Poikilitic gabbro B32. Olivines.

Data Set	90 / 1 .	90 / 2 .	90 / 3 .	90 / 4 .	90 / 5 .	90 / 6 .	90 / 7 .	90 / 8 .	90 / 9 .	90 / 10 .	90 / 11 .	93 / 5 .	93 / 7 .	93 / 8 .
SiO2	38.3871786	38.763743	38.4533318	38.2925287	38.6039576	38.6711285	38.6405963	38.5266092	38.6039576	38.39023186	38.71692692	38.30779478	37.51090309	37.95972715
TiO2	0.01757274	0.0444487	0.02997703	0.02170751	0.00206738	0.03101072	0.01033691	0.04341501	0.027909651	0.015505362	0.028943342	0.029977032	0.011370598	0.039280249
Al2O3	0	0.02177943	0	0.01659385	0	0	0.00622269	0.01970519	0	0	0.006222693	0.035261927	0	0.049781544
Cr2O3	0.02943723	0.00606061	0	0	0	0	0.02510823	0	0	0	0	0	0.015584416	0
FeO	23.7370891	24.2359669	24.0420711	24.1642659	23.9117974	24.4662182	23.8693826	23.7158818	23.87746164	24.10165368	23.70578305	23.99763665	24.15416712	24.25717428
Mno	0.36295846	0.30197357	0.35804033	0.37082748	0.32164612	0.27443201	0.34820405	0.30197357	0.250824953	0.362958462	0.318695235	0.279350144	0.294104553	0.309842589
MgO	36.1632358	36.2191202	36.2111367	36.1782048	36.1821966	36.300951	36.4666086	36.0853967	35.92672472	35.97362775	36.00955348	37.93756748	37.61722975	37.48350621
CaO	0.31586799	0.24500017	0.28144648	0.28448367	0.28853326	0.30574402	0.30574402	0.29055805	0.247024966	0.274359696	0.226777018	0.33510354	0.263223324	0.245000171
Na2O	0	0.00923578	0.00923578	0	0	0	0	0	0	0	0	0	0	0
NiO	0	0.00524504	0.00629404	0	0.00944107	0.00734305	0	0.00314702	0.001049007	0	0	0.004196029	0.002098015	0
Totale	99.01334	99.8525735	99.3915333	99.3286118	99.3196393	100.056828	99.6722034	98.9866866	98.93495253	99.1183368	99.01290173	100.9268876	99.86868087	100.3443122
Fo	72.7842967	72.4576779	72.5649547	72.4367139	72.6856812	72.3386819	72.8535218	72.8099099	72.63204143	72.3809663	72.76259747	73.58162252	73.27888413	73.11381005
Fa	26.8006494	27.1990863	27.0273892	27.1414335	26.9471976	27.3506014	26.7512334	26.8439076	27.07984842	27.20410425	26.87151869	26.11053683	26.39560089	26.54280796

Data Set	93 / 9 .	93 / 10 .	93 / 11 .	93 / 12 .	93 / 13 .	93 / 14 .	93 / 15 .	93 / 17 .	93 / 18 .	93 / 19 .	93 / 20 .	93 / 21 .	93 / 22 .	93 / 23 .
SiO2	37.6208192	37.7409127	37.7215756	37.2137225	37.7022385	35.8163633	37.7093627	37.554666	38.00857875	36.90331134	37.65847563	37.77246269	37.7826401	37.58316275
TiO2	0.0113706	0.02687596	0.04238132	0.02790965	0.02687596	0.03824656	0.03928025	0.01860643	0.042381322	0.046516085	0.036179177	0.023774888	0.034111795	0.015505362
Al2O3	0.02281654	0.01244539	0.03007635	0.02177943	0.27276138	0.02489077	0	0.0134825	0.015556732	0	0	0.002074231	0.03215058	0.035261927
Cr2O3	0.02164502	0	0	0	0	0	0.03896104	0.00779221	0.01991342	0.037229437	0.040692641	0.091774892	0	0.043290043
FeO	24.1814337	24.2056707	23.8299976	23.7421385	23.978449	24.002686	24.059239	24.0945846	23.80576058	23.8168692	24.18345347	24.53589951	24.12084128	23.99460703
Mno	0.35804033	0.32853151	0.32951513	0.33935141	0.36295846	0.32853151	0.34426954	0.37574562	0.408205316	0.362958462	0.416074334	0.335416898	0.258693972	0.331482389
MgO	37.6062524	37.6062524	37.3777249	37.4326114	37.6860874	37.6032586	37.6222194	37.6421782	37.72101518	37.83877173	37.25497867	37.50546082	38.20601249	37.90463556
CaO	0.23690099	0.24297538	0.31991758	0.34016553	0.24297538	0.31384319	0.25613654	0.25208695	0.270310106	0.275372093	0.226777018	0.272334901	0.288533259	0.30776881
Na2O	0.00461789	0	0	0	0.01385367	0.02031872	0	0	0	0	0	0	0	0
NiO	0	0	0.00104901	0	0	0	0.01049007	0.02202915	0.006294044	0.006294044	0.008392058	0	0.008392058	0
Totale	100.063897	100.163664	99.6522375	99.1176785	100.2862	98.1481387	100.079959	99.9811716	100.2980155	99.28732239	99.825023	100.5391988	100.7313755	100.2157139
Fo	73.199543	73.2040592	73.3859228	73.4775447	73.3995737	73.3651276	73.3168271	73.2733727	73.5194922	73.60800614	72.9662613	72.88248305	73.63693462	73.52489632

Fa	26.4044915	26.4325873	26.2464967	26.1439854	26.1987774	26.2706905	26.3019885	26.3110589	26.02846977	25.99082969	26.57073347	26.74718534	26.07977783	26.10977838	

Table 9.1 – Continue. Single mineral phase EMPA analyses. Sample: Poikilitic gabbro B32. Feldspars.

Data Set	82 / 1 .	82 / 2 .	82 / 3 .	82 / 4 .	82 / 5 .	82 / 6 .	82 / 7 .	82 / 8 .	82 / 9 .	82 / 10 .	82 / 11 .	82 / 12 .	82 / 13 .	82 / 14 .
SiO2	47.3494114	47.9590386	46.7794761	47.2099808	45.9632473	47.2791872	47.1285615	46.4537988	47.06546147	47.02169858	46.84461154	46.98404214	47.32396784	47.65066291
TiO2	0.07959419	0.06098776	0.07132466	0.05375192	0.04858347	0.09303217	0.05168454	0.06512252	0.049617157	0.054785611	0.056852992	0.065122518	0.046516085	0.043415012
Al2O3	33.4822367	33.431418	33.2395516	33.4604572	32.6743237	33.3453374	33.1223576	33.5174986	33.77781458	33.66269476	33.42830665	33.72388457	33.52994397	33.5517234
Cr2O3	0	0	0.03636364	0.02164502	0.05541126	0	0	0.004329	0.032034632	0.064069264	0	0	0	0.012987013
FeO	0.57259858	0.53725299	0.54634185	0.56350971	0.56148996	0.5715887	0.58875656	0.54634185	0.513016009	0.579667695	0.618042908	0.607944168	0.642279885	0.629151523
Mno	0.03049245	0	0	0	0	0.03639421	0.04032872	0	0	0	0	0	0.036394209	0.008852645
MgO	0.10478337	0.0648659	0.05987621	0.04490716	0.04889891	0.06686177	0.0459051	0.07983495	0.044907158	0.071851454	0.042911285	0.061872085	0.026944295	0.060874148
CaO	16.6498877	16.6225529	16.8746399	16.6033174	16.8179456	16.4585445	16.513214	17.0315615	17.0619334	16.89286303	17.02751189	16.88780105	16.68025958	16.68937116
Na2O	2.05957908	2.15193689	2.01524733	1.98015137	1.97738063	2.02448311	1.9367432	2.06604413	1.942284665	1.830531719	1.793588597	1.946902555	2.051266876	2.055884767
K2O	0.09336165	0.10175371	0.08496959	0.09231264	0.07552852	0.08811661	0.05454838	0.0723815	0.076577531	0.0576954	0.065038451	0.076577531	0.087067604	0.08496959
SrO														
BaO														
Totale	100.421945	100.929807	99.7077909	100.030033	98.2228093	99.9635457	99.4820995	99.8369128	100.5636466	100.2358575	99.87686431	100.3541466	100.4246403	100.7878922
Ab %	18.1913588	18.8691605	17.6836755	17.654873	17.4669765	18.1121918	17.4515268	17.926136	17.00610462	16.33893124	15.9489743	17.18437202	18.11101427	18.13853818
An %	81.2660568	80.5437756	81.8257333	81.8035759	82.0940376	81.3690956	82.2250618	81.6606388	82.55272593	83.32222486	83.6704928	82.37089134	81.38317353	81.36819814
Or %	0.54258437	0.58706392	0.49059126	0.54155115	0.43898589	0.51871253	0.32341141	0.41322519	0.44116945	0.338843907	0.380532907	0.444736646	0.505812203	0.49326368

Data Set	84 / 4 .	84 / 5 .	84 / 6 .	84 / 9 .	87 / 7 .	87 / 8 .	92 / 11 .	92 / 12 .	92 / 14 .	93 / 3 .
SiO2	47.4644162	47.5712791	45.8960763	46.6980567	50.9359329	46.0751989	47.4145468	50.1512541	47.29241785	46.87514379
TiO2	0.09406586	0.05892037	0.07649312	0.04548239	1.92163114	0.0558193	0.06822359	0.0899311	0.056852992	0.075459426
Al2O3	33.3920076	33.8856746	33.2499228	33.5413522	21.5232579	32.7655899	34.0516131	32.3248158	33.6989938	32.77388678
Cr2O3	0	0	0	0.02597403	0	0	0	0.00606061	0	0
FeO	0.63723051	0.59279606	0.58471707	0.45848281	6.397552	0.50291727	0.68570447	0.70994145	0.744277162	0.591786183
Mno	0	0	0.02852519	0.00196725	0.10918263	0.02360705	0.01475441	0.01475441	0.038361463	0
MgO	0.0758432	0.04490716	0.04690303	0.06386796	1.78730491	0.05388859	0.08781844	0.06287002	0.075843201	0.074845264
CaO	17.1975947	17.0912929	17.1732971	16.9333589	10.8771977	16.9313341	17.0801566	14.8447831	17.12166485	16.38058995
Na2O	1.81298374	1.43339315	1.98107494	1.78527639	4.34543478	1.90995943	1.39829719	2.57678279	1.824066673	2.181491383

K2O	0.10280271	0.08496959	0.07343051	0.0870676	0.71437396	0.07657753	0.10490073	0.16469414	0.113292786	0.071332495
SrO										
BaO										
Totale	100.776944	100.763233	99.1104401	99.6408864	98.6118678	98.394892	100.906015	100.945887	100.9657708	99.02453526
Ab %	15.9256847	13.1095554	17.1977837	15.9400442	40.1380538	16.8774901	12.8215669	23.6654346	16.05685406	19.33886674
An %	83.4801314	86.3791181	82.3827856	83.5484474	55.5202364	82.6772668	86.5455372	75.3393275	83.28694913	80.24505307
Or %	0.59418391	0.51132645	0.41943071	0.51150838	4.3417098	0.44524309	0.63289582	0.99523795	0.656196806	0.416080188

Table 9.1 – Continue. Single mineral phase EMPA analyses. Sample: Poikilitic gabbro B32. Opaque minerals.

Data set	B32_Opq c to big Ol r	B32_Opq c to big Ol r	B32_Opq r-r at big Ol r	B32_Opq r-r at big Ol r	B32_Opq r-r at big Ol r	B32_Opq r-r at big Ol r	B32_Opq 1_r-r	B32_Opq 1_r-r	B32_Opq 1_r-r	B32_Opq 1_r-r	B32_Opq 1_r-r	B32_Opq 1_r-r	B32_Opq 1_r-r	B32_Opq 1_r-r
SiO2	0.07225966	0.04070967	0.15367899	0.06513546	0.14350157	0.40913213	0.127217 7	0.089561 26	0.112969 32	0.081419 33	0.059029 014	0.103809 646	0.075312 88	0.081419 33
TiO2	6.60528402	6.42645551	13.8152771	14.0003078	13.9992741	13.6860658	17.59651 8	17.70195 44	17.61925 916	17.61925 916	17.71332 502	17.77741 385	17.82186 255	17.83633 422
Al2O3	9.7717022	9.98949645	6.02978949	6.44567281	5.98415641	5.50293482	4.524934 91	4.563308 18	4.657685 691	4.685687 809	4.575753 567	4.517675 099	4.603755 685	4.596495 877
Cr2O3	12.5125541	11.8805195	6.85627706	7.11428571	6.86406926	6.70995671	0.319480 52	0.283982 68	0.349783 55	0.254545 455	0.333333 333	0.351515 152	0.289177 489	0.317748 918
FeO	59.5775186	59.4805707	61.4801213	62.1930923	61.866903	59.6280123	69.54800 49	69.23696 37	68.80170 8	69.11880 845	68.65224 665	68.77343 153	68.95520 886	69.03599 878
Mno	0.24393956	0.35607307	0.32558063	0.31771161	0.34230229	0.2921373	0.283284 65	0.361974 83	0.339351 408	0.340335 035	0.319678 862	0.315744 353	0.303940 826	0.378696 498
MgO	6.24309296	6.16724976	6.70014804	6.33190934	7.26697618	4.53562301	5.622376 24	5.699217 38	5.736141 042	5.564495 903	5.591440 198	5.394846 638	5.566491 777	5.542541 293
CaO	0.00303719	0	0.00506199	0.01822315	0.07289261	0.12958687	0.026322 33	0.003037 19	0.005061 987	0.013161 166	0.041508 293	0.032396 717	0.014173 564	0.008099 179
BaO														
V2O3														
NiO														
ZnO														
Total	95.0293883	94.3410746	95.3659346	96.4863382	96.5400754	90.8934489	98.04813 92	97.93999 97	97.62196 016	97.67771 231	97.28631 494	97.26683 298	97.62992 363	97.79733 41

Data set	B32_Opq1_r-r	B32_Opq1_r-r	B32_Opq1_r-r	B32_Opq1_r-r	B32_Opq1_r-r	B32_Opq1_r-r	B32_Opq 1_r-r	B32_Opq 1_r-r	B32_Opq 1_r-r	B32_Opq 1_r-r	B32_Opq 1_r-r	B32_Opq 1_r-r
SiO2	0.09363223	0.10380965	0.07633062	0.0854903	0.1394306	0.30939345	0.099738 68	0.159785 44	0.088543 521	0.134341 895	0.084472 555	0.083454 813
TiO2	17.8363342	17.7019544	17.6037538	17.7887844	17.6978197	17.3267247	17.58204 63	17.79808 77	17.71435 871	17.35153 325	17.46523 924	17.51899 116
Al2O3	4.678428	4.53530606	4.29884373	4.53426895	4.60582992	5.34944173	4.589236 07	4.491747 21	4.780065 319	3.636126 928	4.566419 527	4.613089 724
Cr2O3	0.30562771	0.44415584	0.32034632	0.22770563	0.26147186	0.26753247	0.293506 49	0.275324 68	0.278787 879	0.345454 545	0.296969 697	0.243290 043
FeO	68.7007206	68.70577	69.1925293	68.8744189	69.314724	67.7564884	68.48763 72	69.00873 22	69.31169 439	67.13137 635	69.38844 482	69.01782 105
Mno	0.40525443	0.28820279	0.32558063	0.33049876	0.2921373	0.32361337	0.271481 13	0.241972 31	0.349187 68	0.364925 717	0.293120 926	0.352138 562

MgO	5.56748971	5.59842576	5.36890028	5.31700756	5.45372491	5.55651241	5.55052479	5.51260319	5.67826070	5.47268513	5.80499868	5.57148161
CaO	0.01619836	0	0.04657028	0	0	0.14679762	0.02733473	0	0.04859575	0.07997995	0.06175641	0.01619858
BaO												
V2O3												
NiO												
ZnO												
Total	97.6036853	97.3776245	97.2328549	97.1581746	97.7651383	97.0365041	96.90150 54	97.48825 27	98.24949 328	94.51642 38	97.96142 169	97.41646 517

Table 9.1 – Continue. Single mineral phase EMPA analyses. Sample: Porphyrogabbro. B20. Clinopyroxenes.

Data set	B20_Cpx-c_Opq_Pl	B20_Cpx-c_Opq_Pl	B20_Cpx-c_Opq_Pl	B20_Cpx-c_Opq_Pl	B20_Cpx-c_Opq_Pl	B20_Cpx-c_Opq_Pl	B20_Cpx-c_Opq_Pl	B20_Cpx-c_Opq_Pl	B20_Cpx-c_Opq_Pl	B20_Cpx-c_Opq_Pl	B20_Cpx-c_Opq_Pl	B20_Cpx-c_Opq_Pl	B20_Cpx-c_Opq_Pl	B20_Cpx-c_Opq_Pl
SiO2	51.376	51.517	51.363	50.696	51.021	51.346	51.084	51.041	51.362	51.418	51.139	50.81	50.688	47.871
TiO2	0.843	0.88	0.869	0.941	0.977	0.926	0.962	0.932	0.982	0.986	0.96	1.017	1.039	1.751
Al2O3	2.663	2.8	2.651	2.803	2.866	2.762	2.856	2.952	2.889	2.879	2.941	3.048	3.144	5.687
FeO	5.008	5.399	5.289	5.223	5.519	5.347	5.575	5.546	5.675	5.745	5.708	5.762	5.918	6.238
MnO	0.134	0.153	0.086	0.171	0.122	0.116	0.122	0.072	0.054	0.107	0.176	0.121	0.151	0.112
MgO	16.152	16.436	16.405	16.488	16.254	16.454	16.231	16.105	16.207	16.172	16.267	15.843	16.002	14.436
CaO	21.546	21.37	21.343	21.201	21.645	21.468	21.558	21.615	21.36	21.222	21.045	21.609	21.423	21.284
Na2O	0.269	0.294	0.224	0.233	0.264	0.279	0.223	0.262	0.248	0.266	0.255	0.273	0.278	0.33
K2O	0.001	0.003	0.013	0.004	0	0	0	0	0.003	0	0.015	0.013	0.013	0.012
Cr2O3	0.575	0.689	0.623	0.636	0.572	0.638	0.566	0.592	0.568	0.541	0.381	0.449	0.495	0.603
Total	97.992	98.852	98.243	97.76	98.668	98.698	98.611	98.525	98.78	98.795	98.506	98.496	98.656	97.721
Wo	44.502187	43.6254316	43.8231929	43.5868849	44.1317412	43.7760616	44.0887341	44.2690216	43.78058753	43.58661492	43.30633999	44.42235525	43.89017184	45.44326809
En	46.4185855	46.6855248	46.8679205	47.1648397	46.111009	46.6839389	46.1865302	45.8940423	46.22041785	46.21484089	46.57586356	45.31638228	45.61547038	42.88585548
Fs	8.07378844	8.60293988	8.47657611	8.3814249	8.78318869	8.51047169	8.89943386	8.86590137	9.079136583	9.209906283	9.168216538	9.24567263	9.463685534	10.39585045
N° Mg	85.1836361	84.4399009	84.6839765	84.9109117	83.9997868	84.5809175	83.844462	83.8095133	83.58189921	83.38304322	83.55302209	83.05475729	82.8180273	80.48889339

Data set	B20_Cpx-c_Opq_Pl	B20_Cpx in Pl smecolato_c-r	B20_Cpx in Pl smecolato_c-r	B20_Cpx in Pl smecolato_c-r	B20_Cpx in Pl smecolato_c-r	B20_Cpx in Pl smecolato_c-r	B20_Cpx in Pl smecolato_c-r	B20_Cpx in Pl smecolato_c-r	B20_Cpx in Pl smecolato_c-r	B20_Cpx in Pl smecolato_c-r	B20_Cpx in Pl smecolato_c-r	B20_Cpx in Pl smecolato_c-r	B20_Cpx in Pl smecolato_c-r	B20_Cpx in Pl smecolato_c-r
SiO2	47.844	50.967	50.466	50.637	50.545	50.683	50.465	50.315	50.818	50.871	50.986	50.627	50.694	50.846
TiO2	1.99	1.15	1.184	1.188	1.215	1.213	1.201	1.197	1.242	1.203	1.268	1.183	1.201	1.238
Al2O3	6.216	2.017	2.057	2.008	2.001	1.981	1.904	2.067	2.09	2.035	1.961	2.057	1.997	1.944

FeO	6.545	8.451	8.547	8.235	8.469	8.414	8.396	8.442	8.471	8.155	8.128	8.278	7.935	8.018
MnO	0.13	0.193	0.245	0.212	0.207	0.276	0.247	0.257	0.264	0.247	0.244	0.242	0.284	0.243
MgO	13.922	15.105	14.971	14.873	15.124	15.117	15.079	14.913	15.057	15.299	15.069	15.26	15.423	15.33
CaO	21.517	20.444	20.658	20.459	20.843	20.552	20.663	20.512	20.451	20.314	20.982	20.674	20.557	20.299
Na2O	0.475	0.336	0.349	0.295	0.293	0.277	0.381	0.321	0.323	0.364	0.328	0.396	0.387	0.411
K2O	0	0.006	0.008	0	0.001	0.006	0.008	0	0.004	0	0	0.005	0	0
Cr2O3	0.711	0	0	0.048	0	0.028	0.008	0.025	0	0.033	0.01	0.063	0	0.053
Total	98.639	98.669	98.485	97.907	98.698	98.519	98.344	98.024	98.72	98.488	98.966	98.722	98.478	98.329
Wo	45.9212865	42.0092522	42.339359	42.5211552	42.5131856	42.2406811	42.2670361	42.3520305	42.08217903	41.77683902	42.91957311	42.11904859	42.02986154	41.74062478
En	41.341369	43.1867683	42.6931023	43.010068	42.9221024	43.2308059	42.9172472	42.8432241	43.10950334	43.77781395	42.88879475	43.25730636	43.87508594	43.86088141
Fs	10.9028572	13.5545632	13.6731336	13.3592662	13.4832287	13.4982565	13.405382	13.6053564	13.60556869	13.09068705	12.9774855	13.16369494	12.66320102	12.86911555
N° Mg	79.1309816	76.1116582	75.7423334	76.3004719	76.0958257	76.2057473	76.1989413	75.8977882	76.01066489	76.98077703	76.77045	76.66880304	77.60243244	77.31514853
Dataset	B20_Cpx in Pl smecolato_c-r	B20_Cpx in Pl smecolato_c-r	B20_Cpx in Pl smecolato_c-r	B20_Cpx in Pl smecolato_c-r	B20_Cpx in Pl smecolato_c-r	B20_Cpx in Pl smecolato_c-r	B20_Cpx brught_dark_Ol	B20_Cpx brught_dark_Ol	B20_Cpx brught_dark_Ol	B20_Cpx brught_dark_Ol	B20_Cpx brught_dark_Ol	B20_Cpx brught_dark_Ol	B20_Cpx brught_dark_Ol	B20_Cpx brught_dark_Ol
SiO2	51.048	50.592	51.346	51.698	51.56	51.049	45.361	45.385	47.59	50.068	51.233	50.974	51.069	51.324
TiO2	1.215	1.202	1.188	0.994	0.97	1.206	2.64	2.624	2.168	1.503	1.177	1.175	1.105	1.068
Al2O3	1.965	1.951	2.011	1.795	1.762	2.167	7.473	7.504	5.389	3.617	2.377	2.235	2.039	2.059
FeO	7.452	7.451	7.007	6.544	6.026	5.866	6.745	6.686	6.25	5.887	5.496	5.603	5.575	5.481
MnO	0.204	0.129	0.134	0.162	0.124	0.121	0.159	0.149	0.097	0.094	0.186	0.092	0.099	0.101
MgO	15.511	15.506	15.592	16.109	16.294	15.892	13.035	13.01	13.91	15.043	15.92	15.846	15.928	15.831
CaO	20.324	20.642	21.038	21.012	21.481	20.97	21.523	21.435	20.96	21.029	21.608	20.989	21.145	21.423
Na2O	0.382	0.436	0.493	0.434	0.446	0.508	0.572	0.534	0.642	0.566	0.534	0.512	0.472	0.511

K2O	0.01	0.006	0.003	0	0	0	0.001	0.003	0.009	0.013	0	0.007	0	0
Cr2O3	0.03	0	0.03	0.117	0.061	0.16	0.544	0.549	0.628	0.456	0.439	0.518	0.427	0.481
Total	98.111	97.915	98.812	98.748	98.663	97.779	97.509	97.33	97.015	97.82	98.531	97.433	97.432	97.798
Wo	41.9797189	42.280261	42.8524144	42.604033	43.2534628	43.1658729	46.8301171	46.8810108	45.2167384	44.19797952	44.0842379	43.42222799	43.58639107	44.03214908
En	44.5780468	44.1912782	44.1899561	45.4467467	45.6504431	45.5167822	39.4624797	39.5914743	41.75283624	43.99153833	45.19212133	45.61323824	45.68307895	45.27399742
Fs	12.0143847	11.9123871	11.1404135	10.3567849	9.47095691	9.42502482	11.4552016	11.4140087	10.52413276	9.657754862	8.752131551	9.047723598	8.969876012	8.79321604
N° Mg	78.7703331	78.7671857	79.8656442	81.4406282	82.8180037	82.8454408	77.5025073	77.6219967	79.86851005	81.99835583	83.77559965	83.44755874	83.58757359	83.73650966

Data set	B20_Cpx brught_dark_Ol	B20_Cpx brught_dark_Ol	B20_Cpx brught_dark_Ol	B20_Cpx brught_dark_Ol	B20_Cpx brught_dark_Ol	B20_Cpx brught_dark_Ol	B20_Cpx brught_dark_Ol	B20_Cpx brught_dark_Ol	B20_Cpx brught_dark_Ol
SiO2	51.746	51.46	51.862	51.643	51.078	51.477	51.419	51.28	51.35
TiO2	1.056	1.106	1.129	1.103	1.11	1.135	1.224	1.163	1.218
Al2O3	1.996	2.161	2.229	2.153	2.336	1.955	2.21	2.155	2.348
FeO	5.437	5.56	5.584	5.485	5.523	5.438	5.589	5.64	5.657
MnO	0.168	0.159	0.084	0.089	0.159	0.134	0.137	0.117	0.117
MgO	16.142	16.099	15.839	16.016	16.023	15.962	15.766	15.953	15.74
CaO	21.54	21.232	21.431	21.249	21.274	21.215	20.612	21.071	21.095
Na2O	0.526	0.496	0.493	0.519	0.595	0.489	0.615	0.567	0.56
K2O	0.004	0.016	0.001	0	0	0.005	0.008	0.011	0.027
Cr2O3	0.529	0.491	0.49	0.547	0.518	0.457	0.393	0.323	0.487
Total	98.615	98.289	98.652	98.257	98.098	97.81	97.58	97.957	98.112
Wo	43.7843927	43.4463209	43.9880577	43.5840313	43.4553236	43.6936328	42.9200754	43.2702425	43.56264312
En	45.6543193	45.8365476	45.2346263	45.7081726	45.5395321	45.7418077	45.6785977	45.582427	45.22622289
Fs	8.62643414	8.88045542	8.94614856	8.78140241	8.80576768	8.74203757	9.0839095	9.0402748	9.118412141

N°									
Mg	84.107748	83.7702086	83.488334	83.8842524	83.7966343	83.954808	83.4121738	83.4496015	83.22113648

Table 9.1 – Continue. Single mineral phase EMPA analyses. Sample: Porphyrogabbro. B20. Olivines.

Data set	B20_Ol-c_Pl	B20_Ol-c_Pl	B20_Ol-c_Pl	B20_Ol-c_Pl	B20_Ol-c_Pl	B20_Ol-c_Pl	B20_Ol-c_Pl	B20_Ol-c_Pl	B20_Ol-c_Pl	B20_Ol-c_Pl	B20_Ol-c_Pl	B20_Ol-c_Pl	B20_Ol-c_Pl	B20_Ol-c_Pl
SiO2	39.274	39.158	39.094	40.687	39.212	38.877	39.106	39.119	39.328	39.102	39.976	38.91	39.269	39.134
TiO2	0.012	0.006	0	0.02	0.02	0.017	0.019	0.026	0	0.007	0.03	0.009	0.006	0.024
Al2O3	0.005	0	0	0.047	0.036	0.035	0.016	0.012	0.024	0	0.03	0	0.055	0
Cr2O3	0.06	0.007	0	0	0.026	0.005	0.053	0	0.031	0	0.058	0.084	0	0.005
FeO	17.3	17.384	17.425	17.402	17.498	17.55	17.698	17.397	17.333	17.413	17.747	17.42	17.63	17.739
MnO	0.207	0.273	0.271	0.284	0.292	0.218	0.191	0.259	0.256	0.251	0.237	0.312	0.246	0.272
MgO	42.478	42.736	42.59	39.829	42.764	42.847	42.617	42.844	42.727	42.976	42.799	42.555	42.592	42.805
CaO	0.096	0.089	0.077	0.198	0.144	0.166	0.114	0.132	0.148	0.153	0.131	0.204	0.157	0.174
Na2O	0.007	0.003	0	0.018	0	0	0	0	0.001	0.025	0	0.012	0	0
NiO														
Total	99.439	99.656	99.457	98.485	99.992	99.715	99.814	99.789	99.848	99.927	101.008	99.506	99.955	100.153
Fo	81.219 0056	81.180 494	81.094 3811	80.054 2117	81.075 4424	81.124 9437	80.9382112	81.2200427	81.23634069	81.26011164	80.92174346	81.05013122	80.93976407	80.90035711
Fa	18.556 1194	18.524 862	18.612 4421	19.621 4634	18.610 0211	18.640 5429	18.8556873	18.500992	18.48711476	18.47023717	18.82365728	18.61224354	18.79462484	18.80756275

Data set	B20_Ol-c_Pl	B20_Ol-c_Pl	B20_Ol-c_Pl	B20_Ol-c_Pl	B20_Ol-c_Pl	B20_Ol-c_Pl	B20_Ol-c_Pl	B20_Ol-c_Pl	B20_Ol-c_Pl	B20_A_Ol_c-r	B20_A_Ol_c-r	B20_A_Ol_c-r	B20_A_Ol_c-r	B20_A_Ol_c-r
SiO2	39.313	40.291	39.041	38.066	39.325	38.784	39.153	39.004	39.086	39.54129763	39.96671363	39.36319285	39.83033626	39.79675078
TiO2	0	0	0.025	0	0	0.002	0.029	0.016	0.007	0.007235835	0.029977032	0.005168454	0.032044414	0.035145486
Al2O3	0.037	0.034	0.035	0.027	0.024	0.02	0.006	0.009	0.039	0	0	0	0.021779425	0
Cr2O3	0	0.058	0.082	0.05	0	0	0.041	0.014	0	0	0.113419913	0.038095238	0.073593074	0
FeO	17.48	17.262	17.481	17.318	17.742	17.628	17.153	17.754	17.464	17.7071313	17.55666007	17.65461785	17.53242309	17.55666007

MnO	0.256	0.227	0.301	0.259	0.254	0.225	0.233	0.235	0.248	0.260661226	0.240005053	0.250824953	0.210496235	0.307875335
MgO	42.674	41.758	42.359	44.018	42.349	42.84	42.37	42.803	42.371	41.71376054	42.01813128	42.55901305	42.12790433	41.48423506
CaO	0.159	0.147	0.17	0.145	0.134	0.168	0.132	0.1	0.13	0.10123974	0.150847213	0.119462893	0.094152958	0.065805831
Na2O	0.018	0	0	0.013	0.034	0.007	0	0.003	0.01	0	0	0	0	0
NiO										0.009441066	0.013637095	0	0.010490073	0.005245036
Total	99.937	99.777	99.494	99.896	99.862	99.674	99.117	99.938	99.355	99.34076734	100.0893913	99.99037529	99.93321986	99.2517176
Fo	81.090146	80.972 4723	80.935 8488	81.696 0456	80.747 4726	81.049 1821	81.285567	80.9189171	81.00157085	80.53594533	80.79876689	80.9023456	80.88633941	80.53925024
Fa	18.633 4643	18.777 4351	18.737 3836	18.030 8381	18.977 3602	18.708 9608	18.4604597	18.8286645	18.72905644	19.17812183	18.93901326	18.8267491	18.88403153	19.12114279
Data set	B20_A_Ol_c-r	B20_A_Ol_c-r	B20_A_Ol_c-r	B20_A_Ol_c-r	B20_A_Ol_c-r	B20_A_Ol_c-r	B20_A_Ol_c-r	B20_A_Ol_c-r	B20_A_Ol_c-r	B20_A_Ol_c-r	B20_A_Ol1_c-r	B20_A_Ol1_c-r	B20_A_Ol1_c-r	B20_A_Ol1_c-r
SiO2	39.515 8541	39.998 2636	40.082 7362	39.549 4396	39.733 6508	39.870 0282	40.0074233	39.6491782	39.57997182	40.00233459	40.87250368	39.74688144	39.46191379	39.709225
TiO2	0.0289 4334	0.0237 7489	0	0.0082 6953	0.0237 7489	0.0382 4656	0.02790965	0.00930322	0.017572743	0.012404289	0.028943342	0.020673815	0.034111795	0
Al2O3	0	0.0114 0827	0.0051 8558	0.0020 7423	0.0114 0827	0	0.01244539	0	0.003111346	0	0	0	0.054967121	0
Cr2O3	0	0	0	0.0354 9784	0	0.0138 5281	0	0.01818182	0.03030303	0	0.05974026	0	0	0.001731602
FeO	17.466 7813	17.250 6682	17.266 8262	17.525 354	17.626 3414	17.656 6376	17.6445191	17.47688	17.59503528	17.24258924	18.12622902	18.20903869	17.74348676	17.90405673
MnO	0.2636 1211	0.2636 1211	0.2577 1034	0.2586 9397	0.2527 9221	0.2626 2848	0.26066123	0.21738163	0.23410329	0.220332508	0.29508818	0.254759462	0.285251908	0.308858962
MgO	42.530 0729	41.840 4985	42.107 9456	42.657 8088	42.109 9415	42.250 6506	41.9422881	41.8225357	41.93530252	41.68182656	41.13695304	41.52914222	41.86644488	42.06503431
CaO	0.1285 7447	0.1103 5132	0.1073 1412	0.1174 381	0.1488 2242	0.1346 4885	0.13262406	0.13768605	0.146797623	0.171095161	0.083016587	0.121487688	0.139710841	0.160971187
Na2O	0	0	0	0	0.0027 7073	0	0	0	0.019395139	0	0	0	0.00461789	0
NiO	0	0.0010 4901	0.0052 4504	0.0020 9801	0	0.0094 4107	0.00524504	0	0.008392058	0	0.017833124	0.009441066	0.01153908	0
Total	99.933 8382	99.499 626	99.832 9631	100.15 6674	99.909 5022	100.23 6134	100.033116	99.3311466	99.56998485	99.33058235	100.6203072	99.89142439	99.60204406	100.1498778
Fo	81.043 0593	80.980 216	81.069 2464	81.042 7747	80.760 7442	80.777 6301	80.6759151	80.8161398	80.73987266	80.96740363	79.91937505	80.03489163	80.53987225	80.45436973

Fa	18.6715353	18.7298997	18.6488497	18.6779843	18.9637971	18.9370863	19.0392158	18.9451957	19.00403713	18.78942119	19.75490155	19.68615352	19.14834606	19.20999639
Data set	B20_A_Ol1_c-r	B20_A_Ol1_c-r	B20_A_Ol1_c-r	B20_A_Ol1_c-r	B20_A_Ol1_c-r	B20_A_Ol1_c-r	B20_A_Ol1_c-r	B20_A_Ol1_c-r	B20_A_Ol1_c-r	B20_A_Ol1_c-r	B20_A_Ol1_c-r	B20_A_Ol1_c-r	B20_A_Ol1_c-r	B20_A_Ol1_c-r
SiO2	39.9656959	41.0821585	39.8211766	39.4171332	39.5301025	38.5459463	40.3188522	39.6807282	39.52908473	39.50364119	39.8486556	39.97383782	39.75909434	39.61152181
TiO2	0.02584227	0.00826953	0.02170751	0.01757274	0.03824656	0.01860643	0.01033691	0.04341501	0.008269526	0.024808578	0.035145486	0.029977032	0.012404289	0.007235835
Al2O3	0	0.04667020	0	0.00933404	0	0.04667020	0	0	0	0	0.010371155	0.046670197	0	0.015556732
Cr2O3	0.01558442	0	0.06406926	0	0.00432929	0.01212121	0.03030303	0	0.025974026	0.032034632	0.027705628	0.001731602	0.032034632	0.041558442
FeO	17.8525532	17.4344653	17.7162202	17.6889536	17.8929481	17.781862	17.4839491	17.9010271	17.69501281	17.55464032	17.73237815	17.66774621	17.97979729	17.47082077
MnO	0.29312093	0.28328465	0.31377715	0.23705417	0.29705544	0.28130174	0.25279221	0.25475946	0.237054172	0.271481126	0.246890444	0.242955935	0.302957199	0.247874072
MgO	42.3414628	40.2687481	41.5031959	41.5620741	41.6818266	47.2203761	41.0391552	41.5441113	41.45729077	41.98320349	41.61197098	42.00316223	41.83950058	42.5899491
CaO	0.12553728	0.15894639	0.13059926	0.12553728	0.13667365	0.12756207	0.10123974	0.10326453	0.123512483	0.103264535	0.152872008	0.125537278	0.127562073	0.145785226
Na2O	0	0	0	0.00184716	0	0.00923578	0.01200651	0	0.014777249	0	0	0.005541468	0	0
NiO	0.00314702	0	0.00314702	0.01153908	0.00629404	0	0.00839206	0.01153908	0.010490073	0	0	0.001049007	0.005245036	0
Total	100.622944	99.285425	99.578928	99.070453	99.594758	104.043697	99.2570271	99.5388447	99.10146584	99.47307387	99.66598945	100.0982088	100.0585954	100.130302
Fo	80.615193	80.205105	80.415099	80.515856	80.330811	82.329156	80.4832433	80.307996	80.470644	80.75983102	80.48774891	80.6939104	80.30931907	81.0749657
Fa	19.0677225	19.4789296	19.2531229	19.2234943	19.3446472	17.3920088	19.2350819	19.4121981	19.26792243	18.94345591	19.24092412	19.04089573	19.36028254	18.65693977
Data set	B20_A_Ol1_c-r	B20_A_Ol1_c-r	B20_A_Ol1_c-r	B20_A_Ol1_c-r	B20_A_Ol1_c-r	B20_A_Ol3_c-r	B20_A_Ol3_c-r	B20_A_Ol3_c-r	B20_A_Ol3_c-r	B20_A_Ol3_c-r	B20_A_Ol3_c-r	B20_A_Ol3_c-r	B20_A_Ol3_c-r	B20_A_Ol3_c-r
SiO2	40.7717473	39.7845379	39.5066944	40.4867796	39.3072171	39.4313815	39.4710735	39.5087299	39.59829116	39.54333312	39.5087299	40.37279254	39.7458637	39.09043809
TiO2	0.02790965	0.03824656	0.04238132	0.03411180	0.02687596	0.02170751	0.03928025	0.05375192	0.041347631	0.019640125	0.015505362	0.033078105	0.005168454	0.024808578
Al2O3	0.02489077	0	0.00622269	0	0	0	0.00829692	0.03422481	0	0.039410389	0.001037115	0.024890772	0.016593848	0.017630963

Cr2O3	0.0580 0866	0	0.0779 2208	0	0	0.0121 2121	0.04155844	0.01038961	0.073593074	0.01991342	0.015584416	0	0.007792208	0
FeO	17.298 1323	17.536 4626	17.554 6403	17.469 8109	17.735 4078	18.084 8242	17.7687336	18.2363053	17.92526409	18.01009351	17.73843739	17.84548404	17.7808521	17.64956848
MnO	0.2124 6349	0.3226 2974	0.2449 2319	0.2704 975	0.2242 6702	0.2547 5946	0.26557936	0.24590682	0.231152408	0.275415635	0.302957199	0.344269544	0.187872808	0.217381626
MgO	41.561 0762	41.910 3541	41.985 1994	40.796 6566	42.451 2359	41.943 286	41.6598719	41.7037812	40.39349008	41.7397069	43.54796848	41.28265182	42.33447726	41.43633409
CaO	0.1478 1002	0.1255 3728	0.1802 0674	0.1862 8112	0.1791 9434	0.0830 1659	0.15084721	0.12857447	0.148822418	0.125537278	0.066818228	0.118450496	0.07390501	0.136673649
Na2O	0	0	0	0	0	0	0.0212423	0	0	0.002770734	0	0	0	0
NiO	0.0062 9404	0	0	0	0.0125 8809	0.0041 9603	0.01153908	0.00209801	0.003147022	0.005245036	0	0.009441066	0.003147022	0.009441066
Total	100.10 8332	99.717 7681	99.598 1901	99.244 1375	99.936 7861	99.835 2925	99.4380226	99.923762	98.41510788	99.78106614	101.1970381	100.0310584	100.1556724	98.58227655
Fo	80.880 6281	80.703 5054	80.784 0174	80.386 6123	80.816 5979	80.299 9604	80.4575913	80.0860697	79.85974482	80.26944929	81.13871701	80.17727761	80.76644168	80.5200338
Fa	18.884 4523	18.943 5125	18.948 2284	19.310 5572	18.940 8233	19.422 9244	19.2509879	19.645625	19.8806029	19.42961989	18.5405684	19.44283094	19.02991139	19.2399599
Dataset	B20_A_Ol3_c-r	B20_A_Ol3_c-r	B20_A_Ol3_c-r	B20_A_Ol3_c-r	B20_A_Ol3_c-r	B20_A_Ol3_c-r	B20_A_Ol3_c-r	B20_A_Ol3_c-r	B20_A_Ol3_c-r	B20_A_Ol3_c-r	B20_B_Ol_c-r	B20_B_Ol_c-r	B20_B_Ol_c-r	B20_B_Ol_c-r
SiO2	39.566 7412	39.189 159	39.102 651	39.371 3348	39.425 2751	39.051 7639	39.1392897	39.1667687	39.34894447	39.09654454	39.29500416	39.24818805	39.50669442	38.94591878
TiO2	0.0299 7703	0.0248 0858	0.0423 8132	0.0506 5085	0.0144 7167	0.0444 487	0.03721287	0.03824656	0.059954065	0.036179177	0.002067382	0.027909651	0.019640125	0.011370598
Al2O3	0.0124 4539	0.0259 2789	0.0134 825	0.0165 9385	0	0.0134 825	0	0	0.035261927	0.012445386	0.051855775	0	0	0
Cr2O3	0	0.0060 6061	0.0017 316	0	0.0077 9221	0	0	0	0.018181818	0.03030303	0.012121212	0.03982684	0.001731602	0.05974026
FeO	17.914 1555	17.678 8548	17.778 8324	18.006 054	17.651 5882	17.860 6322	17.6768351	17.9525307	17.8394248	17.59705503	17.87679013	17.72429916	17.67885482	18.15248575
MnO	0.2282 0153	0.2547 5946	0.2734 4838	0.3078 7533	0.3000 0632	0.2813 174	0.23410329	0.24098868	0.230168781	0.311809844	0.224267017	0.307875335	0.225250644	0.275415635
MgO	41.432 3423	42.053 0591	41.537 1257	41.860 4573	41.977 2159	41.880 416	42.243665	41.9043665	42.28258455	43.63678486	40.60205888	40.65993922	40.37951896	40.62600937
CaO	0.1144 0091	0.1164 257	0.0809 9179	0.1417 3564	0.1488 2242	0.0941 5296	0.09010337	0.14679762	0.092128163	0.108326522	0.118450496	0.108326522	0.071880215	0.139710841
Na2O	0	0.0101 5936	0	0	0	0	0.00184716	0	0.010159359	0	0	0.005541468	0	0
NiO	0.0083 9206	0.0052 4504	0.0083 9206	0.0010 4901	0.0062 9404	0	0.01258809	0.01153908	0.009441066	0.017833124	0	0	0	0

Total	99.3066559	99.3644596	98.8390367	99.7557507	99.5314658	99.2262136	99.4356445	99.4612378	99.92624899	100.8472815	98.18261506	98.12190624	97.88357079	98.21065123		
Fo	80.277371	80.692 3617	80.395 3786	80.290 2407	80.648 0867	80.446 8857	80.7825955	80.4116604	80.65975083	81.28218972	79.99144159	80.0741753	80.07839578	79.71249157		
Fa	19.471 4118	19.029 8958	19.303 9119	19.374 2451	19.024 4309	19.246 0905	18.9630492	19.3255951	19.0907788	18.38781353	19.75752122	19.58133373	19.66780081	19.98047335		
Data set	B20_B_Ol_c-r	B20_B_Ol_c-r	B20_B_Ol_c-r	B20_B_Ol_c-r	B20_B_Ol_c-r	B20_B_Ol_c-r	B20_B_Ol_c-r	B20_B_Ol_c-r	B20_B_Ol_c-r	B20_B_Ol_c-r	B20_B_Ol_c-r	B20_B_Ol_c-r	B20_B_Ol_c-r	B20_B_Ol_c-r		
SiO2	39.308 2348	39.335 7138	39.415 0977	39.206 4606	39.160 6623	39.202 3897	38.9652559	39.0843316	39.6308589	39.38456542	39.27566707	38.99985909	39.76112982	39.47514443		
TiO2	0.0299 7703	0.0051 6845	0.0124 0429	0.0351 4549	0.0051 6845	0.0258 4227	0.0113706	0.02584227	0.037212868	0.007235835	0.033078105	0.011370598	0.017572743	0.020673815		
Al2O3	0.0300 7635	0	0	0	0.0093 3404	0	0	0.01555673	0	0.026965003	0.004148462	0.013482501	0	0.017630963		
Cr2O3	0.0320 3463	0	0.0303 0303	0	0.0199 1342	0	0.02164502	0.004329	0	0.01991342	0	0.035497835	0.025974026	0.051948052		
FeO	18.087 8538	17.872 7506	17.831 3458	17.992 9256	18.009 0836	18.052 5082	17.8343754	18.0969427	17.60311427	17.87073089	18.03332061	17.90001724	17.94445169	18.2241868		
MnO	0.2803 3377	0.2803 3377	0.3019 7357	0.2252 5064	0.2301 6878	0.2124 6349	0.23705417	0.20754535	0.249841326	0.247874072	0.265579362	0.353122189	0.209512608	0.230168781		
MgO	40.563 1393	40.218 8511	40.436 4014	40.412 4509	40.766 7185	40.699 8567	40.5132425	40.5351971	40.51723425	40.66093716	40.6349908	40.96131615	40.59108158	40.87249977		
CaO	0.0404 959	0.1174 381	0.1174 381	0.0809 9179	0.0830 1659	0.1397 1084	0.11946289	0.10832652	0.064793434	0.107314125	0.10528933	0.12857447	0.10123974	0.177169545		
Na2O	0	0	0	0.0092 3578	0.0073 8862	0	0	0.00554147	0.00461789	0.017547983	0	0	0	0.017547983		
NiO	0	0.0020 9801	0	0.0062 9404	0.0020 9801	0.0020 9801	0.00419603	0	0.007343051	0.014686102	0	0.015735109	0.008392058	0.005245036		
Total	98.372 1456	97.832 3539	98.144 9638	97.968 7549	98.293 5523	98.334 8692	97.7066025	98.0836128	98.11501599	98.35777001	98.35207374	98.41897518	98.65935427	99.09221518		
Fo	79.739 8545	79.792 3652	79.896 4628	79.812 7101	79.934 3808	79.885 6103	79.9824599	79.7856185	80.17787553	79.99886013	79.82950845	79.99709835	79.94052658	79.78752371		
Fa	19.947 0358	19.891 6369	19.764 5361	19.934 5347	19.809 1994	19.877 4503	19.7516375	19.9822775	19.54122157	19.72405379	19.87405291	19.61106727	19.82503772	19.95719006		
Data set	B20_B_Ol_c-r	B20_B_Ol_c-r	B20_Fe ld in Ol	B20_Fe ld in Ol	B20_Fe ld in Ol	B20_Fe ld in Ol	B20_Cpx brught_dark_Ol	B20_Cpx brught_dark_Ol	B20_Cpx brught_dark_Ol	B20_Cpx brught_dark_Ol	B20_Cpx brught_dark_Ol	B20_Cpx brught_dark_Ol	B20_Cpx brught_dark_Ol	B20_Cpx brught_dark_Ol	B20_Cpx brught_dark_Ol	B20_Cpx brught_dark_Ol
SiO2	39.425 2751	38.982 5575	42.145	39.017	39.045	38.87	38.658	39.006	38.668	39.02	38.75	38.962	39.223	38.872	39.115	39.196

TiO2	0.0072 3584	0.0206 7382	0.13	0.038	0.017	0.029	0	0.023	0.016	0.028	0.006	0.02	0.023	0.015	0.003	0.007
Al2O3	0.0435 5885	0	2.214	0	0.029	0	0.036	0	0.028	0.022	0.029	0.01	0.009	0.017	0	0.015
Cr2O3	0.0458 8745	0.0277 0563	0.007	0.031	0.055	0.017	0	0	0	0.007	0.036	0.036	0.024	0.058	0	0.031
FeO	17.665 7265	17.834 3754	16.213	17.717	17.806	17.609	18.037	17.665	17.782	17.612	17.501	17.421	17.651	17.544	17.638	17.75
MnO	0.2596 776	0.2222 9976	0.223	0.318	0.226	0.29	0.225	0.256	0.272	0.243	0.254	0.253	0.223	0.236	0.258	0.256
MgO	40.791 6669	40.963 312	37.563	42.737	42.574	42.917	42.466	42.81	42.877	42.535	42.381	42.402	42.911	42.627	42.893	42.522
CaO	0.0809 9179	0.0961 7775	0.248	0.081	0.096	0.079	0.115	0.083	0.115	0.095	0.161	0.091	0.123	0.077	0.079	0.121
Na2O	0	0.0193 9514	0.446	0.018	0.03	0	0	0.019	0.015	0.013	0	0	0.021	0	0.033	0.003
NiO	0.0020 9801	0.0125 8809	0.736	0.012	0.022	0.021	0	0	0.001	0.009	0	0	0.009	0.004	0	0
Total	98.322 118	98.179 0851	99.925	99.969	99.9	99.832	99.537	99.862	99.774	99.584	99.118	99.195	100.217	99.45	100.019	99.901
Fo	80.220 6601	80.171 909	84.229 1833	84.668 7304	84.665 8184	84.833 2937	84.469129	84.8019376	84.71984085	84.77226889	84.79188708	84.85704623	84.88168296	84.85722651	84.84370306	84.65395287
Fa	19.489 1873	19.580 8939	15.414 6894	14.882 5817	15.014 0929	14.758 4498	15.2121304	14.8369032	14.89739802	14.88281632	14.84619091	14.7823583	14.80415885	14.8081825	14.79284158	14.98307632

Table 9.1 – Continue. Single mineral phase EMPA analyses. Sample: Porphyrogabbro. B20. Feldspars.

Data set	B20_Pl smecolato_transect	B20_Pl smecolato_transect	B20_Pl smecolato_transect	B20_Pl smecolato_transect	B20_Pl smecolato_transect	B20_Pl smecolato_transect	B20_Pl smecolato_transect	B20_Pl smecolato_transect	B20_Pl smecolato_transect	B20_Pl smecolato_transect	B20_Pl smecolato_transect	B20_Pl smecolato_transect	B20_Pl smecolato_transect	B20_Pl smecolato_transect
SiO2	56.016	57.033	58.676	58.341	50.956	50.719	51.062	52.125	51.886	50.87	51.132	51.423	51.65	51.601
TiO2	0.154	0.155	0.136	0.177	0.109	0.12	0.151	0.122	0.111	0.115	0.134	0.121	0.114	0.137
Al2O3	26.507	25.273	24.634	25.03	30.379	30.122	30.035	30.125	29.796	29.835	29.677	29.626	29.886	29.752
Cr2O3	0.026	0.064	0.026	0	0	0.049	0	0	0.018	0	0.09	0	0	0
FeO	0.442	0.479	0.36	0.402	0.336	0.359	0.396	0.398	0.423	0.431	0.426	0.388	0.34	0.367
MnO	0.035	0	0.032	0.052	0.022	0.024	0.039	0	0.024	0.015	0	0.014	0.002	0
MgO	0.053	0.072	0.022	0.065	0.047	0.044	0.038	0.049	0.034	0.003	0.036	0.009	0.016	0.02
CaO	8.758	8.207	6.756	7.199	13.46	13.056	13.094	12.998	12.847	13.088	12.86	12.588	13.302	12.973
Na2O	6.023	6.012	6.607	6.359	3.673	3.669	3.79	3.926	4.136	3.696	3.923	3.991	3.825	3.858
K2O	1.01	1.149	1.633	1.512	0.366	0.338	0.376	0.377	0.397	0.346	0.365	0.41	0.366	0.387
SrO														
BaO														
Total	99.024	98.444	98.882	99.137	99.348	98.5	98.981	100.12	99.672	98.399	98.643	98.57	99.501	99.095
Ab%	52.2501784	53.1884322	57.8807516	56.1152528	32.3560394	33.0357563	33.6197069	34.5697237	35.97624394	33.12987185	34.81045188	35.58022301	33.50410605	34.19750989
An%	41.9847011	40.1230428	32.7062466	35.1055259	65.5225359	64.9617768	64.1856967	63.2460427	61.75160134	64.82944304	63.05848496	62.01473369	64.38648986	63.54536657
Or%	5.76512053	6.68852493	9.41300184	8.77922125	2.12142468	2.0024669	2.19459639	2.18423352	2.272154715	2.040685112	2.131063158	2.405043294	2.109404093	2.257123536

Data set	B20_Pl smecolato_transect	B20_Pl smecolato_transect	B20_Pl smecolato_transect	B20_Feld in Ol	B20_Feld in Ol	B20_Feld in Ol	B20_Feld in Ol	B20_Feld in Ol	B20_Feld in Cpx	B20_Feld in Cpx	B20_A_An_c-r	B20_A_An_c-r	B20_A_An_c-r	B20_A_An_c-r
SiO2	51.354	51.603	51.508	65.589	66.425	66.17	66.954	66.248	67.057	67.338	56.30655543	56.80626657	57.51766796	56.80728431
TiO2	0.129	0.111	0.107	1.036	1.091	1.1	1.087	1.102	1.05	1.065	0.16125576	0.163323142	0.158154688	0.175727431

Al2O3	29.769	29.709	29.911	16.915	16.864	16.812	17.122	16.65	16.486	16.207	27.36221812	26.80632422	26.87995942	26.63416304
Cr2O3	0.026	0	0.046	0.005	0.031	0	0	0	0.038	0.069	0	0	0	0
FeO	0.389	0.328	0.363	2.481	2.475	2.486	2.606	2.382	1.865	1.897	0.525134497	0.554420844	0.594815806	0.562499836
MnO	0.008	0	0.005	0	0.025	0.059	0.04	0.072	0.029	0.047	0.011803527	0	0.018688918	0
MgO	0.044	0.04	0.016	0.802	0.823	0.789	0.774	0.817	0.667	0.673	0.042911285	0.056882401	0.042911285	0.042911285
CaO	12.764	12.984	12.638	1.302	1.345	1.183	1.245	1.281	1.232	1.161	9.425419803	8.753187929	8.932382269	8.609427498
Na2O	3.791	4.008	4.091	4.195	3.377	3.589	2.509	3.602	3.396	3.522	5.811153168	5.341051934	5.755738484	5.574717184
K2O	0.388	0.388	0.384	6.259	6.214	6.267	5.75	6.261	6.435	6.384	0.869627033	1.010194009	1.030125147	1.064742387
SrO														
BaO														
Total	98.662	99.171	99.069	98.584	98.67	98.455	98.087	98.415	98.255	98.363	100.5160786	99.49165104	100.930444	99.47147297
Ab%	34.1541142	35.0402954	36.115877	46.4419747	41.1381277	42.8983899	35.9436669	42.7309447	40.86200408	42.10849648	50.13141056	49.25918292	50.62403139	50.52826554
An%	63.5458581	62.7277577	61.6535727	7.96527744	9.05413481	7.81382156	9.856036	8.39767623	8.191697374	7.670502462	44.93238955	44.61057966	43.41443816	43.12181527
Or%	2.30002773	2.23194699	2.23055027	45.5927479	49.8077375	49.2877885	54.2002971	48.871379	50.94629855	50.22100106	4.936199887	6.130237424	5.961530448	6.349919188
Dataset	B20_A_An_c-r	B20_A_An_c-r	B20_A_Fel_c-r	B20_A_Fel_c-r	B20_A_Fel_c-r	B20_A_Fel_c-r	B20_A_Fel_c-r	B20_A_Fel_c-r	B20_A_Fel_c-r	B20_A_Fel_c-r	B20_A_Fel_c-r	B20_A_Fel_c-r	B20_A_Fel_c-r	B20_A_Fel_c-r
SiO2	58.0601243	58.9547191	65.5160994	65.2525043	65.0978076	64.5166771	65.0428495	68.3321905	68.57950169	69.2105015	68.76676615	68.41869852	68.79220969	68.45431947
TiO2	0.14471671	0.13851456	0.16125576	0.14885147	0.15918838	0.15608731	0.13334611	1.04816244	1.045061368	1.0078485	1.032657078	1.018185408	1.005781118	1.041960295
Al2O3	26.2338365	25.5638599	20.2818306	20.060925	19.9758816	19.8752814	20.1335231	16.5378437	16.48598792	16.81682776	16.36257117	16.67681717	16.51295292	16.50880446
Cr2O3	0.02164502	0.07012987	0.01471861	0.03809524	0	0.02164502	0	0.04502165	0	0.012987013	0	0.027705628	0.012987013	0.027705628
FeO	0.55442084	0.52614437	0.16763909	0.25145863	0.2140933	0.26155737	0.26357712	1.70870686	1.710726612	1.64003543	1.736983337	1.813733764	1.737993211	1.741022833
MnO	0	0.02655794	0.00196725	0	0	0.00688539	0.0216398	0	0.035410582	0.033443327	0.040328718	0	0.058034009	0.041312345

MgO	0.0379216	0.02794223	0.00299381	0.00698556	0.01397112	0.01097731	0	0.57880338	0.604749734	0.59976005	0.581797186	0.56483226	0.547867333	0.560840513
CaO	7.87746418	7.41479856	0.9344428	0.91115766	0.90710807	0.92836842	0.94254198	0.96177753	0.965827121	0.999236235	0.994174248	0.953678352	0.86458738	0.894959302
Na2O	6.00048667	6.40501386	4.49782516	4.69362371	4.89958162	4.5846415	4.73056683	3.29902084	2.93143677	3.320263134	2.965609158	3.320263134	3.247300467	3.210357344
K2O	1.27769086	1.43818898	9.30259654	9.40435025	9.27217533	9.33826279	9.31833165	6.56154052	6.615039894	6.53951137	6.440904686	6.506992145	6.5437074	6.446149723
SrO														
BaO														
Total	100.208307	100.565869	100.881369	100.767952	100.539807	99.7003836	100.586376	99.0730674	98.97374169	100.1804143	98.92179174	99.30090637	99.32342054	98.92743191
Ab %	53.6031949	55.9451765	40.393171	41.2263983	42.5985842	40.7812235	41.5593287	40.4894343	37.49737822	40.61333251	38.2512609	40.84602016	40.43610971	40.40043214
An %	38.8867679	35.7892949	4.63734399	4.42254099	4.35819251	4.56337794	4.57580232	6.52292655	6.827016923	6.75422476	7.086072014	6.483214329	5.949315411	6.223678236
Or %	7.51003729	8.26552862	54.969485	54.3510607	53.0432233	54.6553985	53.864869	52.9876391	55.67560486	52.63244273	54.66266708	52.67076551	53.61457488	53.37588962

Dataset	B20_A_Fel_c-r	B20_A_Fel_c-r	B20_A_Fel_c-r	B20_A_Fel_c-r
SiO2	68.546934	68.7219855	67.7775213	68.2344873
TiO2	1.00371374	1.05539828	1.02128648	1.05953304
Al2O3	16.2329317	16.4849508	16.3345691	16.3604969
Cr2O3	0.04502165	0.01471861	0	0
FeO	1.70365749	1.74708208	1.91977054	1.75718082
MnO	0.05311587	0	0.01967255	0.05311587
MgO	0.58878274	0.5578467	0.58179719	0.56782607
CaO	0.98101308	0.99923623	1.07820323	0.99619904
Na2O	3.45787627	3.26115414	3.00624659	3.15217193
K2O	6.61399089	6.51118817	6.30977878	6.49335505

SrO				
BaO				
Total	99.2270374	99.3535605	98.0488457	98.674366
Ab%	41.4025073	40.2733024	38.7714444	39.5248545
An%	6.49087436	6.81907241	7.6842099	6.90267958
Or%	52.1066184	52.9076251	53.5443457	53.5724659

Table 9.1 – Continue. Single mineral phase EMPA analyses. Sample: Porphyrogabbro. B20. Biotite (phlogopite).

Data set	B20_A_Bt_c-r	B20_A_Bt_c-r	B20_A_Bt_c-r	B20_A_Bt_c-r	B20_A_Bt_c-r	B20_A_Bt_c-r	B20_A_Bt_c-r	B20_A_Bt_c-r	B20_A_Bt_c-r	B20_A_Bt_c-r	B20_A_Bt_c-r	B20_A_Bt_c-r	B20_A_Bt_c-r	B20_A_Bt_c-r
SiO2	39.28991 55	39.14844 94	39.62271 7	38.96729 14	39.06601 23	39.26040 09	39.24106 39	38.92251 07	39.07211 874	40.44505 22	38.36377 057	39.08738 487	38.98764 619	38.94998 975
TiO2	8.491769 67	8.452489 42	8.415276 55	8.566195 4	8.549656 35	8.450422 04	8.451455 73	8.405973 34	8.401838 572	8.564128 023	8.518645 629	8.475230 617	8.521746 701	8.440085 131
Al2O3	13.37049 3	13.31137 74	13.39123 53	13.27092 99	13.24085 35	13.25226 18	13.18692 35	13.22322 26	13.14336 468	13.89838 476	13.13403 064	13.29582 065	13.22633 392	13.27507 834
Cr2O3	0.097835 5	0.136796 54	0.180952 38	0.103896 1	0.056277 06	0.139393 94	0.145454 55	0.136796 54	0.118614 719	0.228571 429	0.120346 32	0.195670 996	0.259740 26	0.155844 156
FeO	7.463978 98	7.215549 97	7.425603 77	7.296339 89	7.278162 16	7.205451 23	7.339764 47	7.315527 5	7.432672 884	7.435702 506	7.411465 529	7.364001 45	7.334715 103	7.361981 702
Mno	0.004918 14	0.006885 39	0.029508 82	0.071804 79	0.073772 05	0.044263 23	0.012787 15	0.073772 05	0.060984 891	0.052132 245	0.073772 045	0.078690 181	0.096395 472	0.026557 936
MgO	18.53268 53	17.97284 28	17.89899 54	18.02972 52	17.68044 73	18.02573 34	17.60460 41	17.71138 33	17.94490 053	17.12759 024	18.53567 914	18.12353 122	17.91296 655	17.74331 728
CaO	0.028347 13	0	0.015185 96	0.057706 65	0.026322 33	0.026322 33	0.024297 54	0.093140 56	0.070867 818	0.050619 87	0.066818 228	0.002024 795	0.048595 075	0.004049 59
Na2O	0.902335 77	0.780423 46	0.767493 37	0.780423 46	0.609561 52	0.807207 23	0.752716 12	0.615102 99	0.760104 745	0.590166 382	0.611408 677	0.734244 559	0.711155 108	0.678829 876
K2O	9.241754 12	9.353997 9	9.389664 14	9.320429 66	9.336164 77	9.245950 15	9.251195 18	8.942787 04	9.291057 46	9.189303 754	9.184058 718	9.394909 181	9.279518 38	9.318331 65
BaO	0	0	0	0	0	0	0	0	0	0	0	0	0	0
F	0	0	0	0	0	0	0	0	0	0	0	0	0	0
Cl	0	0	0	0	0	0	0	0	0	0	0	0	0	0
Total	97.42403 31	96.37881 22	97.13663 27	96.46474 24	95.91722 93	96.45740 63	96.01026 22	95.44021 66	96.29652 504	97.58165 14	96.01999 55	96.75150 852	96.37881 275	95.95406 541

Data set	B20_A_Bt_c-r	B20_A_Bt_c-r	B20_A_Bt_c-r	B20_A_Bt_c-r	B20_A_Bt_c-r	B20_A_Bt_c-r	B20_A_Bt_c-r	B20_A_Bt_c-r	B20_A_Bt_c-r	B20_A_Bt_c-r	B20_A_Bt_c-r	B20_A_Bt 1_c-r	B20_A_Bt 1_c-r	B20_A_Bt1_c-r
SiO2	39.29703 96	38.78511 56	39.20238 97	38.86857 04	38.82684 3	38.94490 1	39.14844 94	40.71271 82	39.47717 991	37.33178 056	38.77188 496	39.29703 964	37.90069 813	39.51483 635
TiO2	8.475230 62	8.512443 48	8.467994 78	8.411141 79	8.522780 39	8.513477 18	8.399771 19	8.474196 93	8.369794 158	8.403905 954	8.538285 754	7.155207 505	7.196555 135	7.262711 345
Al2O3	13.33523 1	13.29789 49	13.13299 35	13.06558 1	13.34249 09	13.31345 16	13.26055 87	13.79259 9	13.48664 99	12.52939 23	13.21077 718	13.05832 121	12.24211 131	12.95149 831
Cr2O3	0.174891 77	0.130735 93	0.147186 15	0.228571 43	0.157575 76	0.188744 59	0.170562 77	0.180952 38	0.203463 203	0.226839 827	0.276190 476	0.066666 667	0.010389 61	0.106493 506
FeO	7.241806 69	7.210500 6	7.443781 5	7.215549 97	7.153947 65	7.303409 01	7.306438 63	7.379149 56	7.484176 46	7.234737 573	7.420554 396	6.569230 586	6.656079 752	6.586398 444

Mno	0.032459 7	0.086559 2	0.047214 11	0.049181 36	0.037377 84	0.014754 41	0.042295 97	0	0.011803 527	0.049181 363	0.054099 5	0.075739 3	0.021639 8	0.060984 891
MgO	17.82215 43	17.96286 34	17.92494 18	17.60061 23	17.59961 44	17.89799 75	17.58564 33	17.38605 59	17.12359 849	17.08068 721	18.44386 895	19.43282 438	18.08261 581	18.71131 603
CaO	0.031384 32	0.004049 59	0.070867 82	0.028347 13	0.055681 86	0	0	0.057706 65	0.068843 023	0.089090 971	0.050619 87	0.022272 743	0.099214 945	0.026322 332
Na2O	0.734244 56	0.791506 4	0.558764 73	0.821060 9	0.639116 02	0.833067 41	0.875552	0.723161 62	0.682524 188	0.769340 526	0	0.737938 872	0.569847 664	0.361119 022
K2O	9.266930 29	9.317282 64	9.238607 1	9.277420 37	9.263783 27	9.372880 03	9.345605 84	9.103285 16	9.131608 354	9.029854 648	9.313086 613	9.356095 912	9.162029 565	9.216577 944
BaO	0	0	0	0	0	0	0	0	0	0	0	0	0	0
F	0	0	0	0	0	0	0	0	0	0	0	0	0	0
Cl	0	0	0	0	0	0	0	0	0	0	0	0	0	0
Total	96.41137 29	96.09895 17	96.23474 12	95.56603 67	95.59921 1	96.38268 28	96.13487 78	97.80982 54	96.03964 122	92.74481 094	96.07936 771	95.77133 681	91.94118 173	94.79825 818

Data set	B20_A_Bt 1_c-r	B20_A_Bt 1_c-r	B20_A_Bt 1_c-r	B20_A_Bt 1_c-r	B20_A_Bt 1_c-r	B20_A_Bt 1_c-r	B20_A_Bt 1_c-r	B20_A_Bt 1_c-r	B20_A_Bt 1_c-r	B20_A_Bt 1_c-r	B20_A_Bt 1_c-r	B20_A_Bt 1_c-r	B20_A_Bt 1_c-r	B20_A_Bt 1_c-r	B20_A_Bt 1_c-r	B20_A_Bt 1_c-r	B20_A_Bt 1_c-r
SiO2	39.23495 74	39.32960 74	39.02224 94	39.12300 58	39.24309 93	39.37235 25	39.54638 63	38.98255 75	39.83949 593	39.64103 631	39.60541 536	39.28482 674	39.43443 476	39.65426 695	39.19119 451	35.11513 93	39.73263 306
TiO2	7.308193 74	7.257542 89	7.151072 74	7.224464 79	7.175881 32	7.285452 54	7.121095 71	7.200689 9	7.140735 834	7.222397 405	7.260643 963	7.372282 566	7.326800 172	7.323699 1	7.456011 518	6.918492 318	7.538706 78
Al2O3	12.95875 81	12.83223	12.91312 5	12.87890 02	12.88927 14	12.96290 66	13.11639 97	12.98053 75	13.07595 217	12.95772 1	13.07802 64	12.70362 771	13.10913 986	12.98157 466	12.86956 619	11.91749 416	13.10706 563
Cr2O3	0.050216 45	0.047619 05	0.074458 87	0.019047 62	0.010389 61	0.154112 55	0.129004 33	0.035497 84	0.064935 065	0.066666 667	0.127272 727	0.025108 225	0.022510 823	0.025108 225	0.085714 286	0.093506 494	0.025108 225
FeO	6.772215 27	7.015594 91	6.626793 41	6.869163 17	6.662139	6.710612 95	6.674257 49	6.736869 68	7.039831 885	6.810590 48	6.980249 317	6.656079 752	6.682336 477	6.754037 534	6.610635 421	6.958032 088	6.671227 863
Mno	0.065903 03	0.004918 14	0.034426 95	0.004918 14	0.063935 77	0.009836 27	0.006885 39	0.031476 07	0.027541 564	0.014754 409	0.044263 227	0.032459 7	0.012787 154	0.105248 118	0.061968 518	0.029508 818	0.016721 664
MgO	18.66241 71	18.92886 63	18.79015 3	18.78516 34	18.91289 93	18.69135 73	18.63647 08	18.68636 76	19.33802 038	18.63647 077	18.86599 624	18.59854 917	18.72428 921	18.76320 875	18.41792 26	16.51984 67	18.58557 599
CaO	0.022272 74	0.059731 45	0.024297 54	0.022272 74	0.057706 65	0.030371 92	0.028347 13	0.039483 5	0.072892 613	0.048595 075	0.030371 922	0.050619 87	0.037458 704	0.015185 961	0.052644 665	0.186281 122	0.061756 241
Na2O	0.725932 36	0.859851 18	0.691759 97	0.773034 84	0.833990 99	0.664976 2	0.676059 14	0.842303 19	0.688065 656	0.194874 971	0.757334 011	0.807207 226	0.728703 091	0.866316 222	0.781347 041	0.449782 516	0
K2O	9.241754 12	9.327772 72	9.248048 16	9.466241 68	9.303645 55	9.363438 96	9.314135 62	9.329870 73	9.402252 232	9.360291 941	9.367634 992	9.415889 326	9.307841 577	9.313086 613	9.292106 468	8.051130 858	9.257489 227
BaO	0	0	0	0	0	0	0	0	0	0	0	0	0	0	0	0	0
F	0	0	0	0	0	0	0	0	0	0	0	0	0	0	0	0	0

Cl	0	0	0	0	0	0	0	0	0	0	0	0	0	0	0	0	0
Total	95.04262 03	95.66373 4	94.57638 51	95.16621 24	95.15295 89	95.24541 78	95.24904 16	94.86565 35	96.68972 332	94.95339 903	96.11720 816	94.94665 028	95.38630 184	95.80173 213	94.81911 121	86.23921 438	94.99628 468

Table 9.1 – Continue. Single mineral phase EMPA analyses. Sample: Porphyrogabbro. B20. Opaque minerals.

Data set	B20_Opq in Ol_c-r	B20_Opq in Ol_c-r	B20_Opq in Ol_c-r	B20_Opq in Ol_c-r	B20_Opq in Ol_c-r	B20_Opq in Ol_c-r	B20_Opq in Ol_c-r	B20_Opq in Ol_c-r	B20_Opq in Ol_c-r	B20_Opq in Ol_c-r	B20_A_Opq_c-r	B20_A_Opq_c-r	B20_A_Opq_c-r	B20_A_Opq_c-r
SiO2	0.024	0.031	0.034	0.017	0.028	0.054	0.068	0.033	0.049	0.041	0.048851598	0.089561263	0.082437072	0.039691923
TiO2	2.595	2.547	2.57	2.62	2.565	2.614	2.543	2.515	2.581	2.519	61.15934805	60.83063439	61.74234965	61.58316127
Al2O3	8.453	8.182	8.349	8.351	8.267	8.198	8.213	8.255	8.397	8.286	1.190608589	1.238315902	1.20409109	1.18127455
Cr2O3	27.451	27.541	27.531	27.535	27.364	27.332	27.805	27.049	27.073	26.402	0.641558442	0.544588745	0.458874459	0.616450216
FeO	50.041	49.602	50.254	49.504	50.316	49.467	50.053	49.512	50.17	50.638	26.87274802	26.40820597	26.69702994	26.83437281
Mno	0.292	0.301	0.329	0.314	0.293	0.381	0.287	0.292	0.35	0.382	0.093444509	0.053115872	0.064919431	0.097379111
MgO	6.508	6.281	6.676	6.54	6.485	6.686	6.632	6.525	6.459	6.587	6.546465769	6.541476084	6.870795247	7.002522911
CaO	0	0.007	0.03	0.038	0	0.033	0	0.058	0.038	0.085	0.068843023	0.068843023	0.008099179	0
V	0	0	0	0	0	0	0	0	0	0	0	0	0	0
Ba	0	0	0	0	0	0	0	0	0	0	0	0	0	0
Ni	0	0	0	0	0	0	0	0	0	0	0	0	0	0
Zn	0	0	0	0	0	0	0	0	0	0	0	0	0	0
Total	95.364	94.492	95.773	94.919	95.318	94.765	95.601	94.239	95.117	94.94	96.62186808	95.77474124	97.12859603	97.35485278

Data set	B20_A_Opq_c-r	B20_A_Opq_c-r	B20_A_Opq_c-r	B20_A_Opq_c-r	B20_A_Opq_c-r	B20_A_Opq_c-r	B20_A_Opq_c-r	B20_A_Opq_c-r	B20_A_Opq_c-r	B20_A_Opq_c-r	B20_A_Opq_c-r	B20_A_Opq_c-r	B20_A_Opq_c-r	B20_A_Opq_c-r
SiO2	0.04681611	0.04070967	0.01628387	0	0.03358547	0.04376289	0.02035483	0.090579	0.069206431	0.044780632	0.070224172	0.062082239	0.035620957	0.055975789
TiO2	61.7671582	61.5201061	61.8302134	62.0834676	61.7795625	61.2441107	61.4022654	61.6968673	61.48909541	61.22550426	61.56972329	61.70720416	61.69686725	61.75372024
Al2O3	1.20409109	1.17608897	1.20616532	1.20201686	1.20097974	1.16675493	1.18023743	1.18749724	1.207202437	1.21342513	1.178163203	1.098305301	1.242464364	1.188534358
Cr2O3	0.64935065	0.72987013	0.61904762	0.69004329	0.67792208	0.56969697	0.71601732	0.72813853	0.674458874	0.719480519	0.570562771	0.621645022	0.644155844	0.619913432
FeO	26.7455039	26.9010245	26.6576449	26.6445165	26.5940228	26.4849564	26.5011144	26.4698083	27.01110076	26.87476777	26.43446269	27.03533774	26.81417533	26.54049947
Mno	0.05114862	0.10032998	0.09639547	0.05705038	0.108199	0.14360958	0.10426449	0.08360832	0.059017636	0.060001263	0.002950882	0.069837536	0.045246854	0.0757393

MgO	7.03445689	6.87179318	6.90871685	7.15820106	6.83187571	6.88177255	6.87478699	6.93865495	7.011504343	7.042440386	6.917698279	6.928675584	6.975578616	7.166184556
CaO	0	0.00809918	0.01518596	0.00303719	0.02530994	0.02632233	0.0384711	0.01113637	0.017210756	0	0.012148769	0	0.037458704	0.014173564
V	0	0	0	0	0	0	0	0	0	0	0	0	0	0
Ba	0	0	0	0	0	0	0	0	0	0	0	0	0	0
Ni	0	0	0	0	0	0	0	0	0	0	0	0	0	0
Zn	0	0	0	0	0	0	0	0	0	0	0	0	0	0
Total	97.4985255	97.3480217	97.3496533	97.8383329	97.2514572	96.5609863	96.8375119	97.20629	97.53879665	97.18039996	96.75593405	97.52308759	97.49156792	97.4147407

Data set	B20_A_Opq_c-r	B20_A_Opq_c-r	B20_B_Opq_Bt_c-r	B20_B_Opq_Bt_c-r	B20_B_Opq_Bt_c-r	B20_B_Opq_Bt_c-r	B20_B_Opq_Bt_c-r	B20_B_Opq_Bt_c-r	B20_B_Opq_Bt_c-r	B20_B_Opq_Bt_c-r
SiO2	0.08345481	0.35926279	0.03460322	0.04986934	0.04681611	0.10075642	0.05597579	0.05292256	0.04986934	4.705019535
TiO2	61.3175027	58.4211012	61.6079698	61.3981306	61.6379469	61.6813619	61.7175411	61.2420433	60.85957773	55.36034284
Al2O3	1.077563	1.10867646	1.02259588	1.04022684	1.08793415	1.05474646	1.09934243	0.95310914	1.092082617	2.339732558
Cr2O3	0.68484848	0.54632035	0.61038961	0.58268398	0.63030303	0.47965368	0.54805195	0.53593074	0.435497835	0.571428571
FeO	26.656635	25.3316802	27.3706159	27.4938206	27.2039867	27.2706384	27.3393098	26.905064	26.9515182	23.34828765
Mno	0.06787028	0.04032872	0.09442822	0.08557557	0.108199	0.07278842	0.06000126	0.09934635	0.10426449	0.101313609
MgO	8.0962617	6.69715423	7.07138055	6.77599125	6.84684476	6.9805683	6.89973542	6.88776017	6.910712721	8.125201873
CaO	0.04657028	1.88305917	0.04353309	0.01214877	0.04960747	0.0404959	0.01214877	0.02328514	0.005061987	0.12452488
V	0	0	0	0	0	0	0	0	0	0
Ba	0	0	0	0	0	0	0	0	0	0
Ni	0	0	0	0	0	0	0	0	0	0
Zn	0	0	0	0	0	0	0	0	0	0
Total	98.0307063	94.3875832	97.8555163	97.4384469	97.6116381	97.6810095	97.7321065	96.6994614	96.40858492	94.67585151

Table 9.1 – Continue. Single mineral phase EMPA analyses. Sample: Wherlite B15. Clinopyroxenes.

Data set	B15_Cpx-c to Ol_r	B15_Cpx-c to Ol_r	B15_Cpx-c to Ol_r	B15_Cpx-c to Ol_r	B15_Cpx-c to Ol_r	B15_Cpx-c to Ol_r	B15_Cpx-c to Ol_r	B15_Cpx-c to Ol_r
SiO2	51.637	49.48	50.884	51.087	51.749	51.335	51.352	51.3
TiO2	0.761	0.742	0.815	0.77	0.705	0.688	0.729	0.677
Al2O3	2.969	2.722	2.965	2.962	2.566	2.604	2.441	2.515
FeO	5.346	5.188	5.161	5.235	5.129	5.262	5.127	5.351
Mno	0.071	0.123	0.148	0.142	0.158	0.143	0.072	0.103
MgO	15.995	15.968	16.213	16.196	16.174	16.259	16.41	16.547
CaO	22.304	21.935	22.016	21.813	22.155	22.197	22.03	22.011
Na2O	0.248	0.201	0.3	0.233	0.244	0.239	0.242	0.231
K2O	0.008	0.003	0	0	0	0.008	0.006	0.006
Cr2O3	0.968	1.001	1.046	1.038	0.966	0.91	0.914	0.799
Total	99.339	96.362	98.502	98.438	98.88	98.735	98.409	98.741
Wo	45.3508734	45.1653189	44.7971394	44.6476664	45.1181433	44.9701145	44.6832387	44.350941
En	45.2520274	45.7476578	45.9014227	46.1256003	45.8297831	45.8325942	46.311583	46.3909462
Fs	8.48457709	8.33807421	8.19679496	8.36369905	8.15286987	8.32106475	8.11693019	8.41581854
N° Mg	84.2108053	84.5835974	84.8483087	84.6507495	84.8972412	84.6343444	85.0869889	84.6445624

Table 9.1 – Continue. Single mineral phase EMPA analyses. Sample: Wherlite B15. Olivines.

Data set	B15_Ol_c-r	B15_Ol_c-r	B15_Ol_c-r	B15_Ol_c-r	B15_Ol_c-r	B15_Ol_c-r	B15_Ol_c-r	B15_Ol_c-r	B15_Ol_c-r	B15_Ol_c-r	B15_Ol_c-r	B15_Ol_c-r	B15_Ol in Cpx_c-r	B15_Ol in Cpx_c-r	B15_Ol in Cpx_c-r	B15_Ol in Cpx_c-r
SiO2	39.428	38.904	39.001	38.959	39.077	39.217	39.257	39.203	39.042	39.066	39.476	39.393	39.412	39.139	38.914	39.296
TiO2	0.008	0.014	0.027	0.034	0.02	0.018	0.011	0.027	0.026	0.015	0.022	0.023	0.016	0.005	0.018	0.018
Al2O3	0.065	0.01	0.055	0.051	0.035	0.054	0.04	0.02	0.033	0.021	0.04	0.016	0.047	0.019	0.025	0.035
Cr2O3	0	0	0.034	0.094	0	0.01	0.058	0.094	0.014	0	0	0.01	0.044	0.051	0.031	0.048
FeO	17.859	17.803	17.581	17.629	17.631	17.65	17.737	17.603	17.206	17.627	17.616	17.337	17.599	17.554	17.416	17.506
Mno	0.257	0.277	0.206	0.305	0.242	0.264	0.243	0.279	0.27	0.234	0.211	0.173	0.293	0.292	0.18	0.2
MgO	42.694	42.633	42.478	42.782	42.752	42.227	42.546	42.885	42.894	42.368	42.659	42.542	42.782	42.617	42.561	42.888
CaO	0.286	0.286	0.307	0.267	0.332	0.3	0.345	0.258	0.29	0.271	0.3	0.241	0.294	0.3	0.285	0.348
Na2O	0.001	0.001	0.024	0.006	0.027	0.01	0.016	0	0.007	0.004	0.027	0	0.031	0.004	0.024	0.004
NiO																
Total	100.598	99.928	99.713	100.127	100.116	99.75	100.253	100.369	99.782	99.606	100.351	99.735	100.518	99.981	99.454	100.343
Fo	80.7702627	80.7787237	80.9758218	80.9578092	81.0001 69	80.7734834	80.8334224	81.0397862	81.3933 6244	80.8714 0233	81.0066 4976	81.2397 2796	80.9940530 9	80.9741911 6	81.1716987 5	81.1932097 4
Fa	18.953492	18.9230 76	18.8010 596	18.7142 657	18.7393 224	18.9395 974	18.9042 671	18.6606 604	18.3155 4346	18.8748 2195	18.7656 992	18.5725 679	18.6907827 2	18.7105815 7	18.6332527 9	18.5916651 5

Data set	B15_Ol in Cpx_c-r	B15_Ol1_c-r	B15_Ol1_c-r	B15_Ol1_c-r	B15_Ol1_c-r	B15_Ol1_c-r	B15_Ol1_c-r	B15_Ol1_c-r	B15_Ol1_c-r	B15_Ol1_c-r	B15_Ol1_c-r	B15_Ol1_c-r	B15_Ol1_c-r	B15_Cpx-c to Ol_r	B15_Cpx-c to Ol_r	B15_Cpx-c to Ol_r
SiO2	39.484	39.349	39.067	39.259	39.291	39.374	38.935	39.434	39.239	39.306	38.756	39.218	39.313	39.383	39.176	39.279
TiO2	0.014	0.027	0.016	0.014	0.012	0	0.006	0.032	0.013	0	0.033	0.018	0.015	0.015	0.016	0.005
Al2O3	0.018	0.041	0.031	0.019	0	0.016	0.024	0.036	0.041	0.039	0.021	0.031	0.026	0.07	0.072	0.025
Cr2O3	0.051	0.036	0	0	0.048	0.046	0.029	0.123	0.043	0.099	0	0	0.053	0	0.015	0.024
FeO	17.435	17.838	17.56	17.441	17.401	17.576	17.765	17.805	18.096	17.359	17.715	17.523	17.311	17.271	17.491	17.484
Mno	0.258	0.296	0.274	0.224	0.211	0.249	0.294	0.254	0.239	0.144	0.249	0.256	0.206	0.227	0.256	0.198
MgO	42.555	42.52	42.717	42.573	42.752	42.472	42.689	42.716	43.17	42.691	42.24	42.467	42.621	42.263	42.643	43.006
CaO	0.319	0.311	0.262	0.27	0.31	0.282	0.292	0.317	0.298	0.314	0.267	0.283	0.247	0.361	0.27	0.245

Na2O	0.015	0.021	0	0	0.007	0.028	0.01	0.034	0.024	0.01	0	0.01	0.015	0	0	0
NiO														0	0	0.002
Total	100.149	100.439	99.927	99.8	100.032	100.043	100.044	100.751	101.163	99.962	99.281	99.806	99.807	99.59	99.939	100.268
Fo	81.084518	80.6908583	81.0208147	81.1156497	81.2258381	80.9402731	80.8169303	80.8271705	80.7560 6079	81.2993 5815	80.7351 2345	80.9782 0608	81.2615352 2	84.9548072 5	84.8759463 6	85.0588554 6
Fa	18.6361735	18.9899879	18.6839124	18.6418593	18.5463914	18.7901153	18.8668 34	18.8997572	18.9899 1906	18.5448 3359	18.9944 7128	18.7444 4037	18.5153102	14.7202164 7	14.7611636 2	14.6622411 2

Table 9.1 – Continue. Single mineral phase EMPA analyses. Sample: Wherlite B15. Opaque minerals.

Data set	B15_Opq in Ol_c-r	B15_Opq in Ol_c-r	B15_Opq in Ol_c-r	B15_Opq in Ol_c-r	B15_Opq in Ol_c-r	B15_Opq in Ol1_c-r	B15_Opq in Ol1_c-r	B15_Opq in Ol1_c-r	B15_Opq in Ol1_c-r
SiO2	0.06	0.045	0.048	0.031	0.081	0.069	0.08	0.097	0.085
TiO2	3.68	3.614	3.569	3.589	3.644	4.822	4.708	4.816	4.77
Al2O3	15.189	15.109	14.998	15.261	15.381	15.304	15.421	15.5	15.483
Cr2O3	30.911	31.062	30.446	31.333	30.319	26.923	26.704	26.705	26.9
FeO	38.059	37.746	37.957	37.714	37.944	39.321	38.866	39.412	39.383
Mno	0.252	0.354	0.38	0.331	0.3	0.312	0.268	0.289	0.309
MgO	9.716	9.8	9.718	9.626	9.7	9.95	9.533	9.869	9.959
CaO	0	0.003	0	0.039	0.068	0.003	0.031	0.014	0.06
BaO									
V2O3									
NiO									
ZnO									
Total	97.867	97.733	97.116	97.924	97.437	96.704	95.611	96.702	96.949

Table 9.1 – Continue. Single mineral phase EMPA analyses. Sample: Dunite B7. Clinopyroxenes.

Data set	B7_Cpx in Ol_c-r_continua	B7_Cpx in Ol_c-r_continua	B7_Cpx in Ol_c-r_continua	B7_Cpx in Ol_c-r_continua	B7_Cpx in Ol_c-r_continua	B7_Cpx in Ol_c-r_continua	B7_Cpx in Ol_c-r_continua	B7_Cpx1 in Ol	B7_Cpx1 in Ol	B7_Cpx1 in Ol
SiO2	50.333	50.853	51.194	50.885	51.063	51.181	51.407	51.165	51.286	51.779
TiO2	1.161	1.173	1.16	1.211	1.193	1.148	1.218	1.068	1.056	1.029
Al2O3	4.138	3.678	3.57	3.552	3.518	3.57	3.519	3.314	3.278	3.283
FeO	4.182	4.143	4.333	4.171	4.107	4.265	4.49	4.373	4.053	4.169
Mno	0.11	0.147	0.108	0.108	0.088	0.098	0.073	0.113	0.174	0.081
MgO	16.375	16.1	15.841	15.785	16.162	16.06	16.077	16.24	16.892	16.205
CaO	21.307	21.8	21.887	21.726	21.976	21.78	21.678	21.826	21.806	21.175
Na2O	0.649	0.67	0.589	0.625	0.68	0.679	0.608	0.649	0.696	0.681
K2O	0.002	0	0	0.008	0	0	0	0	0	0.005
Cr2O3	0.909	1.036	0.934	0.984	1.069	1.073	0.927	0.956	0.77	0.907
Total	98.257	98.564	98.682	98.071	98.787	98.781	99.07	98.748	99.241	98.407
Wo	43.9049761	44.8119541	45.243429	45.1910739	44.9406984	44.7378668	44.5569123	44.5337211	43.8465603	43.9233035
En	46.9487081	46.0483596	45.5619986	45.6844469	45.9872216	45.9001216	45.9781809	46.105396	47.2597567	46.7704497
Fs	6.72626253	6.64738249	6.99127379	6.77191383	6.55562677	6.83808947	7.20345028	6.96454354	6.36113304	6.74997007
N° Mg	87.4685306	87.3853518	86.696787	87.0903857	87.5232748	87.0338995	86.4550031	86.8766696	88.1368338	87.3880475

Data set	B7_Cpx1 in Ol	B7_Cpx1 in Ol	B7_Cpx1 in Ol	B7_Cpx1 in Ol	B7_Cpx1 in Ol	B7_Cpx1 in Ol	B7_Cpx1 in Ol	B7_Cpx1 in Ol	B7_Cpx1 in Ol
SiO2	51.272	51.372	51.959	51.284	51.346	51.837	51.921	51.317	51.351
TiO2	1.043	1.059	1.008	1.068	1.048	1.05	1.029	1.038	1.048
Al2O3	3.295	3.31	3.301	3.259	3.362	3.371	3.302	3.39	3.304
FeO	4.138	4.248	4.193	4.282	4.13	4.48	4.293	4.33	4.125
Mno	0.145	0.105	0.131	0.094	0.138	0.165	0.083	0.101	0.135
MgO	16.479	16.503	16.215	16.509	16.652	16.383	16.295	16.412	16.73
CaO	21.676	21.99	21.477	21.705	21.78	22.082	21.85	22.001	21.752
Na2O	0.703	0.658	0.667	0.662	0.691	0.697	0.645	0.669	0.692

K2O	0	0	0	0.014	0.005	0	0	0.003	0.01
Cr2O3	0.954	0.877	0.983	0.902	0.925	0.952	0.899	0.989	0.969
Total	98.751	99.245	98.951	98.877	99.152	100.065	99.418	99.261	99.147
Wo	44.1404476	44.4613312	44.2657332	44.1016609	44.067981	44.4884073	44.55465	44.5121074	43.9415922
En	46.691663	46.4270437	46.5009575	46.6731187	46.8794576	45.9253825	46.2324446	46.2006559	47.0244185
Fs	6.5772814	6.70409388	6.74554826	6.79110062	6.52249382	7.0450619	6.83283337	6.83788791	6.50427489
N° Mg	87.6526906	87.3819869	87.3314724	87.2978588	87.7860384	86.7000136	87.1237208	87.1077005	87.8489957

Table 9.1 – Continue. Single mineral phase EMPA analyses. Sample: Dunite B7. Olivines.

Data set	B7_Ol_c-r	B7_Ol_c-r	B7_Ol_c-r	B7_Ol_c-r	B7_Ol_c-r	B7_Ol_c-r	B7_Ol_c-r	B7_Ol_c-r	B7_Ol_c-r	B7_Ol_c-r	B7_Ol_c-r	B7_Ol_c-r	B7_Ol_c-r	B7_Ol_c-r
SiO2	40.114	40.347	40.481	40.095	40.219	39.97	40.272	40.201	40.283	40.603	40.315	40.034	40.347	40.207
TiO2	0.011	0	0.022	0	0.004	0.012	0.013	0	0	0.022	0	0.013	0.016	0.008
Al2O3	0.034	0.012	0.023	0	0.015	0.011	0.029	0.017	0.046	0.024	0.033	0.04	0	0.025
Cr2O3	0.054	0	0.005	0.025	0.071	0	0.049	0.037	0.005	0	0.015	0.005	0	0.012
FeO	13.031	13.237	13.105	12.964	13.359	13.241	13.119	13.174	13.262	12.993	13.039	13.078	13.285	13.416
Mno	0.178	0.21	0.173	0.151	0.213	0.171	0.128	0.254	0.204	0.168	0.172	0.178	0.195	0.209
MgO	46.607	46.599	46.282	46.274	47.019	46.333	46.644	46.798	46.618	46.723	46.733	46.369	46.519	46.626
CaO	0.044	0.059	0.067	0.077	0.132	0.096	0.113	0.099	0.067	0.136	0.059	0.046	0.069	0.065
Na2O	0	0.004	0	0	0.011	0.009	0.001	0.003	0.021	0.021	0.003	0.027	0.027	0.034
NiO														
Total	100.073	100.468	100.158	99.586	101.043	99.843	100.368	100.583	100.506	100.69	100.369	99.79	100.458	100.602
Fo	86.2800749	86.0649239	86.1349923	86.2800328	86.0615521	86.0279233	86.2560236	86.1323454	86.05294654	86.35254173	86.31028304	86.17710976	86.01502244	85.91351478
Fa	13.5327032	13.7147094	13.6820753	13.5600013	13.7169383	13.7916826	13.6094893	13.6020413	13.73309993	13.47104515	13.50923055	13.63493199	13.78011823	13.86768044

Data set	B7_Ol_c-r	B7_Ol_c-r	B7_Ol_c-r	B7_Ol_c-r	B7_Ol_c-r	B7_Ol_c-r	B7_Ol_c-r	B7_Ol_c-r	B7_Ol_c-r	B7_Ol_c-r	B7_Ol_c-r	B7_Ol_c-r	B7_Ol_c-r	B7_Ol_c-r
SiO2	39.947	39.776	40.169	40.05	40.324	40.188	41.212	40.363	40.334	40.883	40.215	40.521	40.21	40.162
TiO2	0	0.006	0.003	0.011	0.012	0	0	0.003	0.006	0.023	0.019	0.018	0.017	0.015
Al2O3	0.042	0	0.009	0.018	0	0.041	0.023	0.015	0.02	0.027	0.016	0.015	0.017	0.022
Cr2O3	0.091	0.002	0	0.034	0.032	0	0.015	0	0.015	0.02	0.044	0.007	0.039	0.032
FeO	13.105	13.365	13.294	13.139	13.183	13.351	13.252	13.053	12.869	13.222	13.107	13.262	13.38	13.369
Mno	0.113	0.151	0.118	0.209	0.128	0.118	0.204	0.145	0.257	0.173	0.245	0.193	0.213	0.199
MgO	46.541	46.802	46.78	46.821	46.586	46.648	45.7	46.172	46.595	45.249	46.639	46.223	46.41	46.141
CaO	0.103	0.067	0.059	0.176	0.107	0.084	0.096	0.069	0.04	0.081	0.069	0.092	0.107	0.065
Na2O	0.003	0.013	0.011	0.033	0	0.009	0.02	0.016	0	0.014	0.014	0.024	0	0

NiO														
Total	99.945	100.182	100.443	100.491	100.372	100.439	100.522	99.836	100.136	99.692	100.368	100.355	100.393	100.005
Fo	86.2559665	86.0563545	86.1435357	86.2099051	86.1839851	86.0589753	85.8215728	86.1789998	86.3505653	85.75640501	86.15955392	85.96049632	85.88570257	85.83763903
Fa	13.6250439	13.7858943	13.7330056	13.5714497	13.6814728	13.8173382	13.9607627	13.6672314	13.37882947	14.0573087	13.58328959	13.83557642	13.89033968	13.95202138
Data set	B7_Ol_c-r	B7_Ol_c-r	B7_Ol_c-r	B7_Ol_c-r	B7_Ol_c-r	B7_Ol_c-r	B7_Ol_c-r	B7_Ol_c-r	B7_Ol_c-r	B7_Ol_c-r	B7_Ol_c-r_continua	B7_Ol_c-r_continua	B7_Ol_c-r_continua	B7_Ol_c-r_continua
SiO2	40.675	39.793	40.275	39.698	39.928	40.172	40.115	38.57	39.945	39.914	39.741	40.213	39.926	40.027
TiO2	0	0.007	0.007	0.015	0.02	0	0.034	0	0.001	0	0	0.005	0.014	0.004
Al2O3	0.013	0	0.015	0.034	0	0.015	0.055	0.011	0.01	0.034	0.01	0	0.013	0.018
Cr2O3	0.039	0.02	0.047	0.042	0.005	0	0.027	0	0	0	0.027	0	0	0.02
FeO	13.404	12.95	13.188	13.227	13.132	13.035	13.45	13.074	13.211	13.106	13.237	13.364	13.284	13.335
Mno	0.288	0.187	0.24	0.158	0.206	0.209	0.166	0.199	0.198	0.216	0.163	0.158	0.223	0.146
MgO	46.312	46.37	46.91	46.115	46.6	46.442	46.293	49.173	46.437	46.295	46.392	46.514	46.405	46.48
CaO	0.13	0.103	0.086	0.096	0.123	0.069	0.159	0.092	0.105	0.053	0.023	0.084	0.057	0.061
Na2O	0	0.008	0.01	0.017	0	0.028	0	0	0.001	0.016	0.024	0	0.01	0.014
NiO														
Total	100.861	99.438	100.778	99.402	100.014	99.97	100.299	101.119	99.908	99.634	99.617	100.338	99.932	100.105
Fo	85.7708893	86.2843119	86.1610323	85.9955717	86.1625317	86.2062521	85.8350745	86.8469141	86.05722581	86.09830894	86.05404858	85.97669279	85.9610354	86.00459809
Fa	13.9260594	13.517985	13.5885103	13.8370234	13.6210585	13.5733277	13.9900477	12.9533952	13.73429362	13.67345121	13.77416335	13.85737476	13.80426145	13.84190996
Data set	B7_Ol_c-r_continua	B7_Ol_c-r_continua	B7_Ol_c-r_continua	B7_Ol_c-r_continua	B7_Ol_c-r_continua	B7_Ol_c-r_continua	B7_Ol_c-r_continua	B7_Ol_c-r_continua	B7_Ol_c-r_continua	B7_Ol_c-r_continua	B7_Ol_c-r_continua	B7_Ol_c-r_continua	B7_Ol_c-r_continua	B7_Ol_c-r_continua
SiO2	39.998	40.052	39.924	39.985	40.104	40.001	40.25	40.203	39.837	40.143	39.941	39.924	39.86	40.347
TiO2	0	0	0	0.01	0.032	0.021	0.02	0.005	0	0.001	0.021	0.006	0	0
Al2O3	0	0.026	0.012	0.01	0.013	0	0	0.004	0.047	0.019	0.013	0.021	0.023	0.003
Cr2O3	0.017	0	0	0.064	0.049	0.061	0	0	0.061	0.047	0.054	0	0	0

FeO	13.214	13.252	13.136	13.136	13.042	13.319	13.43	13.049	13.516	13.553	12.952	13.224	13.21	13.219
Mno	0.173	0.168	0.191	0.189	0.211	0.218	0.228	0.223	0.143	0.155	0.224	0.218	0.135	0.223
MgO	45.87	46.335	45.643	46.32	46.618	46.464	46.154	46.416	47.229	46.539	46.268	47.302	46.531	46.442
CaO	0.098	0.117	0.117	0.128	0.079	0.054	0.136	0.076	0.346	0.061	0.061	0.075	0.084	0.042
Na2O	0	0.01	0.001	0	0	0.027	0	0	0.024	0.014	0	0.02	0	0
NiO														
Total	99.37	99.96	99.024	99.842	100.148	100.165	100.218	99.976	101.203	100.532	99.534	100.79	99.843	100.276
Fo	85.9293152	86.021309	85.9234251	86.1023864	86.2430896	85.9496538	85.7602001	86.1742934	86.03914689	85.81776666	86.22263406	86.24785663	86.13940698	86.02871989
Fa	13.88655	13.801483	13.8722845	13.698002	13.5351263	13.8212271	13.9990931	13.590477	13.81283986	14.01983969	13.54019265	13.52630252	13.71859887	13.7365793
Data set	B7_Ol_c-r_continua	B7_Cpx2 in Ol	B7_Cpx2 in Ol	B7_Cpx2 in Ol										
SiO2	40.308	39.495	39.717	39.849										
TiO2	0.004	0.048	0.007	0.021										
Al2O3	0	0.01	0.014	0										
Cr2O3	0.027	0	0.007	0.017										
FeO	13.405	12.42	13.152	13.465										
Mno	0.166	0.242	0.235	0.218										
MgO	46.939	48.278	46.134	46.181										
CaO	0.08	0.28	0.133	0.088										
Na2O	0	0	0.003	0										
NiO		0.003	0.007	0										
Total	100.929	100.776	99.409	99.839										
Fo	86.04253	89.8756007	88.928118	88.7320422										
Fa	13.7845821	9.80354635	10.7492674	10.9696451										

Table 9.1 – Continue. Single mineral phase EMPA analyses. Sample: Dunite B7. Opaque minerals.

Data set	B7_Opq in Ol_c-r_continua	B7_Opq in Ol_c-r_continua	B7_Opq in Ol_c-r_continua	B7_Opq in Ol_c-r_continua	B7_Opq in Ol_c-r_continua	B7_Opq in Ol_c-r_continua	B7_Opq in Ol_c-r_continua	B7_Opq in Ol_c-r_continua	B7_Opq in Ol_c-r_continua	B7_Opq in Ol_c-r_continua
SiO2	0.023	0.017	0.023	0.065	0.026	0	0.027	0.014	0.046	0.03
TiO2	3.249	3.318	3.272	3.389	3.356	3.322	3.34	3.296	3.296	3.272
Al2O3	17.892	18.196	17.965	17.95	18.072	17.926	17.855	17.858	17.96	18.032
Cr2O3	34.137	34.109	34.701	34.639	34.37	34.53	34.197	34.512	34.178	34.463
FeO	30.426	31.17	30.67	30.543	31.177	30.578	30.557	30.727	30.102	30.494
Mno	0.287	0.261	0.231	0.291	0.291	0.293	0.255	0.247	0.263	0.289
MgO	11.184	11.252	11.167	11.342	11.197	11.311	11.201	11.664	11.464	11.522
CaO	0.021	0.009	0.007	0	0	0	0	0	0.009	0.009
V	0	0	0	0	0	0	0	0	0	0
Ba	0	0	0	0	0	0	0	0	0	0
Ni	0	0	0	0	0	0	0	0	0	0
Zn	0	0	0	0	0	0	0	0	0	0
Total	97.219	98.332	98.036	98.219	98.489	97.96	97.432	98.318	97.318	98.111

Data set	B7_Opq1 in Ol	B7_Opq1 in Ol	B7_Opq1 in Ol	B7_Opq1 in Ol	B7_Opq1 in Ol	B7_Opq1 in Ol	B7_Opq1 in Ol	B7_Opq1 in Ol	B7_Opq1 in Ol	B7_Opq1 in Ol
SiO2	0.03	0.03	0.047	0.088	0.047	0.041	0.063	0.044	0.05	0.038
TiO2	2.966	2.96	3	2.909	2.926	2.952	2.999	2.865	2.931	2.908
Al2O3	18.533	18.214	18.052	18.823	18.427	18.077	18.365	18.061	18.679	18.556
Cr2O3	34.795	35.369	35.139	35.049	34.264	35.09	35.155	34.93	34.485	34.875
FeO	30.244	30.137	29.702	30.606	30.38	30.53	30.083	30.518	30.501	29.939
Mno	0.282	0.255	0.305	0.271	0.319	0.284	0.294	0.275	0.271	0.281
MgO	11.314	11.456	11.508	10.526	11.232	11.103	10.895	10.84	11.207	11.063
CaO	0.033	0	0	0.009	0	0.014	0.021	0	0.005	0.039
V	0	0	0	0	0	0	0	0	0	0
Ba	0	0	0	0	0	0	0	0	0	0
Ni	0	0	0	0	0	0	0	0	0	0

Zn	0	0	0	0	0	0	0	0	0	0
Total	98.197	98.421	97.753	98.281	97.595	98.091	97.875	97.533	98.129	97.699

Table 9.1 – Continue. Single mineral phase EMPA analyses. Sample: Dunite B43. Olivines.

Data set	B43_Ol_c-r	B43_Ol_c-r	B43_Ol_c-r	B43_Ol_c-r	B43_Ol_c-r	B43_Ol_c-r	B43_Ol_c-r	B43_Ol_c-r	B43_Ol_c-r	B43_Ol_c-r	B43_Ol_c-r	B43_Ol_c-r	B43_Ol_c-r	B43_Ol_c-r
SiO2	40.4918683	40.1997765	40.0939313	40.5773586	40.3025684	39.7031186	40.0857894	40.4888151	40.22623775	39.88732979	40.134641	40.47253122	40.18756357	40.18552808
TiO2	0.02480858	0	0.01653905	0.01240429	0.02170751	0.0227412	0.02170751	0	0.042381322	0.038246558	0.024808578	0.009303217	0.024808578	0.054785611
Al2O3	0.06741251	0.01659385	0.05081866	0.0736352	0.02903923	0.0466702	0.04770731	0.01763096	0.057041352	0.014519617	0.060152699	0	0.059115583	0.001037115
Cr2O3	0.01645022	0.04848485	0.03030303	0.00606061	0.01991342	0	0.06320346	0.01818182	0.001731602	0.058874459	0.007792208	0.052813853	0.025974026	0.03030303
FeO	13.86961	14.3482903	14.0513873	14.4664455	14.2432634	14.2281153	14.0362392	14.3674779	14.0241207	14.12813772	14.09683163	14.34324089	13.73731647	14.29577681
Mno	0.18688918	0.2704975	0.17508565	0.19279094	0.20656173	0.20951261	0.20262722	0.20164359	0.177052908	0.170167517	0.196725454	0.219348881	0.23410329	0.236070544
MgO	44.2704748	44.5748455	44.4221612	44.7424989	44.5059879	44.8303173	44.4740539	44.5818311	44.34532002	44.42216116	44.42216116	45.23049002	44.58682074	44.53293215
CaO	0.23993818	0.24904976	0.26626052	0.28043408	0.27638449	0.25309935	0.38268622	0.29562004	0.345227514	0.286508464	0.306756412	0.308781207	0.295620041	0.279421683
Na2O	0	0	0	0	0	0.02031872	0.0083122	0	0	0.02863092	0	0	0	0
NiO	0	0.01573511	0.00629404	0.00839206	0	0.00314702	0.01153908	0	0.010490073	0.006294044	0	0	0	0.002098015
Total	99.1674517	99.7232733	99.1127808	100.36002	99.605426	99.3170402	99.3338655	99.9712004	99.22960324	99.04087025	99.24986914	100.6365093	99.1513223	99.61795305
Fo	84.8788769	84.4578243	84.768342	84.4717282	84.5903744	84.6956964	84.7718545	84.5052788	84.7689432	84.70326608	84.70725996	84.69908788	85.04684227	84.52403913
Fa	14.9175376	15.2509763	15.0418294	15.3214697	15.1865616	15.0794101	15.0087034	15.2775573	15.03876125	15.11237917	15.07960312	15.06753405	14.69944843	15.22138459

Data set	B43_Ol_c-r	B43_Ol_c-r	B43_Ol_c-r	B43_Ol_c-r	B43_Ol_c-r	B43_Ol_c-r	B43_Ol_c-r	B43_Ol_c-r	B43_Ol_c-r	B43_Ol_c-r	B43_Ol_c-r
SiO2	40.6893102	39.5972734	40.1203926	40.4847441	40.2700006	40.1122507	40.3096926	39.9636604	40.70661179	40.30053289	40.4623538
TiO2	0.01653905	0.04134763	0.01550536	0.00723584	0.02480858	0.02480858	0.01550536	0.01240429	0.015505362	0.01343798	0.017572743
Al2O3	0.0404475	0.02385366	0	0.02385366	0.0404475	0.01970519	0.02903923	0.00622269	0.024890772	0.045633082	0.045633082
Cr2O3	0.04675325	0.03290043	0.02857143	0	0.07705628	0.0017316	0.03030303	0	0.126406926	0	0.097835498
FeO	14.398784	14.0402787	14.1230884	14.2442732	14.4371592	14.4028235	13.9776665	14.0513873	14.01503183	14.09380201	13.77872131
Mno	0.25082495	0.17705291	0.1839383	0.15541311	0.18688918	0.20164359	0.13278968	0.19180732	0.194758199	0.231152408	0.23410329
MgO	44.9610471	44.9949769	44.7524783	44.6407093	44.6696495	44.9231255	44.5598764	44.4171715	44.7345154	44.56885788	44.13475535
CaO	0.26626052	0.23791339	0.27942168	0.27739689	0.29562004	0.23993818	0.31991758	0.31789278	0.310806002	0.262210927	0.228801813
Na2O	0	0	0	0	0	0	0	0	0.012930093	0	0.02401303
NiO	0.00734305	0	0	0	0.00839206	0.00104901	0.01153908	0.00419603	0.016784116	0.001049007	0.001049007
Total	100.67731	99.145597	99.503396	99.8336262	100.010023	99.9270758	99.3863295	98.9647423	100.1582405	99.51667618	99.02483892
Fo	84.5434579	84.9412344	84.7909886	84.6754728	84.4819375	84.5732919	84.9139384	84.7515249	84.873432	84.72114529	84.87884886

Fa	15.1885688	14.8688613	15.0110037	15.1570362	15.3172399	15.2110207	14.9422889	15.0405347	14.91662473	15.02920221	14.86534942

Table 9.1 – Continue. Single mineral phase EMPA analyses. Sample: Dunite B43. Opaque minerals.

Data set	B43_Opq-Ol_c-r	B43_Opq1_c-r	B43_Opq1_c-r	B43_Opq1_c-r	B43_Opq1_c-r	B43_Opq1_c-r	B43_Opq1_c-r	B43_Opq1_c-r	B43_Opq1_c-r	B43_Opq1_c-r	B43_Opq1_c-r	B43_Opq in Ol_r-r	B43_Opq in Ol_r-r	B43_Opq in Ol_r-r
SiO2	0.06920643	0.02544354	0.08447255	0.99840453	0.08854352	0.03765644	0.05394031	0.08447255	0.09261448	0.14350156	0.05190482	0.08752578	0.09363223	0.09770319
TiO2	2.44571236	2.97496203	2.90363737	2.74031423	2.98736632	2.99666954	2.91500797	2.90983952	2.91810904	2.89536784	2.83127901	2.26171540	2.39506151	2.41780270
Al2O3	17.0190653	16.9060197	16.0130633	12.8654177	17.2617503	16.8054195	16.8749062	16.7193389	16.6342954	15.5878459	16.3895361	16.6705944	16.7037821	16.7286729
Cr2O3	33.1428571	32.830303	32.2623377	29.2502165	32.9090909	33.1445887	32.791342	32.791342	32.7393939	32.6649350	32.0883116	32.8831168	33.1861471	33.8848484
FeO	29.2843272	29.2439323	28.7935284	26.2839915	29.4418676	29.2873568	29.0651845	29.1207276	29.3489591	28.4451218	29.0894215	28.3451443	28.8218049	28.7450544
Mno	0.24984133	0.21443074	0.25869397	0.25771034	0.26066123	0.35607307	0.22820153	0.27639926	0.22131613	0.25574309	0.31377709	0.27344838	0.35213856	0.21147986
MgO	12.2077615	12.2816089	11.6549045	10.8216273	12.3774108	12.2985738	12.5271013	12.0540793	12.2786150	11.7067972	12.3953736	12.1319183	12.3305077	12.1229369
CaO	0	0	0.06276864	1.28169511	0.03138432	0	0	0.01619836	0	0.04657028	0.01518596	0	0.05163226	0.02632233
V	0	0	0	0	0	0	0	0	0	0	0	0	0	0
Ba	0	0	0	0	0	0	0	0	0	0	0	0	0	0
Ni	0	0	0	0	0	0	0	0	0	0	0	0	0	0
Zn	0	0	0	0	0	0	0	0	0	0	0	0	0	0
Total	94.4187713	94.4767002	92.0334064	84.4993771	95.358075	94.9263379	94.4556839	93.9723975	94.2333032	91.7458828	93.1747899	92.6534636	93.9347066	94.2348209

Data set	B43_Opq in Ol_r-r	B43_Opq in Ol_r-r	B43_Opq in Ol_r-r	B43_Opq in Ol_r-r	B43_Opq c to Ol c	B43_Opq c to Ol c	B43_Opq c to Ol c	B43_Opq c to Ol c	B43_Opq c to Ol c	B43_Opq1 in Ol_r-r	B43_Opq1 in Ol_r-r	B43_Opq1 in Ol_r-r	B43_Opq1 in Ol_r-r	B43_Opq1 in Ol_r-r
SiO2	0.06208224	0.07938385	0.0854903	0.08650804	0.08345481	0.10889835	0.04681611	0.06309998	0.03562095	0.08549029	0.04274514	0.03053224	0.02544354	0.04070966
TiO2	2.37748877	2.3516465	2.33407376	2.30099565	2.97806311	2.92017642	2.86952558	2.89743523	2.86332343	2.43744283	2.50980118	2.55011512	2.52220547	2.46638617
Al2O3	16.7701576	16.8894258	16.7058564	16.7628978	17.5977757	16.9402445	16.9329847	16.9506157	17.2244141	16.5150271	16.4735425	16.6425923	16.4756167	16.4859879
Cr2O3	34.0683983	33.3489177	33.3272727	33.3047619	32.7601732	32.8813853	32.7229437	33.0467532	32.7454545	34.3471861	34.1359307	34.1272727	34.0822510	33.9151515
FeO	28.6531559	28.9207726	28.364332	28.564287	28.9349108	29.0661944	29.3519888	28.9641971	29.3489591	28.9793452	28.8096864	28.5430796	28.3653418	29.0853820
Mno	0.21443074	0.25082495	0.23410329	0.25574309	0.25869397	0.22525064	0.26656299	0.24689044	0.20164359	0.29017004	0.19967633	0.26754661	0.30787533	0.25082495

MgO	11.9852216	12.2546646	12.1818152	12.120941	11.6369417	12.1339142	12.1319183	12.137906	11.78563426	12.30056967	12.04010816	12.00418243	11.91835986	12.18181519
CaO	0.01518596	0	0.00303719	0.04150829	0.00809918	0.02024795	0.02328514	0.01518596	0	0	0.028347127	0	0.018223153	0
V	0	0	0	0	0	0	0	0	0	0	0	0	0	0
Ba	0	0	0	0	0	0	0	0	0	0	0	0	0	0
Ni	0	0	0	0	0	0	0	0	0	0	0	0	0	0
Zn	0	0	0	0	0	0	0	0	0	0	0	0	0	0
Total	94.1461211	94.095636	93.2359808	93.4376428	94.2581124	94.2963118	94.3460254	94.3220836	94.20505008	94.9552314	94.23983764	94.16532118	93.71531705	94.42625744

Data set	B43_Opq1 in Ol_r-r	B43_Opq1 in Ol_r-r	B43_Opq1 in Ol_r-r	B43_Opq1 in Ol_r-r	B43_Opq1 in Ol_r-r	B43_Opq1 in Ol_r-r	B43_Opq1 in Ol_r-r	B43_Opq1 in Ol_r-r	B43_Opq1 in Ol_r-r	B43_Opq1 in Ol_r-r	B43_Opq1 in Ol_r-r
SiO2	0.02646128	0.06513546	0.05902901	0.03765644	0.03460322	0.02544354	0.0488516	0.04783386	0.073277397	0.094649971	0.181158009
TiO2	2.5191044	2.51600333	2.4860263	2.51703702	2.49119475	2.49016106	2.49843059	2.48292523	2.524272858	2.523239168	2.451914505
Al2O3	16.3221237	16.2598967	16.4756168	16.5803654	16.3262721	16.5171014	16.5720685	16.6705945	16.50673023	16.54821485	16.58762524
Cr2O3	34.2181818	34.434632	34.3601732	34.0753247	33.9922078	33.412987	34.2891775	34.4337662	33.76103896	34.39220779	33.43116883
FeO	28.8632097	28.757173	28.8106963	28.8349333	28.5632772	28.8823973	29.2722087	28.4814774	28.75414335	28.96823664	29.26715935
Mno	0.19770908	0.26951387	0.26557936	0.23705417	0.27246475	0.29312093	0.23705417	0.26951387	0.228201526	0.258693972	0.168200263
MgO	12.2776171	12.0949947	11.9622691	12.2127512	11.6010159	12.3015676	12.0490896	12.0760339	12.20676361	12.22372854	13.62383394
CaO	0.02126035	0	0.01619836	0	0.02834713	0.00202479	0.03644631	0	0.026322332	0.041508293	0
V	0	0	0	0	0	0	0	0	0	0	0
Ba	0	0	0	0	0	0	0	0	0	0	0
Ni	0	0	0	0	0	0	0	0	0	0	0
Zn	0	0	0	0	0	0	0	0	0	0	0
Total	94.4456675	94.3973491	94.4355883	94.4951222	93.3093829	93.9248037	95.003327	94.4621449	94.08075026	95.05047922	95.71106014